

**NOVEL ANTIBODY-BASED BIOSENSORS FOR
THE DETECTION OF HAPTENS, PROTEINS &
WHOLE CELLS**

A thesis submitted for the degree of Ph.D.

by

Elizabeth Tully B.Sc. (Hons), DIS

DCU

**Based on research carried out at
School of Biotechnology, Dublin City University,
Dublin 9, Ireland.**

Under the supervision of Professor Richard O'Kennedy

Declaration

I hereby certify that this material, which I now submit for assessment on the programme of study leading to the award of Ph.D., is entirely my own work, that I have exercised reasonable care to ensure that the work is original, and does not to the best of my knowledge breach any law of copyright, and has not been taken from the work of others save and to the extent that such work has been cited and acknowledged within the text of my work.

Signed: Elizabeth Tully
Elizabeth Tully

Date: 20/12/07

Acknowledgements

There are many people who have been part of this journey, all of whom have supported and encouraged me during the course of my PhD, in so many different ways. Firstly; I would like to thank my supervisor, Prof. Richard O’Kennedy for his guidance, enthusiasm and an office door that was always open when I needed it. Thank-you to my examiners, Prof. Paul Engel (external) and Dr Ciaran Fagan (internal), for reading my thesis so thoroughly, and for a surprisingly enjoyable Viva. I would also like to thank the rest of the academic and support staff of the School of Biotechnology and the National Centre for Sensor Research at Dublin City University.

Sincere thanks to both Prof. Seamus Higson (Cranfield University) and Dr. Dmitri Papkovsky (University College Cork) for their invaluable support and guidance on the topics that have since become very close to my heart, impedance and fluorescence. Thanks also to Dr. Tony Killard and Dr. Robert Nooney (Biomedical Diagnostics Institute) for their important contributions, and useful comments on this work and to Dr Stephen Hearty, Dr. Paul Leonard and Dr. Brian Fitzpatrick (Applied Biochemistry Group) for donation of the antibodies used in this research. Thank you to Enterprise Ireland for the generous financial assistance and to the following industrial collaborators; Biotrin International Ltd., Slidepath Ltd., Luxcel Biosciences Ltd. and Microarray Ltd, without whom this work would not have been possible.

To the members of the Applied Biochemistry Group, past and present and the rest of the west-wing post-grads, the people who have made DCU a very special place over the past few years, thank you for driving me mad and keeping me sane! To the fantastic friends and scientists I have met along the way, especially Lynsey, Jo, Steve, Fred, Eva, Sue and little Jen. A very special thank you goes to my partners in crime, Sharon and Sinead, I feel blessed to have gone through this chapter of life with you both by my side. Thank you for the very special moments and here’s to the next chapter!

To my wonderful gang of friends for always being there when I needed you and for forever keeping my spirits up when the days in “PhD-land” got too much. A special mention goes to Alex for the pep talks and the references. Extra thanks also to Emma and Sinead for sorting out my printing issues!

To my amazing family; Evie, Jim, Vicki, Jozzka, John, Jason, Ellie and Luke for their unending support, encouragement and love, especially when I was so narky. Thanks also to my other family Bernie, Greg, Gregory, Amy and Kellie-Ann for making me feel part of yours from day one. To my parents, Madeleine and Sean, thank you for creating an environment in which following this path seemed the right thing to do. I couldn’t have managed without your love and support, so this is for you both!

Finally to my incredible husband Scott, your faith in me knows no bounds, thank you for believing even when I did not. Words can’t describe how your patience, love and support kept me going through the crazy days. I couldn’t have done it without you fumpo; I love you now and always x.

Table of contents	
Declaratton	ii
Acknowledgements	iii
Table of contents	iv
Abbreviations	xiv
Units	xviii
Publications & Presentations	xx
Presentations & Courses	xxi
Abstract	xxii
Chapter 1: Introduction	1
1.0 General Overview	2
1.1 Antibody structure & function	3
1.2 Antigens	6
1.3 Antibody production	7
1.3.1 Polyclonal antibody production	8
1.3.2 Monoclonal antibody production	8
1.3.3 Recombinant antibody production	9
1.4 Antibody Purification	11
1.5 Biosensors & Immunosensors	13
1.5.1 Fluorescence-based detection	16
1.5.1.1 <i>Fluorescent probes</i>	19
1.5.1.2 <i>NIR Probes</i>	23
1.5.1.3 <i>In vivo labeling</i>	24
1.5.1.4 <i>Lanthanides</i>	25
1.5.1.5 <i>Novel fluorophores</i>	27
1.5.1.5.1 Quantum Dots	27
1.5.1.5.2 Porphyrins	30
1.5.1.5.3 Nanoparticles	32
1.5.2 Electrochemical-based detection	34
1.5.2.1 <i>Impedance-based detection</i>	38

1.6 Target molecules for immunosensor development	39
1.6.1 Warfarin	40
1.6.2 <i>Listeria monocytogenes</i>	42
1.6.3 Parvovirus B19	45
1.7 Aims of research	48
Chapter 2: Materials and Methods	49
2.1 Material and equipment	50
2.1.1 Materials	50
2.1.2 Equipment	52
2.1.3 Composition of culture media	55
2.1.4 Standard buffers	56
2.1.5 Bacterial strains	57
2.1.6 Cell culture of mammalian cell lines	58
2.1.7 Cell culture media preparation	58
2.2 Cloning and expression of <i>Listeria monocytogenes</i>-specific proteins	59
2.2.1 Plasmid DNA purification using miniprep purification system	59
2.2.2 Agarose gel electrophoresis for DNA characterisation	60
2.2.3 DNA agarose gel purification	60
2.2.4 Preparation of high efficiency competent bacterial cells	61
2.2.5 Sodium dodecyl sulphate – polyacrylamide gel electrophoresis	61
2.2.6 Coomassie blue staining of SDS-PAGE gels	64
2.2.7 Western blot analysis	64
2.2.8 Primer design for epitope mapping	65
2.2.9 PCR amplification of genes encoding the InlB-specific proteins	65
2.2.10 Direct purification of insert PCR products	66
2.2.11 BamHI/NcoI restriction analysis on <i>E.coli</i> transformed with pQE-60	67
2.2.12 Ligation of InlB insert into pQE60 plasmid DNA	68
2.2.13 Transformation of competent XL-10 Gold <i>E.coli</i> cells with pQE-60 containing the cloned inserts	68
2.2.14 Initial expression of recombinant fragments of InlB protein	69
2.2.15 Optimisation of IPTG concentration	69

2.2.16	Optimisation of sonication conditions	69
2.2.17	Time-course expression cultures	70
2.2.18	Large-scale expression culture	70
2.2.19	IMAC purification of the 6 x His-tagged recombinant proteins	70
2.2.20	Bicinchoninic acid (BCA) assay	71
2.2.21	Sequencing of cloned inserts	72
2.2.22	Expression of anti-InlB scFv	72
2.2.23	Screening of optimised expression conditions of anti-InlB scFv	73
2.3	<i>In vivo</i> biotinylation of Internalin B protein fragments F3, F4 & F5	74
2.3.1	Restriction digests of pAC4 vector and pQE-60 inserts F3, F4 & F5	74
2.3.2	Ligation of InlB insert into pAC4 vector DNA	75
2.3.3	Transformation of electro-competent AVB101 <i>E coli</i> cells with pAC4 vector containing the cloned inserts	75
2.3.4	Expression of <i>in vivo</i> biotinylated InlB protein fragments	76
2.3.5	Purification of <i>in vivo</i> biotinylated protein fragments using a monomeric streptavidin affinity column	76
2.3.6	Characterisation of <i>in vivo</i> biotinylated InlB protein fragments	77
2.3.6.1	<i>Titre of <u>in vivo</u> biotinylated recombinant InlB fragments using extravidin-peroxidase</i>	77
2.3.6.2	<i>Titre of <u>in vivo</u> biotinylated recombinant InlB fragment F3 using streptavidin-Cy5 as tracer molecule</i>	78
2.3.6.3	<i>Optimisation of blocking reagent for fluorescence-based assays using <u>in vivo</u> biotinylated recombinant InlB fragment F3, traced with streptavidin-Cy5</i>	78
2.3.6.4	<i>Direct detection of <u>in vivo</u> biotinylated recombinant InlB fragment F3, traced with fluorescent labels; streptavidin-Cy5, avidin-FITC and streptavidin-linked quantum dots</i>	79
2.4	Antibody purification & characterisation	80
2.4.1	Polyclonal antibody purification and characterisation	80
2.4.1.1	<i>Saturated ammonium sulphate (SAS) precipitation</i>	80
2.4.1.2	<i>Protein G affinity-chromatography</i>	80
2.4.1.3	<i>Checkerboard ELISA for the determination of optimal antigen concentration and antibody dilution</i>	81

2.4.2 Monoclonal antibody purification and characterisation	82
2.4.2.1 Purification of murine IgG by Protein-G affinity chromatography	82
2.4.2.2 Checkerboard ELISA for the determination of optimal coating concentration and antibody dilution	83
2.5 Conjugate Synthesis	84
2.5.1 Preparation of drug-protein conjugates	84
2.5.2 Preparation of biotinylated antibodies	84
2.5.2.1 Biotinylation of antibodies for fluorescence-based immunoassays	84
2.5.2.2 Biotinylation of antibodies for electrical impedance spectroscopy	85
2.5.3 Fluorescent labelling of antibodies and proteins	85
2.6 Analysis of <i>in vivo</i> biotinylated InlB protein fragments and associated antibodies using Biacore	87
2.6.1 Pre-concentration studies	87
2.6.2 Immobilisation of neutravidin on sensor surfaces	87
2.6.3 Non-specific binding studies	88
2.6.4 Regeneration studies	88
2.6.5 Biacore inhibitive immunoassay for the detection of InlB F3	88
2.7 Nanoparticle Synthesis	89
2.7.1 Synthesis of silica dye-doped nanoparticles	89
2.7.2 Surface modification of nanoparticles for antibody conjugation	90
2.7.3 Nanoparticle-antibody conjugate characterisation	90
2.7.3.1 Titre of antibody-nanoparticle conjugates	90
2.7.3.2 Sandwich assay for the detection of human IgG using antibody-conjugated nanoparticles as fluorescent tracer	91
2.8 Development of fluorescence-based immunoassays	91
2.8.1 Determination of optimal fluorescent label working dilution	91
2.8.2 Competitive assay for the detection of warfarin/InlB with Quantum dot-labelled antibodies	92
2.8.3 Competitive assay for the detection of warfarin/InlB with porphyrin-labelled antibodies	93
2.8.4 Immobilisation of biotinylated anti-InlB polyclonal antibody on biochip platform, traced with streptavidin-Cy5	93
2.8.5 Biochip assay for detection of InlB with streptavidin-Cy5, as tracer molecule	94

2.9 Detection of Parvovirus B19	95
2.9.1 Enzyme-linked immunosorbent assay (ELISA) for the detection of Parvovirus B19	95
2.9.2 Fluorescence-based immunoassay (FL) for the detection of Parvovirus B19	95
2.9.3 Chemiluminescence-based immunoassay (CL) for the detection of Parvovirus B19	96
2.9.4 Biomolecule immobilisation on cone platforms	96
2.9.4.1 <i>Investigation of biomolecule immobilisation on cone platforms</i>	97
2.9.4.2 <i>Detection of immobilised anti-VP2 antibody on cone platforms</i>	97
2.9.4.3 <i>Enzyme-based sandwich assay for the detection of VP2 capsid protein on cone platforms</i>	98
2.9.4.4 <i>Chemiluminescence-based detection of HRP on cone platforms</i>	98
2.9.4.5 <i>Fluorescence-based detection of anti-VP2 antibody on cone platforms</i>	98
2.10 Immunostaining application	99
2.10.1 Slide preparation	99
2.10.2 Cell preparation	99
2.10.3 Immunostaining with anti-InlA antibody and fluorescent labels	99
2.10.4 Camera arrangement	100
2.11 Development of labelless reversible immunosensors for the detection of InlB	101
2.11.1 Fabrication of electrode sensor platforms	101
2.11.2 Instrumentation	102
2.11.3 Electrochemical insulation of carbon working electrode with polyaniline	103
2.11.4 Sensor modification	103
2.11.5 Immobilisation of biotinylated antibodies on modified sensor surfaces	103
2.11.6 Electrochemical Impedance Spectroscopy (EIS)	104
2.12 Biocompatibility Testing	105
2.12.1 Culturing of rat aortic smooth muscle cells (RASM)	105
2.12.2 Freezing of cell lines	105
2.12.3 Cell counting	105
2.12.4 Preparation of substrates for biocompatibility testing	106
2.12.5 Cytotoxicity testing of 316L stainless steel substrates	106
2.12.6 Cell proliferation & viability	106

2.12.7 Standard glutaraldehyde fixation for SEM	107
2.12.8 Characterisation of substrates post incubation in culture	107
Chapter 3: Production & Characterisation of <i>Listeria monocytogenes</i>- derived proteins and expression of anti-InlB antibodies	108
3.1 Introduction	109
3.1.1 QIAexpress cloning	110
3.1.2 pAC4 Avidity cloning	111
3.1.3 Protein expression	113
3.1.4 Protein purification using affinity chromatography	115
3.1.5 Chapter outline	116
3.2 Epitope mapping of InlB	117
3.2.1 Cloning of InlB fragments into the pQE-60 expression vector	117
3.2.2 Preparation of genomic DNA	119
3.2.3 Primer design	119
3.2.4 Amplification of InlB gene fragments by PCR	120
3.2.5 Direct purification of PCR products and preparation of pQE60 vector	121
3.2.6 BamHI/NcoI restriction analysis on pQE60 plasmid and purified PCR products containing cloned gene inserts	121
3.2.7 Ligation of vector-insert constructs	122
3.2.8 Transformation of competent XL-10 Gold <i>E.coli</i> cells with pQE-60 containing the cloned inserts	122
3.3 Expression of the recombinant InlB protein fragments (F3, F4 and F5)	122
3.3.1 Determination of InlB protein fragment solubility	124
3.3.2 Optimisation of IPTG concentration for induction of protein expression	125
3.3.3 Optimisation of sonication conditions	127
3.3.4 Time-course analysis on the expression of F3, F4 and F5	128
3.3.5 Large-scale expression culture for purification	130
3.3.6 Purification of the His-tagged InlB protein fragments by IMAC	131
3.3.7 Immunoreactivity of recombinant InlB protein fragments	132
3.3.8 Sequence analysis of recombinant InlB protein fragments	136

3.4 <i>In vivo</i> biotinylation of recombinant Internalin B protein fragments	138
3.4.1 Cloning of InlB fragments into the pAC4 vector	138
3.4.1.1 <i>Isolation of plasmid DNA from pQE-60 clones</i>	138
3.4.1.2 <i>BamHI/NcoI restriction analysis on pAC4 vector-purified plasmid DNA containing cloned gene inserts</i>	139
3.4.1.3 <i>Ligation, transformation and expression of vector-insert constructs</i>	140
3.4.1.4 <i>Confirmation of biotinylation of InlB fragments in pAC4 vector</i>	140
3.4.1.5 <i>Purification of InlB gene products by affinity chromatography</i>	142
3.4.2 Characterisation of <i>in vivo</i> biotinylated recombinant InlB fragments	143
3.4.2.1 <i>Enzyme-based detection of <u>in vivo</u> biotinylated fragments</i>	144
3.4.2.1 <i>Fluorescence-based detection of <u>in vivo</u> biotinylated fragments</i>	145
3.4.2.3 <i>Biacore analysis of <u>in vivo</u> biotinylated fragments</i>	149
3.4.2.3.1 <i>Preconcentration studies of neutravidin on the CM5-chip surface.</i>	150
3.4.2.3.2 <i>Immobilisation of neutravidin/biotinylated F3 onto the CM5-chip surface</i>	151
3.4.2.3.3 <i>Assessment of non-specific binding and regeneration studies</i>	155
3.4.2.3.4 <i>Development of a Biacore inhibition assay for the detection of InlB</i>	158
3.5 Optimisation of expression of anti-InlB scFv from naïve human library	162
3.5.1 <i>Expression of scFv in a non-suppressor strain <i>E. coli</i>, TOP 10F'</i>	162
3.5.2 <i>IMAC purification of anti-InlB scFv</i>	166
3.6 Discussion	167

Chapter 4: Evaluation of novel fluorescent labels and assay formats for antigen detection

4.1 Introduction	174
4.1.1 <i>Absorption and reflection spectroscopy</i>	174
4.1.2 <i>Luminescence</i>	175
4.1.3 <i>Optical-based detection methods</i>	175
4.1.3.1 <i>Optical wave guides</i>	175

4.1.3.2	<i>Surface plasmon resonance</i>	176
4.1.3.3	<i>Applications of optical-based detection</i>	178
4.1.4	Chapter Outline	180
4.2	Fluorescence-based immunoassay (FIA) development	181
4.2.1	Biotinylation of Antibodies	183
4.3	Development of fluorescence-based immunoassays for the detection of InlB	184
4.3.1	Checkerboard assay to determine optimal antigen coating concentration and biotinylated antibody dilution for assay development	185
4.3.2	Optimisation of blocking reagents and diluents	186
4.3.3	Competitive FIA for the detection of InlB F3 in PBS, using quantum dots as the fluorescent label	189
4.3.4	Competitive FIA for the detection of InlB F3 in PBS, using porphyrin-labelled neutravidin as the fluorescent label	193
4.3.5	Biochip application for the detection of InlB	196
4.4	Development of fluorescence-based immunoassays for the detection of warfarin	201
4.4.1	Checkerboard assay to determine optimal antigen coating concentration and biotinylated antibody dilution for assay development	201
4.4.2	Competitive FIA for the detection of warfarin in PBS, using quantum dots as the fluorescent label	203
4.4.3	Competitive FIA for the detection of warfarin in PBS using porphyrin-labelled neutravidin, as the fluorescent label	206
4.5	Immunostaining of <i>Listeria monocytogenes</i> cells	209
4.6	Development and characterisation of ruthenium dye-doped nanoparticles	213
4.6.1	Ruthenium-antibody conjugation	215
4.6.1.1	<i>Detection of hIgG using ruthenium-labelled anti-human IgG</i>	215
4.6.2	Nanoparticle synthesis and characterisation	217
4.6.2.1	<i>Calculation of enhancement effects</i>	218
4.6.2.2	<i>Antibody conjugation to ruthenium dye-doped nanoparticles</i>	222
4.6.3	Nanoparticles as fluorescent labels for use in immunoassays	223
4.6.3.1	<i>Titre of nanoparticle-antibody conjugate</i>	223
4.6.3.2	<i>Sandwich assay for the detection of hIgG using ruthenium dye-doped nanoparticles as fluorescent labels</i>	224

4.7 Development of immunoassays for the detection of Parvovirus B19	229
4.7.1 Enzyme-linked immunosorbent assay for the detection of Parvovirus B19	230
4.7.2 Fluorescence-based immunoassay for the detection of Parvovirus B19	232
4.7.3 Chemiluminescence-based immunoassay for the detection Parvovirus B19	234
4.7.4 Biomolecule immobilisation on cone structures	236
4.7.4.1 Immobilisation of HRP on modified polymer chips for enhanced fluorescence and chemiluminescence-based detection	238
4.7.4.2 Chemiluminescence-based detection on cone platforms	245
4.7.4.3 Fluorescence-based detection on cone platforms	246
4.8 Discussion	249
Chapter 5: The development of a ‘labelless’ immunosensor for the detection of <i>L. monocytogenes</i> cell surface protein fragment, InlB F3	256
5.1 Introduction	257
5.1.1 Affinity sensors	257
5.1.2 Probing biomolecular interactions by impedance spectroscopy	260
5.1.3 Immunosensors based on impedance spectroscopy	261
5.1.4 Electroactive polymers	264
5.1.5 Chapter Outline	266
5.2 Labelless affinity sensing of Internalin B	267
5.2.1 Electrochemical deposition of polyaniline at sensor surface	267
5.2.2 Preparation of biomolecules for affinity immobilisation	269
5.2.3 Affinity immobilisation of antibodies within polymer films	271
5.2.4 Electrochemical impedance interrogation of PANI thin-film carbon electrode platforms	273
5.2.5 Specific recognition of InlB with anti-InlB-doped sensors (sample)	275
5.2.6 Calibration curves showing faradaic and non-faradaic response of anti-InlB-doped electrodes against increasing concentrations of InlB	279
5.2.7 Non-specific recognition of InlB with anti-IgG-doped sensors (control)	283
5.2.8 Comparison of sample and control data	286
5.2.9 Investigation of specific InlB response at lower concentrations	291
5.3 Discussion	297

Chapter 6: Conclusions	300
6.1 Overall conclusions & future work	301
Chapter 7: References	307
Appendix: PECVD of Biocompatible coatings on 316 L stainless steel for arterial stent application	348
A1 Introduction	349
A2 Thin film composition & behaviour	349
A3 Biocompatibility testing	350
A4 Cell proliferation & viability	350
A5 Cytotoxicity testing	352
A6 SEM analysis of substrates post incubation in culture with RASM cells	353
A7 Discussion	354

Abbreviations

A/A ₀	Absorbance reading of bound antibody for each antigen concentration (A) divided by the absorbance reading determined in the presence of zero antigen (A ₀).
Ab	Antibody
AC	Alternating current
Ag	Antigen
AP	Alkaline phosphatase
AT	Annealing temperature
BCA	Bicinchoninic acid
BCIP	5-Bromo-4-Chloro-3'-Indolyphosphate p-toluidine salt
BHI	Brain Heart Infusion
BIA	Biomolecular interaction analysis
bp	Base pairs
BSA	Bovine serum albumin
CCD	Charge coupled device
cDNA	Complementary deoxyribonucleic acid
CDR	Complementarity determining regions of antibody
cfu	Colony forming units
C _H	Constant heavy chain
C _L	Constant light chain
CM	Carboxymethylated
Conc.	Concentration
CV	Coefficient of variation
DNA	Deoxyribonucleic acid
dNTP	Deoxynucleotidyl triphosphates
DMF	Dimethyl Formamide
DMSO	Dimethyl Sulphoxide
<i>E. coli</i>	<i>Escherichia coli</i>
EDC	N-ethyl-N'-(dimethylaminopropyl) carbodiimide
EDTA	Ethylenediaminetetra-acetic acid
ELISA	Enzyme-linked immunosorbent assay

F/F ₀	Fluorescent response of bound antibody for each antigen concentration (A) divided by the fluorescent response determined in the presence of zero antigen (A ₀).
Fab	Antigen binding fragment of an antibody
Fc	Constant region of an antibody molecule
FCS	Foetal calf serum
FIA	Fluorescence immunoassay
FITC	Fluorescein isothiocyanate
Fv	Variable binding region of an antibody
g	relative centrifugal force
GW	Glycine-tryptophan
HABA	4-Hydroxyazobenzene-2-carboxylic acid
HAT	Hypoxanthine, aminopterin and thymidine
HBS	Hepes buffered saline
HGPRT	Hypoxanthine guanine phosphoribosyl transferase
HMDSO	Hexamethyldisiloxane
His	Histidine
hIgG	human Immunoglobulin G
HPLC	High performance liquid chromatography
HRP	Horseradish peroxidase
Ig	Immunoglobulin
IMAC	Immobilised metal affinity chromatography
InIA	Internalin A
InIB	Internalin B
IPTG	Isopropyl-β-D-galactopyranoside
IR	Inter-repeat
ITO	Indium tin oxide
LB	Luria broth
LC	Long chain
LED	Light emitting diode
LEB	Listeria enrichment broth
LFIA	Lateral flow immunoassay
LLO	Listeriolysin O

LOD	Limit of detection
Log	Logarithmic
LRR	Leucine-rich repeats
mAb	Monoclonal antibody
mRNA	Messenger ribonucleic acid
MS	Mass spectroscopy
MTT	3-[4, 5-dimethylthiazol-2-yl]-2, 5-diphenyltetrazolium bromide
MW	Molecular weight
NBT	Nitro-blue Tetrazolium Chloride (NBT)
NCSR	National Centre for Sensor Research
NHS	N-hydroxysuccinimide
NFRU	normalised fluorescence response units
NP	Nanoparticle
NTA	Nitrilotriacetic acid
O ₂	Oxygen
OD	Optical density
OPD	o-phenylenediamine dihydrochloride
OVA	Ovalbumin
pAb	Polyclonal antibody
PAGE	Polyacrylamide gel electrophoresis
PANI	Polyaniline
PBS	Phosphate buffered saline
PBST	Phosphate buffered saline-tween
PCR	Polymerase chain reaction
PECVD	Plasma enhanced chemical vapour deposition
PEG	Polyethylene glycol
PLD	Phospholipase D
PLL	Poly-L-lysine
POC	Point of care
pH	Negative log of the hydrogen ion concentration
pI	Isoelectric point
pNPP	<i>para</i> -nitrophenyl phosphate
Pd-CP	Palladium co-porphyrin
Pt-CP	Platinum co-porphyrin

RF	Radio frequency
RI	Refractive index
rInIB	recombinant InIB
RT	Room temperature
RU	Response units
SAS	Saturated ammonium sulphate
ScFv	Single chain Fv antibody derivative
SD	<i>Standard deviation</i>
SDS	Sodium dodecyl sulphate
SEM	Scanning electron microscope
SOC	Super optimum catabolite
SPR	Surface plasmon resonance
TAE	Tris acetate ethylenediaminetetra acetic acid
TBS	Tris buffered saline
TES	Tris-EDTA sucrose buffer
TEM	Transmission electron microscope
TMB	3,3', 5,5'-tetramethylbenzidine
TY	Tryptone yeast extract
up	<i>Ultra pure</i>
UV	Ultra violet
V _H	Variable heavy chain of antibody
V _L	Variable light chain of antibody
Qdot	Quantum dot
Warf	Warfarin
Z'	Real component of impedance
Z''	Imaginary component of impedance

Units

°C	degrees Celsius
Ω	ohms
μF	microfarads
μg	micrograms
μl	microlitres
μM	micromolar (μmol. L ⁻¹)
bp	base pairs
cm	centimetres
F	farads
FRU	fluorescence response units
g	grams
(k)Da	(kilo) Daltons
kb	kilobases
kg	kilograms
l	litres
m	metres
M	molecular mass (expressed in grams)
mA	milliamps
mg	milligrams
min	minutes
ml	millilitres
mM	millimolar
mol	molar
nm	nanometres
nM	nanomolar
NFRU	normalised fluorescence response units
pg	picograms
ppb	parts per billion
rpm	revolutions per minute
RU	response units
sec	seconds
U	units

V	volts
v/v	volume per unit volume
w/v	weight per unit volume

Peer reviewed journal publications

1. **Tully, E.**, Higson, S.P.J and O’Kennedy, R., (2007), The development of a ‘labelless’ reversible immunosensor for the detection of *L. monocytogenes* cell surface protein, Internalin B, *Biosens. Bioelectronics*. (Accepted for publication).
2. **Tully, E.** and O’Kennedy, R., (2007), Fluorescent Labelling, *Encyclopaedia of Micro and Nanofluidics*, (Submitted).
3. O’Kennedy, R., **Tully, E.** *et al.* (2007). Applications of sensors in food and environmental analysis. In: *Sensors for Chemical and Biological Applications*, Chapter 5, CRC Press (Submitted).
4. **Tully, E.**, Hearty, S., Leonard, P. and O’Kennedy, R , (2006), Development of rapid fluorescence-based immunoassays for the detection of *Listeria monocytogenes*, *Int. J. Bio Macromol.*, 39 (1-3)·127-34.
5. Prasad, G.R., Daniels, S., Cameron, D.C., McNamara, B.P., **Tully E.**, and O’Kennedy, R. (2005), PECVD of biocompatible coatings on 316L stainless steel”, *Surf. Coat. Technol.*, 200, 1031-1035.
6. O’Kennedy, R., Leonard, P., Hearty, S., Daly, S., Dillon, P., Brennan, J., Dunne, L., Darmaninsheehan, A., Stapleton, S., **Tully, E.**, Quinn J., and Chakraborty T., (2004). Advances in biosensors for detection of pathogens in food and feed’, pp 85-104, in *Rapid Methods for Biological and Chemical Contaminants in Food and Feed*, Van Amerongen, A., Barug, D. and Lauwaars, M. (Eds), Wageningen Academic Publishers, The Netherlands.
7. Stapleton, S., **Tully, E.** and O’Kennedy, R. (2004), Immunoassays: Production of Antibodies, *Encyclopaedia of Analytical Science* 2nd ed., pp306-316, Academic Press, New York.

Presentations

1. O’Kennedy, R., Hearty, S., Leonard, P., Byrne, B., Sheehan, A. D., Viguier, C., Gilmartin, N., **Tully, E.**, Stapleton, S., Townsend, S., Hayes, C., McDonnell, B., Donohoe, G., Ryan, M., Darcy, E. and Fitzgerald, J. ‘Antibody engineering’. US-Ireland R&D Partnership Sensors Workshop, Dublin 20th-21st February, 2007.
2. Hearty, S., Leonard, P., Darmanin Sheehan, A., Stapleton, S., **Tully, E.**, Dunne, L., Daly, S., McDonnell, B., Skottrup, P. and O’Kennedy, R. ‘Strategies for the detection of Food Pathogens and Contaminants’. Biacore Food Analysis Symposium. Kempinski Hotel Bristol, Berlin, Germany, 27th September 2006.
3. O’Kennedy, R., Leonard, P., Hearty, S., Brennan, J., Dunne, L., Darmanin Sheehan, A., Stapleton, S., **Tully, E.**, Quinn, J. G. and Chakraborty, T. ‘Advances in biosensors for detection of pathogens in food and water’. Rapid Methods Europe 2004, Noordwijk aan Zee, Netherlands, 25-26th March 2004.
4. Prasad, G.R., **Tully, E.**, Daniels, S., Cameron, D.C. and O’Kennedy, R. ‘Adhesion Improvement of Plasma Polymerised HMDSO Films on 316L Steel by Plasma Pre-treatment and Layering’. Plasma Polymers and Related Materials-Cost Action 527, September 2004, Antalya, Turkey
5. Prasad, G.R., Daniels, S., Cameron, D.C., McNamara, B P., **Tully E.**, and O’Kennedy, R. ‘PECVD of biocompatible coatings on 316L stainless steel’. 9th International Conference on Plasma Surface Engineering, July 2004, Garmisch-Partenkirchen, Germany.
6. **Tully, E.** ‘Quantum dot nanocrystals as biological probes’. Biochip group meeting, National Centre for Sensor Research, Dublin, April 2004.

Courses

1. Successful completion of Nanobiotechnology graduate programme (2003) delivered by Cornell University Nanobiotechnology Centre (NBTC) in conjugation with the NCSR. January – May 2003.

Abstract

The modification of basic sensor platforms, incorporating specially designed materials, enhances the capacity for the development of new and improved biosensors. Novel transduction strategies employ surface modification technologies as a key element in the detection of biologically important molecules. These modifications can be chemical, electrochemical or physical. Surface modification of polymer substrates for biochip applications, thin-film deposition of biocompatible surfaces for implants and electropolymerisation of electrodes for immunoassay development are the basis of much of the research described in this thesis. A number of immunosensing methods were investigated for the generation of improved biosensors for the detection of small haptens, proteins and whole cells. These included fluorescence, chemiluminescence and impedance-based detection systems. Microtitre plates, polymer chips, fluorescence-enhancement chips and screen-printed electrodes were all examined. The specific targets chosen were Internalin B (InlB), an invasion-associated protein of *Listeria monocytogenes*, parvovirus B19, the first human parvovirus and warfarin, the ninth most prescribed drug in the world.

A panel of antibodies and antibody fragments directed against InlB (previously produced) was used for the development of fluorescence and impedance-based assays. A recombinant form of the InlB protein was cloned, expressed in *E.coli* and purified by immobilised metal affinity chromatography (IMAC). An epitope mapping study of InlB was also performed, whereby the recombinant protein was portioned into three fragments to establish the relative location of antibody-binding epitopes on its structure. The *Listeria monocytogenes*-derived proteins, peptides and antibodies were characterised using plate-based methods and subsequently used for the development of immunoassays using novel fluorescent labels and an impedimetric sensor. The recombinant InlB-derived peptides were also cloned into the pAC 4 vector for *in vivo* biotinylation, expressed in *E. coli* and purified using a monomeric streptavidin affinity column. The *in vivo* biotinylated fragments were characterised using SDS-PAGE, Western blotting, immunoassay and Biacore™ (Chapter 3)

Quantum dots and phosphorescent porphyrins were used as labels in the generation of solid-phase immunoassays. Fluorescence-based immunoassays using functionalised dye-doped nanoparticles were also developed. These doped particles were conjugated to specific antibodies and proteins using various surface modification techniques. The optimisation of solid-phase fluorescence-based immunoassays, incorporating labelled antibody-nanoparticle conjugates, for the detection of hIgG was investigated. A number of plate-based assay formats for the detection of parvovirus B19 was also investigated, in conjunction with an industrial partner; Biotrin International Ltd. Enzyme, chemiluminescence and fluorescence-based detection strategies were employed. A series of immobilisation studies was performed to study biomolecule attachment onto cone platforms for detection. (Chapter 4)

Platform technologies using carbon screen-printed electrodes and ultra-thin polymer coatings for antibody-based biosensors were also examined. Antibodies directed against InlB were deposited onto electrodes within conducting polyaniline (PANI) films to produce conductive affinity matrices with clearly defined binding characteristics. The binding of specific antibodies to their target molecules was monitored via electrical impedance spectroscopy (EIS), as the films function as label-free reversible immuno-biosensors, when interrogated with a pulsed potential waveform (Chapter 5).

Finally, the thin-film deposition of biocompatible surfaces for implants was also studied. The adhesion of thin-films to 316L stainless steel substrates was investigated. These films were prepared by plasma-enhanced chemical vapour deposition (PECVD) of hexamethyldisiloxane (HMDSO) and oxygen mixtures. The film properties were found to be dependent on the Oxygen/HMDSO flow ratio and RF (radio frequency) power. Biocompatibility studies were carried out using rat aortic smooth muscle (RASM) cells. Cell proliferation, viability and toxicity were assessed using commercial kits and scanning electron microscopy (SEM) was performed on substrates post incubation in culture to monitor the biocompatibility effects of the films (Appendix).

Chapter 1: Introduction

1.0 General Overview

The binding between an antigen and its homologous antibody, in order to identify the specific antigen or antibody in a complex sample, is the basic principle of immunoassay (Roitt, 1994). Immunochemical techniques capitalise upon the extreme specificity, at the molecular level, of each antibody for its antigen, even in the presence of high levels of contaminating molecules. The selectivity of an immunoassay is based on the innate selectivity of the antibody-antigen reaction and its sensitivity is determined by the detection limit of the label and the affinity of the specific antibody (Van Emon *et al.*, 1989). The multivalency of most antigens and antibodies enables them to interact to form a precipitate. Antibodies and antibody fragments are used in a wide variety of experimental applications for immunoassay, imaging and immunotherapy (Lefranc and Lefranc, 1990). Immunosensing techniques are useful for the detection of biologically important analytes and have wide ranging applications in clinical diagnostics (Luppa *et al.*, 2001; Vo-Dinh *et al.*, 2001; Glockler and Angenendt, 2003). The main advantages of these systems are the provision of accurate, rapid, reproducible results with little sample pre-treatment in a number of biological matrices, such as serum, plasma, urine or cerebrospinal fluid (Aizawa, 1994). Low imprecision, small lot-to-lot variations, high analytical sensitivity and long calibration stability are just some of the advantages of modern immunosensors.

This thesis describes the use of novel antibody-based detection strategies for the immunosensing of haptens, proteins and whole cells, using both novel fluorescence-based and impedance-based methods. The specificity of antigens to recognise their corresponding antibody and form a stable complex is the basis of both the analytical immunoassay in solution and the immunosensor on solid-state interfaces (Luppa *et al.*, 2001). Indeed, the specificity for the measurement of analytes in all immunosensing systems, as in the case of immunoassays, is dependent on the application of binding molecules (Ekins, 1999) and their corresponding antigens. With this in mind a general overview of antibody and antigens and their role in the development of novel antibody-based biosensors is presented.

1.1 Antibody structure & function

An antibody is a glycoprotein molecule used by the immune system to identify and destroy foreign objects like bacteria and viruses (Janeway *et al.*, 1999). Each antibody recognises a unique, specific antigen as its target (Killard *et al.*, 1995). Antibodies exist as one or more copies of a Y-shaped unit, composed of four polypeptide chains. Each Y contains two identical copies of a heavy chain, and two identical copies of a light chain, named as such by their relative molecular weights. Antibodies can be divided into five classes: IgG, IgM, IgA, IgD and IgE, based on the number of Y units and the type of heavy chain. Heavy chains of IgG, IgM, IgA, IgD, and IgE, are known as gamma, mu, alpha, delta, and epsilon, respectively. The light chains of any antibody can be classified as either a kappa or lambda type (based on small polypeptide structural differences); however, the heavy chain determines the subclass of each antibody. Although antibodies can vary in structure, they are generally typified by the immunoglobulin G (IgG) molecule, the most abundant subclass found in the serum of mammals (Stapleton *et al.*, 2004).

The basic four-polypeptide chain structure of an immunoglobulin G (IgG) molecule and the various associated IgG antibody fragments, which may be generated through genetic, enzymatic or chemical manipulations, is shown in Figure 1.1. It consists of two identical heavy chains and two identical light chains, which are held together by a number of disulphide bonds. The antibody chains can be further divided into constant (C) and variable (V) regions based on their amino acid variability. The variable regions, which are located at the N-terminal portions of both the heavy and light chains, form the antigen-binding fragment (Fab). Within this region there are areas of hyper variability, referred to as the hypervariable loops or the complementarity determining regions (CDRs), which are primarily involved in antigen binding (Branden and Tooze, 1991) It is the variation in the amino acid sequence of the CDRs that allows for the generation of a multitude of different antibodies with different binding specificities. The remainder of the variable heavy and light domains exhibit far less variation and these stretches are known as the framework regions (FRs). The crystallisable fragment (Fc) of the antibody is involved in binding surface receptors and plays a number of important physiological roles in immunological responses. This Fc portion is linked to the two Fab domains by a hinge region, which provides flexibility, allowing binding sites on each Fab arm to work independently of each other.

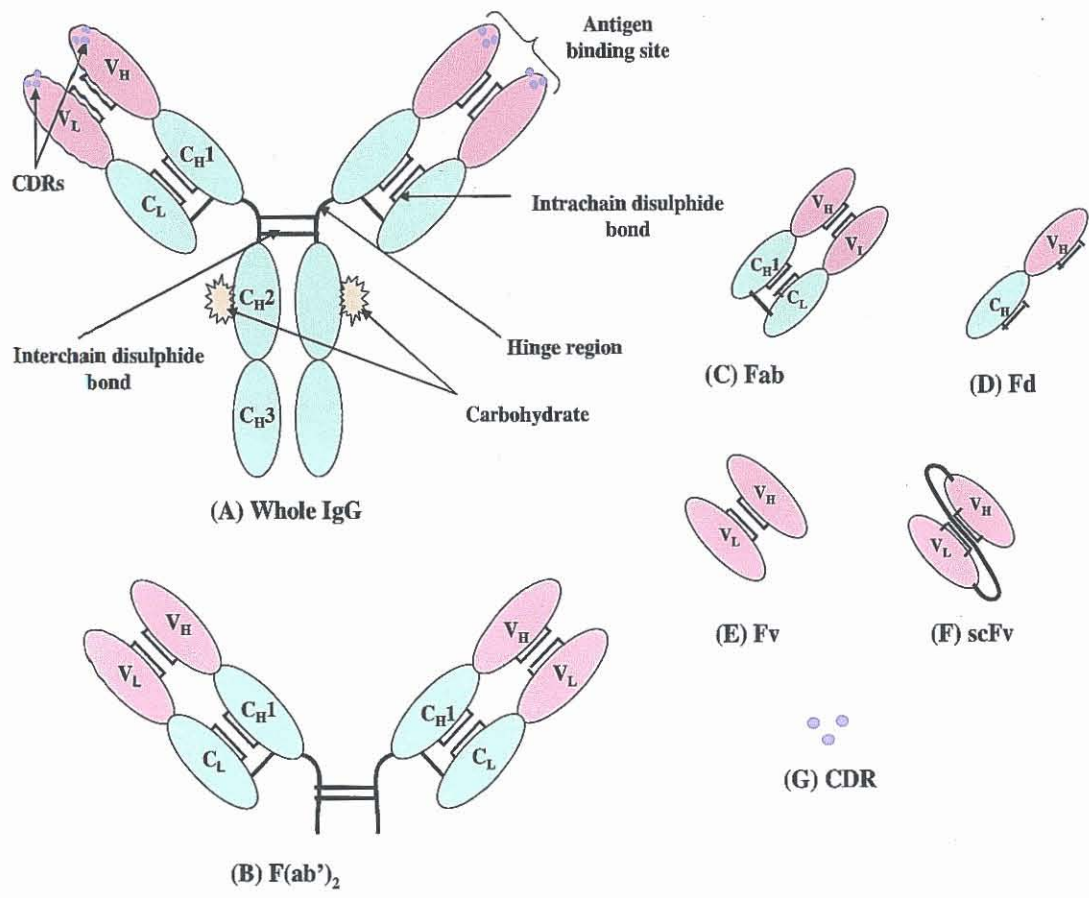


Figure 1.1 Diagrammatic representation of an immunoglobulin G (IgG) molecule and the various IgG antibody fragments, which may be generated through genetic, enzymatic or chemical manipulations. The IgG molecule (A) consists of two identical heavy chains and two identical κ or λ light chains and has a molecular weight of 150-160 kDa. The light chains comprise a variable (V_L) and constant (C_L) domain. The heavy chain consists of one variable (V_H) and three constant (C_{H1} , C_{H2} and C_{H3}) domains with a hinge region connecting the C_{H1} and C_{H2} regions. The heavy and light chains are connected via disulphide bonds; disulphide bonds are also present in the constant and variable regions. The CDRs within the variable domains confer antigenic specificity and contain considerable amino acid sequence variation. The $F(ab')_2$ (B) consists of two antigen binding fragments linked at the hinge regions, with the Fab fragment (C) consisting of one antigen binding domain and the Fd (D) comprising one V_H and one C_H domain. The Fv fragment (E) consists of one V_H and one V_L which, following stabilisation by a synthetic linker, results in the formation of the scFv fragment (F). The CDR (G) represents the smallest antibody fragment capable of antigen binding.

IgG can be cleaved into three parts i.e. two F(ab) regions and one Fc, by the proteolytic enzyme papain or into two parts, one F(ab')₂ and one Fc by the proteolytic enzyme pepsin (Yamaguchi *et al.*, 1995). The number of F(ab) regions on the antibody, corresponds with its subclass, and determines the "valency" of the antibody loosely stated, the number of "arms" with which the antibody may bind its antigen (Benjamini *et al.*, 2000) The lower part of the antibody comprises the Fc fragment, which binds to Fc receptors (Jain *et al.*, 2007). It is not needed for antigen binding, but for the physiological activity of the antibody. This part is glycosylated (in the C_H2 domains), and this glycosylation is important for maintaining the structure and, thus, activity. The highly specific interaction between an antibody and its respective antigen is mainly due to non-covalent forces such as hydrogen bonds. In addition to hydrogen bonds, other weak interactions such as van der Waals forces, hydrophobic interactions and electrostatic forces improve the binding specificity between antibody and antigen. These interactions occur over large and sometimes discontinuous regions of the molecules, improving binding affinity. Avidity is a measure of the overall stability of the antibody-antigen complex. It is controlled by three major factors - the affinity of the antibody for the epitope, the valency of the antigen and antibody, and the structural arrangement of the interacting parts. These characteristics can be altered using antibody engineering techniques to improve the binding capacity and specificity of the antibodies (Chowdhury and Wu, 2005).

Various antibody fragments, including the Fab, Fv and scFv, can be produced using recombinant DNA technology (McCafferty *et al.*, 1990; Winter *et al.*, 1994; Azzazy and Highsmith, 2002). The Fv fragment is one of the smallest antibody fragments required for complete antigen binding. However, a more stable version of the Fv fragment, the single chain Fv fragment (scFv) can be produced by adding a synthetic peptide linker to form a disulphide bridge (Young *et al.*, 1995). Other fragments can also be engineered with the ability to bind antigen, which include both the Fd fragment and the CDR (Burton and Barbas, 1993).

1.2 Antigens

Antigens can be defined as molecules that contain distinct sites or epitopes that are recognised by and interact with various components of the immune system. Immunisation of an animal with an antigen yields monospecific antiserum while mixtures of antigens, such as a cell or unpurified crude preparations, yield multispecific or polyspecific antiserum (Mayer and Walker, 1987). However, not all antigens present can be presumed to elicit the same immune response and the degree of response to a particular antigen may differ from that to another. Generally proteins and large molecules are capable of eliciting good immune responses with the aid of adjuvants (immune stimulants), such as is the case with InlB, a cell surface protein of *Listeria monocytogenes*. Smaller molecules, such as warfarin, with a molecular weight of less than 5,000 Da, are often too small to elicit an immune response on their own. They are referred to as “haptens” and require conjugation to larger carrier molecules to render them immunogenic. Various carrier proteins, such as bovine serum albumin, ovalbumin, keyhole limpet haemocyanin or thyroglobulin, are commonly used for this purpose. However, other carriers composed of synthetic or natural polymers (e.g. dextran, poly-L-lysine), lipid bilayers or synthetic organic molecules have also been used (Hermanson, 1996). Regardless of the type of molecule, a carrier must be highly immunogenic, have the required solubility properties, be non-toxic *in vivo* and possess suitable functional groups for coupling to the hapten.

There are a variety of coupling chemistries available for coupling haptens to carrier molecules (Hermanson, 1996). The choice of method is governed by the functional groups available on both the hapten and the carrier and the desired orientation of the hapten for presentation to the immune system. Conjugation procedures employing the carbodiimide EDC (1-ethyl-3-(3-dimethyl-aminopropyl) carbodiimide hydrochloride) are commonly used for immunogen formation, as the method is both efficient and relatively simple. Another advantage of this cross-linking methodology is that no bridging molecule is introduced between the hapten and carrier, thus eliminating the potential of antibodies being generated against the coupling reagent, which could dilute the desired antibody response against the hapten.

1.3 Antibody Production

Antibodies are produced in reaction to an immune response elicited by a foreign body and can be generated in a variety of ways. It is possible to produce antibodies against a broad range of antigens including larger molecules such as proteins, peptides and carbohydrates or smaller molecules such as hormones and drugs (Delves, 1997). Antibodies can be polyclonal, monoclonal or recombinant in nature. Polyclonal antibody mixtures generally contain multiple epitope specificity and only a finite amount of antibody can be obtained from the serum of an immunised animal. Monoclonal antibodies on the other hand have single epitope specificity and a potentially limitless supply. Recombinant antibodies are produced using phage display technology, whereby hapten, peptide and protein libraries can be presented on the surface of filamentous phage and specific binders selected (Maynard and Georgiou, 2000). Figure 1.2 shows a schematic highlighting the three main types of antibody production.

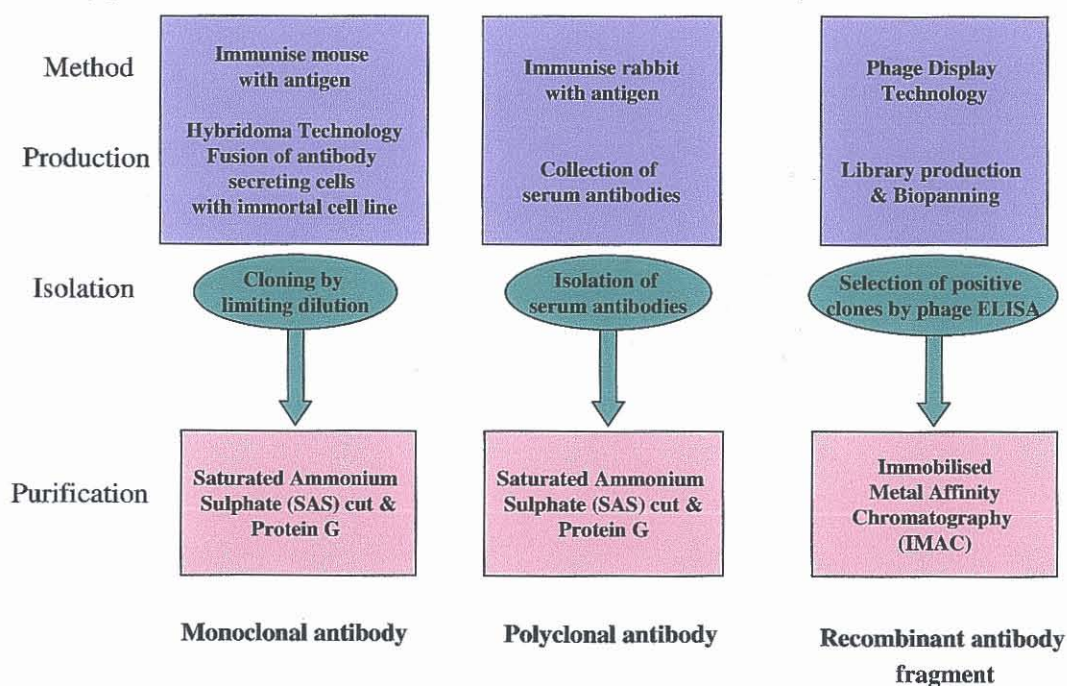


Figure 1.2 Schematic showing the production, isolation and subsequent purification of monoclonal, polyclonal and recombinant antibodies.

1.3.1 Polyclonal antibody production

Antibodies secreted in response to immunisation with a specific antigen are usually polyclonal, in that a mixed population of antigen reactive B-cells is stimulated, which recognise different epitopes on the immunogen (Mayforth, 1993). This system produces heterogeneous antibody populations, with a wide range of binding affinities. Immunisation of an animal with a particular immunogen creates an immune response that is induced against the foreign antigen. Polyclonal antiserum, containing several antibody populations against the immunogen, can be recovered from the immunised animal. Animals, such as rabbits, goats, and sheep, are generally used for polyclonal antibody production, as they are relatively easy to handle for immunisation and bleeding purposes. When a sufficient titre of antibody is obtained, the animal is bled and the antibodies are purified from the serum. Polyclonal antibodies can be produced quickly and relatively cheaply and do not require the same amount of expertise or time as monoclonal antibody production. They can also be very specific and high concentrations can be purified from small amounts of serum. However, polyclonal antiserum contains a heterogeneous population of antibodies, which can be hard to reproduce in subsequent immunisations. Unlike monoclonal antibody production, a consistent source of antibodies cannot be generated.

1.3.2 Monoclonal antibody production

During monoclonal antibody production, however, the antibody molecule is derived from a single clone of B-cells and each antibody secreted by the clone has identical antigen binding specificity. In other words monoclonal antibodies provide single epitope specificity and potentially limitless amounts of identical antibody. Monoclonal antibodies are most commonly produced by employing the hybridoma technique, first described by Köhler and Milstein in 1975. In this method, spleenocytes (normal B cells) from an immunised animal are fused with myeloma cells (tumour B cells) using a fusion medium such as polyethylene glycol (PEG). Stock myeloma cell lines selected for the fusion process are specifically chosen because they are derived from a common ancestor MOPC-21 known to have lost the ability to produce IgG, so that the only antibody produced is derived from the antigen-sensitised spleenocyte. The resultant hybrid cell is known as a hybridoma and inherits antigen specificity from the spleenocytes and immortality from the myeloma cells, thus creating a permanent cell line, which secretes a homogeneous antibody of desired

specificity. Cloning is undertaken to ensure that all hybridomas are derived from a single parent that secretes the required antibody and that non-secretors arising either in the original fusion wells or as spontaneous variants, do not outgrow the antibody-secreting hybrids (Hadas and Theilen, 1987). This ensures that the hybridomas secrete antibody that is homogeneous and monospecific. Early cloning allows selection of cells that have chromosomes for antibody production, otherwise variants not producing IgG will overgrow. There are two common methods used to clone out hybridomas, soft agar and limiting dilution. In soft agar the cells are plated out on a semi-solid medium such as low agar plates and single cells produce colonies that are further expanded, whereas limiting dilution involves seeding the cells at a known concentration in 96 well plates. It is important to seed at very low densities to ensure monoclonality and so growth conditions must be optimised to ensure that such low cell densities can survive. This is achieved by the use of special media such as Briclone. However, it is necessary to carry out several rounds of cloning before the presence of a stable monoclonal antibody-secreting hybridoma can be assumed. Hybridomas can become unstable over time and hence stocks of original clone must be maintained by cryopreservation (De Leij *et al.*, 1983).

1.3.3 Recombinant antibody production

The use of phage display vectors for displaying polypeptides on the surface of bacteriophage and bacteria, combined with *in vitro* selection technology, has changed the way in which antibodies are generated (Dillon *et al.*, 2003). Recombinant antibody technology has several advantages over conventional antibody production, including speed, the possibility of altering affinity and specificity and the ability to generate novel functionalities, (Hoogenboom *et al.*, 1998; Soderlind *et al.*, 1999; Borrebaeck, 2000). The emergence of this technique has made it possible to generate high binding affinity molecules against a number of chosen targets, resulting in potentially limitless applications (Krebber *et al.*, 1997; Hayhurst and Georgiou, 2001; Cao and Lam, 2003). These targets include bacterial pathogens such as *Brucella abortus*, toxins like aflatoxin, tumour markers and small haptens including drugs of abuse, antibiotics and therapeutic drugs such as warfarin. The scFv is one of the most commonly used antibody fragments and recombinant scFvs with specific affinities have also been produced and applied to the detection of illicit drugs (Brennan *et al.*,

2003; Dillon *et al.*, 2003) and food contaminants (Leonard, 2003; O'Kennedy *et al.*, 2005).

Recombinant antibodies consist of only the antigen binding domains and are produced from immune tissue or hybridoma cell lines through the use of recombinant DNA technology. Recombinant antibodies are maintained in bacteria and offer a stable reproducible genetic source. Recombinant antibody technology represents a fusion of cDNA library procedures and phage display technology to create and screen large numbers of immunoglobulin clones (Mc Cafferty *et al.*, 1990; Posner *et al.*, 1993). Phage display technology was first introduced by Smith (1985). This technique allowed the expression of antibody fragments on the surface of filamentous phage as a fusion partner to a phage coat protein. Phage particles which display the antibody fragment of interest are subsequently selected using a method known as biopanning, which enables the isolation of high affinity antibodies (Barbas, *et al.*, 1991; Hoogenboom *et al.*, 1998). Large antibody repertoire libraries can be generated from a variety of naive, immunised and synthetic sources.

Recombinant antibodies have already contributed greatly in the analytical and diagnostic fields (Mazuet *et al.*, 2006; Padoa and Crowther, 2006). They are especially ideal for tumour targeting where small, rapidly-penetrating but high affinity molecules are essential. With the development of new expression vectors it is now also possible to express antibody fragments on a large scale, link the fragment to an enzyme allowing direct detection or engineer a histidine (His) tag into the antibody sequence to facilitate purification by immobilized metal affinity chromatography (IMAC), (Brennan *et al.*, 2003). Recombinant antibody fragments can also be expressed as fusion proteins coupled to reporter molecules (Casaedi *et al.*, 1990). These advances in antibody engineering have had a positive influence on immunodiagnosics in general with the creation of efficient and stable biomolecules for use in immunosensing technology (Hock, 1997).

1.4 Antibody Purification

Purification of antibodies is carried out to improve the functional activity of the antibody by removing any interfering immunoglobulins or contaminants. There are a number of methods available for antibody purification and the choice of technique is dependent on a number of factors. These include the level of purity required, the antibody class, antibody source and intended application (Roque *et al.*, 2007). Antibodies may be separated according to charge or size, using traditional protein purification techniques. A precipitation technique such as saturated ammonium sulphate (SAS) precipitation isolates the IgG molecules from other serum proteins, thus stabilising the antibody and reducing lipid content. Purification by ion exchange chromatography is based on the fact that γ globulins are the least negatively charged of the serum proteins. This makes them easy to purify using positively charged ion exchange matrices. Polyclonal antiserum is subjected to SAS precipitation to remove crude proteins prior to purification using affinity chromatography to isolate IgG

Affinity purification techniques purify antibodies by capturing them on a gel matrix containing a covalently coupled analyte (Muronetz and Korpela, 2003). Purified antibody can be acquired by coupling antigen to an affinity column. The most commonly used method of affinity purification exploits the ability of Protein A and Protein G to bind specifically to certain portions of the IgG molecule (Dancette *et al.*, 1999; Fahrner *et al.*, 1999). When Protein A and Protein G are immobilised onto Sepharose the purification of monoclonal and polyclonal antibodies is possible. Protein G purification was the method chosen for the purification of the polyclonal and monoclonal antibodies used in this research. A heterogeneous mixture of molecules in solution, containing the protein of interest (in this case, SAS cut polyclonal serum or monoclonal antibody supernatant) is added to a column containing the affinity partner (Protein G) immobilised on some matrix (Sepharose resin). Target molecules are captured by their immobilised affinity partner, on a solid or stationary phase. Contaminating molecules in the solution are not captured since they do not exhibit the same affinity properties of the target molecule for the immobilised capture molecules. The solid medium can then be removed from the mixture, washed, and the target molecule released in a process known as elution (Huse *et al.*, 2002).

The use of affinity chromatography for the highly selective purification of recombinant antibodies has been reported by many authors (Casey *et al.*, 1995; Cho *et al.*, 2000). Immobilized metal ion affinity chromatography (IMAC) is an important technique employed for antibody fragment purification and was used in the research described in this thesis. IMAC is based on the specific covalent binding of amino acids, allowing proteins with an affinity for metal ions to be retained in a column containing immobilized metal ions, such as cobalt, nickel, copper, zinc, or iron (Kipriyanov *et al.*, 1997). Porath and associates (1975) were first to introduce the use of IMAC, while working on the fractionation of proteins from human serum. It is now possible to engineer a histidine tag into an antibody fragment sequence which will bind the metal chelate column, thus facilitating purification (Müller *et al.*, 1998). IMAC is now routinely used for the purification of recombinant proteins and antibody fragments, due to relatively low costs, high recovery, high stability and high purification yield, (Arnold, 1991).

Following purification, determination of the class and subclass of the antibody can be performed in a number of ways including radioimmunoassay (RIA), enzyme-linked immunosorbent assay (ELISA) and immune precipitation, using subclass-specific antisera. Commercially available antibody isotyping kits are used for this purpose. In the case of monoclonal antibodies, determination of the antibody class does not prove that the antibody is truly monoclonal. However, if the antibody was produced from a hybridoma that has undergone a rigorous and technically satisfactory cloning procedure and the antibody shows evidence of monoclonal specificity as established by a predetermined classification, it is assumed that the antibody exhibits monoclonality.

Antibody specificity is investigated by performing cross-reactivity studies with the antigen and other structurally similar antigens using ELISA, RIA, Biacore, Western and Dot Blotting. The affinity of the antibody for its specific antigen can be investigated using ELISA or biosensors. Biacore is a real-time surface plasmon resonance (SPR)-based biosensor that can be used to study biomolecular interactions without the need for labelling. The antibody-antigen interaction can be studied using Biacore, thus providing valuable information on the kinetics of association and dissociation (Alfthan, 1998).

1.5 Biosensors & Immunosensors

One of the most important issues in analytical biochemistry is selectivity, particularly at low analyte concentrations and in the presence of interfering substances. In recent years, high selectivity has been obtained by advances in analytical instrumentation such as high-performance liquid chromatography, gas chromatography, mass spectrometry and atomic absorption spectroscopy (Ashwin *et al.*, 2005; Jin *et al.* 2007). However, these powerful instruments are not applicable for *in situ* operation and can only be used in specialised laboratory environments. Therefore there is a need for highly selective sensors that are rapid and simple to use, for a number of applications, such as medical, environmental and industrial (Darmanin-Sheehan *et al.*, 2003). Biosensors are generally defined as analytical devices incorporating either a biological material or a biologically-derived material intimately associated with a physicochemical transducer or transducing microsystem, which may be optical, electrochemical, thermometric, piezoelectric, magnetic or micromechanical (Turner *et al.*, 1986). Figure 1.3 shows the general layout of a biosensor.

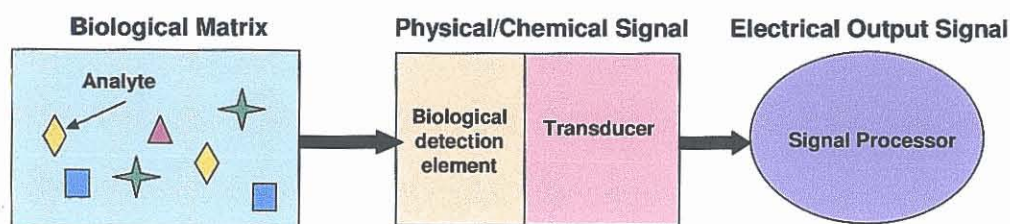


Figure 1.3 Schematic layout of a biosensor consisting of biological detection element and signal processing unit – (Adapted from Eggins, 1996). A biological matrix containing the analyte of interest is applied to a biological detection element which transduces the resultant physical or chemical signal that occurs upon biocomplex formation. The signal is then converted to a readable output (usually electronic), using a signal processor and software.

Biosensors are concerned with sensing and measuring a particular chemical or biological species, known as an analyte, (Byfield and Abuknesha, 1994). The recognition element must be biologically sensitive i.e. a molecule that is capable of either reacting with the analyte or catalysing a reaction involving the analyte. This element is immobilised at the transducer by a suitable method such as covalent attachment or physical entrapment. The transducer can take a number of different forms, but basically converts an observed change (physical or chemical) into a measurable signal whose magnitude is proportional to the concentration of the analyte under investigation (Luppa *et al.*, 2001). Biosensors combine the specificity and sensitivity of biological systems with the computing power of a signal processor (Buerk, 1993). Many types of molecules qualify for bio-recognition, and these include enzymes, receptors, peptides, DNA and living cells (Scouten *et al.*, 1995; Rao *et al.*, 1996; Quinn and O’Kennedy, 1999). However, if antibodies or antibody fragments are applied as the biological element, the device is known as an immunosensor (Taylor, 1991). Immunosensors can either be direct or indirect. Direct sensors are able to detect the physical changes occurring during immune complex formation, whereas indirect sensors use signal-generating labels, which allow more sensitive and versatile detection modes when incorporated into the complex (Blum and Coulet, 1991).

The most significant obstacles in immunosensor development are related to immobilisation, orientation and retention of the specific properties of immunomolecules on transducer surfaces. The optimum density and orientation of antibodies at immunosensor surfaces is a critical parameter. A wide variety of materials can be used as sensing surfaces for immunosensor applications and these include but are not limited to polymers, metals, glass and plastics (Darmanin-Sheehan *et al.*, 2003). Therefore, antibody immobilisation techniques must be tailored for the type of material used at the sensor surface (Turkova, 1999) and a suitable method of immobilisation derived (Lu *et al.*, 1996). In doing so, optimal biomolecule immobilisation is achieved and therefore maximum antibody functionality and reaction kinetic parameters are retained. There are four main types of immobilisation currently used at immunosensor surfaces. These include amongst others; the oriented coupling of antibodies by binding to Fc receptors such as protein A or G on the surface (Quinn and O’Kennedy, 1999), affinity coupling of biomolecules using other binding partners at the surface, such as biotin-avidin, (Schetters, 1999), coupling to

solid supports via an oxidised carbohydrate moiety (Kang *et al.*, 2007) and the binding of Fab or scFv fragments to the surface via a sulphhydryl group in the C-terminal region of the antibody fragment (Domen *et al.*, 1990).

The regeneration of the binding sites of antibodies on immunosensor surfaces is also an important consideration. Antibody regeneration using acidic or alkaline solutions can be potentially harmful to the binding ability of the antibody and can lead to denaturation of the molecule. There are a number of different approaches that can be used to solve this problem. One method is to displace the antigenic analyte using a highly concentrated solution of a related antigen with weak affinity to the surface-bound antibody; however this is only useful for small molecules (haptens). A more robust approach is to use antibody engineering techniques to improve the chemical stability of antibodies as whole molecules or as Fab fragments. Phage display techniques, (Winter *et al.*, 1994) offer such a tool and can be helpful in the selection of antibody fragments with improved stability for biosensor applications (Jung *et al.*, 1999).

Biosensors can be categorised based on the detection principle used. The five principal classes of transducer used in biosensors are; electrochemical, optical, thermometric, piezoelectric and magnetic. Electrochemical sensors may be subdivided into potentiometric, amperometric, or conductimetric sensors. Potentiometric sensors measure the change in charge density at the surface of an electrode (Ghindilis *et al.*, 1998; Purvis *et al.*, 2003). Amperometric sensors monitor currents generated when electrons are exchanged either directly or indirectly between a biological system and an electrode (Skladal *et al.*, 2002; Kameswara Rao *et al.*, 2005). Conductimetric sensors measure changes in ionic conductance (Kim *et al.*, 2000). Optical biosensors correlate changes in concentration or mass, to direct changes in the characteristics of emitted light (Myong Song *et al.*, 2005; Leung *et al.*, 2007). Other physicochemical sensors, such as thermometric, piezoelectric, and magnetic sensors, monitor biological interactions through changes in heat, mass or magnetic properties (Eggins, 1996). The research described in this thesis focuses on the use of both optical and electrochemical-based methods, namely fluorescence-based and impedance-based sensors for the detection of haptens, proteins and whole cells.

1.5.1 Fluorescence-based Detection

The use of fluorescence to facilitate measurements in biological systems has increased dramatically and includes applications in spectroscopy (Hoshina *et al.*, 2007), flow cytometry (Manger *et al.*, 2007), clinical chemistry (Hernández-Caraballo & Marco-Parra, 2003), *in situ* hybridisation (Baylis *et al.*, 2007), immunoassay (Tully *et al.*, 2006), immunocytochemistry (Buchwalow *et al.*, 2005), immunohistochemistry (Peiró *et al.*, 2007) and microarrays (Rucker *et al.*, 2005).

Luminescence is the emission of light from any substance occurring when an electron returns from an electronically excited state to ground state. There are two main categories of luminescence; fluorescence and phosphorescence and these are dependent on the nature of the excited state of the electrons involved in the process.

Fluorescence is the property whereby some atoms and molecules absorb light at a particular wavelength and subsequently emit light of longer wavelength after a brief interval, termed the fluorescence life-time (Lackowicz, 1999). Photons from an external source are absorbed by the fluorophore and this produces excited singlet state electrons. The time taken for these electrons to return to the lower energy level is known as the excited state life-time. The emission of light occurs as fluorescence from an excited electron singlet state, where all the electrons in the molecule are spin-paired. The return to ground states occurs, with the emission of photons. Emission rates are fast, being in the region of 10^8 s^{-1} , and fluorescence life-times are relatively short. Many fluorophores have sub-nanosecond life-times and, therefore, the fluorescence emitted by these dyes is short-lived.

Phosphorescence is the emission of light from triplet-excited states, whereby one set of electron spins is unpaired. This means that electrons in the excited orbital have the same spin as ground state electrons. Therefore, transition to ground state is not possible and emission rates are slow (in the region of 10^3 - 10^1 s^{-1}). Phosphorescent life-times have durations in the millisecond range. Following exposure to light, phosphorescent substances glow for several minutes as the excited phosphors return to the ground state very slowly. Figure 1.4 shows a modified Jablonski diagram depicting both fluorescence and phosphorescence-based light emission.

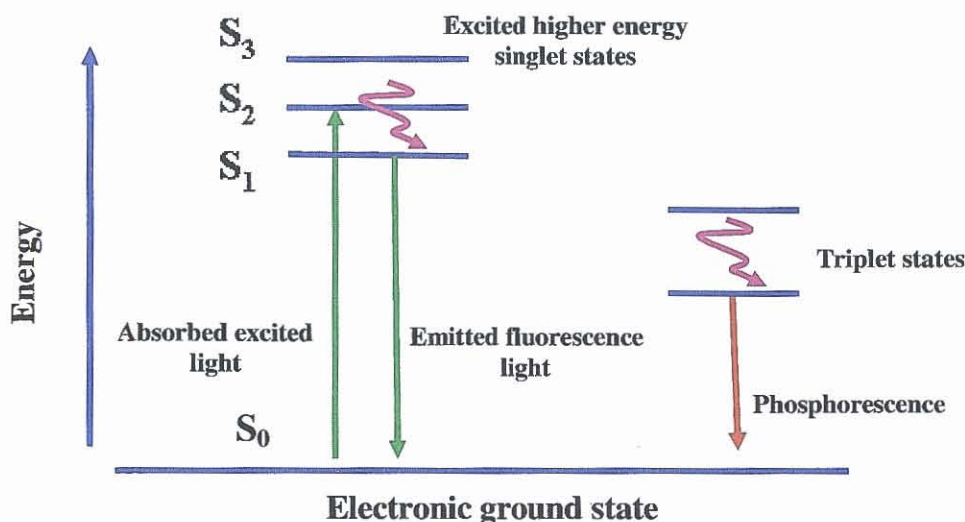


Figure 1.4 When a photon provided by an external light source is absorbed by a fluorophore, it is excited from a vibrational level in the electronic ground state (S_0) to a higher electronically excited state. The electronic state of an organic molecule can be either a singlet state whereby all electrons in the molecule are spin-paired or a triplet state where one set of electrons is unpaired. The excited singlet states (S_{1-3}) are reached after initial absorption. A molecule in this energy level will quickly fall to the lowest vibrational level of this state by energy loss through collision. Fluorescence occurs as photon of light is emitted; returning the fluorophore to ground state. The Jablonski diagram shows the possible routes by which an excited molecule can return to ground state via unstable triplet states. A quick return to ground state results in fluorescence, whereas a delayed return is known as phosphorescence - (Adapted from Lackowicz, 1999).

Biological molecules can be tagged with a fluorescent chemical group (fluorophore) using simple chemical reactions which allows sensitive and quantitative detection of the molecule. A number of processes involved in fluorescence emission can have an effect on the fluorescence characteristics of a fluorophore. These include collisions with quenchers, rotational and translational diffusion and complex formation with solvent/solute. Fluorescent molecules absorb photons of energy at one wavelength and subsequently emit energy at another wavelength (Wolfbeis, 1993). During the absorption process (excitation), the quantum energy levels of some fluorophores increases with photon uptake. This absorption band is not isolated at a discrete

(single) photon energy level but spread over a range of wavelengths, giving rise to a peak of maximal absorbance. The extinction coefficient (E) is measured at the absorbance peak maximum and is specific for each fluorophore. The ratio of total photon emission over the entire range of fluorescence to the total photon absorption (range 0-1) is known as the quantum yield (Q). The higher the quantum yield the brighter the fluorescence (photon emission) will be. Another characteristic that is an important consideration for a fluorophore is the size of its Stokes shift. Stokes Law states that the emission wavelength of a given fluorophore should be longer and of lower energy than the excitation wavelength, so that the emission spectrum should be separated sufficiently from its excitation spectrum (Mason, 1993).

The intensity of emitted fluorescence can be decreased by a number of processes and this is known as quenching. Collisional quenching occurs when the excited state fluorophore is de-activated upon contact with some other molecule in solution. Fluorophores can form non-fluorescent complexes with quenchers and static quenching can occur in the ground state, since no diffusion or molecular collisions are occurring. Quenching can also happen by other non-molecular mechanisms such as attenuation of the incident light by the fluorophore itself or the presence of another absorbing species in the sample (Hermanson, 1996). Another problem encountered with the use of fluorescence for analysis is over labelling. Decreases in emission intensities can occur, as the level of probe attachment to biological molecule is increased. This happens since fluorophores can self-quench at high label levels, due to the energy transfers from excited state molecules to ground state dimers.

However, fluorescence-based detection is a safe, rapid, non-invasive technique suitable for many biological applications (Hall *et al.*, 1999; Sutherland, 2002; Lochner *et al.*, 2003) and has many advantages over other light-based investigative methods. Changes in concentration can be monitored very rapidly and samples are not affected or destroyed in the process. A fluorescence emission spectrum is a plot of fluorescence intensity versus wavelength (nm) or wavenumber (cm^{-1}). Emission spectra vary widely from fluor to fluor and are dependent on chemical structure and environmental conditions e.g. pH, buffer components, solvent polarity and dissolved oxygen.

1.5.1.1 Fluorescent probes

Detection of labels for use in biological applications can be performed by either spectrophotometric or radioactive methods (Wolfbeis, 1993). The use of spectrophotometric probes includes both chromogenic (coloured) labels and fluorescent labels. Chromogenic labels are mainly used for the non-covalent staining of structural features within cells as the coloured pigments in the dye bind to specific areas in the cell. However, there are a number of problems associated with these tags. The sensitivity of visible wavelength dyes is generally not sufficient for detection of low concentrations of antigen and, even if a biomolecule is covalently modified with the chromogen, a relatively large amount of dye is required.

Fluorescent probes (fluorophores) are relatively small molecules that are used to label biomolecules such as proteins, antibodies and nucleic acids. They contain functional groups and specific physical and chemical characteristics that confer suitability for their use as detection moieties. To date, thousands of fluorescent probes are known each with varying spectral properties. Fluorescent labels have provided excellent sensitivity for a range of assay systems that can be applied to the determination of almost any analyte. Fluorescent tags have a number of attributes including large quantum emission yield upon excitation and easy conjugation to biomolecules via reactive groups that make them highly suitable for biological detection. The physical and chemical properties exhibited by an ideal fluorescent label are shown in Table 1.1

Table 1.1 List of ideal properties for fluorescent probes

<i>Properties</i>	<i>Ideal fluorescent probe</i>
<i>Light emitted</i>	Narrow band of emission
<i>Stability</i>	Emits brightly; photostable
<i>Stokes shift</i>	Large shift with good distance between excitation and emission wavelengths
<i>Quantum yield</i>	High quantum yield, approaching 1
<i>Fluorescence life-time</i>	Long life-time
<i>Light source</i>	Broad excitation range; inexpensive

These include high quantum yield and a large Stokes shift to ensure good separation of excitation and emission wavelengths. A large Stokes shift will increase the fluorescent signal generated as interference from Rayleigh scattered excitation light is decreased. The aromatic ring system contained in most fluorophores generates the luminescence and, as the ring gets larger, the emission shifts to red and the quantum yield increases. Aromatic ring constituents affect the fluorescent behaviour of each dye. Ring activators i.e. electron donating groups increase the quantum yield of a fluorophore whereas electron withdrawing groups decrease it. The presence of heavy atoms can also diminish the quantum yield by enhancing the probability of the excited singlet state going into triplet transition. Energy decay from a triplet excited state causes phosphorescence instead of fluorescence. The phosphorescent band is located at longer wavelengths and, hence, at lower energies, relative to the fluorescence spectrum (Lackowicz, 1999). Polycyclic structures in the aromatic ring system are important to maintain fluorescent properties. Co-planar structures, i.e. rings in the same dimensional plane, show the greatest fluorescence. Malachite green and rhodamine have very similar structures, yet the oxygen bridges on the upper phenyl rings of rhodamine confer a planar shape, thus enhancing its luminescent qualities (Hermanson, 1996).

Intrinsic fluorophores are naturally occurring whereby the intrinsic fluorescence originates within the aromatic amino acids such as tryptophan, tyrosine and phenylalanine. The indole groups of tryptophan residues are the dominant source of UV absorbance/emission in proteins. Emission of tryptophan is very sensitive to local environmental changes and can be used as a reporter group for protein conformational changes. The emission maximum of proteins reflects the average exposure of tryptophan residues to the aqueous phase. Tryptophan fluorescence is subject to quenching by iodide, acrylamide and disulphide groups and also by nearby electron-deficient groups and protonated histidine residues (Suresh Kumar *et al.*, 2007). Extrinsic fluorophores, on the other hand, are added to samples to provide fluorescence when the molecule of interest is non-fluorescent or the intrinsic fluorescence is too weak. Proteins with weak intrinsic fluorescence can be labelled with fluorophores that have longer excitation and emission wavelengths than their constituent aromatic amino acids. There are huge numbers of such fluorophores. Reagents are available that can be used for both the covalent and non-covalent

labelling of proteins. In the case of covalently bound probes a variety of reactive groups is available for effective coupling with amine, sulphhydryl and histidine side chains in proteins. Ideally, for labelling of biomolecules, each fluorophore should have several analog forms each with a different reactive group suitable for coupling to a different specific functional group on the target molecule. Popular organic labels include derivatives of fluorescein, rhodamine, coumarin, and cyanine, as shown in Table 1.2.

Table 1.2 List of common organic fluorophores.

Fluorophore	Mr (Da)	λ_{ex} (nm)	λ_{em} (nm)	Fluorescent lifetime (ns)	Quantum Yield (Q)	Reacts with
Fluorescein isothiocyanate (FITC)	389	494	520	~ 4.1	0.75	Amines
NHS-fluorescein	457	491	518	~ 4.0	0.75	Amines
Iodoacetamido-fluorescein	515	491	520	~ 4.0	0.75	Sulphydryls
Fluorescein-5-maleimide	427	490	515	~ 4.0	0.75	Sulphydryls
Fluorescein-5-thiosemicarbazide	421	492	516	~ 4.0	0.75	Aldehyde/Ketone
5-(((2-(Carbohydrazino)methyl)-thio)-acetyl)-aminofluorescein	493	490	516	~ 4.0	0.75	Aldehyde/Ketone
Tetramethylrhodamine-5-(6)-isothiocyanate	444	544	570	~1.5	0.25	Amine
NHS-rhodamine	528	546	579	~1.5	0.25	Amine
Lissamine rhodamine sulphonyl chloride	577	556	576	~2.1	0.25	Amine
Texas red sulphonyl chloride	577	556	576	~4.2	0.25	Amine
Tetramethylrhodamine-5-(6)-iodoacetamide	569	540	567	~	0.25	Sulphydryls
Lissamine rhodamine B sulphonyl hydrazine	573	560	585	~	0.25	Sulphydryls
Texas red hydrazine	621	580	604	~	0.25	Sulphydryls
7-Amino-4-methyl-coumarin-3-acetic-acid	233	345	450	~	0.49	Amines (using EDC activation)
Cyanine 3 (Cy3)	767	550	570	~0.2	~0.25	Amines
Cyanine 5 (Cy5)	792	649	670	~0.3	~0.29	Amines

There are many techniques available for the direct and indirect labeling of biomolecules with fluorescent tags for biological applications (Sun *et al.*, 2006; Tirat *et al.*, 2006; Lundberg *et al.*, 2007). The selection of an appropriate fluorescent tag is dependent on a number of parameters such as sample type, mode of action, immobilisation strategy, excitation and emission characteristics of the fluorophore and the type of analyte being detected. Fluorescence-based detection of antibody-antigen binding interactions was traditionally performed with organic fluorescent tags such as FITC or rhodamine (Hermanson, 1996) which display a number of advantageous properties such as long absorption maxima, insensitivity to solvent polarity, high molar extinction co-efficients and the availability of a wide variety of reactive derivatives. Fluorescein derivatives are characterised by a multi-ring aromatic structure, due to the planar nature of an upper, fused, three-ring system (Figure 1.5).

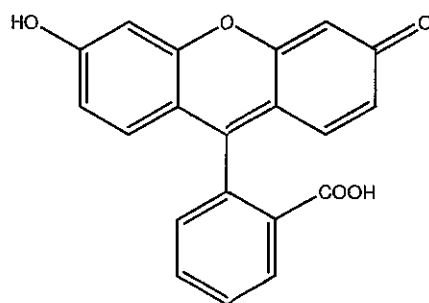


Figure 1.5 Structure of Fluorescein

Derivatives of the basic structure of fluorescein involve substitution of carbons number 5 or 6 of the lower ring, for modification and labeling of biomolecules. The effective excitation wavelength range is between 488-495nm, while the emission spectrum lies between 518-525nm, depending on the derivative. The quantum yield of fluorescein derivatives can be up to 0.75 (Hermanson, 1996). However, quick photobleaching can occur when the dye is dissolved in buffers, exposed to light or pH variations or subjected to long-term storage. The main applications of FITC include; labelling of antibodies to detect antigens in cells, tissues, immunoassays, blots, chips, and microarrays, identification of molecules separated by capillary zone electrophoresis and use as a label in flow cytometry.

There are significant problems associated with the use of organic fluorophores, such as fluorescein, in biological applications. These molecules often have narrow excitation spectra and broad emission bands and so multiplexing of assays is difficult as spectral overlap can take place. Quenching, photobleaching and autofluorescence can also occur, affecting the generated signal, and giving rise to skewed or invalid results. Therefore, the need for more photostable and robust labels was identified. The following sections (Sections 1.5.1.2-1.5.1.5) give a general overview of the development of more stable, sensitive fluorescent labels and their associated technologies.

1.5.1.2 Near-infrared (NIR) Fluorescent Probes

Near-infrared (NIR) detection of biomolecules has a number of advantages over conventional fluorophores, including low fluorescence background, since very few naturally occurring molecules can undergo electronic transitions in this low energy region of the spectrum (Basheer *et al.*, 2007). Scatter is also reduced at higher wavelengths at this end of the spectrum thus reducing sample photodecomposition. NIR probes have high quantum yields, large Stokes shifts, photochemical stability and a high tolerance to quenching. Good examples of NIR probes are the cyanine dyes. These molecules have emission maximums between 600-800nm. The quantum yields of these probes in aqueous solutions are very low. However, on binding to analytes changes in absorption and emission wavelengths are increased as the fluorescent lifetime increases. Figure 1.6 shows the basic structure of a cyanine dye.

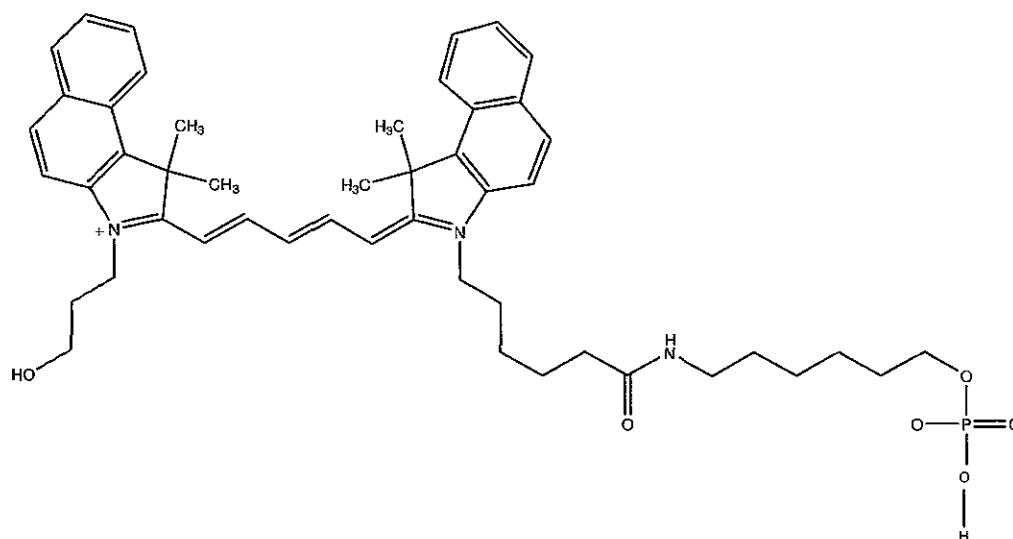


Figure 1.6 Structure of Cyanine 5

Cyanine dye fluorophores fluoresce brightly and contain a (-CH=CH-)₃ group linking two nitrogen-containing heterocyclic rings, as shown in Figure 1.6. They can be functionalised with NHS-ester, maleimide, isothiocyanate and hydrazine chemistries for biomolecule attachment and exhibit high molar extinction coefficients and favourable quantum yields. The small size of these dyes reduces steric hindrance, and therefore, loss of activity (Hermanson, 1996). Cyanine dyes are used for standard fluorescence, fluorescence resonance energy transfer (FRET), time-resolved fluorescence (TRF) and fluorescence polarisation applications. Cyanine dyes can be used to label proteins both covalently and non-covalently (Song *et al.*, 2004).

1.5.1.3 *In vivo* labelling

The green fluorescent protein (GFP) from the jellyfish, *Aequorea victoria*, is a versatile reporter for monitoring gene expression and protein localisation in a variety of cells and organisms (Tsien, 1998; Kukar *et al.*, 2002). GFP emits bright green light on excitation. The chromophore in GFP is intrinsic to the primary structure of the protein, and fluorescence from GFP does not require additional gene products, substrates or other factors. GFP fluorescence is stable, species-independent and can be monitored non-invasively using the techniques of fluorescence microscopy, fluorescence-activated cell sorting (FACS), flow cytometry and fluorescence resonance energy transfer (FRET). Since the first use of GFP in living organisms, live cell fluorescence microscopy has become an indispensable tool for cell biologists. In recent years many fluorescent reporters suitable for *in vivo* experiments have been developed, including a wide range of fluorescent proteins in various colours (Awais *et al.*, 2007). The technique of labelling genes and proteins *in vivo* for microarray purposes has become an important tool in the development of gene and protein expression analysis (Todman *et al.*, 2005). *In vivo* labelling methods give accurate pictures of what is happening in the natural dynamic environment and these techniques are a vital tool for fluorescence-based detection, especially for microarray applications.

1. 5.1.4 Lanthanides

Fluorescence typically occurs from aromatic molecules (Basheer *et al.*, 2007) e.g. naturally occurring fluorescent substances such as quinine, fluorescein, rhodamine B, acridine orange and 7-hydroxycoumarin. In contrast to aromatic organic molecules, atoms are generally non-fluorescent in the condensed phase. However, the lanthanides, a group of elements including terbium and europium, do not follow this rule. Fluorescence occurs in these molecules as a result of electron transitions between orbitals. Lanthanides exhibit long decay-times due to the shielding effect of electron transitions between the orbitals and short emission rates because of their low extinction co-efficients (Lamture *et al.*, 1996).

Long life-time probes are those with fluorescent life-times greater than those of traditional organic probes (1-10ns). Lanthanides are transition metals with fluorescent life-time decay times between 0.5-3ms (Handl and Gillies, 2005). Transition metal ligand complexes are made up of metal and organic ligands. They contain mixed singlet-triplet states and have intermediate lifetimes of 400 nanoseconds to microseconds. Their absorption co-efficients are very low and emissive rates slow, giving rise to long life-times. They are not directly excited but use chelated organic liquids as conduits. Lanthanides can substitute chemically for calcium in calcium-dependent proteins. They can be used with proteins that do not have intrinsic binding sites and are particularly useful in immunoassay applications (Gudgin-Dickson *et al.*, 1995). Biological samples can exhibit autofluorescence, which can be limiting, since autofluorescence from the sample decays on a nanosecond timescale, as does the fluorescence of most probes. However, due to the long decay time of lanthanides, they continue to emit following the disappearance of autofluorescence. Time-gated detection can be used with lanthanides whereby steady state intensity measurements are taken over a period of time following pulsed excitation. This principle of time-gated detection of long life-time probes is illustrated in Figure 1.7.

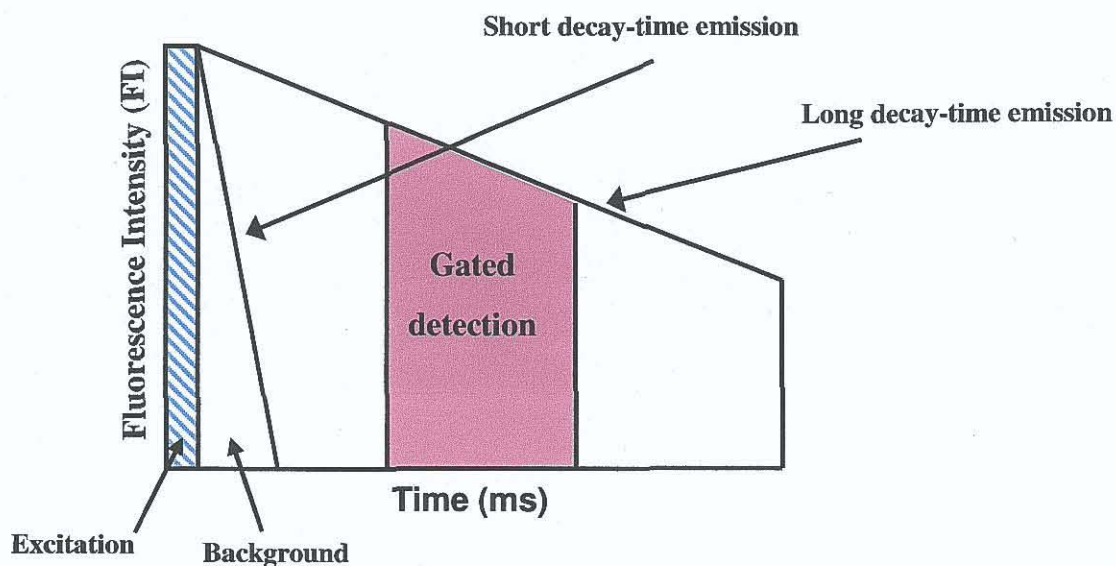


Figure 1.7 Principle of time-gated fluorescence detection. Time-gated fluorescence detection is used to monitor the fluorescence of a sample as a function of time, after excitation by a flash or pulse of light. This figure shows a schematic of the system used with lanthanide molecules whereby steady-state intensity measurements of emitted fluorescence are taken over a period of time following pulsed excitation. Time resolution is optically gated, whereby a short laser pulse acts as a gate for the detection of emitted fluorescence and only fluorescence that arrives at the detector at the same time as the gated pulse is collected. In time-gated detection systems, the detector is turned on after excitation and the fluorescence intensity generated is integrated. This method is useful for long lifetime probes.

1.5.1.5 Novel Fluorophores

The evolution of novel fluorophores that exhibit greater stability and brightness, has led to improved sensitivity and reproducibility in biological monitoring (Chan *et al.*, 2002). The advent of inorganic fluorophores such as quantum dots, nanocrystals and nanoparticles has revolutionised fluorescence-based detection methods. These novel fluorescent molecules exhibit large Stokes shift, high quantum yields and can be excited with a broad range of excitation sources (Seydack, 2005). Functionalisation of the polymer shell of such molecules is generally quite simple and allows direct coupling of the probe to biomolecules. Novel fluorescent probes have higher quantum yields and high resistance to photodegradation and the main advantages of such probes are their narrow predictable emissions, extreme photostability and brightness (Bruchez *et al.*, 1998; Tan^b *et al.*, 2004; Goldman *et al.*, 2005). Quantum dots, dye-doped nanoparticles and phosphorescent porphyrin dyes were used in the development of novel immunoassays described in this thesis.

1.5.1.5.1 Quantum Dots

Quantum dots are tiny light-emitting particles on the nanometer scale. They are a new class of biological label with improved characteristics and properties that are superior to traditional organic dyes and fluorescent proteins. Recent advances have led to quantum dot bioconjugates that are highly luminescent and stable (Chan and Nie, 1998; Mattoussi *et al.*, 2000; Goldman *et al.*, 2004). These bioconjugates raise new possibilities for studying genes, proteins and drug targets in single cells, tissue specimens and even in living animals (Ackerman *et al.*, 2002; Gao and Nie, 2003; Mulvaney *et al.*, 2004; Goldman *et al.*, 2006; Kerman *et al.*, 2007).

Quantum dots are nanocrystalline semi-conductors that exhibit unique light emitting properties that can be customised by changing the size or composition of the dots (Alivisatos, 2004). They are typically 2-8nm in size and covered with a layer of organic material that allows functionalisation of the surface for biomolecule attachment (Bruchez *et al.*, 1998; Seydack, 2005). The colour is determined by the size of the particles and the composition of the materials used, which in turn dictate the optical properties. Smaller dots fluoresce at shorter wavelengths (blue), while larger dots emit at longer wavelengths, (red). One of the main advantages of nanocrystalline fluorophores is that they absorb light over a broad spectral range. By

absorbing all wavelengths shorter than their emission wavelength (blue wavelengths), a single light source is required for the excitation of multiple coloured dots. This simplifies instrumentation, lowering costs and enabling multiplexing of assays (Goldman *et al.*, 2004). Typically in fluorescence-based measurements, when dealing with ordinary fluorescence labeling using proteins, such as green fluorescent protein, or organic dyes, such as rhodamine, it is difficult to utilise more than two or three colours at once. Each of the fluorophores must first be excited with a specific wavelength of light, which can block the emitted colour of a second or third fluorescent probe. However, with quantum dots the same wavelength of light can be used to excite different sized dots (and therefore colours), thus facilitating simple multiplexing of assays. Figure 1.8 shows a schematic representation of the basic quantum dot structure.

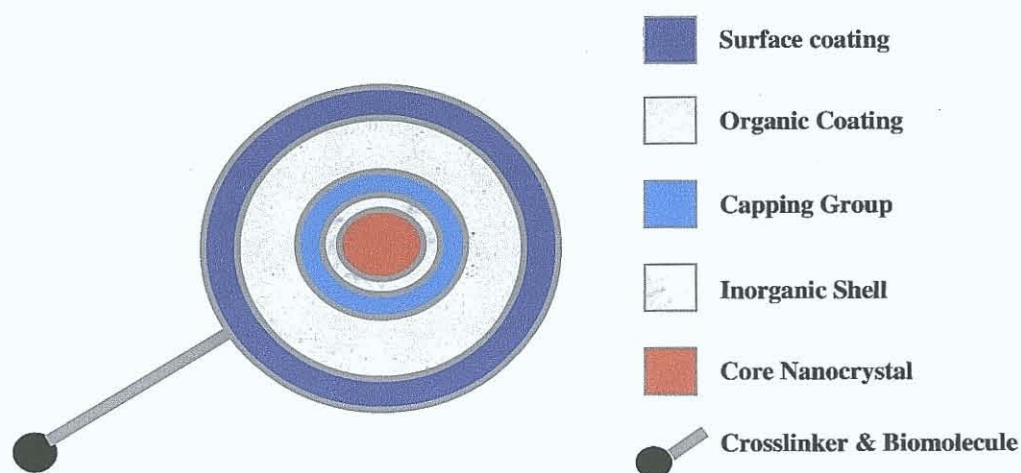


Figure 1.8 Schematic depicting the component layers of a quantum dot. An inorganic zinc sulphide (ZnS) shell encapsulates the core nanocrystal composed of cadmium selenide (CdSe). The inorganic shell is subsequently capped and an organic layer and a polymer surface coating are applied to enable biomolecule attachment. For the quantum dots used in this thesis the polymer shell is directly coupled to streptavidin through a carbodiimide-mediated coupling reaction for biomolecule attachment.

For the research described in this thesis, streptavidin conjugated quantum dots were purchased from the Quantum Dot Corporation, (USA). These unique fluorescent probes have an emission maximum near 605nm and can be excited with a range of excitation sources. The quantum dots comprise of a cadmium selenide (CdSe) core shell coated with a zinc sulphide (ZnS) semi-conducting inorganic coating to improve optical properties. This is further functionalised by coating with a polymer shell to allow direct coupling to biomolecules. In this case the polymer shell was directly coupled to streptavidin through a carbodiimide-mediated coupling reaction as shown in Figure 1.8.

The narrow emission spectra of nanocrystals give rise to sharper colours and high spectral resolution, which improves assay sensitivity since nanocrystals emit more light than their constituent dye. Quantum dots are not liable to photobleaching, exhibit excellent photostability and, relative to conventional fluorophores, are up to 100 times more stable (Seydack, 2005). It is this photostability that allows repeated interrogation of the materials over longer periods. Quantum dots have high excitation cross sections, in that they absorb much of the light with which they are irradiated, and high quantum yields whereby they re-emit more than 50% of the light they absorb (Sun *et al.*, 2001). This gives rise to strong fluorescence signals, thus increasing detection sensitivity.

The potential uses of quantum dots in biological applications include drug delivery, diagnostics, drug discovery, genetic analysis and observation of biomolecular interactions (Aoyagi and Kudo, 2005; Kerman *et al.*, 2007; Lucas *et al.*, 2007). In the research described in this thesis, quantum dots were investigated as novel labels for the development of immunoassays for the detection of InlB and warfarin. An imaging application was also performed using quantum dots as the fluorescent label for the immunostaining of *L. monocytogenes* whole cells.

1.5.1.5.2 Porphyrins

Organic fluorescent labels such as FITC, Cy5 and rhodamine can exhibit high optical background in immunoassay applications, which reduces sensitivity (Wolfbeis, 1993). The use of long-decay fluorescent probes and time-resolved detection allows for a significant decrease in background and, therefore, an increase in sensitivity. The lanthanide chelates, such as europium and terbium have traditionally been used as probes for the time-resolved fluorescent detection of analytes (Yuan and Wang, 2006). Functionalised derivatives of these dyes are available commercially for both homogenous and heterogeneous assays. However, an enhancement step is often necessary, such as dissociative enhancement (DELFLIA) or addition of enzyme labels to improve performance, resulting in an enzyme-amplified lanthanide luminescence system (Gudgin-Dickson *et al.*, 1995; Handl and Gillies, 2005).

Another group of structures, the metalloporphyrins, is particularly suitable for biological applications, due to their relatively long decay times. Metalloporphyrins provide a realistic alternative to fluorescent lanthanide chelate labels. Phosphorescent metalloporphyrins, such as the water-soluble platinum and palladium complexes of coproporphyrin, have a number of advantages as labels for immunoassay development (Hemmilá & Mukkala, 2001). Palladium (II) and platinum (II) complexes of porphyrins were first synthesised and studied by Eastwood and Gouterman (1970). These complexes of porphyrin and related tetrapyrrolic pigments emit strong phosphorescence at room temperature, which is characterised by long lifetimes falling into the sub-millisecond range and long-wave spectral characteristics. These include high quantum yields of up to 40%, simple laser excitation at 532nm and broad red emission (600-750nm). It is these features that make porphyrin dyes useful as probes for a number of bioanalytical applications, particularly those employing time-resolved fluorescent detection (Papkovsky, 1991 and 1993). The basic structure of porphyrin consists of four pyrrole units linked by four methene bridges (Figure 1.9).

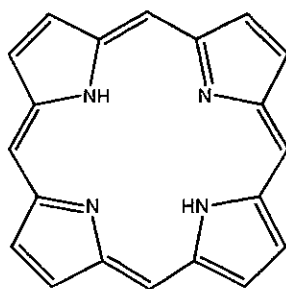


Figure 1.9 Structure of porphyrin

Metalloporphyrins can be synthesised to have either isothiocyanate reactive groups or maleimide reactive groups, allowing conjugation to be tailored exactly to suit the substance being labelled. There are two main conjugation strategies for porphyrin attachment to proteins. The first involves the activation of the porphyrin by carbodiimide, followed by nucleophilic attack of the primary amino groups of the biomolecule to produce bioconjugates via the amide bond. The second method employs carbodiimide to preactivate the porphyrin in the presence of an active ester, which results in a porphyrin derivative, with active functional groups that can react with the amino groups of a biomolecule (O’Riordan *et al.*, 2001; Papkovsky and O’Riordan, 2005).

Novel derivatives of platinum and palladium coproporphyrin were made available for the development of novel immunoassays, in association with an industrial partner Luxcel Biosciences Ltd. (UCC, Cork). The derivatives were used to make phosphorescent conjugates of antibodies and neutravidin. The labels and conjugates were then evaluated in solid phase immunoassays using a commercial phosphorescence-based detector, and investigated as novel probes for the detection of both InlB and warfarin.

1.5.1.5.3 Nanoparticles

Fluorescent labeling of biological materials using organic fluorescent dyes is widely employed in immunoassays and biological imaging (Lackowicz, 1999). However, organic fluorophores have limitations such as poor photostability and brightness, especially for samples with high background fluorescence (Trau *et al.*, 2002). Indeed even the highly luminescent quantum dots described by Chan and Nie (1998) have certain characteristics which limit their effectiveness. These include poor solubility in water, blinking and highly toxic cadmium components. Fluorescent nanoparticles exhibit considerable advantages in detection over both organic fluorescent dye molecules and quantum dots. The superiority of nanoparticles is apparent in their stability, brightness and ease of functionalisation for bioconjugation.

Organically modified silicate materials have become an attractive field of study due to the versatility and flexibility associated with their preparation (Pham *et al.*, 2007). Dye-doped silica nanoparticles display high stability and retain their optical activity, thus providing a viable method for the production of tailored materials with unique properties for biological applications. Ow *et al.* (2005) described a class of highly fluorescent core-shell nanoparticles, up to 20 times brighter and more photostable than their constituent fluorophore. The fabrication of such molecules employs a microemulsion technology. This method encapsulates fluorescent dye molecules into a silica matrix, giving rise to dye-doped nanoparticles with a high intensity fluorescent signal. The excellent photostability of doped nanoparticles is due to exclusion of oxygen by the silica encapsulation. Surface modification post-fabrication allows efficient conjugation to biomolecules. Silica is easy to modify, either through NHS activation, silanisation or carboxyl modification (Lian *et al.*, 2004). Scanning electron microscopy (SEM), transmission electron microscopy (TEM) and fluorescence spectroscopy are used to characterise the doped nanoparticles to determine size uniformity, quantum yield, fluorescent life-time and fluorescent intensity. Each nanoparticle encapsulates thousands of fluorescent dye molecules in the protective silica matrix, providing a highly amplified and reproducible signal for fluorescence-based bioanalysis. Figure 1.10 shows a schematic depicting the structure of dye-doped nanoparticles.

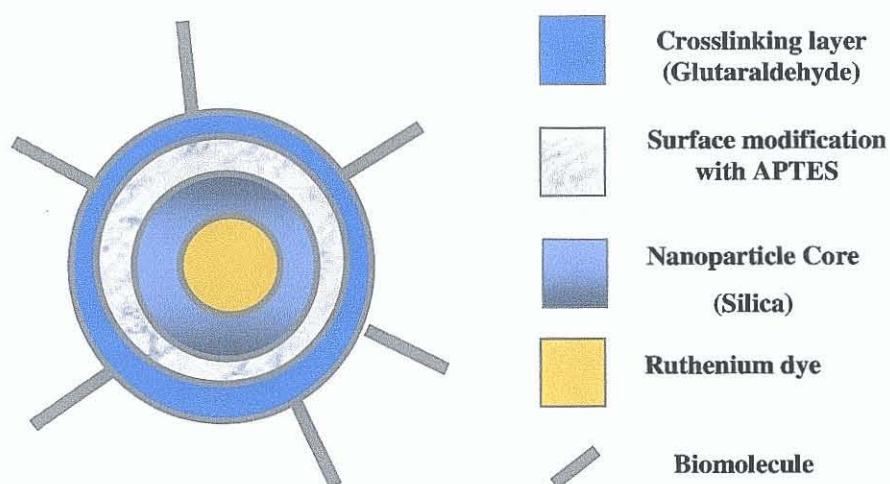


Figure 1.10 Schematic depicting the component layers of ruthenium dye-doped silica nanoparticles. A silica shell encapsulates the constituent dye (ruthenium) using a water in oil microemulsion technique. The silica surface of the doped nanoparticles is modified for biomolecule attachment by silanisation with aminopropyltrimethoxysilane (APTES) and subsequent glutaraldehyde crosslinking.

Traditional immunoassays employ the use of one or more fluorescent dye molecules linked to an antibody, to trace the antibody-antigen binding interaction. Nanoparticles have been successfully conjugated to antibodies, proteins, streptavidin and avidin (Santra *et al.*, 2001; Ye *et al.*, 2005; Dahint *et al.*, 2007). The efficiency of the conjugation process can be monitored and the conjugation rate predicted, with respect to the initial ratio of biomolecule to nanoparticle (NP) by applying mathematical formulae which take into account the size of the nanoparticles, their capacity for binding (mg protein present per mm^2 of nanoparticle surface) and the mean diameter of the nanoparticles. Functionalisation of the polymer shell of such molecules is generally quite simple and allows direct coupling of the probe to biomolecules (Lian *et al.*, 2004). In this research, ruthenium dye-doped silica-shell nanoparticles were investigated in association with Dr. Robert Nooney of the Biomedical Diagnostics Institute (BDI), DCU. Nanoparticles were synthesised using a microemulsion method and conjugated to antibodies for the development of fluorescence-based immunoassays with improved sensitivities.

1.5.2 Electrochemical-based detection

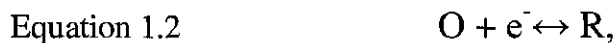
Over the past 30 years electrochemical sensors have been used as tools for the detection of a wide range of analytes (Pejic and DeMarco, 2006). These sensors are dependent on the condition and stability of the membrane/electrode surface and the behaviour of immobilised biomolecules at this interface. Electrical impedance spectroscopy (EIS) has been used to provide information on the various processes occurring at electrochemical sensor surfaces (i.e., adsorption, film formation, rate of charge transfer, ion exchange, diffusion and mass transport) since the understanding of these processes assists the development of improved immunosensing strategies. Biosensors have experienced rapid, extensive improvement as a result of studying the electrochemical phenomena occurring at sensor surfaces. Advanced sensor materials and coupling strategies have been developed to maintain the bioactivity of biomolecules, thus enriching generated signals. Enhancement of bio-immobilisation matrices with materials such as hydrogels, sol-gel-derived composites, polymer thin-films and lipid membranes (Xu *et al.*, 2006) has assisted in the evolution of smart, novel immunosensors. Continued improvements in surface chemistries at electrode interfaces, immobilisation strategies, protein engineering techniques and transduction system design have aided in the creation of a new generation of electrochemical immunosensors

Electrochemistry involves the study of the interrelationship of electrical potentials and their associated currents with chemical systems and their underlying chemistries (Bard and Faulkner, 1980). It is the study of reactions in which charged particles cross the interface between two phases of matter, typically an electronic conductor (electrode) and a conductive solution (electrolyte). Electrochemistry may be used as a fundamental analytical tool (Pejic and DeMarco, 2006) as well as having numerous industrial applications. Processes taking place at the surface of the electrode produce an imbalance in the electrical charges of both the electrode and the electrolyte. This is known as a potential difference and is the determining factor of the resultant electrochemical reaction. The unit of measurement of potential difference, voltage (V), can be described using Equation 1.1.

$$\text{Equation 1.1} \quad V = J/C,$$

whereby a volt is simply the energy (J) required to move a charge (c).

The application of a potential to an electrode supplies electrical energy and alters the energy level of the electrons within the electrode since they possess charge (Buerk, 1993). An electrochemical cell is a device capable of producing electric current from energy released by a redox reaction. This kind of cell is also known as galvanic cell, named after Luigi Galvani, the 18th century scientist responsible for conducting some of the first experiments on chemical reactions involving electric current. In a galvanic cell the anode is defined as the electrode where oxidation occurs and the cathode is the electrode where reduction takes place. The electrodes in galvanic cells have different dissolving rates (unequal amounts of electrons in each metal) which cause a difference in electrode potential between the electrolyte and the electrodes. If an electrical connection, such as a wire or direct contact, is formed between the anode and cathode, electrical current will flow between the metal electrodes (Bard and Faulkner, 1980). The application of a potential to an electrode can, therefore, supply electrical energy, thus altering the energy level of the electrons within a metal electrode since they possess charge. If we consider a single electron transfer reaction as described in Equation 1.2;



where *O* is a molecule in an oxidised state, *R* is a molecule in a reduced state and *e* is an electron.

It can be assumed that there are arbitrary amounts of (*O*) and (*R*) in the solution and so the total current flowing, *i*, is determined by calculating the sum of the reductive *i_c*, and oxidative *i_a*, currents, as shown in Equation 1.3.

$$\text{Equation 1.3} \quad i = i_a + i_c = nFAk_{\text{red}} [O]_0 - nFAk_{\text{ox}} [R]_0,$$

where *A* is the electrode area (cm²), *F* is the Faraday constant i.e. amount of electric charge in one mole of electrons (~9.65 x 10⁴ Coulomb/mol), *n* is the number of electrons transferred, [*O*]₀ and [*R*]₀ are the surface concentrations of either (*O*) or (*R*), respectively.

The free energies of activation for the electrode reaction are related to both the chemical properties of the reactants, the transition state of the reactants and their response to applied potential. The Butler-Volmer equation, (Equation 1.4) provides further information on the fundamental relationship between current flow and applied voltage.

$$\text{Equation 1.4} \quad i = i_0 \left\{ \frac{[O]_0}{[O]_{bulk}} e^{\frac{-\alpha n F (E - E_e)}{RT}} - \frac{[R]_0}{[R]_{bulk}} e^{\frac{(1-\alpha) n F (E - E_e)}{RT}} \right\},$$

where, F is the Faraday constant ($\sim 9.65 \times 10^4$ Coulomb/mol) n is the number of electrons transferred, E is the applied voltage, E_e is the voltage established by the mixture of (O) and (R) at equilibrium, $[]_0$ are the surface concentrations of either (O) or (R), respectively, and the α term reflects the sensitivity of the transition state to the applied voltage.

If α is equal to zero, then the transition state shows no dependence on potential. Typically, however, α tends to approximate to 0.5. This means that the transition state responds to potential in a manner halfway between the reactants' and the products' response. Current flow therefore responds to changes in the value of α , the value of i_0 (the exchange current density) and changes in potential.

Electrochemical reactions involve the interfacial transfer of charge between an electrode and a species in solution (Eggs, 1996). The exponential relationship of applied potential to rate of electron transfer would suggest that it is possible to transfer unlimited amounts of material to and from the electrode surface. However, for a fixed electrode surface area, the reaction rate is controlled by the rate constant and the surface concentration of the reactant. If the rate constant is sufficiently large so that any reactant close to the electrode surface is immediately converted into reaction product, then the current will be controlled by the amount of fresh reactant reaching the surface over time from the bulk solution (Lower, 1994). This important factor shows that mass transport of reaction materials greatly affects measured current.

Specifically there are three forms of mass transport, which can affect an electrochemical experiment, namely diffusion, convection, and migration (Brett and Oliveira Brett, 1993). Diffusion occurs in all solutions and arises from local differences in concentrations of reactants (Bakker *et al.*, 2004). Entropy forces act to try and equalise these differences and are the main driving forces for diffusion. Convection, however, results from the action of a force on the solution, for example a stirrer or gravity, whereas migration is an electrostatic effect arising from the application of a polarising potential at an electrode, thus creating a charged interface. Charged species within the local solution will become attracted to, or repelled from, the electrode.

The common feature connecting electrochemical sensors is that they rely on the detection of an electrical property and are normally classed according to the mode of measurement, i.e., potentiometric, conductimetric or amperometric, (Pejic and DeMarco, 2006). The most important consideration in electrochemical sensor design is the understanding of the relationship between surface chemistry and reactivity. Examination of the processes occurring at surface layers and the interaction of such layers with biomolecules during electrochemical interrogation is the fundamental principle behind electroanalytical techniques (Eggins, 1996)

Surface modification and immobilisation techniques that are specific for the detection method employed and the electrical processes occurring at the sensor surface are paramount to ensuring optimal sensor operation. This can involve tailoring surface chemistries at electrode surfaces to improve biomolecule adsorption or altering the bulk electrical conduction properties of the sensor by modifying the membrane composition (Schultze, 2000). Understanding how various parameters influence the response mechanism and interfacial reaction kinetics will assist with the development of electrochemical sensors with new and improved response characteristics. Electrochemical impedance spectroscopy (EIS) is a non-destructive steady-state technique that is capable of probing these phenomena over a range of frequencies (Macdonald, 1987; Fletcher, 2001).

1.5.2.1 Impedance-based detection

Electrical impedance spectroscopy (EIS) is an effective method for probing the features of surface-modified electrodes (Bard and Faulkner, 1980, Stoyanov 1989 and Stoyanov *et al.*, 1991). When a small-amplitude perturbing sinusoidal voltage signal is applied to the electrochemical cell, the resulting current response can be measured. The impedance is calculated as the ratio between the system voltage phasor, $U(j\omega)$, and the current phasor, $I(j\omega)$, which are generated by a frequency response analyser during the experiment. Complex impedance can be presented as the sum of the real, $Z_{re}(\omega)$, and imaginary, $Z_{im}(\omega)$ components that originate mainly from the resistive and capacitive components of the cell, respectively.

$$\text{Equation 1.5} \quad Z(j\omega) = \frac{U(j\omega)}{I(j\omega)} = Z_{re}(\omega) + jZ_{im}(\omega),$$

where $\omega = 2\pi f$, $j = \sqrt{-1}$, ω is equal to the Warburg impedance ($\text{rad}\cdot\text{s}^{-1}$) and f is the excitation frequency (Hz)

One of the most important parameters governing impedance spectroscopy is the applied frequency. At very low frequencies the impedance value is determined by the DC-conductivity of the electrolyte solution, whereas at very high frequencies, the inductance of the electrochemical cell and connecting wires contribute to the resulting impedance spectra. To eliminate these effects, useful impedance spectra are recorded at frequencies where only the interfacial properties of the modified electrodes control the resulting data ($10 \text{ mHz} < f < 100 \text{ kHz}$). Experimental results can be analysed graphically as in the case of Faradaic impedance spectra, usually by the use of the Nyquist coordinates (Z_{im} vs. Z_{re}), in the frame of the theoretical model (Ghindilis and Kurochkin, 1994). Thus, impedance spectroscopy provides a suitable transduction technique to follow the interfacial interactions of biomolecules at electrode surfaces (Cheng *et al.*, 2002; Szymańska *et al.*, 2007). EIS is a powerful method for the characterisation of the structural features of sensing interfaces and for explaining the actual events occurring at these surfaces. In this thesis, the development of a labelless impedance-based sensor for the detection of InIB is described.

1.6 Target molecules for immunosensor development

Immunoassays rely on the specific interaction between antibody and antigen for analyte determination (Ekins, 1999). Recent advances in antibody technology have allowed for the standardisation of antibody preparations and revolutionised their use as clinical and diagnostic tools. Given the unique specificity of antibodies and the use of antibody libraries, common biosensor formats can now be easily and quickly adapted for the detection of specific analytes in solution without the need for developing individual chromatographic assay separation techniques (Hock, 1997).

Point of care (POC) diagnostic instruments are becoming more important in the current climate and the need for rapid, disposable polymer biochips for the detection of clinically important analytes is a key issue. Photostable fluorescent probes can be used to multiplex assays in chip format and the use of novel fluorescent labels such as quantum dots and nanoparticles, in the development of biochip and microarray platforms is paramount in the advancement of such systems. Characterisation of novel fluorescent labels on solid-phase platforms is an essential step, prior to transfer to biochip, as are comparative studies based on traditional immunochemical techniques such as ELISA. This allows determination of the advantages of novel labels with respect to assay performance, speed and detection limits attainable.

The work in this thesis describes the development of novel antibody-based biosensors that employ both optical and electrochemical transduction methods for the detection of a hapten, bacterial proteins and whole cells. Three distinctly different target molecules were chosen for the development of the antibody-based biosensors described in this research. Internalin B (InIB), an invasion-associated protein of *Listeria monocytogenes*, parvovirus B19, the first human parvovirus and warfarin, the ninth most prescribed drug in the world. The following sections give a general overview of structure and function of each target and their clinical importance for detection.

1.6.1 Warfarin

Warfarin, a synthetic derivative of 4-hydroxycoumarin, is the most widely prescribed oral anticoagulant for the management of a wide variety of thromboembolic disorders such as atrial fibrillation and deep vein thrombosis (Hirsh *et al.*, 2001). It is a vitamin K antagonist and, therefore, an indirect anti-coagulant. Vitamin K is a necessary element for the synthesis of a number of clotting factors in the blood (II, VII, IX and X). The production of these clotting factors is dependent on the carboxylation of glutamic acid residues, a process requiring the presence of vitamin K, a co-factor in the production of carboxylase (Cooke *et al.*, 1997). The carboxylation of glutamate residues on the N-terminal portion of the clotting factors determines the required structure for the binding of calcium ions. It is these calcium ions that control the interaction of the clotting factors with negatively charged phospholipid surfaces such as platelets, thereby greatly enhancing the coagulation cascade and fibrin formation (Mueller, 2004). Warfarin reduces the rate at which these factors are produced, thus producing an anticoagulant effect. Figure 1.11 shows the basic structure of warfarin.

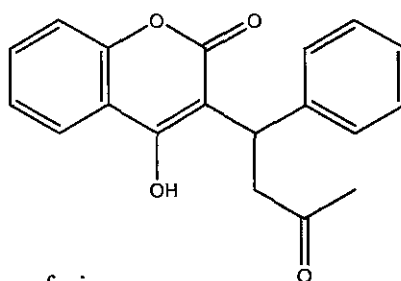


Figure 1.11 Structure of warfarin

The amount of functional vitamin K-dependent clotting factors produced can be reduced by up to 50% by the administration of warfarin therapy (Majerus *et al.*, 1996). Warfarin is nearly always administered orally and is absorbed rapidly, with peak blood levels attained after 90 minutes (King *et al.*, 1995). The plasma half-life is between 36-42 hours; however, plasma concentrations do not correlate well with anticoagulant effect, implying variable hepatic metabolism in different individuals (Prandoni and Wright, 1942). Warfarin can be detected in the plasma one hour after oral administration, and peak concentrations occur two to eight hours later. The drug is highly bound to plasma proteins (~99%) and is metabolised in the liver and kidneys, with the subsequent production of inactive metabolites that are excreted in the urine and stool.

There is currently a wide range of analytical techniques available for the determination of warfarin in biological fluids, ranging from chromatography to phosphorescence-based measurements (Capitán-Vallvey *et al.*, 1999; Osman *et al.*, 2005; Hou *et al.*, 2007). However, these analytical techniques involve lengthy sample pre-treatment and post-column reactions for the determination of unbound warfarin in plasma samples. The current trend in warfarin therapy is towards lower intensity treatment. Consequently, there is the need to develop more sensitive analytical techniques capable of detecting lower concentrations of warfarin in biological fluids.

Fitzpatrick and O’Kennedy (2004) describe the development of a Biacore-based inhibition immunoassay for the determination of warfarin in plasma ultrafiltrate. This format demonstrated a range of detection from approximately 4-250 ng/ml, which is within the clinical range and showed good reproducibility and robustness. The use of surface plasmon resonance technology for the detection of warfarin provides a viable alternative to traditional chromatographic techniques. However, recent advances in polymer technology and fluorescence-based detection methods have identified the importance of microarray and biochip formats in immunoassay development (Bashir, 2004; Wacker *et al.*, 2004). Therefore, improved fluorescent labels such as quantum dots and porphyrin dyes were evaluated for the development of sensitive and reproducible immunoassays for the detection of warfarin. The use of these novel fluorescent labels in plate-based assays and validation of such assays would then facilitate transfer of such optimised reagents to chip-based methods for the detection of warfarin

1.6.2 *Listeria monocytogenes*

Listeria monocytogenes is an important food-borne pathogen with an extremely high mortality rate of approximately 30%. *Listeria monocytogenes* is a gram-positive facultatively anaerobic rod-shaped bacterium that grows between 1 - 45°C (Jones and Seeliger, 1992). It is responsible for most food-borne outbreaks of listeriosis and belongs to the bacterial genus *Listeria*. Currently, there are six recognized species of *Listeria* (*L. innocua*, *L. ivanovii*, *L. monocytogenes*, *L. grayi*, *L. seeligeri*, *L. welshimeri*), with *L. monocytogenes* the principal human pathogen. *L. monocytogenes* can be readily isolated from a number of sources such as, soil, water, plants, fertilizer and processed foods, even when stored at 4°C (Southwick and Purich, 1996).

Listeriosis is most prevalent in immunocompromised patients, with the risk of infection up 1000 times more likely than that of the general public (Jensen *et al.*, 1994). The elderly, pregnant women and newborns are also especially at risk to listeriosis, however, the general population can also be susceptible (Hof, 2003). In most cases of infection, symptoms present as those commonly associated with food poisoning and include fever, vomiting, diarrhoea and headache. In more severe cases, listeriosis can cause gastroenteritis, meningitis, septicaemia, and meningo-encephalitis. Links have also been found between listeriosis infection and spontaneous abortion and stillbirth (Doganay, 2003). The ability of the bacteria to cross the intestinal, bloodbrain and foeto-placental barriers during infection is an important consideration in understanding the pathogenic effect of the disease. In all infected tissues, *Listeria* is intracellular owing to its capacity to survive in phagocytic cells and also to invade and survive in non-phagocytic cells (Cossart *et al.*, 2003). The bacteria rely on actin-based motility to spread from cell to cell, escaping the internalisation vacuole by this method. A family of bacterial cell-wall surface proteins known as the internalins aid in this process by promoting entry into epithelial cells and hepatocytes (Dramsi *et al.*, 1995).

The life cycle of *L. monocytogenes* in host cells is described in detail by Southwick and Purich (1996) and involves a number of distinct stages. The initial entry of the bacteria into the host cells is dependent on virulence factors. Phagocytosed *L. monocytogenes* survive the phagocytic vacuole by activation of listeriolysin O (LLO)

and the bacterial metalloprotease (Mpl) as the pH inside the phagolysosome drops (Cossart, 2002). This disrupts the phagosomal membranes and allows the bacteria to escape into the cytosol. Within the cytosol the *L. monocytogenes* cells replicate and direct cell-to-cell spread using actin-based motility. The internalin family of proteins are involved in the invasion of host cells, with Internalin A (InlA) and Internalin B (InlB) the most important. The structure of the internalins is characterised by the presence of two distinct repeat regions separated by an inter-repeat region (Schubert *et al.*, 2001). The proteins generally comprise a short N-terminal conserved cap region, followed by several leucine-rich repeats (LRR), an inter-repeat ('IgG-like') region and a second repeat region known as the B repeats (Bierne and Cossart, 2002). The research described in this thesis focuses on the study of Internalin B (InlB) and Figure 1.12 illustrates the InlB amino acid structure and the regions and domains into which it can be divided.

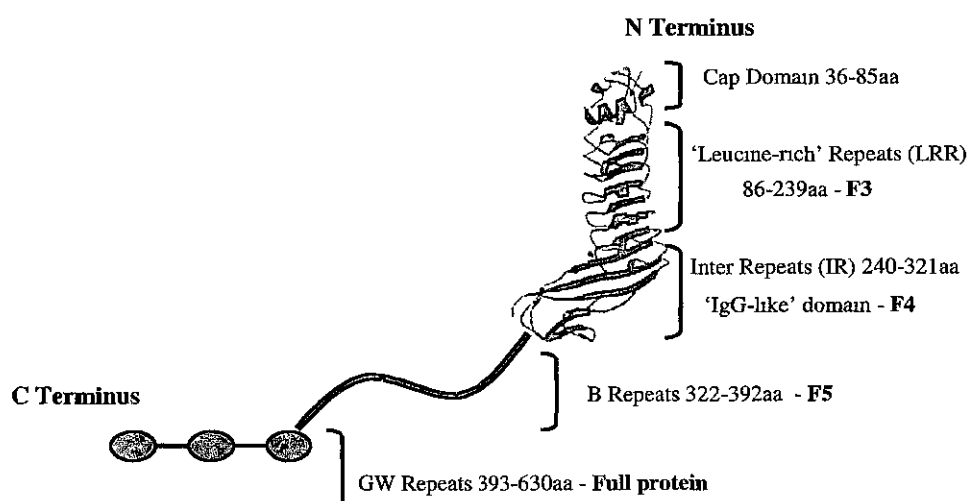


Fig. 1.12 Internalin B amino acid structure. The amino acid sequence of the InlB protein is organised into a number of distinct domains. Schematic domain organization of full length InlB, comprising an N-terminal signal sequence (residues 1-35), cap domain (36-85), LRR-domain (86-239), IR-region (240-321), B-repeat (322-392) and three GW-modules (393-630). This schematic also shows how the full recombinant Internalin B protein was divided into three smaller peptide fragments for epitope mapping F3, F4 and F5. F3 covers amino acids 0-239, F4 covers amino acids 0-321 and F5 covers amino acids 0-392 (Adapted from Schubert *et al.*, 2001; Freiberg *et al.*, 2004).

InlB promotes invasion into the host cell by activation of phosphatidylinositol-3-kinase (Ireton and Cossart, 1997). The InlB protein contains four distinct domains, similar to the other members of the internalin family. The amino terminal part of the protein incorporates the internalin domain, housing the cap domain, 'leucine-rich' repeats (LRR) and inter-repeat (IR) region and is involved in Met recognition. The LRR provide a structural framework for the formation of protein-protein interactions (Kobe and Kajava, 2001), whereas the carboxy-terminal anchors the protein to the cell via the GW repeat domains. These repeats cause a loose association of the protein to the bacterial surface through non-covalent interactions with lipoteichoic acid. This is a membrane-anchored polymer that is present on the surface of Gram-positive bacteria (Jonquieres *et al.*, 1999)

L. monocytogenes can be found in a wide variety of foods such as soft cheeses, pate, processed meats, chicken, shellfish and milk (Rea *et al.*, 1992; Dalton *et al.*, 1997; Hollingsworth, 1999; de Valk *et al.*, 2001). The isolation of *L. monocytogenes* from these foodstuffs and the link of food-poisoning outbreaks to *Listeria*-contaminated samples, have prompted the development of more rapid and sensitive methods for detection. Traditionally, recognition of *L. monocytogenes* in a sample was performed using immunoassays which target the whole bacterial cell (Mena *et al.*, 2004). These methods can be both dangerous and time-consuming in that pathogenic bacterial cells are involved. An improved technique for the detection of *Listeria*, employing the *L. monocytogenes* cell surface proteins InlB as antigenic determinant, was investigated for the development of optimised systems described in this thesis. The use of *L. monocytogenes*-derived recombinant proteins such as InlB in assay development eliminates the need to culture and handle pathogenic cells and a constant supply of antigen can be maintained. Both electrochemical and optical-based sensing methods were examined for the enhanced detection of InlB. Novel fluorescent labels were characterised on solid-phase platforms prior to transfer to a biochip for enhanced detection of InlB. Impedance-based detection of InlB was also investigated and the development of a novel platform for the labelless sensing of InlB via impedimetric transduction described.

1.6.3 Parvovirus

Parvovirus is a small un-enveloped single stranded DNA virus (Coon, 2003). The members of the parvo-viridae are among the smallest of all DNA viruses. Its members infect many species, from insects to higher animals, but only one member, parvovirus B 19, is able to cause human disease. Infection with Parvovirus B19 is common in humans and symptoms range from completely asymptomatic infection to serious and potentially fatal conditions in a minority of the population (Brown, 2004). Figure 1.13 shows an x-ray crystallographic image of Parvovirus B19, the human strain of this disease.

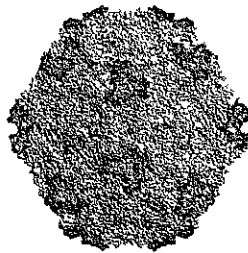


Fig 1.13 X-ray crystallographic image of the Parvovirus B19 capsid protein VP2 particle (obtained from Barbel Kaufmann *et al.*, 2005).

Parvovirus B19 can cause many illnesses ranging from a deadly infection to anaemia and arthropathy, depending on the age and immune status of the affected patient (Coon *et al.*, 2003). In children, infection commonly manifests as Fifth disease or *erythema infectiosum*, whereas in adults, especially women, polyarthropathy is common. In immunosuppressed patients manifestation is as pure red cell aplasia, and during pregnancy as *hydrops fetalis* or intrauterine death (Young and Brown, 2004). Many assays are available to test for parvovirus infections and these include antibody serology studies, DNA-based methods such as PCR and various methods based on antigen detection. Parvovirus first emerged in the 1970's as a disease affecting dogs and cats caused by the tiny virus effecting eukaryotes. In both species, parvovirus causes serious problems for newborns and can be fatal; older animals can suffer some effects, but they are mild and temporary. The virus can stay active in soil for long periods of time, so dogs must be vaccinated close to birth, immediately after maternal antibodies wane. In 1975, Cossart *et al.*, discovered the human form, Parvovirus B19, to be the causative agent of Fifth disease, a mild rash on the body, typically described by doctors as a "slapped-cheek" pattern on the face. Transmission is greatest during

viraemia prior to symptoms arising and the virus is mainly spread via aerosol droplets through the respiratory route. It is usually transmitted by hand-to-mouth contact, blood or blood products but can also be spread transplacentally to the foetus during active maternal infection, with infection rates of up to 33% reported (Anonymous, 1990). During outbreaks, which predominantly occur in winter and spring time, infection rates of up to 50% have been noted in the school and home, respectively (Anderson, 1987).

Parvovirus B19 preferentially infects and replicates in erythroid cells. Erythrocytes will lyse causing erythropoiesis, following Parvovirus B19 infection and lymphocyte, granulocyte and platelet counts may also fall during infection. The incubation period for the virus is usually 4-14 days and all non-immune individuals are susceptible (which can be up to 50% of the population). The highest risk of infection for pregnant women is during epidemics and following exposure to infected children (Valeur-Jensen, 1999). Persons with pre-existing anaemia and congenital or acquired immunodeficiencies are also highly susceptible. The consequences of parvovirus infection during pregnancy are extremely serious (De Yong *et al.*, 2004), the main risk being foetal anaemia which can lead to Non-Immune Hydrops Fetalis (NIHF), resulting in miscarriage. It has been estimated that maternal Parvovirus B19 infection occurs in approximately 1 in every 400 pregnancies and up to 20% of NIHF is parvovirus B19 related (Jordan, 1996). The majority of foetal losses due to B19 infection occur in the second trimester and most pregnant women are asymptomatic, therefore, the only way to identify patients at risk is to screen for parvovirus B19 antibodies and treat appropriately.

Parvovirus B19 infection is also a major concern for transplant patients. Parvovirus B19 can cause acute or chronic aplastic anaemia in organ transplant recipients and can contribute to some cases of rejection (Murer *et al.*, 2000). Patients who have undergone an organ transplant are at risk of developing Parvovirus B19 due to acquired infection from the transplanted organ and blood transfusions. However, intravenous immunoglobulin (IVIG) therapy has been shown to be effective in treating chronic Parvovirus B19 infection in transplant patients.

Parvovirus B19 has been associated with persistent chronic anaemia and with transient aplastic crisis in children with sickle cell disease. Reports suggest that Parvovirus B19 can be transmitted through blood transfusions and plasma-derived products (Prowse *et al.*, 1997). B19 is a non-enveloped virus and is resistant to high temperatures and most solvent-detergent treatments. Despite this fact, routine screening of blood products for B19 DNA does not occur. It was suggested that individual donors should be screened for B19 IgG and those with continually high levels could be identified. The blood or plasma from these donors could then not be used for treatment of any immunocompromised or other high risk patients, thereby reducing the risk of B19 infection (Yoto *et al.*, 1995). Although intravenous immunoglobulin (IVIg) therapy is effective for the treatment of Parvovirus B19 infection in humans, work is currently being carried out to produce a vaccine.

There are many different diagnostic tests available for the detection of Parvovirus B19 (Beersma *et al.*, 2005; Peterlana *et al.*, 2006; Wong & Brown, 2006). However, with the increasing use of microarray and chip-based technologies in diagnostics, there is a need for the development of sensitive and reproducible assays that employ fluorescence-based methods for the detection of Parvovirus-associated antigens. The successful development of fluorescence and chemiluminescence-based immunoassays for the detection of Parvovirus antigens in plate-based assays would facilitate further investigation of these methods and their potential transfer to novel chip-based formats.

1.7 Aims of research

The overall aim of this thesis was the development of novel biosensing strategies for the detection of haptens, proteins and whole cells. Assays were developed for the detection of InlB, warfarin and Parvovirus B19, using antibody-based methods. The research sought to exploit novel antigens, antibodies, labels and immobilisation strategies. Optical and electrochemical-based techniques were investigated using a number of detection methods including microscopy, biosensors and immunoassays.

Chapter 3 describes the production and characterisation of *L. monocytogenes*-specific recombinant InlB protein fragments. Recombinant InlB protein was sub-divided into three shorter overlapping peptide fragments which were cloned into both the pQE-60 vector for His purification and the pAC4 vector for *in vivo* biotinylation. Following high-level expression, the recombinant proteins were purified using immobilised metal affinity chromatography (IMAC) and avidin affinity chromatography. Extensive characterisation of the cloned proteins using SDS-PAGE, Western blotting and Biacore was performed. The InlB protein fragments were subsequently used in the development of novel biosensing strategies for the detection of InlB.

Chapter 4 describes the development of fluorescence-based biosensing strategies for the detection of InlB, warfarin, Parvovirus B19 and human IgG. Solid-phase plate based methods were employed to investigate novel fluorescent labels, such as quantum dots, porphyrins and dye-doped nanoparticles. Subsequent transfer to a biochip format was undertaken for some of the assays and optimisation of immobilisation strategies explored.

Chapter 5 describes the development of a labelless impedance-based immunosensor for the detection of InlB. Electrochemical impedance spectroscopy techniques were used to investigate 'labelless' detection via impedimetric transduction. Sensors were fabricated by electropolymerising planar screen printed carbon electrodes with polyaniline to produce a conductive substrate and biomolecules were subsequently incorporated onto the polyaniline layer. Upon exposure to a range of concentrations of antigen solution, complex plane impedance analyses were performed to assess the impedance of the polymer, thereby allowing the amount of bound antigen to be determined.

Chapter 2: Materials and Methods

2.1 Material and equipment

2.1.1 Materials

All reagents and chemicals were of analytical grade and supplied by Sigma-Aldrich Co. (Poole, Dorset, U.K), unless listed below (Table 2.1).

Table 2.1: Reagents and chemicals used and the relevant suppliers.

Reagent	Supplier
Acetic acid Hydrochloric acid	Riedel de-Haen AG, Wunstorfer, Strabe 40, D-30926, Hannover, Germany.
Sodium di-hydrogen orthophosphate Di-sodium hydrogen orthophosphate Sodium chloride	BDH Laboratory Supplies , Poole, Dorset, BH15 1TD, UK.
Amino-propyltriethoxy-silane (APS)	Fisher Scientific UK, Bishop Meadows Rd., Loughborough, Leics. LE115RG.
pAC 4 vector AVB 101 <i>E. Coli</i>	Avidity Corporation, 1899 Gaylord St., Denver, CO 80206, USA.
BamHI enzyme NcoI enzyme NotI enzyme T4 DNA ligase	Biosciences, 13 Charlemont Tce., Crofton Rd., Dun Laoghaire, Co. Dublin.
Bicinchoninic acid assay (BCA) kit Neutravidin Immunopure Avidin Biotin-Sulfo-NHS Pre-stained MW markers (Blueranger)	Pierce Biotechnology Inc., North Meridian Rd., PO box 117, Rockford, IL., 61105, USA.
Ni-NTA resin pQE-60 vector	QIAGEN, QIAGEN House, Fleming Way, Crawley, West Sussex, UK.

DNA Purification System Wizard Mini Prep Kit	Promega Corporation, 2800 Wood Hollow Rd., Madison, WI., 53711-5399, USA.
PCR primers Sequencing	MWG-Biotech Ltd., Milton Keynes, MK12 5RD, UK.
Quantum Dot Streptavidin Conjugate	Quantum Dot Corporation, 26118 Research Rd., Hayward, CA., 94545, USA.
Foetal calf serum L-glutamine (200mM) Non-essential amino acids (100x) Sodium Pyruvate (100mM)	Gibco BRL, Trident House, Renfrew Rd., Paisley, PA4 9RF, Scotland, UK
Osmium Tetroxide	Fluka Chimie AG, Industriestrasse 25, 9471 Buchs, Switzerland
Platinum Porphyrin dye	Luxcel Biosciences, University College Cork, Lee Maltings, Cork.
Cy 5 reactive dye	Amersham Pharmacia Biotech AB, SE-751 84, Uppsala, Sweden.
Tryptone (L0021) Agar Technical (L0013) Yeast Extract (L0042) Brain heart infusion broth (BHI) (CM225) Listeria enrichment broth (LEB) (CM863)	Oxoid, Basingstoke, Hampshire, RG24 8PW, UK.

2.1.2 Equipment

Table 2.2: List detailing equipment used and the relevant suppliers.

Equipment	Supplier
3015 pH meter	Jenway Ltd., Gransmore Green, Felsted, Dunmow, Essex, UK.
Atto dual minislab AE-6450 Atto AE-6100 Hybrid PCR express	Medical Supply Company (MSC), Damastown, Mulhuddart, Dublin 15, Ireland.
Beckman ultracentrifuge (L8-70M) Beckman centrifuge (J2-21)	Beckman-Coulter Inc., 4300N Harbour Boulevard, Fullerton, CA 92834-3100, USA.
Biacore™ 1000 & 3000	Biacore AB, 2 Meadway Court, Meadway, Stevenage, Herts., SG1 2EF, UK.
Nikon Diaphot inverted microscope Nikon Fluorescent microscope (TE2000)	Nikon Corporation, 2-3 Marunouchi 3-chome, Chiyoda-ku, Tokyo, Japan.
Ultrafiltration Stirred Cell (8400)	Amicon Inc., 72 Cherry Hill Drive, Beverly, MA., 01915, USA.
Stuart Platform Shaker (STR6)	Lennox, P.O. Box 212A, John F.Kennedy Drive, Naas Rd., Dublin 12.
Biometra T gradient Uno II Thermocycler	Anachem Ltd., Anachem House, Charles St., Luton, Bedfordshire, UK.

Trans-Blot Semi-Dry Electrophoretic Transfer Cell (170-3940) Econo-Pac™ chromatography column	BioRad Laboratories Inc., BioRad House, Maylands Ave., Hemel Hempstead, Hertfordshire, UK.
Eppendorf centrifuge (5810 R)	Eppendorf AG, 10 Signet Court, Swann Rd., Cambridge, UK.
Eppendorf tubes	Sarstedt, Drinagh, Wexford, Ireland.
Grant waterbath (Y6)	Grant Instruments (Cambridge) Ltd., 29 Station Rd., Shepreth, Royston, Hertfordshire, UK.
Heraeus Christ Labofuge 6000	Heraeus Instruments Inc. 111-a Corporate Blvd. South Plainfield, NJ, USA.
Image Master VSD gel documentation system	Amersham Pharmacia Biotech AB, SE-751 84, Uppsala, Sweden.
NUNC Maxisorb plates	NUNC, Kamstrup DK, Roskilde, Denmark.
Orbital incubator (100X400.XX1.C)	Sanyo Gallenkamp Plc, Monarch Way, Belton Park, Loughborough, Leicester, UK.
SB1 Blood tube rotator	Stuart Scientific, Holmethrope Industrial Est., Redhill, Surrey, UK.
Stuart platform shaker (STR 6)	Lennox, John F Kennedy Industrial Est., Naas Rd., Dublin 12, Ireland.
Tomy Autoclave (SS 325)	Mason Technology, Greenville Hall, 228 South Circular Rd., Dublin 8, Ireland.
UV-160A spectrophotometer	Shimadzu Corp., Albert-Hahn-Str. 6-10, 47269 Duisburg, Germany.

Safire ² Platereader	Tecan Austria GmbH, Untersbergstrasse 1a, A-5082 Grodig / Salzburg, Austria.
CM5 Sensor Chips	Biacore AB, Sovereign Court, 230 Upper 5th Street, Milton Keynes, MK9 2HR, UK.
Carbon screen-printed electrode assemblies	Microarray Ltd., The Fairbairn Building, 72 Sackville Street, Manchester, M60 1QD, UK.
QIcam Fast 1394 monochromatic camera	4401 Still Creek Drive, Suite 100 Burnaby BC Canada V5C 6G9
Image Pro Plus fluorescent imaging software	Slidepath, INVENT, Dublin City University, Dublin 9.
Hitachi S 300N Scanning Electron Microscope	Hitachi Corp. Ltd., 6-6 Marunouchi 1-chome, Chiyoda-ku, Tokyo, Japan.
Sycopel PCI-100 MK3 Potentiostat PC interface	Sycopel Scientific Ltd, 15 Sedling Rd Wear Ind. Est., Washington, Tyne & Wear NE38 9BZ, UK.
ACM Auto AC DSP frequency response analyser	ACM Instruments, 125 Station Rd, Cark, Grange-over-Sands, Cumbria, UK, LA11 7NY, UK.
Philup's CM12 Tunneling Electron Microscope (TEM)	Philips Medical Systems, The Observatory, Castlefield Road, Reigate, Surrey RH2 0FY, UK.
PD-10 Desalting Columns	Amersham Pharmacia Biotech AB, SE-751 84, Uppsala, Sweden.
Vivaspin Concentrator (5000 MWCO)	Vivascience AG, Sartorius Group, 30625 Hannover, Germany.

2.1.3 Composition of culture media

Table 2.3: Composition of culture media used.

Culture Media*	Formulation
2x Tryptone Yeast extract (2x TY) medium	Tryptone 16 g/l, Yeast extract 10 g/l, NaCl 5 g/l.
Luria Broth medium	Tryptone 10 g/l, Yeast extract 5 g/l, NaCl 10 g/l.
Super Broth medium	MOPS 10 g/l, Yeast Extract 20 g/l, Tryptone 30 g/l.
Terrific Broth medium	Tryptone 12 g/l, Yeast extract 24 g/l, Glycerol 4 ml/l, KH ₂ PO ₄ 17mM, K ₂ HPO ₄ 72mM.
Super Optimal Catabolite (SOC) medium	Tryptone 20 g/l, Yeast extract 5 g/l, NaCl 0.5 g/l, KCl 2.5mM, MgCl ₂ 20mM, Glucose 20mM.
Brain Heart Infusion	BHI 54.4 g/l.
Listeria-Enrichment Broth	LEB 37 g/l.

* Solid medium was prepared by adding 15 g/l of bacteriological agar to the above medium

2.1.4 Standard buffers

Table 2.4: Composition of buffers used.

Solution	Composition
Phosphate buffered saline (PBS)	150mM NaCl, 2.5mM KCl, 10mM Na ₂ HPO ₄ , 18mM KH ₂ PO ₄ , pH 7.4 .
Phosphate buffered saline -Tween (PBST)	150mM NaCl, 2.5mM KCl, 10mM Na ₂ HPO ₄ , 18mM KH ₂ PO ₄ , 0.05% (v/v) Tween 20, pH 7.4 .
Hepes Buffered saline (HBS)	10mM Hepes, 150mM NaCl, 3.4mM EDTA, 0.05% (v/v) Tween 20, pH 7.4
Tris Buffered Saline (TBS)	10mM Tris-HCl, 150mM NaCl, pH 8.0.
Aniline hydrochloride monomer solution	0.2M aniline hydrochloride, 0.5M KCl, 0.3M HCl, pH 1.0.
Sodium cacodylate buffer*	0.1 M Sodium Cacodylate, pH 7.3.
Sodium phosphate buffer	0.1M Na ₂ HPO ₄ , pH 4.3 with 1M HCl.

Denaturing buffer	8M Urea, 100mM NaH ₂ PO ₄ , 10mM Tris, pH 8.0.
Carbonate buffer	0.2M Na ₂ CO ₃ , 0.2M NaHCO ₃ , pH 9.5.
Tris-acetate/EDTA electrophoresis buffer (TAE)	40mM Tris-acetate , 1mM EDTA, pH 8.0.
Tris-EDTA sucrose buffer (TES)	200mM Tris-HCl, 0.5M Sucrose, 0.5mM EDTA, pH 8.0.
Alkaline-Cetyl Trimethyl Ammonium Bromide (CTAB) solution	3mM CTAB, 1mM NaOH, pH 8.0.

* Denotes toxic material. Use according to manufacturer's instructions and with extreme caution.

2.1.5 Bacterial strains

Table 2.5: Bacterial host strains and their genotypes

Bacterial strain	Genotype
XL-1 Blue <i>E. coli</i>	<i>RecA endA1 gyrA96 thi-1 hsdR17 supE44 relA1 lac [F'proAB lac^f ZΔM15 Tn10 (Tet^r)]</i>
AVB 101 <i>E. coli</i>	<i>K12 strain [MC1061 araD139 delta(ara-leu)7696 delta(lac)l74 galU galK hsdR2(r_Km_{K+}) mcrB1 rpsL(Str^r)]</i>
INVαF' <i>E. coli</i>	<i>F'endA1 recA1 hsdR17 (r_k⁻, m_k⁺) supE44 thi-1 gyrA96 relA1 ø80lacZΔM15 Δ (lacZYA-argF) U16 λ</i>
TG1 <i>E. coli</i>	<i>F' traD36 lac^f Δ(lacZ)M15 proA⁺B⁺/supE Δ(hsdM-mcrB)5 (r_k⁻m_k⁺McrB⁻) thi Δ(lac-proAB)</i>

XL-10 Gold <i>E. coli</i>	<i>Tet^R Δ (μxpA) 183Δ(mcrCB-hsdSMR-mrr) 173 endA1 supE44 thi-1, recA1 gyrA96, relA1, lacHte [F' proAB lacI^qZΔM15 Tn10 (Tet^R) Amy Cam^R]</i>
TOP 10 F' <i>E. coli</i>	<i>F'(lacI^q Tn10(Tet^R)) mcrA delta(mrr-hsdRMS-mcrBC) phi80lacZdeltaM15 deltalacX74 deoR recA1 araD139 delta(ara-leu)7697 galU galK rpsL (Str^R) endA1 nupG</i>

2.1.6 Cell culture of mammalian cell lines

Table 2.6: Mammalian cell lines

Abbreviation	Cell Line
BAEC	Bovine Aortic Endothelial cells
HASM	Human Aortic Smooth Muscle cells
RASM	Rat Aortic Smooth Muscle cells
Sp2/O (ATCC CRL 1581)	Mouse myeloma cells

2.1.7 Cell culture media preparation

Table 2.7: Cell culture media preparation

Media	Composition
BAEC/RASM/HASM Growth Media	Dulbecco's Modification of Eagle's Medium (DMEM) Supplemented with – Foetal Calf Serum 10% (v/v), L-glutamine (2mM), Penicillin /Streptomycin 1% (v/v).
Monoclonal Antibody Growth Media	Dulbecco's Modification of Eagle's Medium (DMEM) Supplemented with – Foetal Calf Serum 10% (v/v), L-glutamine (2mM), Sodium Pyruvate 1% (v/v), Non-essential amino acids 1% (v/v), Gentamycin (25μg/ml).

2.2 Cloning and expression of *Listeria monocytogenes*-specific protein fragments in pQE-60 vector.

E. coli XL-10 Gold cells containing the plasmid pQE-60, bearing the Internalin B (InlB) gene, were kindly donated by Dr. Paul Leonard, Applied Biochemistry Group, Dublin City University. The previously expressed recombinant InlB protein was used as a template for the cloning and expression of smaller InlB protein fragments into the pQE-60 vector (Qiagen Ltd., Crawley, West Sussex, UK).

2.2.1 Plasmid DNA purification using miniprep DNA purification system

A Promega Wizard™ Plus SV Miniprep DNA purification system was used to purify plasmid DNA as follows: single colonies of *E. coli* cells harbouring the plasmid were inoculated in 5ml of LB broth, containing the appropriate antibiotics, and grown while shaking at 37°C overnight. The overnight culture was centrifuged at 10,000 x g for 20 min. The supernatant was discarded and the tube was blotted on tissue paper to remove any remaining supernatant. The bacterial pellet was completely resuspended in 250µl of cell resuspension solution (50mM Tris-HCl, pH 7.5, 10mM EDTA and 10µg RNase A) by repeated pipetting. The resuspended pellet was then transferred to a sterile 1.5ml microcentrifuge tube and 250 µl of cell lysis solution (0.2M NaOH and 1% (w/v) SDS) was added and mixed gently by inverting the tube four times. The suspension was then incubated at room temperature for approximately 5 min, until the cell suspension cleared, to ensure complete cell lysis. Alkaline protease solution (10µl) was then added and mixed by inverting the tube four times. After five minutes incubation, 350µl of neutralisation solution (buffer containing 4.09 M guanidine hydrochloride, 0.795 M potassium acetate and 2.12 M glacial acetic acid, pH 4.2) was added and mixed by inversion. The bacterial lysate was then centrifuged at 10,000 x g for 10 mins at room temperature. The cleared bacterial lysate was transferred to a spin column and centrifuged at 10,000 x g for 1 minute at room temperature, after which the spin column was removed and the flow-through discarded. The spin column was re-inserted into the collection tube and 750µl of column wash solution (162.8mM potassium acetate, 22.6mM Tris-HCl, pH 7.5 and 0.109mM EDTA) previously diluted with ethanol to 95% (v/v) final concentration, was added. The column was then centrifuged at 10,000 x g for 1 min at room temperature and the flow-through discarded. Wash solution (250µl) was added to the column, which was then

centrifuged at 10,000 x g for 2 min at room temperature. The spin column was then transferred to a sterile 1.5ml microcentrifuge tube and the plasmid DNA was eluted from the column by adding 100µl of autoclaved upH₂O. The column was centrifuged at 10,000 x g for 1 min at room temperature. The eluted plasmid DNA was then stored at -20°C.

2.2.2 Agarose gel electrophoresis for DNA characterisation

DNA samples were analysed by horizontal electrophoresis in agarose gels containing 0.5µg/ml ethidium bromide*, using an Atto horizontal gel apparatus. Gels were prepared by dissolving 0.5g electrophoresis grade agarose in 50ml 1xTAE and boiling the mixture in a microwave oven (this gives a 1% w/v gel). Ethidium bromide was added to the solubilised agarose to yield a final concentration of 0.5µg/ml. When the solution had cooled sufficiently, the gel was poured into a horizontal gel platform, combs inserted and the gel left to solidify. Once set, the gel was placed in the electrophoresis unit filled with 1x TAE buffer and the comb removed. A loading dye was incorporated into the DNA samples (1µl of dye to 5µl of sample) to facilitate loading. The samples were resolved by applying a direct current of appropriate voltage. Mini- and maxi-gels were run at 100V for 1 hour or until the tracking dye reached the base of the gel. Gels were then visualised on a UV transilluminator and photographed using a UV image analyser (Image master VSD system, Amersham Pharmacia).

* Denotes toxic material. Use according to manufacturer's instructions and with extreme caution.

2.2.3 DNA agarose gel purification

DNA was purified from the agarose gel using a Wizard™ PCR-prep purification kit. DNA was electrophoresed on a 1% (w/v) low melt agarose gel at 70V for approximately 1 - 2 hours. The gel was then visualised under ultra violet (UV) light and the bands of interest excised from the gel using a sterile scalpel and placed in a sterile 1.5ml microcentrifuge tube. The gel bands were then incubated in a 70°C water bath until the gel was completely melted. Immediately after the gel melted 1ml of resin was added. The gel resin-mix was then flushed through a Wizard mini-column using a 5ml syringe barrel. The mini-column was then washed with 2ml of 80% (v/v) propanol. The syringe barrel was then removed and the mini-column placed in a fresh

1.5ml microcentrifuge tube. The column and eppendorf were then centrifuged at 10,000 x g for 2 min, to remove the propanol. The column was once again transferred to a fresh 1.5ml microcentrifuge tube and 50µl of upH₂O added. This was incubated at room temperature for 1 min and the column was then centrifuged at 10,000 x g for 20 s. The eluted DNA was collected in a sterile microcentrifuge tube and stored at -20°C.

2.2.4 Preparation of high efficiency competent bacterial cells for transformation.

High efficiency competent cells were prepared as previously described by Inoue *et al.*, (1990). A single *E. coli* colony was inoculated in 5ml of 2x TY, containing the appropriate antibiotics, and grown overnight at 37°C, while shaking. 100ml of 2x TY was inoculated with the overnight culture and the culture incubated, while shaking at 37°C, until the optical density at 550nm (OD₅₅₀) was between 0.3 and 0.4. The cells were then left on ice for 15 min and centrifuged at 3200 x g for 20 min at 4°C. The supernatant was decanted and the pellet was resuspended in 20ml of cold 100mM MgCl₂. The cells were centrifuged at 3200 x g for 20 min at 4°C and the pellet was resuspended in 20ml of cold 50mM CaCl₂. The cells were incubated on ice for 30 min and collected by centrifugation at 3200 x g for 20 min at 4°C. The supernatant was decanted and the cells were resuspended in 2ml of CaCl₂. The CaCl₂-competent *E. coli* were flash frozen in 200µl aliquots and stored at -80°C.

2.2.5 Sodium dodecyl sulphate – polyacrylamide gel electrophoresis (SDS-PAGE)

SDS-PAGE analysis was used to assess protein purity and determine the apparent molecular mass of proteins. Protein electrophoresis was performed using an Atto dual minislabs AE-6450 electrophoresis system. Polyacrylamide gel electrophoresis was carried out using the discontinuous system in the presence of sodium dodecyl sulphate (SDS), as described by Laemmli (1970). Table 2.8a details the composition of the gels, running buffer and sample loading buffer. Samples for analysis (approx. 1 mg/ml) were diluted with the sample loading dye (4:1, sample: buffer) and boiled for 10 min prior to loading. Boiled samples (20µl) were added to the gel and electrophoresed alongside appropriate molecular weight markers (Table 2.8b). Initially the gels were electrophoresed at 15mA per plate until the samples migrated

through the stacking gel and then they were electrophoresed at 20mA per plate until the sample had migrated to the end of the gel (approximately 90 min).

Table 2.8a: Composition of SDS-PAGE gels and buffers

Solution	Composition
Stacking gel	5% (w/v) acrylamide, 0.13% (w/v) bis-acrylamide, 125mM Tris, 0.1% (w/v) SDS, 0.15% (w/v) ammonium persulphate, 0.25% (v/v) TEMED.
Separating gel	10% (w/v) acrylamide, 0.27% (w/v) bis-acrylamide, 375mM Tris, 0.1% (w/v) SDS, 0.08% (w/v) ammonium persulphate, 0.08% (v/v) TEMED.
Sample loading buffer	60mM Tris, 25% (v/v) glycerol, 2% (v/v) SDS, 14.4 mM 2-mercaptoethanol, 0.1% (w/v) bromophenol blue.
Electrophoresis buffer	25mM Tris, 192mM Glycine, 0.1% (w/v) SDS.

Table 2.8b: Molecular weight markers used in SDS-PAGE analysis

Product	Molecular weight standards (Daltons)
<p>Sigma Wide Range (M4038)</p> <p>Molecular weight range: 6,500- 205,000 Da</p>	<p>Aprotinin, bovine lung (6,500), α-Lactalbumin, bovine milk (14,200), Trypsin inhibitor, soybean (20,000), Trypsinogen, bovine pancreas (24,000), Carbonic anhydrase, bovine erythrocytes (29,000), Glyceraldehyde-3-phosphate dehydrogenase, rabbit muscle (36,000), Ovalbumin, chicken egg (45,000), Glutamic dehydrogenase, bovine liver (55,000), Albumin, bovine serum (66,000), Phosphorylase B, rabbit muscle (97,000), β-Galactosidase, <i>E. coli</i> (116,000), Myosin, rabbit muscle (200,000).</p>
<p>Pierce Blueranger™ pre-stained marker (26681)</p> <p>Molecular weight range: 18,300- 215,000 Da</p>	<p>Lysozyme (18,300), Trypsin inhibitor (28,000), Carbonic anhydrase (39,200), Ovalbumin (60,000), Bovine serum Albumin (84,000), Phosphorylase (120,000), Myosin (215,000).</p>
<p>Amersham Rainbow™ pre-stained marker (RPN800)</p> <p>Molecular weight range: 10,000- 250,000 Da</p>	<p>Recombinant Protein (10,000), Recombinant Protein (15,000), Recombinant Protein (25,000), Recombinant Protein (30,000), Recombinant Protein (35,000), Recombinant Protein (50,000), Recombinant Protein (75,000), Recombinant Protein (105,000), Recombinant Protein (160,000), Recombinant Protein (250,000).</p>

2.2.6 Coomassie blue staining of SDS-PAGE gels

SDS-PAGE gels were stained for 4 hours using Coomassie blue to allow visualisation of the protein bands, and then destained overnight in destaining solution (Table 2.9).

Table 2.9: Composition of Coomassie blue staining and destaining solutions.

Solution	Composition
Coomassie blue staining solution	0.1% (w/v) Coomassie Brilliant Blue R-250 , 25% (v/v) methanol, 10% (v/v) acetic acid
Destaining solution	14% (v/v) methanol, 10% (v/v) acetic acid.

2.2.7 Western blot analysis

Proteins were transferred from SDS-PAGE gels (*Section 2.2.5*) to nitrocellulose membrane by electrophoretic means using a BioRad semi-dry blotter (Trans-Blot SD Semi-Dry Electrophoretic Transfer Cell 170-3940). The SDS-PAGE gel, nitrocellulose and Whatman chromatography paper were pre-soaked in Bjerrum and Schafer-Nielson transfer buffer, pH 9.2 (48 mM Tris, 39mM Glycine 0.0375% (w/v) SDS 20% (v/v) methanol) for 20 min. The gel was transferred to the membrane for 20 min at 15V. The membrane was blocked overnight at 4°C with PBS (Table 2.4) containing 5% (w/v) powdered milk. The blocked membrane was then washed using PBS (Table 2.4) using 3 x 10min washes. The membrane was probed with the primary antibody, made up to the appropriate working dilution in PBS (Table 2.4) containing 1% (w/v) powdered milk. The antibody solution was left to incubate for 1.5 hours at room temperature, and the membrane washed as before. An enzyme-labelled secondary antibody diluted to 1/2000 in PBS (Table 2.4) containing 4% (w/v) powdered milk was added and the blot incubated and washed as before. Colour development was then observed following addition of the appropriate substrate, (BCIP-NBT for alkaline-phosphatase labelled antibody or TMB for horseradish-peroxidase labelled antibody), and the reaction stopped after 5 min, by addition of 50mM EDTA.

2.2.8 Primer design for Epitope Mapping

Forward and reverse DNA primers were designed for the genes encoding the InlB protein based on DNA sequences previously submitted to GenBank. The Internalin B recombinant protein was portioned into three smaller fragments and primers designed to code for portioning the protein at these points, (F3, F4 and F5). The F3, F4 and F5 primers were based on the sequence of the recombinant InlB protein cloned and expressed by Chakraborty and associates (1995) from *L. monocytogenes* (Accession number AJ01234-GenBank). NcoI and BamHI restriction enzyme sites were incorporated into the forward and reverse primers, respectively, for subsequent directional cloning into the high-level expression vector pQE-60. The DNA sequences of the forward and reverse primers for each of the three fragments F3, F4 & F5 of the InlB gene are shown in Table 2.10.

Table 2.10: The nucleotide sequences of the InlB-specific forward and reverse primers.

Primer	DNA sequence
InlB forward	NcoI site 5'- CAT GCC ATG*GGA GAG ACT ATC ACC GTG CCA ACG C- 3' * start codon
P3 reverse	BamHI site 5'- CGC GGA TCC ACA TTC TTG GCT AAA TAA TTC- 3'
P4 reverse	BamHI site 5'- CGC GGA TCC TAC TGT GTA AAC CTC TTT CAG TGG- 3'
P5 reverse	BamHI site 5'- CGC GGA TCC TTG TTT AAG CGA GTT ATC TTC TCG - 3'

2.2.9 PCR amplification of genes encoding the InlB specific proteins

Standard polymerase chain reactions (PCRs) were set up as detailed in Table 2.11. The PCRs were used to amplify the genes encoding F3, F4 and F5 using the PCR cycle detailed in Table 2.12. A temperature gradient PCR was performed to determine the optimum annealing temperature for subsequent reactions and the optimum temperature was calculated to be 55°C.

Table 2.11: The components for a standard PCR reaction.

Component	Volume in reaction
dNTP mix (10mM)	1µl
Thermo buffer, containing Mg ²⁺ (10X)	5µl
Forward primers (0.5nM/µl)	1µl
Reverse primers (0.5nM/µl)	1µl
Template DNA (5-7ug)	1µl
Sterile upH ₂ O	38.5µl
Taq polymerase (1U/µl)	2.5µl
Total volume of reaction:	50µl

Table 2.12: The stages and steps for a standard PCR reaction.

Stage	Step	Number of cycles
1	Step 1: 95°C for 10 min	1
2	Step 1: 95°C for 1 min Step 2: 55°C for 30 s Step 3: 72°C for 1 min	30
3	Step 1: 72°C for 10 mins	1

2.2.10 Direct Purification of insert PCR Products

Direct purification of the PCR amplifications of each of the inserts F3, F4 & F5 was performed using a commercial kit (Promega Wizard™ PCR Prep DNA purification system). Direct purification buffer (50mM KCl, 10mM Tris-HCl, pH 8.8, 1.5mM MgCl₂ & 0.1% (v/v) Triton® X-100) was added to 200µl of the PCR reaction (pooled) and vortexed briefly to mix. Once the PCR reaction / buffer mixture was sufficiently combined, 1ml of resin was added. A wizard minicolumn was prepared for each sample by attaching a 3ml luer lock syringe (with the plunger removed) to a minicolumn with a collection tube. The resin/DNA mix was transferred to the

syringe/column assembly and the plunger inserted to push the DNA/resin slurry through the column. The syringe was then detached from the minicolumn, the plunger removed from the barrel and the barrel re-attached to the column. Two ml of isopropanol 80% (v/v) was added to the syringe and pushed through, using the plunger, to wash the column. The syringe was then removed completely and the minicolumn transferred to a fresh microcentrifuge tube. The column was then centrifuged at 10,000 x g for 2 min at room temperature. The minicolumn was transferred to another clean microcentrifuge tube and 50ul of 'nuclease-free' water added and let sit for 1 min. The column was then centrifuged at 10,000 x g for 20 s at room temperature. The eluted DNA was stored at -20°C.

2.2.11 BamH1/Nco1 restriction analysis on *E. coli* transformed with pQE-60

BamH1/Nco1 restriction enzyme analysis was carried out on the pQE-60 plasmid DNA isolated from the transformed XL-10 Gold *E. coli*. Overnight cultures of the clones for analysis were inoculated in 5ml of LB with appropriate antibiotics and grown while shaking, overnight at 37°C. The plasmid DNA was purified from each clone using the Wizard Plus™ SV Miniprep DNA purification system, (Section 2.2.1). BamH1/Nco1 restriction enzyme digests were set up as follows, (Table 2.13).

Table 2.13: Components for restriction digest

Component	Volume in reaction
NE buffer 2 (10X)	5µl
BSA (10mg/ml)	0.5µl
Plasmid DNA	10µl
UpH ₂ O (Sterile)	30 5µl
BamH1 (10U/µl)	2µl
Nco1 (10U/µl)	2µl
Total Volume of reaction:	50µl

2.2.12 Ligation of InlB insert into pQE60 plasmid DNA

A single XL-10 gold *E. coli* colony harbouring pQE-60 was grown overnight in 5ml of LB broth containing 100 µg/ml ampicillin, while shaking at 37°C. The pQE-60 plasmid DNA was purified using the Promega Wizard Plus™ Miniprep DNA purification system (Section 2.2.1). The pQE-60 plasmid DNA was then linearised using a BamH1 / Nco1 restriction digest as described in Section 2.2.11 and the linearised plasmid was gel purified, following agarose gel electrophoresis, using the Wizard™ PCR-prep purification kit (Section 2.2.3). The DNA encoding the gene of interest was then directionally cloned into the linearised pQE-60 using T4 DNA ligase. The ligation reaction was set up as shown in table 2.14.

Table 2.14: Components of ligation reaction

Component	Volume in reaction
pQE-60 DNA	4µl
Gene of insert	4µl
T4 DNA ligase (1U/µl)	1µl
Ligation buffer (10X)	1µl
Total volume of reaction:	10µl

The ligation reaction was incubated at 14°C for at least 4 hours, but preferably overnight. The ligation mixture was then centrifuged at 10,000g for 30 seconds and stored at -20°C.

2.2.13 Transformation of competent XL-10 Gold *E.coli* cells with pQE-60 containing the cloned inserts

CaCl₂-competent XL-10 Gold *E. coli* were prepared as described in Section 2.2.4. The competent XL-10 Gold *E. coli* were then transformed with the pQE-60, containing the gene of interest (InlB F3, F4, or F5). Vials containing the ligation reaction were centrifuged at 10,000 x g for 30 seconds and then placed on ice. 2µl of the overnight ligation reaction was added to 50µl of competent XL-10 Gold *E. coli* cells and mixed gently. The vials were then incubated on ice for 30 min. The transformation reaction was then exposed to heat shock, by placing the vials in a 42°C water bath for 30 s and

then directly back on ice. SOC medium (250µl) was then added to each transformation reaction. The transformation reaction was then incubated at 37°C for 1 hour, while shaking at 225rpm. Each transformation reaction (150µl) was then spread onto LB agar plates, containing antibiotics (100µg/ml ampicillin, 25µg/ml chloramphenicol and 10µg/ml tetracycline). The plates were then incubated, inverted, at 37°C for at least 18 hours.

2.2.14 Initial expression of recombinant fragments of InlB protein

Ten ml of LB broth (10 g tryptone, 5 g yeast extract and 10 g NaCl per litre) containing 100 µg/ml ampicillin, 25µg/ml chloramphenicol and 10µg/ml tetracycline was inoculated with 100µl of an overnight culture of *E. coli* XL-10 Gold cells containing the InlB gene fragments (from a single colony). The culture was incubated shaking at 37°C until the optical density at 550nm (OD₅₅₀) reached 0.5. Protein expression was then induced following addition of 1mM IPTG. The culture was further incubated, at 37°C, while shaking for 4 hours and then centrifuged at 3,200 x g for 20 min. The supernatant was discarded and the pellet resuspended in 500µl of denaturing buffer and sonicated for 30 s with 3 s pulses at 220V. The lysed cells were then centrifuged at 20,000 x g for 15 min and the supernatant analysed using SDS-PAGE for assessment of protein expression.

2.2.15 Optimisation of IPTG concentration

In order to determine optimal concentration of IPTG for maximum protein expression, several “small-scale” expression cultures (10ml) were performed. The growth conditions for each culture were identical to those described in *Section 2.2.14*, with the exception that various IPTG concentrations (ranging from 0 – 1mM), were used for induction of protein expression.

2.2.16 Optimisation of sonication conditions

In order to determine optimal conditions for sonication for maximum protein expression, several “small-scale” expression cultures (10ml) were performed. The growth conditions for each culture are the same as those described in *Section 2.2.14*, except that a range of sonication times from 0-60 seconds were examined for optimal protein isolation. Sonication was performed at 220watts using 3 second pulses.

2.2.17 Time course expression cultures

A “small-scale” expression culture (10ml) was carried out as described in *Section 2.2.14*. A 1ml sample was taken pre-induction with IPTG and then at hourly intervals for up to five hours. The culture was allowed grow and following overnight induction a final 1ml sample was taken.

2.2.18 Large-scale expression culture

LB broth (10ml) containing 100 µg/ml ampicillin, 10 µg/ml tetracycline and 25 µg/ml chloramphenicol was inoculated with 20µl of XL-10 Gold *E. coli* harbouring the pQE-60 plasmid. The culture was grown at 37°C overnight, while shaking. The overnight culture was then used to inoculate 500ml of LB broth for large scale expression. The culture was incubated at 37°C, while shaking, until the optical density at 550nm (OD₅₅₀) reached 0.5. Protein expression was then induced following addition of 0.1mM IPTG. The culture was incubated, at 37°C, while shaking, for a further 4 hours and then centrifuged at 3,200 x g for 20 min. The supernatant was discarded and the pellet resuspended in 25ml of IMAC purification buffer and sonicated three times for 30 s followed by a 30 s interval. This was repeated three times. The lysed cells were then centrifuged at 3,200 x g for 15 mins and the supernatant analysed using SDS-PAGE (*Section 2.2.5*) for protein expression and the His-tagged recombinant proteins purified using IMAC (*Section 2.2.19*).

2.2.19 IMAC purification of the 6xHis-tagged recombinant proteins and antibody fragments

Ni-NTA resin (2ml) was loaded into an empty Econo-Pac™ chromatography column (BioRad International Inc.) and allowed to settle to form a 1ml packed column. All purification steps were performed at 4°C to optimise Ni-binding. IMAC wash buffer (20ml), as described in Table 2.15, was added to the packed column for equilibration. The sample for purification was filtered to remove protein aggregates and applied to the column. The ‘flow-through’ fraction was collected and re-applied to the column three times. The column was then washed with 2 x 20ml of wash buffer (Table 2.15) and the wash fractions retained. The protein was eluted from the column using 5ml of elution buffer (Table 2.15), and collected in 5 x 1ml fractions. The eluted fractions were then pooled and concentrated in a Vivaspin concentrator and buffer exchanged

into PBS (Table 2.4) at 4°C. The concentration of the purified protein was then determined using a BCA assay (Section 2.2.20) and the purified protein was stored in 1ml fractions at -20°C.

Table 2.15: Buffers used during the IMAC purification of His-tagged proteins

Solution	Composition
Wash buffer	50mM NaH ₂ PO ₄ , 300mM NaCl, 20mM Imidazole, pH 8.0
Elution buffer	50mM NaH ₂ PO ₄ , 300mM NaCl, 250mM Imidazole, pH 8.0.

2.2.20 Bicinchoninic acid (BCA) assay

BCA reagents were supplied as components of the BCA protein assay kit (Pierce, 23225). Reagent A contained an optimised formulation of sodium carbonate, sodium bicarbonate, bicinchoninic acid and sodium tartarate in a 0.1 M NaOH solution. Reagent B consisted of an aqueous solution of 4% (w/v) cupric sulphate. Bovine serum albumin protein standards in a concentration range from 0.25 to 2 mg/ml were prepared in PBS (Table 2.4). Each standard (10µl) was added to a 96-well microtitre plate in triplicate. This was repeated for the samples under investigation (protein samples of unknown concentration). The BCA working reagent was prepared by mixing reagents A & B in the ratio of 50:1. A 200µl aliquot of working reagent was added to each well and the plate was allowed develop at 37°C for 30 min. Absorbance values were measured at 562nm using a Tecan Safire plate reader. The blank (0µg) absorbance value was subtracted and a standard curve of net absorbance at 562nm versus concentration (µg/ml) was constructed and used to calculate the protein concentration of the test samples.

2.2.21 Sequencing of cloned inserts

Plasmid DNA for sequencing was purified from overnight cultures using the Promega Wizard Plasmid DNA purification kit (Section 2.2.1). The plasmid DNA was quantified by determining its absorbance at 260nm. DNA (20µg) was dispensed into a fresh 1.5ml microcentrifuge tube and vacuum dried. Sequence analysis was then conducted by MWG-Biotech and the results given in Section 3.3.8. The web-based bioinformatics tools listed in Table 2.16 were used for the analysis and alignment of cloned sequence data, with known DNA sequences.

Table 2.16: Web-based bioinformatics tools and their source location

Tool	Source Location
Translate tool	www.expasy.org
BLAST	www.expasy.org
Swiss-model	http://swissmodel.expasy.org
Multialn	http://prodes.toulouse.inra.fr/multaln/multaln.html

2.2.22 Expression of anti-InlB scFv

An anti-InlB human scFv clone, previously isolated from a naive phage display library by Dr. Paul Leonard, was used in this research for the development of immunoassays for the detection of InlB. SB broth (Table 2.3) containing 100µg/ml ampicillin, 25 µg/ml chloramphenicol was inoculated with a single colony of TOP 10F⁺ *E. coli* containing the anti-InlB scFv plasmid. The cultures were grown at 37°C overnight, while shaking. The overnight cultures were then used to inoculate 500ml of SB containing 100µg/ml ampicillin, 25 µg/ml chloramphenicol and 2% (w/v) glucose. The culture was incubated at 37°C, while shaking for 8 hours. The culture was then centrifuged at 3,200 x g for 20 min at 4°C and resuspended in fresh SB broth containing 100µg/ml ampicillin, 25 µg/ml chloramphenicol, to remove all glucose from the medium. Protein expression was induced following addition of 1mM IPTG and the culture was incubated shaking at 30°C overnight. The culture was centrifuged at 3,200 x g for 20 min, the supernatant discarded and the pellet resuspended in 25ml of IMAC wash buffer (Table 2.15) and sonicated for 30 s. The lysed cells were then centrifuged at 3200g for 15 mins and the supernatant retained for purification by IMAC (Section 2.2.19).

2.2.23 Screening of optimised expression conditions of anti-InlB scFv by ELISA

A 96-well microtitre plate was coated with InlB recombinant protein (20ug/ml). The plate was incubated for 1 hour at 37°C and the contents emptied. The plate was then washed three times with PBS (Table 2.4) containing 0.05% (v/v) Tween and three times with PBS (Table 2.4). The plate was blocked using 200µl of PBS (as before), containing 4% (w/v) powdered milk and incubated at 4°C overnight. Anti-InlB scFv lysates from each expression study (*Section 3.5.1*) were added to the plate neat 100µl/well, in triplicate. The plate was incubated at 37°C for 1 hour and washed as before. HRP-labelled anti-cmyc antibody previously diluted to 1/1,000 with PBS (as before) containing 1% (w/v) Marvel, was added to the plate (100µl/well) and the plate incubated at 37°C for 1 hour. Following the wash step (as before), 100µl/well of TMB substrate was added and, after 30 min incubation at 37°C, the absorbance at 620nm was determined using a Tecan Safire plate reader. The absorbance value of each sample was plotted to determine which conditions were optimal for the expression of the anti-InlB scFv

2.3 *In vivo* biotinylation of Internalin B protein fragments F3, F4 & F5

The pAC4 vector for *in vivo* biotinylation of recombinant proteins (Avidity Corporation, USA), has both a BamH1 and Nco1 restriction site, thus allowing easy transfer of inserts from Qiagen's pQE-60 vector into the pAC 4 vector.

2.3.1 Restriction digests of pAC4 vector & pQE-60 inserts F3, F4 & F5

A single XL-1 Blue *E. coli* colony harbouring pAC4 was grown overnight in 5ml of LB broth containing 100 µg/ml ampicillin and 10 µg/ml tetracycline at 37°C, while shaking. The pAC4 vector plasmid DNA was purified using the Promega Wizard Plus™ Miniprep DNA purification system (*Section 2.2.1*) and linearised using a BamH1 / Nco1 restriction digest as described in *Section 2.2.11*. BamH1/Nco1 restriction enzyme analysis was also carried out on pQE-60 plasmid DNA isolated from XL-10 Gold *E. coli* containing the InlB F3, F4 & F5 fragments. Overnight cultures were prepared by inoculating a single colony of each fragment in 5ml of LB, with appropriate antibiotics and growing overnight at 37°C, while shaking. The plasmid DNA was purified from each clone using the Wizard Plus™ SV Miniprep DNA purification system (*Section 2.2.1*) and BamH1/Nco1 restriction enzyme digests were set up as described in *Section 2.2.11*.

The resulting restricted products (pAC4 vector & pQE-60 inserts F3, F4 & F5) were analysed by horizontal electrophoresis (*Section 2.2.2*), on a 1% (w/v) agarose gel. The gels were visualised on a UV transilluminator (Image master VSD system, Amersham Pharmacia) and the appropriate bands were cut, and purified, using the Wizard™ PCR-prep purification kit (*Section 2.2.3*).

2.3.2 Ligation of InlB insert into pAC4 vector DNA

The DNA encoding the genes of interest was cloned into the linearised pAC4 using T4 DNA ligase. The ligation reaction was set up as shown (Table 2.17).

Table 2.17: Components of ligation reaction

Component	Volume in reaction
pAC4 DNA	4 μ l
Gene of insert (F3, F4 or F5)	4 μ l
T4 DNA ligase (1U/ μ l)	1 μ l
Ligation buffer (10X)	1 μ l
Total volume of reaction:	10 μ l

The ligation reaction was incubated at 14°C for at least 4 hours, but preferably overnight. The ligation mixture was then centrifuged at 10,000 x g for 30 seconds and stored at -20°C.

2.3.3 Transformation of electro-competent AVB101 *E.coli* cells with pAC4 containing the cloned inserts

Electro-competent AVB101 *E. coli* (Avidity Corporation, US) were transformed with pAC4 containing the genes of interest (InlB F3, F4, or F5). Ligations and electroporation cuvettes (0.2cm, B10-Rad) were incubated on ice for 10 minutes. At the same time the electro-competent AVB101 cells were thawed on ice. Each ligation was added to the cells (300 μ l), mixed gently, transferred to a chilled cuvette and incubated in ice for 1 minute. The sample was the electroporated at 2.5kV, 25 μ F, 200 Ω ($\tau \approx 4$ msec). The cuvette was immediately flushed with 1ml SOC, followed by 1ml SOC (x2) at room temperature and transferred to 50ml polypropylene tube. The cells were incubated at 37°C for one hour with shaking at 250rpm. Each transformation reaction (150 μ l) was then spread onto LB agar plates, containing antibiotics (100 μ g/ml of ampicillin and 25 μ g/ml chloramphenicol). The plates were then incubated, inverted, at 37°C for at least 18 hours.

2.3.4 Expression of *in vivo* biotinylated InlB protein fragments

Twenty ml of LB broth containing 100 µg/ml ampicillin and 25µg/ml chloramphenicol was inoculated with a single colony of AVB101 *E. coli* containing the InlB gene fragments, (F3, F4 and F5). The cultures were incubated at 37°C, while shaking until the optical density at 550nm (OD₅₅₀) reached 0.5. Protein expression was then induced following addition of 1mM IPTG and 50mM D-biotin. The AVB101 strain contains the pACYC184 plasmid with an IPTG inducible birA gene to overexpress biotin ligase. The culture was further incubated, for 4 hours, at 37°C, while shaking and then centrifuged at 3,200 x g for 20 mins. The supernatant was discarded and the pellet resuspended in 1ml of PBS and sonicated for 30 s with 3 sec pulses at 220V. The lysed cells were then centrifuged at 20,000 x g for 15 min and the supernatant analysed using SDS-PAGE for assessment of protein expression.

2.3.5 Purification of *in vivo* biotinylated protein fragments using a monomeric avidin affinity column.

The biotinylated InlB fragments were purified using immobilised monomeric avidin (Pierce, 20267). The monomeric avidin was equilibrated at room temperature for 10 min and 4ml of resin was used to pack a clean, empty PD-10 column (Amersham Pharmacia). The resin was allowed to settle to form a 2ml packed column of immobilised monomeric avidin. The column was then washed twice with 8 ml of PBS (Table 2.4). Biotin blocking/elution buffer (2mM D-biotin in PBS, as before) was added (6ml), to block non-reversible biotin binding sites. Biotin was then removed from the reversible binding sites by the addition of 12ml of regeneration buffer (0.1 M glycine, pH 2.8). The column was washed with 8ml of PBS (as before) and the biotinylated protein was applied to the column. When the entire sample had passed through the column, 0.25 ml of PBS was added to force sample completely into the resin bed. The biotinylated sample was left to incubate on the column for 1 hour at room temperature, to maximize binding. The column was then placed in a fresh collection tube and 12ml of PBS (as before) was added and collected in 2ml fractions until all non-bound protein was removed. The bound biotinylated molecule was eluted with the addition of Biotin blocking/elution buffer (as before) and 500µl fractions of purified protein were collected until no further protein was detected (Absorbance at 280nm ≤ 0.05). The fractions were then analysed at 280 nm in quartz cuvettes and

fractions containing the majority of protein were pooled and stored in 0.01% (w/v) azide. The column was regenerated by washing twice with 4 ml of regeneration buffer and once with 5 ml of PBS. The column was stored in PBS containing 0.01% (w/v) sodium azide at 4°C

2.3.6 Characterisation of *in vivo* biotinylated proteins

The *in vivo* biotinylated protein fragments were characterised using the following methods; SDS-PAGE (Section 2.2.5) for protein expression analysis, Western Blotting (Section 2.2.7) with an anti-biotin antibody and Biacore analysis (Section 2.6), to assess binding with the associated anti-InIB polyclonal antibody. Enzyme and fluorescence-based analysis was also performed (Sections 2.3.6.1-2.3.6.4)

2.3.6.1 Titre of *in vivo* biotinylated recombinant InIB fragments using extravidin-peroxidase

Anti-InIB polyclonal antibody at a concentration of 10µg/ml in 0.1M carbonate buffer (pH 9.6) was used to coat the wells of a microtitre plate (100µl/well). The plate was incubated for 1 hour at 37°C and the contents emptied. The plate was then washed three times with PBS (Table 2.4) containing 0.05% (v/v) Tween 20 and three times with PBS (Table 2.4). The plate was blocked using 200µl of PBS (Table 2.4), containing 2% (w/v) BSA and incubated at 4°C overnight. Serial *in vivo* biotinylated recombinant InIB fragment (F3, F4 & F5) dilutions ranging from 1/5 – 1/5120 were then prepared in PBS (Table 2.4) containing 0.2% (w/v) BSA and 100µl of each dilution added to the wells in triplicate. The plate was incubated at 37°C for 1 hour and washed as before. Extravidin-Peroxidase, previously diluted to 1/1,000 with PBS (as before) containing 1% (w/v)BSA, was added to the plate (100µl/well) and the plate incubated at 37°C for 1 hour. Following the wash step, 100µl/well of TMB substrate was added and, after 30 mins incubation at 37°C, the absorbance at 450nm was determined using a Tecan Safire plate reader.

2.3.6.2 Titre of *in vivo* biotinylated recombinant InlB fragment F3, using streptavidin-Cy5 as tracer molecule

Anti-InlB polyclonal antibody at a concentration of 10µg/ml in 0.1M carbonate buffer (pH 9.6) was used to coat the wells of a microtitre plate (100µl/well). The plate was incubated for 1 hour at 37°C and the contents emptied. The plate was then washed three times with PBS (Table 2.4) containing 0.05% (v/v) Tween 20 and three times with PBS (Table 2.4). The plate was blocked using 200µl of PBS (Table 2.4), containing 2% (w/v) BSA and incubated at 4°C overnight. Serial *in vivo* biotinylated recombinant InlB fragment F3 dilutions ranging from 1/5 – 1/5120 were then prepared in PBS (Table 2.4) containing 0.2% (w/v) BSA and 100µl of each dilution added to the wells in triplicate. The plate was incubated at 37°C for 1 hour and washed as before. Streptavidin-Cy5, previously diluted to 1/1,000 with PBS (as before) containing 1% (w/v) BSA, was added to the plate (100µl/well) and the plate incubated at 37°C for 1 hour. Following the wash step, the fluorescence response of bound antigen was determined using a Tecan Safire plate reader with excitation at 649nm and emission at 670nm.

2.3.6.3 Optimisation of blocking reagent for fluorescence-based assays using *in vivo* biotinylated recombinant InlB fragment F3, traced with streptavidin-Cy5

Anti-InlB polyclonal antibody at a concentration of 10µg/ml in 0.1M carbonate buffer (pH 9.6) was used to coat the wells of a microtitre plate (100µl/well). The plate was incubated for 1 hour at 37°C and the contents emptied. The plate was then washed three times with PBS (Table 2.4) containing 0.05% (v/v) Tween 20 and three times with PBS (Table 2.4). The plate was blocked using 200µl of PBS (Table 2.4), containing 1% (w/v) BSA and incubated at 4°C overnight. Serial *in vivo* biotinylated recombinant InlB fragment F3 dilutions ranging from 1/5 – 1/5120 were then prepared in PBS (Table 2.4) containing 0.1% (w/v) BSA and 100µl of each dilution added to the wells in triplicate. The plate was incubated at 37°C for 1 hour and washed as before. Streptavidin-Cy5, previously diluted to 1/1,000 with PBS (as before) containing 1% (w/v) BSA, was added to the plate (100µl/well) and the plate incubated at 37°C for 1 hour. Following the wash step, the fluorescence response of bound antigen was determined using a Tecan Safire plate reader with excitation at 649nm and emission at 670nm.

2.3.6.4 Direct detection of *in vivo* biotinylated recombinant InlB fragment F3, traced with fluorescent labels; streptavidin-Cy5, avidin-FITC and streptavidin-linked quantum dots

Anti-InlB polyclonal antibody at a concentration of 10 μ g/ml in 0.1M carbonate buffer (pH 9.6) was used to coat the wells of a microtitre plate (100 μ l/well). The plate was incubated for 1 hour at 37°C and the contents emptied. The plate was then washed three times with PBS (Table 2.4) containing 0.05% (v/v) Tween 20 and three times with PBS (Table 2.4). The plate was blocked using 200 μ l of PBS (Table 2.4), containing 1% (w/v) BSA and incubated at 4°C overnight. Serial *in vivo* biotinylated recombinant InlB fragment F3 dilutions ranging from 1/5 – 1/5120 were then prepared in PBS (Table 2.4) containing 0.1% (w/v) BSA and 100 μ l of each dilution added to the wells in triplicate. The plate was incubated at 37°C for 1 hour and washed as before. The fluorescent label (streptavidin-Cy5, avidin-FITC and streptavidin-linked quantum dots), previously diluted to 1/1,000 with PBS (as before) containing 1% (w/v) BSA, was added to the plate (100 μ l/well) and the plate incubated at 37°C for 1 hour. Following the wash step, the fluorescence response of bound antigen was determined using a Tecan Safire plate reader. Excitation and emission was performed at 649nm and 670nm for streptavidin-Cy5 wells, 494nm and 518nm for avidin-FITC wells and 450nm and 605nm for streptavidin-quantum dot wells. The fluorescent response was normalised against background fluorescence and the results plotted using normalised fluorescence response units (NFRU).

2.4 Antibody Purification & Characterisation

2.4.1 Polyclonal antibody purification and characterisation

Rabbit serum containing polyclonal antibodies directed against InlB was obtained from Dr. Paul Leonard (Applied Biochemistry Group, DCU). The polyclonal antibodies were initially purified from the rabbit serum using saturated ammonium sulphate precipitation followed by protein G affinity chromatography.

2.4.1.1. Saturated ammonium sulphate (SAS) precipitation of polyclonal serum

SAS (3.6ml) was added 'drop-wise' to 3.6ml of the rabbit serum, on ice. The mixture was then left stirring on ice for one hour. The precipitated mixture was then centrifuged at 3,200 x g for 20 min at 4°C. The supernatant was discarded and the pellet was resuspended in 3.6ml of 45% (w/v) SAS. The resuspended pellet was then centrifuged at 3,200 x g for 20 min at 4°C. The supernatant was again discarded and the pellet resuspended in 3.6ml of 45% (w/v) SAS. The resuspended pellet was then centrifuged at 3,200 x g for 20 min at 4°C. The pellet was finally resuspended in 1.8ml of PBS (Table 2.4) and the solution was dialysed overnight at 4°C in PBS (as before).

2.4.1.2 Protein G affinity-chromatography of SAS-purified polyclonal serum

A 2ml suspension of immobilised Protein G (immobilised on Sepharose 4B) was equilibrated in an empty PD-10 desalting column (Amersham Biosciences) with 20ml of sterile filtered running buffer, PBS (Table 2.4). The column was stoppered when the running buffer reached the top of the gel. The SAS-purified sample (2ml) was added to the column. The effluent was monitored at 280 nm, and fractions containing protein (i.e. Absorbance 280nm \geq 0.05) collected. Running buffer was continually added to prevent the column running dry. After all the protein was collected the fractions were passed over the column two more times. The gel was washed with 20ml of wash buffer (Table 2.18) and any protein collected at this stage was kept and stored in 0.01% (v/v) azide. The column was then equilibrated using running buffer, which was allowed to pass through the column for five mins. The running buffer was allowed reach the top of the gel and then 1.5ml of elution buffer (Table 2.18) was added. The elution buffer was allowed to run into the column. Then the column was stoppered and the elution buffer was left within the column for 15 min. The stopper

was removed and 500µl fractions of protein were collected into tubes containing 50 µl of neutralising buffer (Table 2.18), once protein was detected. Fractions were collected until no further protein was detected (Absorbance at 280nm ≤ 0.05). The fractions were then analysed at 280 nm in quartz cuvettes and fractions containing the majority of protein were pooled and stored in 0.01% (w/v) azide. The protein G column was then washed using running buffer and stored in 20% (v/v) methanol.

Table 2.18: Composition of buffers used during the protein G purification of rabbit IgG polyclonal antibodies.

Solution	Composition
Running & Wash buffer (PBS)	0.15M NaCl, 2.5mM KCl, 10mM Na ₂ HPO ₄ , 18mM KH ₂ PO ₄ , pH 7.4.
Elution buffer	0.1M Glycine/HCl, pH 2.7.
Neutralising buffer	2M Tris/HCl, pH 8.6.

2.4.1.3 Checkerboard ELISA for the determination of optimal antigen concentration and antibody dilution

A 96-well microtitre plate was coated with different InlB-F3 recombinant protein concentrations, ranging from 0 to 50µg/ml, by adding 100µl of each concentration per well. The plate was incubated for 1 hour at 37°C and the contents emptied. The plate was then washed three times with PBS (Table 2.4) containing 0.05% (v/v) Tween and three times with PBS (Table 2.4). The plate was blocked using 200µl of PBS (as before), containing 2% (w/v) BSA and incubated at 4°C overnight. Serial biotinylated anti-InlB polyclonal antibody dilutions ranging from 1/50 – 1/12,800 were then prepared in PBS (as before), containing 1% (w/v) BSA and 100µl of each dilution added to the wells in triplicate. The plate was incubated at 37°C for 1 hour and washed as before. Extravidin-Peroxidase, previously diluted to 1/1,000 with PBS (as

before) containing 1% (w/v) BSA, was added to the plate (100µl/well) and the plate incubated at 37°C for 1 hour. Extravidin-peroxidase is a commercially available conjugate (Sigma-Aldrich) prepared from egg white avidin and linked to horseradish peroxidase for detection. It is a tetrameric protein containing four high affinity binding sites for biotin. Extravidin combines the high specific activity of avidin with the low background staining of streptavidin, a biotin binding protein produced by the bacteria *Streptomyces avidinii*. Following the wash step, 100µl/well of TMB substrate was added and, after 30 min incubation at 37°C, the absorbance at 450nm was determined using a Tecan Safire plate reader.

2.4.2 Monoclonal antibody purification and characterisation

Monoclonal antibodies to warfarin were produced by Dr. Brian Fitzpatrick (Applied Biochemistry Group, DCU). A direct ELISA format was used to screen the hybridoma-clone supernatants for specific antibody production, and 'positive' wells were propagated and cloned by limiting dilution. Stocks of positive antibody-secreting clones were frozen down for subsequent rounds of cloning out. A frozen stock of both the anti-warfarin monoclonal antibody and anti-InlB monoclonal antibody was obtained and grown up for subsequent rounds of cloning out by limiting dilution, to ensure monoclonality. Once sufficient antibody-containing supernatant was collected, the antibodies were concentrated for purification using an Amicon ultrafiltration system.

2.4.2.1 Purification of murine IgG by Protein-G affinity chromatography

Supernatants from hapten-specific antibody-secreting hybridomas were collected and concentrated 10-fold using an Amicon concentration device. 10 mls of concentrated supernatant were passed through a PD-10 column containing Protein G immobilised on Sepharose 4B. The eluate was collected and passed through the column a second time. The column was then washed with 25 ml of PBS (Table 2.4) containing 0.05% (v/v) Tween 20 and the retained protein eluted with 0.1 M glycine-HCl (pH 2.5). 850 µl fractions were collected in eppendorf tubes containing 150 µl of Tris-HCl (pH 8.5) to return the pH to ~7.0 to prevent antibody denaturation. The absorbance of each fraction was then measured at 280 nm for protein concentration determination. Purified antibodies were stored at -20°C prior to further use.

2.4.2.2 Checkerboard ELISA for the determination of optimal antigen coating concentration and antibody dilution

A 96-well microtitre plate was coated with different warfarin-BSA conjugate concentrations, ranging from 50µg/ml to 0µg/ml, by adding 100µl of each concentration per well. The plate was incubated for 1 hour at 37°C and the contents emptied. The plate was then washed three times with PBS (Table 2.4) containing 0.05% (v/v) Tween 20 and three times with PBS (Table 2.4). The plate was blocked using 200µl of PBS (Table 2.4), containing 2% (w/v) BSA and incubated at 4°C overnight. Serial biotinylated anti-warfarin monoclonal antibody dilutions ranging from 1/50 – 1/12,800 were then prepared in PBS (Table 2.4) containing 1% (w/v) BSA and 100µl of each dilution added to the wells in triplicate. The plate was incubated at 37°C for 1 hour and washed as before. Extravidin-Peroxidase (as per *Section 2.4.1.3*) was diluted to 1/1,000 with PBS (as before) containing 1% (w/v) BSA, was added to the plate (100µl/well) and the plate incubated at 37°C for 1 hour. Following the wash step, 100µl/well of TMB substrate was added and, after 30 min incubation at 37°C, the absorbance at 450nm was determined using a Tecan Safire plate reader.

2.5 Conjugate Synthesis

2.5.1 Preparation and characterisation of 4'-azowarfarin-protein conjugates

A 50ml solution containing 0.1 M HCl and 7 mM potassium bromide was used to dissolve 350 mg of 4'-aminowarfarin. A 0.014 M solution of sodium nitrite (10ml) was added dropwise to the solution containing 4'-aminowarfarin, and maintained with continuous stirring on an ice-bath for 1 hour. The activated 4'-aminowarfarin solution was then added dropwise to 10 ml of a 5% (w/v) solution of BSA, and the pH maintained between 9.0-9.5 with the simultaneous addition of 0.1 M NaOH, and stirred overnight at 4°C (Sato *et al.*, 1982). The resulting dark brown solution was then dialysed against several changes of PBS, pH 7.4, and lyophilised prior to further studies. The drug-protein conjugates following lyophilisation were characterised by UV spectroscopy. A direct comparison of the reference spectra obtained for the drug-protein conjugate to 4'-aminowarfarin and a 'control' protein (i.e. a protein solution which had undergone the same chemical procedure as the conjugate solution, except the drug solution had been omitted from the coupling step) was made from 200-400 nm

2.5.2 Preparation of biotinylated antibodies

2.5.2.1 Biotinylation of antibodies for fluorescence-based immunoassays (FIA)

Antibodies, at a concentration of ~1mg/ml, were dialysed overnight to remove any traces of azide, for subsequent use in the biotinylation reaction. Long-chain biotin (Sulfo-NHS-LC-Biotin, Pierce, 21335) was dissolved in DMSO to prepare a 10mM stock solution of biotin. The extent of biotin labeling depends on the distribution of amino groups on the protein, the protein concentration and the amount of reagent used. Experiments were performed using a 20-fold molar excess of biotin reagent to label 1mg antibody (in 1ml PBS, Table 2.4), which results in conjugation of 4-6 biotin groups per antibody molecule. The biotin stock solution (13µl) was added to 1ml of antibody (concentration 1mg) and the solution was incubated end on end, overnight, at 4°C. The biotin conjugate was subjected to gel filtration to stop the reaction and to remove any unbound biotin using a PD-10 desalting column (Amersham Pharmacia). The conjugate concentration and biotin/protein ratio was determined using commercial HABA/Avidin reagent (Sigma Aldrich, H2153).

2.5.2.2 Biotinylation of antibodies for electrical impedance spectroscopy (EIS)

Antibodies were biotinylated to facilitate immobilisation onto the neutravidin-modified polymer films with biotinamidohexanoic acid-3-sulfo-N-hydroxysuccinimide (BAC-sulfo-NHS), using the procedure outlined in the Sigma Immunoprobe biotinylation kit (BK101). The strong affinity between avidin and biotin (affinity constant $K_a = 10^{15} \text{ M}^{-1}$) allows direct coupling of the biotinylated antibodies to the modified electrode. The extended spacer arm from the hexanoic acid improved the interaction between avidin and the biotinylated antibody by overcoming steric hindrances present at the biotin binding sites. A molar ratio of 10:1 biotin to antibody was used to ensure efficient labelling and the antibody was subjected to fast gel filtration post-biotinylation to remove any unreacted biotin. An avidin-HABA (4-Hydroxyazobenzene-2-carboxylic acid) assay was then performed to determine the degree of biotinylation; dye/protein ratio and biotin-antibody conjugate concentration. Biotinylated antibodies were diluted in PBS, comprising 0.13 mM NaH_2PO_4 , 0.528 mM Na_2HPO_4 and 0.51 mM NaCl, pH 7.4, and stored at -20°C at a concentration of 1 mg/ml.

2.5.3 Fluorescent labelling of antibodies and proteins

A standard protocol for the fluorescent labelling of biomolecules is difficult to derive as optimisation of labelling condition such as buffer pH and concentration is highly specific for each dye. Gel filtration is used to remove sodium azide, which is often found as a preservative in biological preparations and interferes with the labelling process. Typically, phosphate buffered saline comprising 0.13 mM NaH_2PO_4 , 0.528 mM Na_2HPO_4 and 0.51 mM NaCl, pH 7.4 or 0.5M carbonate buffer, pH 9.6, are used for labelling reactions. The amount of fluorescent labelling reagent used for each reaction is dependent on the amount of protein to be labelled. By using the appropriate molar ratio of labelling reagent to protein, the extent of conjugation can be optimally controlled. For protein concentrations in the range of 2-5mg/ml, a 10-fold molar excess is used, for concentrations $<2\text{mg/ml}$, a 15 molar excess is used and for protein concentrations $<1\text{mg/ml}$, 20 molar excess of dye is used.

Using ruthenium dye as an example, the label was dissolved in an organic solvent (DMSO) at a concentration of 10mg/ml (as most fluorescent dyes are insoluble in aqueous solution). Taking into account an optimal 20 fold molar excess based on the antibody concentration (1mg/ml), the appropriate volume of label was determined and added to the protein stock. The dye/protein solution was left to react overnight at 4°C. Excess dye was removed via centrifugation using a commercial Vivaspin column at 3,200 x g (or by dialysis). The conjugate concentration and dye/protein ratio were then determined spectrophotometrically. The level of label incorporation can be measured by determining the absorbance at or near the characteristic extinction maximum of the label. It is also important to determine the dye/protein ratio for all derivatives prepared with tags. The equations below are used to calculate this information.

Equation. 2.1

$$\frac{A_{280} - (A_{\text{max}} \times CF) \times DF}{\epsilon_{\text{protein}}}$$

where A_{280} is the absorbance of the dye/protein conjugate at 280nm; A_{max} is the absorbance of the conjugate at the excitation maximum wavelength for the dye; CF is the correction factor i.e. A_{280} dye / A_{max} dye, DF is the dilution factor, $\epsilon_{\text{protein}}$ is the protein molar extinction co-efficient.

Equation 2.2

$$\left(\frac{A_{\text{max}}}{\epsilon_{\text{dye}} \times \text{Conc.}} \right) \times DF$$

where A_{max} is the absorbance of the conjugate at the excitation maximum wavelength for the dye; ϵ_{dye} is the dye molar extinction co-efficient; Conc. is the dye/protein conjugate concentration in moles per l and DF is the dilution factor.

2.6 Analysis of *in vivo* biotinylated InIB protein fragments and associated antibodies using Biacore

Analysis was performed using a Biacore 3000TM instrument operated with the Biacore 3000 Control Software package version 3.1.1. All data analysis was performed using Biaevaluation 4.0.1. Research grade CM5 (carboxymethylated 5) sensor chips were employed and Hepes Buffered Saline (HBS), pH 7.4, containing 10mM HEPES (4-(2-hydroxyethyl)piperazine-1-ethanesulphonic acid), 150mM NaCl, 3.4mM EDTA and 0.05% (v/v) Tween 20, was used as the running buffer. This was freshly prepared, filtered (pore size 0.22 μ m) and degassed using a vacuum filtration apparatus (Millipore sintered glass filtration unit) before use. All samples were syringe filtered (0.2 μ m pore size) to remove any particulate matter.

2.6.1 Preconcentration studies

Neutravidin was prepared in 10mM sodium acetate buffer that had been adjusted with 10% (v/v) acetic acid to a range of pH values. The protein sample, at the respective pH, was passed over an underivatized chip surface, at a flow rate of 10 μ l/min for 1 minute, and the amount of electrostatic interaction monitored. The pH which gave the highest degree of binding, *i.e.* maximum response, was chosen as the buffer for subsequent immobilisations.

2.6.2 Immobilisation of neutravidin/biotinylated F3 onto sensor surfaces

Immobilisation of neutravidin was carried out according to standard amine coupling chemistry. Briefly, the carboxymethylated dextran surface was activated by mixing equal volumes of 100mM NHS (N-hydroxysuccinimide) and 400mM EDC (N-ethyl-N-(dimethyl-aminopropyl) carbodiimide hydrochloride) and injecting the mixture over the sensor chip surface for 8 minutes at a flow rate of 10 μ l/min. Neutravidin at a concentration of 50 μ g/ml in 10mM sodium acetate buffer, at pH 4.6, was injected over the activated surface for 40 minutes at a flow rate of 5 μ l/min. Unreacted NHS groups were capped by an injection of 1M ethanolamine, pH 8.5, for 7 minutes. Loosely bound neutravidin protein was removed using three 30sec pulses of 5mM NaOH. *In vivo* biotinylated InIB protein fragment F3 (60 μ g/ml) was subsequently immobilised on the neutravidin surface using a manual 6 minute injection, at a flow rate of 5 μ l/min. The F3 fragment was stabilised on the surface of the chip with a 30 second pulse of EDC/NHS.

2.6.3 Non-specific binding studies

Anti-InIB polyclonal antibody at the optimal assay dilution (1/20) was simultaneously injected over both the blank neutravidin surface (reference flow cell) and the neutravidin surface with the immobilised biotinylated InIB F3. The binding response following each injection was monitored and used to determine the degree of non-specific binding of the antibodies to the neutravidin surface in the absence of biotinylated F3.

2.6.4 Regeneration studies

A known concentration of antibody was passed over the chip surface, at the optimised flowrate, and the surface regenerated by passing over various concentrations of NaOH ranging from 1-100mM to assess the stability of the immobilised protein surface. This cycle of binding and regeneration was usually completed for more than 50 cycles; however, due to low stocks of anti-InIB polyclonal antibody, only 10 regenerations were performed. After each cycle of injection of antibody and subsequent regeneration, the binding signal was measured to assess the stability and suitability of the immobilised surface for assay purposes.

2.6.5 Biacore inhibitive immunoassay for the detection of InIB

Standards of free InIB-F3 were prepared at varying concentration ranges. Each standard was incubated with an equal volume of anti-InIB polyclonal antibody and allowed equilibrate for 30 minutes at room temperature. Each sample was then injected over the immobilised protein surface, in triplicate, and the surface regenerated with the appropriate concentration of sodium hydroxide, 27.5mM, as determined from *Section 2.6.4*. A calibration curve was then constructed by plotting the change in response (RU) for each standard against the log of concentration and a four-parameter equation fitted to the data using Biaevaluation software 4.0.1.

2.7 Nanoparticle Synthesis

2.7.1 Synthesis of silica dye-doped nanoparticles

Dye-doped high brightness nanoparticles were synthesised* by Dr. Robert Nooney of the Biomedical Diagnostics Institute (BDI), National Centre for Sensor Research (NCSR), using a microemulsion method adapted from Santra *et al.* (2001). A microemulsion was formed by mixing Triton X surfactant, hexanol co-solvent and cyclohexane oil phase together. Separately an aqueous solution of 20mM Ru (bpy)₃Cl₂ (ruthenium bipyridine salt) was prepared and the pH adjusted to 1.6 with the addition of 1N HCl. The aqueous Ru (bpy)₃Cl₂ solution was added to the oil phase with rapid stirring. To ensure formation of the water in oil microemulsion the solution was sonicated and stirred for a further five minutes. Following this, tetraethylorthosilicate (TEOS) was added. After 30 minutes of gentle mixing on a blood rotor, NH₄OH was added to initiate polymerisation. This mixture was left to further react for 24 hours at room temperature. To prevent aggregation of the nanoparticles, 3-(trihydroxysilyl) propyl-methyl phosphonate, monosodium salt, 42% (w/v) in water was added for 5 minutes. Aminopropyltrimethoxysilane (APTES) was then added for conjugation with antibodies and the solution stirred for a further 24 hours. The NPs were separated from the solution with the addition of an excess of absolute ethanol to break the microemulsion state. The solidified silica nanoparticles were then harvested by centrifugation for 10 minutes and washed twice in absolute ethanol. The nanoparticles were washed once more with deionised water and characterised using a transmission electron microscope (TEM) for imaging and size measurements. The modified particles were stored in deionised water at 4 °C for antibody attachment.

* Please note that due to the proprietary nature of these methods (Biomedical Diagnostics Institute, DCU) details on actual volumes and experimental conditions cannot be given. The methods used were adapted from Santra *et al.*, (2001), Tan^b *et al.*, (2004) and Qhobosheane *et al.*, (2001).

2.7.2 Surface modification of nanoparticles for antibody conjugation

Amino-activated-nanoparticles in deionised water were centrifuged at 20,000 x g for 10 minutes and dried overnight in a 60°C oven. The dried particles (2mg) were suspended in 900µl of 0.1M phosphate buffer, pH 7.4, supplemented with differing ratios of glutaraldehyde and BSA*. Antibodies were attached to the amino-modified nanoparticles using glutaraldehyde crosslinking. This mixture was left to react for 24 hours at 4°C, with gentle stirring. The nanoparticle mix was then centrifuged at 20,000 x g for 10 minutes and the resultant pellet washed twice with 0.1M phosphate buffer, pH 7.4. The amine/glutaraldehyde modified nanoparticles were resuspended in 1ml of 0.1M phosphate buffer, pH7.4, containing 0.25mg of polyclonal anti-human IgG antibody. This was left to react for 24 hours at 4°C, with gentle stirring. The antibody-conjugated nanoparticles were then separated by washing twice in 0.1M phosphate buffer, pH 7.4 and stored in 0.1M phosphate buffer, pH 7.4, containing 0.1% (w/v) BSA and 0.02% (w/v) NaN₃.

** Please note that due to the proprietary nature of these methods (BDI, DCU) details on actual volumes and experimental conditions cannot be given.*

2.7.3 Nanoparticle-antibody conjugate characterisation

2.7.3.1 Titre of antibody-nanoparticle conjugates

Black Fluoronunc™ 96-well microtitre plates were coated with 100µl/well of human IgG (5µg) and incubated for 1 hour at 37°C. The plates were then emptied and washed 3 times with PBS (Table 2.4), containing 0.05% (v/v) Tween 20 (PBST) and three times with PBS (Table 2.4). The plates were then blocked by adding 200µl/well of PBS containing 1% (w/v) BSA and incubated for 1 hour at 37°C. The plates were washed as before and serial dilutions of the various anti-human IgG nanoparticle conjugates (with differing glutaraldehyde concentrations) were prepared in PBS containing 0.1% (w/v) BSA. These were added to the plates (100µl/well) in triplicate and incubated at 37°C for 1 hour and washed as before. Following the final wash step, the fluorescent response was determined using a Tecan Safire² monochromator-based microplate reader, with excitation at 453nm and emission at 618nm.

2.7.3.2 Sandwich assay for the detection of human IgG using antibody-conjugated nanoparticles as fluorescent tracer molecule

Black Fluoronunc™ 96-well microtitre plates were coated with 100µl of anti-human IgG (5µg) and incubated for 1 hour at 37°C. The plates were then emptied and washed 3 times with PBS (Table 2.4), containing 0.05% (v/v) Tween 20 and three times with PBS (Table 2.4). The plate were then blocked by adding 200µl/well of PBS (Table 2.4) containing 1% (w/v) BSA and incubated for 1 hour. Free human IgG dilutions, ranging from 0.005ng/ml to 500,000 ng/ml, were prepared in PBS containing 0.1% (w/v) BSA. The plates were washed (as before) and 100µl of the free human-IgG dilutions (in triplicate) were added to each well and incubated for 1 hour at 37°C. The plates were then washed again and 100µl of the anti-hIgG-conjugated nanoparticles; previously diluted to 1/100 with PBS containing 0.1% (w/v) BSA was added to each well. The plates were then incubated at 37°C for 1 hour before washing (as before). Following the final wash step, the fluorescent response was determined using a using a Tecan Safire² monochromator-based microplate reader, with excitation at 453nm and emission at 618nm. The fluorescent response was normalized against a zero control (blank well containing no fluorescent molecules).

2.8 Development of fluorescence-based immunoassays

2.8.1 Determination of optimal fluorescent label working dilution

Black Fluoronunc™ 96-well microtitre plate were coated with the appropriate amount of coating antigen as determined by checkerboard ELISA (100µl/well); either 20µg/ml InIB or 50µg/ml Warfarin-BSA and incubated at 37°C for 1 hour. The plates were washed 3 times with PBST (Table 2.4), PBS containing 0.05% (v/v) Tween 20 and 3 times with PBS (Table 2.4). The plates were then blocked with 200µl/well of 1% (w/v) BSA diluted in PBS. Powdered milk was not used as a blocking reagent in this case, since milk contains biotin which could interfere with the produced signal. Following incubation for 1hr at 37°C the plates were washed as before. A 1/300 dilution of the biotinylated anti-InIB polyclonal antibody or anti-warfarin monoclonal antibody was prepared in PBS (Table 2.4) containing 0.1% (w/v) BSA and 100µl added to each well of the plate (in triplicate) The plates were then incubated for 1 hour at 37°C and washed as before. The avidin-linked fluorescent conjugate (Table 2.19), was titrated from a 10nm working stock. Dilutions ranging from 1/2 to 1/4,096

were prepared in 0.2M borate buffer, pH 8.2 and added to the plate 100µl/well (in triplicate) and the plate incubated at 37°C for 30mins. Following the wash step, the fluorescent response was determined using a Tecan Safire² monochromator-based microplate reader with excitation and emission wavelengths dependent on the fluorophore used. The fluorescent response was normalized against a zero control (blank well containing no fluorescent molecules).

Table 2.19: Excitation and emission wavelengths of fluorescent labels

Fluorescent Probe	Excitation Wavelength (nm)	Emission Wavelength (nm)
Quantum dot streptavidin conjugate	450	605
Streptavidin-Cy5	649	670
Porphyrin-labelled Neutravidin	380	650
Avidin-FITC	494	518

2.8.2 Development of a competitive assay for the detection of InIB/warfarin with quantum dot-labelled antibodies

Black FluoronuncTM 96-well microtitre plates were coated with either 50µg/ml warfarin-BSA conjugate or 20µg/ml InIB-F3 and incubated for 1 hour at 37°C. The plates were then emptied and washed 3 times with PBS (Table 2.4) containing 0.05% (v/v) Tween 20 and three times with PBS (Table 2.4). The plates were blocked by adding 200µl of PBS containing 1% (w/v) BSA to each well and incubated for 1 hour at 37°C. Free warfarin or purified InIB-F3 dilutions, ranging from 1.5ng/ml to 50000ng/ml, were prepared in PBS (Table 2.4) containing 0.1% (w/v) BSA. The plates were washed as before and 50µl of free hapten/protein dilution was added to each well (in triplicate) along with 50µl of the biotinylated anti-warfarin/anti-InIB antibody previously diluted to 1/300 in PBS containing 0.1% (w/v) BSA. The plates were then incubated at 37°C for 1 hour and washed as before. The quantum dot-streptavidin conjugate was diluted to a working solution of 1/500 of the original stock (2nM concentration as determined in *Section 2.8.1*) in the supplied incubation buffer, (0.2M borate buffer, pH 8.2), added to the plate (100µl/well) and the plate incubated

at 37°C for 30min. Following the wash step, the fluorescent response was determined using a Tecan Safire² monochromator-based microplate reader with excitation at 450nm and emission at 605nm. The fluorescent response was normalized against a zero control.

2.8.3 Development of competitive assay for the detection of warfarin/InIB with porphyrin-labelled antibodies

Black FluoronuncTM 96-well microtitre plates were coated with either 50µg/ml warfarin-BSA conjugate or 20µg/ml InIB-F3 and incubated for 1 hour at 37°C. The plates were then emptied and washed 3 times with PBS (Table 2.4) containing 0.05% (v/v) Tween 20 and three times with PBS (Table 2.4). The plates were blocked by adding 200µl of PBS containing 1% (w/v) BSA to each well and incubated for 1 hour at 37°C. Free warfarin or purified InIB-F3 dilutions, ranging from 1.5ng/ml to 50000ng/ml, were prepared in PBS containing 0.1% (w/v) BSA. The plates were washed as before and 50µl of free hapten/protein dilution was added to each well (in triplicate) along with 50µl of the biotinylated anti-warfarin/anti-InIB antibody previously diluted to 1/300 with PBS containing 0.1% (w/v) BSA. The plates were then incubated at 37°C for 1 hour and washed as before. The porphyrin-labeled neutravidin conjugate was diluted to a working solution of 1/500 of the original stock in 0.2M borate buffer, pH 8.2, and added to the plates (100µl/well) for 30 min at 37°C. Following the final wash step, the fluorescent response was determined using a Tecan Safire² microplate reader with excitation at 380nm and emission at 650nm. The fluorescent response was normalized against a zero control.

2.8.4 Immobilisation of biotinylated anti-InIB polyclonal antibody on biochip platform, traced with streptavidin-Cy5

Biotinylated anti-InIB antibody was immobilised by passive adsorption onto polystyrene (PS) cone platforms (1/100 of stock) and left to react for two hours at room temperature. The platforms were then washed 5 times with PBS (Table 2.4) containing 0.05% (v/v) Tween 20 and five times with PBS (Table 2.4) to remove any unbound antibody. The platforms were blocked by immersing the chip in PBS (as before) containing 1% (w/v) BSA and incubating the chip for 1 hour at 37°C. The blocked platforms were subsequently washed as before and streptavidin-Cy5 diluted

in PBS was added to the antibody spots on the cone surface (1/500 dilution). This was left to react for two hours at room temperature, after which the platforms were washed as before. The fluorescent signal generated from the immobilised biotinylated anti-InIB antibody, traced with streptavidin-Cy5, was detected using a CCD camera with exposure times of 5-10 seconds.

2.8.5 Biochip assay for detection of InIB with streptavidin-Cy5 as tracer molecule

InIB-F3 recombinant protein fragment was immobilised by passive adsorption onto polystyrene (PS) cone platforms (20ng/ μ l) and left to react for two hours at room temperature. The platforms were then washed 5 times with PBS (Table 2.4) containing 0.05% (v/v) Tween 20 and five times with PBS (Table 2.4) to remove any unbound antigen. The platforms were blocked by immersing the chip in PBS (as before) containing 1% (w/v) BSA and left to incubate for 1 hour at 37°C. The blocked platforms were washed as before and biotinylated anti-InIB polyclonal antibody was spotted onto the InIB-F3 immobilised cones (1/100 dilution) and left to react for two hours at room temperature. The platforms were then emptied and washed as before to remove any unbound antibody. Streptavidin-Cy5 diluted in PBS (as before) was then added to the antibody-antigen spots on the cone surface (1/500 dilution). This was left to react for two hours at room temperature, after which the platforms were washed as before. The fluorescent signal generated from the immobilised biotinylated anti-InIB antibody, traced with streptavidin-Cy5 was detected using both a CCD camera with exposure times of 5-10 seconds.

2.9 Detection of Parvovirus B19

2.9.1 Enzyme-linked immunosorbent assay (ELISA) for the detection of Parvovirus B19

Microtitre plates were coated with 4µg of coating antibody (anti-parvovirus B19 antibody) and incubated for 1 hour at 37°C. The plates were emptied and washed 5 times with TBS (Table 2.4) containing 0.05% (v/v) Tween 20 (TBST), and blocked to prevent non-specific binding with blocking solution (200µl/well). This blocking solution comprised of PBS (Table 2.4) containing 10% (w/v) sucrose and 1% (w/v) BSA. The plates were incubated for 1 hour at 37°C and washed as before with TBST. Recombinant VP2 capsid protein dilutions were prepared in low pH sample diluent (Biotrin International, Dublin), at concentrations ranging from 1pg-10µg/ml. Each VP2 concentration was added to the plates in triplicate (100µl/well) and incubated at 37°C for 1 hour. The plates were washed as before and peroxidase-labelled anti-VP2 antibody added, previously diluted to 1/10000 with enzyme conjugate diluent, (100µl/well) and incubated at 37°C for 1 hour. The plates were washed, as before, and TMB substrate added (100µl/well). After 10 minutes incubation at 37°C the absorbances at 620 nm were determined using a Tecan Safire² plate reader.

2.9.2 Fluorescence-based immunoassay (FL) for the detection of Parvovirus B19

Microtitre plates were coated with 4µg of coating antibody (anti-Parvovirus B19 antibody), and incubated for 1 hour at 37°C. The plates were then emptied and washed 5 times with TBS (Table 2.4) containing 0.05% (v/v) Tween 20 and blocked to prevent non-specific binding with blocking solution (as before, *Section 2.9.1*). The plates were then incubated for 1 hour at 37 °C. Recombinant VP2 capsid protein dilutions were prepared in low pH sample diluent (Biotrin International, Dublin), at concentrations ranging from 1pg-10µg/ml. The plates were washed as before and each VP2 concentration was added in triplicate (100µl/well), and incubated at 37 °C for 1 hour. The plates were washed (as before) and biotin-labelled anti-VP2 antibody, previously diluted to 1/800 with enzyme conjugate diluent, (Biotrin International, Dublin) was added (50µl/well) along with avidin-FITC conjugate previously diluted in the same diluent to 20µg/ml, (50µl/well). The plates were incubated at 37°C for 1 hour, washed as before and the fluorescence response determined using a Tecan Safire² plate reader with excitation at 494 nm and emission 518 nm.

2.9.3 Chemiluminescence-based immunoassay for the detection Parvovirus B19

Microtitre plates were coated with 4µg of coating antibody (anti-Parvovirus B19 antibody), and incubated for 1 hour at 37°C. The plates were then emptied and washed 5 times with TBS (Table 2.4) containing 0.05% (v/v) Tween 20 and blocked to prevent non-specific binding with blocking solution (as before, *Section 2.9.1*). The plates were then incubated for 1 hour at 37 °C. Recombinant VP2 capsid protein dilutions were prepared in low pH sample diluent (Biotrin International, Dublin), at concentrations ranging from 1pg-10µg/ml. The plates were washed as before and each VP2 concentration was added in triplicate (100µl/well), and incubated at 37 °C for 1 hour. The plates were washed, as before, and peroxidase-labelled anti-VP2 antibody, previously diluted to 1/10000 with enzyme conjugate diluent was added (100µl/well), and incubated at 37°C for 1 hour. The plates were washed, as before, and luminol/iodophenol/hydrogen peroxide substrate was added, (100µl/well). The luminescence response was determined using a Biotek plate reader.

2.9.4 Biomolecule immobilisation on cone platforms

Plate-based assays for the detection of Parvovirus B19 were reproduced on optical enhancement cone structures (Optical sensors group, Biomedical Diagnostics Institute, DCU) using the same antibodies, antigen and reagents provided by Biotrin International, Dublin. Both polycarbonate (PC) and polystyrene (PS) cone platforms were made available for investigation. A number of surface modification strategies for optimal biomolecular immobilisation were examined. These included treatment of the polymers with an oxygen plasma prior to immobilisation, modification of the platforms with glutaraldehyde and the use of indium tin oxide (ITO)-coated polymer materials with and without aminopropyl-tri-ethoxysilane (APTES). A matrix approach was taken for each modification step, in that each method was examined in series, with appropriate controls. The success of each strategy was evaluated by determining the amount of horseradish peroxidase (HRP) successfully immobilised on each modified surface. This was achieved by immobilising a range of concentrations of HRP (0-1000µg/ml) on the modified platforms and assessing HRP incorporation with TMB substrate. Once an optimal method was chosen, the procedure was repeated for the anti-VP2 antibody (Biotrin International, Dublin) for further assay development.

2.9.4.1 Investigation of biomolecule immobilisation on cone platforms

Dilutions of plant HRP were prepared in PBS (Table 2.4) and 20µl of each concentration (0-1000 µg/ml) was added to the modified cone platforms and left to react for two hours at room temperature. The platforms were then emptied and washed 5 times with PBS (Table 2.4) containing 0.05% (v/v) Tween and five times with PBS (Table 2.4). The amount of bound HRP was determined by adding TMB (3,3',5,5'-Tetramethylbenzidine dihydrochloride) substrate to each of the cone assemblies. The TMB substrate was prepared by dissolving 1mg of TMB in 200µl dimethylsulphoxide (final concentration of DMSO was 2% w/v). This TMB solution was added to 9.8ml of 100mM citric acid buffer, pH 5.5, and mixed to homogeneity. To this solution, immediately prior to assay, 3µl of H₂O₂ (30%, v/v) was added and mixed to give a final concentration of 0.03% (v/v) H₂O₂ in the reaction solution.

Twenty microlitres of prepared TMB substrate was added to each cone assembly and the platforms were covered to protect from light as the reaction proceeded. Fifteen microlitres of the reacted TMB substrate from each cone was then pipetted into an appropriate well in a microplate and 135µl of reaction solution was added and mixed for 3min (1/10 dilution, total volume of reaction in each well is 150µl). The absorbances for all samples were read at 620nm. This method was based on the fact that TMB substrate produces a blue colour in the presence of HRP catalytic activity, which can be spectrophotometrically measured at 620nm (Ryan *et al.*, 1994).

2.9.4.2 Detection of immobilised anti-VP2 antibody on cone platforms

HRP-conjugated anti-VP2 antibody was immobilised via glutaraldehyde crosslinking on polystyrene (PS) cone platforms (0-1000µg/ml) and left to react for two hours at room temperature. The platforms were washed 5 times with PBS (Table 2.4) containing 0.05% (v/v) Tween 20 and five times with PBS (Table 2.4) to remove any unbound antibody. The amount of bound HRP-conjugated anti-VP2 antibody was determined using TMB substrate, (as before, *Section 2.9.4.1*).

2.9.4.3 Enzyme-based sandwich assay for the detection of VP2 on cone platforms

Polystyrene cone platforms were treated with differing percentage concentrations of glutaraldehyde; 2.5%, 1% and 0.25% (v/v), prepared in PBS (Table 2.4). Anti-VP2 coating antibody (3.91 μ g) was spotted on the cones of each platform and incubated for 2 hours at RT. The platforms were washed 5 times with TBS (Table 2.4) containing 0.05% (v/v) Tween (TBST), and blocked to prevent non-specific binding with blocking solution (200 μ l/well), as before, *Section 2.9.1*. The platforms were incubated for 2 hours at RT and washed as before with TBST. Recombinant VP2 capsid protein dilutions were prepared in low pH sample diluent (Biotrin International, Dublin), at concentrations ranging from 1ng – 10,000ng/ml. Each VP2 concentration was added in triplicate (3 cones) and incubated at RT for 2 hours. The chip platforms were washed as before and peroxidase-labelled anti-VP2 antibody (previously diluted to 1/10000 with enzyme conjugate diluent) was added to each cone and incubated at RT for 2 hours. The platforms were washed, as before, and TMB substrate (prepared as per *Section 2.9.4.1*) was added (20 μ l/cone). The absorbances for all samples were read at 620nm.

2.9.4.4 Chemiluminescence-based detection of HRP on cone platforms

The immobilisation of HRP via glutaraldehyde crosslinking on polystyrene (PS) cone platforms (0-1000 μ g/ml) was visualised by the *in situ* addition of luminol/iodophenol substrate to cone platforms using a 5ml luer-lock syringe. The detection of the chemiluminescence signal generated from immobilised-HRP, was captured with a CCD camera using an exposure time of ~40 s.

2.9.4.5 Fluorescence-based detection of anti-VP2 antibody on cone platforms

Anti-VP2 antibody-biotin conjugate was immobilised via glutaraldehyde crosslinking on polystyrene (PS) cone platforms (1/800 dilution as per *Section 2.9.2*) and left to react for two hours at RT. The platforms were then emptied and washed 5 times with PBS (Table 2.4) containing 0.05% (v/v) Tween and five times with PBS (Table 2.4) to remove any unbound antibody. Streptavidin-Cy5 prepared in PBS (as before) was then added to the antibody spots (0-1000 μ g/ml) and left to react for two hours at RT. The platforms were emptied and washed as before. The fluorescent signal generated from the immobilised biotin anti-VP2 antibody traced with streptavidin-Cy5 was detected using a CCD camera with exposure times of 5-10 seconds.

2.10 Immunostaining Application

2.10.1 Slide Preparation

Glass microscope slides were cleaned in 50:50 MeOH: HCl solution for thirty minutes. They were then rinsed three times in de-ionised water and left to air dry for thirty minutes in a slide rack. Two types of poly-L-lysine were investigated for optimal coating of the glass slides. The first method involved the use of stock poly-L-lysine solution diluted 1/10 (v/v) in sterile filtered PBS (Table 2.4). This solution was spotted onto clean slides and left to incubate for two hours. It was then rinsed off with ultra pure water and left to air-dry overnight. The second method utilized poly-L-lysine hydrobromide diluted 0.1% (w/v) in sterile molecular grade water. This solution was spotted onto clean slides and left to incubate for two hours. It was then rinsed off with ultra pure water and left to air-dry overnight.

2.10.2 Cell Preparation

1ml of *Listeria monocytogenes* cells were used to inoculate 50ml of Brain Heart Infusion (BHI) medium (Table 2.3). This was grown at 200rpm for 4 hours at 37°C, while shaking. The cells were then sub-cultured by inoculating 3ml into 50ml of *Listeria* Enrichment Broth (LEB) (Table 2.3) and growing overnight at 37°C, while shaking at 200rpm. The culture was then centrifuged at 3,200 x g to pellet the cells. The pellet was resuspended in a 1/10 dilution of PBS (Table 2.4), to wash the cells and re-centrifuged at 3,200 x g. This was repeated three times and the cells were finally resuspended in 2.5% (v/v) glutaraldehyde in PBS (Table 2.4). A series of dilutions (Neat, 1/25, 1/50, 1/100) of the cell suspension were prepared in PBS (as above), and spotted onto the poly-L-lysine coated slides. The cells were left to fix for thirty minutes at room temperature.

2.10.3 Immunostaining with anti-InlA antibody and quantum dots

Once the cells had been fixed for thirty minutes, the slides were washed three times in PBS (Table 2.4). A 2% (w/v) solution of BSA was prepared in PBS (as before) and used to block the slides for 1h at RT, to prevent non-specific binding. The slides were washed again in PBS and the primary antibody was prepared. An anti-InlA monoclonal antibody was biotinylated (*Section 2.5.2.1*) and subsequently diluted 1/100 (40µg/ml) in a 1% (w/v) solution of BSA prepared in PBS (as before). This was

added to each slide and incubated for 1hr at RT, after which the slides were washed three times in PBS (as before). A 20nM solution of avidin-linked fluorescent label (quantum dots, Cy5 or FITC) was diluted in incubation buffer (0.2M borate, pH8.2), added to each slide and incubated at RT for thirty minutes. The slides were washed three times in PBS (as before), and mounted with 90% (v/v) glycerol for imaging.

2.10.4 Camera arrangement

For each fluorescent label a specific emission filter was purchased from Chroma Technology and inserted into the filter block of a Nikon fluorescent microscope with 12-bit cooled QICAM fast monochromatic camera (Figure 2.1) and Image Pro Plus software. The slides were viewed using the oil immersion lens and an objective of 40x. The resulting images were processed using the image pro software.

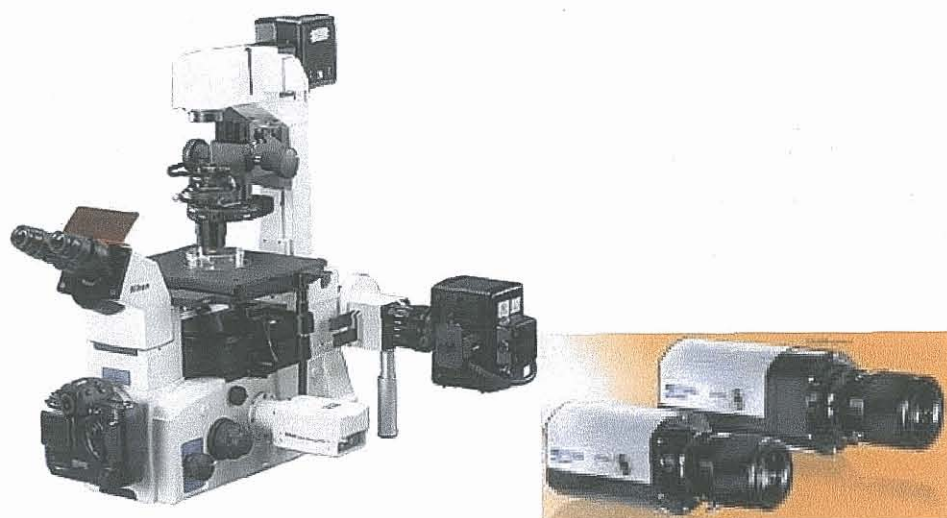


Figure 2.1. *Nikon Fluorescent microscope (TE2000, Nikon Inc.) and 12-bit cooled QICAM fast monochromatic camera (1394, QImaging™) used for the fluorescent imaging of quantum dot-labelled bacterial cells. This set up was controlled with Image Pro Plus software, supplied by Slidepath, DCU.*

2.11 Development of labelless reversible immunosensors for the detection of InIB

2.11.1 Fabrication of electrode sensor platforms

Screen-printed electrode sensor platforms were provided by Microarray Ltd. (Manchester, UK) as shown in Figure 2.2. The actual size of the sensor is 60x20mm and the area of the working and the counter electrodes are 22mm² and 72mm², respectively.

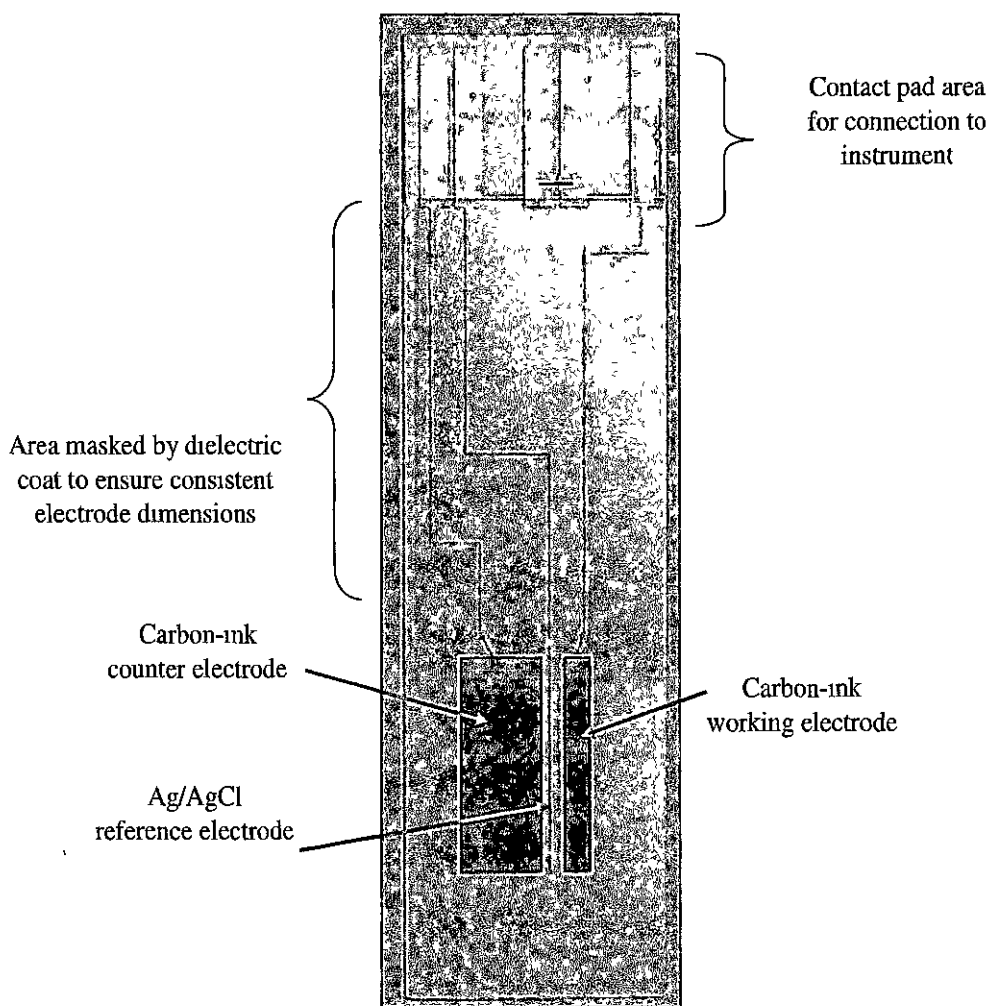


Figure 2.2 Screen-printed electrode sensor platform (Microarray Ltd., Manchester, UK)

2.11.2 Instrumentation

A Sycopel PCI-100 MK3 Potentiostat computer interface was used in conjunction with a 'Ministat Potentiostat' for electrochemical deposition (Figure 2.3). All current/charge transients were recorded using compatible PC and Sycopel software. AC Impedance measurements were performed using an ACM Auto AC DSP frequency response analyser (Figure 2.4). The test frequency varied from 10000Hz to 1Hz a.c. and a 5mV amplitude perturbation was used. The potentiostat was linked to compatible PC utilising ACM software for data acquisition.

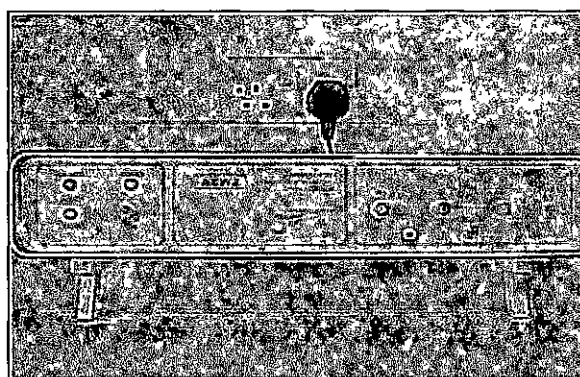


Figure 2.3 AEW2 'Mini Potentiostat' used in conjunction with Sycopel PCI-100 MK3 Potentiostat computer interface for all electrochemical deposition investigations.

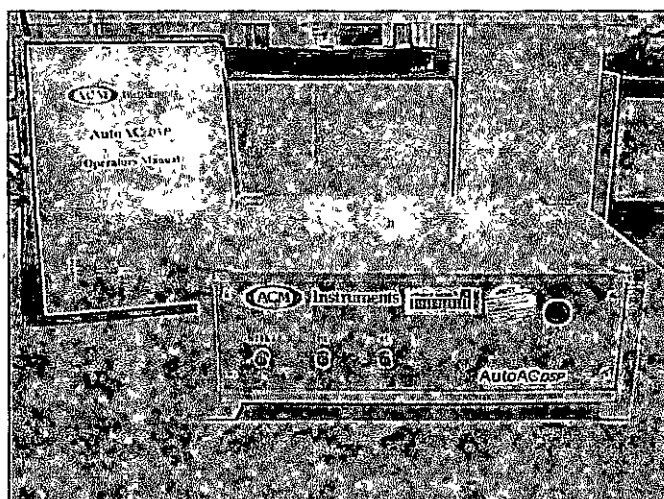


Figure 2.4 ACM Auto AC DSP frequency response analyser used in conjunction with Sycopel impedance software for all electrical impedance measurements.

2.11.3 Electrochemical insulation of carbon working electrode with polyaniline

The monomer solution used was thoroughly purged with N₂ for 20 minutes in a sealed cell to provide an oxygen-free atmosphere. The cycle number and potentiodynamic sweep rates were determined for each set of electrodes prior to deposition (data not shown). The insulation of planar carbon electrodes was achieved by sequentially scanning the working electrode potential from -200mV to 800mV (vs. Ag/AgCl) and back to the starting potential, at a scan rate of 50mV/s. A 0.2M aniline hydrochloride solution was prepared in a 0.5 M KCl, pH 1.0. The conducting films increased in thickness, as more charge was passed with each potential sweep. The optimisation of cycle number and the polymerisation time was dependent on the quality of the monomer solution and previous studies have shown that 15 cycles was sufficient for optimal electrodeposition of the polymer thin-films.

2.11.4 Sensor modification

Potentiodynamic cyclic voltammetry was employed for the electrodeposition of polyaniline (PANI) as a planar thin-film over the working electrode of the carbon sensor. After 15 cycles the sensor was subjected to a single linear sweep to 800mV, removed from the set-up, rinsed in aniline buffer at pH 1.0 and left to air-dry overnight. Water-soluble biotin-sulpho-NHS (30µl), at a concentration of 10 mg/ml was placed on the polymer-coated working electrode surface for 24 hours. The sensors were then rinsed with deionised water. Neutravidin (30µl), at a concentration of 10µg/ml was then placed on the working electrode for 1 hour. Finally, the sensor surface was thoroughly rinsed with de-ionised water.

2.11.5 Immobilisation of biotinylated antibodies on modified sensor surfaces

Biotinylated antibody (100µl of a 1mg/ml solution) was added to the sensor surface. This solution was left to incorporate at the working electrode for 1 hour at room temperature and any unbound material rinsed off with deionised water. Finally, any non-specific interactions were blocked by adding 10⁻⁶ M bovine serum albumin (BSA) in PBS (Table 2.4) to the sensors for 1 hour at room temperature. The modified sensors were washed with deionised water and left in PBS, (as above), overnight at 4° C.

2.11.6 Electrochemical Impedance Spectroscopy (EIS).

A Gill AC DSP Frequency Response Analyser was used to perform electrochemical impedance spectroscopy (EIS). Data processing and interpretation of the electrochemical impedance measurements were analysed, over a frequency range from 10,000Hz to 1Hz, (5mV amplitude perturbation). Following the immobilisation of antibody molecules at the sensor surfaces, EIS was performed to interrogate the electrodes. A baseline trace was recorded initially in PBS, (Table 2.4), alone. Antibody-loaded sensors (electropolymerised carbon thin-film), were then exposed for 30 minute time periods to increasing concentrations of antigen by serial addition. After 30 minutes exposure to a single concentration, the working electrode was flushed with PBS, (as before) and the impedance trace was then recorded in PBS, (pH 7.4) alone between 10,000Hz to 1Hz. This process was then repeated for the full range of antigen concentrations from 1ng/ml-100ng/ml.

Complex plane impedance analyses were used to relate the changes in sensor output to the antibody/antigen binding events at the electrode-polymer interface. These changes included the differing redox states of the polymer, the faradaic charge transfers and also the capacitive transduction events. Results were plotted in representative Nyquist and Bode forms as well as a percentage change in impedance from the baseline response.

2.12 Biocompatibility Testing

2.12.1 Culturing of rat aortic smooth muscle cells (RASM)

Cell culture medium was made as per Table 2.7. The medium was poured off carefully and the cells washed gently with PBS (Table 2.4). The cells were harvested by adding 3ml of 10x trypsin-EDTA to the flask and incubating for three minutes, at 37°C. The flask was then tapped gently to dislodge harvested cells. 9 ml of medium was added to neutralize the trypsin and the contents transferred to a sterile universal tube. The cells were centrifuged at 1,600 x g for 10 minutes. The medium was then poured off gently and the pellet resuspended in 1ml PBS (as above). An additional 9 mls of PBS (as above) was added to the resuspended pellet and the solution centrifuged again at 1600g for 10 minutes to wash pellet. The supernatant was poured off and 1ml medium added to the tube to resuspend the pellet. The cell suspension was then added to 30ml of medium using an appropriate split ratio (1:4), and transferred to T-75 flasks for incubation at 37°C in 5% CO₂. The cells were fed every two days by pouring off medium and gently adding 14 ml of new medium to the flask taking care not to disturb cells.

2.12.2 Freezing of cell lines

The cells were trypsinised and then pelleted by centrifugation at 1,600 x g for 10 minutes. The pellet was resuspended in foetal calf serum with 10% (v/v) DMSO and aliquoted into 1ml cryovials. The cryovials were frozen in the vapour phase of liquid nitrogen for two hours before transferring to liquid phase for long-term storage. The vials were labeled with cell line, stock, date and passage.

2.12.3 Cell Counting

The cells were trypsinised to harvest as before. The pelleted cells were resuspended in 1ml fresh medium and 50µl of cell suspension removed to a sterile eppendorf. 10µl of Trypan Blue was added to the cell suspension and incubated at RT for five minutes. A haemocytometer was used to count the cells using the following formula to calculate number of cells/ml;

$$N \times DF \times 25 \times 10^4$$

where N is the average number of cells counted and DF is dilution factor of cells to dye. Dead cells are stained blue, while healthy cells remain white. Percentage viability is calculated by expressing blue cells (dead) over white cells (alive) as a percentage.

2.12.4 Preparation of substrates for biocompatibility testing

Substrates were placed in a beaker of methanol with a magnetic stirrer for five to ten minutes. The stainless steel substrates were subsequently rinsed in de-ionised water. They were then placed in aluminium foil and autoclaved at 121°C.

2.12.5 Cytotoxicity testing of 316L stainless steel substrates

An MTT (3-[4,5-dimethylthiazol-2-yl]-2,5-diphenyltetrazolium bromide) assay kit (Roche Diagnostics), was used to assess the toxicity of treated and untreated substrates on RASM cells in culture. Cells were seeded with the treated and untreated substrates as per the plate layout with the plates in triplicate. Cells were grown in 24 well plates with substrates for 48 h and 72h at high density. 100µl (x6) of suspension from each sample was removed to a 96 well plate and incubated with the yellow MTT solution for approx. 4 h. After this incubation period, purple formazan salt crystals were formed. These salt crystals are insoluble in aqueous solution, but may be solubilised by adding the solubilisation solution and incubating the plates overnight in humidified atmosphere (37°C, 5% CO₂). The solubilised formazan product was spectrophotometrically quantified using a Tecan Safire plate reader. An increase in number of living cells results in an increase in the total metabolic activity in the sample. This increase directly correlates to the amount of purple formazan crystals formed, as monitored by the absorbance at 503nm.

2.12.6 Cell Proliferation & Viability

The cells were seeded with substrates in triplicate (1x10⁴cells/ml). The plates were incubated for 24 h at 37°C in 5% CO₂ and fed as before. After 24 hours, samples were removed from each well and retained for subsequent testing; the plates were then incubated for a further 24, 48 and 96 h in the same environmental conditions (37°C in 5% CO₂) At each time point (24 h, 48 h and 96h) the cells were trypsinised for assessment with Trypan Blue stain to determine cell proliferation, density and

viability. The substrates were retained for cell adhesion testing, on completion of the entire time course.

2.12.7 Standard Glutaraldehyde Fixation for SEM

Samples were removed from culture medium, rinsed with PBS (Table 2.4) and incubated at room temperature for 1 hour in PBS (as before) containing 2.5% (v/v) glutaraldehyde. The samples were then washed in 0.1M cacodylate buffer, pH 7.4 (Table 2.4) and incubated for a further 2 hours at 4°C in 1% (v/v) osmium tetroxide in 0.1M cacodylate buffer, pH 7.4. The glutaraldehyde/osmium tetroxide-modified substrates were then washed briefly in 0.1M cacodylate buffer, pH 7.4. Dehydration was performed on each of the samples to remove any traces of moisture, by incubating the substrates in a graded series of ethanol concentrations from 50, 60, 70, 80, and 90% (v/v), for 15 minutes each. Finally the substrates were incubated 2 x 10 min in 100% (v/v) ethanol and dried overnight in a bell chamber under vacuum.

2.12.8 Characterisation of substrates post incubation in culture

Two techniques were used for the characterisation of substrates post incubation in culture. In order to assess cell adhesion, cells were fixed with glutaraldehyde/PBS, as per *Section 2.12.7*. Scanning electron microscopy was used to study the morphology of adherent RASM cells and to compare the cell adhesion response on the different surfaces. All tests were performed on a Hitachi S 300N scanning electron microscope (SEM) located in the School of Chemical Sciences, DCU. The samples were immobilised on a 25mm aluminum stub and fixed in place using a sticky carbon disc. The secondary electron detector mode was used and measurements were taken using a relatively high KV (~20KV) since large magnifications were not required. The parameters for each sample were individually optimised to give the highest resolution, by altering the following conditions of gun alignment, shift, tilt, spot size, beam current and stigmata. In order to assess the effect of culture conditions on the substrates, the cells were first removed by trypsinisation. The substrates were then passed on to colleagues in the School of Engineering, (DCU) for evaluation, whereby contact angle measurement was used to assess hydrophobicity and hydrophilicity of the substrates post incubation in culture.

Chapter 3:
Production & characterisation of *Listeria*
***monocytogenes*-derived proteins and**
expression of anti-InlB antibodies.

3.1 Chapter introduction

This chapter describes the cloning and expression of the *L. monocytogenes* invasion-associated protein Internalin B (InlB) peptide fragments into two vector systems, the pQE-60 vector (Qiagen Ltd.) and the pAC4 vector (Avidity Corporation). The Internalin B protein was previously cloned and expressed in pQE-60 (Leonard, 2003). The InlB protein was sub-divided into three shorter overlapping peptide fragments with molecular weights of 23, 34 and 45kDa, respectively. Expression of the InlB fragments in *E. coli* XL-10 Gold cells, using the Qiagen system allows purification of His-tagged proteins using immobilised metal affinity chromatography (IMAC). Expression of recombinant InlB protein fragments in *E. coli* AVB101 cells, using the Avidity system enables *in vivo* biotinylation of the fragments and subsequent affinity purification using monomeric avidin.

The cloning and subsequent expression of recombinant *L. monocytogenes* protein fragments offers several advantages over the isolation of native proteins from whole *L. monocytogenes* cells. Cloning eliminates the need for growing large-scale cultures of this bacterial pathogen and provides an unlimited supply of the recombinant proteins that may have incorporated affinity tags enabling one-step purification and enhanced functionality. The fusion of a polyhistidine tag at the C terminus of each protein fragment enables easy purification and expression, while the addition of a Biotin AviTag to the fragments allows *in vivo* expression of biotin on each fragment. The incorporation of such tags into the recombinant protein fragments generated improved reagents which could be used in association with anti-InlB antibodies, for the development of enhanced assays for the detection of InlB. An overview of both vector systems is presented here and a description of protein expression and purification is also described.

3.1.1 QIAexpress cloning

High-level expression of 6xHis-tagged proteins in *E. coli* is achieved using the QIAexpress pQE vectors, which enable selective purification of cloned proteins using nickel-nitrilotriacetic acid (Ni-NTA). The pQE plasmids belong to the pDS plasmid family (Bujard *et al.*, 1987) which were derived from the plasmids pDS56/RBSII and pDS781/RBSII-DHFERS (Stuber *et al.*, 1990). The 6xHis tag is an affinity tag of six consecutive histidine residues and is uncharged at physiological pH. Depending on the intended use of the expressed protein pQE vectors incorporating either C- or N-terminal 6xHis tags are available. When incorporating C-terminal His tags the cloned insert must be in-frame with the ATG start codon and the 6xHis tag thus ensuring only full-length proteins are purified. The pQE-60 expression vector incorporates a number of important features which contribute to the high level expression of recombinant proteins in *E. coli* (Figure 3.1).

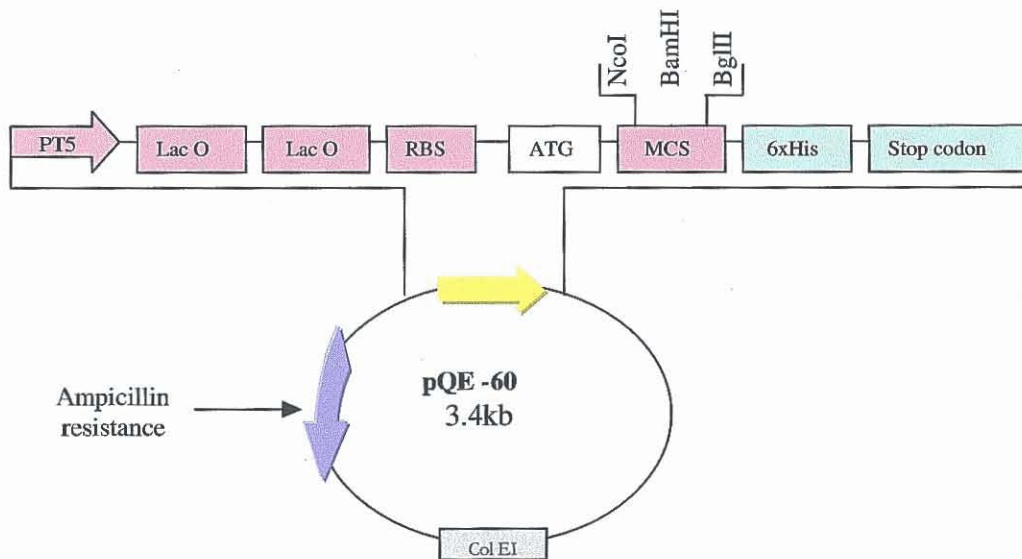


Figure 3.1 pQE-60 vector used for C-terminal 6xHis tag constructs. PT5: T5 promoter with a repression module to regulate expression of proteins in *E. coli*; Lac O: Two lac operator sequences for increased lac repressor binding and therefore efficient repression of T5; RBS: synthetic ribosomal binding site for efficient translation; ATG: start codon; MCS: multiple cloning site with Nco I, Bam HI and Bgl III restriction sites; 6xHis: affinity tag of 6 consecutive histidine residues; Stop codons: Stop codons in all three reading frames; Col E1: Col E1 origin of replication.

The RNA polymerase from *E. coli* recognises the phage T5 promoter found in the plasmid, which also harbours two lac operator sequences that increase lac repressor binding, therefore allowing efficient repression of the T5 promoter. The plasmid also comprises a synthetic ribosomal binding site, RBSII, for increased translation and a sequence coding a 6xHis-tag located 3' to the cloning region. A multiple cloning site and translational stop codons in all reading frames facilitate preparation of the expression construct. The β -lactamase gene (*bla*), which confers ampicillin resistance and the *colE1* origin of replication are also important features that are encoded for in the pQE-60 plasmid.

3.1.2 pAC4 Avidity cloning

The Biotin AviTag is a unique peptide sequence, 15 residues long, that is recognised by biotin ligase (Schatz, 1993). In the presence of ATP, the ligase specifically attaches biotin to lysine residue in the sequence of target molecules. Avidity Corporation (Colorado, USA) has developed a series of vectors, namely AviTag pAC4, pAC5 & pAC6 that enable the efficient fusion of the Biotin AviTag to proteins and antibodies. Efficient biotinylation of Biotin AviTag-fused proteins can be achieved by expressing in a specialised *E. coli* strain (AVB101) also from Avidity Corporation. The AVB101 strain contains the pACYC184 *ColE1* compatible plasmid with an IPTG-inducible *birA* gene to over express biotin ligase (pBirAcm). This strain is recommended for protein expression because of its robust growth and the absence of the OmpT and Lon proteases. Elevated levels of biotin ligase in the cells ensure complete biotinylation of Biotin AviTag-fused proteins. The Biotin AviTag can be easily introduced at either the N- or C- terminus of any cloned target protein (Tatsumi *et al.*, 1996). The InlB protein fragments were sub-cloned from the pQE-60 vector as BamHI/NcoI constructs and transferred into the pAC4 vector for subsequent expression in *E. coli* AVB101 cells. The main advantage of the pAC4 vector is that it has multiple cloning sites, a high copy number plasmid and a strong IPTG-inducible promoter which facilitates simple transfer of the recombinant protein fragments to this expression system. In addition the Biotin AviTag has only one fifth of the bulk of alternative biotinylation tag sequences that are over 85 amino acid residues long. This greatly reduces steric problems. Figure 3.2 shows the vector map of the pAC4 expression vector.

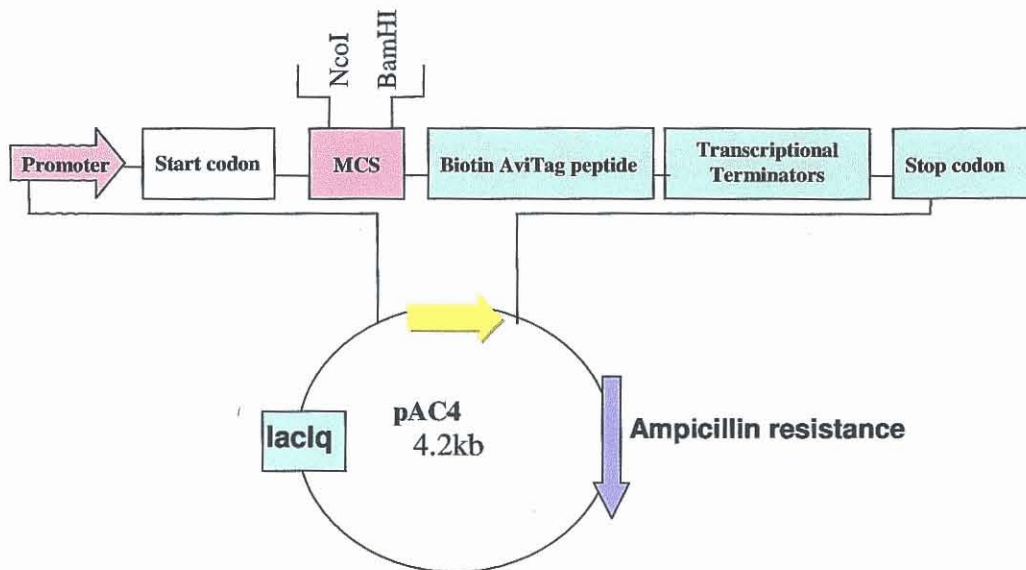


Figure 3.2 pAC4 vector used for C-terminal AviTag protein fusions. Promoter: promoter with a repression module to regulate expression of proteins in *E. coli*; Start codon: start codon; MCS: multiple cloning site with *Nco* I and *Bam* HI restriction sites; Biotin AviTag peptide: 15 residue peptide sequence recognised by biotin ligase, for creation of a biotinylated-fusion protein; Transcriptional terminators; transcriptional terminators are also encoded on the plasmid, which prevent read-through transcription and increase construct stability; Stop codon: Stop codons in all three reading frames; Ampicillin resistance: the β -lactamase gene (*amp*) confers ampicillin resistance.

The plasmid has an IPTG-inducible Trc promoter, which is recognised by the RNA polymerase from *E. coli*. A multiple cloning site and translational stop codons in all reading frames facilitate preparation of the expression construct. A glutamic acid residue which has been shown to greatly enhance biotinylation rates of the AviTag (Beckett *et al.*, 1999) is also included. Other important features that are encoded in the pAC4 plasmid are the β -lactamase gene (*bla*) confers ampicillin resistance and the *lac* I^q inserted at *Eco*RV site (thus disrupting the *tet*^R gene).

3.1.3 Protein expression

E. coli is the most frequently employed host with many available expression systems for producing proteins (Makrides, 1996). High-level recombinant protein expression using pQE-60 is induced upon addition of isopropyl- β -D-thiogalactoside (IPTG). IPTG binds to the lac repressor protein resulting in its dissociation. This allows the host strain's RNA polymerase to transcribe the sequence downstream of the promoter sequence with the resultant transcript being translated into the specific recombinant protein sequence required. However, sometimes the levels of protein expression are low despite the use of strong transcriptional and translational signals. In such cases, there are a number of approaches that can be used to optimise expression levels.

Examination of the codon usage of the heterologous protein can be advantageous since not all mRNA codons are used equally. The so-called major codons are those that occur in highly expressed proteins, whereas the minor or rare codons tend to be in genes expressed at a low level. If the codon usage of your target protein differs significantly from the average codon usage of the expression host, this can cause significant problems during expression such as decreased mRNA stability, premature termination of translation, frameshifts, deletions and misincorporations (Kane, 1995). If any of these problems occur, protein synthesis can be inhibited and the observed levels of expression are often low. However, expression levels in such situations can be improved by replacing codons that are rarely found in highly expressed *E. coli* genes with more favourable codons throughout the whole gene (Lainé *et al.*, 2002). A high GC content in the 5'-end of the gene of interest can also cause interrupted translation and lower levels of expression. Thus, higher expression levels can be obtained by changing G and C residues at the 5'-end of the coding sequence to A and T residues without changing the amino acids. The addition of a fusion partner can also improve expression levels (Murby *et al.*, 1996). Fusion of the N-terminus of a heterologous protein to the C-terminus of a highly-expressed fusion partner often results in high level expression of the fusion protein (La Vallie *et al.*, 1993).

Another problem with protein expression is that in many cases the expressed protein is insoluble and accumulates in so-called inclusion bodies (Makrides, 1996; Choi *et al.*, 2005). This is especially true under conditions of high level expression. Several strategies are available to improve the solubility of the expressed protein by reducing the rate of protein synthesis, thus improving levels of soluble expression. This can be achieved by lowering the growth temperature, growth time, inducer concentration or by using a lower copy number plasmid. Co-expression of chaperones and foldases can also improve soluble protein expression (Bessette *et al.*, 1999). Molecular chaperones promote cellular targeting by transiently interacting with folding intermediates (Georgiou and Valax, 1996). Foldases such as disulphide oxidoreductase (DsbA), disulphide isomerase (DsbC) and protein disulphide isomerase (PDI) also exhibit chaperone activity and co-expression of one or more of these foldases with the target protein can lead to higher levels of soluble protein.

Periplasmic expression also has a positive effect on protein expression since the oxidising environment of the periplasm allows for the formation of disulphide bonds, which do not occur in the reducing environment of the cytoplasm (Hockney, 1994). Secretion of the target protein in the periplasm is achieved by the addition of a leader sequence (signal peptide) to the N-terminus of the target protein and results in reduced proteolysis, thus increasing soluble expression (Humphreys *et al.*, 2000). The most common leader sequences are *pelB* and *ompT*. *E. coli* does not express large proteins (> 70 kDa) very efficiently and, therefore, expression of smaller peptide fragments of the target protein can also improve expression levels and solubility.

In this chapter the high level expression and purification of InlB protein fragments from two vector systems is presented. His-tagged recombinant InlB protein fragments, from the pQE-60 vector are expressed upon the addition of IPTG whereas *in vivo* biotinylated recombinant proteins fragments cloned into the pAC4 vector are induced upon the addition of both IPTG and biotin. The pAC series of vectors are used to express C-terminal AviTag-protein fusions. The pAC4 vector allows co-expression of the AviTag plasmid and the pBirA gene. The expression of an anti-InlB scFv isolated from a naive human library is also described and the optimisation of growth, induction and purification conditions is shown.

3.1.4 Protein purification using affinity chromatography

Affinity Chromatography can be used to separate biochemical mixtures, based on highly specific biologic interactions such as antigen with an antibody or a protein with a hexahistidine tag and a metal ion (e.g. Ni⁺). A heterogeneous mixture of molecules in solution, containing the protein of interest (6xHis tagged protein, biotin-tagged protein) is added to a column containing the affinity partner immobilised on a matrix (Ni-NTA resin or monomeric avidin on Sepharose). The target molecule for purification binds to the column while other impurities pass through. Subsequently the captured target molecule can be specifically eluted and the associated fractions collected.

Hochuli and co-workers (1987) applied IMAC for the purification of recombinant proteins containing engineered N- or C-terminal histidine tags. Methods used to elute the His-tagged protein of interest included changing the pH, or adding a specific molecule, such as imidazole which competes for binding to Ni²⁺ on the column. One of the main advantages of IMAC purification is its suitability for protein purification under both native and denaturing conditions since the interaction between the Ni-NTA and the 6xHis tagged recombinant protein does not depend on the tertiary structure. There are several commercially available chelating ligands available. However, for the purpose of this research, nitrilotriacetic acid (NTA) containing four metal-chelating sites was used, since it binds to the metal ions more stably and retains them under stringent washing and eluting conditions. IMAC purification was used to purify recombinant InlB protein fragments cloned from Qiagen's pQE-60 vector, whereas affinity chromatography using immobilised monomeric avidin on Sepharose was used to purify *in vivo* biotinylated recombinant InlB clones from Avidity's pAC4 vector. Both of these systems are described in this chapter.

3.1.5 Chapter outline

This chapter outlines the production and characterisation of Internalin B-derived protein fragments. The successful expression and purification of a recombinant form of Internalin B, a cell surface protein of *Listeria monocytogenes* is described. The entire InlB recombinant protein was sub-divided into three shorter overlapping peptide fragments with molecular weights of 23, 34 and 45kDa, respectively. Identification of the antibody binding regions was achieved by probing the expressed polypeptide domains with a panel of InlB-associated antibodies. Purification of the InlB fragments by immobilised metal affinity chromatography (IMAC) was optimised and purity monitored by electrophoresis and Western blotting.

The InlB protein fragments were also successfully cloned into another expression system, Avidity's pAC4 vector for *in vivo* biotinylation. Purification of the *in vivo* biotinylated InlB fragments was performed via affinity chromatography using monomeric streptavidin. Characterisation of cloned proteins was monitored by electrophoresis, Western blotting, Biacore and fluorescence-based detection methods. Finally an anti-InlB antibody fragment (scFv), previously isolated from a naive human library was studied and optimisation of expression and purification conditions was investigated.

The expression and purification of the InlB protein fragments, epitope mapping and recombinant anti-InlB antibody expression were investigated for the subsequent application of these reagents as antigens and antibodies in novel immunoassay formats for the improved detection of InlB.

3.2 Epitope mapping of InlB

An epitope mapping study of the *Listeria monocytogenes* invasion-associated protein marker, InlB, was undertaken in order to identify peptide fragments that could be employed as antibody binding sites for immunoassay development. Epitope mapping is used for the determination of the relative location of epitopes on the surface of antigens, thus facilitating the definition of antigenic sites (Westwood and Hay, 2001). This is particularly useful for the successful development of improved immunoassays with greater sensitivity and reproducibility. Synthetic peptide technology facilitates the production of a series of overlapping peptides, offset with respect to each other by one amino acid, which can be used to mimic the linear antibody-binding region. However, synthetic peptide technology is limited in that only a small number of overlapping peptides (routinely 96) can be conveniently synthesised at once, which is normally too short to cover the whole protein of interest (Westwood and Hay, 2001). In order to define the antibody-binding domains of the *Listeria monocytogenes* invasion-associated protein marker, InlB, shorter overlapping peptide fragments were cloned to determine which InlB polypeptide domain was most immunoreactive. This section describes the cloning and expression of the peptide fragments in the pQE-60 expression vector (Qiagen Ltd.). Identification of the antibody binding regions was achieved by probing the expressed polypeptide domains with a panel of anti-InlB antibodies and antibody fragments.

3.2.1 Cloning of InlB Fragments into the pQE-60 expression vector

In order to express high levels of the correct InlB gene products, the InlB gene sequence was directionally cloned into the Qiagen pQE-60 expression vector (Section 3.1.1). The InlB recombinant protein was sub-divided into three shorter fragments. This was achieved by designing specific primers incorporating suitable restriction sites, compatible with chosen expression systems for transformation into *E. coli* (Sections 2.2.8-2.2.14). The pQE-60 plasmids containing the cloned inserts were then transformed into competent XL-10 Gold *E. coli*, since they harbour the *lac I^f* mutation and produce enough *lac* repressor to efficiently block transcription, making them ideal for storing and propagating pQE plasmids (Qiagen Ltd, 2000). Transformants were screened by growing up single colonies of each fragment in small-scale cultures. Factors affecting the expression and recovery levels of the recombinant proteins were optimised individually for each fragment. Figure 3.3 illustrates an overview of the processes involved in the cloning of the InlB protein fragments.

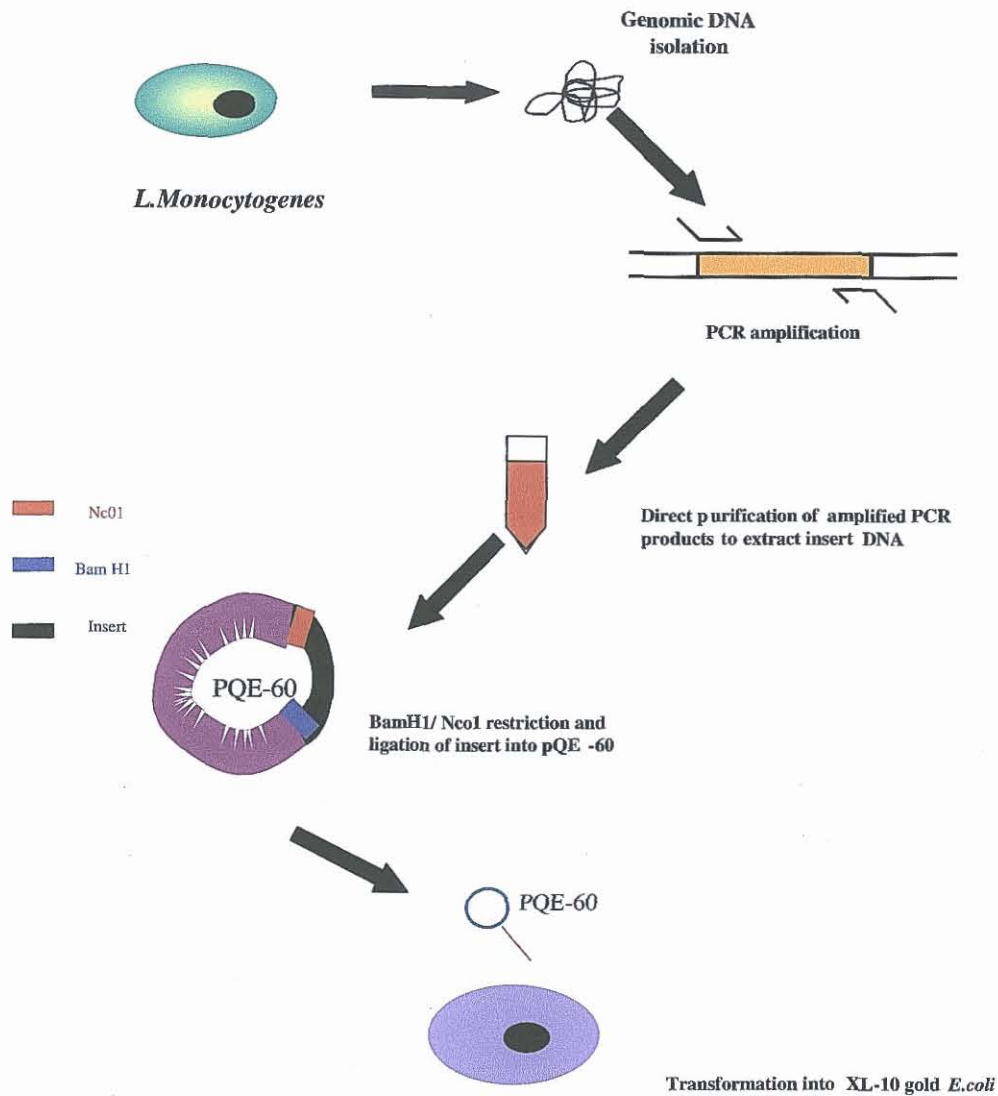


Figure 3.3 Overview of the processes involved in the cloning of the *InlB* gene sequence for epitope mapping. DNA from *Listeria monocytogenes* was prepared and the *InlB* gene sequence (and *InlB* gene fragments) amplified by using specific PCR primers. Fresh PCR products (PCR A overhangs degrade over time) were directly purified using a commercial kit (Promega Wizard Direct PCR Purification). This eliminated the need for sub-cloning into the pCR 2.1 vector (TA cloning). Purified plasmid DNA from directly amplified PCR products were directionally cloned into the pQE-60 expression vector by digestion with *NcoI* and *BamHI* restriction enzymes. The pQE-60 vectors, containing gene inserts, were finally transformed into *E. coli* XL10 Gold cells.

3.2.2 Preparation of genomic DNA

E. coli XL-10 Gold cells containing the plasmid pQE60, bearing the Internalin B (InlB) gene, were donated by Dr. Paul Leonard, Applied Biochemistry Group, DCU(Section 2.2).

3.2.3 Primer design

Forward and reverse DNA primers were designed for the genes encoding each section of the InlB protein based on DNA sequences previously submitted to GenBank. The primers were based on the sequence of the recombinant InlB protein cloned and expressed from *L. monocytogenes* (Accession number AJ012346). The InlB protein is 621 amino acids long. In order to perform accurate epitope mapping, primers were designed to divide the protein into three distinct regions F3, F4, F5 as shown below in Figure 3.4.

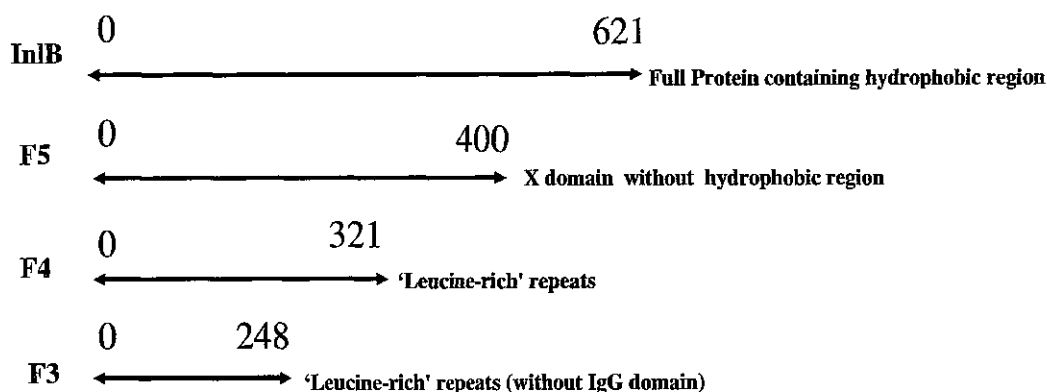


Figure 3.4 Schematic of InlB epitope mapping. The full InlB recombinant protein was portioned into three distinct regions F3, F4 and F5. The expression of smaller protein fragments enabled the identification of antibody-binding domains.

The entire InlB protein consisting of amino acids 0-621 includes the hydrophobic region and had previously been expressed and purified (Leonard, 2003). The X domain (F5), which does not include the hydrophobic region of the protein, comprises amino acids 0-400. The 'leucine-rich' repeats which contain the IgG domain (F4) is made up of amino acids 0-321. The F3 region from 0-248 amino acids represents the 'leucine-rich' repeat region with no IgG domain.

3.2.4. Amplification of InlB gene fragments by PCR

Listeria monocytogenes (AJ012346-Genbank) genomic DNA was used as the template for the amplification of the InlB gene fragments. Primers were engineered (Section 2.2.8), for directional cloning of the fragments into the pQE-60 plasmid. Since proteins expressed from pQE-60 contain a C-terminal 6xHis tag, the genes were cloned in frame with the 3' sequence encoding the 6xHis tag. A standard PCR reaction was used to amplify the DNA sequences (Section 2.2.9). The optimum annealing temperature for use with each gene was determined using a temperature gradient PCR. This involved carrying out several standard PCR reactions with varying annealing temperatures, ranging from 58 - 65°C. The optimum annealing temperature for the amplification of each fragment was determined to be 63°C. Figure 3.5 shows the optimised PCR amplification of each InlB gene fragment by PCR.

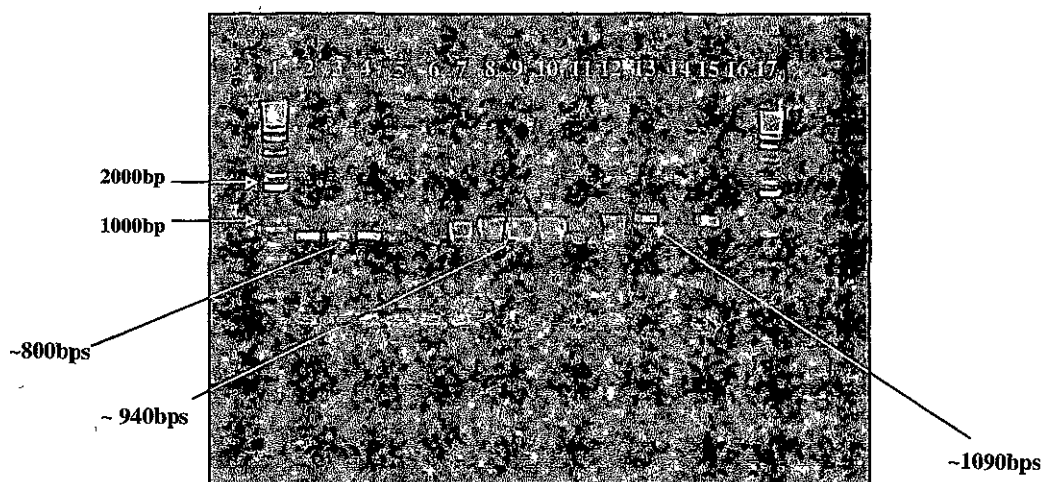


Figure 3.5 Agarose gel showing the amplification of the InlB gene fragments for mapping of anti-InlB antibody binding domains. Lanes (1) and (17): show a 1kb plus DNA ladder; Lanes (2)-(5): show the amplification of the F3 insert with bands visible at approximately 797bps as predicted from primer design; Lane (6): is a negative control for F3 (no template DNA); Lanes (7)-(10): show the amplification of the F4 insert with bands visible at approximately 943bps as predicted from primer design; Lane (11): is a negative control for F4 (no template DNA); Lanes (12)-(15): show the amplification of the F5 insert with bands visible at approximately 1085bps as predicted from primer design; Lane (16): is a negative control for F5 (no template DNA).

3.2.5 Direct Purification of PCR products and preparation of pQE60 vector

The amplified PCR products for each insert (F3, F4 & F5) were pooled and directly purified using a commercial kit, the Promega Wizard direct purification kit (Section 2.2.10). This kit removes the need to sub-clone the vector and inserts into a selection system, such as TA cloning system, by allowing direct purification of amplified PCR products. The purified PCR products can then be restricted and ligated into the vector of choice. The pQE-60 vector stock was grown up under normal conditions (Leonard, and the pQE60 plasmid DNA purified using the Promega Wizard Plus miniprep DNA purification system.

3.2.6 BamHI and NcoI restriction analysis on pQE60 plasmid and purified PCR products containing cloned gene inserts

The pQE-60 plasmid DNA was then linearised using a BamHI / NcoI restriction digest (Section 2.2.11). A BamHI/NcoI restriction digest was also carried out on the direct PCR purified inserts containing the cloned genes of interest, (Figure 3.6).

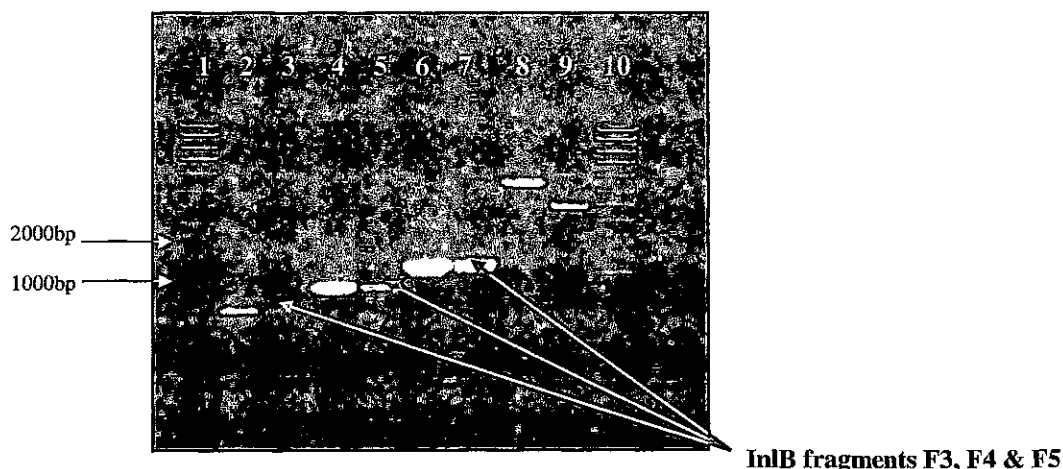


Figure 3.6 Restriction Digest on pQE-60 vector and InlB cloned inserts F3, F4 & F5. Lane (1): 1kb plus DNA ladder; Lane (2): BamHI/NcoI restricted F3 gene fragment, Lane (3): unrestricted F3 gene fragment; Lane (4): BamHI/NcoI restricted F4 gene fragment; Lane (5): unrestricted F4 gene fragment; Lane (6): BamHI/NcoI restricted F5 gene fragment; Lane (7): unrestricted F5 gene fragment; Lane (8): BamHI/NcoI restricted pQE-60 vector; Lane (9): unrestricted pQE-60 vector; Lane (10): 1kb plus DNA ladder.

3.2.7 Ligation of vector-insert constructs

The linearised plasmid DNA from the vector (pQE-60) and inserts (F3, F4 & F5) was subsequently gel purified, following agarose gel electrophoresis, using the Wizard PCR-prep purification kit (Sections 2.2.2-2.2.3). The gel purified vector and insert constructs were subsequently ligated (Section 2.2.12). The T4 DNA ligase directionally cloned the DNA encoding the gene fragments of interest into the linearised pQE-60, for transformation into competent XL-10 Gold *E.coli* cells.

3.2.8 Transformation of competent XL-10 Gold *E.coli* cells with pQE-60 containing the cloned inserts

Competent XL-10 Gold *E coli* were prepared using the methods described by Inoue *et al.*, 1990, (Section 2.2.4). The competent XL-10 Gold *E coli* were then transformed with the pQE-60, containing the gene of interest (Section 2.2.13).

3.3 Expression of the recombinant InlB protein fragments

Positive clones were screened by picking single colonies from each transformation plate, for growth and induction. High-level recombinant protein expression was induced upon addition of isopropyl- β -D-thiogalactoside (IPTG). XL 10-Gold cells are endonuclease-deficient (*endA1*), which greatly improves the quality of plasmid miniprep DNA, and recombination-deficient (*recA*), which ensures insert stability. Overnight expression cultures were prepared (Section 2.2.14). Following growth and induction the bacterial cell pellet was resuspended in PBS (Table 2.4) and sonicated for 30s to lyse the cells. The cultures were finally centrifuged at 3,200 x g for 20 min, to remove cell debris and the supernatant (cell lysate) analysed by SDS-PAGE. The approximate size of each expressed protein was determined prior to small-scale expression analysis. The amino acid sequence of each insert was placed into a software tool from the EMBL database and the molecular weight and pI calculated accordingly. These approximate values were confirmed by SDS-PAGE analysis and the theoretical sizes matched up to the actual values. SDS-PAGE analysis on the F3, F4 and F5 initial expression cultures yielded the appropriate bands at 23, 34 and 45kDa, respectively.

The SDS-PAGE analysis on the initial small-scale expression cultures of the InlB fragments in XL-10 Gold can be seen in Figure 3.7.

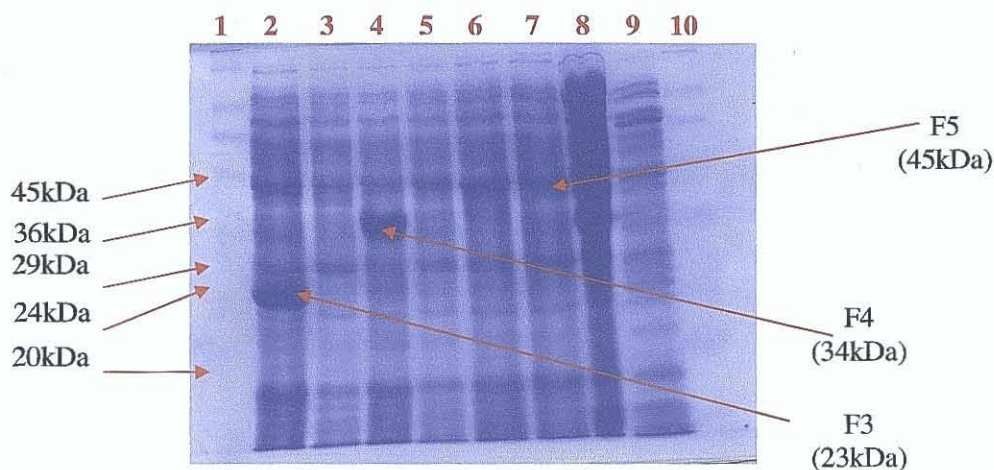


Figure 3.7 SDS-PAGE analysis of the expression of InlB fragments under native conditions. Lanes (1) and (10): Sigma wide range molecular weight markers consisting of aprotinin (6.5 kDa), α -lactoalbumin (14.2 kDa), trypsin inhibitor (20.1 kDa), trypsinogen (24 kDa), carbonic anhydrase (29 kDa), glyceraldehyde-3-phosphate dehydrogenase (36 kDa), ovalbumin (45 kDa), glutamic dehydrogenase (55 kDa), bovine albumin (66 kDa), fructose-6-phosphate kinase (84 kDa), phosphorylase B (97 kDa), β -galactosidase (116 kDa) and myosin (205 kDa); Lane (2): F3 induced sample; Lane (3): F3 un-induced sample; Lane (4): F4 induced sample; Lane (5): F4 un-induced sample; Lane (6): F5 induced sample; Lane (7): F5 non-induced sample; Lane (8): PLD induced sample (control); Lane (9): InlB induced sample.

This indicates that the three recombinant proteins fragments F3, F4 and F5, were successfully expressed in XL-10 Gold from the high-level expression vector pQE-60. In order to obtain the maximum yield of protein, optimisation of several parameters such as, lysis buffer, IPTG concentration, sonication conditions and induction time was necessary. For optimisation, a number of small-scale expression experiments were carried out before proceeding to large-scale expression.

3.3.1 Determination of InlB fragment (F3, F4 and F5) protein solubility

The high-level expression of recombinant proteins in *E. coli* may result in the formation of insoluble inclusion bodies, consisting of aggregates of the expressed protein. Therefore optimisation of lysis buffer for soluble protein isolation was performed. Single colonies of XL-10 Gold *E. coli*, harbouring pQE-60 encoding the F3, F4 & F5 fragments, were picked from a freshly streaked plate and used to inoculate small-scale (10ml) cultures (Section 2.2.14). Following growth and induction the bacterial cells were pelleted by centrifugation, at 3,200 x g for 20 min, and the supernatant discarded. The bacterial pellets were resuspended in PBS (0.15M NaCl, 2.5mM KCl, 10mM Na₂HPO₄, 18mM KH₂PO₄, pH 7.4) and sonicated (Section 2.2.14). Following centrifugation, at 20,000 x g for 15 min, the supernatant (soluble protein) was analysed by SDS-PAGE. Alternatively, the pellet was resuspended in 1ml of denaturing buffer (8M Urea, 100mM NaH₂PO₄, 10mM Tris, pH 8.0) and sonicated (as before). Following centrifugation, at 20,000 x g for 15 min, the supernatant (insoluble protein) was analysed using SDS-PAGE. The protein solubility determination for each of the fragments can be seen in Figure 3.8.

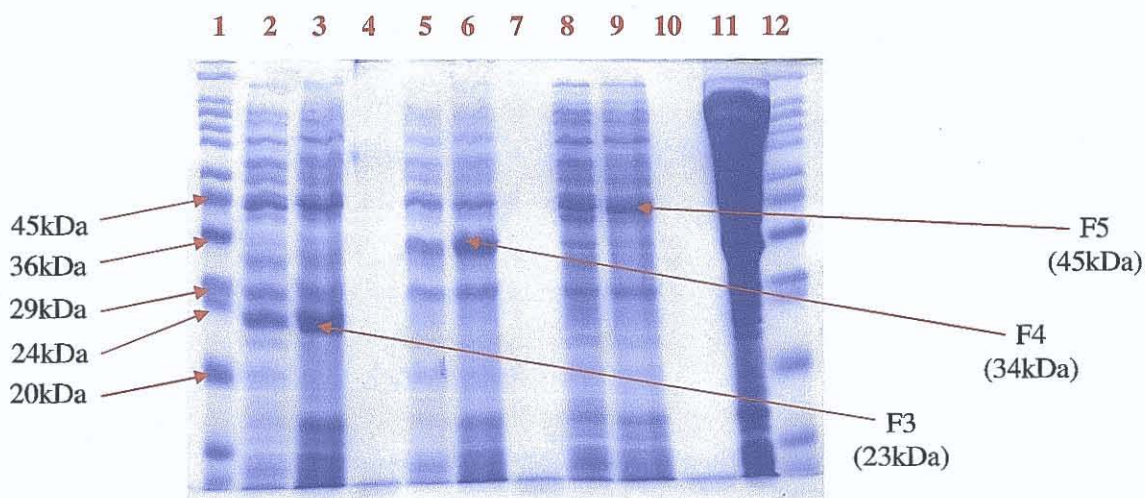


Figure 3.8 SDS-PAGE analysis on the expression of InlB fragments under native and denaturing conditions. Lanes (1) and (12): Sigma wide range molecular weight markers (as before); Lanes (2), (5) and (8): bacterial cell pellet resuspended in PBS for F3, F4 & F5 respectively; Lanes (3), (6) and (9): bacterial cell pellet resuspended in denaturing buffer for each fragment F3, F4 and F5; Lanes (4), (7) and (10): Empty lanes; Lane (11): PLD control.

Although, some soluble expression was observed (Lanes 2, 5 and 8, respectively), the majority of the expressed F3, F4 and F5 protein fragments forms insoluble inclusion bodies, which were solubilised using 8M urea (Lanes 3, 6 and 9, respectively). This suggests the need for denaturing buffer (containing 8M urea) for the subsequent isolation of recombinant InlB fragments, following high-level expression in XL-10 Gold *E. coli*.

A web-based bioinformatics program was also used to determine the solubility of the recombinant proteins (Harrison, 2000). Based on the amino acid sequence of the protein this model uses the approximate charge average, to determine protein solubility. This program estimated the percentage chance of insolubility for each fragment, which was determined as 68%, 72% and 73% for the F3, F4 and F5 fragments, respectively. This confirmed the need for denaturing buffer, containing 8M urea, for the solubilisation and isolation of the recombinant InlB protein fragments, following expression in XL-10 Gold *E. coli*.

3.3.2 Optimisation of IPTG concentration for induction of protein expression

Expression of F3, F4 & F5, from pQE-60, is rapidly induced upon addition of isopropyl- β -D-thiogalactoside (IPTG). The IPTG binds to the *lac* repressor protein and inactivates it. Once the *lac* repressor is inactivated, the host cell's RNA polymerase can transcribe the sequence downstream from the promoter. However, the concentration of IPTG required for induction must be optimised, so that the highest level of protein expression is achieved without the level of protein expression and IPTG concentration becoming toxic to the cell. Several small-scale expression cultures were set up and a concentration range of IPTG from 0-1mM, was used for induction to determine optimal IPTG concentrations for maximum protein expression (*Section 2.2.15*).

Single colonies of XL-10 Gold *E. coli*, harbouring pQE-60 encoding the F3, F4 & F5 fragments, were picked from a freshly streaked plate and used to inoculate small-scale (10ml) cultures (*Section 2.2.14*). Each culture was then induced with varying concentrations of IPTG, ranging from 0.01 to 1mM and incubated for a further 4 hours. The cultures were then centrifuged and the supernatants discarded. The bacterial cell pellets was resuspended in denaturing buffer (8M Urea, 100mM NaH₂PO₄, 10mM Tris, pH 8.0) and sonicated (as before) and the supernatants retained for SDS-PAGE analysis.

Figure 3.9 shows the gel pictures obtained for the expression of F3 in XL 10-Gold *E. coli*, following induction with the various IPTG concentrations. Variations in IPTG concentration did not seem to affect the level of protein expression so the lowest concentration of 0.1mM was chosen for F3 as optimal. The same IPTG concentration gradient was investigated for both F4 and F5, (figures not shown). Basal level expression of F3 was visible following induction with zero concentration of IPTG.

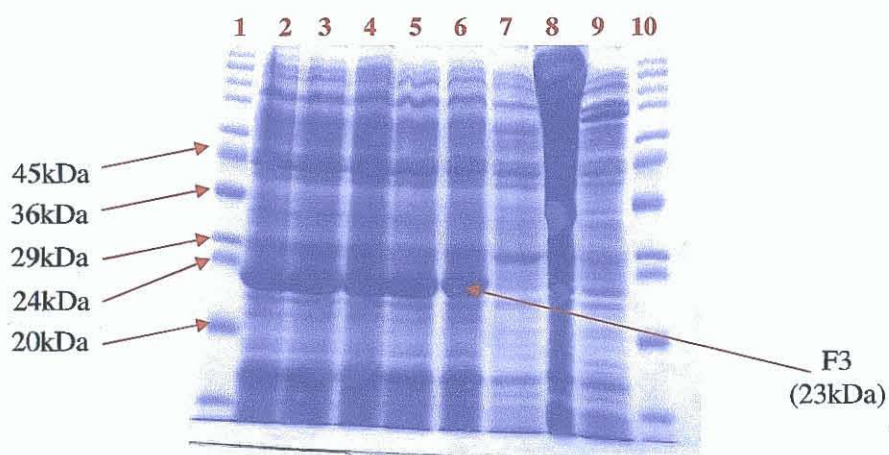


Figure 3.9 Optimisation of IPTG concentration for the induction of InlB F3- expression under denaturing conditions. Lanes (1) and (10): Sigma wide range molecular weight markers; Lane (2): induction of F3 expression using 1mM IPTG; Lane (3): induction of F3 expression using 0.5 mM IPTG; Lane (4): induction of F3 expression using 0.1 mM IPTG; Lane (5): induction of F3 expression using 0.05 mM IPTG; Lane (6): induction of F3 expression using 0.01 mM IPTG; Lane (7): induction of F3 expression using 0 mM IPTG; Lane (8): PLD control; Lane (9): InlB lysate.

3.3.3 Optimisation of Sonication Conditions

Following intracellular protein expression the bacterial cells must be lysed to isolate the recombinant protein. For the isolation of inclusion bodies the pelleted bacteria were resuspended in denaturing buffer, containing 8M urea, and then sonicated. Sonication is used to isolate an expressed protein from within the cell cytoplasm. It involves sonically pulsing cells with sonic waves, thus disrupting the cell membrane and releasing cytoplasmic extracts. However, the bacterial cells should only be sonicated for the minimum time necessary because prolonged sonication may destroy the protein and cleave the 6xHis tag (Qiagen, 2000). Therefore, the optimum sonication time for the isolation of the F3, F4 and F5 fragments from XL 10-Gold *E. coli* was investigated. Several small-scale (10ml) expression cultures were set up (Section 2.2.14) and a range of sonication times from 0-60s were examined to determine optimal conditions for maximum protein expression (Section 2.2.16). Figure 3.10 shows the SDS-PAGE analysis of sonication conditions for the expression the F3 fragment under denaturing conditions.

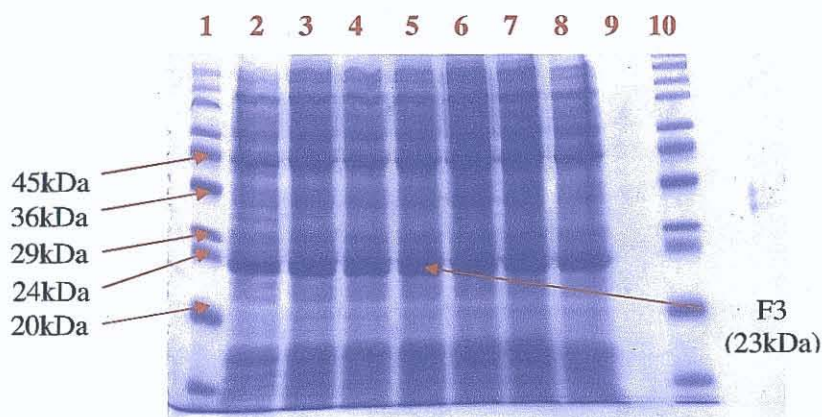


Figure 3.10 *Optimisation of sonication conditions for expression of InlB F3 under denaturing conditions. Lanes (1) and (10): Sigma wide range molecular markers; Lane (2): 0 sec sonication; Lane (3): 10 sec sonication; Lane (4): 20 sec sonication; Lane (5): 30 sec sonication; Lane (6): 40 sec sonication; Lane (7): 50 sec sonication; Lane (8): 60 sec sonication; Lane (9): Empty lane.*

Increased sonication did not seem to have a major effect on protein expression. The intensity of the 23kDa band gradually increased as the sonication time increased up until 30 seconds, after which time the band intensities levelled off. This suggested that a 30 second sonication pulse was sufficient for the isolation of F3. The same sonication conditions were investigated for both the F4 and F5 fragments, (figures not shown) with the same results

reported, whereby increased sonication had a minimal effect on protein expression. Therefore a sonication time of 30 seconds was chosen as optimal for the expression of the three InlB protein fragments.

3.3.4 Time-course analysis on the expression of F3, F4 and F5

Following optimisation of the parameters for protein expression a time-course analysis on the level of protein expression was carried out in order to determine the optimal induction time (Section 2.2.17). This is important in order to get a balance between the amount of soluble protein in the cells, the formation of inclusion bodies, and protein degradation. By checking the recombinant protein present at various times after IPTG induction, the optimal induction period can be established. Several small-scale (10ml) expression cultures were set up (Section 2.2.14) and a range of induction times were examined, whereby 1ml samples were taken at intervals of 1, 2, 3, 4, 5, 6 and 18h post induction. Figures 3.11-3.13 show the SDS-PAGE analysis of variations in induction time for the expression of each fragment.

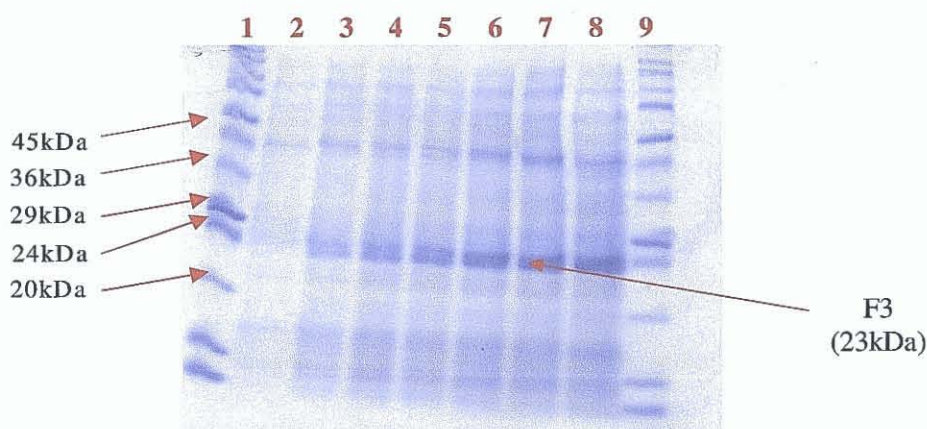


Figure 3.11 Time course expression analysis on F3 in XL-10 Gold *E. coli*. Lanes (1) and (9): Sigma wide-range molecular weight marker; Lane (2): Non-induced control; Lane (3): F3 expression 1 hour post IPTG induction; Lane (4): F3 expression 2 hours post IPTG induction; Lane (5): F3 expression 3 hours post IPTG induction; Lane (6): F3 expression 4 hours post IPTG induction; Lane (7): F3 expression 5 hours post IPTG induction; Lane (8): F3 expression following overnight induction using IPTG. A band representing F3 is clearly visible at 23kDa.

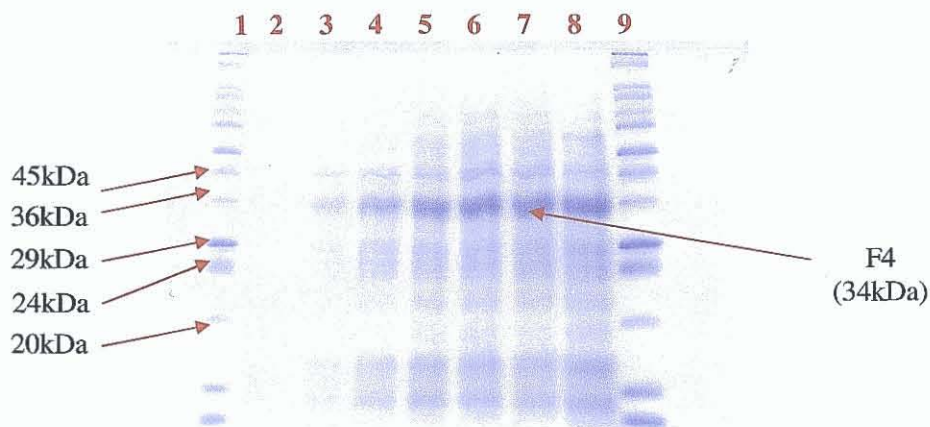


Figure 3.12 Time course expression analysis on F4 in XL-10 Gold *E. coli*. Lanes (1) and (9): Sigma wide-range molecular weight marker; Lane (2): Non- induced control; Lane (3): F4 expression 1 hour post IPTG induction; Lane (4): F4 expression 2 hours post IPTG induction; Lane (5): F4 expression 3 hours post IPTG induction; Lane (6): F4 expression 4 hours post IPTG induction; Lane (7): F4 expression 5 hours post IPTG induction; Lane (8): F4 expression following overnight induction using IPTG. A band representing F4 is clearly visible at 34kDa.

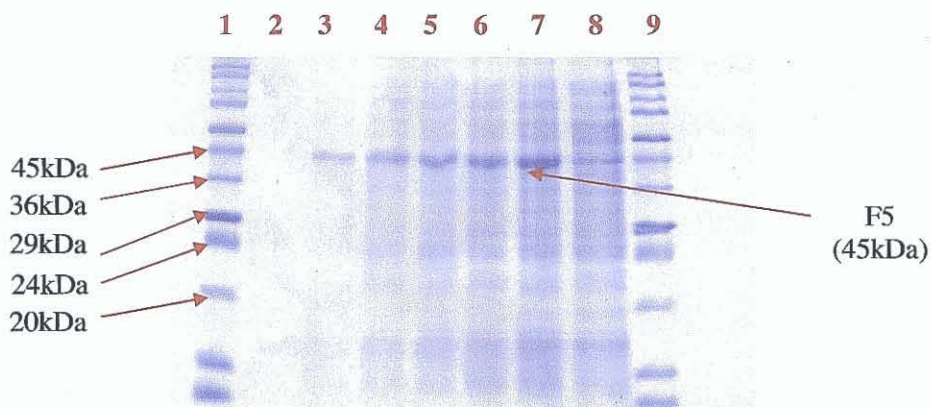


Figure 3.12 Time course expression analysis on F5 in XL-10 Gold *E. coli*. Lanes (1) and (9): Sigma wide-range molecular weight marker; Lane (2): Non- induced control; Lane (3): F5 expression 1 hour post IPTG induction; Lane (4): F5 expression 2 hours post IPTG induction; Lane (5): F5 expression 3 hours post IPTG induction; Lane (6): F5 expression 4 hours post IPTG induction; Lane (7): F5 expression 5 hours post IPTG induction; Lane (8): F5 expression following overnight induction using IPTG. A band representing F5 is clearly visible at 45kDa.

SDS-PAGE analysis on the time course analysis for F3, F4 and F5 suggested the optimal induction period for protein expression was 4 hours, after which no major difference in the levels of protein expression were observed (Figures 3.10, 3.11 and 3.12). Although slightly higher levels of F4 and F5 expression were observed following a 5-hour induction period, 4 hours was selected to minimise proteolytic degradation of the proteins and 6x His-tag cleavage.

3.3.5 Large-scale expression culture for purification

LB (10ml) containing 100 µg/ml ampicillin, 10 µg/ml tetracycline and 25 µg/ml chloramphenicol was inoculated with a single colony of InlB F3, F4 and F5 in XL-10 Gold *E. coli* containing the pQE-60 plasmid. The cultures were grown as described in Section 2.2.18 and protein expression was then induced following addition of 0.1mM IPTG. The culture was incubated shaking at 37°C for 4 hours and then centrifuged at 3,200 x g for 20 min. The supernatant was discarded and the pellet resuspended in 25ml of IMAC wash buffer (Table 2.15) and sonicated for 30s. The lysed cells were then centrifuged at 3,200 x g for 15 min and the supernatant analysed for protein expression, using SDS-PAGE (Figure 3.13).

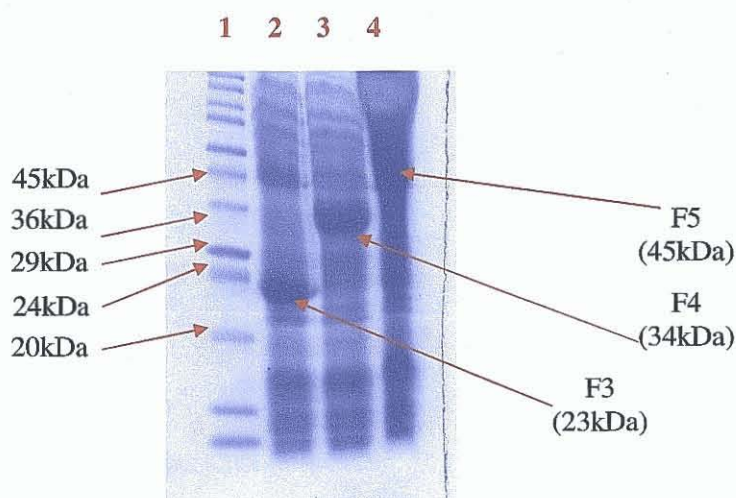


Figure 3.13 Expression of InlB protein fragments under optimal expression and growth conditions. Lane (1): Sigma-wide molecular weight marker; Lane (2): F3 fragment; Lane (3): F4 fragment; Lane (4): F5 fragment.

3.3.6 Purification of the His-tagged InlB protein fragments by IMAC

InlB protein fragments engineered to express a 6xHis affinity tag, encoded at the C terminal were purified by binding to Ni-NTA resin. The high-affinity interaction between histidine residues and Ni⁺⁺ ions enabled specific purification of His-tagged recombinant proteins and the high surface concentration of the NTA ligand was sufficient for the binding of approximately 5-10mg of 6xHis tagged protein per millilitre of resin. *E.coli* cells harbouring an InlB gene insert (F3 fragment) were induced with IPTG for 4 hours and the recombinant gene products purified (Section 2.2.19). The purification monitoring gel from the pre-optimised expression of the InlB F3 fragment had a faint protein band at the predicted M_R 23 kDa (data not shown). Low yields of protein were recovered since purification parameters had not been optimised. The pre-optimised IMAC purification was performed at room temperature and an excess amount of resin was used which explains the low yields observed (Barbas *et al.*, 2001). A number of factors were investigated to improve purification conditions. These included reaction temperature, amount of resin used, amount of imidazole used to elute the protein from the column, wash buffer composition and lysate preparation. Figure 3.14 shows the optimised purification gel for InlB F3.

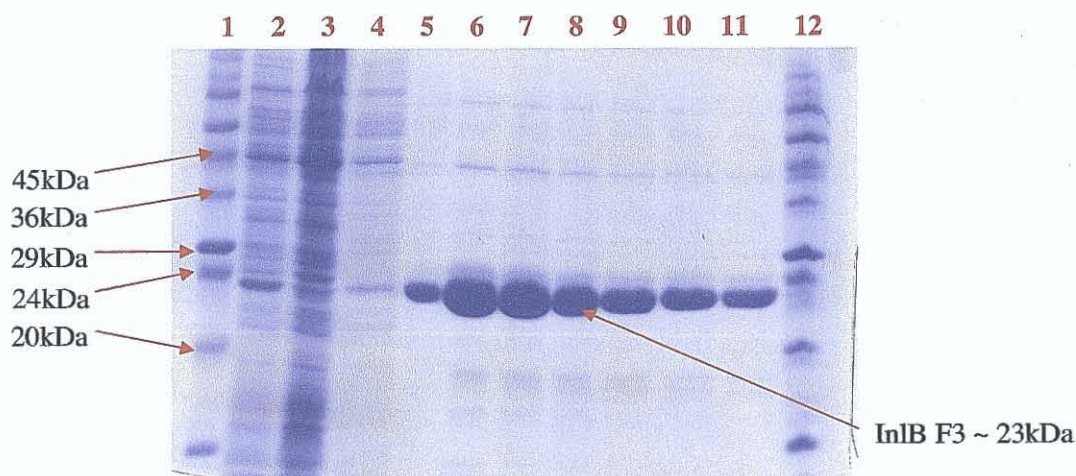


Figure 3.14 SDS-PAGE Analysis on optimised IMAC-purification of InlB recombinant protein fragment F3. Lanes (1) and (12): Sigma wide-range molecular weight marker; Lane (2): Crude cytoplasmic lysate from XL-10 Gold following F3 Expression; Lane (3): Flow-through from IMAC column following application of crude lysate; Lane (4): Wash fraction 1; Lanes (5)-(11): Eluted fractions 1-7, The elution of the InlB protein resulted in the presence of a concentrated protein band at the expected molecular weight of ~ 23kDa.

The conditions used for purification are important factors in recovery of functional protein. Limiting the amount of resin used to purify His-tagged protein minimises the purification of non-specific proteins in the sample by introducing competition for binding to the resin. The pellet from the centrifuged lysate was resuspended in IMAC wash buffer (50mM NaH₂PO₄, 300mM NaCl, 20mM imidazole, pH 8.0) and sonicated three times for 30s. The lysed cells were centrifuged (*Section 2.2.19*) and the lysate filtered before purification. The protein was eluted with elution buffer that had a high concentration of imidazole (50mM NaH₂PO₄, 300mM NaCl, 250mM imidazole, pH 8.0), since imidazole competes for binding to Ni²⁺ on the column. The higher the concentration of imidazole tolerated by the protein, the cleaner the eluant will be. The optimised IMAC purification of the InlB recombinant protein fragments was performed at 4°C which improved binding of specific His-tagged proteins to the Ni-NTA resin (Barbas *et al.*, 2001). The eluted fractions (Lanes 5-11) show concentrated protein bands at the predicted M_R of 23 kDa.

3.3.7 Immunoreactivity of recombinant InlB Protein fragments

To confirm the presence of a His tag for IMAC purification, *E. coli* lysates harbouring the recombinant protein fragments were probed with a commercial anti-His tag-specific monoclonal antibody. The recombinant proteins were electrophoresed alongside a prestained molecular weight marker using SDS-PAGE (*Section 2.2.5*). Figure 3.15 (A) shows the Coomassie stained gel with bands representing the F3 (Lane 2), F4 (Lane 3) and F5 (Lane 4) InlB fragments and the full InlB protein clearly visible at 23, 34, 45 and 60kDa, respectively. The proteins were transferred to nitrocellulose for Western blot analysis (*Section 2.2.7*). The nitrocellulose blots were probed with an anti-His tag-specific monoclonal antibody, since the pQE-60 vector has a His tag for purification. Figure 3.15 (B) shows the His blot with bands clearly visible at 23, 34, 45 and 60kDa representing the F3, F4 and F5 fragment and the full InlB protein, respectively. This blot confirms the presence of a 6xHis tag in each of the clones, indicating that the tag is not hidden within the protein structure.

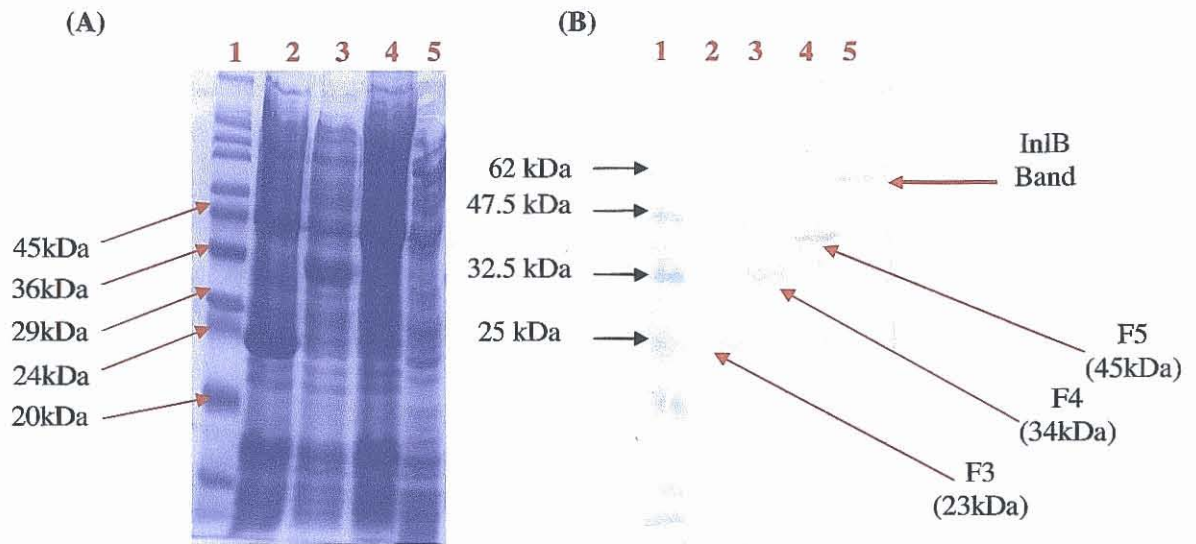


Figure 3.15 SDS-PAGE gel and Western Blot of InlB peptide fragments (F3, F4 and F5) probed with anti-His tag-specific monoclonal antibody to confirm presence of the His tag. (A) Coomassie stained gel. Lane (1): Sigma-wide molecular weight marker; Lane (2): F3 fragment; Lane (3): F4 fragment; Lane (4): F5 fragment; Lane (5) InlB protein; (B) His blot. Lane (1): Pierce pre-stained marker; Lane (2): F3 fragment; Lane (3): F4 fragment; Lane (4): F5 fragment; Lane (5) InlB protein. Bands visible at 23, 34, 45 and 60kDa confirm presence of the His-tag in each fragment and in the previously cloned full protein (Leonard, 2003).

To determine the potential for use of the recombinant InlB protein fragments in immunoassay development with fluorescence and impedance-based detection methods, the immunoreactivity of the proteins was assessed by Western blotting using a panel of anti-InlB antibodies. Figures 3.16-3.18 show the detection of the InlB protein fragments (F3, F4 and F5) via Western blotting with an anti-InlB polyclonal antibody, anti-InlB monoclonal antibody and anti-InlB antibody fragment (scFv). Phospholipase D (PLD) is a diagnostic marker for *Corynebacterium pseudotuberculosis* infection and although it is not specific for *L. monocytogenes* or its associated proteins, it has shown minor crossreactivity (Dercksen *et al.*, 2000). It was therefore assessed as a control in these experiments.

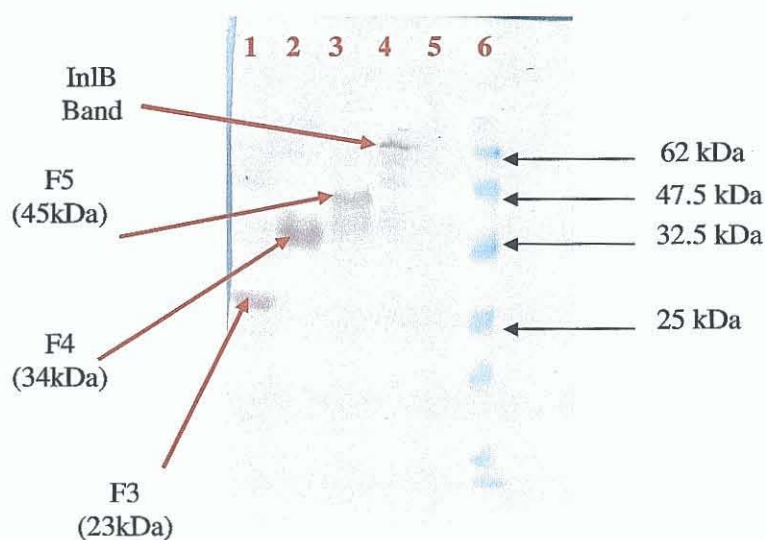


Figure 3.16 Western Blot of InlB peptide fragments (F3, F4 and F5) probed with anti-InlB polyclonal antibody to determine location of the antibody-binding site. Lane (1): F3 fragment; Lane (2): F4 fragment; Lane (3): F5 fragment; Lane (4) InlB protein; Lane (5) PLD is not recognised by anti-InlB antibodies (negative control); Lane (6): Pierce pre-stained marker; Bands visible at 23, 34 and 44 kDa confirm presence of an epitope detected by the polyclonal antibody in each of the InlB fragments, indicating that the antibody binding site is located in the F3 fragments (0-248 amino acids).

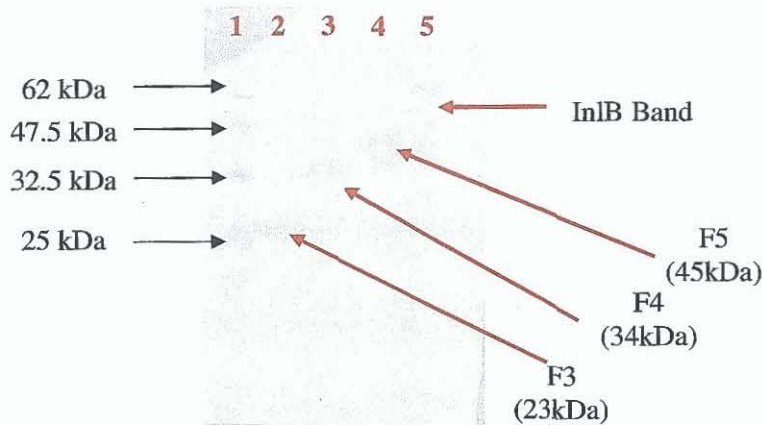


Figure 3.17 Western Blot of InlB peptide fragments (F3, F4 and F5) probed with anti-InlB monoclonal antibody to determine location of the antibody-binding site. Lane (1): Pierce pre-stained markers; Lane (2): F3 fragment; Lane (3): F4 fragment; Lane (4): F5 fragment; Lane (5) InlB protein; Bands visible at 23, 34 and 44 kDa confirm presence of an epitope detected by the monoclonal antibody in each of the InlB fragments, indicating that the antibody binding site is located in the F3 fragments (0-248 amino acids).

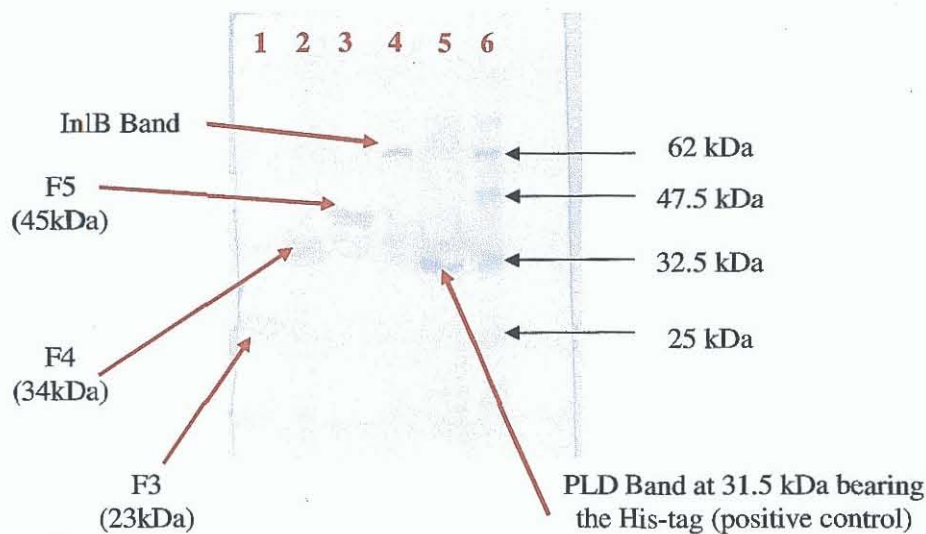


Figure 3.18 Western Blot of InlB peptide fragments (F3, F4 and F5) probed with anti-InlB scFv to determine location of the antibody-binding site. Lane (1): F3 fragment; Lane (2): F4 fragment; Lane (3): F5 fragment; Lane (4) InlB protein; Lane (5) PLD (positive control) is also recognised by the HRP labelled anti-His antibody used for detection; Lane (6): Pierce pre-stained marker; Bands visible at 23, 34 and 44 kDa confirm presence of an epitope detected by the scFv antibody fragment in each of the InlB fragments, indicating that the antibody binding site is located in the F3 fragment (0-248 amino acids).

The rInlB protein fragments (F3, F4 and F5) could be specifically detected with each of the anti-InlB antibodies (polyclonal, monoclonal and scFv) raised against the native form of the full InlB protein. Bands visible at 23, 34 and 45kDa, respectively, confirmed the presence of the epitope detected by the anti-InlB monoclonal and scFv antibodies in each of the fragments and a major epitope recognised by the anti-InlB polyclonal antibody. This indicated that the location of an important epitope for antibody-binding was found in the F3 fragment (amino acids 0-248). This showed that the F3 peptide fragment could be used for the generation of improved immunoassays for the detection of InlB, whereby the part of the InlB protein containing the most immunoreactive domain could be used as the antigenic determinant in assay development.

3.3.8 Sequence analysis of recombinant InlB protein fragments

The pQE-60 plasmid DNA containing the F3, F4 and F5 inserts was purified from the XL-10 Gold *E. coli*. A Comfort read (in both directions) was then obtained from MWG-Biotech on each plasmid and the nucleotide sequence returned. The amino acid sequences were then deduced from the nucleotide sequences using a web-based translation tool (Table 2.15). The translated amino acid sequences were aligned with the published amino acid sequence of Internalin B (Accession number AJ012346) using the multialin program (Table 2.15). The aligned sequences were imported into the BLAST database, to check for similarities with the known sequence of Internalin B. Figures 3.19-3.21 show the alignments of the cloned fragments (F3, F4 and F5) with the published protein sequence, displaying 100% identity with the sequence provided by Genedoc (AJ012346).

F3 InlB AJ012346	MGETITVPTPIKQIFSDDAFAETIKDN ETITVPTPIKQIFSDDAFAETIKDN
F3 InlB AJ012346	LKKKSVTDAVTQNELNSIDQIIANNSDIKSVQGIQYLPNVTKLFLNGNKLTDIKPLANLK LKKKSVTDAVTQNELNSIDQIIANNSDIKSVQGIQYLPNVTKLFLNGNKLTDIKPLANLK
F3 InlB AJ012346	NLGWLFLDENKVKDLSSLKDLKKLKSLSLSEHNGISDINGLVHLPQLESYLGNNKITDIT NLGWLFLDENKVKDLSSLKDLKKLKSLSLSEHNGISDINGLVHLPQLESYLGNNKITDIT
F3 InlB AJ012346	VLSRLTKLDTLSLEDNQISDIVPLAGLTKLQONLYLSKNHISDLRALAGLKNLDVLELFSQ VLSRLTKLDTLSLEDNQISDIVPLAGLTKLQONLYLSKNHISDLRALAGLKNLDVLELFSQ
F3 InlB AJ012346	EC EC

Figure 3.19 Amino acid sequence of cloned *InlB* F3 sequence aligned with the sequence obtained from Genebank (Accession number AJ012346). The text in red indicates the end of the signal peptide, while the text in blue is the amino acid sequence of the F3 fragment.

```

F4 InlB MGETITVPTPIKQIFSDDAFAETIKDNLKKKSVTDAVTQNELNSIDQIIA
AJ012346 ETTITVPTPIKQIFSDDAFAETIKDNLKKKSVTDAVTQNELNSIDQIIA

F4 InlB NNSDIKSVQGIQYLPNVTKLFLNGNKLTDIKPLANLKNLGLFLDENKVK
AJ012346 NNSDIKSVQGIQYLPNVTKLFLNGNKLTDIKPLANLKNLGLFLDENKVK

F4 InlB DLSSLKDLKCLKSLSLSEHNGISDINGLVHLPQLESLYLGNNKITDITVLS
AJ012346 DLSSLKDLKCLKSLSLSEHNGISDINGLVHLPQLESLYLGNNKITDITVLS

F4 InlB RLTKLDLTSLEDNQISDIVPLAGLTKLQNLVLSKNHISDLRALAGLKNLD
AJ012346 RLTKLDLTSLEDNQISDIVPLAGLTKLQNLVLSKNHISDLRALAGLKNLD

F4 InlB VLELFSQECLNKPINHQS NLVVPNTVKNTDGS LVTPEIISDDGDYEKPNV
AJ012346 VLELFSQECLNKPINHQS NLVVPNTVKNTDGS LVTPEIISDDGDYEKPNV

F4 InlB KWHLPEFTNEVSFIFYQPVTIGKAKARFHGRVTQPLKEVY TV
AJ012346 KWHLPEFTNEVSFIFYQPVTIGKAKARFHGRVTQPLKEVY TV

```

Figure 3.20 Amino acid sequence of cloned *InlB* F4 sequence aligned with the sequence obtained from Genebank (Accession number AJ012346). The text in red indicates the end of the signal peptide, while the text in blue is the amino acid sequence of the F4 fragment.

```

F5 InlB MGETITVPTPIKQIFSDDAFAETIKDNLKKKSVTDAVTQNELNSIDQIIA
AJ012346 ETTITVPTPIKQIFSDDAFAETIKDNLKKKSVTDAVTQNELNSIDQIIA

F5 InlB NNSDIKSVQGIQYLPNVTKLFLNGNKLTDIKPLANLKNLGLFLDENKVK
AJ012346 NNSDIKSVQGIQYLPNVTKLFLNGNKLTDIKPLANLKNLGLFLDENKVK

F5 InlB DLSSLKDLKCLKSLSLSEHNGISDINGLVHLPQLESLYLGNNKITDITVLS
AJ012346 DLSSLKDLKCLKSLSLSEHNGISDINGLVHLPQLESLYLGNNKITDITVLS

F5 InlB RLTKLDLTSLEDNQISDIVPLAGLTKLQNLVLSKNHISDLRALAGLKNLD
AJ012346 RLTKLDLTSLEDNQISDIVPLAGLTKLQNLVLSKNHISDLRALAGLKNLD

F5 InlB VLELFSQECLNKPINHQS NLVVPNTVKNTDGS LVTPEIISDDGDYEKPNV
AJ012346 VLELFSQECLNKPINHQS NLVVPNTVKNTDGS LVTPEIISDDGDYEKPNV

F5 InlB KWHLPEFTNEVSFIFYQPVTIGKAKARFHGRVTQPLKEVYTVSYDVDGTV
AJ012346 KWHLPEFTNEVSFIFYQPVTIGKAKARFHGRVTQPLKEVYTVSYDVDGTV

F5 InlB IKTKVEAGTRITAPKPPTKQGYVFKGWYTEKNGGHEWNFNTDYMSGNDFTLAYV
AJ012346 IKTKVEAGTRITAPKPPTKQGYVFKGWYTEKNGGHEWNFNTDYMSGNDFTLAYV

```

Figure 3.21 Amino acid sequence of cloned *InlB* F5 sequence aligned with the sequence obtained from Genebank (Accession number AJ012346). The text in red indicates the end of the signal peptide, while the text in blue is the amino acid sequence of the F5 fragment.

3.4 *In vivo* biotinylation of recombinant Internalin B protein fragments

3.4.1 Cloning of InlB fragments into the pAC4 vector

The pAC4 vector for *in vivo* biotinylation of recombinant proteins was purchased from Avidity Corporation, USA. This vector has both a BamH1 and Nco1 restriction site, thus facilitating easy transfer of InlB protein fragments (F3, F4 and F5) from Qiagen's pQE-60 vector into the pAC 4 vector.

3.4.1.1 Isolation of plasmid DNA from pQE-60 clones

The pAC4 vector stock with InlB insert in AVB101 cells was cultured and the vector DNA purified (Section 2.2.1). AVB101 cells are *endA*⁻ and as a result they are not compatible with the Promega mini-prep kit. Therefore, the vector was transferred into XL-I Blue *E. coli* for optimal purification of vector DNA. The purified pAC4 vector was digested with BamH1 and Nco1 (Section 2.2.11) to remove existing InlB insert and subsequently purified (Section 2.2.3) for ligation with InlB fragments (F3, F4 and F5). This is shown in Figure 3.22.

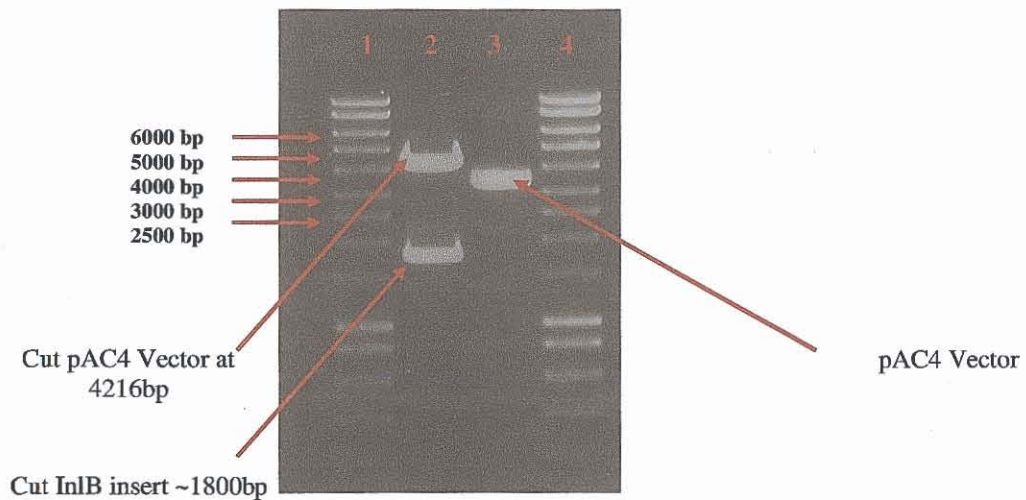


Figure 3.22 Agarose gel showing the restriction of the pAC 4 vector in XL-1 Blue for purification of plasmid DNA. Lanes (1) and (4): Hyperladder DNA ladder; Lane (2): Digested pAC 4 vector in XL-1 Blue *E. coli* with InlB gene removed; Lane (3): Undigested pAC4 vector.

3.4.1.2 BamHI/NcoI restriction analysis on pAC4 vector purified plasmid DNA containing cloned gene inserts

The pAC 4 vector in XL-1 Blue *E.coli* and the InlB pQE-60 inserts (F3, F4 and F5) in XL-10 Gold *E. coli* were restricted using a BamHI/NcoI double digest (Section 2.3.1). The resulting restricted products were run on a 1% (w/v) agarose gel and the appropriate bands were cut for purification, (Figure 3.23).

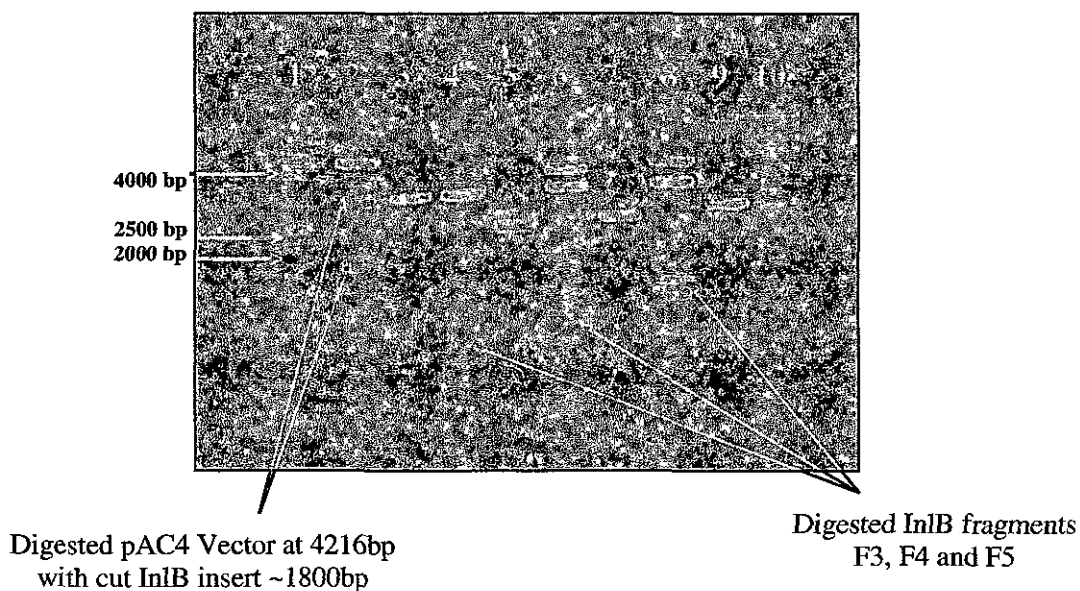


Figure 3.23 Agarose gel showing the restriction of the pAC4 vector and InlB pQE-60 inserts. Lanes (1) and (10): Hyperladder DNA ladder; Lane (2): Digested pAC 4 vector in XL-1 blues with InlB insert; Lane (3): Undigested pAC4 vector; Lane (4): Digested F3 insert in pQE-60; Lane (5): Undigested F3 insert in pQE-60; Lane (6): Digested F4 insert in pQE-60; Lane (7): Undigested F4 insert in pQE-60; Lane (8) Digested F5 insert in pQE-60; Lane (9): Undigested F5 insert in pQE-60.

3.4.1.3 Ligation, Transformation and Expression of vector-insert constructs

A gel purification kit was used to purify cut pAC4 vector and InlB insert bands, for ligation and transformation into AVB 101 *E. coli*. (Section 2.2.3). The gel purified InlB inserts were cloned into linearised pAC4 using T4 DNA ligase (Section 2.3.2) and subsequently transformed into electrocompetent AVB101 *E. coli*, (Section 2.3.3). Positive clones were screened by picking single colonies from each transformation plate, for growth and induction (Section 2.3.4). High-level recombinant protein expression was induced upon addition of 1mM IPTG and 100 μ M biotin and the resulting pellets washed with PBS to remove any free biotin. The clones were then analysed using SDS-PAGE and Western blotting to confirm the presence of the biotin AviTag prior to purification via affinity chromatography, using immobilised monomeric avidin.

3.4.1.4 Confirmation of biotinylation of InlB fragments in pAC4 vector

Confirmation of *in vivo* biotinylation of the InlB protein fragments cloned into the pAC4 vector was determined by SDS-PAGE analysis and Western blotting. The fragments were expressed (Section 2.3.4) and subsequently analysed using SDS-PAGE (Section 2.2.5). To confirm the presence of a biotin tag on the *in vivo* biotinylated proteins, *E. coli* lysates harbouring the recombinant protein fragments were probed with a commercial anti-biotin antibody. The recombinant proteins were electrophoresed alongside a prestained molecular weight marker using SDS-PAGE. Figure 3.24 (A) shows the Coomassie blue-stained gel of the *in vivo* biotinylated protein fragments F3, F4 and F5 lysates, diluted 1/10 in PBS (Lanes 2-4). Biotinylated anti-InlB polyclonal antibody (Section 2.5.2.1) was used as a positive control (Lane 5), while unbiotinylated fetuin protein was used as a negative control (Lane 6). The proteins were transferred to nitrocellulose for Western blot analysis (Section 2.2.7). The nitrocellulose blot was probed with a commercial anti-biotin antibody, since the pAC4 vector has a biotin AviTag peptide which should be present on each cloned protein fragments. Figure 3.24 (B) shows the blot probed with the anti-biotin antibody with bands clearly visible at 23, 35 and 44kDa representing the F3, F4 and F5 fragment, respectively. This blot confirms the presence of a biotin tag in each of the clones.

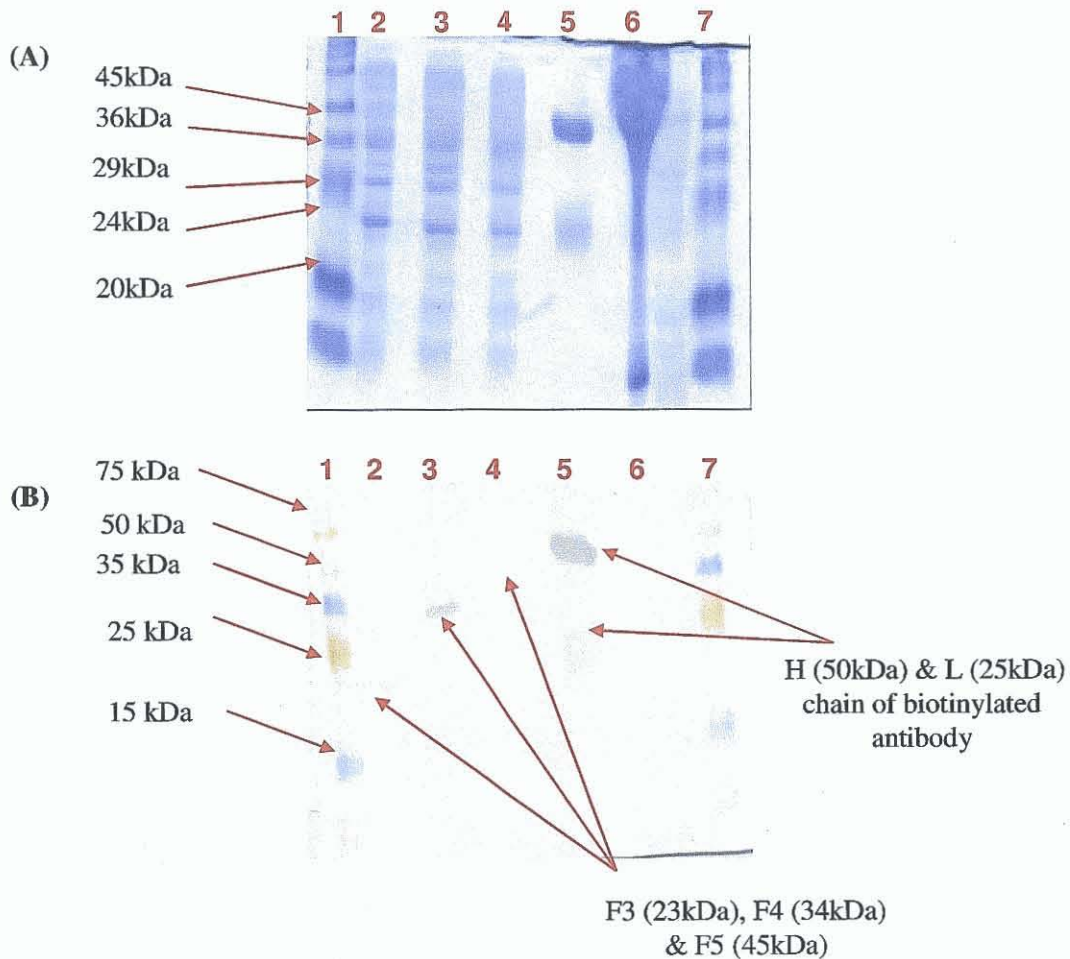


Figure 3.24 SDS-PAGE gel and Western Blot of InlB peptide fragments (F3, F4 and F5) probed with anti-biotin antibody to confirm presence of the biotin AviTag. (A) Coomassie stained gel; Lanes (1) and (7): Sigma wide-range molecular weight marker; Lane (2): InlB F3 protein fragment, diluted 1/10; Lane (3): InlB F4 protein fragment, diluted 1/10; Lane (4): InlB F5 protein fragment, diluted 1/10; Lane (5): Positive control, anti-InlB biotinylated polyclonal antibody; Lane (6): Negative control, non-biotinylated fetuin. (B) Nitrocellulose blot probed with anti-biotin antibody; Lanes (1) and (7): Amersham Rainbow prestained molecular weight marker; Lane (2): InlB F3 protein fragment; Lane (3): InlB F4 protein fragment; Lane (4): InlB F5 protein fragment; Bands are visible at 23, 34, 45 kDa, respectively, for each of the protein fragments indicating the presence of a biotin tag on each cloned protein, as expected. Lane (5): Positive control, anti-InlB biotinylated polyclonal antibody with heavy and light chains of the antibody clearly visible at 50 and 25 kDa, respectively, indicating presence of biotin; Lane (6): Negative control, fetuin which has no biotin tag and therefore was not detected by the anti-biotin antibody.

3.4.1.5 Purification of *in vivo* biotinylated InIB fragments by affinity chromatography

Immunopure® immobilised monomeric avidin (Pierce), was used for the affinity purification of the *in vivo* biotinylated InIB protein fragments (Section 2.3.5). Avidin monomers have a much lower biotin-binding affinity than native tetrameric avidin enabling dissociation of biotinylated molecules using mild elution conditions. During immobilisation of monomeric avidin polymeric forms of avidin with strong binding characteristics are immobilised and, therefore, biotin-containing buffer was used to block these high affinity biotin-binding sites. The biotin molecules were eluted from the avidin monomers with a glycine solution which frees only the reversible binding sites. The *in vivo* biotinylated fragments were then applied to the support for purification and eluted by ligand competition using a biotin-containing solution (2mM biotin in PBS, pH 7.4).

ImmunoPure® immobilised monomeric avidin is produced using a procedure that results in a high-binding capacity support with minimal non-specific binding and excellent recovery of biotinylated molecules. The monomeric avidin column is supplied as a 50% slurry containing 4% (w/v) beaded agarose. The binding capacity of the column is approximately 1.2 mg biotinylated protein per ml of settled gel (Instruction manual # 20227, Pierce Biotechnology, Inc., 2005). Biotinylated protein was incubated on the column for one hour at room temperature. Purified fractions were eluted using 2mM biotin in PBS (0.15M NaCl, 2.5mM KCl, 10mM Na₂HPO₄, 18mM KH₂PO₄, pH 7.4) and 2ml fractions were collected and monitored spectrophotometrically at 280nm for protein content. The fractions that contained protein were pooled and quantified for characterisation using fluorescence-based immunoassay and Biacore. Figure 3.25 shows the elution profile for the *in vivo* biotinylated InIB fragment, F3, following affinity purification using monomeric avidin immobilised on Sepharose.

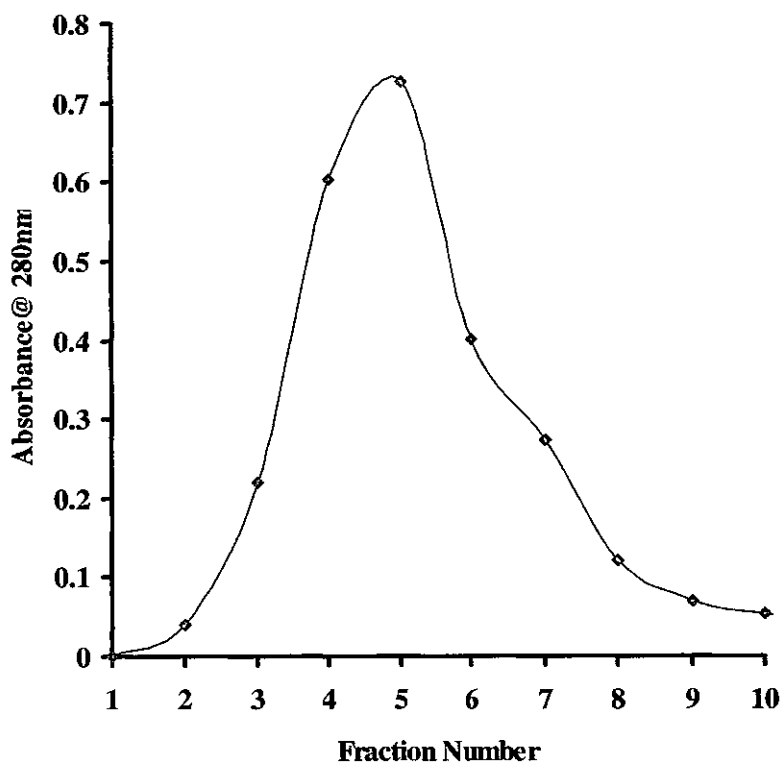


Figure 3.25 Elution profile of *in vivo* biotinylated InlB fragment F3 following affinity purification using a monomeric streptavidin column (10ml capacity). *In vivo* biotinylated fragments were incubated on the column for one h at room temperature and eluted in 2ml fractions using 2mM biotin in PBS (0.15M NaCl, 2.5mM KCl, 10mM Na₂HPO₄, 18mM KH₂PO₄, pH 7.4). Eluted fractions were monitored for protein content at 280nm and those containing protein (Fractions 3-8) were collected and pooled for subsequent characterisation.

3.4.2 Characterisation of *in vivo* biotinylated recombinant InlB fragments

The *in vivo* biotinylated InlB protein fragments, cloned from the pAC4 vector, were purified using affinity chromatography and characterised using both fluorescence-based and Biacore-based methods. The following sections describe the characterisation of the *in vivo* biotinylated fragments and their potential use as novel reagents for improved detection of InlB.

3.4.2.1 Enzyme-based detection of *in vivo* biotinylated fragments

Each of the purified biotinylated InIB fragments was titrated against immobilised anti-InIB polyclonal antibody and traced with extravidin peroxidase (*Section 2.3.6.1*). This assay was performed to ensure that the *in vivo* biotinylated fragments retained functionality post purification and would still bind an associated InIB-derived antibody. Anti-InIB polyclonal antibody at a concentration of 10 μ g/ml in 0.1M carbonate buffer (Table 2.4) was used to coat the wells of a microtitre plate. The plates were washed and blocked as per *Section 2.3.6.1*. The concentration of each fragment (F3, F4 and F5) was determined spectrophotometrically post-purification and stock solutions were prepared at a concentration of 500 μ g/ml. Doubling dilutions (1/10 to 1/5120) of each fragment were prepared from these stocks in PBS (0.15M NaCl, 2.5mM KCl, 10mM Na₂HPO₄, 18mM KH₂PO₄, pH 7.4) containing 0.2% (w/v) BSA and subsequently added to the plate. The amount of bound *in vivo* biotinylated fragment was determined using extravidin peroxidase (Sigma-Aldrich) and TMB substrate. Figure 3.26 shows a titre of the *in vivo* biotinylated InIB protein fragments against immobilised anti-InIB polyclonal antibody.

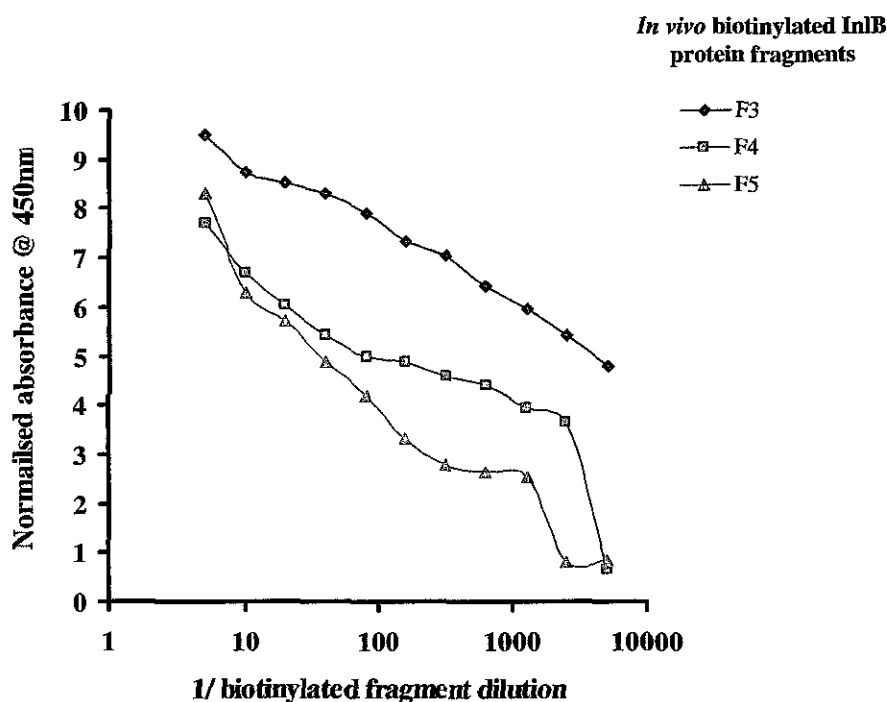


Figure 3.26 Titre of *in vivo* biotinylated protein fragments against immobilised antibody. Anti-InIB polyclonal antibody was coated on the plate (10 μ g/ml) and a range of dilutions (1/10 to 1/5120) of each of the biotinylated fragments (F3, F4 and F5) was added. The amount of bound protein was detected using extravidin-peroxidase and TMB substrate.

From Figure 3.36, it is apparent that the F3 fragment gave the most linear response with the highest level of biotinylation. This indicated that the efficiency of *in vivo* biotinylation of the F3 fragment was superior to both the F4 and F5 fragments. The F3 fragment is also the portion of the InlB protein that is the most immunoreactive, in that it contains the antibody-binding domain, as previously determined by SDS-PAGE and Western blotting (Section 3.3.7) For both these reasons subsequent studies focused only on this part of the InlB protein, the F3 fragment.

3.4.2.2 Fluorescence-based detection of *in vivo* biotinylated fragments

The *in vivo* biotinylated F3 fragment was further investigated using a streptavidin-linked fluorescent label. Streptavidin-Cy5 (Amersham) was used to detect the amount of *in vivo* biotinylated protein bound to immobilised antibody (Section 2.3.6.2). Anti-InlB polyclonal antibody at a concentration of 10µg/ml in 0.1M carbonate buffer (Table 2.4), was used to coat the wells of a microtitre plate. The plates were washed and blocked as per Section 2.3.6.2. Doubling dilutions (1/10 to 1/5120) of biotinylated and non-biotinylated F3 fragment were prepared in PBS (0.15M NaCl, 2.5mM KCl, 10mM Na₂HPO₄, 18mM KH₂PO₄, pH 7.4) containing 0.2% (w/v) BSA and subsequently added to the plate. The amount of immobilised InlB F3 protein was detected using Streptavidin-Cy5 (Amersham) at a dilution of 1/1000. PBS (as before) was also used in some wells as a control, to determine the extent of non-specific binding. Figure 3.27 shows the titre of both the biotinylated and non-biotinylated F3 fragments, against immobilised anti-InlB polyclonal antibody and traced with streptavidin-Cy5.

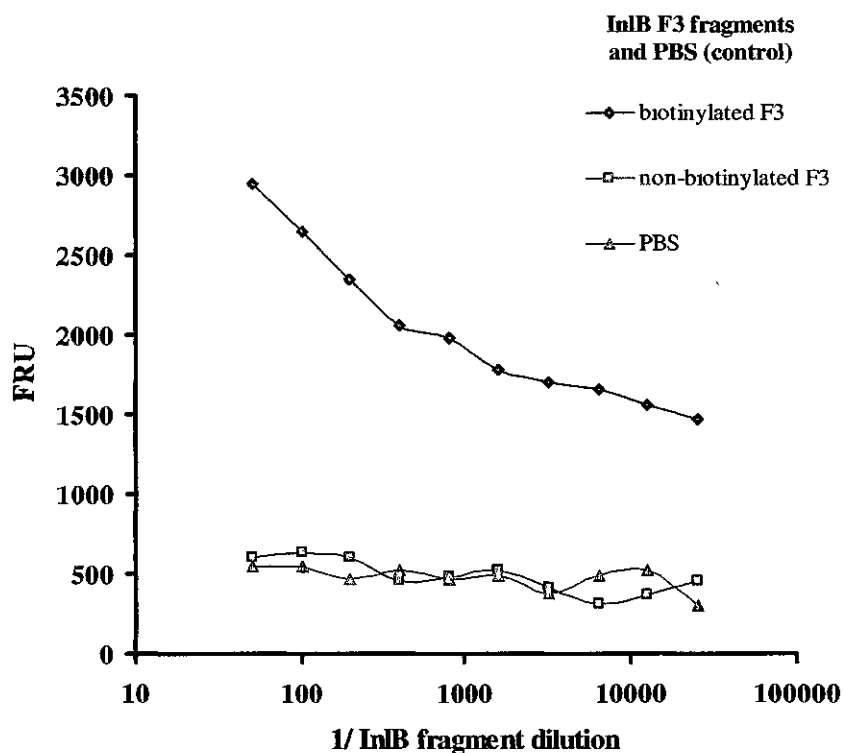


Figure 3.27 Assessment of specific interactions between biotinylated F3 fragment and fluorescent label (streptavidin-Cy5). Biotinylated and unbiotinylated protein fragments were added to immobilised antibody and the amount of bound protein was detected using streptavidin-Cy 5. The fluorescence response units (FRU) were plotted against the InIB fragment dilution.

Non-biotinylated F3 and PBS (0.15M NaCl, 2.5mM KCl, 10mM Na₂HPO₄, 18mM KH₂PO₄, pH 7.4) were used as negative controls in this experiment, with both showing minimal interaction with the streptavidin-Cy5. This was due to the fact that although the non-biotinylated F3 fragment binds immobilised anti-InIB antibody, it did not have a biotin tag to allow subsequent detection of bound antigen with streptavidin-Cy5. It behaved in the same manner as PBS, which as a buffer had no binding capabilities for subsequent detection with Cy5. This indicated that only negligible amounts of non-specific binding was taking place and that the blocking solution, 2% (w/v) BSA in PBS (0.15M NaCl, 2.5mM KCl, 10mM Na₂HPO₄, 18mM KH₂PO₄, pH 7.4) was sufficient. Only the specific interaction between the biotinylated InIB F3 protein fragment bound to immobilised anti-InIB polyclonal antibody and traced with streptavidin-Cy5 was observed.

The assay was repeated over a wider range of F3 protein fragment dilutions to assess the operating range of the biotinylated F3 protein as reagent for immunoassay development. Figure 3.28 shows a titre of the both the biotinylated and non-biotinylated F3 fragments against immobilised anti-InlB polyclonal antibody, traced with Streptavidin-Cy5, whereby the fluorescent response was normalised against a zero control (well containing no fluorescent molecules). The normalised fluorescence response units (NFRU) were plotted against the InlB F3 fragment dilution (both biotinylated and non-biotinylated) bound to immobilised antibody and traced with Cy5. The *in vivo* biotinylated F3 fragment was successfully traced using streptavidin-linked Cy5, which highlights its potential use as a viable antigen for further fluorescence-based assay development.

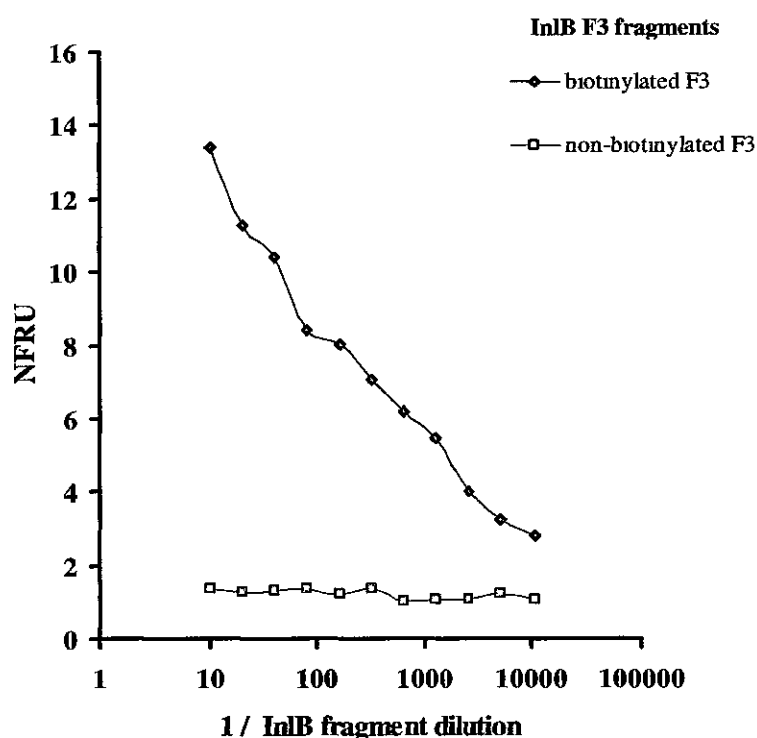


Figure 3.28 Fluorescence-based detection of InlB F3 protein fragments. Anti-InlB polyclonal antibody was coated on the plate (10µg/ml) and a range of dilutions (1/10 to 1/5120) of both the biotinylated and non-biotinylated F3 fragment was added. The amount of bound protein was detected using streptavidin-Cy5. The fluorescent response was normalised against the background fluorescence (NFRU) and plotted against the InlB F3 fragment dilution (both biotinylated and non-biotinylated).

Finally, the use of the *in vivo* biotinylated F3 fragment as a useful reagent for fluorescence-based detection was further investigated using three avidin-linked fluorescent labels; streptavidin-linked quantum dots, streptavidin-Cy5 and avidin-FITC (Section 2.3.6.4). Anti-InIB polyclonal antibody (10µg/ml) was used to coat the wells of a microtitre plate and blocked using PBS containing 2% (w/v) BSA. Biotinylated F3 fragment dilutions prepared in PBS containing 0.2% (w/v) BSA were added to the plate and the amount of bound protein traced with the fluorescent labels (Figure 3.29).

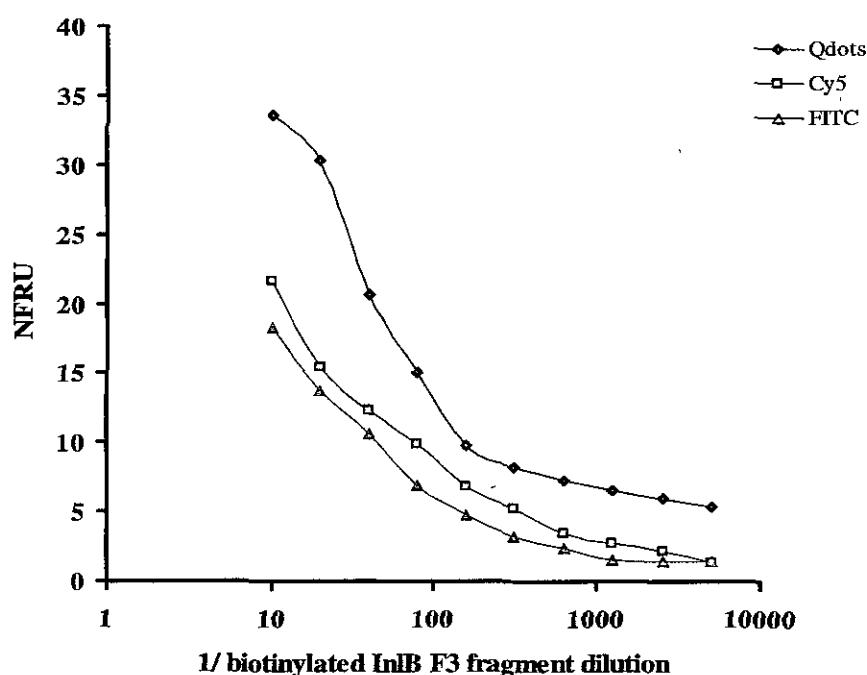


Figure 3.29 Direct detection of biotinylated F3 fragment using three fluorescent labels; Quantum dot-streptavidin conjugate (Qdots), Streptavidin-Cy5 (Cy5) and Avidin-FITC (FITC). Anti-InIB polyclonal antibody was coated on the plate (10µg/ml) and a range of dilutions (1/10 to 1/5120) of the biotinylated InIB F3 fragment was added. The amount of bound protein was detected using quantum dots, Cy5 and FITC. The fluorescent response was normalised against the background fluorescence (NFRU) and plotted against the biotinylated InIB F3 fragment dilution.

Figure 3.29 shows that the biotinylated fragment F3 could be successfully traced with three different avidin-linked fluorescent labels. This highlights the potential use of the *in vivo* biotinylated fragment as a reagent for future fluorescence-based immunoassay development.

3.4.2.3 Biacore analysis of *in vivo* biotinylated fragments

This section focuses on the use of Biacore-based methods (Section 4.1.3.2) for the characterisation of *in vivo* biotinylated recombinant InlB F3. The biotinylated F3 fragment was used as the capture antigen for the preliminary development of a Biacore inhibition assay for detection of InlB F3, using the anti-InlB polyclonal antibody. A Biacore carboxymethylated 5 (CM5) chip was covalently immobilised with the avidin-derivative, neutravidin for the specific capture of the biotinylated fragment (F3) on the surface of the chip. The chip consists of three layers: glass, a thin gold film and a matrix layer. The matrix layer is attached to the gold film through an inert linker layer. In the case of the CM5 chip the matrix layer is carboxymethylated dextran, which allows the covalent immobilisation of neutravidin on the sensor surface. Biotinylated InlB F3 was then immobilised on the neutravidin surface and anti-InlB polyclonal antibody, incubated with decreasing concentrations of InlB F3 protein fragment, injected over the surface. The shift in binding response after each injection was recorded and the results presented in Section 3.4.2.3.4. Figure 3.30 shows a diagrammatic representation of a CM5 chip and the assay format used for the detection of InlB, with biotinylated F3 as capture antigen.

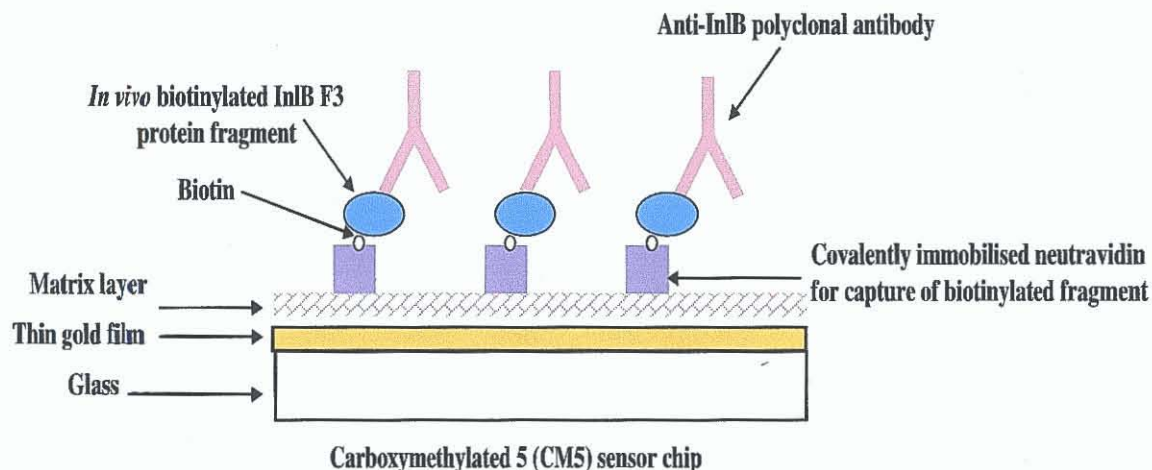
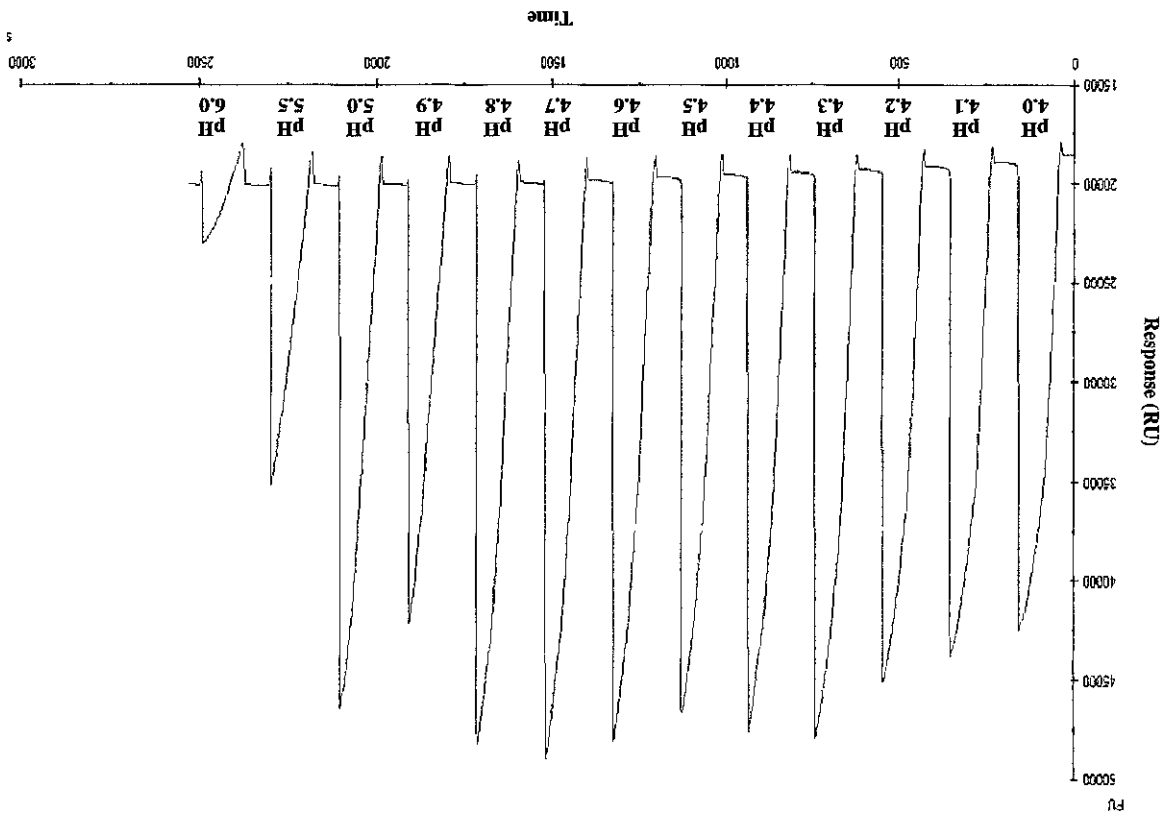


Figure 3.30 Diagrammatic representation of the surface of a carboxymethylated 5 (CM5) sensor chip. The chip consists of three layers: glass, a thin gold film and a matrix layer. The matrix layer is attached to the gold film through an inert linker layer. In the case of the CM5 chip the matrix layer is carboxymethylated dextran, which allows the covalent immobilisation of neutravidin onto the sensor surface. Neutravidin was used to capture the *in vivo* biotinylated InlB F3, for subsequent use in the development of an inhibition assay for the detection of InlB using the anti-InlB polyclonal antibody.

Figure 3.31 Typical preconcentration of neuravidin to the CM-dextran sensor chip at various pH increments and passed over a blank CM-dextran surface at 10µl/min for one minute and the amount of electrostatic interaction monitored. The optimal pH for the immobilisation of neuravidin onto the CM-dextran surface was found to be pH 4.6/4.7.



3.4.2.3.1 Preconcentration studies of neuravidin on the CM5-chip surface. Low ionic strength buffers, such as 10mM sodium acetate, enable the electrostatic adsorption of positively charged proteins to the negatively charged surface of the dextran chip. This maximises the amount of protein immobilised at the sensor surface, thus increasing the potential yield of immobilised ligand. To maximise the amount of neuravidin immobilised on the CM dextran surface, 50µg/ml of neuravidin, diluted in 10mM sodium acetate buffer at various increments pH (4.0-6.0) were injected over a blank CM dextran surface and the degree of preconcentration recorded (Section 2.6.1). From Figure 3.31, the optimal neuravidin preconcentration was determined in sodium acetate buffer, pH 4.7, which was used for all subsequent neuravidin immobilisations.

3.4.2.3.2 Immobilisation of neutravidin/biotinylated F3 onto the CM5-chip surface

In order to immobilise a ligand onto a CM5 sensor chip, three main phases are involved in the process. Firstly the surface is activated, the ligand is subsequently immobilised on the activated surface and finally the surface is deactivated or 'capped' to block any remaining sites left active by the immobilisation process. Molecules can be covalently coupled to the CM5 chip surface via amine, thiol, aldehyde or carboxyl groups. These chips have a high binding capacity, advantageous for capture assays and high surface stability providing accuracy and precision. The most commonly used surface chemistry for the immobilisation of biomolecules on CM5 sensor chip surfaces is EDC (N-ethyl-N'-(dimethylaminopropyl) carbodiimide) and NHS (N-hydroxysuccinimide) chemistry. The use of carbodiimide-EDC in conjunction with NHS activates the carboxyl groups of the CM-dextran surface, transforming them to active NHS esters that can be used to covalently immobilise the protein, in this case neutravidin, via its amino groups. The chip surface is then deactivated with 1M ethanolamine hydrochloride, pH 8.5, and all non-covalently bound protein is removed by reducing the electrostatic interaction between the CM-dextran surface and the protein.

Immobilisation of neutravidin on the dextran surface was performed as described in *Section 2.6.2*. Neutravidin (50µg/ml), diluted in 10mM sodium acetate buffer, pH 4.6 (*Section 3.4.2.3.1*) was injected over the EDC/NHS activated sensor chip surface for 40 minutes at a flow rate of 5µl/min. Approximately 25,000 RU of neutravidin was immobilised on the surface (Figure 3.32).

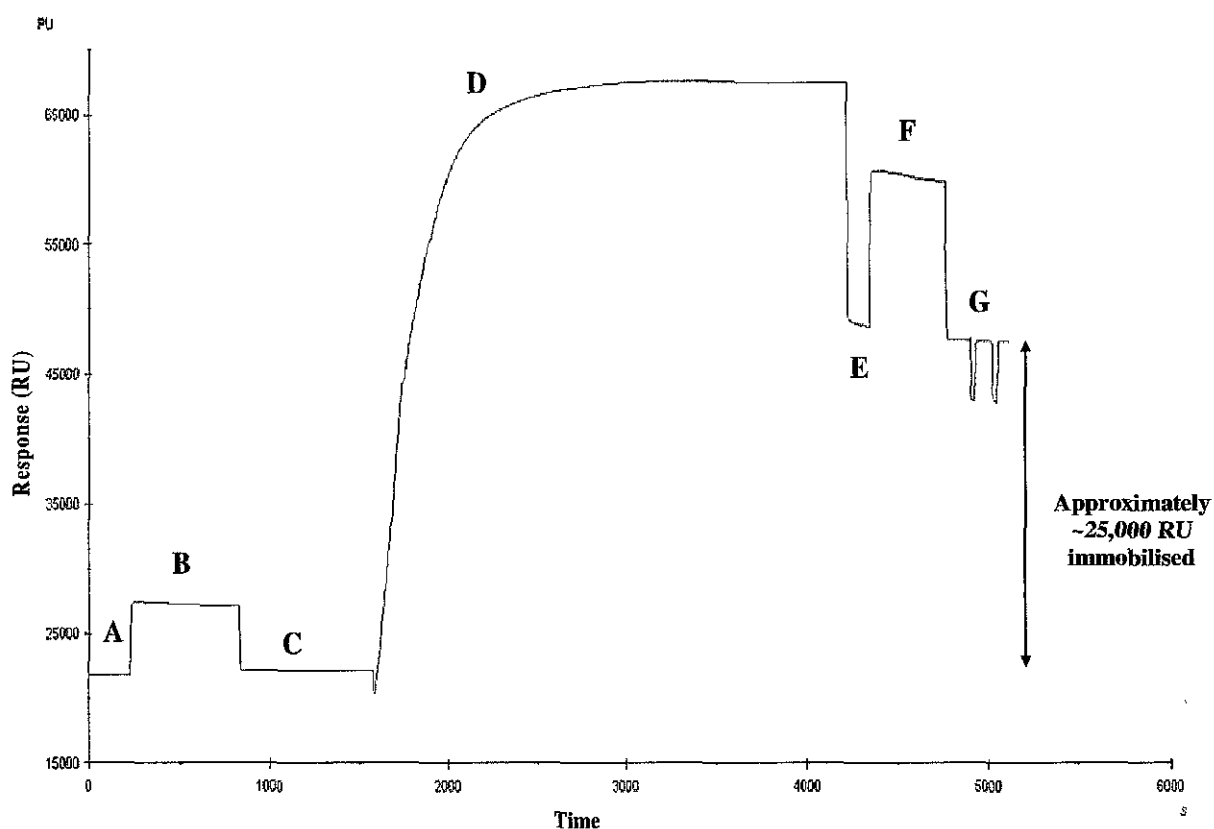


Figure 3.32 Typical immobilisation of neutravidin onto a CM-dextran chip surface. (A) HBS buffer is passed over the chip surface and the baseline response is recorded. (B) The CM-dextran surface is activated with an equal volume of 100mM NHS and 400mM EDC, which causes an increase in SPR signal due to a bulk refractive index change. (C) HBS buffer is passed over the surface again, post-activation and the baseline response measured. (D) Neutravidin (50 μ g/ml) diluted in 10mM sodium acetate buffer, pH 4.6, is passed over the surface for 40 minutes, a large increase in SPR signal is observed as the bulk refractive index changes. (E) HBS buffer is passed over the surface and the amount of bound neutravidin recorded. (F) The surface is deactivated or 'capped' using IM ethanolamine hydrochloride, pH 8.5, which removes non-covalently bound neutravidin and blocks any remaining NHS esters. (G) The surface is regenerated with two 30 second pulses of 5mM NaOH, to ensure all immobilised neutravidin is bound covalently, before a measurement of total immobilised neutravidin is recorded. Approximately 25,000 response units (RU) of neutravidin were bound to the sensor chip surface post immobilisation.

The biotinylated InIB F3 protein fragment, diluted in HBS buffer to a concentration of 60µg/ml was manually injected over the surface for six minutes, at flow rate of 5µl/min. Approximately 450 RU of biotinylated F3 was immobilised on the surface. Although the affinity between neutravidin and biotin is strong (Green, 1965), dissociation of the biotinylated fragment occurred as soon as HBS buffer solution was passed over the surface. This was possibly due to the efficiency of the *in vivo* biotinylation process. Theoretically, *in vivo* biotinylation of recombinant proteins using the pAC4 vector system should be up to 90% efficient (Tatsumi *et al.*, 1996), however, this is difficult to control. Further optimisation of growth and expression conditions would be required to ensure maximum potential biotinylation of the cloned protein. Therefore an alternative strategy for stabilisation of the surface was investigated.

The immobilised biotinylated F3 protein fragment was subjected to a 30s pulse of 400mM EDC/100mM NHS at a flow rate of 5µl/min, to stabilise the biotinylated protein on the surface (Karlsson *et al.*, 2000; Markgren *et al.*, 2001). This treatment activates the carboxyl groups in the protein, whereby subsequent reaction with primary amines (also in the protein) results in intra- and intermolecular cross-links. Intermolecularly cross-linking monomers that were not covalently fixed to the matrix, therefore, enhances the stability of the surface, whereby the chemically modified surface showed an almost constant baseline level and improved binding capacity. Initial experiments post-crosslinking showed that the biotinylated fragment became tightly bound to neutravidin surface and was not dissociated even upon washing with buffer for several hours (not shown). The surface was then regenerated with a 30s pulse of 5mM NaOH to ensure all immobilised biotinylated F3, cross-linked with EDC/NHS stayed on the surface, before a measurement of total immobilised biotinylated F3 was recorded. Approximately 900 response units (RU) of cross-linked biotinylated F3 were bound to the sensor chip. Figure 3.33 shows the manual injection and stabilisation of the biotinylated fragment with EDC/NHS.

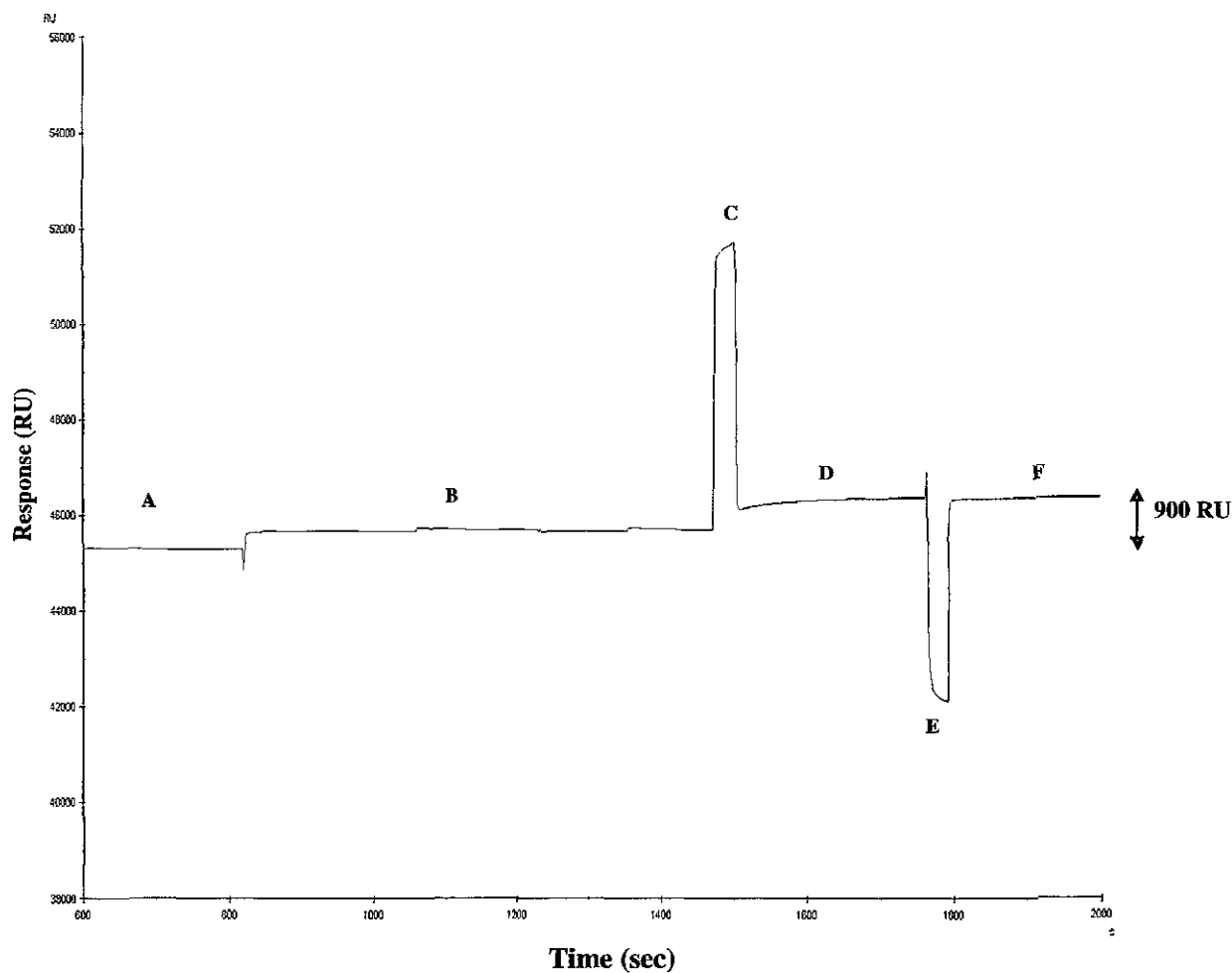


Figure 3.33 Immobilisation of biotinylated F3 protein onto neutravidin surface and subsequent cross-linking using EDC/NHS. (A) HBS buffer is passed over the chip surface and the baseline response is recorded. (B) A manual injection of *in vivo* biotinylated InlB F3 protein is passed over the surface for 7 minutes. (C) The biotinylated F3 protein is stabilised on the surface with 30 second pulse of 400mM EDC/100mM NHS, which causes an increase in SPR signal due to a bulk refractive index change.(D) HBS buffer is passed over the surface again, post cross-linking with EDC/NHS and the baseline response measured (E) The surface is regenerated with a 30 second pulses of 5mM NaOH to ensure all immobilised biotinylated F3 protein is tightly bound, before a measurement of the amount of biotinylated F3 is recorded. (F) Approximately 900 response units (RU) of biotinylated F3 are bound to the sensor chip surface post immobilisation and stabilisation with EDC/NHS.

3.4.2.3.3 Assessment of non-specific binding and regeneration studies

The degree of non-specific binding of the polyclonal anti-InIB antibody to the neutravidin/biotinylated fragment immobilised on the CM5 chip was assessed. This was achieved by passing the polyclonal anti-InIB antibody (diluted 1/20) over the neutravidin surface when both in the presence (flow cell 2) and absence (flow cell 1) of biotinylated F3. Figure 3.34 shows the overlay plots obtained following injection of anti-InIB polyclonal antibody on the neutravidin surfaces with and without biotinylated F3. Injection of the anti-InIB polyclonal antibody over both surface resulted in approximately 300 response units of binding to the neutravidin surface with immobilised biotinylated F3, while negligible binding (< 10 RU) was observed for the neutravidin surface with no biotinylated F3.

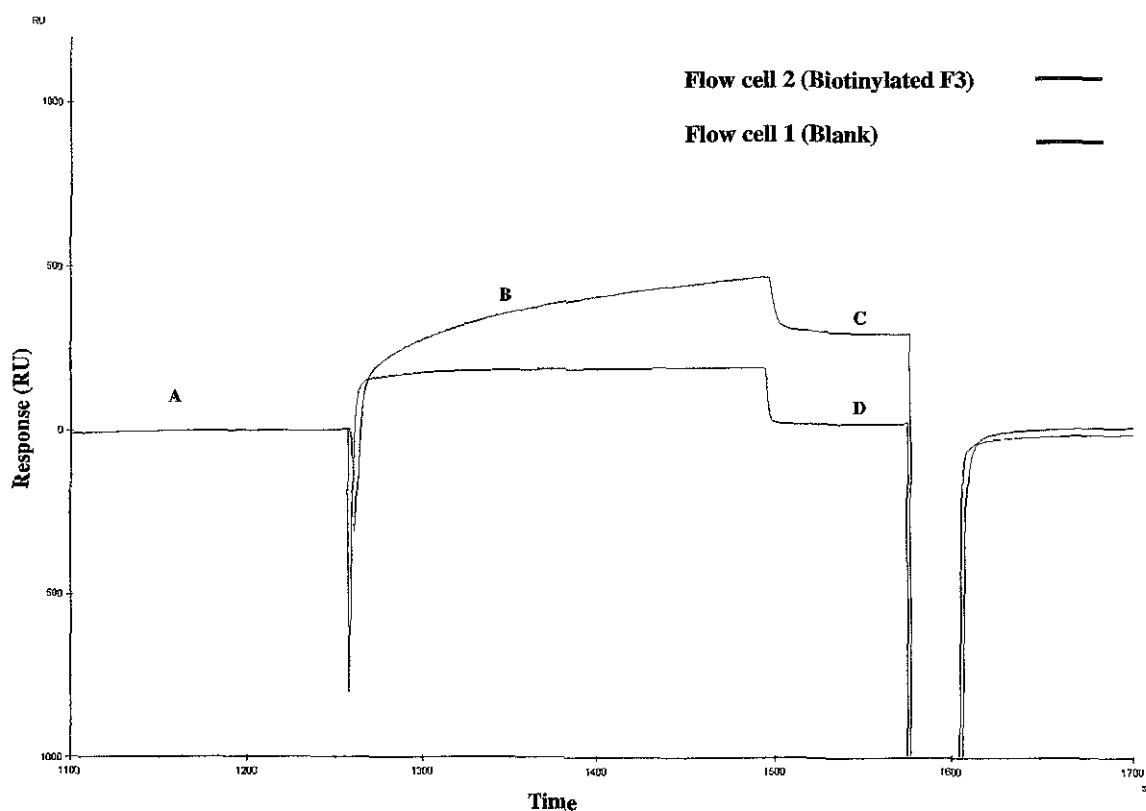


Figure 3.34 Overlay plot showing simultaneous injection of the anti-InIB polyclonal antibody over neutravidin-immobilised surfaces both with and without biotinylated F3 protein. (A) HBS buffer is passed over the chip surface and the baseline response is recorded. (B) A manual injection of anti-InIB polyclonal antibody is passed over both surfaces for 2 minutes. (C) Approximately 300RU of anti-InIB polyclonal antibody was captured on the biotinylated F3 protein surface. (D) Negligible binding was observed for the neutravidin surface containing no biotinylated F3.

Optimisation of the anti-InIB polyclonal antibody dilution and effective regeneration conditions were also investigated. The anti-InIB polyclonal antibody was diluted to 1/20 in HBS buffer and injected over the immobilised neutravidin/biotinylated F3 surface at a flow-rate of 10 μ l/min. Initial studies showed little dissociation of the polyclonal antibody from the immobilised surface. A regeneration solution consisting of 27.5mM NaOH enabled complete removal of the bound polyclonal antibody using a 30 second pulse at a flow-rate of 10 μ l/min. The efficiency of the regeneration process was then evaluated by performing multiple (i.e. 10) binding-regeneration cycles on the chip surface. At this point, stocks of anti-InIB polyclonal antibody were in short supply and so only ten regenerations were performed to demonstrate proof of principle, that the surface could be regenerated effectively. Over the 10 binding-regeneration cycles the antibody binding capacity varied slightly but it did not significantly affect the assay performance. The binding of the anti-InIB polyclonal antibody to the neutravidin/biotinylated F3 surface was highly reproducible, with approximately 300RU of the antibody binding to the surface each time. This indicates that the regeneration solution of 27.5mM NaOH for the anti-InIB polyclonal antibody did not affect antibody binding throughout the regeneration study and was sufficient for complete removal of bound antibody.

Figure 3.35 shows regeneration studies using the polyclonal antibody, diluted 1/20 in HBS running buffer and passed over the surface using a 2 minute pulse at 10 μ l/min. The bound antibody was completely removed using a 30 second pulse of 27.5mM NaOH.

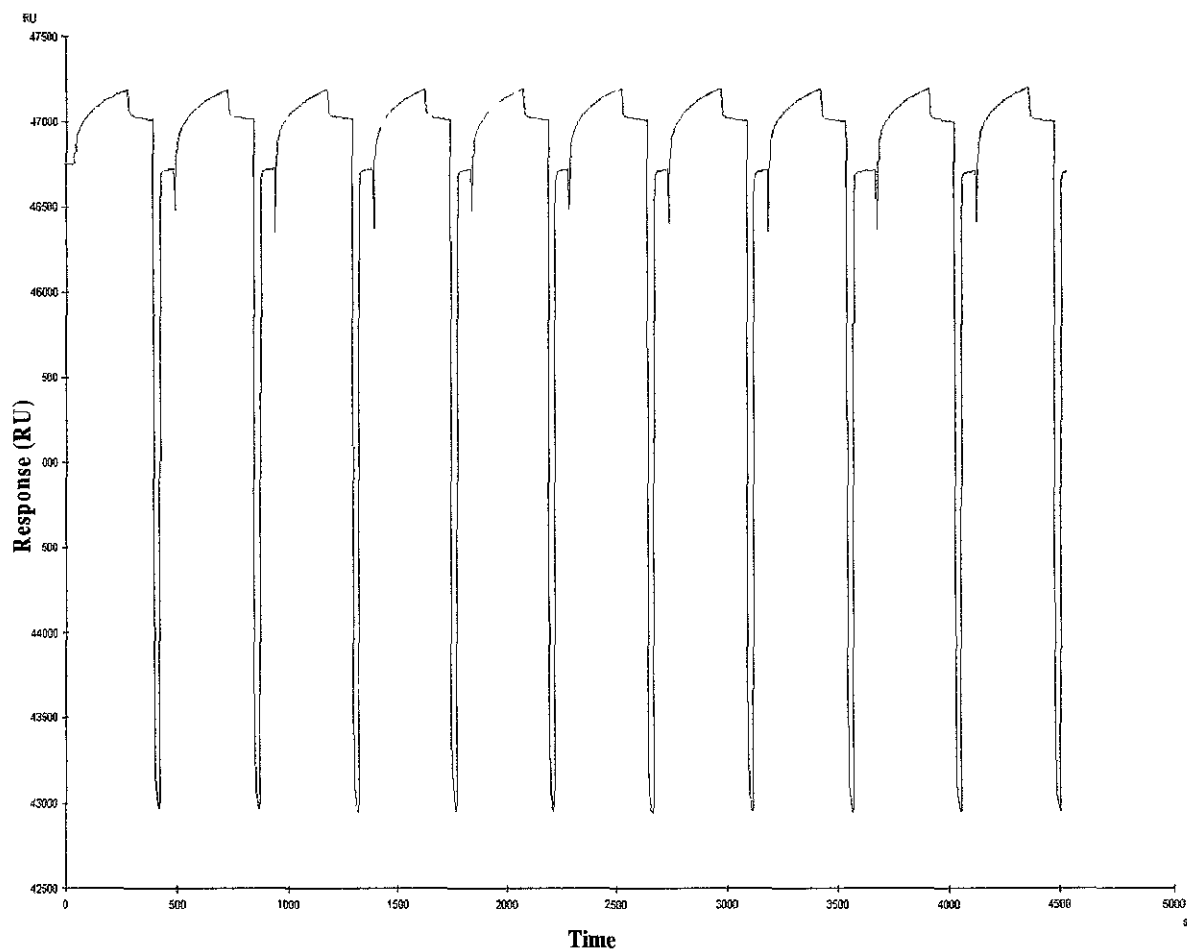


Figure 3.35 *Regeneration studies using the polyclonal antibody, diluted to 1/20 in HBS running buffer and passed over the surface using a 2 minute pulse at 10 μ l/min. The bound antibody was completely removed using a 30 second pulse of 27.5mM NaOH. In order to conserve polyclonal antibody stocks, only 10 regeneration cycles were performed. However 10 cycles were sufficient to highlight that the surface was regenerable with approximately 300 RU of antibody going on and being removed during each cycle.*

3.4.2.3.4 Development of a Biacore inhibition assay for the detection of InlB

Following optimisation of the various assay parameters, a preliminary inhibition assay, incorporating the polyclonal antibody, was developed for the detection of InlB F3 (*Section 2.6.5*). This assay employed neutravidin for the specific and directed immobilisation of *in vivo* biotinylated InlB F3 protein on the CM5 sensor chip. Free (non-biotinylated) InlB F3 standards, ranging in concentration from 0- 1250ng/ml were prepared in HBS. Each free InlB F3 concentration was incubated with an equal volume of the anti-InlB polyclonal antibody diluted 1/10 (to ensure a final dilution of 1/20) and allowed to equilibrate for 30 min at 37°C. The equilibrated samples were then passed over the sensor surface, in random order, and followed by regeneration of the biotinylated F3 sensor surface using 27.5mM NaOH.

Figure 3.36 shows a typical overlay sensorgram showing the antibody binding responses of the polyclonal antibody in the presence of a range of free InlB F3 standards.

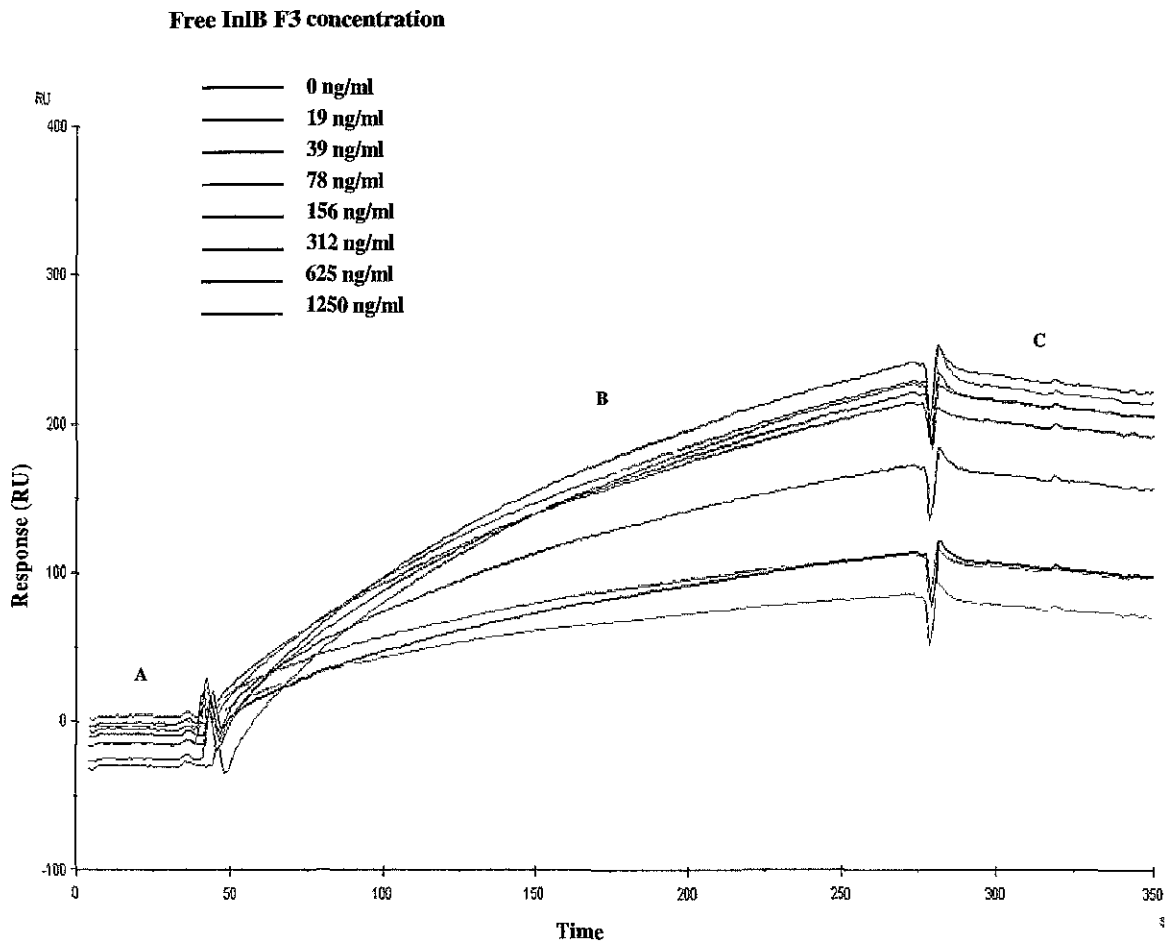


Figure 3.36 Typical overlay sensorgram showing the antibody binding responses of the anti-InlB polyclonal antibody in the presence of a range of free InlB F3 standards. Free InlB F3 dilutions, ranging in concentration from 19 – 1250 ng/ml, were pre-incubated with an equal volume of the anti-InlB polyclonal antibody and passed over the sensor surface. The sensor surface was regenerated using 27.5mM NaOH. (A) The normalised baselines of each sensorgram when HBS is injected over the chip surface. (B) The binding of increased free antibody with decreasing InlB F3 protein concentrations. (C) Baseline shift when buffer is passed over the surface after each injection.

Figure 3.37 shows the use of the *in vivo* biotinylated InlB F3 protein as a capture antigen, for the sensitive detection of InlB in a Biacore-based inhibition assay.

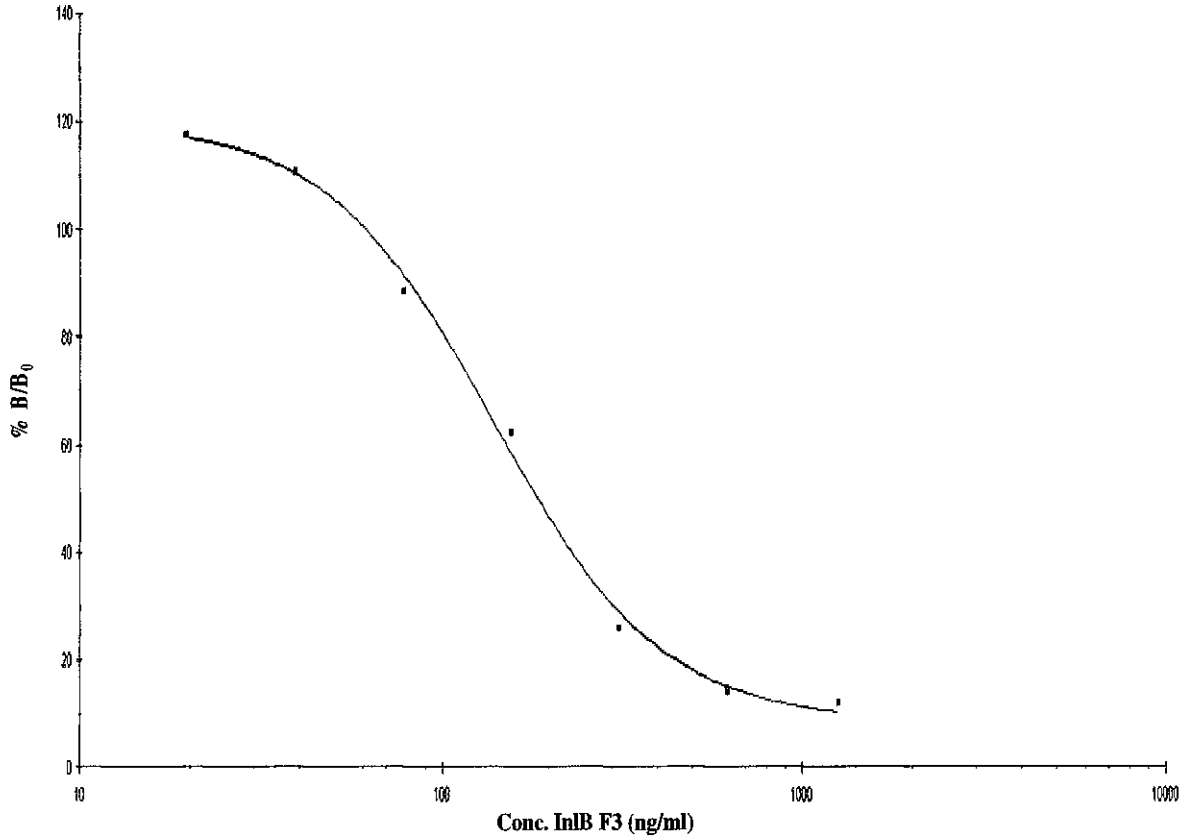


Figure 3.37 Calibration curve for the detection of free InlB F3, using a Biacore-based inhibition assay. Anti-InlB polyclonal antibody was incubated with various InlB F3 concentrations and injected over a neutravidin/biotinylated F3 surface. A 4-parameter equation was fitted to the data set using Biaevaluation 3.1 software. The percentage B/B_0 was determined and plotted against log concentration of free InlB F3. B/B_0 is calculated as the mean response at each antigen concentration (A) minus the mean response at excess antigen (A excess) divided by the mean response determined in the presence of zero antigen (A_0) minus the mean response at excess antigen concentration (A excess). The B/B_0 value is expressed as a percentage to determine the percentage inhibition at each antigen concentration. Each point on the curve is the mean of three replicate measurements and CVs of between 0.48-3.05% were found.

This calibration curve demonstrates a proof of principle concept showing the use of the biotinylated InlB protein fragment as a reagent for further assay development. Unfortunately, this calibration profile is only based on the mean value of three replicates since the stocks of the anti-InlB polyclonal antibody were depleted. Further reproducibility studies would be required for assay validation, possibly with an alternative anti-InlB antibody. However, overall this section demonstrates the potential use of the *in vivo* biotinylated protein as useful tool for the sensitive detection of InlB.

3.5 Optimisation of expression of anti-InIB scFv from naïve human library

An anti-InIB human scFv clone, previously isolated from a naïve phage display library by Dr. Paul Leonard, was made available (Leonard, 2003). The antibody fragment was expressed in a suppressor host strain TG1 *E.coli*. This host strain produces a suppressor tRNA which allows read-through of the amber stop codon located between the scFv and gene 3 sequences of the pCANTAB vector. Suppression of the amber stop codon is only about 20% efficient; therefore, a small amount of soluble antibody is produced in addition to phage-displayed antibodies in this strain. To switch to optimal expression of soluble recombinant antibodies it was necessary to transform the scFv into a non-suppressor strain, namely TOP 10F' *E.coli*. In this strain of *E.coli*, the amber stop codon is recognised and only soluble antibodies are produced, thus allowing optimal expression of antibody for subsequent purification (Barbas *et al.*, 2001).

3.5.1 Expression of anti-InIB scFv in a non-suppressor strain *E. coli*, TOP 10F'

The BMV library is a large non-immunised scFv phage display library developed by Vaughan *et al.* (1996). ScFv fragments were cloned into the phagemid vector pCANTAB6 by Dr. Paul Leonard, which enabled the production of phage-displayed scFv in the presence of helper phage and soluble scFv in the presence of IPTG. A positive clone (G3) from successful rounds of panning against Internalin B was obtained in TG1 *E. coli*. Although the scFv was expressed in these cells, the efficiency was sub-optimal and so electroporation of the plasmid DNA into a non-suppressor strain was performed. A stock of anti-InIB scFv clone G3 in TG1 *E.coli* were streaked out onto LB agar and a single colony from the plate was picked and used to inoculate an overnight culture. The plasmid DNA was purified using a wizard mini-prep kit (*Section 2.2.1*) for subsequent electroporation into competent TOP 10F' *E.coli*. Positive transformants were screened for the scFv insert by performing a double restriction digest with Sfi1/Not1. Figure 3.38 shows an agarose gel of the restricted clone with the scFv band visible at ~800bp.

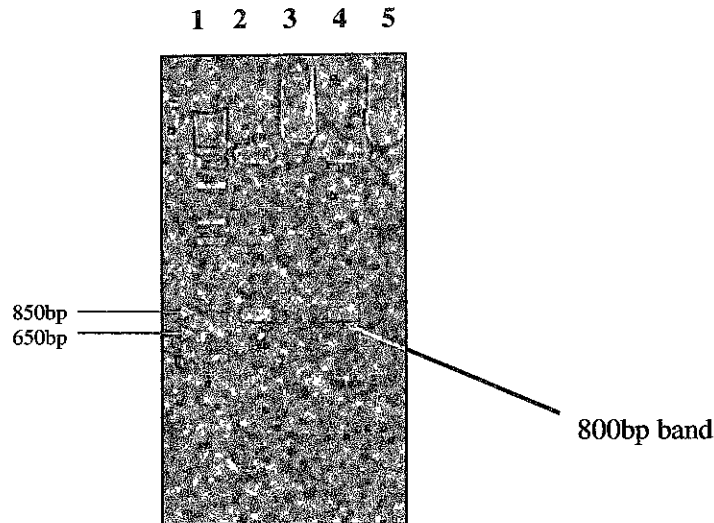


Figure 3.38 Agarose gel showing the *SfiI/NotI* restriction digest of transformed anti-InIB scFv clone G3 in TOP 10F' *E. coli*. Lane (1): DNA Hyperladder; Lanes (2) and (4): Digested anti-InIB G3 clone with ~800bp band confirming the presence of the scFv insert; Lanes (3) and (5): Undigested anti-InIB G3 clone.

Once in the non-suppressor strain, TOP 10F' *E. coli*, the expression conditions of the anti-InIB scFv were subsequently examined to assess what methods produced the maximum expression yield of antibody fragment. Many factors can affect protein expression (*Section 3.1.3*) and so optimisation of growth and expression parameters were investigated. The various parameters assessed included culture media, IPTG concentration, lysis buffer and lysis method. Four different culture media were evaluated, Super broth (SB), Terrific broth (TB), Luria Bertani (LB) and 2xTY (Table 2.3). Each of these media preparations were used to culture eight small scale (5ml) cultures, which were grown as per *Section 2.2.22*, but with the following parameters varied; IPTG concentration: 1mM or 2mM; Lysis buffer: Tris-EDTA sucrose buffer (TES) comprising 200mM Tris-HCl, 0.5M Sucrose, 0.5mM EDTA, pH 8.0 or phosphate buffered saline (PBS) comprising 150mM NaCl, 2.5mM, KCl, 10mM Na₂HPO₄, 18mM KH₂PO₄, pH 7.4; Lysis method: Freeze/Thaw (F/T) or Sonication. Figure 3.39 shows a schematic detailing the parameters investigated for optimal expression of the anti-InIB scFv.

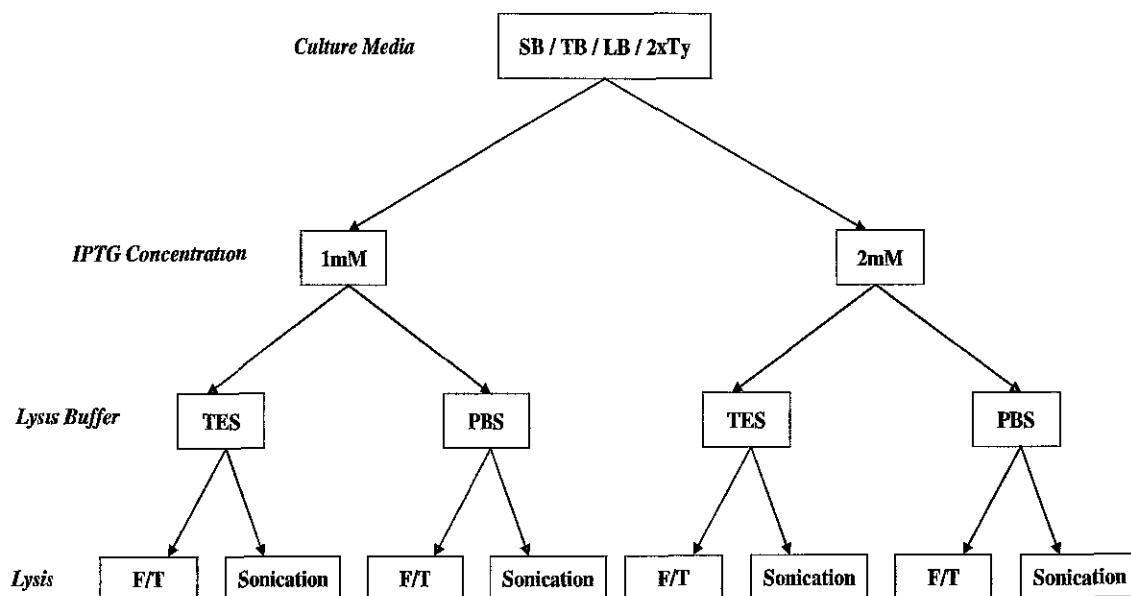


Figure 3.39 Parameters investigated for optimal expression of anti-InIB scFv. A number of expression conditions were varied in several small scale cultures, using four types of culture media; Super Broth (SB), Terrific Broth (TB), Luria Bertani broth (LB) and 2xTY broth; Two IPTG concentration were evaluated: 1mM and 2mM, two lysis buffers were assessed: Tris-EDTA Sucrose (TES) and phosphate buffered saline (PBS) and two lysis methods were investigated: freeze/thaw (F/T) and sonication. Each of the four culture medium were used to prepare eight small-scale cultures in which the above expression conditions were varied as per the matrix shown.

Single colonies of the anti-InIB scFv clone G3 in TOP 10F⁹ *E. coli* were used to inoculate 5ml overnight cultures using the various culture media (SB, TB, LB and 2xTY) under investigation. Different IPTG concentration, lysis buffer and lysis method were investigated for each medium and the results of the expression analysis were assessed by performing a direct ELISA on the lysates from each culture (Section 2.2.23). The results are shown in Figure 3.40.

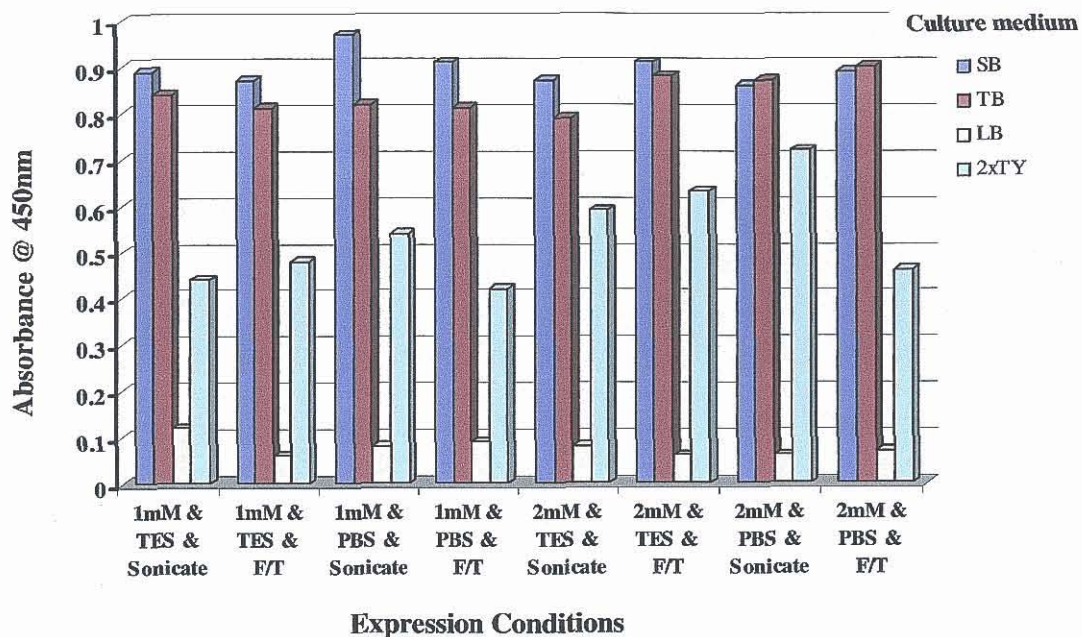


Figure 3.40 Optimisation of expression conditions of anti-InlB scFv. Four culture medium; Super broth (SB), Terrific Broth (TB), Luria Bertani broth (LB) and 2xTY were investigated for optimal antibody expression, while varying the following expression conditions; IPTG concentration, lysis buffer and lysis method, as detailed in figure 3.39. The optimal conditions for expression of the anti-InlB scFv were determined to be culture using Super Broth, induction with IPTG at a concentration of 1mM, use of PBS as lysis buffer and sonication as lysis method. This was determined as the value which gave the highest absorbance at 450nm.

These optimal expression conditions of culture using Super Broth, induction with IPTG at a concentration of 1mM, use of PBS as lysis buffer and sonication as lysis method were used in a large scale expression culture (500ml) for IMAC purification of the anti-InlB scFv.

3.5.2 IMAC purification of anti-InlB scFv

The presence of a His-tag on the anti-InlB scFv, allowed it to be purified using IMAC (Section 2.2.19). SB broth containing the appropriate antibiotics was inoculated with a single colony of TOP 10F' *E. coli* containing the anti-InlB scFv plasmid. The cultures were grown using the optimised growth and induction conditions described in Section 2.2.22. The culture was centrifuged at 3,200 x g for 20 min, the supernatant discarded and the pellet resuspended in 25ml of lysis buffer (PBS) and sonicated for 30s. The lysed cells were then centrifuged at 3,200 x g for 15 min and the supernatant retained for purification by IMAC. Initial purification was sub-optimal and so optimisation of the purification process was undertaken. Figure 3.41 shows the optimised purification gel for the anti-InlB scFv. The main difference between the improved purification method and the original technique is as follows; the pellet from the centrifuged lysate was resuspended in IMAC wash buffer (50mM NaH₂PO₄, 300mM NaCl, 30mM Imidazole, pH 8.0), with a higher imidazole concentration (30mM) and sonicated three times for 30s. This produced a cleaner purified sample, since the higher the concentration of imidazole tolerated by the protein the cleaner the eluant (Barbas *et al.*, 2001). The eluted fraction (Lane 2) shows a concentrated protein band at the predicted molecular weight of 30 kDa with minimal contaminating proteins, left in the sample (Figure 3.41).

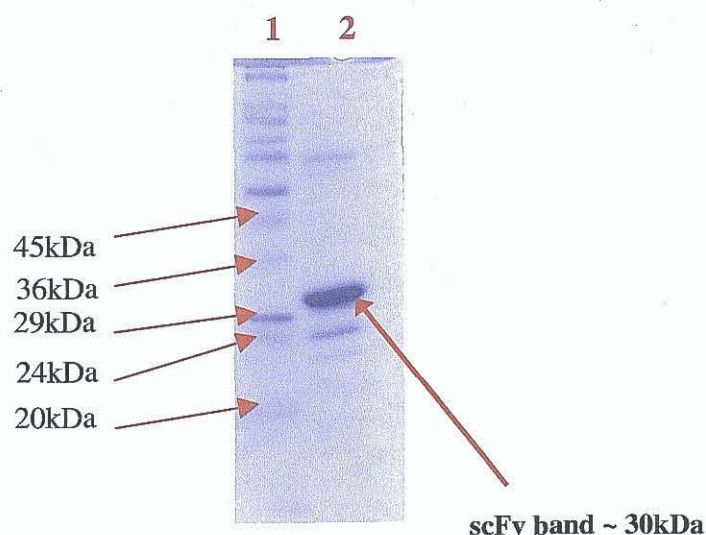


Figure 3.41 SDS-PAGE analysis on an optimised IMAC purification of anti-InlB scFv. Lane (1): Sigma wide-range molecular weight marker; Lane (2): Purified anti-InlB scFv fraction. The elution of the scFv with 250mM imidazole resulted in the presence of a concentrated protein band at the expected molecular weight of ~ 30kDa.

3.6 Discussion

This aim of this chapter was to generate recombinant InlB protein fragments for subsequent use in the development of novel immunoassay formats, using fluorescence and impedance-based detection. The cloning and subsequent high-level expression of InlB-associated proteins, F3, F4 and F5 into two vector systems (Qiagen's pQE-60 for His-tag purification and Avidity's pAC4 for *in vivo* biotinylation) was undertaken.

Firstly, InlB protein fragments F3, F4 and F5 with relative molecular weights (M_R) of 23, 34 and 45 kDa respectively, were derived from Internalin B, a cell surface protein of *L. monocytogenes*, which had been previously cloned and expressed (Leonard, 2003). The InlB recombinant protein was portioned into three shorter overlapping peptide fragments (F3, F4 and F5) to determine the relative location of the epitope for antibody binding, within the full InlB protein (Figure 3.4) using specifically engineered forward and reverse primers. The InlB-specific primers were based on the nucleotide sequence (Accession number AJ01234) of InlB previously submitted to GenBank by Chakraborty and associates (1995). An Nco1 restriction site was engineered into the forward primers and a BamH1 site into the reverse to enable the directional cloning into pQE-60. Since proteins expressed from pQE-60 contain a C-terminal 6xHis tag, the genes were cloned in frame with the 3'-sequence encoding the 6xHis tag. The authentic ATG start codons within the protein sequences were used to initiate protein expression using the optimised Shine-Dalgarno region of the pQE-60.

A standard PCR reaction was then used to amplify the genes encoding the InlB protein fragments F3, F4 and F5. The PCR amplified genes were then directly purified using a commercial kit (Section 2.2.10) which eliminated the need to sub-clone the vector and inserts into a selection system such as the TA cloning kit. Following direct purification of the amplified PCR products, the genes encoding the F3, F4 and F5 fragments (~800, ~950 and ~1090 bps, respectively) were confirmed following a BamH1/Nco1 restriction digest (Figure 3.6). The BamH1/Nco1 restricted genes encoding each fragment were then gel-purified and directionally cloned into the high-level expression vector pQE-60 using T4 DNA ligase (Section 3.2.7). The pQE-60 plasmids containing the cloned inserts were transformed into CaCl₂-competent XL-10 Gold *E. coli*, a fast growing *E. coli* that allows a sufficiently high transformation rate (Section 3.2.8). Following the successful cloning of the F3, F4 and F5 genes into the high-level expression vector pQE-60 the suitability of XL-

10 Gold *E. coli* as a host strain was investigated. Initial small-scale expression cultures were carried out on the F3, F4 and F5 XL-10 Gold *E. coli* clones (Section 3.3) and following protein expression the cell lysates were analysed using SDS-PAGE (Figure 3.7). Strong bands at 23, 34 and 45 kDa respectively for the F3, F4 and F5 clones (as predicted from the EMBL database protein predict tool), confirmed the suitability of XL-10 Gold *E. coli* as a host strain for the expression of the InlB protein fragments from the high-level expression vector pQE-60.

High-level protein expression within *E. coli* host strains can often result in the formation of insoluble aggregated folding intermediates. There are many approaches available for the expression of soluble proteins such as the co-expression of chaperones (Hannig and Makrides, 1998), which assist in protein folding and the use of gene fusions to improve expression levels (Smith and Johnson, 1988; Murby *et al.*, 1996). However, these methods can often be time-consuming. A more simple solution is the solubilisation of inclusion bodies using a strong denaturant such as 8M urea. This method is not without its drawbacks and can often result in non-functional, inactive protein. The functionality of the protein may be restored by removing the denaturant (via a buffer exchange methods such as dialysis or ultracentrifugation), thus isolating the active protein from the inclusion bodies

Solubility determination studies on the recombinant InlB proteins (Figure 3.8) indicated that the high-level expression of F3, F4 and F5 resulted in the formation of insoluble inclusion bodies, which could be solubilised using 8M urea (Lanes 3, 6 and 9, respectively). A web-based bioinformatics program, used to determine the solubility of the recombinant proteins (Harrison, 2000), predicted that the F3, F4 and F5 proteins had a 68%, 72.9% and 73% chance of insolubility, confirming the need for denaturing buffer, containing 8M urea, to ensure high-level recovery of the InlB protein fragments following expression in XL-10 Gold *E. coli*. As described in Section 3.1.1, the expression of recombinant proteins from pQE-60 is under the control of an optimised promoter-operator element consisting of the phage T5 promoter, which is recognised by *E. coli* RNA polymerase, and two *lac* operator sequences, which increase *lac* repressor binding. The *lac*^q gene contained on the F' episome of XL-10 Gold *E. coli* ensures the production of high levels of the *lac* repressor protein and tightly regulates recombinant protein expression. High-level protein expression from pQE-60 is rapidly induced upon addition of

isopropyl- β -D-thiogalactoside (IPTG), which binds to the *lac* repressor protein and inactivates it. However, optimisation of IPTG concentration for induction of the protein fragments was assessed to ensure minimal toxicity to the host cell (Liu^c *et al.*, 1999). Varying IPTG concentrations ranging from 0.01–1mM were investigated. Figures 3.9 show the SDS-PAGE analysis on F3 expression, variations in IPTG concentration did not seem to affect the level of protein expression and so the lowest concentration of 0.1 mM was chosen as optimal (Lane 6). Basal level expression of F3 was visible following “induction” with zero concentration of IPTG (Lane 7).

Recovery of intracellular proteins from each fragment (F3, F4 and F5) involved resuspending the pelleted bacteria in 8M urea denaturing buffer and pulsing the resuspension with sonic waves using a sonicator. Sonication perforates the cell membrane and allows the cell contents to be released. However, over-sonication can be detrimental, leading to co-purification of *E. coli* host proteins (Ausubel *et al.*, 1994) and so the lowest useful sonication time was chosen. This is the sonication time which gave the maximum expressed protein (strongest band on SDS-PAGE gel) in the shortest time. The SDS-PAGE analysis on the optimisation of sonication time for the F3 protein suggested that a 30 second sonication pulse was sufficient for the isolation of protein, from XL-10 Gold *E. coli* (Figure 3.10). The same sonication conditions were investigated for both the F4 and F5 fragments, (figures not shown) with the same results reported, whereby sonication over 30 seconds had a minimal effect on protein expression.

Time course expression cultures were also carried out to determine the optimal induction period, post IPTG addition, for InlB fragment expression. Intracellular protein content is a balance between the amount of soluble protein in the cells, the formation of inclusion bodies and protein degradation. Analysis on the levels of protein expression at hourly intervals post IPTG induction was used to determine the optimal induction time. SDS-PAGE analysis (Figures 3.11-3.13) on the time-course expression cultures for the InlB protein fragments suggested that a 4-hour induction period enabled sufficient levels of protein production. Slightly higher levels of InlB F3, F4 and F5 expression were observed following a 5-hour induction period. However, the 4-hour induction period appeared satisfactory and minimised the risk of potential proteolytic degradation and 6xHis tag cleavage (Makrides, 1996).

The genes encoding the F3, F4 and F5 recombinant proteins were sequenced for comparison with the known nucleotide and amino acid sequences of InlB previously submitted to GenBank. Nucleotide and amino acid sequence alignments were then used to compare the cloned InlB fragments F3, F4 and F5 described in this chapter with the sequences previously submitted to GenBank and the NCBI database. Amino acid sequence analysis on the each fragments showed 100% homology between the cloned F3, F4 and F5 fragments with the full recombinant 60 kDa protein previously identified by Chakraborty *et al.*, (1995), (Accession number AJ01234).

The immunoreactivities of the recombinant proteins were then determined using Western blotting. The recombinant proteins were electrophoresed using SDS-PAGE (Fig. 3.15 A) with the bands representing the expressed F3, F4 and F5 visible at 23, 34 and 45 kDa, respectively. The proteins were then transferred to nitrocellulose for Western blotting. Initially the nitrocellulose was probed with an anti-His antibody to ensure the recombinant proteins were expressed in frame. The presence of the bands at 23, 34 and 45 kDa confirm the proteins were fully expressed in frame with a 6xHis tag (Fig. 3.15 B).

The ability of the recombinant proteins to bind associated anti-InlB antibodies was subsequently examined. Nitrocellulose containing the transferred proteins was probed with three anti-InlB-derived antibodies (polyclonal, monoclonal and scFv). This allowed identification of the relative location of epitopes on the surface of the protein, thus determining antigenic sites (Rao *et al.*, 1996). It can be clearly seen that the antibody-binding region is located in the first 0-248 amino acids of the protein (F3), as the panel of antibodies used to investigate immunoreactivity bind the three fragments and the full protein. This showed that the location of the antibody-binding domain is in the first portion of the recombinant protein, the F3 fragment. This information is useful for further assay development, whereby the first section of the protein containing the 'leucine-rich' repeats with no IgG domain (Schubert *et al.*, 2001; Kobe and Kajava, 2001; Freiberg *et al.*, 2004) is the most immunoreactive portion of the protein, containing all epitopes for antibody binding. This eliminates the need to grow and purify the rest of the recombinant protein as all the antigenic sites are contained within this first section (F3), thus making antigen preparation far simpler.

Since F3 was identified as the most immunoreactive portion of the InlB protein, it was subsequently used for further assay development. The optimised parameters for protein expression were applied for the large-scale production of F3 and the protein was purified using immobilised metal affinity chromatography (IMAC). Figure 3.14 shows the optimised purification of F3, using imidazole elution, whereby high levels of purity were obtained. The concentration of the purified protein was subsequently estimated using a BCA assay (Section 2.2.21). A standard curve was constructed using BSA and concentration values for the purified protein obtained from it. The final concentration of purified F3 was calculated to be 1.5mg/ml.

The recombinant protein fragments (F3, F4 and F5) were also subcloned into another vector system (pAC4) for *in vivo* biotinylation (Schatz, 1993). *In vivo* biotinylation of proteins has been shown to be extremely useful in analysing protein-protein interactions (Tan^a *et al.*, 2004; Krepiy *et al.*, 2006). The pAC4 vector has both a BamHI and NcoI restriction site, thus facilitating easy transfer of InlB protein fragments (F3, F4 and F5) from Qiagens pQE-60 vector into the pAC 4 vector. The InlB inserts (Section 3.4.1.2) with the genes encoding the F3, F4 and F5 fragments (~800, ~950 and ~1090 bps, respectively) were directionally cloned into the pAC4 expression vector for *in vivo* biotinylation, using T4 DNA ligase (Section 3.2.7) and subsequently transformed into electrocompetent AVB101 *E. coli*, (Section 2.3.3). Positive clones were screened by picking single colonies from transformation plate, for growth and induction (Section 2.3.4). High-level recombinant protein expression was induced upon addition of 1mM IPTG and 100µM biotin and the resulting pellets washed with PBS to remove any free biotin.

Characterisation of the *in vivo* biotinylated InlB protein fragments cloned from the pAC4 vector system was undertaken using traditional immunochemical techniques, SDS-PAGE and Western blotting, prior to purification via affinity chromatography, using immobilised monomeric avidin. The recombinant proteins were electrophoresed using SDS-PAGE (Fig. 3.24 A) and the proteins transferred to nitrocellulose for Western blotting. The nitrocellulose was probed with an anti-biotin antibody to confirm the presence of the biotin AviTag. The presence of the bands at 23, 34 and 45 kDa confirm the proteins were fully expressed in frame with the biotin AviTag (Fig. 3.24 B). The *in vivo* biotinylated InlB protein fragments cloned from the pAC4 vector were purified using affinity chromatography and characterised using both fluorescence-based and Biacore-based

methods This highlighted the potential use of these cloned InlB proteins as novel reagents for enhanced assay development.

The *in vivo* biotinylated fragments were investigated using direct binding assay with an anti-InlB polyclonal antibody. Both extravidin-peroxidase and streptavidin-Cy5 were used to detect the amount of *in vivo* biotinylated protein bound to immobilised anti-InlB antibody (Figures 3.36-3.38). The F3 fragment gave the most sensitive response, which indicated that the *in vivo* biotinylation efficiency of the F3 fragment was superior to both the F4 and F5 fragments. Demonstration that the biotinylated fragment F3 could be successfully traced with three different avidin-linked fluorescent labels was also shown. This highlights the potential use of the *in vivo* biotinylated fragment as a reagent for future fluorescence-based immunoassay development. Biacore-based methods (Section 4.1.3.2) were also used for the characterisation of *in vivo* biotinylated InlB F3. The biotinylated F3 fragment was used as the capture antigen for the preliminary development of a Biacore inhibition assay for detection of InlB F3, using the anti-InlB polyclonal antibody. A range of detection of between 19-1250 ng/ml was derived and CVs of between 0.48-3.05% were found. However, as stocks of the anti-InlB polyclonal antibody were depleted, the preliminary assay was only based on three replicates and as such, could only demonstrate a proof of principle concept. However, it did demonstrate the potential use of the biotinylated InlB protein fragment as a reagent for further assay development for the sensitive detection of InlB.

Overall, the cloning, expression and purification of the F3, F4 and F5 gene sequences in *E. coli* using the two strategies described in this chapter, showed a safe and reliable method for the production of InlB-derived recombinant protein fragments. Following optimisation of the various parameters required for high-level protein expression the recombinant proteins were purified using IMAC and monomeric avidin affinity chromatography. The ability of the proteins to recognise InlB-associated antibodies was confirmed using SDS-PAGE, Western blotting, fluorescence-based immunoassay and Biacore methods. The recombinant proteins described in this chapter are important for the development of novel immunoassays for the detection of InlB using both fluorescence and impedance-based technology (Chapters 4 and 5).

**Chapter 4: Evaluation of novel fluorescent
labels and assay formats for antigen detection**

4.1 Introduction

Sensors based on optical phenomena are widely used for the sensitive detection of biological molecules (Luppa *et al.*, 2001). This is mainly due to the advantages of applying visible radiation which include a non-destructive operation mode, rapid signal generation and high levels of accuracy for clinical applications (Aizawa, 1994). Changes in optical phenomena such as adsorption, fluorescence, luminescence, scatter or refractive index (RI) can occur when light is reflected at sensing surfaces and these changes form the physical basis for optical sensor technology. The light coming from a source can be either transmitted through or reflected back from the sample via optical waveguides, which direct the light to a suitable detector (Eggins, 1996). Photodiodes or photomultipliers are generally used as the detectors in such systems and optical filters are available for applications where specific wavelengths are to be monitored (Wolfbeis, 1993). The main operational principles for optical biosensors include absorption and reflection spectroscopy, including surface plasmon resonance and luminescence-based detection, including chemiluminescence, fluorescence and phosphorescence (Buerk, 1993).

4.1.1 Absorption & Reflection Spectroscopy

Absorption spectroscopy refers to the interaction of electromagnetic radiation with matter. It is used to characterise the intensity of transmitted light through a uniform medium as a function of the incident light, when the optical properties are affected by chemical concentration (Buerk, 1993). A spectrum of light will be absorbed at a particular wavelength, which is distinct for each chemical species. This is due to the fact that they absorb energy at different wavelengths since differing chemical bonds experience differing vibrational and rotational movements; therefore variations in light absorption occur for each molecule. Absorption spectroscopy can be affected by light scattering, disturbances from external light sources and non-uniform optical properties in a chemical species, all of which make acquisition of a specific absorption peak difficult. However, this method is a useful optical tool for the analysis of biological molecules such as protein or DNA, both of which have known absorption peaks at 260nm and 280nm, respectively. Reflection spectroscopy on the other hand measures light reflected back from the surface where changes in the intensity of the reflected light represent both the physical and chemical events occurring in the medium. Light transmitted through an optical fibre penetrates into the surface material to depth that is dependent on the difference in refractive index of the material.

4.1.2 Luminescence

Luminescence can be defined as the emission of light from atoms or molecules as a result of a transition from an electronically excited state to a lower energy state (Lackowicz, 1999). Luminescence-based detection encompasses three basic phenomena; fluorescence, phosphorescence and chemiluminescence. The principles of fluorescence and phosphorescence-based detection have already been discussed in detail (*Section 1.5.1*). Chemiluminescence occurs by the oxidation of a substance to produce visible light in the absence of any exciting illumination and without the emission of heat. No external source of light is required to initiate the reaction and the whole sample is involved. Luminol is one of the best known chemiluminescent species and is used extensively in immunoassay techniques (Dotsikas and Loukas, 2004) where it reacts with oxygen, hydrogen peroxide or peroxidase. When luminol reacts with these molecules, a chemical reaction occurs producing an excited state and the decay of this excited state to a lower energy level is responsible for the emission of light. In theory, one photon of light should be produced for each molecule of reactant, but in actual practice, non-enzymatic reactions seldom exceed 1% quantum efficiency (Eggins, 1996). The key difference between chemiluminescence and fluorescence or phosphorescence is that no radiation is absorbed. The energy required to emit light comes from the energetics of the chemical reaction. Chemiluminescent-based detection has been used extensively in biosensor technology for the detection of various analytes (Ji *et al.*, 2006; Liu *et al.*, 2007; Luo *et al.*, 2007).

4.1.3 Optical-based detection

4.1.3.1 Optical wave guides

Optical fibres are waveguides for light, in that light waves are propagated along the fibre by total internal reflection (TIR). Total internal reflection depends on the angle of incidence and the refractive indices of the media. Waveguides can be either extrinsic or intrinsic. Extrinsic waveguides transmit light from a light source to a light collector. In the intrinsic mode, the phase polarisation and intensity of the light are modulated within the waveguide by a measurand lying within the penetration depth for the evanescent field adjacent to the guide (Eggins, 1996). Optical waveguides can be glass, quartz, polymer film or fibers made of high refractive index (RI) material embedded between lower index dielectric materials. Excitation light travelling through an optical waveguide is confined by total internal reflection at the interface, defined by the waveguide surface. TIR occurs only under a particular set of conditions and is dependent on many factors, including the

wavelength, incidence angle, and the relative refractive indices of the waveguide and the surrounding medium (Kumar *et al.*, 1994). The surrounding medium has to be of a lower refractive index than the waveguide in order to achieve TIR. Optical waveguides operate when an evanescent field develops at the sensor's surface, generated by the excitation of the light itself in the dielectric layer. Laser light is transmitted into the device and when it encounters a biomolecule immobilised on the surface, multiple reflections occur. Some of the light, however, penetrates the biolayer and as this light is reflected back into the waveguide, a shift in phase occurs that interferes with the transmitted light. Thus, any changes occurring at the biomolecule interface (such as during immunocomplex formation) can be detected by monitoring the changes in interference (Székács *et al.*, 2003; Wu *et al.*, 2006).

4.1.3.2 Surface Plasmon Resonance

SPR is a sensing technique that can be used to monitor 'real-time biospecific reactions'. Refractive index (RI) changes occurring in close proximity to a thin metal surface at the interface between a glass sensor surface (high refractive index) and a buffer (low refractive index) are detected via an evanescent field generated at the site of total internal reflection (Homola *et al.*, 1999). The evanescent field penetrates the metal film, with exponentially decreasing amplitude from the metal-sensor interface and surface plasmons oscillate and propagate along the surface of the metal film (Mullett *et al.*, 2000). Surface plasmons absorb some of the light energy from this evanescent field, thus changing the TIR light intensity. The resonance angle at which this intensity minimum occurs is a function of the refractive index of the solution close to the metal layer on the opposing face of the sensor surface. Surface plasmon resonance (SPR) occurs in the visible region in free electron-like metals such as silver and gold, when the thickness of the metal film is a fraction of the wavelength. Changes in the optical properties of this region will, therefore, influence the SPR angle, which is the basis of the SPR technology for biosensing purposes (Liedberg *et al.*, 1995). The general principle of SPR measurement is depicted in Figure 4.1. SPR biosensors allow direct monitoring of the biospecific interactions taking place at sensor surfaces. They do this by measuring changes in the intensity and the resonance angle of reflected light, caused by the alterations in RI at the surface interface.

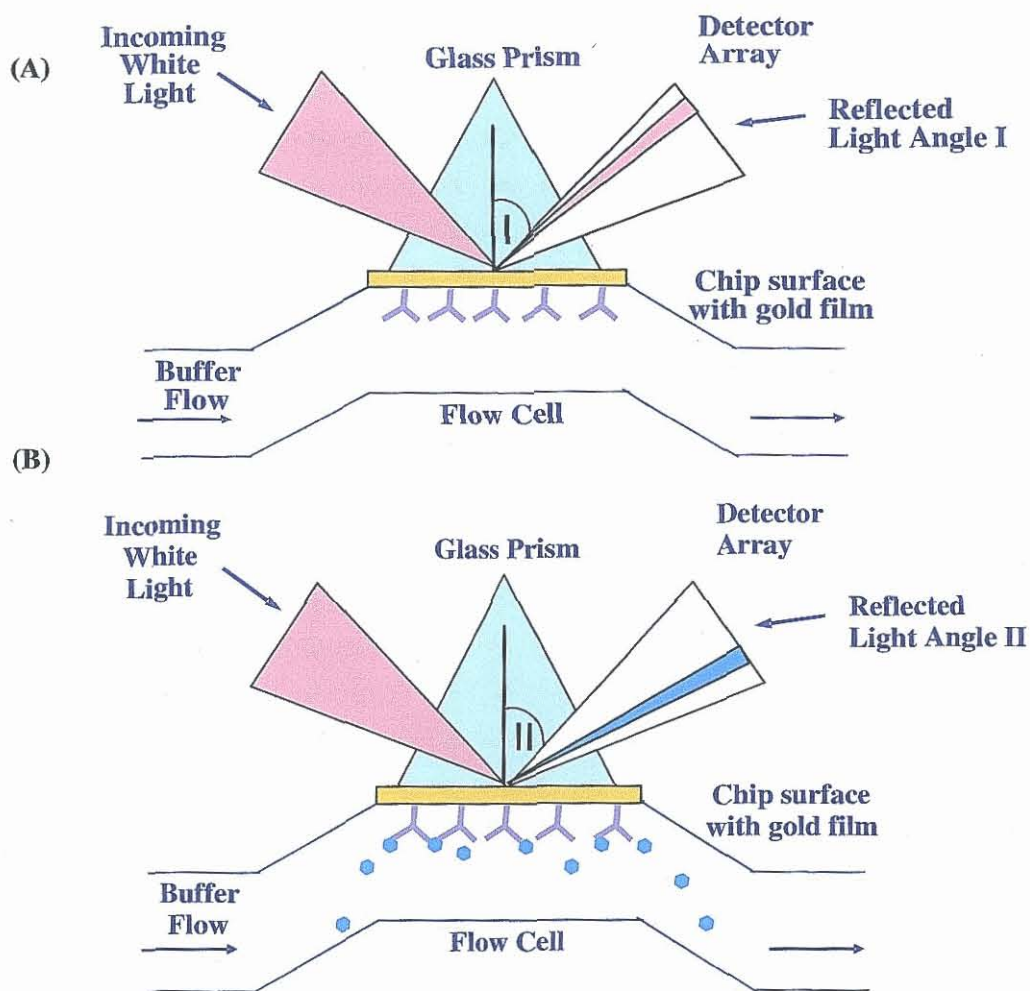


Figure 4.1 Schematic showing principle of operation of a surface plasmon resonance-based biosensor. Monochromatic *p*-polarised light is focused onto a metal thin film surface immobilised with a biological sample (antibody), via a glass prism under conditions of total internal reflection (TIR). (A) As buffer is passed over the surface, the dip in reflected light intensity is recorded (shown in pink) at reflected light angle I. (B) On introduction of antigen, a subsequent binding event occurs which changes the optical properties of the system. Changes in the refractive index at the interface between the surface and a solution flowing over the surface (buffer containing corresponding antigen), alter the angle at which reduced-intensity polarized light is reflected from the supporting glass plane (shown in blue) at reflected light angle II. The changes in angle are caused by association or dissociation of molecules from the sensor surface and are, therefore, proportional to the mass of bound material (Anonymous, 2007).

4.1.3.3 Applications of optical-based detection

There are many applications of optical sensors in clinical chemistry and diagnosis (Cullum and Vo-Dinh, 2000; Alivisatos, 2004; Goldman *et al.*, 2004; Medintz *et al.*, 2005). Optical immunosensors utilise both labelled and label-free technologies. The optical detection of the immunological reactions using labelled immunospecies has been described by many authors (O’Riordan *et al.*, 2002; Sutherland, 2002; Lochner *et al.*, 2003; Tully *et al.*, 2006). Labels can be fluorescent but enzymatic, biological and chemiluminescence species are also utilised (Nimeri *et al.*, 1994; Matz *et al.*, 1999).

Rowe^b *et al.* (1999) describe the use of an array biosensor employing labelled antibodies coupled to a glass chip, for the simultaneous detection of bacterial, viral and protein analytes. The array biosensor utilises evanescent wave excitation to interrogate patterns of fluorescently-labelled antibodies, immobilised on planar waveguides. This system detects and measures analytes in buffer and in a number of physiological fluids and is relatively unaffected by non-specifically bound components from complex samples. Optical detection via a thermoelectrically cooled CCD camera captures the fluorescent signal from bound analytes upon excitation with a laser diode.

While labelled antibodies and antigens give rise to highly specific and sensitive results, improvement in optical transduction and associated technologies can enhance collected signals. Stranik *et al.* (2005) describe the use of a chip-based sensor employing metallic nanoparticles in conjunction with fluorescently-labelled antibodies for the detection of bovine serum albumin (BSA). A plasmonic enhancement effect is reported whereby the presence of metallic particles in the vicinity of a fluorophore dramatically alters the fluorescence emission and absorption properties of the fluorescent dye. The effect, which is associated with the surface plasmon resonance of the metallic surface, depends on parameters such as metal type, particle size, fluorophore type, and fluorophore-particle separation and is a useful tool for the optical detection of biologically important analytes, in this case BSA.

Label-free optical methods are also widely used in biosensors and a number of sensitive systems exist (Wei *et al.*, 2003; Muller-Renaud *et al.*, 2004; Mauriz *et al.*, 2007). Label-free evanescent wave-related sensors represent a valuable alternative to traditional solid-phase immunoassay technology (Huang *et al.*, 2006) and surface plasmon resonance (SPR) can also be employed for the immunosensing of biomolecules (Leonard, 2003 and Leonard *et al.*, 2005). However, label-free systems are often prone to non-specific binding effects and poor analytical sensitivity to analytes with low molecular weight (Berger *et al.*, 1998) is also common. The problem of non-specific binding is also a major issue, however; this can be reduced by applying a reference sensing region to the label-free optical sensor; the Biacore™ system (Biacore AB, Uppsala, Sweden) allows users to use a flow cell as reference cell. Subtraction of the sample response from the reference cell response allows deduction of a true signal; therefore, the effects of non-specific binding are corrected for.

Biosensors are used for the analysis of complex fluids and, in recent years, the fabrication of biosensors able to distinguish multiple analytes in a single sample has become an increasingly well recognised research goal (Ekins and Chu, 1993). Several research groups have described advances in multianalyte sensor arrays using optical methods (Bakaltcheva *et al.*, 1998). The types of optical devices fabricated for interrogation of such arrays varies depending on the type of molecule attached to the sensor surface and the mode of immobilisation. Instruments for the analysis of small biological elements (nucleotides, amino acids, RNA) can be based on total internal reflection fluorescence and confocal microscopy, where high resolution and pattern recognition are key elements (Sapsford *et al.*, 2002; Zhang *et al.*, 2006;). The approach taken for the detection of larger molecules such as antibodies or longer nucleic acid strands (Wadkins *et al.*, 1998; Blawas and Reichert, 1998; Charles *et al.*, 2004) is significantly different. These molecules are involved in highly specific binding interactions, whereby a detection event at a single spot is sufficient for identification. The central element for antibody-based optical sensor systems is planar optical waveguides. Waveguides are used to direct excitation light to biomolecule-linked fluorophores bound to the waveguide surface (Rowe^a *et al.*, 1999) and form the basis of the chip-based immunosensors described in this research.

4.1.4 Chapter Outline

This chapter focuses on the development of enhanced detection strategies using luminescence-based methods for the quantification of a number of important targets. The incorporation of novel antigens (Chapter 3) and fluorescent labels (with improved optical properties) into fluorescence-based systems with enhanced detection capabilities is shown. The combination of such technologies highlights the potential use of novel labels in the development of better detection systems with greatly increased sensitivities. The detection of warfarin, listerial proteins, human IgG and whole *Listeria* cells is described.

The use of novel fluorescent labels with superior optical properties in solid-phase plate-based immunoassays, polymer chip-based systems and for the immunostaining of bacterial cells, on modified glass surfaces is shown. Antibodies, coupled to fluorescent-tracer molecules (phosphorescent porphyrin labels and quantum dots) via streptavidin-biotin attachment, were assessed in plate-based formats for the detection of warfarin and Internalin B. The synthesis and characterisation of ruthenium dye-doped high-brightness nanoparticles was also explored and use of such particles for the detection of human IgG examined. The assays described in this chapter highlight the potential use of novel labels in the development of improved fluorescence-based strategies for the detection of important analytes. Optimisation of assay parameters and comparison of assay sensitivities and limits of detection with current techniques are discussed. Polymer chip-based strategies for the detection of InlB and the parvovirus capsid protein, VP2 were also investigated using a CCD set-up. The immobilisation and subsequent detection of biomolecules on modified polymer chips was explored and the potential use of such biochips with enhanced labels discussed.

The incorporation of immunoreagents with better specificity for antibody-antigen recognition coupled with novel fluorescent labels into detection systems with enhanced signal capturing properties (biochips with cone structures) facilitates the improved detection of target analytes. In this chapter, the potential use of such formats is discussed and associated obstacles examined.

4.2 Fluorescence immunoassay (FIA) development

There are a number of important parameters that must be investigated for successful fluorescence-based immunoassay development. These are the choice of analyte, choice of label, conjugation strategy, assay format and detection system. The chosen targets *Listeria monocytogenes* cell surface protein Internalin B, warfarin and Parvovirus B19 are all of commercial and clinical significance. Antibodies directed against these targets had been produced and fully characterised by ELISA and Biacore-based assays, prior to this research (Fitzpatrick and O’Kennedy, 2004; Leonard *et al.*, 2005; Hearty *et al.*, 2006; Tully *et al.*, 2006). In this chapter the use of quantum dots and porphyrin-derivatives in the development of novel assays for the detection of the target analytes previously listed is described.

The main advantages of novel fluorescent probes such as quantum dots are their narrow predictable emission, extreme photostability, multiple tunable colours, brightness, broad excitation, large Stokes shift and high quantum yields (West and Halas, 2000). Functionalisation of the polymer shell of such molecules is relatively simple and allows direct coupling of the label to biomolecules. In the case of quantum dots, the polymer shell is directly coupled to streptavidin through a carbodiimide-mediated covalent reaction. The commercially available streptavidin-conjugated quantum dots used in this research emit brightly at 605nm and can be excited with a broad range of sources.

The selected porphyrin dyes used here, emit strong phosphorescence at room temperatures, which is characterised by long lifetimes in the sub-millisecond range and long-wave spectral characteristics (Martsev *et al.*, 1995). These features make the dyes useful as probes for a number of bioanalytical applications since they can provide high sensitivity and selectivity, together with easy detection using a simple instrumental set-up. Novel derivatives of platinum and palladium coproporphyrin were used to make phosphorescent conjugates of antibodies, avidin, biotin and neutravidin (O’Riordan *et al.*, 2001). These labels and conjugates have previously been evaluated in solid phase immunoassays using commercial phosphorescent detectors. Successful use of these probes was reported for a number of plate-based assays formats (Papkovsky, 1991). A simple conjugation procedure was used for labelling biomolecules such as neutravidin or antibodies with this dye. A carbodiimide preactivates the porphyrin dye (platinum or palladium coproporphyrin) in organic solvent in the presence of N-hydroxysuccinimide.

Proteins are subsequently conjugated to the porphyrin derivative via their amino groups (O’Riordan *et al.*, 2001).

Initially direct binding assays were performed to investigate label sensitivities and fluorescence signal to noise ratios, whereby coating concentration, blocking solution, antibody dilution and label dilution were optimised. Competitive immunoassays for the detection of InlB using both an anti-InlB polyclonal antibody and an anti-InlB scFv were developed. Competitive immunoassays for the detection of warfarin using an anti-warfarin monoclonal antibody were also investigated using quantum dots and porphyrin dye as the fluorescent tracer molecules.

Dye-doped nanoparticles were prepared and optimisation of the conjugation strategy with antibodies was examined. Silica nanoparticles are easy to modify, either through NHS activation, silanisation or carboxyl modification (Lian *et al.*, 2004). Ruthenium dye-doped nanoparticles were surface-modified for both avidin and antibody attachment. Human IgG was used as the target molecule for the nanoparticle development, described in this chapter. Initially, InlB was chosen as the target molecule, however, the anti-InlB polyclonal antibody was in short supply and so a commercial source (Sigma) of antibody and antigen was selected. This was deemed necessary as large quantities of reagent were required for the optimisation of antibody-nanoparticle conjugation and assay development.

The following sections (*Sections 4.3-4.6*) describe the optimisation and associated problems in the development of fluorescence-based immunoassays for the detection of InlB, warfarin and human IgG, using novel fluorescent labels.

4.2.1 Biotinylation of Antibodies

Biotin is a vitamin, which binds with high affinity to the tetrameric protein avidin (also streptavidin and neutravidin), with a dissociation constant (K_d) in the order of 10^{-15} mol/l (Green 1965; Wilchek and Bayer, 1988). Biotin is a relatively small molecule of 244 daltons and it can be conjugated to proteins without significantly altering the biological activity of the protein, via amino, carboxyl or sulfhydryl groups. A protein can be reacted with several molecules of biotin that, in turn, can each bind a molecule of avidin. This greatly increases the sensitivity of many assay procedures. The highly specific interaction between streptavidin and biotin allows biotin-containing molecules, in this case biotinylated antibodies, to be discretely bound with streptavidin-linked fluorescent conjugates i.e. quantum dots or porphyrin dye. Polyclonal, monoclonal and scFv antibodies were biotinylated (*Section 2.5.2.1*) and subsequently used in association with avidin-linked fluorescent probes.

A long chain analog of biotin, with an extended spacer arm (22.4 Å) to reduce steric hindrances was used to biotinylate the antibodies for this application. Long-chain biotin forms a stable amide bond with primary amines at pH 7-9. The optimal antibody concentration for successful biotinylation was determined to be approximately 1mg/ml and a 10-20 molar excess of biotin was used to promote efficient biotinylation. The HABA/avidin method is used to determine the degree of biotinylation of antibodies and recombinant proteins biotinylated 'in-house'. The method is based on the binding of the dye HABA to avidin and the ability of biotin to displace the dye. The displacement of dye is accompanied by a change in absorbance with a known extinction co-efficient; therefore, the biotin labelling levels can be determined spectrophotometrically (*Section 2.5.2.1*).

4.3 Development of fluorescence-based immunoassays for the detection of InlB

Fluorescence-based immunoassays (FIA) for the detection of InlB a cell surface protein of *Listeria monocytogenes* were developed, using quantum dots and porphyrin dye as fluorescent labels. The F3 fragment of the recombinant InlB protein was used as the antigen for the development of these assays since it was deemed to contain the most immunoreactive portion of the protein (*Section 3.3.7*). InlB-F3 was grown under optimum conditions (*Section 2.2.18*), subsequently purified using immobilised metal affinity chromatography (IMAC) and the concentration of purified protein determined (*Sections 2.2.19 and 2.2.20*)

Rabbit anti-serum containing polyclonal antibodies directed against InlB was obtained from Dr. Paul Leonard and made available for this application. The polyclonal antibodies were initially purified from the rabbit serum using saturated ammonium sulphate precipitation followed by protein G affinity chromatography, (*Sections 2.4.11 and 2.4.1.2*). The purified anti-InlB polyclonal antibody was subsequently biotinylated (*Section 2.5.2.1*), for use in the development of fluorescence-based immunoassays for the detection of free InlB. Extensive characterisation of this antibody was undertaken previously (Leonard, 2003; Leonard *et al.*, 2005; Hearty *et al.*, 2006). However it was necessary to repeat the checkerboard ELISA for the biotinylated anti-InlB polyclonal antibody, using an avidin-conjugated probe (extravidin-peroxidase).

4.3.1 Checkerboard assay to determine optimal antigen coating concentration and biotinylated antibody dilution for assay development

In order to determine the optimal working dilution of the biotinylated antibody and the optimal recombinant InIB-F3 coating concentrations, a checkerboard ELISA was performed (Section 2.4.1.3). Varying concentrations of InIB-F3 ranging from 0 – 40 μ g/ml were coated on a microtitre plate and dilutions of biotinylated antibody from 1/50 to 1/12800 were added to each InIB-F3 concentration. The amount of bound antibody was detected using extravidin peroxidase and the resulting response was measured using a Tecan Safire² plate reader (Figure 4.2).

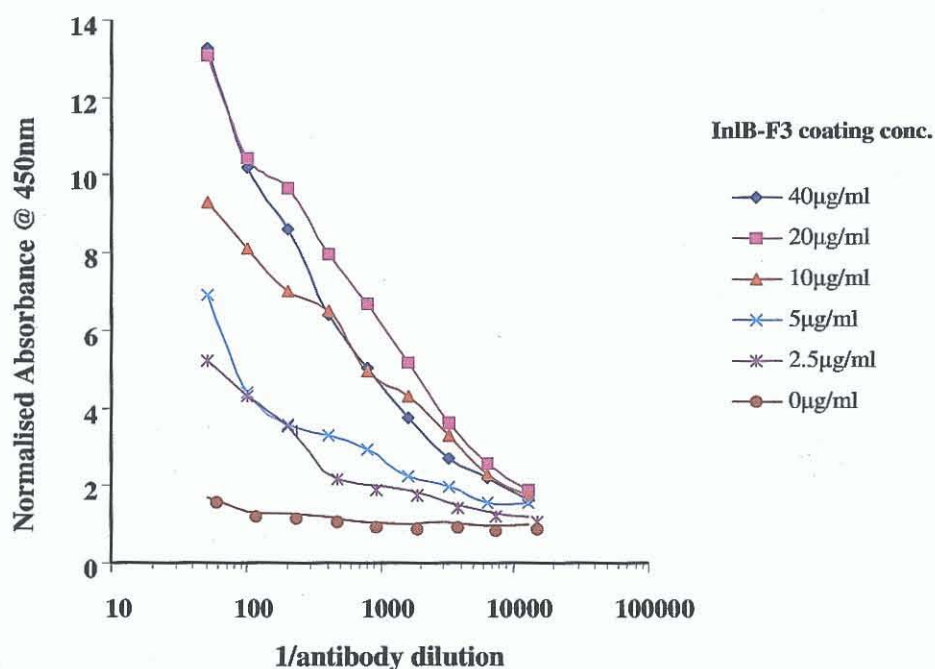


Figure 4.2 Checkerboard ELISA for the determination of optimal InIB-F3 coating concentration and biotinylated antibody dilution for use in a competitive fluorescence-based immunoassay (FIA). Varying InIB-F3 coating concentrations ranging from 0 – 40 μ g/ml and biotinylated antibody dilutions from 1/50 – 1/12800 were assayed and the amount of bound biotinylated antibody was determined using, extravidin peroxidase.

The optimal coating concentration of InIB-F3 was 20 μ g/ml and the optimal biotinylated anti-InIB antibody dilution that gave the greatest change in absorbance per change in antibody dilution was determined to be 1/300.

4.3.2 Optimisation of blocking reagents and diluents

In order to reduce non-specific binding (NSB) a number of blocking solutions were examined. When no protein was coated on the surface, a signal was observed following the addition of varying dilutions of biotinylated antibody. Therefore, it was necessary to optimise the blocking reagent to establish the best solution that kept NSB to a minimum. Casein, glycerol, gelatin, BSA, OVA, Tween 20 and Triton X have been reported as suitable solutions for reducing NSB in immunoassays.

In order to determine the optimal blocking solution for this assay format, varying concentrations of BSA, Tween 20 and glycerol were investigated. Plates were coated with recombinant InlB protein fragment F3 (InlB-F3) at the optimal concentration (20µg/ml) and blocked with the following range of solutions: PBS containing 0.1-2% (w/v) BSA, 0.01-0.5% (w/v) Tween 20 and 10% (v/v) glycerol. Biotinylated antibody*, diluted 300-fold was added to the plate and the fluorescence measured following the addition of streptavidin-Cy5 at a dilution of 1/1000. The fluorescent response was normalised by subtracting the response in the absence of fluorescent tracer molecule (streptavidin-Cy5) from all values. The fluorescence response units (FRU) for each blocking solution were plotted both in the presence and absence of coating antigen (InlB-F3) to evaluate which blocking solution reduced non-specific binding (NSB) of the biotinylated anti-InlB antibody to the plate. The results of blocking solution optimisation are shown in Figure 4.3.

** Optimisation of blocking solution for fluorescence-based immunoassays was initially performed using a biotinylated anti-InlB polyclonal antibody. The optimal blocking solution was determined to be PBS containing 1% (w/v) BSA in this case. The selected blocking solution was subsequently assessed for compatibility with both a biotinylated anti-warfarin monoclonal antibody and warfarin-BSA conjugate and an anti-InlB scFv and InlB-F3, which were also used for fluorescence-based immunoassay development, whereby it was also found to be suitable for use with these alternative antibody-antigen pairs (data not shown).*

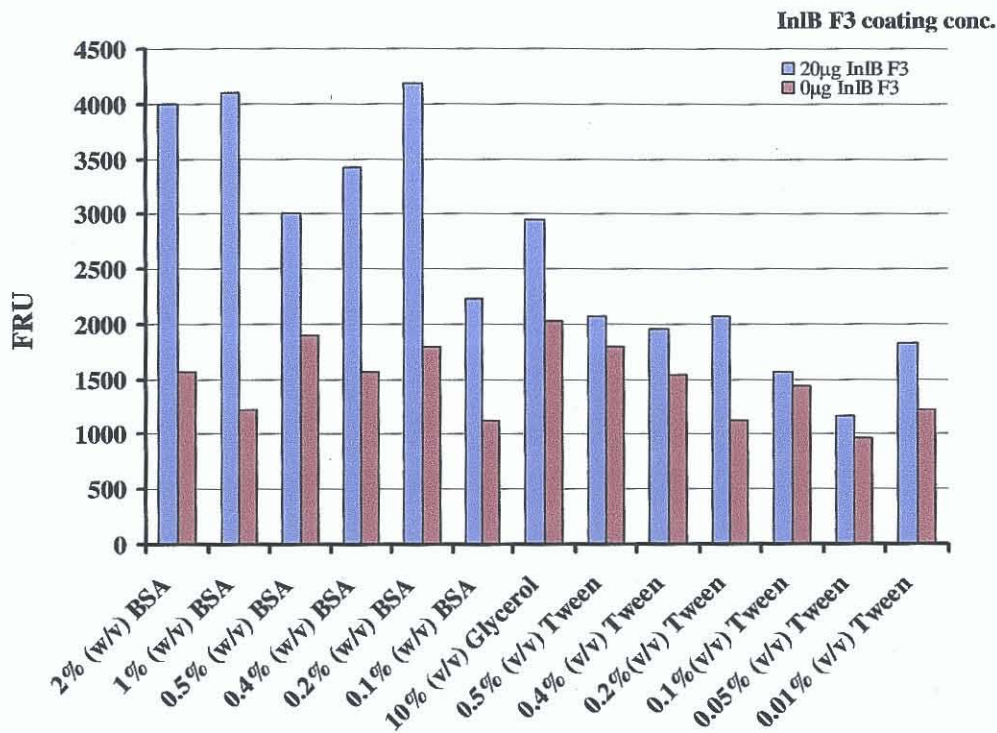


Figure 4.3 Selection of blocking reagent. Plates were coated with 20µg InlB-F3 and with PBS containing no protein. A 1/300 dilution of biotinylated antibody was prepared in PBS and traced with streptavidin-Cy5 to determine the optimal blocking solution to reduce non-specific binding. The fluorescence response units (FRU) for each blocking solution were plotted both in the presence and absence of coating antigen (InlB-F3)

The variation between blocking solutions suggested that non-specific binding was occurring between the biotinylated antibody and the plate surface. Interactions involving solutions containing Tween 20 showed a high degree of NSB. The use of Tween 20 was not suitable since studies have shown that non-ionic detergents can prevent attachment of proteins to polystyrene or nitrocellulose membranes (Gardas and Lewartowska, 1988). When the blocking solutions contained BSA, however, only minimal interactions were observed, when no antigen (InlB-F3) was coated on the plate surface. In order to maximize the signal for fluorescence-based immunoassays, the solution which gave the largest difference in observed specific and non-specific response was chosen. PBS containing 1% (w/v) BSA was found to be the most suitable blocking reagent for this

format since the solution significantly reduced the NSB of the biotinylated antibody to the plate.

A titre of biotinylated antibody against the optimal coating concentration of recombinant InlB-F3 (20 μ g/ml) was performed using PBS containing 1% (w/v) BSA as a blocking agent. From Figure 4.4 it can be seen that the use of BSA as a blocking solution greatly reduced non-specific binding interactions and resulted in only specific binding between immobilised InlB-F3 and the biotinylated anti-InlB polyclonal antibody. For subsequent assay development, plates were blocked with PBS containing 1% (w/v) BSA.

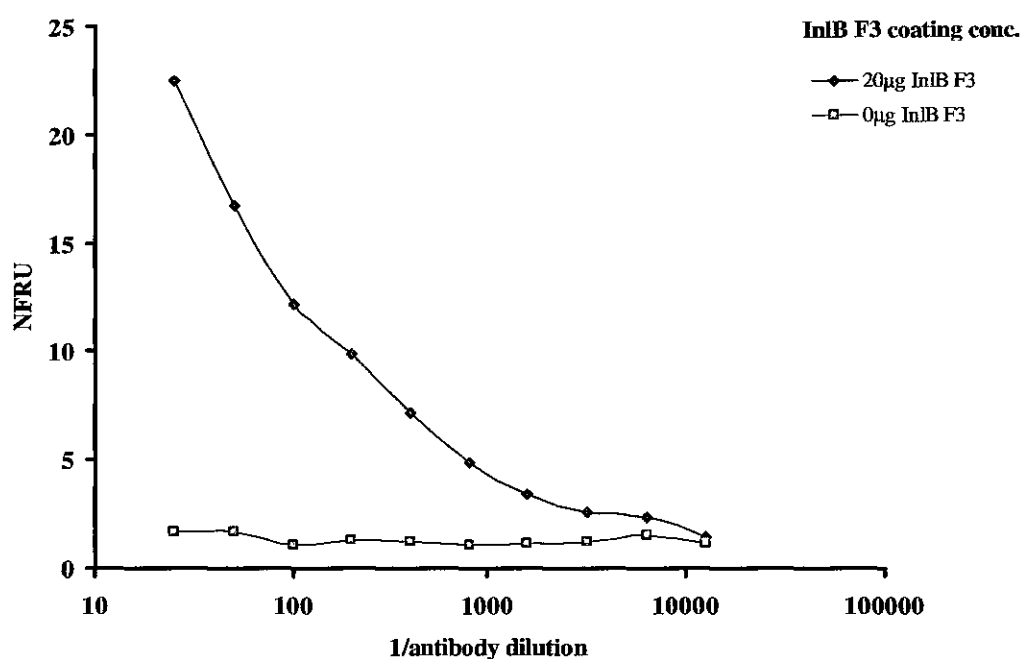


Figure 4.4 Titre of biotinylated antibody labelled with streptavidin-Cy5. PBS containing 1% (w/v) BSA was used as the blocking solution to ensure that non-specific binding interactions between the biotinylated anti-InlB polyclonal antibody and the plate surface were reduced. The fluorescent response was normalised by subtracting the response in the absence of fluorescent tracer molecule (streptavidin-Cy5) from all values and the normalised fluorescence response units (NFRU) plotted against biotinylated antibody dilution both in the presence and absence of coating antigen (InlB-F3).

4.3.3 Competitive fluorescence-based immunoassay (FIA) for the detection of InlB-F3 in PBS, using quantum dots as fluorescent label

A model competitive FIA was developed using the optimised dilutions determined from the checkerboard assay, where the biotinylated anti-InlB polyclonal antibody competes for binding to free InlB-F3 in solution and immobilised InlB-F3 on the plate. A microtitre plate was coated with 20µg/ml of InlB-F3 and blocked with PBS containing 1% (w/v) BSA. Standards of InlB-F3 were prepared in PBS ranging from 1.5 to 50,000ng/ml and mixed with an equal volume of biotinylated anti-InlB polyclonal antibody to give a final dilution of 1/300 (Section 2.8.2). Quantum dots were used at a concentration of 2nM, (Section 2.8.1).

Results were normalised by dividing the mean fluorescence obtained at each InlB-F3 concentration (F) by the fluorescence values determined in the presence of zero antigen (F_0). These values (F/F_0) were plotted against the logarithm of InlB-F3 concentration using Biaevaluation 4.0.1 software and a four-parameter equation was fitted to the data. The four parameter function provides an accurate representation of the sigmoidal relationship between the measured response and the logarithm of concentration observed for immunoassays (Findlay *et al.*, 2000).

Figure 4.5 shows the FIA inter-day calibration curve using the polyclonal antibody, where the lower limit of detection for the competitive assay was determined to be 12ng/ml. This limit of detection is defined as the lowest concentration that could be statistically determined as different from the F_0 value and is calculated by determining as the mean value of the blank (F_0) plus 3 times the standard deviation.

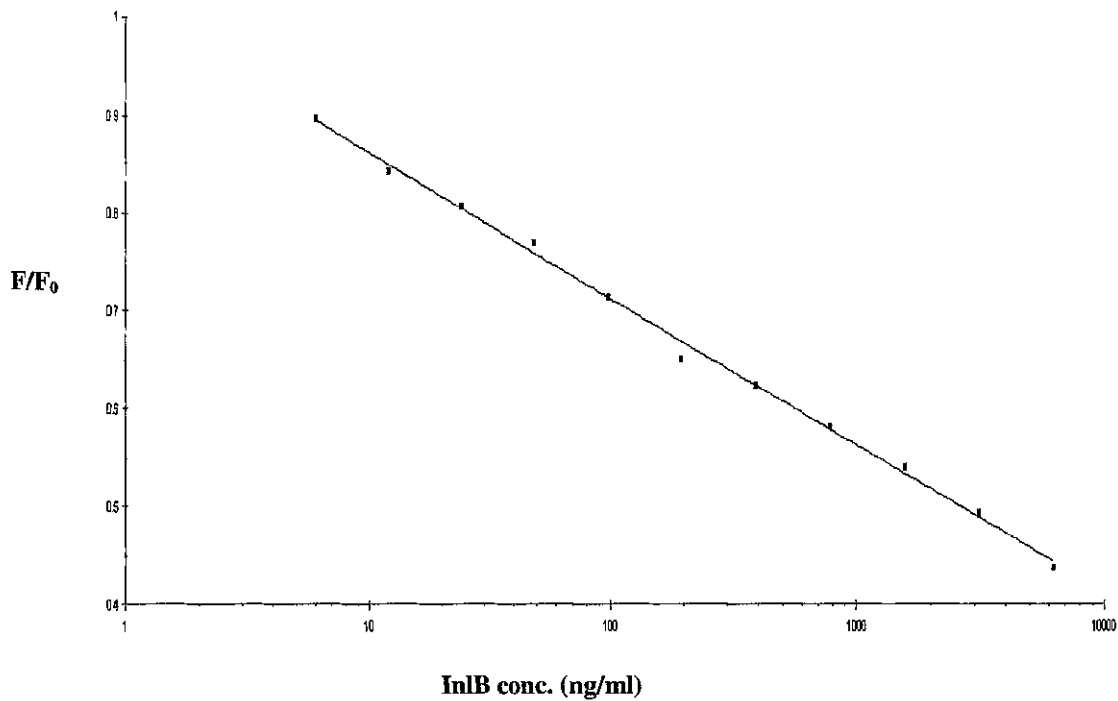


Figure 4.5a Inter-day calibration curve for competitive FIA for the detection of free InlB-F3 in PBS using the anti-InlB polyclonal antibody and streptavidin-linked quantum dots as the fluorescent label. Results were normalised by dividing the mean fluorescence obtained at each InlB-F3 concentration (F) by the fluorescence values determined in the presence of zero antigen (F_0). A lower limit of detection of 12ng/ml was determined by calculating the mean of the blank value (F_0) plus 3 times the standard deviation.

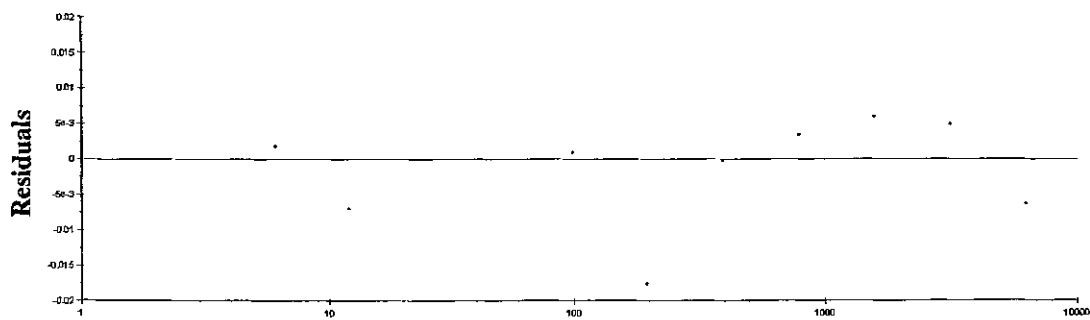


Figure 4.5b Residuals of Bisevaluation plot using 4-parameter equation fit for data shown in Fig 4.5a, a competitive fluorescence-based immunoassay for the detection of InlB-F3, using streptavidin-linked quantum dots as the fluorescent label.

In order to measure the accuracy of the fluorescence-based immunoassay using quantum dots as the label, intra-day and inter-day assay variability studies were performed, whereby three sets of standards were assayed over three days. The coefficients of variation (CV's) were determined to assess the reproducibility and precision of the analytical method, expressing the standard deviation as a percent function of the mean. Inter-day assay CV's ranged from 0.37% to 8.43% (Table 4.1), which are well within the 20% limits suggested by Findlay *et al.* (2000).

Table 4.1. Inter-day FIA coefficient of variation (CVs) for the detection of free InIB-F3 using the InIB-specific polyclonal antibody and streptavidin-linked quantum dots. Three sets of each standard were assayed over three days and the CVs calculated. Back-calculated concentrations were determined using Biaevaluation 4.0.1 software and expressed as a percentage of the theoretical concentrations (% recovery).

Concentration (ng/ml)	F/F ₀ ± SD	CV (%)	Back calculated concentration (ng/ml)	Recovery (%)
6250	0.44± 0.02	4.56	6889	110
3125	0.49± 0.00	0.40	2898	92
1563	0.54± 0.00	0.37	1424	91
781	0.58± 0.01	2.57	741	94
391	0.62± 0.02	2.88	392	100
195	0.65± 0.04	6.60	256	131
98	0.71± 0.01	2.10	96	98
49	0.77± 0.03	4.41	41	83
24	0.81± 0.05	5.70	23	96
12	0.84± 0.07	8.43	13	111

The assay was found to be accurate with the percentage recovery of back-calculated values determined to be between 83-111% of the measured concentrations. This was in line with the percentage accuracies suggested by Findlay *et al.*, (2000) whereby the values should be within a 25% acceptance limit. This was true for all concentrations except for the concentration of 195ng/ml. This point on the curve was askew in both the inter and intra-day variability studies and had a percentage recovery of 131%, which is outside of the suggested range.

An anti-InlB recombinant antibody fragment (scFv) isolated from a naive human library (Vaughan *et al.*, 1996) by Dr. Paul Leonard, was also used to develop a competitive assay for the detection of free InlB-F3. The scFv was biotinylated as detailed in *section 2.5.2.1*. A model competitive assay was developed where the biotinylated anti-InlB scFv competes for binding to free InlB-F3 in solution and immobilised InlB-F3 on the plate. Standards of InlB-F3 were prepared in PBS ranging from 1.5 to 50,000ng/ml and mixed with an equal volume of biotinylated anti-InlB scFv to give a final dilution of 1/300. Quantum dots were used at a concentration of 2nM, (*Section 2.8.1*). Intra-assay variability studies were performed to demonstrate the reproducibility of the competitive FIA. Results were normalised by dividing the mean fluorescence obtained at each InlB-F3 concentration (F) by the fluorescence values determined in the presence of zero antigen (F₀). These values (F/F₀) were plotted against the logarithm of InlB-F3 concentration using Biaevaluation 4.0.1 software and a four-parameter equation was fitted to the data. Figure 4.6 shows the FIA inter-day calibration curve using the scFv antibody fragment, where the lower limit of detection for the scFv competitive assay was determined to be 12ng/ml.

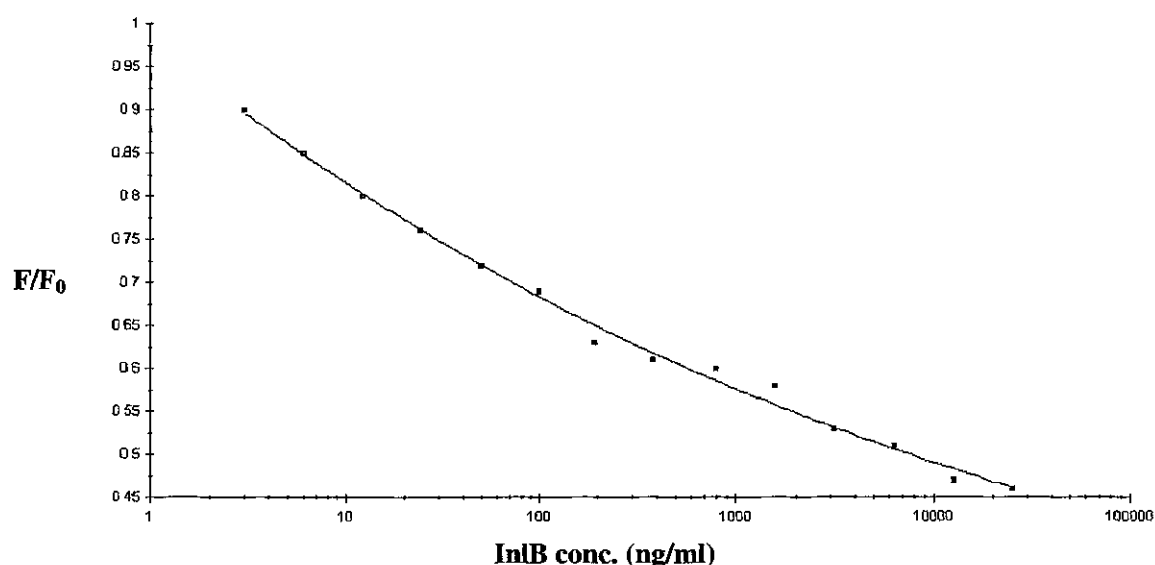


Figure 4.6 Intra-day calibration curve for competitive FIA for the detection of free InlB-F3 in PBS using the anti-InlB scFv. Results were normalised by dividing the mean fluorescence obtained at each InlB-F3 concentration (F) by the fluorescence values determined in the presence of zero antigen (F₀). A lower limit of detection of 12ng/ml was determined by calculating the mean of the blank value (F₀) plus 3 times the standard deviation.

Efficiency of biotinylation was a problem in this format. Entire antibody molecules were biotinylated via conjugation to a chemically active biotin derivative (*Section 2.5.2.1*), however scFv molecules are less stable than their whole IgG counterparts and more sensitive to chemical modifications. Additionally, their monovalent nature can be a disadvantage when the triggering of biological responses is desired. The anti-InlB scFv was also far less concentrated than polyclonal or monoclonal stocks and thus biotinylation was more difficult. This had an effect on the reproducibility of this assay format, whereby only intra-assay variability studies were performed. Santala and Lamminmäki, (2004) describe an alternative method which can be used for site-specific biotinylation of recombinant antibodies. This method uses the enzyme biotin ligase to catalyse the attachment of a biotin to a lysine residue in specific protein substrates, which in turn can be genetically linked to the antibody to generate a fusion protein. Enzymatic biotinylation of the scFv molecules would therefore produce a more stable and efficiently biotinylated complex (Sibler *et al.*, 1999; Cloutier *et al.*, 2000), which could be explored in future work.

4.3.4 Competitive fluorescence-based immunoassay (FIA) for the detection of InlB in PBS, using porphyrin-labelled neutravidin as the fluorescent label

Fluorescence-based immunoassays for the detection of InlB-F3 were also developed using an anti-InlB polyclonal antibody, with porphyrin-labelled neutravidin as the fluorescent label. Standards of InlB-F3 were prepared in PBS ranging from 1.5 to 50,000ng/ml and mixed with an equal volume of biotinylated anti-InlB polyclonal antibody to give a final dilution of 1/300 (*Section 2.8.3*). Porphyrin-labelled neutravidin was used at a concentration of 2nM (*Section 2.8.1*).

Results were normalised by dividing the mean fluorescence obtained at each InlB-F3 concentration (F) by the fluorescence values determined in the presence of zero antigen (F_0). These values (F/F_0) were plotted against the logarithm of InlB-F3 concentration using Biaevaluation 4.0.1 software and a four-parameter equation was fitted to the data. Figure 4.7 shows FIA inter-day calibration curve using the polyclonal antibody for the detection of free InlB-F3 in PBS, where the limit of detection for the competitive assay was determined to be 87ng/ml. The limit of detection was determined as the mean of the blank (F_0) plus 3 times the standard deviation.

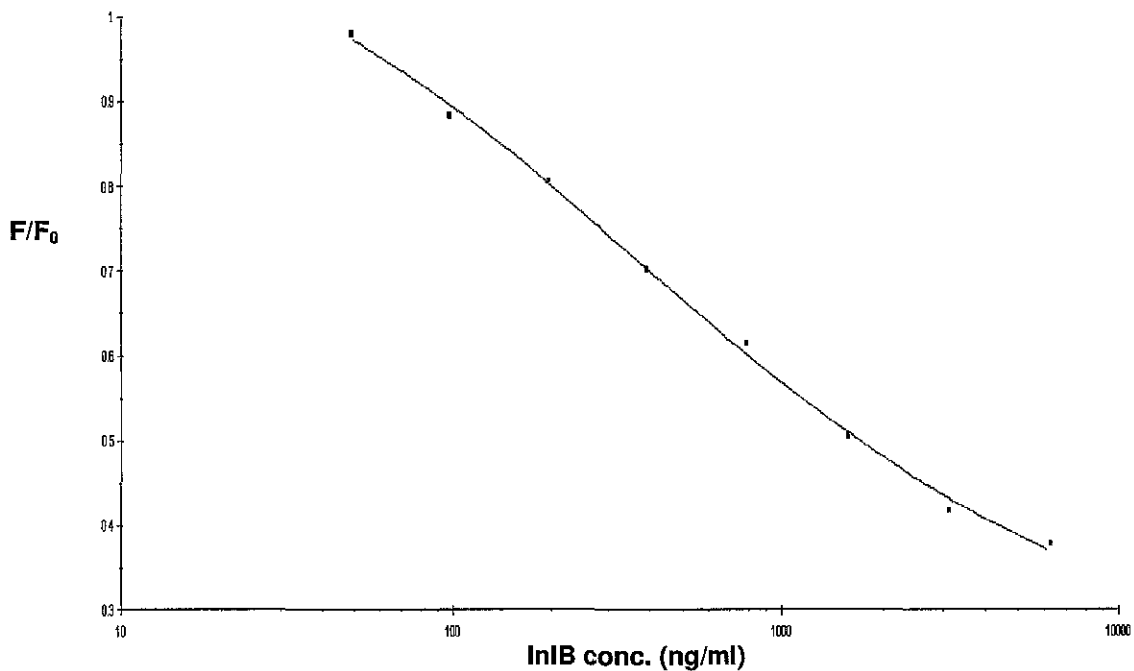


Figure 4.7a *Inter-day calibration curve for competitive FIA for the detection of free InIB-F3 in PBS using the anti-InIB polyclonal antibody and porphyrin-labelled neutravidin as the fluorescent label. Results were normalised by dividing the mean fluorescence obtained at each InIB-F3 concentration (F) by the fluorescence values determined in the presence of zero antigen (F_0). A lower limit of detection of 87ng/ml was determined by calculating the mean of the blank value (F_0) plus 3 times the standard deviation.*

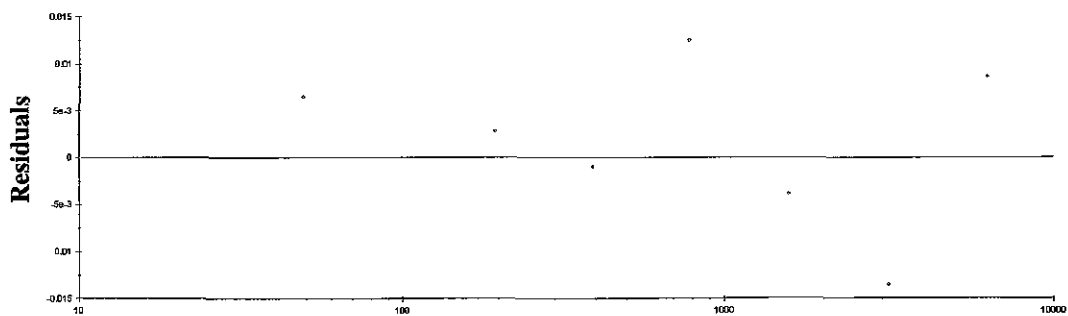


Figure 4.7b *Residuals of Biaevaluation plot using 4-parameter equation fit for data shown in Fig 4.7a, a competitive fluorescence-based immunoassay for the detection of InIB-F3, using porphyrin-labelled neutravidin as label.*

Intra-assay and inter-assay variability studies were performed to demonstrate the reproducibility of the competitive FIA. Inter-day assay CV's ranged from 0.71% to 3.43%, (Table 4.2).

Table 4.2. *Inter-day FIA coefficient of variation (CVs) for the detection of free InIB-F3, using the InIB-specific polyclonal antibody and porphyrin-labelled neutravidin. Three sets of each standard were assayed over three days and the CVs calculated. Back-calculated concentrations were determined using Biaevaluation 4.0.1 software and expressed as a percentage of the theoretical concentrations (% recovery).*

Concentration (ng/ml)	F/F ₀ ± SD	CV (%)	Back calculated concentration (ng/ml)	Recovery (%)
62500	0.38± 0.01	3.43	5604	89
3125	0.42± 0.01	1.91	3584	114
1563	0.50± 0.01	1.77	1612	103
781	0.61± 0.01	2.11	716	91
391	0.70± 0.00	0.71	393	100
195	0.80± 0.01	0.74	191	98
98	0.89± 0.01	1.92	107	110
48	0.98± 0.01	1.01	46	93

The assay was found to be accurate with the percentage recovery of back-calculated values determined to be between 89-114% of the measured concentrations. This was in line with the percentage accuracies suggested by Findlay *et al.* (2000).

4.3.5 Biochip application for the detection of InIB

A novel, disposable, antibody-based bio-chip sensor was developed by the research group led by Prof. MacCraith of the National Centre for Sensor Research (NCSR), DCU (Blue *et al.*, 2005; Stranik *et al.*, 2005). This system utilises patented optical enhancement platforms which demonstrate up to an 80-fold increase in the collection of luminescence/fluorescence, thereby improving sensitivity. The optical enhancement platforms used in the biochip system are illustrated in Figure 4.8.

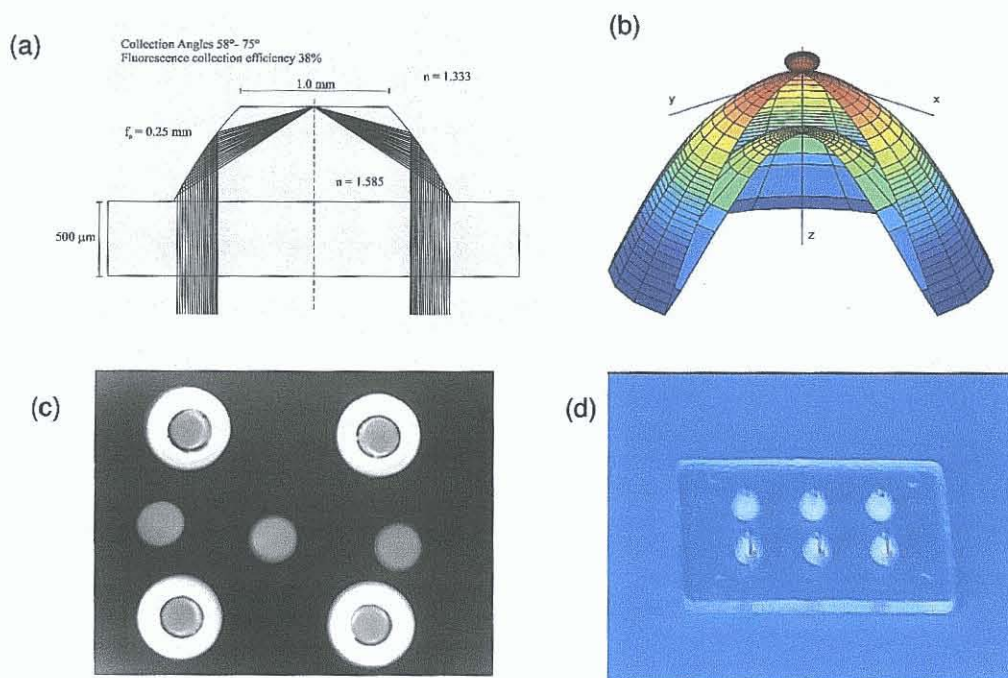


Figure 4.8 Optical enhancement platforms. (a) Cone-shaped structure of polymer platform illustrating the light emission rays emitted from a surface-confined fluorophore. (b) Anisotropic emission study showing the majority of light is waveguided at high angles, thus enhancing captured fluorescence (c) Typical enhancement performance of cones vs. flat surfaces showing 25-80 fold signal enhancement. (d) Image of the polymer chip platform incorporating patented cone structures for enhanced fluorescence capture.

The polystyrene chips are produced by micro-injection moulding and the use of enhanced cone structures for fluorescent detection greatly increases signal amplification. Biochips with enhanced cone structures are used as the substrate for the immobilisation of fluorescently-labelled antibodies and antigens. The signal generated during immunocomplex formation produces a fluorescence that can be captured using a photomultiplier tube and CCD camera. The excitation and detection set-up employs a laser diode as the light source, as shown in Figure 4.9. This allows biotinylated antibodies bound to antigen on the chip surface to be traced with streptavidin-linked fluorescent dyes. These dyes fluoresce upon excitation with a laser light and the resultant signal is recorded with a cooled charged coupled device (CCD) camera.

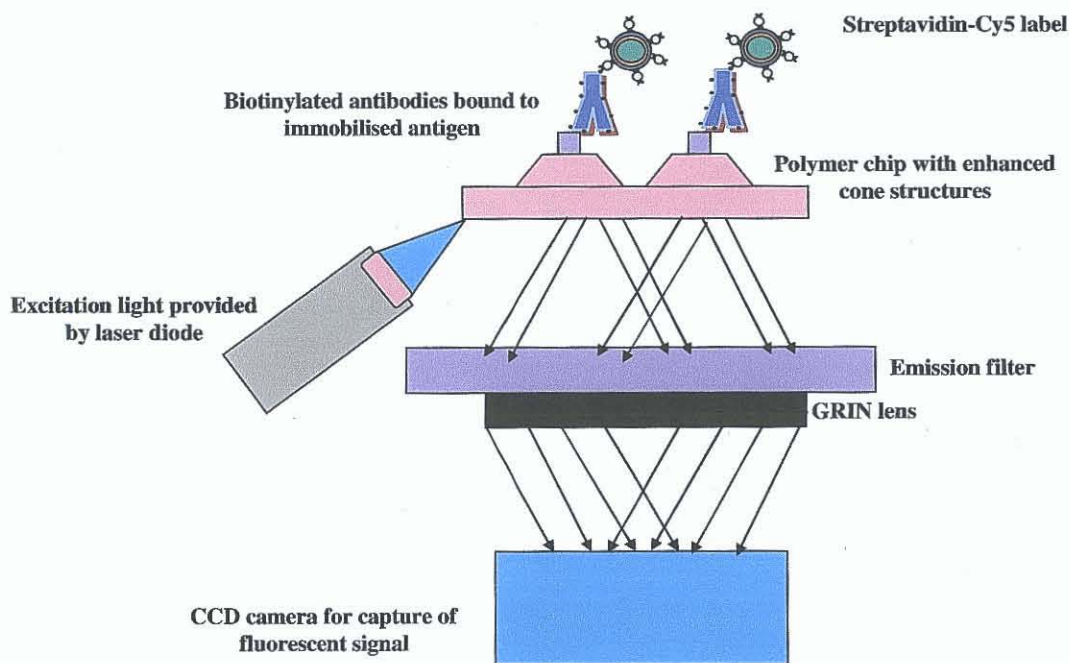


Figure 4.9 Antigen is immobilised on a polymer chip with optical enhancement structures (cone). Biotinylated antibody binds to immobilised antigen on chip surface and bound antibodies are traced using a streptavidin-linked fluorophore (streptavidin-Cy5). A laser light is used to excite any bound fluorescently-labelled antibody and background fluorescence is reduced by an optical filter. The resulting fluorescent signal is captured using a charge coupled device (CCD) camera and the signal is monitored on a laptop with imaging software.

A proof of principle experiment was set up initially, to evaluate biomolecule immobilisation, detection capabilities and the degree of captured fluorescence using the CCD set-up. A simple assay using a biotinylated antibody spotted onto the cone surfaces and detected with the addition of streptavidin-Cy5 was performed. Biotinylated anti-InlB polyclonal antibody was immobilised on the surface of the polystyrene cone structures by passive adsorption and any remaining binding sites on the biochip blocked using PBS containing 1% (w/v) BSA (Section 2.8.4). Following washing bound biotinylated antibody was detected with the addition of Strep-Cy5 and the fluorescent signal generated was captured with a cooled CCD camera. The resulting images are shown in Figure 4.10.

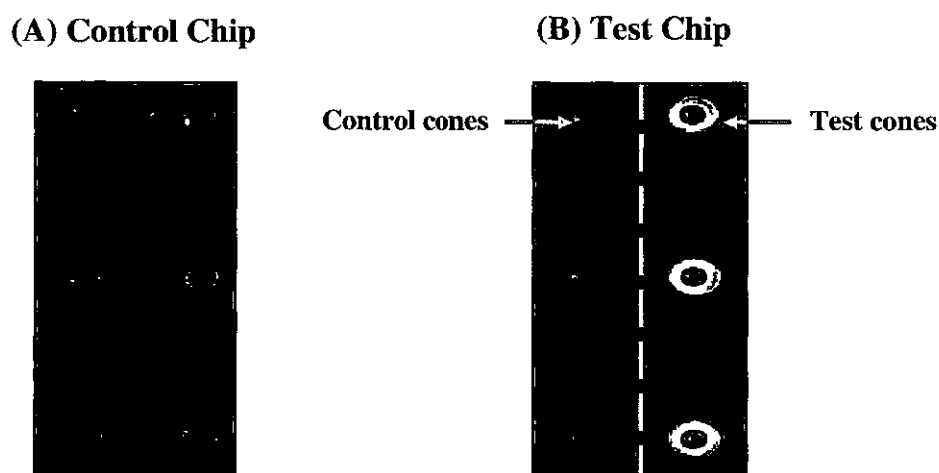
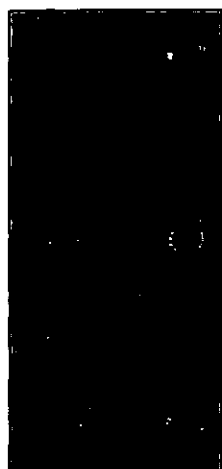


Figure 4.10 Preliminary chip-based assay (A) Captured image of blank control chip (B) Captured image of test chip. Biotinylated anti-InlB polyclonal antibody was immobilised on the surface of the right hand side of the chip (test cones) while the left hand side was left blank (control cones). Following the addition of Strep-Cy5 to the entire chip surface, the fluorescence was captured with a CCD camera.

The fluorescent signal from a blank chip was recorded to estimate the degree of background fluorescence (A), where the mean fluorescent intensity (n=6) was found to be $26,983 \pm 2,204$. The fluorescent signal was then recorded for the test chip (B); antibody immobilised (test) cones (n=3) were calculated to have a mean fluorescent intensity of $317,630 \pm 5,395$, whereas the control cones (n=3) had a mean value of $31,889 \pm 2,457$. CVs were calculated to determine the reproducibility of spot intensities and were found to be 1.70% and 7.71%, for the antibody immobilised (test cones) and control cones, respectively. Normalised values (minus background fluorescence from chip A) were therefore calculated to be 290,647 and 4,906 for the antibody immobilised and control surfaces respectively (B). The results from Figure 4.10 showed that bound biotinylated antibody could be detected using the CCD detection set-up, when traced with streptavidin-Cy5.

The next step in the development of a biochip-based assay was to assess the system's capabilities for the detection of biotinylated antibody, bound to immobilised antigen on the cone structures. Recombinant InlB-F3 was immobilised on the surface of the polystyrene cone structures by passive adsorption and any remaining binding sites on the biochip blocked using PBS containing 1% (w/v) BSA (*Section 2.8.5*). Following washing, biotinylated anti-InlB polyclonal antibody was added to the chip and incubated for 1 hour. Bound biotinylated antibody was detected with the addition of Strep-Cy5 and the fluorescent signal generated was captured with a cooled CCD camera. The resulting images are shown in Figure 4.11.

(A) Control Chip



(B) Test Chip

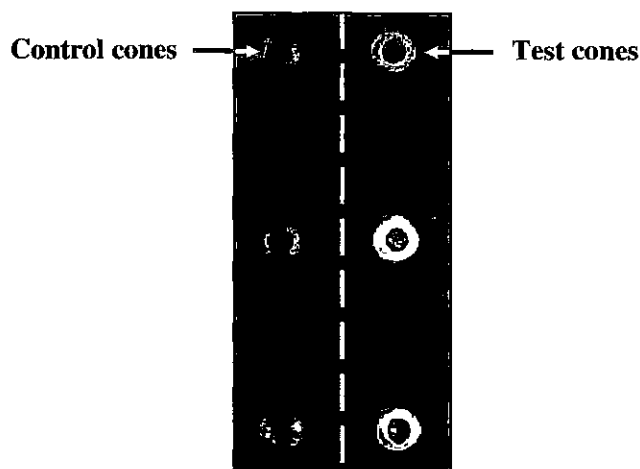


Figure 4.11 (A) Captured image of blank control chip (B) Captured image of test chip. *InlB-F3* was immobilised on each of the six cones by passive adsorption. The chip was then washed and blocked, as per section 2.8.6. Biotinylated anti-*InlB* polyclonal antibody was spotted onto the surface of the right hand side of the chip (test cones) while the left hand side was left blank (control cones). Following the addition of *Strep-Cy5* to the entire chip surface, the fluorescence was captured with a CCD camera.

The fluorescent signal from a blank chip was recorded to estimate the degree of background fluorescence (A), where the mean fluorescent intensity ($n=6$) was found to be $41,447 \pm 2,550$. The fluorescent signal was then recorded for the test chip (B); test cones ($n=3$) with biotinylated anti-*InlB* polyclonal antibody bound to *InlB-F3* and traced with streptavidin-Cy5, were calculated to have a mean fluorescent intensity of $356,764 \pm 26,163$, whereas the control cones ($n=3$) with no biotinylated antibody present, had a mean value of $42,717 \pm 6,546$. CVs were calculated to determine the reproducibility of spot intensities and were found to be 7.33% and 15.32%, for the antibody immobilised and control cones, respectively. Normalised values (minus background fluorescence from chip A) were calculated to be 315,317 and 1,270 for the test and control surfaces, respectively (B).

4.4 Development of fluorescence-based immunoassays for the detection of warfarin

Anti-warfarin monoclonal antibody was previously produced by Dr. Brian Fitzpatrick (Applied Biochemistry Group, DCU). Although extensive characterisation of the antibody had been undertaken previously (Fitzpatrick and O’Kennedy, 2004), a different clone of the monoclonal antibody was selected from cryogenically frozen hybridoma stocks. Therefore, it was deemed necessary to repeat the checkerboard ELISA for the anti-warfarin monoclonal antibody. Supernatants from warfarin-specific antibody-secreting hybridomas were collected for concentration and purification (*Section 2.4.2.1*). The purified anti-warfarin monoclonal antibody was subsequently biotinylated (*Section 2.5.2.*), for use in the development of fluorescence-based immunoassays for the detection of free warfarin.

4.4.1 Checkerboard assay to determine optimal antigen coating concentration and biotinylated antibody dilution for assay development

A standard checkerboard ELISA was set up as described in *Section 2.4.2.2* to determine the optimal conjugate coating concentration and monoclonal antibody dilution for use in a competitive assay. For this purpose, anti-warfarin monoclonal antibody was biotinylated, (*Section 2.5.2.1*), for use in a competitive assay and traced using an avidin-conjugated probe (extravidin-peroxidase, Sigma). Wells of a microtitre plate were coated with varying concentrations of warfarin-BSA and blocked with PBS containing 1% (w/v) BSA. Varying concentrations of the biotinylated anti-warfarin-specific monoclonal antibody were then added to the plate and the amount of bound antibody detected with the addition of extravidin-peroxidase (Figure 4.12).

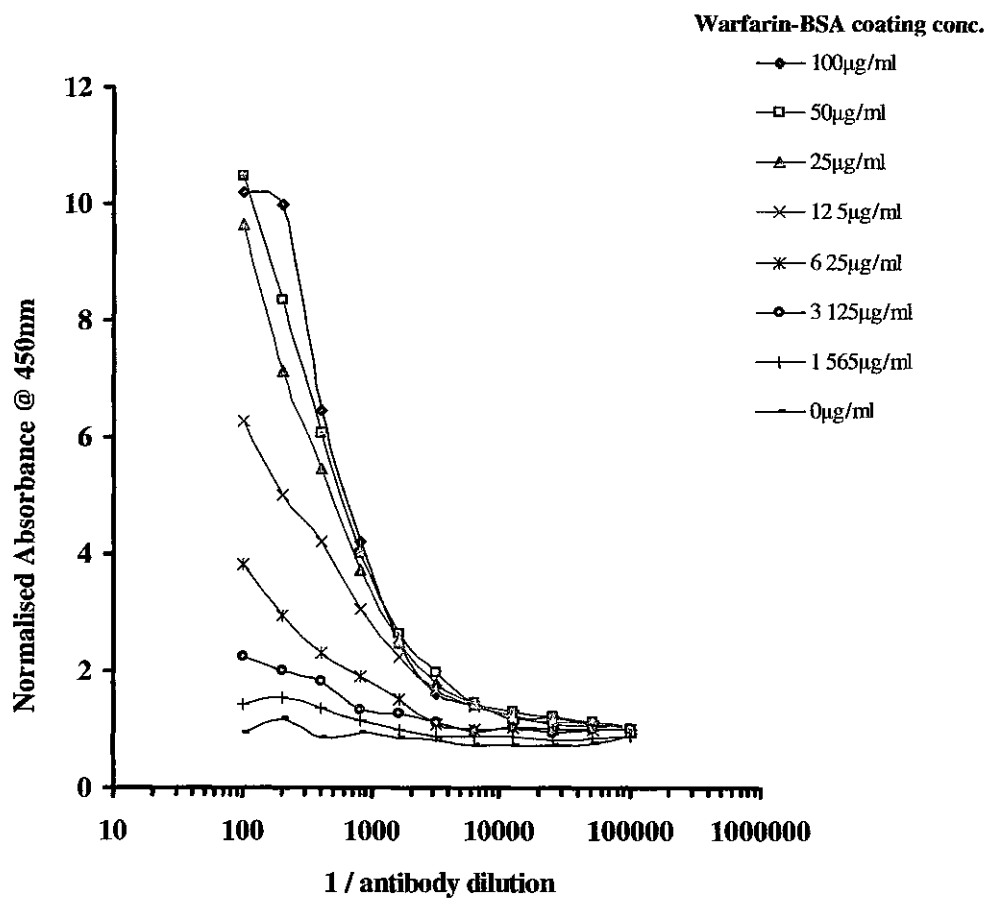


Figure 4.12 Checkerboard FIA for the determination of optimal warfarin-BSA conjugate coating concentration and biotinylated anti-warfarin monoclonal antibody dilution for use in a competitive FIA. Varying warfarin coating concentrations ranging from 0 - 100µg/ml and biotinylated antibody dilutions from 1/100 - 1/10000 were assayed. The amount of bound biotinylated antibody was determined using, extravidin peroxidase conjugate at a dilution of 1/1000.

A 50µg/ml warfarin-BSA coating concentration and biotinylated antibody dilution of 1/300 were chosen for use in a competitive FIA for the detection of free warfarin.

4.4.2 Competitive fluorescence-based immunoassay (FIA) for the detection of warfarin in PBS, using quantum dots as the fluorescent label

An anti-warfarin monoclonal antibody was used to develop a competitive assay for the detection of free warfarin in PBS, using quantum dots as the fluorescent label (*Section 2.8.2*). A model competitive assay was developed where the biotinylated anti-warfarin monoclonal antibody competes for binding to free warfarin in solution and immobilised warfarin-BSA on the plate. Standards of warfarin were prepared in PBS ranging from 1.5 to 50,000ng/ml and mixed with an equal volume of biotinylated anti-warfarin antibody to give a final dilution of 1/300 (*Section 2.8.2*). Quantum dots were used at a concentration of 2nM (*Section 2.8.1*)

Results were normalised by dividing the mean fluorescence obtained at each warfarin concentration (F) by the fluorescence values determined in the presence of zero drug (F_0). These values (F/F_0) were plotted against the logarithm of warfarin concentration using Biaevaluation 4.0.1 software and a four-parameter equation was fitted to the data. Figure 4.13 shows the FIA inter-day calibration curve using the monoclonal antibody, where the lower limit of detection for the competitive assay was determined to be 201ng/ml. This was determined as the mean of the blank (F_0) plus 3 times the standard deviation of the blank.

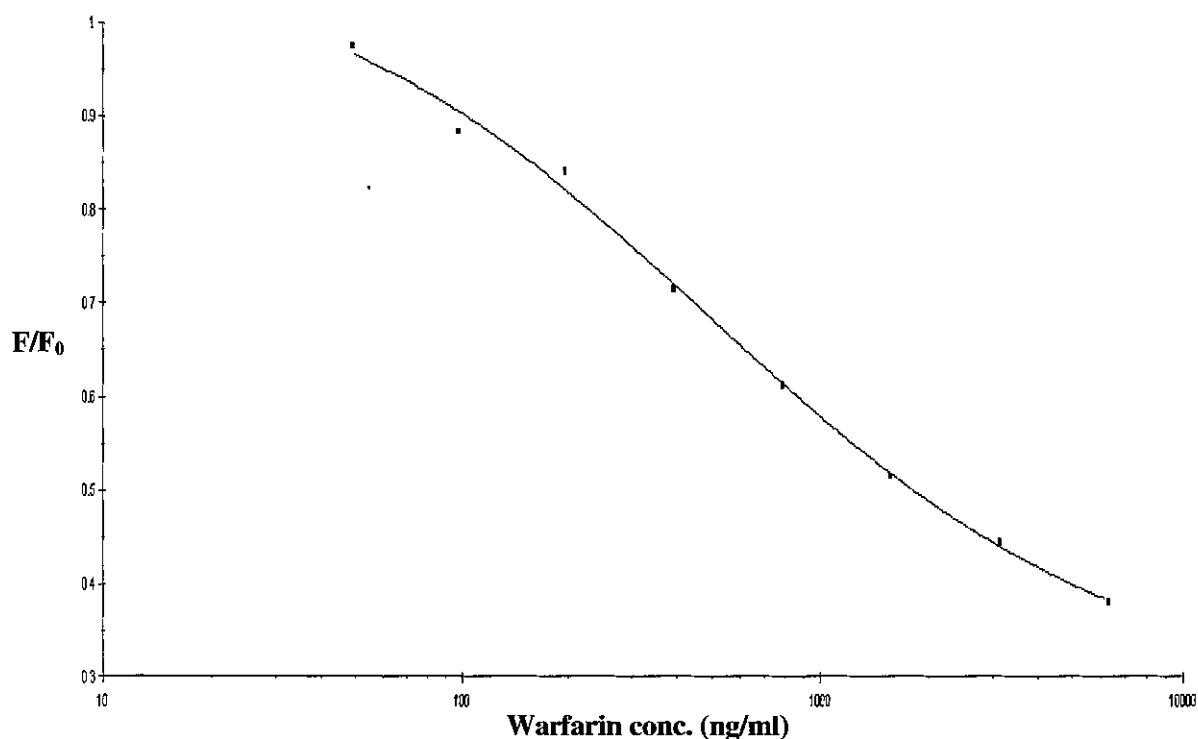


Figure 4.13a Inter-day calibration curve for competitive FIA for the detection of free warfarin in PBS using the anti-warfarin monoclonal antibody and quantum dots as fluorescent label. Results were normalised by dividing the mean fluorescence obtained at each warfarin concentration (F) by the fluorescence values determined in the presence of zero drug (F_0). A limit of detection of 201ng/ml was determined as the mean of the blank value (F_0) plus three times the standard deviation of the blank.

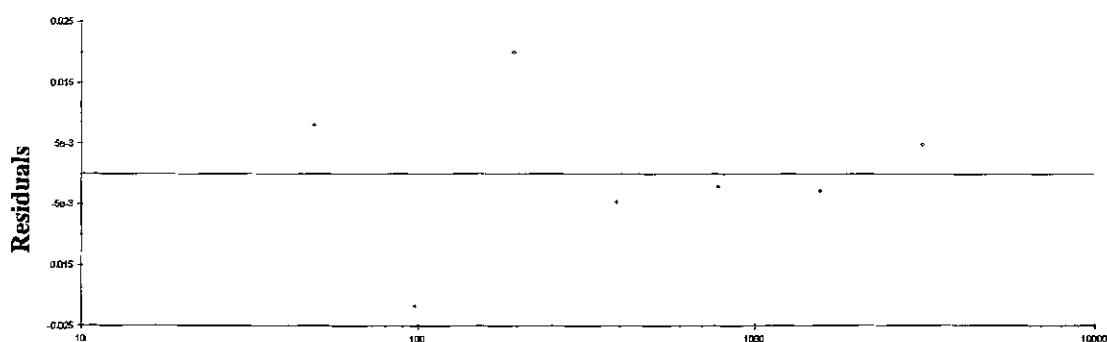


Figure 4.13b Residuals of Biaevaluation plot using 4-parameter equation fit for the data shown in Figure 4.13a, a competitive fluorescence-based immunoassay for the detection of free warfarin, using quantum dots as label.

Inter-assay variability studies were performed to demonstrate the reproducibility of the competitive FIA for the detection of warfarin, using quantum dots as the fluorescent label. Inter-day assay CV's ranged from 1.36% to 9.90%, (Table 4.3).

Table 4.3 *Inter-day FIA coefficient of variation (CVs) for the detection of free warfarin using the warfarin-specific monoclonal antibody and quantum dots. Three sets of each standard were assayed over three days and the CVs calculated. Back-calculated concentrations were determined using Biaevaluation 4.0.1 software and expressed as a percentage of the theoretical concentrations (% recovery).*

Concentration (ng/ml)	F/F₀ ± SD	CV (%)	Back calculated concentration (ng/ml)	Recovery (%)
6250	0.38± 0.01	3.41	6413	102
3125	0.44± 0.04	9.90	2975	95
1563	0.51± 0.01	1.36	1597	102
781	0.61± 0.02	3.43	792	101
391	0.72± 0.02	3.20	403	103
195	0.84± 0.07	8.60	168	85

The assay was found to be accurate with the percentage recovery of back-calculated values determined to be between 85-103% of the measured concentrations. This was in line with the percentage accuracies suggested by Findlay *et al.* (2000).

4.4.3 Competitive fluorescence-based immunoassay (FIA) for the detection of warfarin in PBS, using porphyrin-labelled neutravidin as the fluorescent label

The anti-warfarin monoclonal antibody was used to develop a competitive assay for the detection of free warfarin in PBS, using porphyrin-labelled neutravidin as the fluorescent label (*Section 2.8.3*). A model competitive assay was developed where the biotinylated anti-warfarin monoclonal antibody competes for binding to free warfarin in solution and immobilised Warfarin-BSA on the plate. Standards of warfarin were prepared in PBS ranging from 1.5 to 50,000ng/ml and mixed with an equal volume of biotinylated anti-warfarin antibody to give a final dilution of 1/300. Porphyrin-labelled neutravidin was used at a concentration of 2nM (*Section 2.8.1*) as determined by conjugate titre.

Results were normalised by dividing the mean fluorescence obtained at each warfarin concentration (F) by the fluorescence values determined in the presence of zero drug (F_0). These values (F/F_0) were plotted against the logarithm of warfarin concentration using Biaevaluation 4.0.1 software and a four-parameter equation was fitted to the data. Figure 4.14 shows the FIA inter-day calibration curve using the monoclonal antibody, where the lower limit of detection for the competitive assay was determined to be 228ng/ml using the three sigma method as before, whereby the limit of detection is calculated as the mean value of blank sample (F_0) plus 3 standard deviations.

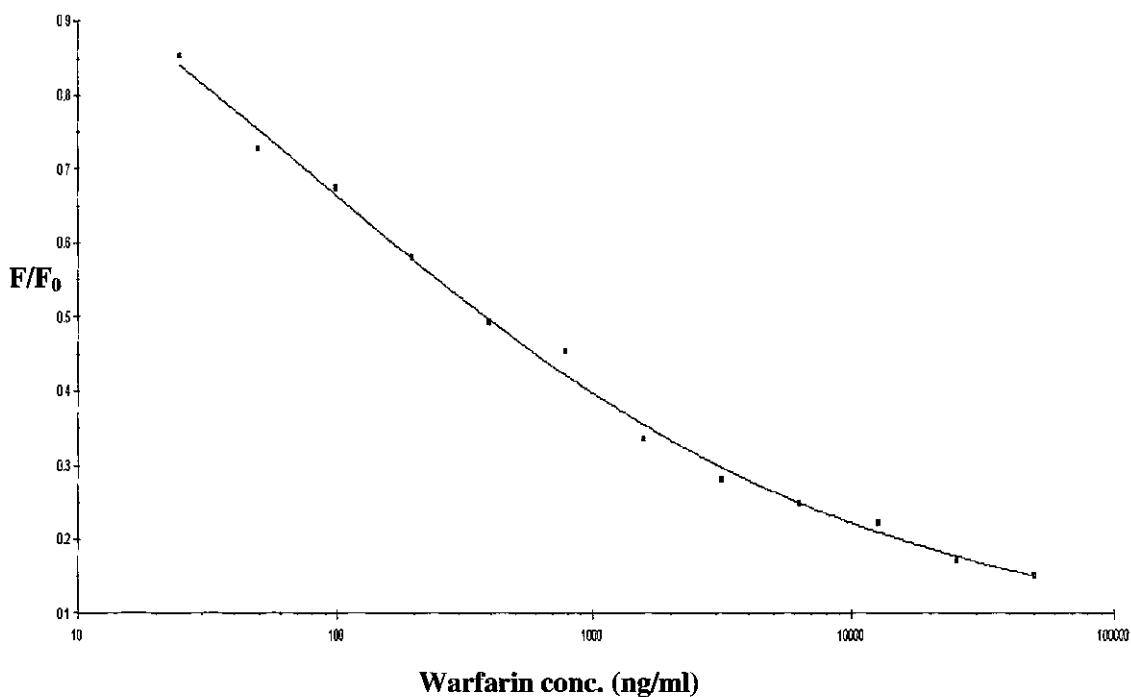


Figure 4.14a Inter-day calibration curve for competitive FIA for the detection of free warfarin in PBS using the anti-warfarin monoclonal antibody and porphyrin-labelled neutravidin fluorescent label. Results were normalised by dividing the mean fluorescence obtained at each warfarin concentration (F) by the fluorescence values determined in the presence of zero drug (F_0). A limit of detection of 228 ng/ml was determined as the mean of the blank value (F_0) plus three times the standard deviation of the blank.

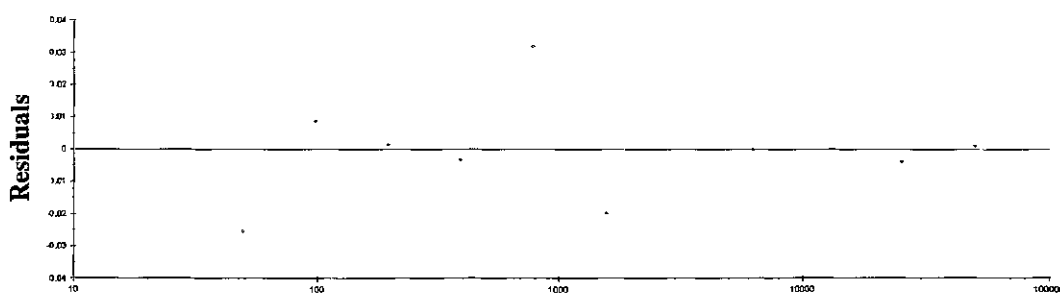


Figure 4.14b Residuals of Biaevaluation plot using 4-parameter equation fit for data shown in Figure 4.14a, a competitive fluorescence-based immunoassay for the detection of free warfarin, using porphyrin-labelled neutravidin as the fluorescent label.

Inter-assay variability studies were performed to demonstrate the reproducibility of the competitive FIA. Inter-day assay CV's ranged from and 0.40 to 14.54%, (Table 4.4). The assay was found to significantly less accurate than the quantum dot-based assay for the detection of warfarin (Section 4.4.2).

Table 4.4 *Inter-day FIA coefficient of variation (CVs) for the detection of free warfarin using the warfarin-specific monoclonal antibody and porphyrin-labelled neutravidin. Three sets of each standard were assayed over three days and the CVs calculated. Back-calculated concentrations were determined using Biaevaluation 4.0.1 software and expressed as a percentage of the theoretical concentrations (% recovery).*

Concentration (ng/ml)	F/F ₀ ± SD	CV (%)	Back calculated concentration (ng/ml)	Recovery (%)
50000	0.15±0.01	9.20	48539	97
25000	0.17± 0.00	0.57	27413	109
12500	0.22± 0.03	14.54	9818	78
6250	0.26± 0.03	12.15	6246	99
3125	0.28± 0.03	8.86	3879	124
1563	0.34± 0.04	11.30	1958	125
781	0.45± 0.03	5.50	577	73
391	0.49± 0.00	0.40	402	103
195	0.58± 0.08	12.93	193	98

Back-calculated values were found to be within 78-125% of the measured concentrations, which is at the far end of the limits suggested by Findlay *et al.* (2000) which states that the values should lie within ± 25% accuracy.

4.5 Immunostaining of *Listeria monocytogenes* cells

Quantum dots were successfully used as a suitable label for fluorescence-based immunoassay for the detection of InlB (Section 4.2), and so their applicability as reagents for immunostaining were also investigated. Quantum dots conjugates were used to stain bacterial cells immobilised on treated glass slides. Immunostaining of *Listeria monocytogenes* whole cells using quantum dots was compared to other more traditional probes such as Cy5 and FITC. *L. monocytogenes* cells employ surface bound proteins known as Internalins to promote invasion into host cell, with Internalin A (InlA) and Internalin B (InlB) being the best characterised. The use of the Internalin B fragments and associated antibodies for epitope mapping and subsequent development of fluorescence-based immunoassays was described earlier (Section 4.2). However, Internalin A protein is more readily accessible on the cell surface and therefore it is more suitable for immunostaining applications. A monoclonal antibody directed against InlA (Hearty *et al.*, 2006) was used for the specific and non-specific immunostaining of whole cells (Section 2.10.3). The antibody was biotinylated as before (Section 2.5.2.1). *Listeria monocytogenes* and *Bacillus cereus* whole cells were investigated, with the *Bacillus* cells used as a negative control. The fluorescent signal was captured using a Nikon fluorescent microscope and 12-bit cooled QICAM fast monochromatic camera (Section 2.10.4) with suitable optical filters for the sensitive detection of the fluorescent labels.

The multicolour sensitivity and stability of quantum dots makes them ideal for the analysis of complex samples for histology, pathology and cytology in immunostaining applications. Quantum dots are similar in size to organic dyes so can be substituted for current fluorescent techniques. The immunolabelling of *Listeria monocytogenes* for fluorescent detection with quantum dots was carried out in collaboration with industrial partners (Slidepath Ltd., DCU) who have access to sophisticated image analysis equipment and software. Glutaraldehyde (Seveus *et al.*, 1994) was used to fix *Listeria monocytogenes* whole cells on Poly-L-Lysine treated glass slides (Section 2.10.1). The cells were then incubated with previously biotinylated anti-InlA monoclonal antibody and traced using a range of streptavidin-conjugated fluorescent probes. The resulting labelled cells were imaged using a fluorescent microscope with monochrome camera and Image Pro™ Software (Figures 4.15-4.17).

Figure 4.15 clearly show the use of streptavidin-linked quantum dots and a biotinylated anti-InlA monoclonal antibody for the imaging of whole *L. monocytogenes* cells.

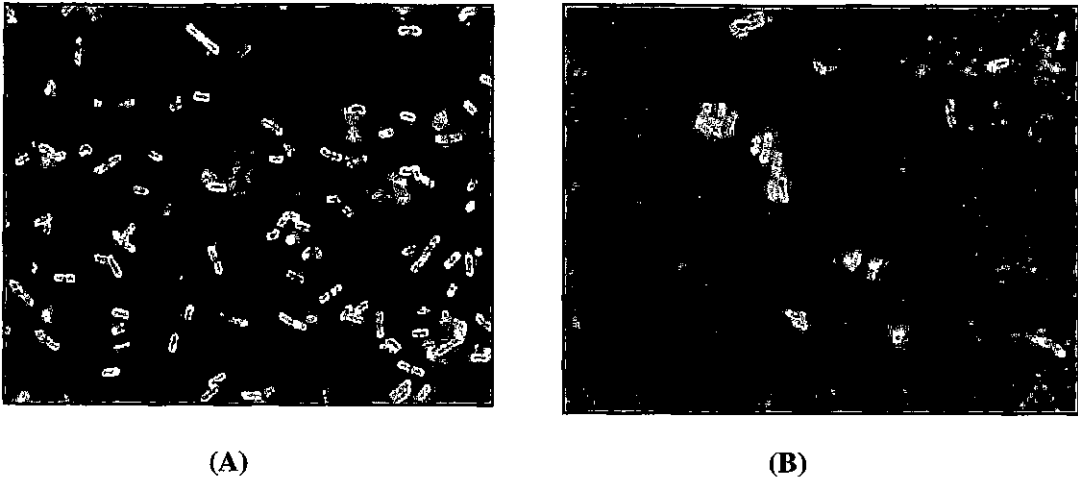


Figure 4.15 Use of anti-InlA antibody-linked red light-emitting quantum dots (605nm), for the visualisation of *L. monocytogenes* cells on poly-L-lysine-treated glass slides. The images show different dilutions of *L. monocytogenes* cells, fixed with glutaraldehyde, immunostained and visualised under fluorescence at a total magnification of 400x. (A) 1/10 dilution of *L. monocytogenes* cells and (B) 1/25 dilution of *L. monocytogenes* cells.

Figure 4.15 (A) & (B) clearly emphasise the suitability of quantum dots for the immunostaining of bacterial cells. The specificity of the biotinylated anti-InlA antibody in targeting the cell surface protein InlA is evident in the clear staining of the cell wall of the *L. monocytogenes* cells, as shown particularly in figure 4.16 (B) where a more dilute concentration of cells was fixed to the glass slide using glutaraldehyde. The strong affinity between the biotinylated antibody which targets the cell wall protein, InlA, and the streptavidin linked quantum dots gives a clear image of the immunostained cell.

In order to evaluate quantum dots as a superior fluorescent label for immunostaining, the use of avidin-FITC and streptavidin-Cy5 (traditional organic probes) was also investigated. The use of these fluorescent tracers as immunostaining probes gave lower quality results whereby the images were more blurred and less bright. Figure 4.16 (A) & (B) show the immunostaining of *L. monocytogenes* cells with FITC and Cy5 probes.

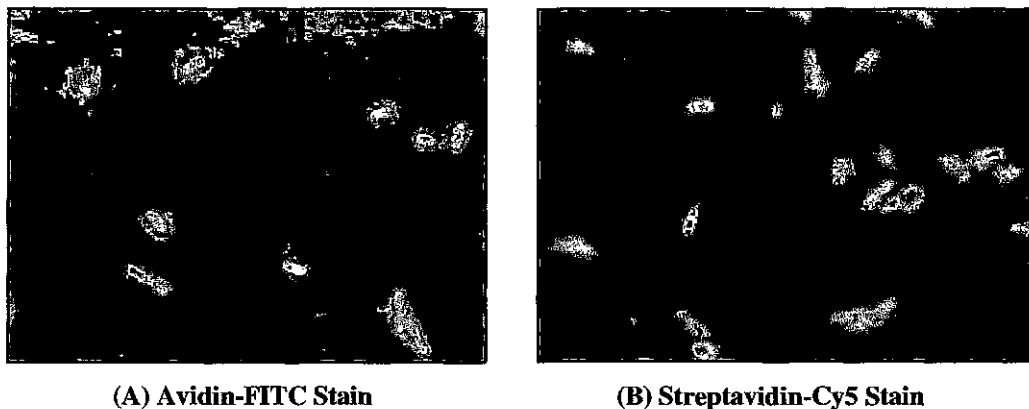


Figure 4.16 (A) Antibody-linked avidin-FITC immunostaining of *L. monocytogenes* cells on poly-L-lysine treated glass slide. (B) Antibody linked streptavidin-Cy5 immunostain of *L. monocytogenes* cells on poly-L-lysine treated glass slides. The image shows *L. monocytogenes* cells fixed with glutaraldehyde, immunostained and visualised under fluorescence at a total magnification of 400x.

Bacillus cereus is an endemic, soil-dwelling, Gram-positive, rod shaped, beta haemolytic bacterium that causes foodborne illness. Generally speaking, *Bacillus* foodborne illnesses occur due to survival of the bacterial spores when food is improperly cooked, which is further compounded with the storage of food at unsuitable temperatures. Bacterial growth results in production of enterotoxin, and ingestion causes diarrhoea. It is similar in structure and mode of action to *L. monocytogenes* and for these reasons was chosen as the control cells in these experiments. Cells were stained in exactly the same way as *L. monocytogenes* cells (Section 2.10.3) using a biotinylated anti-InlA monoclonal antibody and avidin-conjugated fluorescent probes. Since InlA is not a cell surface protein of *B. cereus*, InlA can be used as a negative control for these investigations (Figure 4.17).



Figure 4.17 (A) Antibody-linked streptavidin-Qdot immunostain of *B. cereus* cells on poly-L-lysine treated glass slide. The image shows *B. cereus* fixed with glutaraldehyde, immunostained with biotinylated anti-InlA antibody and streptavidin-linked quantum dots. The cells were visualised under fluorescence at a total magnification of 400x (negative control). (B) Bright field view of *B. cereus* cells on glass slides fixed with glutaraldehyde and visualised at a total magnification of 400x

From Figure 4.17 (A) & (B) it is evident that the anti-InlA antibody did not specifically target any cell surface protein in *B. cereus* and so the cells were not stained when streptavidin-linked quantum dots were added to the slide. The *B. cereus* cells could therefore be used as a negative control to show that the anti-InlA antibody was only specific for *L. monocytogenes* cell surface protein InlA and therefore could be used for the specific immunostaining of *L. monocytogenes* cells using quantum dots.

4.6 Development and characterisation of ruthenium dye-doped nanoparticles

Luminescence-based methodologies are widely employed throughout the biological and chemical sensor areas. However, autofluorescence arising from the system detection platform or the matrix can often cause interference, thus preventing the achievement of lower detection limits. Ruthenium complexes are designed specifically to have long fluorescence life-times close to 500 nanoseconds. These labels are laser-excitatable metal ligand complexes and can be used to label amines on biomolecules under mild conditions. Labeling of proteins with ruthenium is via a ruthenium-activated ester for acylation of amino acid side chains. The main advantages of ruthenium-based dyes as protein-labels include high photostability, good water solubility, a lack of dye-dye interactions and large Stokes shifts. In addition, the fluorescence signal of long-lived fluorophores such as ruthenium can be gated to eliminate the emission from short-life-time fluorophores and autofluorescence from cells and biomolecules to further improve sensitivity (Castellano *et al.*, 1998). The optical properties of ruthenium dyes have an excitation maximum at 453nm and an emission maximum at 618nm. The structure of the ruthenium NHS ester for antibody labelling is shown in Figure 4.18

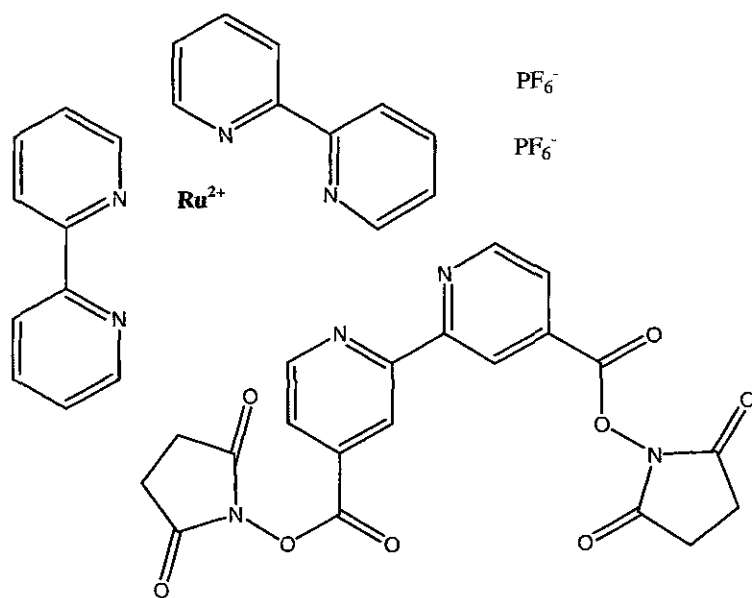


Figure 4.18 Structure of Ruthenium-NHS ester used for antibody labelling (Fluka, product number 96632, Bis(2,2'-bipyridine)-4,4'-dicarboxybipyridine-ruthenium-di-(N-succinimidyl-ester)bis(hexafluorophosphate).

The work described in this thesis focused on three main target analytes, namely the *L. monocytogenes* cell surface protein InlB, the anti-coagulant warfarin and the Parvovirus B19 capsid protein, VP2. Initially it was proposed to use InlB protein fragment F3 and its associated polyclonal antibody for the characterisation and investigation of ruthenium dye-doped nanoparticles in fluorescence-based immunoassays. However, since the work involved in nanoparticle synthesis and characterisation employed completely new technologies and methods a large amount of antibody was required for the optimisation of numerous conjugations and assay parameters. Therefore, it was proposed to employ a cheap commercially available antibody-antigen pair for all nanoparticle-based assay development, since the anti-InlB polyclonal antibody was in short supply and so the selected analyte for nanoparticle studies was human IgG (hIgG).

Ruthenium-NHS (Figure 4.18) was conjugated to anti-hIgG polyclonal antibody (*Section 2.5.3*) for use in fluorescence-based immunoassays for the detection of hIgG. The development and optimisation of a solid-phase fluorescence-based immunoassay using a labelled antibody-ruthenium conjugate was then compared to antibody-conjugated ruthenium dye-doped nanoparticles in a sandwich assay format. (Lian *et al.*, 2004). The use of nanoparticles to improve the performance and sensitivity of immunoassays is an emerging technology. Seydack (2005) described the use of nanoparticles in immunoassays resulting in improved detection limits, multiplexing of assays, reduction in photobleaching, signal amplification and improved sensitivity. In the work described in this thesis, ruthenium dye-doped nanoparticles were fabricated in association with Dr. Robert Nooney, Biomedical Diagnostics Institute (BDI) in Dublin City University for use as fluorescent tags in novel immunoassay formats. Here, the preparation and characterisation of ruthenium dye-doped nanoparticles is discussed and their application in solid-phase applications demonstrated.

4.6.1 Ruthenium-antibody conjugation

Ru-NHS is a functionalised succinimidyl ester of ruthenium that reacts with primary amines to form stable dye-protein conjugates. The NHS ester labelling reaction proceeds rapidly at slightly alkaline pH values resulting in a stable amide-linked derivative. Sodium bicarbonate buffer (Table 2.4) was determined to be the optimal buffer for ruthenium labelling of antibodies. This was established by performing a number of conjugation reactions with various buffers and comparing conjugate activity by titration. Ruthenium-NHS was conjugated to the anti-hIgG polyclonal antibody (*Section 2.5.3*). Unreacted dye was removed from the antibody-dye conjugate by gel filtration or dialysis and the conjugate concentration and dye/protein ratio were calculated spectrophotometrically.

4.6.1.1 Direct detection of hIgG using ruthenium labelled anti-human IgG

Human IgG was physically adsorbed onto the polystyrene plate surface. Immunoassays were established in the traditional manner with blocking and washing steps included. The performance of the ruthenium-antibody conjugate was assessed via traditional fluorescence-based immunoassay, for subsequent comparison with nanoparticles. Anti-human IgG was labelled with Ru-NHS (*Section 2.5.3*). The conjugate concentration was determined spectrophotometrically as 1.7mg/ml and dye/protein ratio calculated to be 2.7 (*using equations 2.1 and 2.2, Section 2.5.3*) To demonstrate proof of principle that the ruthenium antibody remained active post-conjugation, a plate was coated with human IgG (5µg/ml) and subsequently blocked with PBS containing 1% (w/v) BSA to prevent non-specific binding. The ruthenium-labelled anti-human antibody was diluted in PBS (1/2-1/512) and added to the plate. After one hour the amount of bound fluorescently-conjugated antibody was determined by reading at optimal excitation (453nm) and emission (618nm) wavelengths. The fluorescent signal generated was normalised against a zero control, where no fluorescent material was added to the well (Figure 4.19).

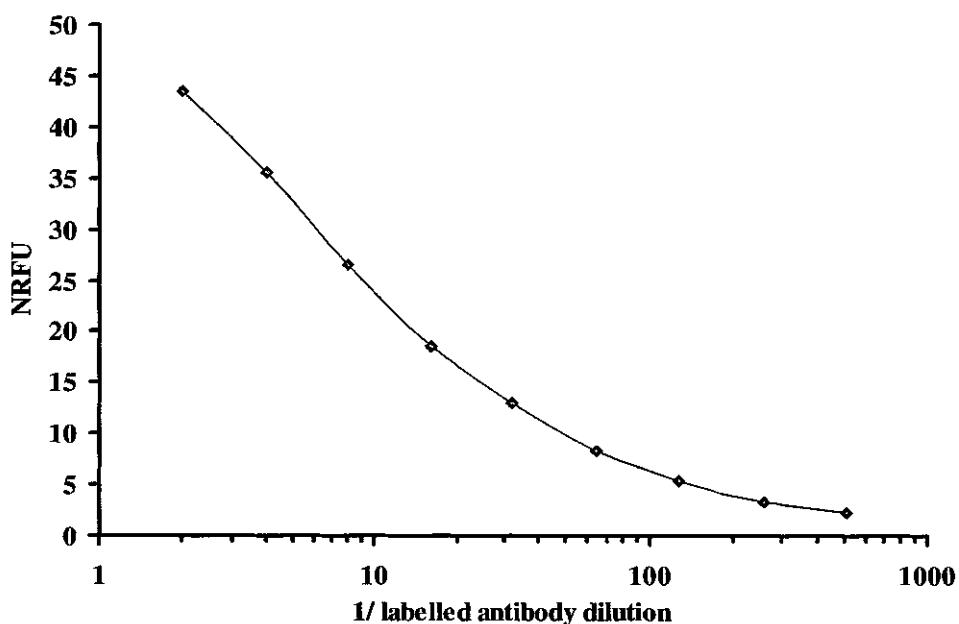


Figure 4.19 *Fluorescent response of ruthenium conjugated anti-human IgG in solid-phase direct binding assay. The fluorescent response was normalised against the background fluorescence and the normalised response plotted (NFRU).*

Figure 4.19 shows the use of ruthenium-labeled anti-hIgG in a direct binding format with immobilised hIgG, demonstrating that the labelled antibody retained antigen-binding functionality post-conjugation. This conjugate would be directly compared to ruthenium dye-doped nanoparticle-antibody conjugates, in a sandwich assay format for the detection of hIgG, to determine the advantages of nanoparticles as detection moieties for increased assay sensitivity.

4.6.2 Nanoparticle synthesis and characterisation

Nanoparticles are microscopic particles with at least one dimension of less than 100 nm. Nanoparticle research is currently an area of intense interest, due to a wide variety of potential applications in biomedical, optical, and electronic fields. Many materials have been investigated for the fabrication of nanoparticle probes and these include semiconductor nanocrystals (Matoussi *et al.*, 2000), metals such as gold or silver, (Schneider *et al.*, 2000), polystyrene latex (Sun *et al.*, 2004) and dye-doped silica (Santra *et al.*, 2000). Silica shell dye-doped nanoparticles have a number of advantages over conventional fluorescent labels in that they are inherently brighter than their constituent dye, the silica surface displays an easily modifiable chemistry for attachment of biomolecules and the fabrication of such particles is both reproducible and robust. Silica nanoparticles have been successfully utilised in both bioseparation and bioanalysis applications. The fabrication and use of these ultrasensitive labels in fluorescence-based immunoassays is described here.

Ruthenium dye-doped high-brightness nanoparticles were synthesised in association with Dr. Robert Nooney, Biomedical Diagnostics Institute (BDI) as described in *Section 2.7*. Modification of the synthesised nanoparticles for antibody conjugation was investigated for use in fluorescence-based immunoassays for the detection of human IgG. A reverse microemulsion technique adapted from the methods described by Santra *et al.* (2001), Quoboshene *et al.* (2001) and Tan^b *et al.* (2004) was used for nanoparticle synthesis (*Section 2.7.1*). The main advantages of dye-doped nanoparticles for immunoassays are stability, brightness and ease of functionalisation for bioconjugation. Fabrication by microemulsion, whereby the dye is encapsulated within a silica matrix, provides good photostability, since oxygen is excluded by the silica encapsulation. The microemulsion method is both isotropic and thermodynamically stable (Wang^b *et al.*, 2004). Nanodroplets of water form in the bulk-oil phase, which acts as a confined medium for discrete particle formation. The microemulsion yields monodispersed and highly uniform nanoparticles, but takes 24–48 hours to complete.

After the initial microemulsion stage, the nanoparticle surface is subsequently functionalised for interaction with target molecules for biological applications. However, prior to functionalisation the nanoparticles were characterised using fluorescence analysis for calculation of enhancement effects, transmission electron microscopy (TEM) for concentration and size determination and dynamic light scattering analysis to measure the zeta potential of the particles.

4.6.2.1 Calculation of enhancement effects of dye-doped nanoparticles

A study of the relative brightness of ruthenium dye-doped nanoparticles and a comparison with the brightness of a single dye molecule was performed to calculate the fluorescent enhancement effects of dye-doped nanoparticles. A known mass of dried ruthenium dye-doped silica NPs (60 nm in diameter) were dispersed in ultra pure water*. The particles remained aggregated due to cross linking. Therefore, NaOH was added to dissolve the silica and free the dye. A fluorescence study was then performed on the freed dye and compared against a series of dilutions of pure Ru(bpy)₃Cl₂ in solution phase. The emission profile (between 500-800nm) of 60nm silica nanoparticles was compared to pure dye, Ru(bpy)₃Cl₂. The pure dye concentration was 0.5x10⁻⁵ mol/l and the nanoparticle concentration was calculated as 10⁻¹⁰ mol/l, using equations 4.1- 4.3.

$$\text{Equation 4.1} \quad \text{Volume of sphere cm}^3 = \frac{4\pi r^3}{3}$$

where r = radius of the nanoparticles

$$\text{Equation 4.2} \quad \text{Mass (g/l)} = P \times V$$

where P = density of nanoparticle (silica is 2.6g/ cm³) and V = volume of nanoparticles

$$\text{Equation 4.3} \quad \text{Number of mol/l} = \text{mass} \times N_A$$

where N_A = Avogadro's Constant (6.0221415 × 10²³ mol⁻¹)

Based on these values the relative brightness of the nanoparticles was calculated to be 39,000 times brighter than the constituent ruthenium dye. Figure 4.20 shows the emission spectra of the nanoparticles and ruthenium dye between 500-800nm.

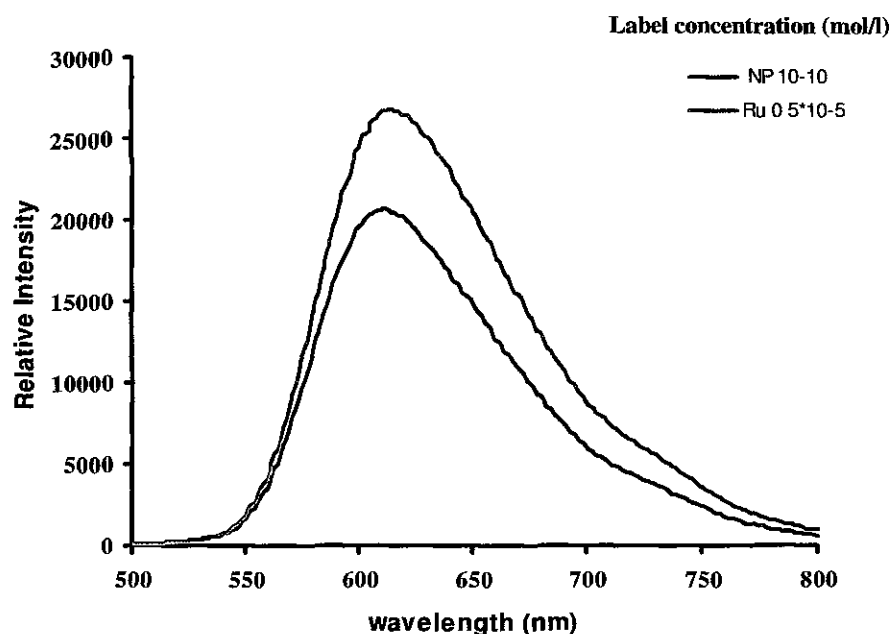


Figure 4.20 Comparison of emission spectra of ruthenium dye-doped silica nanoparticles and constituent dye $\text{Ru}(\text{bpy})_3\text{Cl}_2$ for calculation of enhancement effect. The nanoparticles were determined to be approximately 39,000 times brighter than the ruthenium dye, used to dope the particles.

The enhancement effect of the nanoparticles can be calculated by determining the relative fluorescent intensity of a known concentration of both the ruthenium dye-doped nanoparticles and their constituent dye. A scan of the emission spectra between 500 and 800nm was performed and the resultant fluorescent response plotted for both the nanoparticles (concentration 10^{-10} mol/l) and the ruthenium dye (concentration 0.5×10^{-5} mol/l). By calculating the relative intensity of a single mole of nanoparticle and comparing this with the relative intensity of a single mole of dye, an enhancement ratio can be determined. Based on these data, the nanoparticles are approximately 39,000 times brighter than ruthenium dye.

** Please note that due to the proprietary nature of these methods (BDI, DCU) details on actual volumes and experimental conditions cannot be given. The methods used were adapted from Santra *et al.* (2001), Qhobosheane *et al.* (2001) and Tan^b *et al.* (2004).*

Transmission electron microscopy (TEM) analysis was also performed to determine the actual size and concentration of the particles (Figure 4.21).

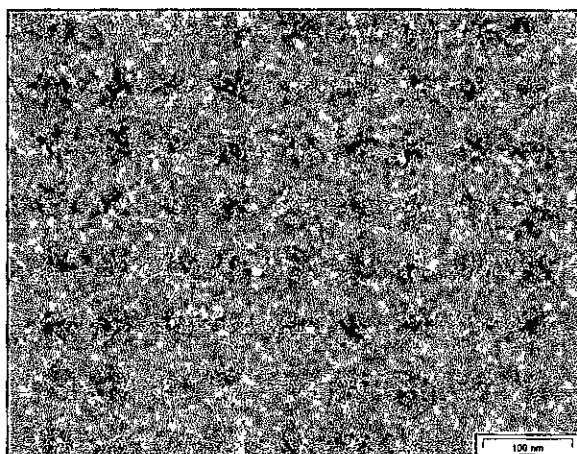


Figure 4.21 Transmission electron microscopy (TEM) micrograph of the high brightness ruthenium dye-doped nanoparticles. Assuming a particle size of $60\text{nm} \pm 2\text{nm}$ and a mass of 2 mg/ml , the number of particles/ml was determined as 7.36×10^{12} and the concentration of nanoparticles was $1.22 \times 10^{-8}\text{ mol/l}$ (Scale = 100nm).

Santra *et al.* (2001) described aggregation issues with dye-doped silica nanoparticles formed by microemulsion. In correlation with these findings, aggregation problems were observed, which altered the actual size of the particles. Dynamic light scattering analysis was performed (by BDI collaborators) to measure the zeta potential of the aggregating particles and the actual zeta potential determined as 19.7 mV . This potential is below 20 mV which is commonly thought of as the threshold for stable nanoparticles (Tan^b *et al.*, 2004). The low surface potential could have contributed to the aggregation of the nanoparticles and so addition of a protecting group, was required.

To reduce aggregation of the dye-doped nanoparticles, 3-(trihydroxysilyl) propyl-methyl phosphonate, monosodium salt was added particles (Section 2.7.1). NaOH was then added to dissolve the silica and free the dye. A fluorescence study was performed on the freed dye and compared against a series of dilutions of pure $\text{Ru}(\text{bpy})_3\text{Cl}_2$ in solution phase. The results of the fluorescence study were as follows. Nanoparticles and ruthenium dye were diluted to a concentration of $1 \times 10^{-6}\text{ mol/l}$ in ultra pure water and the fluorescence measured. The relative intensity of the dye was determined to be 3578 at

this concentration while the nanoparticles gave a value of 6.58×10^7 . The ratio of brightness and therefore enhancement was approximately 18,381. These nanoparticles were less bright than those in Figure 4.20 for two reasons. Firstly, addition of protecting groups essentially reduces the ability of the nanoparticles to collide with other particles and secondly, the release of ruthenium dye from the silica matrix reduces its fluorescence as quenching by oxygen in the atmosphere can occur (Bagwe *et al.*, 2006). Figure 4.22 shows a TEM micrograph of the nanoparticles with THPMP and APTES added.

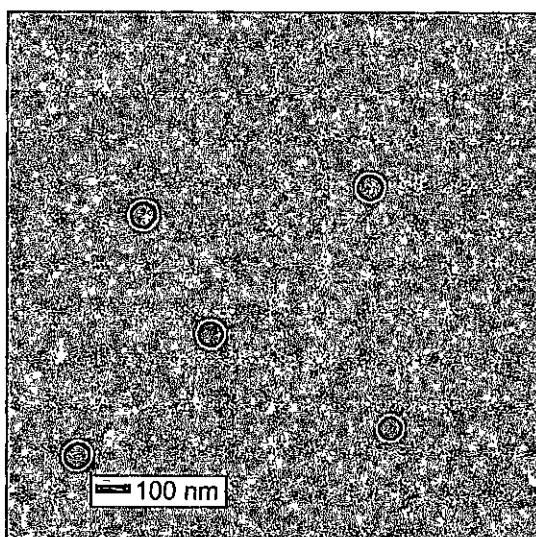


Figure 4.22 Transmission electron microscopy (TEM) micrograph of the high brightness ruthenium dye-doped nanoparticles with protecting groups THPMP and APTES added. The average particle size was calculated as $77.9\text{nm} \pm 5.09\text{ nm}$ (Scale = 100nm).

Dynamic light scattering analysis showed that the diameter of the nanoparticles with the protecting groups THPMP and APTES added was 93.2 nm and the surface zeta potential was calculated to be 36.4 mV. The TEM analysis values are smaller than those obtained from dynamic light scattering analysis, since it includes the hydrodynamic radius which is the shell of solvating water molecules that move around with the nanoparticles. After the addition of glutaraldehyde and antibody (anti-human IgG) the particle size rose to 102nm.

4.6.2.2 Antibody conjugation to ruthenium dye-doped nanoparticles

The surface modification of ruthenium dye-doped nanoparticles for biomolecule attachment was a two-fold process. Silica is easy to modify using a number of methods such as NHS activation, silanisation, carboxyl modification (Lian *et al.*, 2004). In this case, aminopropyltrimethoxysilane (APTES) modification (*Section 2.7.1*) was used to add amino groups to the silica shell. This was followed by glutaraldehyde crosslinking for antibody attachment. This method has been extensively used by many authors for biomolecule conjugation to amine modified surface (Nakanishi *et al.*, 1996; Hermanson, 1996).

Modification of the protocols described by Santra *et al.* (2001), Smith *et al.* (2006) and Tan^b *et al.* (2004) was undertaken to optimise biomolecule attachment. High-brightness ruthenium dye-doped nanoparticles were conjugated to polyclonal anti-hIgG antibody as described in *Section 2.7.2*. The antibody-modified particles were centrifuged at 20,000 x g and then resuspended in 0.1M phosphate buffer (1ml) containing 0.2% (w/v) BSA and 0.02% (v/v) NaN₃ and stored at 4 °C for used in fluorescence-based immunoassays for the detection of human IgG.

4.6.3 Nanoparticles as fluorescent labels for use in immunoassays

4.6.3.1 Titre of nanoparticle-antibody conjugate

A number of anti-human IgG antibody-nanoparticle conjugates were prepared using differing ratios of glutaraldehyde and BSA for biomolecule crosslinking to amino-functionalised particles. Each conjugate was titrated against immobilised human IgG (5 μ g) and the fluorescent response measured (*Section 2.7.3.2*) using a Tecan Safire² monochromator-based microplate reader, with excitation at 453nm and emission at 618nm, (Figure 4.23).

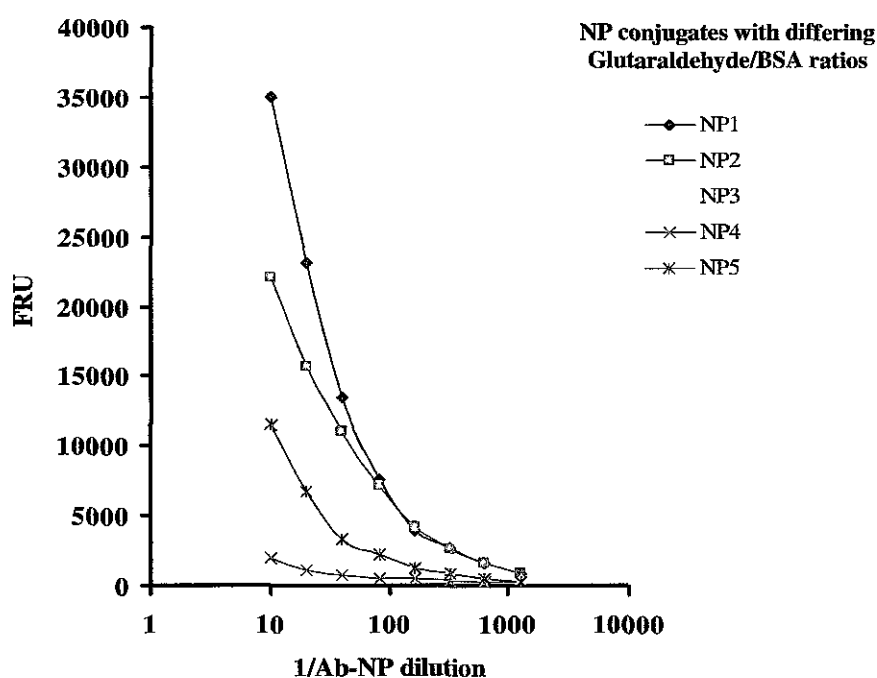


Figure 4.23 Fluorescent response of anti-human IgG-nanoparticle conjugates in a solid-phase direct binding assay, titrated against immobilised human IgG, for selection of optimal antibody-nanoparticle conjugate. The antibody-nanoparticle (Ab-NP) conjugates were prepared using varying ratios of glutaraldehyde-BSA for antibody crosslinking. The fluorescent response from each conjugate was plotted against conjugate dilution (1/10-1/1024).

Different ratios of glutaraldehyde-BSA were used for antibody conjugation; the sample which gave the highest fluorescent signal was selected for further assay development. This synthesis of this antibody-nanoparticle conjugate did not utilise any BSA and had glutaraldehyde at a final concentration of 0.1% (v/v), as per *Section 2.7.2*.

4.6.3.2 Sandwich assay for the detection of hIgG using ruthenium dye-doped nanoparticles and ruthenium dye as fluorescent label

The anti-human IgG antibody-nanoparticle conjugate was compared to ruthenium labeled anti-human IgG using a fluorescence-based sandwich assay. A black Fluoronunc™ 96-well microtitre plate was coated with anti-human IgG (5µg) and the assay performed as described in *Section 2.7.3.2*. Free human IgG dilutions, ranging from 0.005 - 500,000 ng/ml were prepared in PBS containing 0.1% (w/v) BSA and added to the plate in triplicate. Bound antigen was subsequently detected using anti-hIgG-conjugated nanoparticles and ruthenium labeled anti-human IgG (both previously diluted to 1/100). The plate was incubated at 37°C for 1 hour and washed as before. Following the wash step, the fluorescent response was determined using a Tecan Safire² monochromator-based microplate reader, with excitation at 453nm and emission at 618nm. The fluorescent response was normalized against a zero control (blank well containing no fluorescent molecules) and the normalised fluorescence plotted against the logarithm of human IgG concentration in ng/ml.

Figure 4.24 shows the calibration curve for a fluorescence-based sandwich assay for the detection of hIgG. Three sets of each standard were assayed over two days and the CVs calculated. CVs of between 0.41-7.60% and 0.36-4.73% were determined for the ruthenium nanoparticle assay and ruthenium dye assay, respectively.

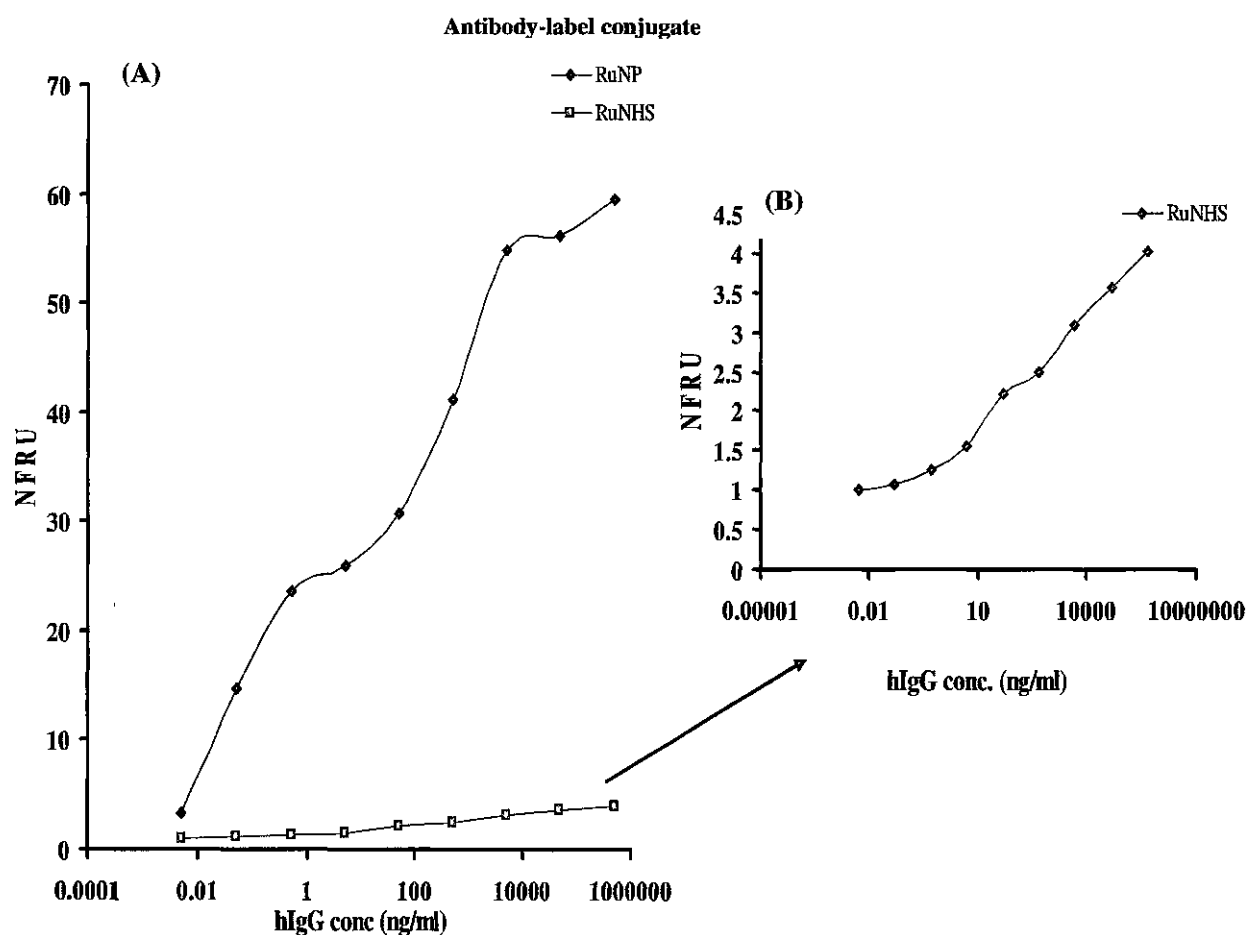


Figure 4.24 Fluorescence-based detection of human IgG in PBS, using a sandwich assay format. Both an anti-human IgG antibody-nanoparticle conjugate (RuNP) and ruthenium labeled anti-human IgG (RuNHS) were used for the detection of hIgG. The fluorescent response of each conjugate was normalised against a zero control (blank well containing no fluorescent molecules) and the normalised fluorescence (NFRU) plotted against the logarithm of human IgG concentration (ng/ml), for direct comparison of assay sensitivities. (A) Graph depicting the normalised fluorescent response vs. hIgG concentration using both the antibody-nanoparticle conjugate and ruthenium-labelled antibody for detection. (B) Graph depicting the normalised fluorescent response vs. hIgG concentration using the ruthenium-labelled antibody for detection (enlarged for clarity).

The assays were repeated twice and data fitted to a 4 parameter equation using Biaevaluation™ software. A calibration curve was constructed for determination of the lower limit of detection (mean value of the blank plus 3 times the standard deviation) of hIgG in a sandwich assay format for both the nanoparticle and ruthenium dye-antibody conjugates. Using ruthenium dye-doped nanoparticles as fluorescent label, a lower limit of detection of 1.3 pg/ml was calculated. Figure 4.25 shows the calibration curve for the fluorescence-based detection of hIgG using ruthenium dye-doped nanoparticles as fluorescent label.

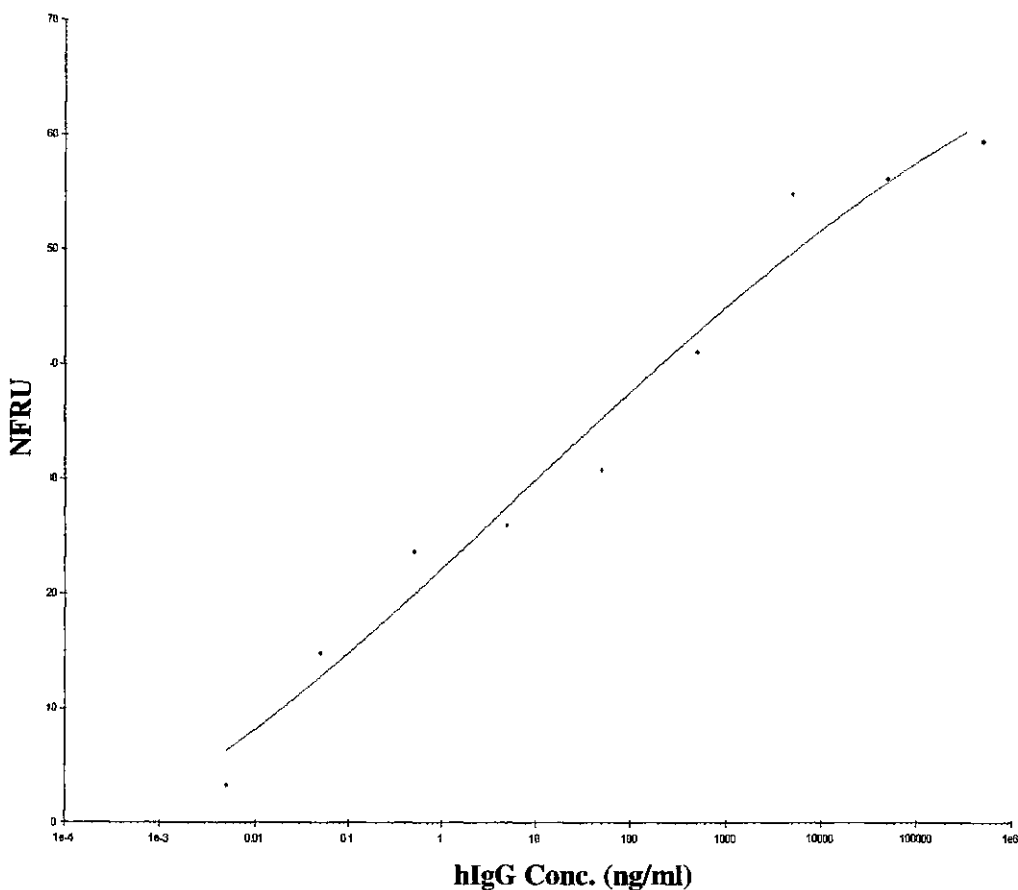


Figure 4.25 Calibration curve for the fluorescence-based detection of hIgG using ruthenium dye-doped nanoparticles as fluorescent label. The lower limit of detection was determined to be 0.0013ng/ml (1.3pg/ml) calculated from the mean value of the blank plus 3 times the standard deviation. The fluorescent response was normalised against a zero control (blank well containing no fluorescent molecules) and the normalised fluorescence (NFRU) plotted against the logarithm of human IgG concentration (ng/ml).

The same analysis was performed for the assay incorporating ruthenium dye as the fluorescent label, for direct comparison of assay sensitivities. The assay was repeated twice and data fitted to a 4 parameter equation using Biaevaluation™ software. A calibration curve was constructed for determination of the lower limit of detection (mean value of the blank plus 3 times the standard deviation) for the detection of hIgG using ruthenium dye as fluorescent label and a lower limit of detection of 84 pg/ml was determined. Figure 4.26 shows the calibration curve for the fluorescence-based detection of hIgG using ruthenium dye as fluorescent label.

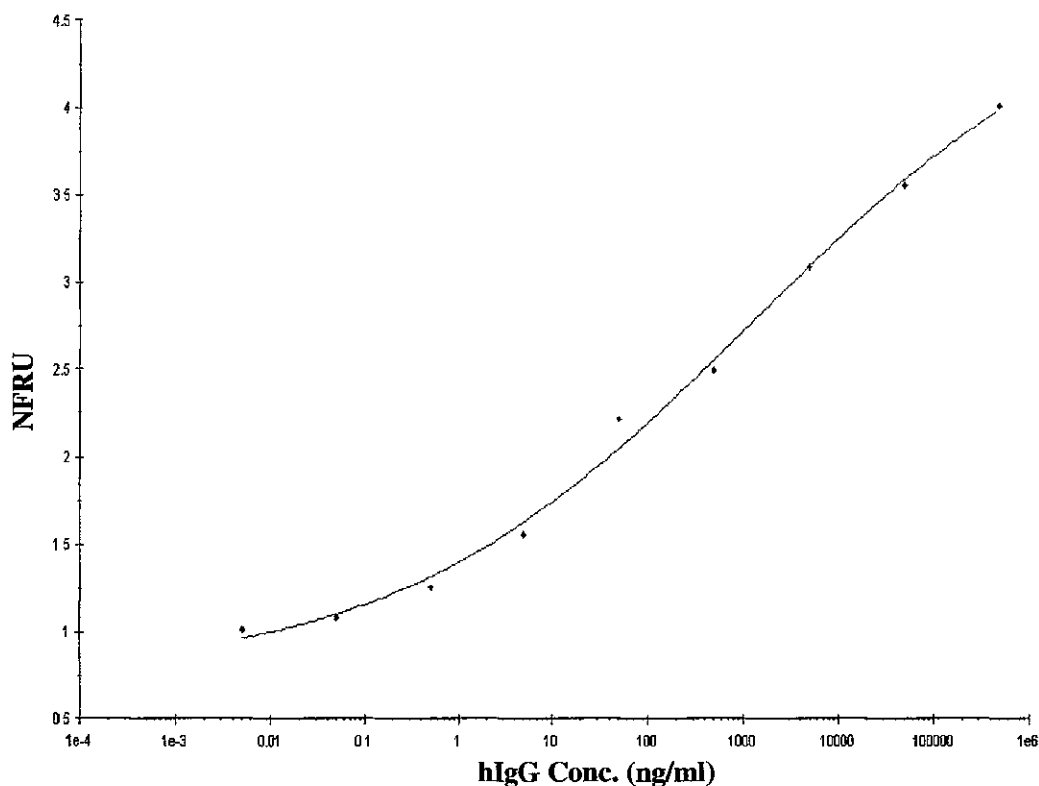


Figure 4.26 Calibration curve for the fluorescence-based detection of hIgG using ruthenium-dye as fluorescent label. The lower limit of detection was determined to be 0.084ng/ml (84pg/ml) calculated from the mean value of the blank plus 3 times the standard deviation. The fluorescent response was normalised against a zero control (blank well containing no fluorescent molecules) and the normalised fluorescence (NFRU) plotted against the logarithm of human IgG concentration (ng/ml).

Fluorescence-based detection of hIgG using ruthenium dye-doped nanoparticles as the fluorescent label was approximately 60 times more sensitive than detection with pure ruthenium dye. This demonstrates the potential use of dye-doped nanoparticles in immunoassay development, whereby the limitations (photobleaching, quenching) associated with the use of organic dyes could be overcome. Doping of highly functional nanoparticles that are easily modified for biomolecule attachment, with fluorescent dye molecules allows development of immunoassays with enhanced sensitivities.

4.7 Development of immunoassays for the detection of Parvovirus B19

In conjunction with industrial partners at Biotrin International Ltd. (Dublin, Ireland), a series of assays were developed, comparing various methods for the detection of Parvovirus B19. Commercial antibodies and a recombinant capsid protein (VP2), specific for Parvovirus B19 were donated by the research partners at Biotrin for assay development. A standard ELISA-based antigen capture assay, previously developed at Biotrin Ltd. was used as the model system. A recombinant VP2 structural protein was added to antibody-coated wells of a microtitre plate and subsequently detected with an anti-Parvovirus B19 enzyme conjugated antibody. This assay detects antigen in viraemic plasma at 10^8 genome equivalents/ml and is sensitive to approximately 10pg/ml of recombinant antigen (Doyle *et al.*, 2000). Fluorescence and luminescence-based detection methods were investigated for the same antigen capture assay for the detection of Parvovirus B19. Comparative studies were performed between the three methods and sensitivity, reproducibility and specificity assessed.

The main aim of validating these detection methods in solid phase plate-based assays was to transfer the assay for the detection of Parvovirus B19 onto enhanced cone platforms. In order to assess the suitability of Parvovirus detection on cone platforms, initially plate-based comparative studies were performed, investigating fluorescence and chemiluminescence-based detection and comparing these methods to the existing ELISA-based strategy. Reagents, antibodies and antigens* were supplied by Biotrin for use in a 96-well plate format and subsequently transferred to chip-based platforms. The chips utilised for this project, were the novel luminescence enhancement platforms designed and fabricated by NCSR researchers, previously described for the detection of InIB (Section 4.3).

** Please note that due the proprietary nature of the commercial reagents provided by the industrial partners (Biotrin International Ltd., Dublin) all buffer and reagent formulations have been omitted. These reagents are referred to only by generic terms (low pH diluent, blocking solution, and enzyme conjugate diluent) on the request of the industrial partners, Biotrin International Ltd.*

In order to evaluate the suitability of the cone structures for the development of chip-based assays for the detection of Parvovirus B19, a number of immobilisation strategies were first investigated. These immobilisation approaches were performed on both cone and planar surfaces and included passive adsorption, silanisation on indium tin oxide (ITO), plasma-enhancement via sputtering and glutaraldehyde activated cross-linking. Each method was investigated with immobilised horseradish peroxidase (HRP). Finally, the anti-VP2 antibody was immobilised on the cone structures using the best method for attachment and the optical enhancement generated from the immobilised immunoreagents was assessed.

4.7.1 Enzyme-linked immunosorbent assay for the detection of Parvovirus B19

An ELISA-based assay for the detection of Parvovirus B19 was investigated to see if limits of detection achieved by Biotrin researchers could be reproduced. A microtitre plate was coated with 4 µg/ml of coating antibody (anti-VP2 capture antibody from Parvovirus B19) and incubated (*Section 2.9.1*). Recombinant VP2 capsid protein dilutions were prepared in low pH sample diluent in concentrations ranging from 1pg – 10 µg/ml. Bound antigen was subsequently detected using horse-radish peroxidase-labelled anti-VP2 antibody with TMB as substrate (*Figure 4.27*).

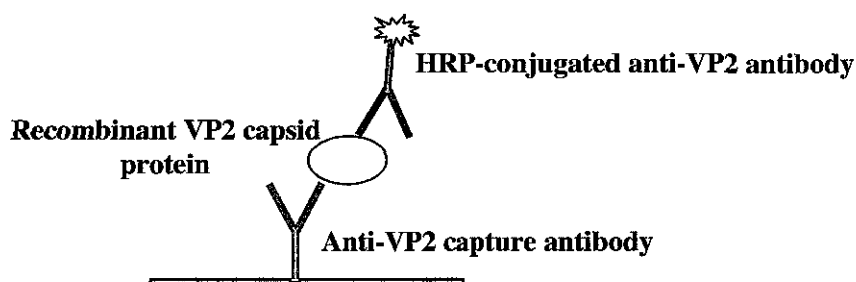


Figure 4.27 Schematic showing solid-phase assay format for the ELISA-based detection of Parvovirus B19 capsid protein VP2. An anti-VP2 antibody is used in a sandwich assay format to capture varying amounts of recombinant VP2 capsid protein. Bound protein is detected using a HRP-conjugated anti-VP2 antibody, which is subsequently traced using TMB substrate.

Figure 4.28 shows the calibration curve for an ELISA-based sandwich assay for the detection of Parvovirus B9 capsid protein VP2. Three sets of each standard were assayed over three days and the CVs calculated. CVs of between 0.44-18.66% were found.

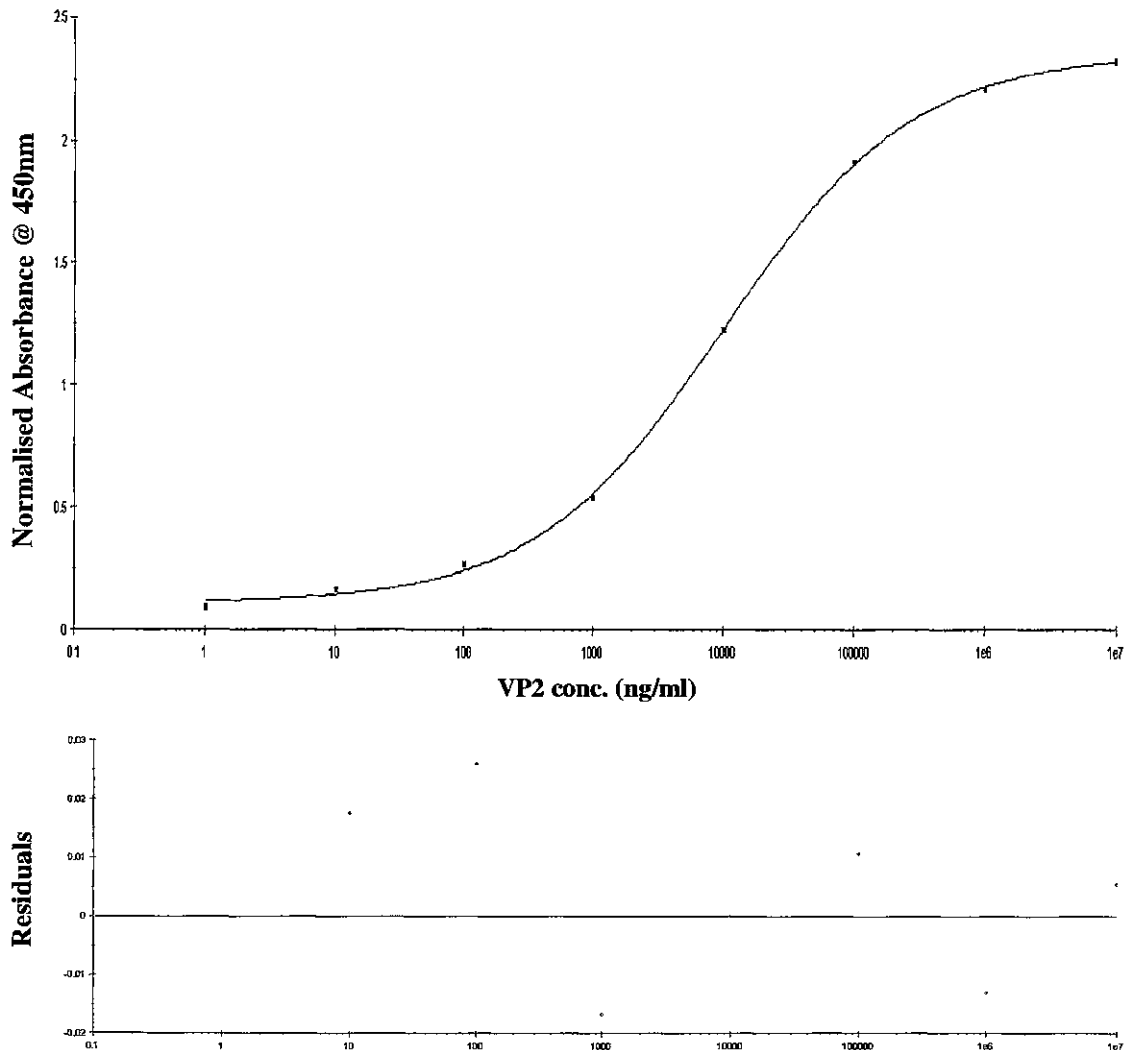


Figure 4.28 Calibration curve for ELISA-based detection of Parvovirus B19 VP2 capsid protein in PBS using a sandwich assay format. Residuals of Biaevaluation plot using 4-parameter equation fit for data are also shown. The lower limit of detection was determined to be 3 pg/ml, (mean value of the blank plus 3 times the standard deviation).

A lower limit of detection of 3 pg/ml for Parvovirus B19 capsid protein VP2 was calculated as the mean value of the blank (sample containing no VP2 capsid protein) plus 3 times the standard deviation of the blank. This was lower than the detection limit achieved by the Biotrin assay (10pg/ml) and suggested successful replication of the ELISA-based sandwich assay for the detection of VP2. The next step was to investigate the sensitivity and reproducibility of the VP2 assay using fluorescence and chemiluminescence-based detection methods. An avidin-FITC label was chosen for the fluorescence-based assay, while a luminol substrate was used for chemiluminescence-based detection of VP2. Optimisation of the assay using both fluorescence and chemiluminescence-based detection would allow transfer of the assay to chip format, which was the overall aim of the collaboration.

4.7.2 Fluorescence-based immunoassay for the detection of Parvovirus B19

A fluorescence-based immunoassay (FLA) for the detection of Parvovirus B19 was investigated. A microtitre plate was coated with 4 µg/ml of coating antibody (anti-VP2 capture antibody from Parvovirus B19) and incubated (*Section 2.9.2*). Recombinant VP2 capsid protein dilutions were prepared in low pH sample diluent (*proprietary*) in concentrations ranging from 1 pg – 10 µg/ml. Bound antigen was subsequently detected using biotin-labelled anti-VP2 antibody and avidin-FITC (Figure 4.29).

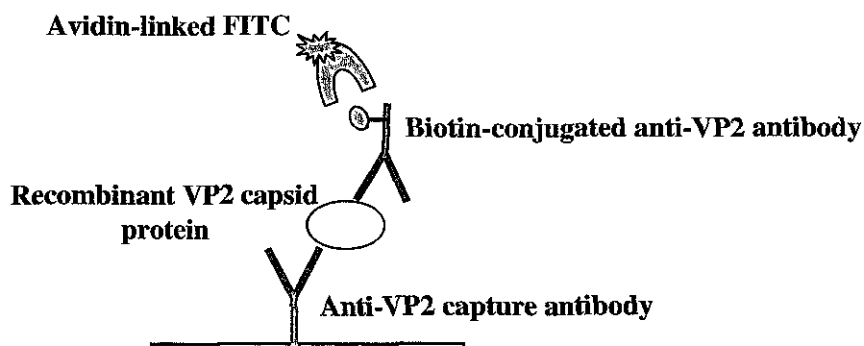


Figure 4.29 Schematic showing solid-phase assay format for the ELISA-based detection of Parvovirus B19 capsid protein VP2. An anti-VP2 antibody is used in a sandwich assay format to capture varying amounts of recombinant VP2 capsid protein. Bound protein is detected using a biotin-conjugated anti-VP2 antibody, which is subsequently traced using an avidin-FITC label.

Figure 4.30 shows the calibration curve for a fluorescence-based sandwich assay for the detection of Parvovirus B9 capsid protein VP2. Three sets of each standard were assayed over three days and the CVs calculated, CVs of between 0.39-6.02% were determined.

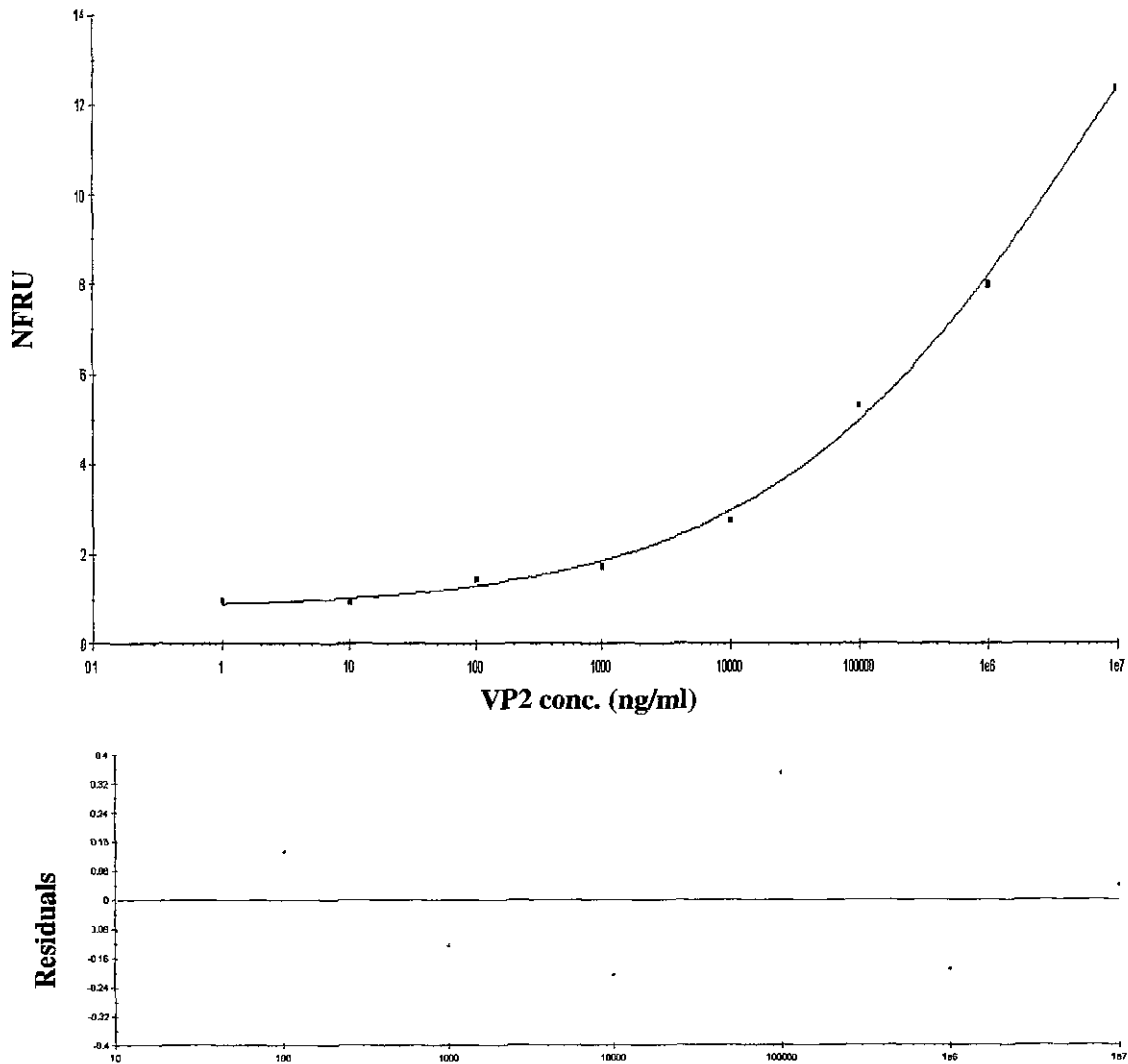


Figure 4.30 Calibration curve for the fluorescence-based detection of Parvovirus B19 VP2 capsid protein in PBS using a sandwich assay format. Residuals of Biaevaluation plot using 4-parameter equation fit for data are also shown. The lower limit of detection was determined to be 17 pg/ml, calculated from the mean value of the blank plus 3 times the standard deviation and the fluorescent response was normalised against the background fluorescence (NFRU).

The fluorescence-based assay produced a limit of detection less sensitive than the equivalent ELISA assay. The limit of detection for the fluorescence-based assay was determined to be 17 pg/ml, when calculated from the mean value of the blank (sample containing no VP2 capsid protein) plus 3 standard deviations. This was thought to be related to the immunoreagents used in the fluorescence-based assay which employed a biotinylated anti-VP2 antibody, as opposed to the HRP-conjugated anti-VP2 antibody used in the ELISA-based method. Fluorescence-based detection is generally more sensitive than enzyme-based methods, however, since there were proprietary issues concerning the reagents and buffers; optimisation of biotinylation and assay conditions were not permitted.

4.7.3 Chemiluminescence-based immunoassay for the detection of Parvovirus B19

A chemiluminescence-based immunoassay (CIA) for the detection of Parvovirus B19 was investigated. A microtitre plate was coated with 4 µg/ml of coating antibody (anti-VP2 capture antibody from Parvovirus B19) and incubated as described in *Section 2.9.3*. Recombinant VP2 capsid protein dilutions were prepared in low pH sample diluent in concentrations ranging from 1pg – 10 µg/ml. Bound antigen was subsequently detected using horseradish peroxidase-labelled anti-VP2 antibody and luminol/iodophenol substrate (Figure 4.31).

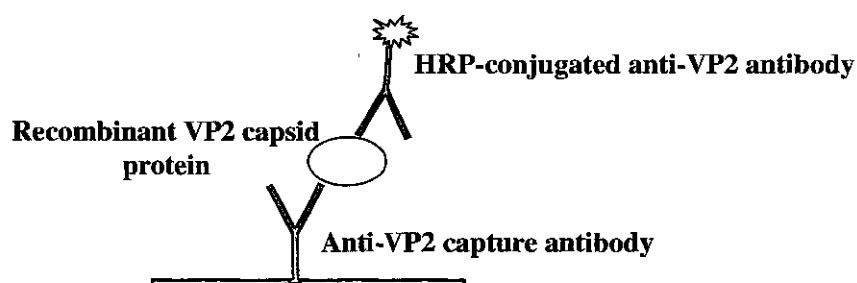


Figure 4.31 Schematic showing solid-phase assay format for the ELISA-based detection of Parvovirus B19 capsid protein VP2. An anti-VP2 antibody is used in a sandwich assay format to capture varying amounts of recombinant VP2 capsid protein. Bound protein is detected using a HRP-conjugated anti-VP2 antibody, which is subsequently traced using a luminol/iodophenol substrate.

Figure 4.32 shows the calibration curve for a chemiluminescence-based sandwich assay for the detection of Parvovirus B9 capsid protein VP2. Three sets of each standard were assayed over three days and the CVs calculated, CVs of between 1.11-9.16% were reported.

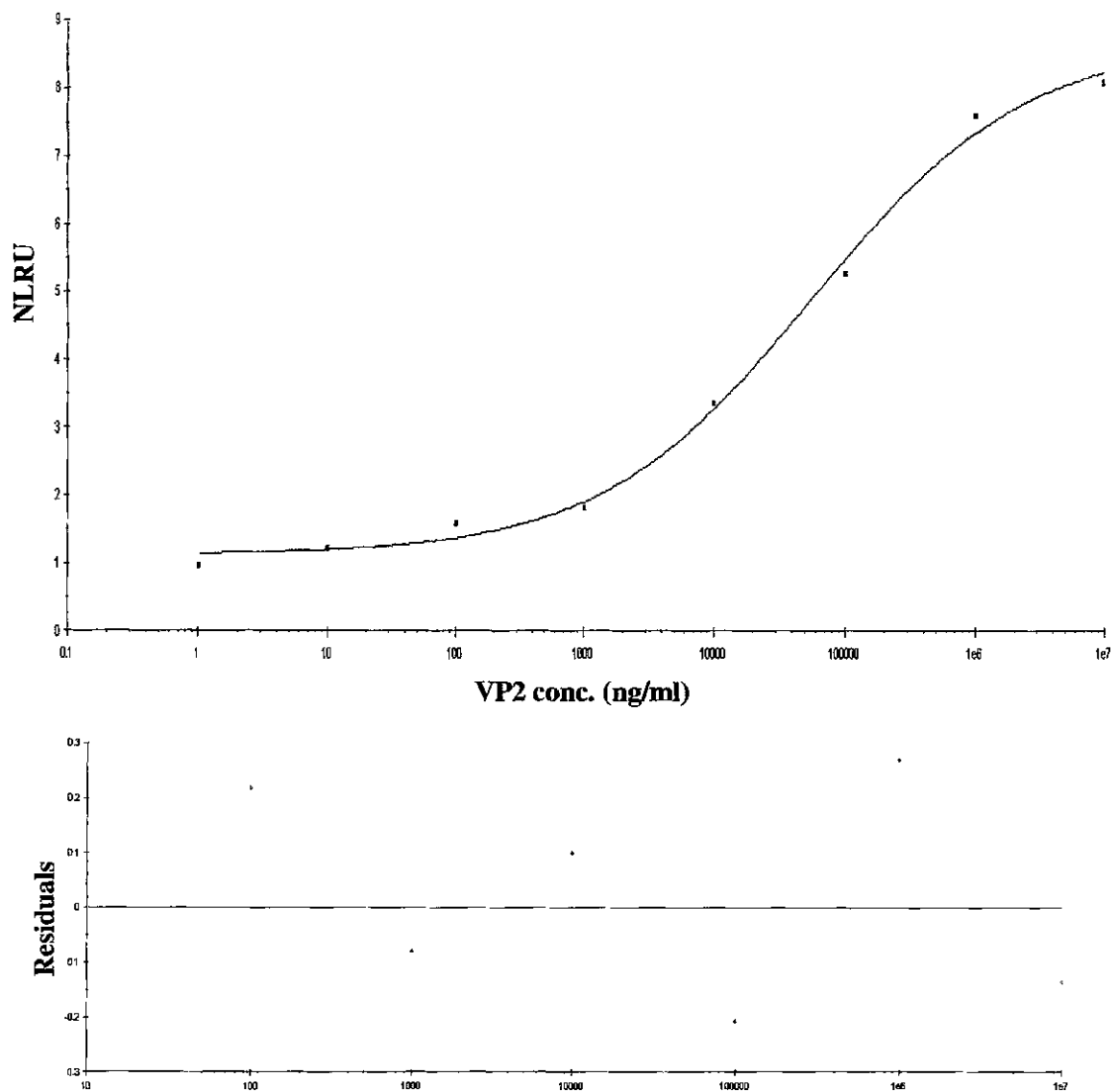


Figure 4.32 Calibration curve for the chemiluminescence-based detection of Parvovirus B19 capsid protein VP2 in PBS using a sandwich assay format. Residuals of Biaevaluation plot using 4-parameter equation fit for data are also shown. . The lower limit of detection was determined to be 38 pg/ml calculated from the mean value of the blank plus 3 times the standard deviation and the chemiluminescent response was normalised against the background luminescence (NLRU).

The chemiluminescence assay also established an LOD of 38 pg/ml, which was less sensitive than both the ELISA and the fluorescence-based assays. Although, the chemiluminescence-based assay used the same HRP-conjugated anti-VP2 antibody as the ELISA, it was far less sensitive. It has been suggested that chemiluminescence possesses much better signal-to-noise ratios than absorbance-based assays (Kricka, 2003). However, it did not perform significantly better in this assay format. In conclusion, the successful transfer from ELISA based detection on solid phase to fluorescent and chemiluminescent versions of the assay were established, the former being 4 times less sensitive than the established ELISA with an LOD of 17 pg/ml and the latter being almost 10-fold less sensitive with an LOD of 38 pg/ml reported.

4.7.4 Biomolecule immobilisation on cone structures The plate-based immunoassay for the detection of Parvovirus B19 capsid protein VP2 was successfully reproduced using enzyme-based detection. The assay was also successfully replicated in plate-based format using both fluorescence and chemiluminescence-based detection, albeit at slightly less sensitive LODs. The next phase involved transfer of the plate-based assays to a chip-based format using a polymer platform with cone structures for enhanced fluorescence and chemiluminescence-based detection. The microtitre plates used in the plate-based assays were MaxiSorb™ plates (Nunc, Denmark), which have a high affinity to biomolecules due to their mixed hydrophilic/hydrophobic domains. The MaxiSorb™ polystyrene surfaces therefore, promote biomolecule attachment through passive adsorption onto well surfaces (Anonymous, 1998). The polymer chips do not exhibit the same characteristics and so a number of surface modification strategies for biomolecule immobilisation were evaluated (*Section 2.9.4*). Both polycarbonate (PC) and polystyrene (PS) cone platforms were investigated for biomolecule immobilisation. The polymer chips were adapted in a number of ways to assess what kind of modification processes provided optimal biomolecule attachment.

Polymer chips were treated with an oxygen plasma and subsequently modified with aminopropyl-tri-ethoxysilane and glutaraldehyde prior to biomolecule immobilisation. The use of indium tin oxide (ITO)-coated polymer materials with and without aminopropyl-tri-ethoxysilane treatment was also examined. Each strategy was evaluated first using horseradish peroxidase (HRP), before being used to assess the immobilisation of the anti-VP2 coating antibody. The most consistent surface modification technique (that gave the highest levels of HRP immobilisation), was subsequently used in the fluorescence and chemiluminescence-based assays for the detection of Parvovirus B19 capsid protein VP2, on the chip platforms. Figure 4.33 shows a schematic of the surface modification techniques evaluated for biomolecule immobilisation on cone platforms.

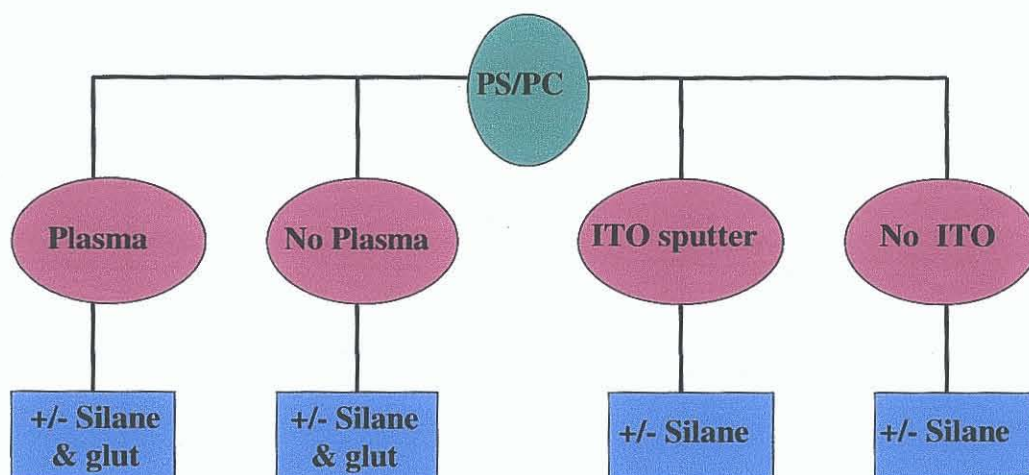


Figure 4.33 Schematic of surface modification techniques evaluated for biomolecule immobilisation on cone platforms. PC - polycarbonate; PS - polystyrene; Plasma - Oxygen plasma treatment; ITO - Indium tin oxide sputtering; Glut - Glutaraldehyde modification; Silane - Aminosilanisation. Both polycarbonate (PC) and polystyrene (PS) cone platforms were subjected to surface modification treatments. An oxygen plasma was sputtered onto the polymer chips, followed by silanisation to facilitate glutaraldehyde cross-linking. Another batch of chips were coated with indium tin oxide and subsequently treated with aminopropyl-tri-ethoxysilane. Negative controls were prepared for each surface modification step (whereby no treatment occurred) and the strategies were evaluated by assessing the amount of immobilised HRP post-modification.

Plasma treatment is a useful tool for biomolecule attachment to polymer surfaces for immunosensor applications (Wu *et al.*, 2000; Li *et al.*, 2004). The treatment of polymer surfaces with oxygen plasma is reported to enhance immobilisation of biomolecules (Jo *et al.*, 2000; Michalzik *et al.*, 2005) and, therefore, was assessed in this study. Glutaraldehyde is frequently used in biochemistry applications as an amine-reactive homo-bifunctional cross-linker, promoting biomolecule immobilisation in a number of sensor platforms (Lu *et al.*, 1997; Liu^a *et al.*, 1999; Deng *et al.*, 2004). Silanisation of the surface with aminopropyl-tri-ethoxysilane (APTES) allowed glutaraldehyde crosslinking and covalent immobilisation of antibodies to the chip surface. The use of glutaraldehyde both in the presence and absence of oxygen plasma treatment and silane was assessed. The sputtering of polymer surfaces with indium tin oxide (ITO) for enhanced immobilisation of biomolecules was reported by Fang *et al.* (2003), and this method was also investigated. Direct silanisation is a commonly used method for the immobilisation of biomolecules at chip surfaces (Nisnevitch *et al.*, 2000; Betty *et al.*, 2004). Thus, this method was also examined. Plant horseradish peroxidase (Sigma) is a cheap, robust molecule that is easily detected using TMB substrate and so was chosen as the test molecule for immobilisation for these preliminary studies.

4.7.4.1 Immobilisation of HRP on modified polymer chips for enhanced fluorescence and chemiluminescence-based detection

Both polycarbonate and polystyrene chips were investigated. Plant horse-radish peroxidase (HRP) was immobilised on the surface of modified cone structures (*Section 2.9.4.1*) and any remaining binding sites on the biochip blocked using PBS (0.15M NaCl, 2.5mM KCl, 10mM Na₂HPO₄, 18mM KH₂PO₄, pH 7.4) containing 1% (w/v) BSA. Following washing, bound HRP was detected following the addition of TMB substrate (*Section 2.9.4.1*). The CCD detection set-up (*Section 4.4.4*) used to assess the amount of bound biomolecule on chip surfaces, is only suitable for measuring fluorescence and chemiluminescence and does not have absorbance-detection capabilities. Therefore, reacted TMB substrate from each cone was transferred to wells of a microplate containing 135µl of unreacted substrate (1/10 dilution) and the absorbances for each sample was read at 620nm using a Safire² plate reader. Figure 4.34 shows the results for polycarbonate chips, modified as detailed in Figure 4.33.

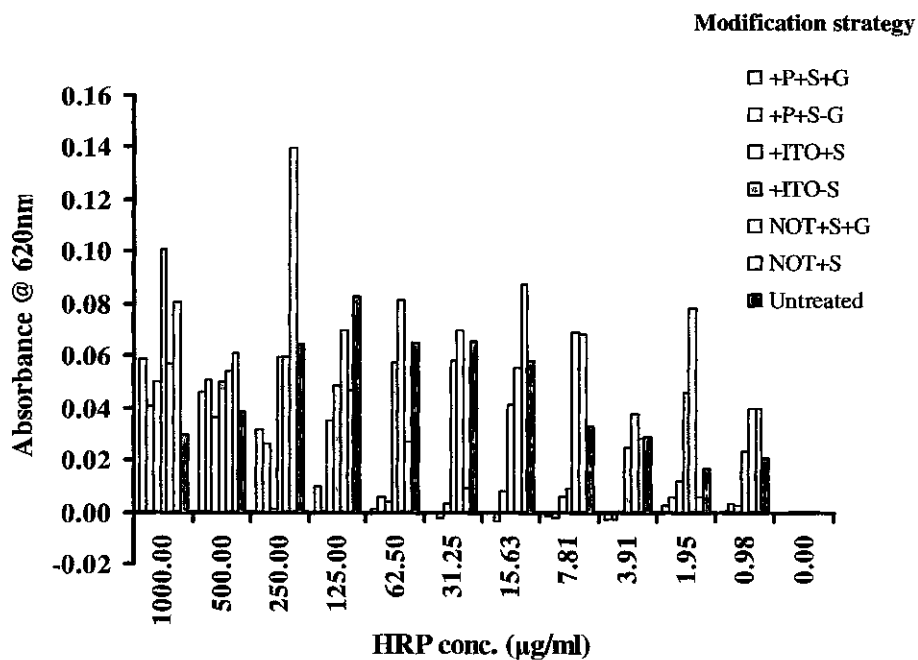


Figure 4.34 Immobilisation studies on polycarbonate. *P* - oxygen plasma treatment; *S* - silanisation with aminopropyl-tri-ethoxysilane; *G* - glutaraldehyde treatment; *ITO* - indium tin oxide sputtering; *NOT* - no treatment. The strategy that gave the most consistent immobilisation results for the polycarbonate chips was no plasma treatment but with both silanisation and glutaraldehyde modification. Controls included completely untreated chips. The background absorbance was subtracted from all values.

From Figure 4.34 it was determined that the oxygen plasma treatment was not enhancing HRP immobilisation either with or without subsequent glutaraldehyde crosslinking. The indium tin oxide sputtered chips that were silanised showed good levels of HRP immobilised at higher concentrations, however, this levelled off at the lower end of the concentration range. From this data, the most promising strategies were silanisation with glutaraldehyde treatment and silanised chips with no pre-treatment. These methods gave the most consistent immobilisation throughout the entire concentration range of HRP.

The polystyrene chips were evaluated in exactly the same way as the polycarbonate chips, except that the oxygen plasma pre-treatment and ITO sputtering strategies were not investigated, since they showed no obvious benefits on the polycarbonate cones. Figure 4.35 shows the results for polystyrene chips modified as detailed in Figure 4.33.

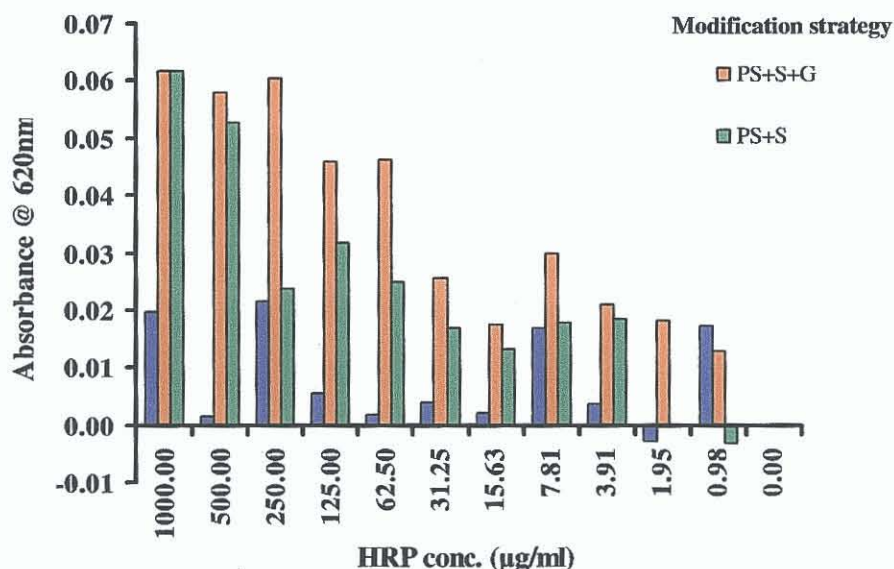


Figure 4.35 Immobilisation studies on polystyrene. G - glutaraldehyde treatment; S - silanisation with aminopropyl-tri-ethoxysilane, Untreated - no treatment. The strategy that gave the most consistent immobilisation results for polystyrene chips was determined to be glutaraldehyde crosslinking of HRP via the amino groups of aminopropyl-tri-ethoxysilane on the chip. Controls included completely untreated chips. The background absorbance was subtracted from all values.

The next phase involved assessing which polymer material was most suitable for use with glutaraldehyde for the immobilisation of HRP. A range of HRP concentrations (0-1000µg/ml) were spotted onto the cone platforms of both polycarbonate and polystyrene chips, in the presence and absence of silane/glutaraldehyde to determine which chip material was optimal (Figure 4.36).

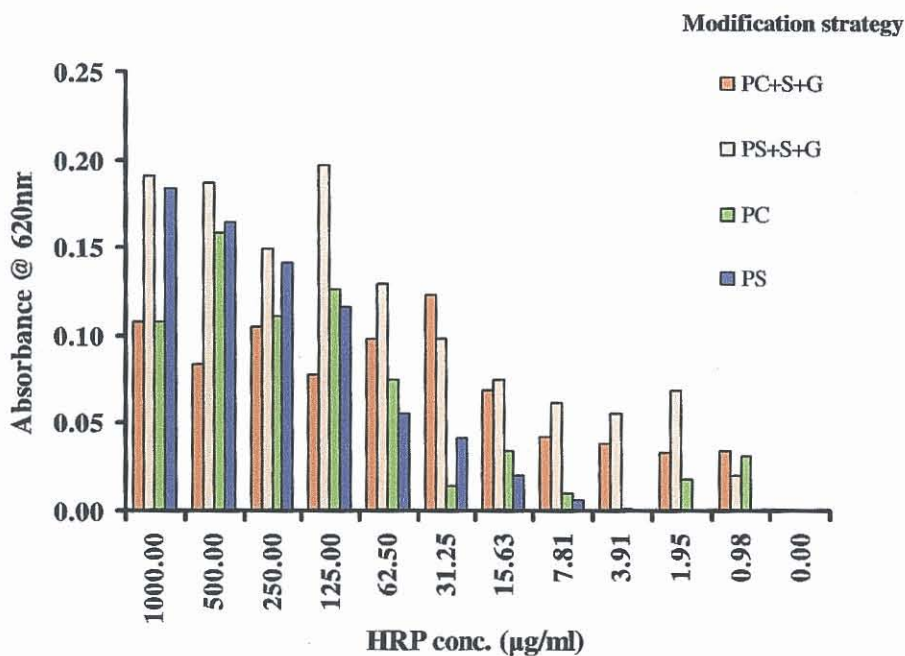


Figure 4.36 Immobilisation studies to determine optimal polymer type for biomolecule immobilisation. , PS - polystyrene; PC - polycarbonate; G - glutaraldehyde treatment; S - silanisation with aminopropyl-tri-ethoxysilane (APTES). Polystyrene chips with silane/glutaraldehyde modification showed the most consistent immobilisation of HRP. The background absorbance was subtracted from all values.

Polystyrene chips that were modified with silane and glutaraldehyde consistently showed the most uniform immobilisation levels of HRP. Therefore, polystyrene was deemed to be the optimal chip material since it produced the most reproducible results of HRP immobilisation. This was further improved by modifying the chip surfaces with aminopropyl-tri-ethoxysilane to assist in the immobilisation of HRP by glutaraldehyde crosslinking.

A consistent strategy for HRP immobilisation was defined on polystyrene chips that had been modified with silane/glutaraldehyde. The next phase involved the immobilisation of HRP-conjugated anti-VP2 antibody on the chip surface, using this immobilisation technique. A range of HRP-conjugated anti-VP2 antibody concentrations (0-1000 μ g/ml) were prepared and spotted onto the optimally-modified cones of polystyrene chips (Section 2.9.4.2). The amount of bound antibody was detected in the same way as immobilised HRP, using TMB substrate (Figure 4.37).

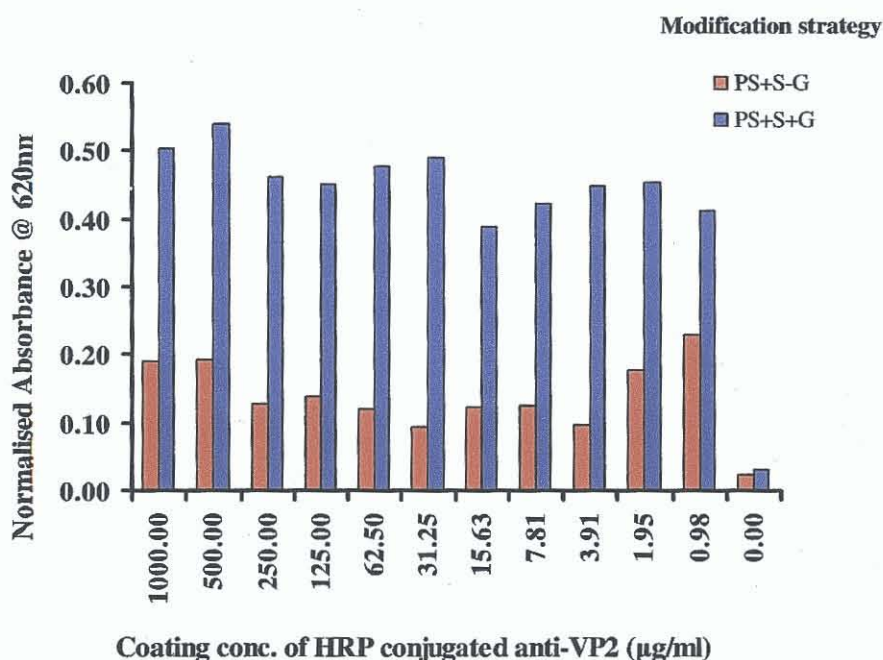


Figure 4.37 Immobilisation of antibodies. PS - polystyrene; G - glutaraldehyde treatment; S - silanisation with aminopropyl-tri-ethoxysilane (APTES). Polystyrene platforms were treated with aminopropyl-tri-ethoxysilane and subsequently investigated both with and without glutaraldehyde to determine the optimal coating concentration of HRP-conjugated anti-VP2 antibody for assay development on cone platforms.

Figure 4.37 shows that the presence of glutaraldehyde had a positive effect on immobilisation. Glutaraldehyde can be used to cross link biomolecules to polymer surfaces via activated functional groups (Lu *et al.*, 1997; Figueiro *et al.*, 2006). In this case amino groups were available from the aminosilanisation of the surface prior to the addition of glutaraldehyde. There seemed to be little variation in signal with decreasing concentrations of anti-VP2 coating antibody and so a low concentration was chosen, to

conserve antibody supplies. An anti-VP2 antibody concentration of 3.91 μ g/ml was selected for use in the further chip-based studies.

Figure 4.38 shows the different percentage glutaraldehyde solutions for use in chip-based assays for the detection of Parvovirus B19 capsid protein VP2. An ELISA-based assay was performed (*Section 2.9.4.3*) using varying percentage concentrations of glutaraldehyde for immobilisation of the coating antibody, 2.5%, 1% and 0.25% (v/v).

Anti-VP2 coating antibody (3.91 μ g) was spotted on modified cones and incubated for 2 hours at RT. The chip platforms were washed and blocked in the same way as the plate-based assay. Recombinant VP2 capsid protein dilutions were prepared in low pH sample diluent (Biotrin International, Dublin), at concentrations ranging from 1ng – 10,000ng/ml (*Section 2.9.4.3*). Each of the VP2 concentration was added in triplicate (3 cones) and incubated at RT for 2 hours. The chip platforms were washed, as before, and peroxidase-labelled anti-VP2 antibody added to detect the amount of capsid protein bound to each cone. TMB substrate (20 μ l/cone) was used to trace the HRP-conjugated anti-VP2 antibody bound to the differing concentrations of VP2 capsid protein. After 10 minutes incubation, 15 μ l of the reacted TMB substrate from each cone was pipetted into a microplate and 135 μ l of reaction solution was added and mixed for 3mins (1/10 dilution, total volume of reaction in each well is 150 μ l). The absorbances for all samples were read at 620nm and normalised against the background absorbance.

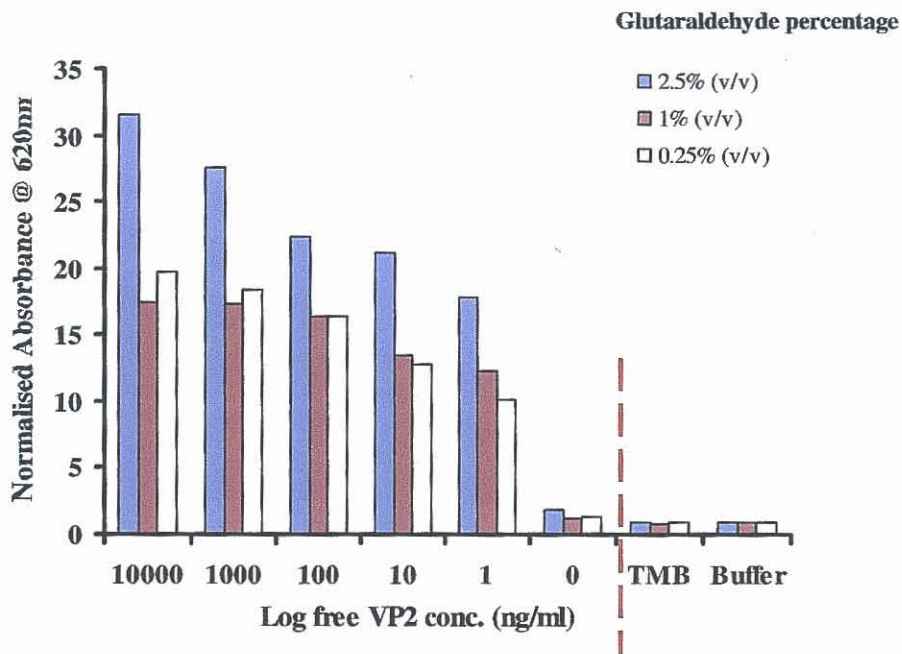


Figure 4.38 Determination of optimal percentage glutaraldehyde concentration for VP2 sandwich assay on polystyrene cone platforms. The ELISA-based assay was reproduced on the cone platforms using varying concentrations of glutaraldehyde for coating antibody immobilisation. The optimal concentration of glutaraldehyde was determined to be 2.5% (v/v). Both TMB substrate and buffer were also tested as negative controls, to determine background absorbance, which was subtracted from all test values.

Various surface modification methods were investigated to evaluate the most suitable strategy for biomolecule attachment onto the cone platforms, allowing the transfer of the plate-based assays to a chip format. Directed immobilisation of antibodies onto the cone platforms using glutaraldehyde crosslinking via aminosilane modification allowed transfer of the ELISA-based assay to chip format, where a detection limit of 1ng/ml was achieved. This strategy also was investigated for both chemiluminescence and fluorescence-based detection of VP2, to see if the plate-based assays could be replicated in chip format in the same manner as the ELISA-based assay.

4.7.4.2 Chemiluminescence-based detection on cone platforms

In order to assess compatibility of the CCD detection set-up for transfer of the chemiluminescence-based VP2 assay to a chip platform, the chemiluminescence-based detection of HRP was firstly investigated. HRP was immobilised as before and detected using a chemiluminescent substrate, using the CCD set-up (Section 4.4.4). The immobilisation of HRP (0-1mg/ml) via silane/glutaraldehyde crosslinking on polystyrene (PS) cone platforms was visualized by the *in situ* addition of luminol/iodophenol substrate using a luer lock syringe (Section 2.9.4.4). The detection of the generated chemiluminescent signal from immobilised-HRP was captured with a CCD camera. However, very long exposure times were required (~40 s). A number of problems such as deposition/light-capture issues were encountered. Figure 4.39 shows the chemiluminescent detection of immobilised HRP.

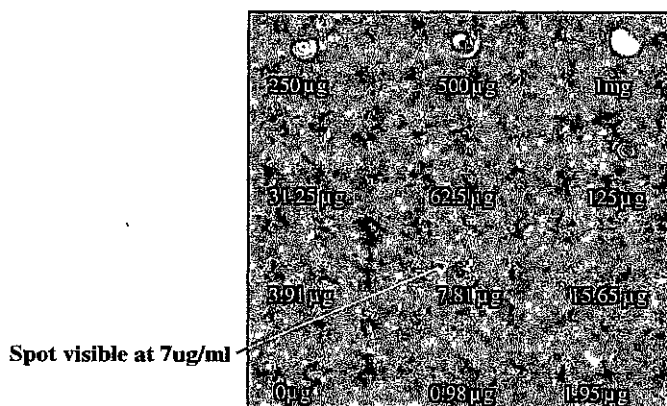


Figure 4.39 Chemiluminescent detection of immobilised HRP on glutaraldehyde-treated polystyrene cones. Luminol/iodophenol substrate was added to cone platforms and the generated luminescent signal from immobilised HRP at each spot was captured with a CCD camera. This was performed to assess the lowest amount of HRP detectable using this substrate and detection set-up. A faint spot was visible at 7.81 µg/ml. However, some concentrations above this point are not visible, indicating that the method was sub-optimal.

From Figure 4.39, a number of immobilised HRP spots are visible; however the sequence of spot intensities from the highest concentrations (1mg) to the lowest concentration (0µg) does not follow the expected pattern. Spot intensities (representing decreasing concentrations of immobilised HRP) decrease from 1mg/ml down to 125µg/ml, as expected, but after this point, at 62.5µg/ml, 31.25µg/ml and 15.65µg/ml, no chemiluminescent signal is apparent. However, on the cone representing 7.81µg/ml, there is a faint spot visible, even though concentrations above this point were undetectable. This indicated that this strategy was unsuitable for full transfer to a chip format at this point, due to significant problems in set-up and detection, whereby the accurate quantification of individual spot intensities was not possible. These problems were associated with concentration issues of luminol at the optical interface, which exhibited limited sensitivity for chemiluminescent HRP detection in this format. If this strategy were to be explored further, a surface-immobilised chemiluminescent label would be investigated.

4.7.4.3 Fluorescence-based detection of VP2 capsid protein on cone platforms

The transfer of the fluorescence-based detection of VP2 capsid protein from a plate-based method to cone platforms was evaluated. The immobilisation of biotin conjugated anti-VP2 antibody via glutaraldehyde crosslinking onto polystyrene cone platforms (Section 2.9.4.5) was performed. This allowed bound anti-VP2 antibody to be visualised with the addition of streptavidin-linked Cy5. Figure 4.40 shows a schematic of this format.

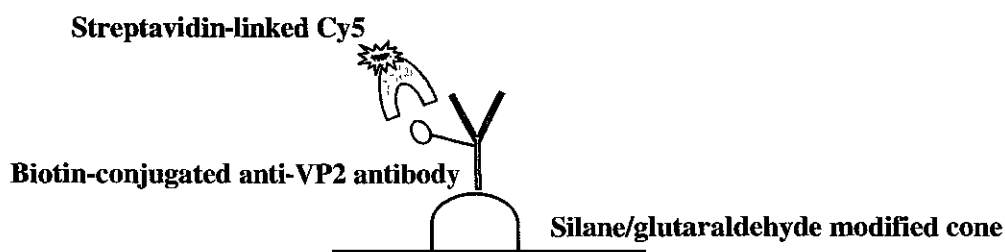


Figure 4.40 Fluorescence-based detection of biotin-conjugated anti-VP2 antibody immobilised on polystyrene cone platforms. Bound antibody was traced with streptavidin-Cy5 and the fluorescent signal generated was captured using both a CCD and CMOS camera.

A range of biotin-conjugated anti-VP2 antibody concentrations (0-1000 μ g/ml) were spotted onto cone surfaces of the chip. Four antibody concentrations (1000 μ g/ml, 125 μ g/ml, 7.81 μ g/ml and a control, 0 μ g/ml) were also spotted onto planar areas on the chip surface. This allowed visualisation of the enhancement effects of the cone structures, which are reported to enhance collected fluorescence up to 80 fold (Blue *et al.*, 2005). The fluorescent signal generated from the immobilised biotin-conjugated anti-VP2 antibody spots was traced with streptavidin-Cy5 and detected using a charged coupled device (CCD) camera, with an exposure time of 5 secs. The successful demonstration of fluorescence-based anti-VP2 antibody detection is shown in Figure 4.41.

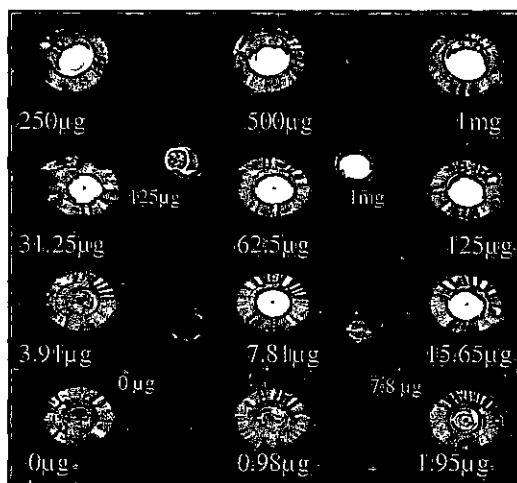


Figure 4.41 CCD image of immobilised biotin-conjugated anti-VP2 antibody, traced with streptavidin-Cy5. The concentrations of the antibody spots depicted in white text are on cone surface, whereas antibody concentrations on planar surfaces are show in red. A clear enhancement from antibody immobilised on the cone surfaces is evident and shows that the fluorescence-based detection of VP2 is possible using this setup.

Figure 4.41 shows the captured fluorescence and associated enhancement of bound biotin-conjugated anti-VP2 antibody, traced with streptavidin-Cy5. Spot intensities (representing decreasing concentrations of immobilised biotin-conjugated anti-VP2 antibody) decrease as expected, from 1mg/ml down to 7.81 μ g/ml, since there were fewer antibodies available for the reaction with streptavidin-Cy5. The fluorescent signal strengths from antibody immobilised on the cone parts of the chip were considerably higher than the comparative signals on the planar areas of the polymer surface at the same concentration. This is particularly evident at 7.81 μ g/ml, where the signal from the cone (white text) is significantly brighter than the signal from the planar surface at the same concentration (red text). This is a key outcome and clearly demonstrates proof of principle for enhanced fluorescence-based detection using the chip format.

Further improvements in detection setup, chip fabrication and fluorescent tracer molecules would be necessary for optimisation of this method if it is to achieve widespread use in immunoassay-based applications.

4.8 Discussion

The work described in this chapter involved the development of improved fluorescence-based detection methods for the immunosensing of various analytes. The chosen targets were warfarin, a small hapten, the bacterial protein InlB, *L. monocytogenes* bacterial cells and human IgG. Details of assay limits of detection are shown in table 4.5.

Table 4.5: Fluorescence-based assay limits of detection

Assay (Label)	LOD
InlB polyclonal assay (Qdots)	12ng/ml
InlB polyclonal assay (Porphyrin)	87ng/ml
InlB scFv assay (Qdots)	12ng/ml
Warfarin monoclonal assay (Qdots)	201ng/ml
Warfarin monoclonal assay (Porphyrin)	228ng/ml
Parvovirus VP2 protein (ELISA)	3pg/ml
Parvovirus VP2 protein (Chemiluminescence-based)	38pg/ml
Parvovirus VP2 protein (Fluorescence-based)	17pg/ml
Human IgG (Ruthenium-doped nanoparticles)	1.3pg/ml
Human IgG (Ruthenium label)	84pg/ml

The use of biochip-based systems using traditional fluorescent labels such as FITC and Cy5 have been reported by several authors (Rowe-Taitt *et al.*, 2000; Rubina *et al.*, 2005; Sapsford *et al.*, 2006). Microarray-based systems were successfully demonstrated for the detection of biotoxins, tumour markers, DNA and clinically important analytes (Ekins *et al.*, 1999; Feldstein *et al.*, 1999; Rowe^a *et al.*, 1999; Espina *et al.*, 2004). However, sensitivity is often limited by the spectral characteristics of the fluorescent probe and the quantum yield of the emitting molecules. The performance of a fluorescence-based immunoassay depends on both the specificity and affinity of the immunomolecules involved and also on the label/detection system chosen. Moreover, within the label/detection system association, there are two major considerations; one based on the specific activity of the labelled molecule and secondly, the sensitivity of the detection system for that molecule (Marquette *et al.*, 2006). In fluorescence-based detection platforms, the background noise of the measurement set-ups (photo-multiplier tube, CCD camera) is usually very low. As a consequence, in equivalent conditions of immunological reactivity and signal detection, the sensitivity of the assay is directed by the label activity or the labelling quality. Therefore, the use of improved fluorescent probes is a key consideration for the accurate and sensitive detection of analytes.

The application of enhanced fluorescent probes in immunosensing technology is an area of expanding recent interest (Seydack, 2005; Hun and Zhang, 2007). Fluorescent silica nanoparticles display excellent optical properties and are particularly useful as sensitive and photostable fluorescent probes for improved immunosensing and bioanalytical applications (Zhao *et al.*, 2004). With this in mind, this chapter focused on the use of novel fluorescent labels and biochip platforms for the improved detection of target analytes.

Fluorescence-based immunoassays for the detection of InlB were established using both streptavidin-linked quantum dots and porphyrin-labeled neutravidin as fluorescent labels (Section 4.2). The polyclonal antibody-based competitive assay using quantum dots as label has a limit of detection (LOD) of 12ng/ml (Table 4.5). This was determined by calculating the mean value of the blank (F_0) plus three times the standard deviation. The LOD for the scFv competitive assay was determined to be 12ng/ml (Table 4.5) and the polyclonal antibody-based competitive assay using porphyrin-labeled neutravidin as label has a limit of detection (LOD) of 87ng/ml (Table 4.5). These assays successfully demonstrated the use of quantum dots and porphyrin for the fluorescence-based detection of InlB. However, significant problems were encountered with the commercially acquired quantum dots. Large batch-to-batch variations were found and the fluorescent signal strengths of stock solutions were inconsistent. Many assays incorporating quantum dots, particularly those based on immunofluorescence, have been reported to be less sensitive than other assays (Jamieson *et al.*, 2007). The large size of quantum dots, relative to current fluorophores reduces their ability to access and label immunomolecules, and uncertainty over the toxicity of these molecules is a key issue. In addition, the fundamental characteristics of their surface chemistry and physiochemical properties in assay situations are poorly understood. For this reason the quantum dots were not further investigated as potential labels for the transfer of fluorescence-based detection of InlB to a biochip-based system.

However, the fluorescence-based detection of InlB in a biochip format was attempted with the near infra red label (NIR) Cy5; using specialised polymer platforms with cone structures for enhanced fluorescence capture (Section 4.3). The successful detection of anti-InlB polyclonal antibody, bound to immobilised antigen (InlB-F3) and traced with Cy5 was demonstrated using a CCD detection set-up (Section 4.3.5). This highlighted the

potential use of the cone platforms for further chip-based detection of analytes using alternative fluorescent labels. The use of dye-doped nanoparticles in such a system would greatly improve assay sensitivities.

Although little has been published on the use of quantum dots in solid-phase immunoassays, many authors have reported on their suitability for imaging applications (Mattheakis *et al.*, 2004; Sukhanova *et al.*, 2004). Quantum dots were therefore investigated for the imaging of *L. monocytogenes* bacterial cells using antibodies directed against InlA; a readily accessible cell surface protein on *L. monocytogenes*. The multicolour sensitivity of quantum dots makes them ideal for the analysis of complex samples using immunostaining techniques, (Wang *et al.*, 2004; Jaiswal *et al.*, 2003 and 2004). The main advantage of quantum dots for the immunostaining of bacterial cells is the ability to multiplex without the need for multiple excitation sources, thus facilitating double or even triple immunostaining of the cells. Whole *L. monocytogenes* cells were imaged using biotinylated anti-InlA monoclonal antibody tagged with streptavidin-linked quantum dots. This method was then compared to both FITC and Cy 5 staining (Section 4.5). The superior optical properties of quantum dots as imaging molecules was apparent when compared with these organic probes and the studies presented here show that quantum dots do have potential for use in imaging applications. However, only when the significant concerns regarding quantum dot stability and toxicity are fully addressed, will it be possible to fully assess their potential for use in fluorescence-based immunoassays.

The most commonly used detection methods for *L. monocytogenes* to date, include culture, biochemical testing, ELISA and nucleic acid amplification (Dunbar *et al.*, 2003). The majority of assays for detection are cell-based giving the value of *L. monocytogenes* whole cells in the sample. Dunbar *et al.* describe the use of microsphere-associated fluorescence-based detection of *L. monocytogenes* cells using a Luminex™ LabMAP microsphere system. Limits of detection achieved are $10^6/10^7$ genome equivalents for *L. monocytogenes*. The most common high-throughput screening system for detection of *L. monocytogenes* in food samples is the mini-VIDAS *L. monocytogenes* (LMO), (Mena *et al.*, 2004), where antibodies specific for the bacteria are used in an enzyme-linked fluorescence-based immunoassay. These methods were useful for determining the number of *L. monocytogenes* cells in a sample and, therefore, are unsuitable for direct comparison to the assay sensitivities reported in this chapter for the detection of InlB.

However, by employing internalin proteins and associated antibodies in immunoassay development, alternative strategies for detection are created. This is an important breakthrough as the use of *L. monocytogenes*-associated proteins eliminates the need to culture and handle dangerous pathogenic whole cells, when characterising novel immunoassay formats. Overall, it was demonstrated that anti-InlB antibodies and recombinant InlB fragments, could be used to generate specific assays for the detection of *L. monocytogenes* cell surface proteins. The use of avidin-linked fluorescent labels such as quantum dots and platinum-porphyrin dye was demonstrated for the detection of InlB in plate-based assays, while Cy5 was successfully used for the detection of both InlA and InlB in both chip-based and immunostaining formats.

Nanoparticles are highly complex, spectroscopically tailored tags that improve assay sensitivity, reproducibility and multiplexing capabilities, therefore, their potential use as labels for fluorescence-based detection was examined. Silica nanoparticles were doped with ruthenium dye for use in fluorescence-based assays for the detection of human IgG (Section 4.6). Antibody nanoparticles were prepared using methods adapted from Santra *et al.* (2001), Tan^b *et al.* (2004) and Qhobosheane *et al.* (2001) by amino-modification using APTES and glutaraldehyde crosslinking. The antibody-coated nanoparticles were utilised in a sandwich assay formats for the detection of human IgG and directly compared with an assay using ruthenium-labeled anti-human IgG. The dye-doped nanoparticles demonstrate a huge potential for improved fluorescence-based immunoassays with doped particles between 20,000-40,000 times brighter than their constituent dye. Comparison of the antibody-conjugated particles to dye-conjugated antibodies in a sandwich assay format for the detection of human IgG, gave normalised fluorescent signals up to 60 times brighter than the ruthenium dye-conjugated antibodies. Limits of detection of 1.3 pg/ml and 84 pg/ml (Table 4.5), were determined for the nanoparticles and ruthenium dye, respectively. The target detection limits were calculated using the 3 sigma method (mean of blank plus 3 x SD).

These results were better than the findings of Lian *et al.* (2004) who reported on the use of nanoparticles in immunoassays for the detection of human IgG using similar doped nanoparticles, fabricated in a comparable manner. They achieved a LOD of 1.9ng/ml for the detection of human IgG using FITC-doped nanoparticles. This suggests that the ruthenium dye-doped nanoparticles presented in this chapter are far superior to the particles described by Lian and co-workers. They have wide-ranging potential in the future of fluorescence-based detection, with improved detection limits, reduced photobleaching and increased sensitivity.

Lian *et al.* (2004) however, did demonstrate the use of doped particles in both solid-phase and biochip applications. The applications of nanoparticles in immunoassay formats included direct and indirect binding assays for the detection hIgG, using avidin nanoparticles in direct comparison with Texas red and quantum dots. Lian *et al.* also investigated the use of nanoparticles in a protein microarray application with high detection sensitivity reported. The main advantages of these probes over conventional small organic dyes and luminescent quantum dots is their ease of preparation, small lot to lot variability (as was significantly observed with commercial quantum dots) high functionality for biomolecule attachment, good photostability and absence of toxic constituent materials (as with quantum dots). Therefore, the potential applications of dye-doped nanoparticles are endless and the integration of this technology with chip-based detection methods should dramatically increase assay sensitivity even further.

The use of novel fluorescent probes for the detection of a hapten, namely warfarin, the ninth most prescribed drug in the world, was also investigated. Fluorescence-based immunoassays for the detection of warfarin were demonstrated using quantum dots and porphyrin as fluorescent labels (*Section 4.4*). The fluorescence-based immunoassays for the detection of warfarin were not as sensitive as conventional ELISA techniques. The limit of detection of free warfarin in ELISA was found to be 1.5ng/ml (Fitzpatrick and O'Kennedy, 2004). However, in the fluorescence-based immunoassays; the limits of detection were 201ng/ml and 221ng/ml (Table 4.5), respectively, for quantum dots and porphyrin. Problems were encountered with quantum dot stability (as before) and this could have led to decreased assay sensitivities. Issues with the protein-drug conjugate (warfarin-BSA) were also experienced which also could have also had an effect on assay performance. Frozen stocks of warfarin-BSA were thawed unintentionally (when a

freezer defrosted), which affected the functionality of the conjugate. Preparation of fresh warfarin-BSA was unsuccessful due to limitations in conjugate characterisation. However, these assays did demonstrate the potential of novel labels for the fluorescence-based detection of haptens and assay sensitivities could be improved through more efficient biotinylation of the monoclonal antibody or fresh preparation of the drug-conjugate. The use of more stable fluorescent labels such as dye-doped nanoparticles in association with the biochip cone platforms, described in *Sections 4.3.5 and 4.7*, could provide more sensitive fluorescence-based detection of warfarin, in line with the assay sensitivities previously established using ELISA and Biacore (Fitzpatrick and O'Kennedy, 2004).

Chip-based methods for the detection of Parvovirus B19 capsid protein VP2 were examined in association with an industrial partner (Biotrin International Ltd. Dublin). The immobilisation of biomolecules on chip surfaces was investigated for the development of chip-based assays for the detection of parvovirus B19 (*Section 4.7*). Successful optimisation of biomolecule immobilisation on polymer chips was achieved using HRP and various surface modification techniques (*Section 4.7.7*). Transfer of an enzyme-based assay for the detection of Parvovirus B19 capsid protein VP2, from plate to chip was demonstrated. Fluorescence and chemiluminescence-based detection of the VP2 capsid protein on chip platforms was not successful. Problems with detection set-up were encountered, however, proof of principle showing fluorescent detection of immobilised anti-VP2 antibody was shown. The fluorescent signal strengths from antibody immobilised on the cone parts of the chip and traced with fluorescent dye, were significantly higher than the same reagents immobilised on the planar surface of the chip. This demonstrates the potential of these cone-based platforms for use in biochip applications, whereby comparison of fluorescent signal from cones to planar surfaces showed a clear enhancement of collected fluorescence (Blue *et al.*, 2005). Further improvements to cone platforms and detection set up will enable this technology to become a useful tool for biochip applications. Significant developments have been ongoing within the NCSR to further improve the optical enhancement structures. These have included changes in the material used for fabrication, in the design of the cone to a paraboloidal structure, increasing the light collection efficiency still further, and improved precision in fabrication leading to better defined optical performance. Work is

also underway to improve the optical detection set-up, which would enable the use of novel fluorophores such as nanoparticles in the chip-based systems.

Future trends in fluorescent-based detection of biological molecules lie with a number of emerging technologies that combine nanotechnology with biomolecules for biochemical analysis. In this chapter, novel approaches for the enhanced fluorescence-based detection of molecules were examined, utilising improved reagents, novel probes and superior fluorescence capture systems. The benefits obtained through the use of novel labels on classical microtitre plates were presented and discussed and preliminary studies showing the application and potential transfer of these labels to protein biochips were also shown. Labels with better spectral properties including greater photostability, solubility in aqueous solution and high brightness (such as those described in this chapter) will play an important role in the future of immunodetection. The development of polymer biochips with cone structures for enhanced fluorescence capture will also have a significant influence in the area of fluorescence-based analysis. However, the approaches presented here are still in an early phase of development, and considerable improvements in sensitivity and limit of detection can be expected with further study and development. It is expected that improved labels and chip-based technologies will revolutionise biochemical analysis and the future of clinical diagnostics.

Chapter 5:
**The development of a ‘labelless’
immunosensor for the detection of
L.monocytogenes cell surface protein
fragment, InlB F3**

5.1 Introduction

Immunosensing devices transduce antigen-antibody interactions into directly measurable signals and allow simple, rapid and sensitive quantification of analytes in biologically complex samples (Byfield and Abuknesha, 1994). These devices incorporate either antigen or antibody at the sensor surface and subsequent probing with the opposite form, results in a highly specific immunocomplex. There are two main types of immunosensors; direct and indirect. Indirect immunosensors employ labels (fluorescent tags, enzymes, radio-isotopes, etc.), whereas direct methods are 'label-free'. The main difference between these sensor types is that direct immunosensors detect physical changes during immunocomplex formation, whereas, indirect immunosensors use signal generating labels that allow sensitive detection of the complex. In simple terms, labelled immunosensors are based on the direct detection of a specific label, whereas unlabelled types rely on a change in physical properties. The use of labels can often result in longer analysis times, with extra steps required, thus increasing the complexity of the procedure. Enzymes and fluorescent tags are by far the most commonly used components in indirect biosensors, whereas most affinity sensors are based on antibodies. The theory and background of the development of basic biosensors and immunosensors was discussed in Chapter 1. Here a more detailed account of affinity-based immunosensors is presented, in relation to an impedance-based sensor, developed for the detection of Internalin B.

5.1.1 Affinity Sensors

Affinity sensors detect the binding events occurring at sensor surfaces. They are excellent tools for the biosensing of biologically important reactions and subsequent detection of analytes in complex matrices (Tijssen, 1985). Affinity sensors are generally ligand-based solid-state devices, in which immunochemical reactions are coupled to a transducer (Buerk, 1993). The fundamental basis of these sensors is the specificity of the molecular recognition of antigens by antibodies to form a stable complex, whereby the binding of such a complex is monitored electrochemically or optically (Mullett *et al.*, 2000; Skottrup *et al.*, 2007; Pohanka *et al.*, 2007). The biological component in affinity immunosensors (either antibody or antigen) can be immobilised at the sensor surface via a number of methods, as shown in Table 5.1.

Table 5.1 Methods of immobilisation of biological components at biosensing surfaces

Method	Mode of Action	Example
Adsorption	Biological component is directly adsorbed onto a suitable surface.	Direct adsorption onto polymer chip.
Entrapment	Biological component is trapped within a matrix.	Physical entrapment of antibody within polymer matrix.
Microencapsulation	Biological element is trapped between membranes.	Use of self-assembled monolayers to entrap antibodies.
Covalent Attachment	Biological component is immobilised at the sensor surface via a series of covalent chemical bonds.	Use of thiols to immobilise antibodies on polymer chip surfaces.
Cross-linking	Biological component is chemically bonded to the sensor surface via use of a bifunctional agent.	Glutaraldehyde fixation of antibodies on polymer chip surfaces.

The other vital element in bioaffinity immunosensor fabrication is the type of detector involved. The direct detection of bioaffinity reactions can be performed with piezoelectric, optical, and electrochemical transduction methods (Dong *et al.*, 2000; Sadik *et al.*, 2002; Slavik *et al.*, 2002). Electrochemical transducers are most popular for affinity-based immunosensors and include potentiometric, amperometric and conductimetric devices

The selectivity of an immunosensor is based on the unique relationship between antibodies and their corresponding antigens. Antibodies bind specifically with their respective antigen providing ultra-high sensitivity and selectivity for immunosensors. The bonding between antigens and antibodies is dependent on a number of forces such as hydrogen bonds, hydrophobic bonds, electrostatic forces, and Van der Waals interactions. While these are all bonds of a weak, non-covalent nature, the associations between antigen and antibody can be quite strong. Antigens can exhibit multivalency, either through the existence of multiple copies of the same epitope or through the presence of multiple epitopes, which are recognized by multiple antibodies. Interactions involving multivalency produce more stabilized complexes; however, multivalency can also result in steric hindrances, which can reduce the possibility for binding (Benjamin, 2000). All antigen-antibody binding follows the basic thermodynamic principles of a reversible bimolecular interaction. The affinity constant K_A is determined as follows:

$$\text{Equation 5.1} \quad K_A = \frac{[\text{Ab-Ag}]}{[\text{Ab}][\text{Ag}]}$$

Where $[\text{Ab}]$ and $[\text{Ag}]$ are the molar concentrations of unoccupied binding sites on the antibody and antigen respectively, and $[\text{Ab-Ag}]$ is the molar concentration of the antibody-antigen complex. The time taken to reach equilibrium is dependent on the rate of diffusion and the affinity of the antibody for the antigen, and can vary widely (Aalberse *et al.*, 2001). The affinity constant for antibody-antigen binding can span a wide range, extending between 10^5 mol^{-1} to 10^{12} mol^{-1} and can be affected by a number of factors such as the temperature, pH and solvent.

5.1.2 Probing biomolecular interactions by impedance spectroscopy.

Bioelectronics is a rapidly progressing field that employs principles and techniques from chemistry, biochemistry, physics and materials science (Willner, 2002). The main features of a bioelectronic device include a conductive or semiconductive support for biomolecule immobilisation and an electronic transducer for processing of the biological functions occurring at the interface. Biomolecules that can be integrated with electronic transducers include proteins such as enzymes (Willner and Katz, 2000; Morrin *et al.*, 2003), receptors (Goepel and Heiduschka, 1995) antibodies or antigens (Rogers, 2000), oligonucleotides or DNA fragments (Yang *et al.*, 1997; Davis and Higson, 2005), or low molecular weight molecules exhibiting affinity interactions with other biomaterials such as biotin (Anzai *et al.*, 1998). There are a number of different electronic methods that can be employed to transduce the biological functions occurring at the electronic supports (Sethi, 1994). These include electrical transduction such as current (Xu *et al.*, 2006), potential changes (Ghindilis and Kurochkin, 1994), piezoelectric transduction (Ben Dov *et al.*, 1997), field effect transistor transduction (Zayats *et al.*, 2000), photoelectrochemical transduction (Pardo-Yissar *et al.*, 2003) and others such as surface plasmon resonance (Liedberg *et al.*, 1995; Jordan and Corn, 1997; Raitman *et al.*, 2002).

Electrochemical immunosensors are used extensively for the direct detection of antibody-antigen interactions. Their main advantages are that they are non-invasive and require little sample pre-treatment (Grant *et al.*, 2003). Electrochemical immunosensors involve the formation of a recognition complex between the sensing biomaterial and the analyte under investigation in a monolayer or thin-film configuration on an electronic transducer (Kharitonov *et al.*, 2000; Ouerghi *et al.*, 2002; Davis and Higson, 2005). The formation of a complex on a conductive or semi-conductive surface may alter the capacitance and the resistance at the surface-electrolyte interface (Katz and Willner, 2003) and this can be exploited to determine the concentration of the required analyte.

Impedance spectroscopy is a powerful tool for the analysis of the interfacial property changes of modified electrodes, upon the occurrence of biorecognition events at modified surfaces (Guan *et al.*, 2004). The immobilisation of biomolecules at electrode or semiconductor surfaces alters both the capacitance and interfacial electron transfer resistance of the surface (Berggren and Johansson, 1997). Impedance spectroscopy permits analysis of the changes occurring, that originate from the underlying biorecognition events. Thus, impedance spectroscopy (Nahir and Bowden, 1996; Pejčić and DeMarco, 2006), including non-Faradaic impedance measurements resulting in capacitance sensing (Bart *et al.*, 2005), is becoming an attractive electrochemical tool to characterise biomaterial films associated with electronic elements.

5.1.3 Immunosensors Based on Impedance Spectroscopy

Impedance spectroscopy is a useful electrochemical tool for the characterisation of biological thin-films involved in the transduction of biomolecular interactions at electrode surfaces (Ameur *et al.*, 1997; Sargent and Sadik, 1999). Electrical Impedance Spectroscopy (EIS) methods can be employed to investigate 'labelless' detection of analytes via impedimetric transduction. Several methodologies for the electrochemical transduction of antibody-antigen binding on modified electrode surfaces have been reported (Sadik *et al.*, 2002; Grant *et al.*, 2005).

Conductive polymers are excellent platforms for the immobilisation of biomolecules at electrodes. Sargent and Sadik, (1999) have investigated the binding mechanisms of antibody-antigen interactions on conducting polypyrrole films using impedance spectroscopy. While the charge transfer mechanisms are yet to be fully understood, it has been accepted now for sometime that antibody-antigen affinity associations may be monitored electrochemically via AC and other current transient approaches (Grant *et al.*, 2003 and 2005). Concentration-dependent impedance measurements are based on the theory of charge-generation and transportation at the polymer interface. This is due to the fact that proteins in solution act as polyelectrolytes and hence, as an antibody is a protein, its electrical charge will be affected on binding an antigen (Prasad and Lal, 1999). The impedance of the system increases as antigen

concentrations are increased, especially at lower frequencies (Katz *et al.*, 1998). The impedimetric response of an antibody-loaded film may be represented as either a Bode or Nyquist plot. A Bode plot shows the module of impedance of the system versus frequency and is indicative of the overall result. A Nyquist plot however, illustrates the real impedance of the system vs. the imaginary components (Kharitonov *et al.*, 2000). Although several processes can contribute to both the real and imaginary components, in most cases it can be assumed that Z' corresponds to charge transfer processes while Z'' refers to the capacitive component (Katz *et al.*, 2001). The typical shape of a faradaic impedance spectrum can be presented in the form of a Nyquist plot (Figure 5.1).

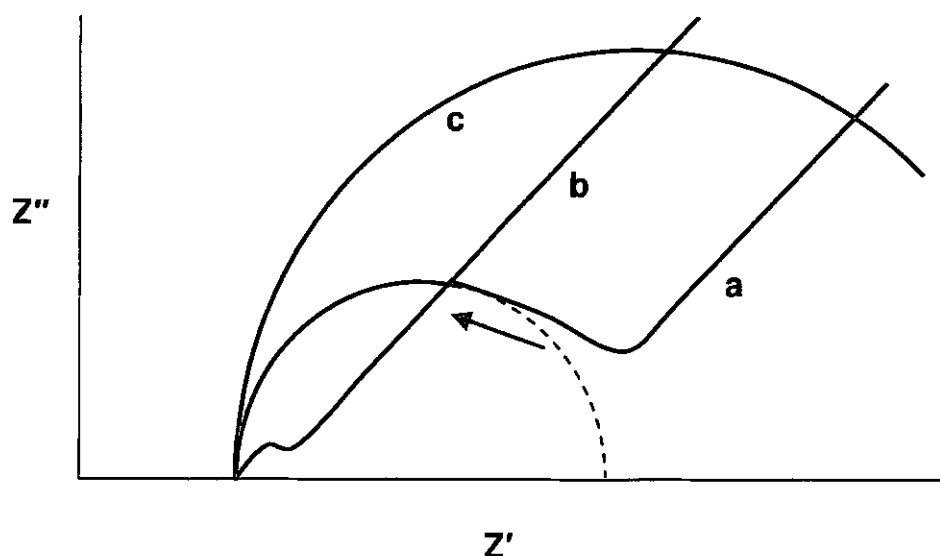


Figure 5.1 Schematic Faradaic impedance spectra presented in the form of a Nyquist plot. (a) A modified electrode where the impedance is controlled by diffusion of the redox probe (low frequencies) and by the interfacial electron transfer (high frequencies). (b) A modified electrode where the impedance is mainly controlled by diffusion of the redox probe. (c) A modified electrode where the impedance is controlled by the interfacial electron transfer within the entire range of the applied frequencies. The arrow shows the direction of the frequency increase.

A classical Nyquist plot consists of a semicircle region representing the capacitive component and a straight line with a slope of 45° that indicates the contribution made by the resistive component to the total impedance of the circuit, as shown in Figure 5.1, curve a. The semicircular portion is normally observed at higher frequencies and corresponds to electron transfer-limited processes; the linear part, however, is characteristic of the lower frequency ranges and corresponds to electrochemical processes that are diffusionally limited (Brett and Oliveira Brett, 1993). When electron transfer processes are fast, the impedance spectrum changes to include only the linear part, curve b, whereas a slow electron-transfer step is represented by a large semicircle region with no straight line, curve c. The electron transfer kinetics and diffusional characteristics can be extracted from the spectra. The semicircle diameter equals to the electron transfer resistance R_{et} . The intercept of the semicircle with the Z' -axis at high frequencies ($\omega \rightarrow \infty$) is equal to the solution resistance; R_s . Extrapolation of the circle to lower frequencies yields an intercept corresponding to $R_s + R_{et}$. Equivalent circuits are often included to help illustrate this; however, an equivalent circuit is not included here, since due to the complexity of the polymer/antibody/antigen interaction, many equivalent circuits could be equally valid. Once antigen is introduced to the system and binding occurs at the polymer interface, the shape of the Nyquist plot become more difficult to interpret. Both the real (Z') and imaginary (Z'') components tend to increase as antigen concentration increases, with the increases in the real component dominating the total increase in impedance, i.e. the faradaic component of the impedance increases more dramatically and is frequency independent (Ameur *et al.*, 1997). This principle forms the basis of the 'labelless'-immunosensor described here.

One of the most important parameters governing the technique is the applied frequency. At low frequencies ($f < 1\text{MHz}$), the impedance value is basically determined by the DC-conductivity of the electrolyte solution. At high frequencies ($f > 100\text{kHz}$), inductance of the electrochemical cell and connecting wires could contribute to the impedance spectra. Thus, the analytically meaningful impedance spectra are usually recorded at frequencies where they are mainly controlled by the interfacial properties of the modified electrodes ($10\text{mHz} < f < 100\text{kHz}$).

InIB contains four distinct domains, similar to the other members of the internalin family. This division of the recombinant protein into smaller truncated sections F3, F4 and F5, (Tully *et al.*, 2006) facilitated expression of only the most immunoreactive portion of the recombinant protein for immunosensing applications. The fragment F3 comprises of the N-terminal signal sequence, cap domain and 'Leucine-rich' repeat (LRR)-domain and was chosen as the target antigen for the development of an affinity sensor for the detection of InIB. The recombinant InIB F3 fragment was used in conjunction with an anti-InIB polyclonal antibody, for the development of a labelless, impedimetric immunosensor. Labelless affinity sensors are a new generation of biosensors and address a number of problems associated with the rapid diagnosis of food-borne pathogens by allowing cost-effective, specific and sensitive detection.

5.1.4 Electroactive Polymers

In order to produce conductive surfaces suitable for biomolecule attachment at the electrode, electroactive polymers are employed. These include, but are not limited to, polyacetylene, polypyrrole, polythiophene and polyaniline (Eggins, 1996; Lillie *et al.*, 2001; Li *et al.*, 2005). These conducting polymers are easily prepared by the electrochemical oxidation of the substrate at the electrode surface (Ramanavicius *et al.*, 2006). Factors which influence the suitability of a particular polymer for sensor applications are the type of solvent used and the counter anion in the solution, both of which can have a major effect on the polymer's conducting properties. The electrically conducting polymer polyaniline was used to develop the sensor surfaces for the labelless detection of Internalin B described here. Polyaniline exists in three well-defined oxidation states: leucoemeraldine, emeraldine and pernigraniline, as shown in Figure 5.2.

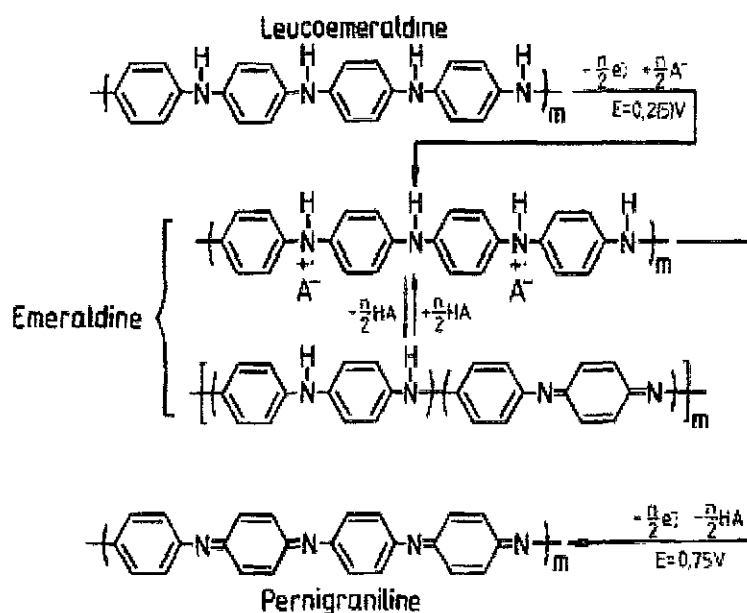


Figure 5.2 Generalised Scheme of the oxidative and non-oxidative doping of polyaniline: n , number of aniline units, $m = 4n$, (adapted from Eggs, 1996).

The accepted mechanism for the electropolymerisation of aniline (Eggs, 1996) is illustrated in Figure 5.2. The formation of the radical cation of aniline oxidation on the electrode surface is considered to be the rate determining step. This is followed by the coupling of radicals and the elimination of protons. The dimer formed undergoes oxidation on the electrode surface, along with aniline. The radical cation of the dimer couples with the aniline radical cation, resulting in propagation of the chain. The polymer formed is doped by the acid present in the solution. Leucoemeraldine and pernigraniline represent the fully reduced and fully oxidised forms, respectively. In emeraldine the ratio of amine to imine nitrogen atoms is ~ 0.5 . Electrically conducting emeraldine is produced either by standard chemical or electrochemical oxidation. During electrochemical polymerisation at pH 1.0, aniline is formed as its electrically conductive emeraldine form. Conducting polymers are those that permit some electrical conductivity in at least one redox state (Grennan *et al.*, 2006). The polymer may be oxidised or reduced, so the conductivity of the polymer depends on its redox state. Polyaniline has three redox states, as shown in Figure 5.2 which permit the polymer to exhibit either reasonable conductivity or insulating behaviour via its

polarisation. Polyaniline is easily electropolymerised from an aqueous solution of aniline monomer. Biomolecules may be immobilised within the polyaniline (PANI) matrix and for the purposes of this research anti-InIB antibodies have been immobilised within PANI via an avidin-biotin coupling method (Cui *et al.*, 2003; Dong *et al.*, 2004). Although only minute quantities of the biological component (antibody) are required, higher purity offers greater reliability (Turner *et al.*, 1989) and so a highly concentrated and pure sample of antibody is necessary.

5.1.5 Chapter Outline

The main objective of this chapter was to explore the development a labelless affinity biosensor for the rapid detection of Internalin B, a cell surface protein of the bacterial pathogen, *Listeria monocytogenes*. The methods utilised include electrochemical polymerisation and biotin-avidin coupling for site-specific immobilisation of antibodies onto specialised bio-modified surfaces. An anti-InIB polyclonal antibody was used for the development of 'labelless' immunosensor for the detection of Internalin B. The anti-InIB polyclonal antibody was specifically immobilised at the electrode surface via a series of surface modification steps. The sensors were then probed with varying concentrations of InIB antigen (F3 fragment) and impedimetric responses recorded. An anti-IgG antibody was also immobilised at electrode surfaces, as a control and subsequently exposed to the same concentrations of InIB antigen. Impedimetric data for the control sensors were also recorded. The antibodies act as the capture biocomponents for the antigen under investigation. They are used for impedimetric investigations into the binding event and associated processes, using the concepts described by Grant *et al.* (2003), to obtain affinity binding and signal transduction processing for the electrode platform assemblies. Complex plane impedance analyses were used to relate the differing redox states of the polymer to possible charge transfer mechanisms occurring at the interface and to explain how these may be used to modulate the impedance of the polymer. The planar electrodes and impedimetric detection methods were subjected to reproducibility and control analysis studies for assay validation.

5.2 Labelless affinity sensing of Internalin B

5.2.1 Electrochemical deposition of Polyaniline (PANI) at sensor surface

The electrochemical formation of polymer layers of controlled thickness at electrode surfaces via potentiometric deposition, gives rise to a reproducible method for biosensor fabrication. In this case, polyaniline (PANI) was used, as it can be easily electropolymerised from an aqueous solution of aniline monomer. Potentiodynamic cyclic voltammetry was employed and PANI was laid down as a planar thin-film over the working electrode of a carbon sensor as described in *Section 2.11.3* (and by Barton *et al.*, 2004). A typical cyclic voltammogram for the electrodeposition of polyaniline (PANI) is shown in Figure 5.3. The working electrode potential was scanned from -200mV to $+800\text{mV}$ (vs. Ag/AgCl) at a sweep rate of 50 mV/s . The buffer species, cycle number and polymerisation time were investigated to determine the most efficient and reproducible method for polymerisation of the PANI films.

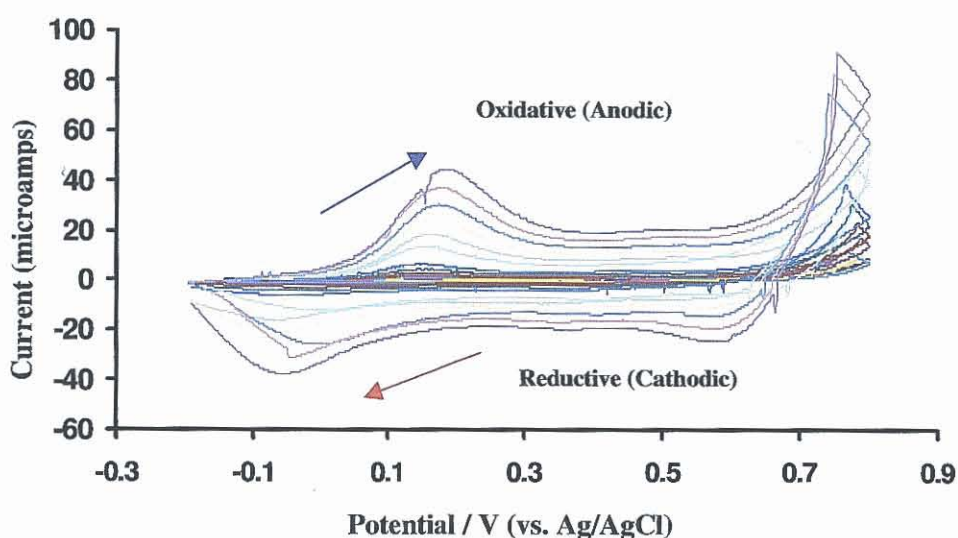


Figure 5.3 Cyclic voltammogram showing the potentiodynamic electrodeposition of polyaniline (PANI) as a thin-film on planar carbon screen-printed electrodes. The working electrode potential was scanned from -200mV to 800mV (vs. Ag/AgCl) and peak increases in anodic and cathodic current transients were recorded.

Peak increases in both anodic and cathodic current transients were insignificant after 15 cycles, indicating that optimum conductive deposition had occurred and the polymerisation was complete within ten minutes (Barton *et al.*, 2004). The controlled potential electrolysis of an aqueous solution containing monomers produces a suitable surface for antibody immobilisation. The main advantage of electrochemical polymerisation is that films can be prepared easily in a rapid one-step procedure. Furthermore, this method enables exact control of the thickness of the polymer layer based on the measurement of the electrical charge passed during the electrochemical polymerisation.

The exact mechanism of polymerisation is not fully understood and many authors have reported possible mechanisms (Gospodinova and Terlemezyan, 1998; Losito *et al.*, 2001.). Anodic polymerisation is, however, known to proceed via a two-electron oxidation (Losito *et al.*, 2001). The electropolymerisation of PANI is a self-regulating process since PANI is an insulating polymer and so the working electrodes become fully insulated after 15 potential sweeps. This limits the deposition of further polymer, thus regulating the final thickness of the film.

Electrochemical polymerisation is generally carried out in an acidic aqueous solution of aniline. A low pH is required to solubilise the monomer and generate emeraldine salt, the conducting form of polyaniline (Eggins, 1996). Constant potential or potentiodynamic techniques are employed since the over-oxidation potential for PANI is close to that required for monomer oxidation. A short-term increase of the applied potential to 800mV (vs. Ag/AgCl) during deposition was reported to give more adherent films (Barbero *et al.*, 1993) and therefore is utilised in this case. The growth of PANI is self-catalysing, whereby the greater the amount of polymer deposited at the surface, the higher the rate of polymer formation. The mechanism for this, as described by Zotti *et al.* (1998), involves the adsorption of the anilinium ion onto the most oxidised form of PANI, followed by electron transfer to form the radical cation and subsequent reoxidation of the polymer in its most oxidised state. During the electrochemical polymerisation at pH 1.0, aniline is formed as the electrically conductible emeraldine form.

5.2.2 Preparation of biomolecules for affinity immobilisation

Antibody biotinylation was performed prior to all other sensor fabrication steps and the biotinylated antibodies were stored frozen in working aliquots of 1mg/ml at -20°C. To remove sodium azide preservative, the antibody was subjected to gel-filtration using a Sephadex (G25) gel-filtration column prior to protein labelling, since sodium azide can have an adverse effect on the biotinylation of antibodies.

The avidin-biotin system provides a powerful tool for research and analysis due to the specific and high affinity ($K_a = 10^{15} \text{ M}^{-1}$) interaction between avidin and biotin. Biotinylated antibodies, enzymes and other biological molecules are increasingly used as highly specific probes in immunological methods (Heggeness and Ash, 1977; Gretch *et al.*, 1987; Wilchek and Bayer, 1988,). There are a number of commercial products and techniques available for the simple biotinylation of biological molecules. One of the most reliable commercially available kits is the ImmunoProbe™ Biotinylation kit from Sigma. This kit can be used to prepare biotin-labelled polyclonal and monoclonal antibodies for use in a wide variety of applications such as ELISA, immunoblotting, immunohistochemistry and other immunosensing techniques. This kit may also be used for conjugation of biotin to other proteins, peptides, hormones or cytokines.

Biotinylation is often performed with N-hydroxysuccinimide (NHS) esters of biotin or biotinamidohexanoic acid (BAC), (Wilchek and Bayer, 1988). The extended spacer arm from the hexanoic acid greatly improves the interaction between avidin and the biotinylated macromolecules by overcoming steric hindrance present at the biotin binding sites of avidin (Green, 1965). For this application using the Sigma ImmunoProbe™ Kit, biotinylation was performed with BAC-SulfoNHS, (Section 2.5.2.2). Sulphonation of the hydroxysuccinimide increases the polarity of the reagent, allowing it to dissolve easily in aqueous buffer. The ester provides a carbonyl carbon adjacent to the ester linkage, as a target for primary amine side-chains of accessible lysine residues, which joins the biotinamidocaproate to the protein via an amide bond (Immunoprobe biotinylation kit bulletin, Sigma). This derivative is soluble in water and biotinylation proceeds at near neutral pH values. The reagent is particularly useful when mild reaction conditions are required, for the biotinylation of sensitive biomolecules such as antibodies, enzymes and cell surface proteins (Gretch

et al., 1987). Following the labelling reaction, the biotinylated protein was separated from unreacted or hydrolysed reagent by a fast-gel filtration step, using a PD-10 desalting column (Amersham Pharmacia). The column, prepacked with Sephadex G-25, was used for the separation of unreacted BAC-SulfoNHS and buffer exchange. The column with a bed volume of 9.1ml and a bed height is 5 cm was pre-swollen in water containing 0.1% (w/v) Kathon® CG as preservative. Figure 5.4 shows the elution profile of the biotinylated anti-InIB antibody, using 10ml of PBS (0.15M NaCl, 2.5mM KCl, 10mM Na₂HPO₄, 18mM KH₂PO₄, pH 7.4), collected in 1ml fractions. The protein content of each fraction was monitored by measuring absorbance at 280 nm and the fractions containing protein were pooled (Fractions 3-7).

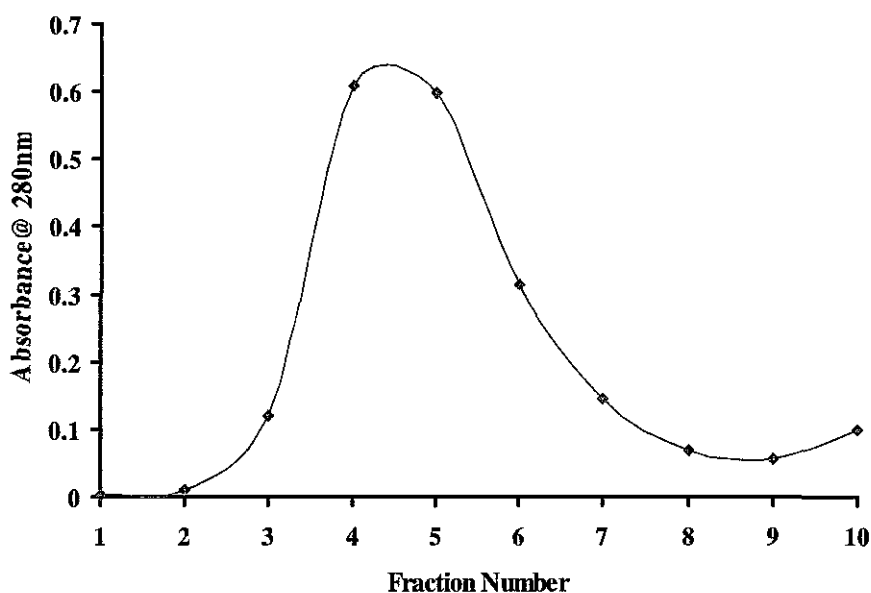


Figure 5.4 Elution profile of biotinylated anti-InIB polyclonal antibody following separation of unreacted biotin by fast-gel filtration using a PD-10 desalting column (bed volume of 9.1ml and bed height of 5 cm). Elution was performed using PBS (0.15M NaCl, 2.5mM KCl, 10mM Na₂HPO₄, 18mM KH₂PO₄, pH 7.4) and 10 x 1ml fractions were collected. The protein content of each fraction was determined by measuring the absorbance at 280nm and the fractions containing the majority of the biotinylated antibody (Fractions 3-7) were pooled for calculation of biotin content using the avidin-HABA assay.

The extent of biotinylated protein and ratio of biotin to protein were determined by the avidin-HABA assay (Green, 1965). The absorption of avidin-HABA complex at 500nm decreases proportionally with increased concentration of biotin as the HABA dye is displaced from avidin due to the higher affinity of avidin for biotin. Using a ratio of BAC-Sulpho-NHS/ IgG of 10.1, the level of biotin incorporation was determined to be approximately 4 moles of biotin per mole of anti-InIB antibody, which is in line with predicted values (Immunoprobe biotinylation kit bulletin, Sigma)

5.2.3 Affinity immobilisation of antibodies within polymer films

The major advantage of affinity immobilisation techniques is that there is no biomolecule present when the polymer matrix is formed PANI can thus be electrogenerated at the carbon sensor surface using optimum deposition conditions and any low pH effects on antibody are rendered irrelevant, as the antibody is immobilised after polymer deposition. A 0.2M aniline solution was prepared in a pH1.0 chloride buffer (0.5M KCl) to provide sufficient counter-ions for polymerisation. Cyclic voltammetry was then performed at a scan rate of 50mV/s from -200mV to +800mV and back to the starting potential (vs. Ag/AgCl). A linear sweep from -200mV to +800mV was performed at the end of cyclic voltammetry to leave the polyaniline in its conductive emeraldine salt form. The biotin NHS ester salt was prepared in deionised water at a concentration of 1mg/ml. The PANI-coated sensors were submerged in the biotinylating solution (30µl) for 24hours. The biotin coupled to the primary amines at the end of the polyaniline chain and to secondary amines throughout the polymer.

Neutravidin biotin-binding agent was prepared in de-ionised water at a concentration of 10ug/ml. The neutravidin (30µl) was added to the working electrodes of the biotinylated sensors, by pipetting, and left to incubate for 1 hour (*Section 2.11.4*) The sensors were then thoroughly flushed with de-ionised water to remove any non-specifically weakly absorbed matter. The biotinylated antibody at a concentration of 1mg/ml was defrosted and the sensor working electrodes were covered in the antibody solution (100µl) for another 1 hour period. De-ionised water was then used again to thoroughly flush the sensors and remove any non-specifically bound antibody at the end of the exposure

Avidin-biotin attachment bridges were formed on the polymer films, by taking advantage of the strong specific biological interactions between avidin and biotin (Ouerghi *et al.*, 2002; Dong *et al.*, 2004). Biotinylated antibodies were specifically coupled to the biotinylated polymer films via neutravidin. This method allowed controlled immobilisation of biomolecules at the sensor surface. A schematic representation of the immobilisation approach is illustrated in Figure 5.5.

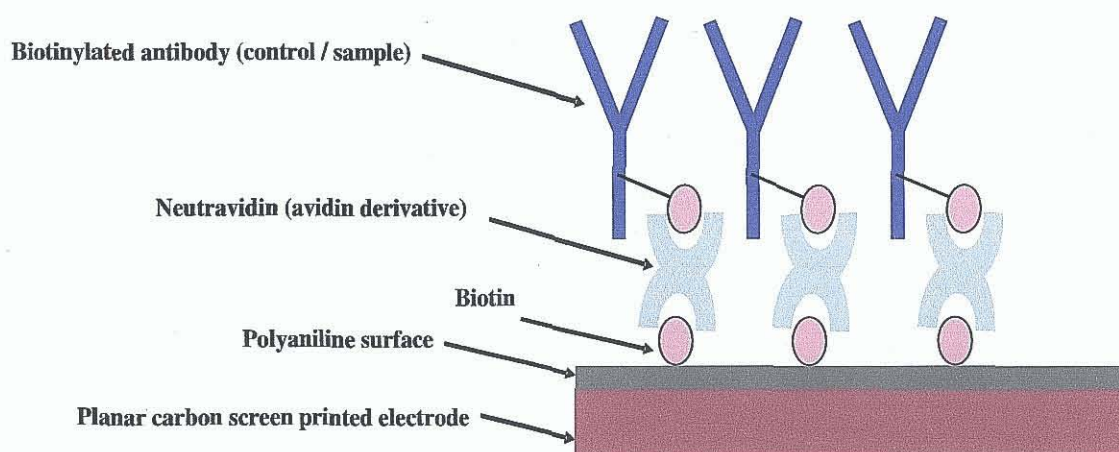


Figure 5.5 Schematic representation of biomolecule immobilisation onto polyaniline (PANI) sensor surfaces via biotin-avidin coupling. Biotinylated antibodies, both sample (anti-InlB antibody) and control (anti-IgG antibody) were specifically coupled to the biotinylated polymer (polyaniline) films using the avidin derivative neutravidin, which formed avidin-biotin bridges. This method allowed controlled immobilisation of biomolecules at the sensor surface.

This approach for antibody immobilisation provides orientation-specific attachment of a monolayer of antibodies at the surface of the polyaniline film. Optimum deposition criteria can be utilised for polyaniline electrogeneration (low pH), since the antibody is immobilised post-PANI deposition, and therefore, antibody attachment can occur at neutral pH. In order to reduce any non-specific binding effects, BSA blocking solution was prepared at a concentration of 10^{-6} M in de-ionised water and the electrode surfaces were submerged in this solution, for 1 hour at room temperature. BSA does not contain endogenous biotin and therefore is compatible for use in biotin/avidin systems as a blocking agent.

5.2.4 Electrochemical impedance interrogation of PANI thin-film carbon electrode platforms

Following electropolymerisation of the sensor surfaces with PANI, the electrodes were modified as described in *Section 2.11.4* and sample and control antibodies were site-specifically coupled to the sensors as per *Section 2.11.5*. Impedimetric data were collected for the InIB-doped sensor between 10,000Hz -1Hz in PBS (0.15M NaCl, 2.5mM KCl, 10mM Na₂HPO₄, 18mM KH₂PO₄, pH 7.4) i.e. buffer containing no antigen, as a baseline trace. Four sensors were used for each experiment (two sample and two control) and each sensor was interrogated in triplicate for reproducibility analysis (six replicates in total). After 30 minutes exposure to buffer alone (baseline trace), the sensor was flushed thoroughly with 50ml of PBS (as above) and the impedance spectrum was recorded. This sensor was then exposed to increasing antigen (1-100ng/ml) and the process was repeated for the full range of concentrations. Six-matched sensor pairings (sample and control) were evaluated at each concentration and the corrected responses plotted. Spectra were analysed over the full frequency range and for clarity represented in terms of percentage impedance changes from the baseline impedance trace

The probing of the modified sensors with antigen (InIB F3 fragment), demonstrated the principle of a labelless detection method for the *L. monocytogenes* cell surface protein InIB. Impedimetric data were collected for the anti-InIB-doped sensors after exposure to increasing antigen concentrations (1ng/ml-100ng/ml), as described in *Section 2.11.6*. Impedances were recorded for each InIB concentration over a range of frequencies from 10,000-1 Hz. For construction of a calibration curve, a frequency of 1Hz was chosen for interrogations since this is the frequency which allowed the greatest changes in impedimetric response to be observed. Initial examination of the total overall impedance (Z) of each of the films at various concentrations of InIB, allowed construction of a calibration curve. Three replicate measurements were recorded on two separate electrodes for each antigen concentration and CVs of less than 5% were determined (Figure.5.6).

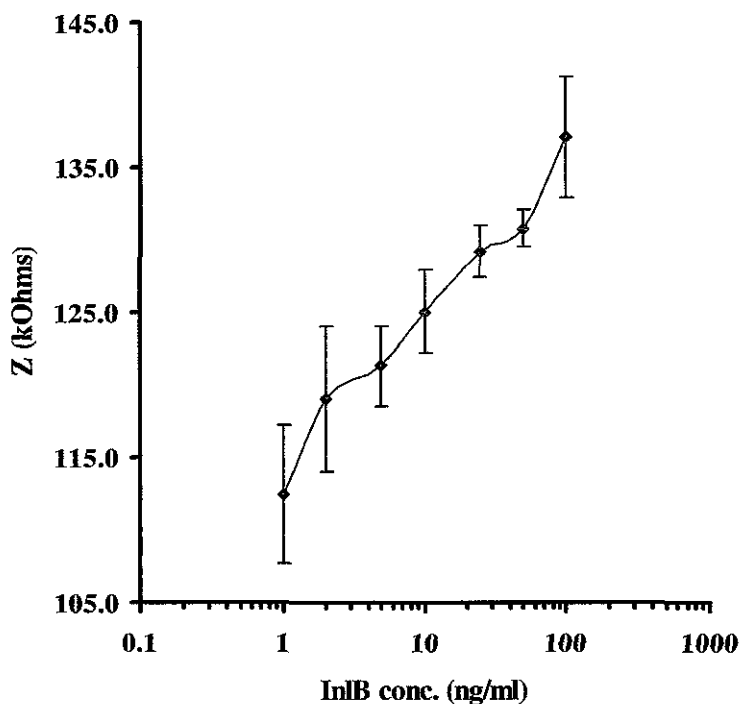


Figure 5.6 Calibration curve of InlB concentration at 1Hz. The calibration curve was generated as a result of exposure of an anti-InlB loaded PANI-film to increasing concentrations of InlB (1-100ng/ml). The curve displays total impedance (Z) against InlB concentration (ng/ml). Error bars are calculated from the standard deviations of the mean value of three replicates on two separate electrodes and CVs of less than 5% were found.

Initial examination of the total impedance of the anti-InlB loaded PANI thin-film electrodes at various concentrations of InlB (1-100ng/ml) gave CVs of less than 5% and the calibration profile showed near-linear behaviour between 1-100ng/ml. It can be clearly observed from Figure 5.6 that the anti-InlB-loaded PANI thin-film electrodes provide specific recognition sites for InlB detection. Increasing changes in total impedance (Z) were attributed to the changes occurring at the electrode/polymer interface, as a result of immunocomplex formation, whereby antibody-antigen binding affected the electrochemical activity of the modified electrode surface.

5.2.5 Specific recognition of InlB with anti-InlB-doped sensors (sample)

In order to differentiate between the individual components of the total impedance of the system, both the capacitive and faradaic components of the composite impedimetric response were investigated. Electrochemical impedance spectra obtained for anti-InlB-doped PANI thin-film electrodes, exposed to increasing InlB concentrations were presented in the form of a Nyquist plot (Figure 5.7). The Nyquist plot depicted the real (Z') and imaginary (Z'') components of the AC impedance of the sensors, following exposure to InlB antigen (1 – 100ng/ml).

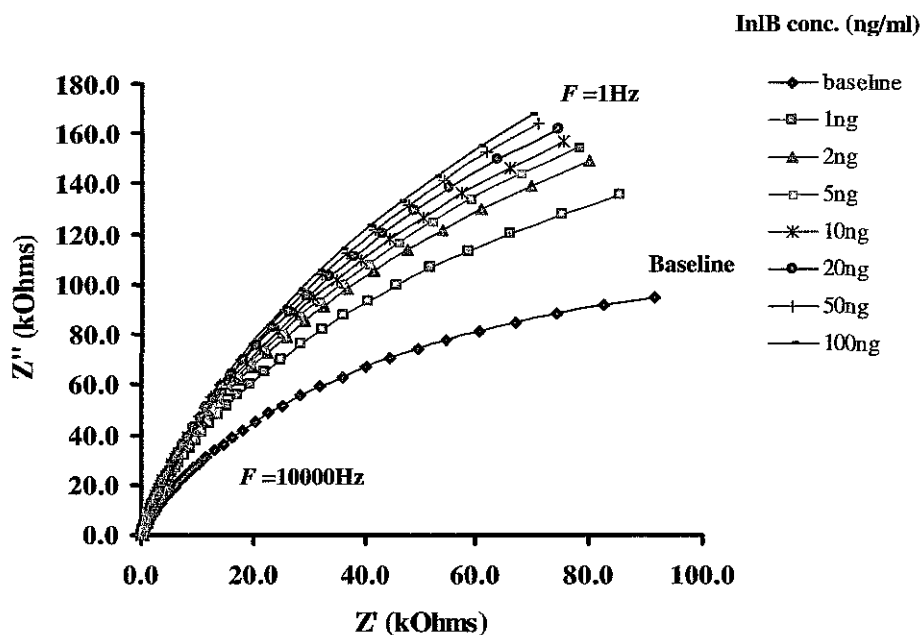


Figure 5.7 Nyquist plot showing the faradaic component (Z') against the capacitive component (Z'') for anti-InlB-doped PANI-films on carbon electrodes, following exposure to various concentrations of InlB (1-100ng/ml).

From Figure 5.7 it is apparent that the real (Z') component and the imaginary (Z'') component of impedance both increased with decreasing frequency from the baseline trace. The impedance spectrum is indicative of a surface-modified electrode system where the electron transfer is slow. However, Figure 5.7 also shows that the increase in the real component (Z') dominated the total increase in impedance. It can therefore be deduced that a charge-transfer mechanism between the antibody/antigen had occurred, since a response corresponding to a change in the real component (Z')

accounted for the largest increase in impedance observed (Stoynov, 1989; Pejicic and De Marco, 2006). The real component yields data that are frequency independent whereas the imaginary component is frequency dependent (Grant *et al.*, 2005). The imaginary component (Z'') decreased slowly at greater antigen concentrations (towards 100ng). This was expected as a change in the capacitive component is indicative of frequency independent changes in the conductivity of the polymer film, due to double layer charging effects. It was found that the Faradaic (real) component of the impedimetric response acted as the dominant component of the ac impedimetric response of anti-InIB loaded PANI films on exposure to increasing concentrations of InIB,

For clarity, the vector quantity impedance can also be represented in the form of a Bode plot (vs. log frequency). Data were plotted for the low frequency region (10Hz to 1Hz) where the differences in the spectra obtained are greatest. The normalised impedimetric response (Z/Z_0) was then obtained by dividing the mean impedimetric response at each InIB concentration (Z) by the mean impedimetric response at zero InIB concentration (Z_0), i.e. the baseline signal with no antigen (Ouerghi *et al.*, 2002). This gave a normalised response that can be plotted against frequency in the form of a Bode plot as shown in Figure 5.8.

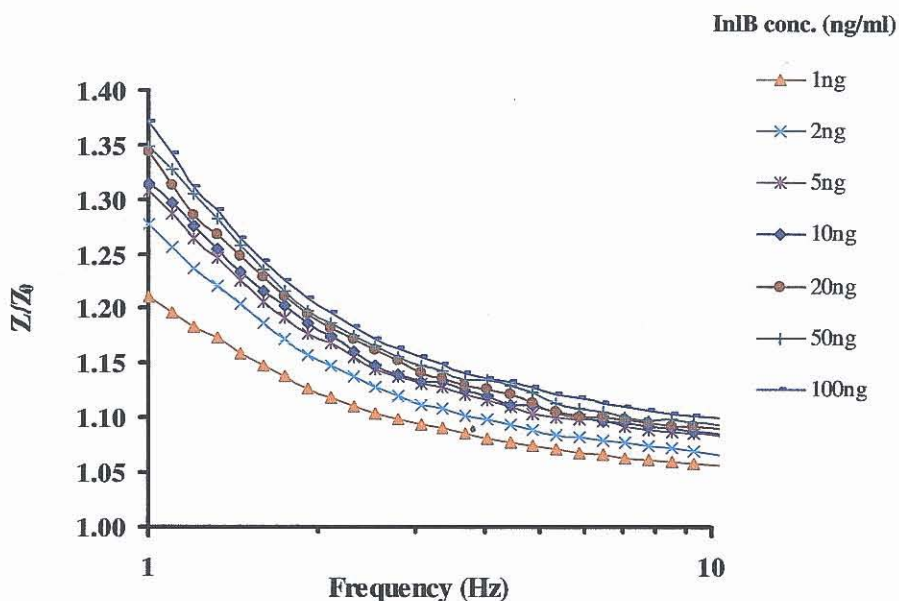


Figure 5.8 Bode plot showing the faradaic and non-faradaic changes in total impedance for anti-InIB-doped PANI-films on carbon electrodes following exposure to various concentrations of InIB, normalised from baseline trace (Z/Z_0).

The impedance of the system increased with exposure to increasing InIB antigen concentration from the baseline trace up to 100ng/ml. The interaction of the protein and the formation of stable antibody/antigen complexes could possibly account for the changes in the resistive and capacitive properties of the conducting polymer thin-film electrode. These effects were observed at frequencies lower than 10Hz. Figure 5.9 represents the data plotted as a percentage change in impedance from the baseline values, in the lower frequency range ($f \leq 10\text{Hz}$), for the full range of antigen concentrations (1-100ng/ml).

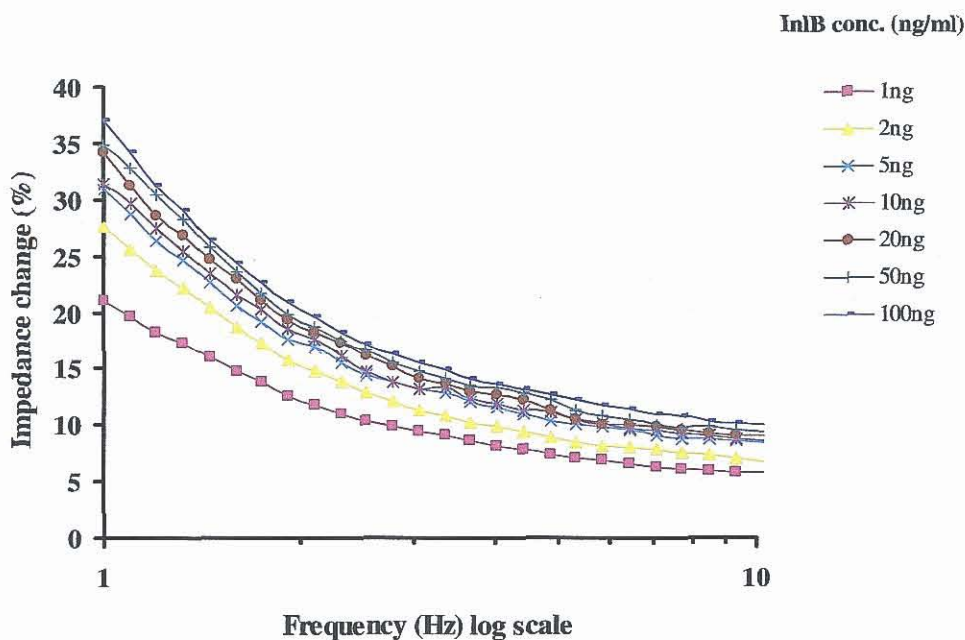


Figure 5.9 Percentage impedance change from the baseline trace for increasing InlB antigen concentrations (1-100ng/ml), in the frequency range 1- 10Hz, for InlB sensors. The percentage impedance change increases for increasing InlB antigen concentrations between 1-10Hz.

Figure 5.9 shows that the greatest percentage difference was observed at the applied frequency of 1Hz, where the range of impedance change over concentrations from 1-100ng/ml is 21-37%. The percentage impedance change at 1Hz was used to form the basis of a calibration profile for differentiation of the various concentrations of InlB, applied to the anti-InlB-doped PANI films on carbon host electrodes.

5.2.6 Calibration curves showing faradaic and non-faradaic response of anti-InIB-doped electrodes against increasing concentrations of InIB

The percentage impedance change from the baseline at 1Hz was used to form the basis of a calibration profile for differentiation of various concentrations of InIB, applied to anti-InIB antibody-doped PANI films on carbon planar electrodes. Figure 5.10 is the calibration profile obtained at 1Hz where the greatest percentage impedance increases at each concentration were noted.

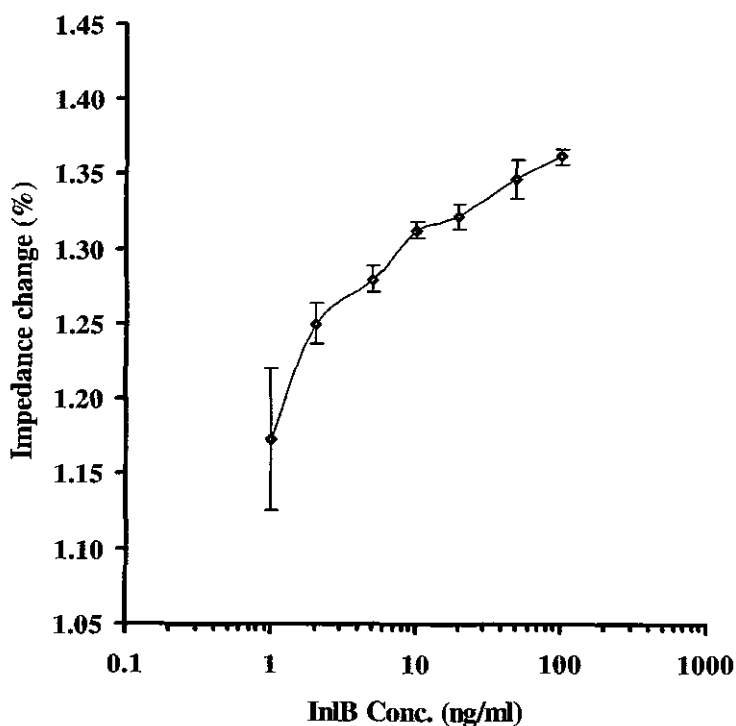


Figure 5.10 Calibration curve of InIB concentration at 1Hz. The curve was generated as a result of exposure of anti-InIB-loaded PANI-films to increasing concentrations of InIB at 1 Hz. The curve displays the percentage change in impedance for each InIB concentration (ng/ml), normalised against the baseline response (zero antigen). Error bars are calculated from the standard deviations of the mean value of three replicates on two separate electrodes (six replicates in total).

The faradaic response was represented as percentage impedance change for InlB-doped PANI thin-film carbon electrodes, following exposure to increasing InlB concentrations. The mean impedance value at each concentration (Z) was normalised against the mean impedance value at zero antigen concentration i.e. Z/Z_0 (Ouerghi *et al.*, 2002). This calibration profile suggests that the technique offers a viable approach for the labelless impedimetric detection and subsequent quantification of InlB antigen F3.

An alternative method of representing the response of the anti-InlB doped polyaniline coated electrodes to increasing concentrations of InlB is by observing the non-faradaic or capacitive response of the system. In order to successfully use the anti-InlB-doped PANI-coated electrodes as a capacitance-based immunosensor, the type of biomaterial immobilisation strategy was important. The polymer layer should be insulating to prevent interferences from redox couples in the electrolyte solution and high faradaic background currents, otherwise increases in resistive current will apply, thus decreasing the capacitance response (Pan, 2007). The biomolecule immobilisation layer also needed to be as thin as possible in order to detect the tiny capacitance changes caused by antibody–antigen interactions. The capacitive response (C) can be calculated from the imaginary (Z'') value at the predicted characteristic frequency (Hays *et al.*, 2006), using the following equation;

$$\text{Equation 5.2} \quad C = 1 / (2\pi f Z'')$$

where the characteristic frequency (f) was determined as the frequency (Hz) where the phase angle is closest to 90° , indicating that the system exhibits near ideal capacitor behaviour (Berney *et al.*, 1998). For InlB-doped sensors, the characteristic frequency was calculated to be approximately 28 Hz, as shown in Figure 5.11 and Table 5.2.

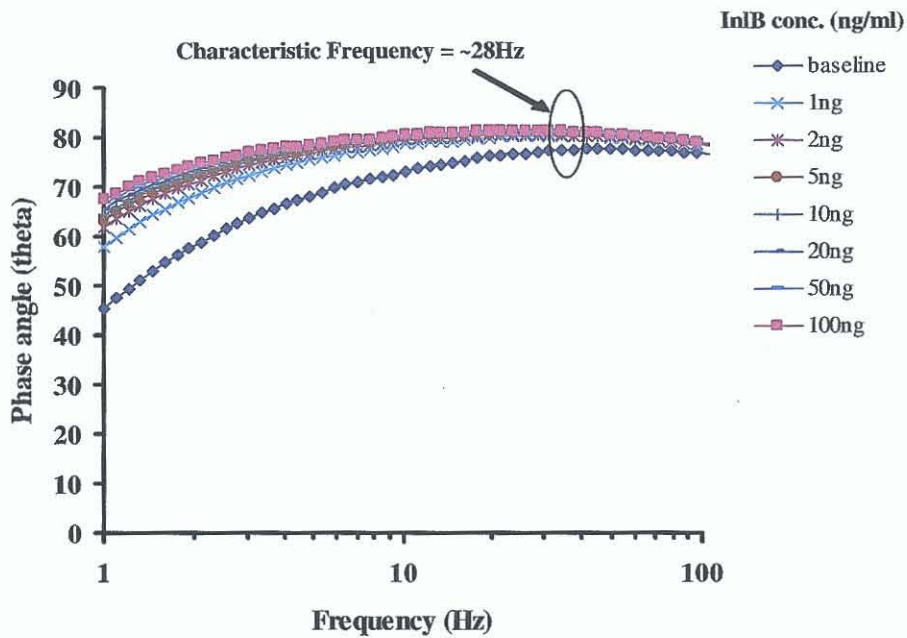


Figure 5.11 Plot showing frequency vs. phase angle for each concentration of InIB (1-100ng/ml). The characteristic frequency, where the phase angle is closest to 90° was determined to be approximately 28 Hz.

The phase angle values at each antigen concentration were investigated and the frequencies where values were closest to 90° were examined to determine the characteristic frequency (Table 5.2).

Table 5.2 Determination of characteristic frequency for InIB-doped sensors

Frequency (Hz) →	34.30	31.26	28.48	25.95	23.64	21.54
InIB Conc. (ng/ml) ↓						
0ng	77.14	76.98	76.81	76.52	76.32	76.16
1ng	79.97	79.97	80.01	79.91	79.87	79.84
2ng	80.26	80.31	80.44	80.36	80.36	80.28
5ng	80.53	80.60	80.63	80.59	80.56	80.56
10ng	80.62	80.68	80.73	80.73	80.73	80.70
20ng	80.78	80.83	80.84	80.77	80.70	80.68
50ng	80.82	80.86	80.89	80.87	80.91	80.90
100ng	80.90	80.95	81.01	80.98	80.99	81.01

In this case, a frequency of 28.48 Hz was chosen as the characteristic frequency since the phase angle values at this frequency were closest to 90°. The non-faradaic response of the immunosensor was determined from this characteristic frequency value using Equation 5.2 and a calibration curve was constructed. Figure 5.12 shows the calibration curve for the non-faradaic capacitive response against InlB concentration for anti-InlB-doped PANI electrodes at the characteristic frequency of 28.48 Hz.

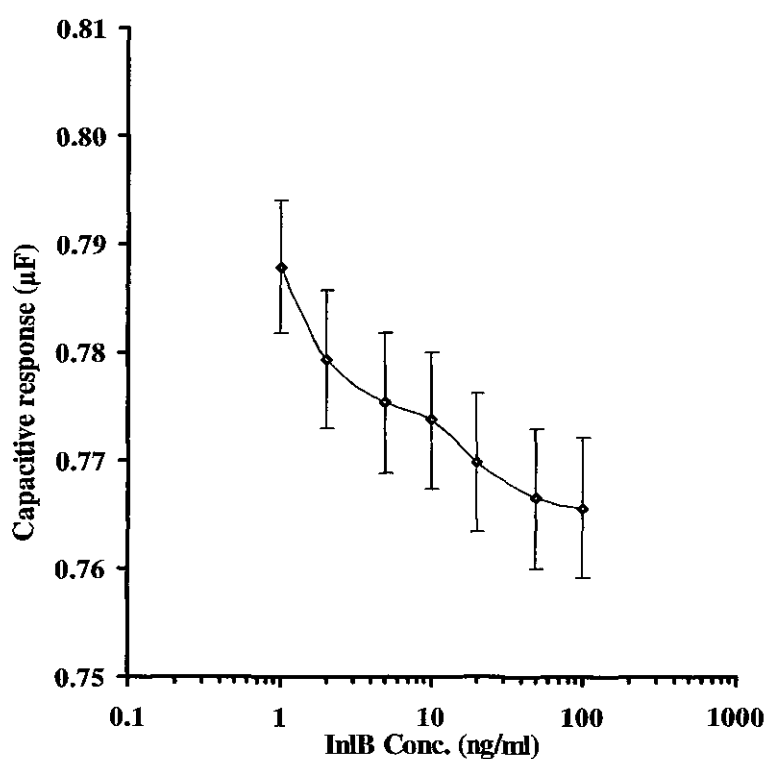


Figure 5.12 Calibration curve of the non-faradaic capacitive response against InlB concentration (ng/ml) for anti-InlB-doped PANI-coated carbon electrodes at the characteristic frequency of 28Hz. The characteristic frequency is the frequency where the phase angle is closest to 90°. Error bars are calculated from the standard deviations of the mean value of three replicates on two separate electrodes (six replicates in total).

5.2.7 Non-Specific recognition of InlB with anti-IgG-doped sensors (control)

Using the same experimental procedures for InlB antigen exposure, the anti-IgG-doped thin-films were exposed to increasing concentrations of InlB antigen. Control experiments using anti-IgG-doped electrodes were used to validate the specificity of the observed impedance responses for the anti-InlB-doped electrodes. Alfonta *et al.* (2001) employed this method of using a non-specific antibody for control sensors. Control sensors were fabricated in exactly the same way as the anti-InlB-doped sensors and were exposed to increasing concentrations of InlB under the same experimental conditions. The impedimetric responses were then compared and specific impedance changes reported. Figure 5.13 shows the spectra obtained from the control sensors, represented in the form of a Nyquist plot. This graph depicts the faradaic and capacitive components of the AC impedance, of the control anti-IgG-doped PANI-films following exposure to the same concentration range of InlB antigen (1-100ng/ml).

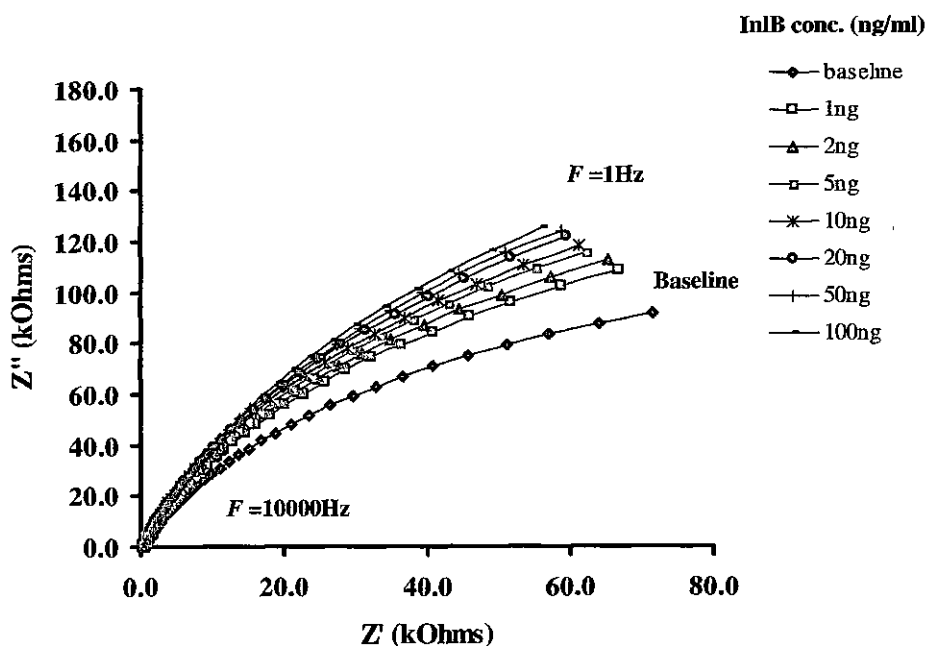


Figure 5.13 Nyquist plot showing the faradaic component (Z') against the capacitive component (Z'') for anti-IgG-doped (control) PANI-films on carbon electrodes, following exposure to various concentrations of InlB (1-100ng/ml).

The faradaic component of the Nyquist Plot (Z') increased for increasing concentrations of InlB exposed to the control sensors. However, the signal responses were much lower than that of the specific response of Internalin B in the sample Nyquist plots, (Figure 5.7). Saturation of the films (as the antigen concentration increased), led to a decrease in the overall impedance (Z) observed on the control sensors. It is possible that excess analyte could have given rise to an alternative conduction pathway, which in turn reduced the total impedance within the cell (Sadik *et al.*, 2002). Figure 5.14 shows the normalised impedance changes (Z/Z_0) from the baseline trace for the lower frequencies (1-10Hz), for the control sensors in the form of a Bode plot. This figure for InlB recognition on anti-IgG-doped films can be directly compared to Figure 5.8 (anti-InlB-doped films).

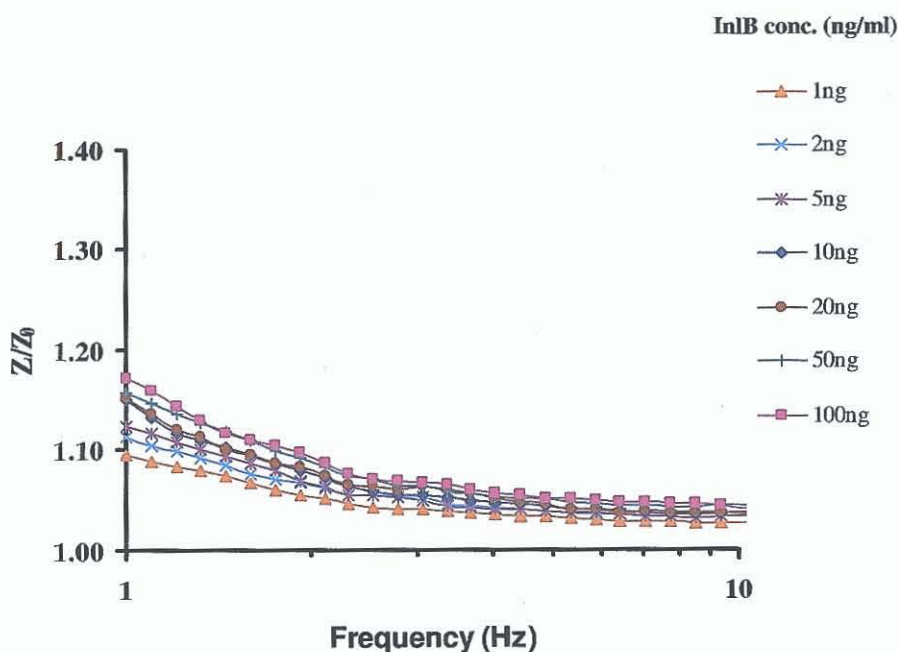


Figure 5.14 Bode plot showing the faradaic and non-faradaic changes in total impedance for anti-IgG-doped PANI-films on carbon electrodes following exposure to various concentrations of InlB, normalised from the baseline trace (Z/Z_0).

The Bode plot for InlB recognition on the anti-IgG-doped sensors (control) followed a similar pattern to that obtained for increasing InlB concentrations on the anti-InlB doped sensors, (Figure 5.8). The changes observed with respect to the baseline trace for the control sensors, were comparable, albeit at much smaller values, indicating that

the impedimetric response of the control sensors was not specific. Any increases in impedance were due to non-specific interactions occurring at the electrode/solution interface and were not a result of immunocomplex formation. Figure 5.15 depicts the percentage impedance changes from the baseline trace for the control sensors. The values of the specific responses obtained from the anti-InlB-doped sensors, where a percentage change of 17% was reported, were greater than the control results (8%) and as such differentiation between the two were possible.

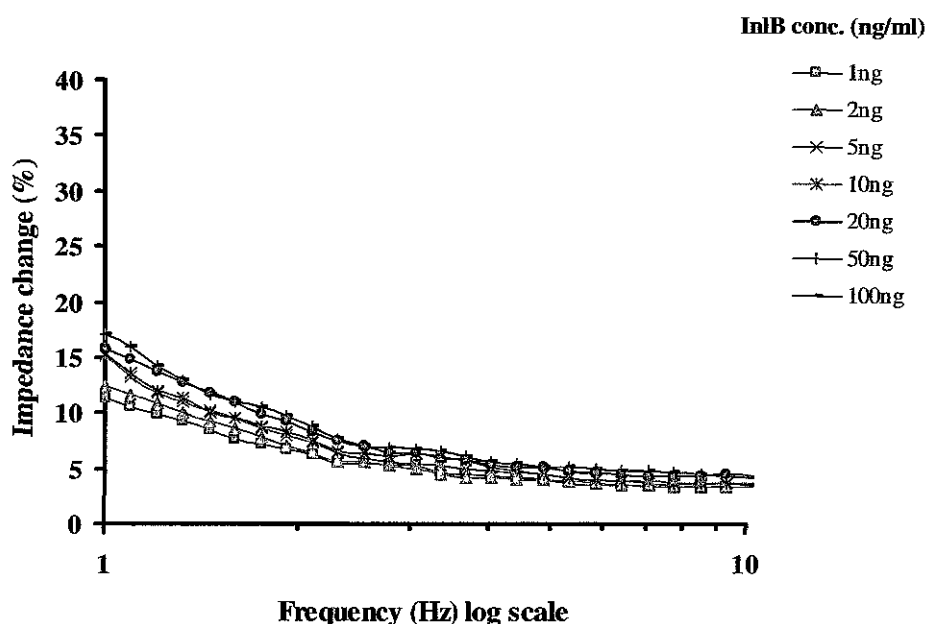


Figure 5.15 Percentage impedance change from the baseline trace for increasing InlB antigen concentration in the frequency range 1-10Hz, for IgG (control) sensors. The percentage impedance change increases for increasing InlB antigen concentrations, between 1-10Hz. However, the overall increase in impedance is low (<8%).

For the control sensors, the total change in percentage impedance at 1Hz was <8%. This increase in impedance was attributed to polymer effects at the electrode surface (Souteyrand *et al.*, 1994). Non-specific interactions were minimised by blocking and the specific sample response determined by subtraction of the control response. Ameur *et al.* (1997) reported a method for determining the specific signal of an impedimetric sensor, as the difference in response to the injection of antigen between a sample and a reference sensor (sample and control).

5.2.8 Comparison of sample and control data

Figure 5.16 shows the calibration profile obtained at 1 Hz, for InlB recognition on the control sensors. This figure can be directly compared to Figure 5.10 for InlB recognition on the sample sensors (anti-InlB-doped) where the specific antibody-antigen response is shown.

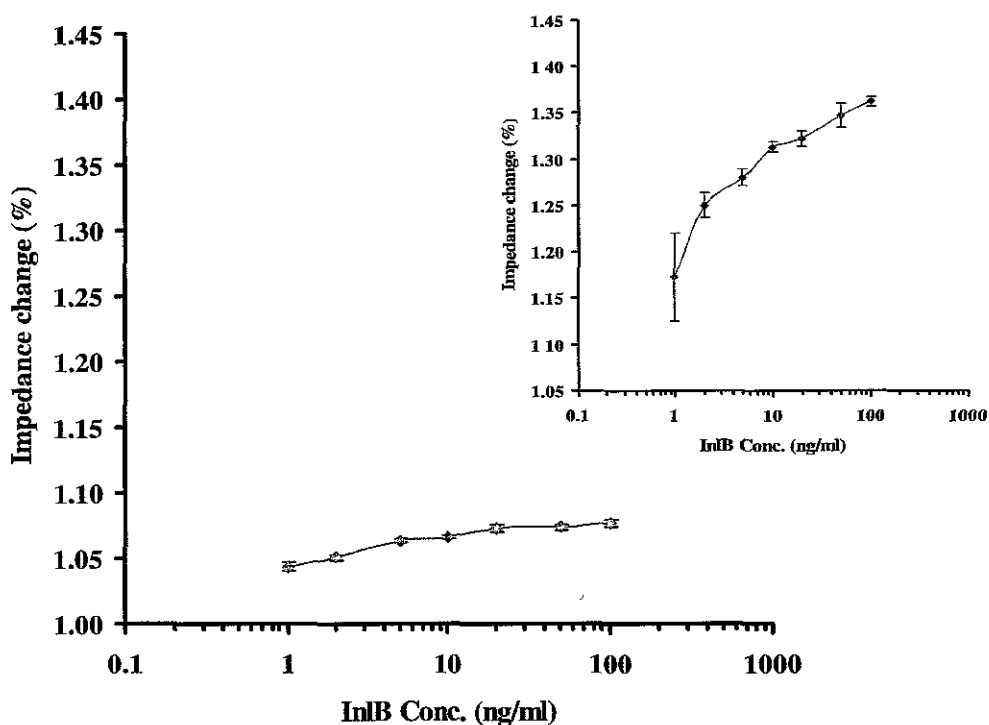


Figure 5.16 Calibration curve of InlB concentration at 1 Hz. The curve was generated as a result of exposure of anti-IgG-loaded PANI-films (control sensors) to increasing concentrations of InlB at 1 Hz. The curve displays the percentage change in impedance for each InlB concentration (ng/ml), normalised against the baseline response (zero antigen). Error bars are calculated from the standard deviations of the mean value of three replicates on two separate electrodes (six replicates in total). However, they are difficult to distinguish from the symbols used to plot the data points, since the error is so small, indicating that the overall percentage change was minimal.

Figure 5.16 suggests that the anti-IgG doped PANI thin-films showed a small degree of interaction with InlB antigen and to a certain extent this was to be expected due to the anti-IgG antibody being polyclonal in nature. It is also possible that irreversible non-specific adsorption of InlB to the conductive film may have occurred, due to polymer effects at the electrode surface. The percentage change in impedance for the sample sensors using the anti-InlB antibody and InlB antigen was greater, showing a definite interaction and therefore this technique could be employed for the specific detection of InlB. Control experiments were also carried out to investigate the observed resistive and capacitive changes of the PANI thin-film electrodes with no antibody present, to assess and subsequently minimise non-specific interactions at the sensor surface. Impedance effects were observed at the electrode/solution interface for thin-films containing no immobilised antibody. This provided additional information on polymer behaviour at the electrode surface, and, as such assisted in the understanding of the non-specific impedance effects on control sensors. The thin-film electrodes were exposed to InlB over the full concentration range previously employed (1-100ng/ml) and the impedance data were recorded as before (Section 2.11.6). Figure 5.17 shows the Nyquist plot depicting the real and imaginary components of impedance (Z' & Z'').

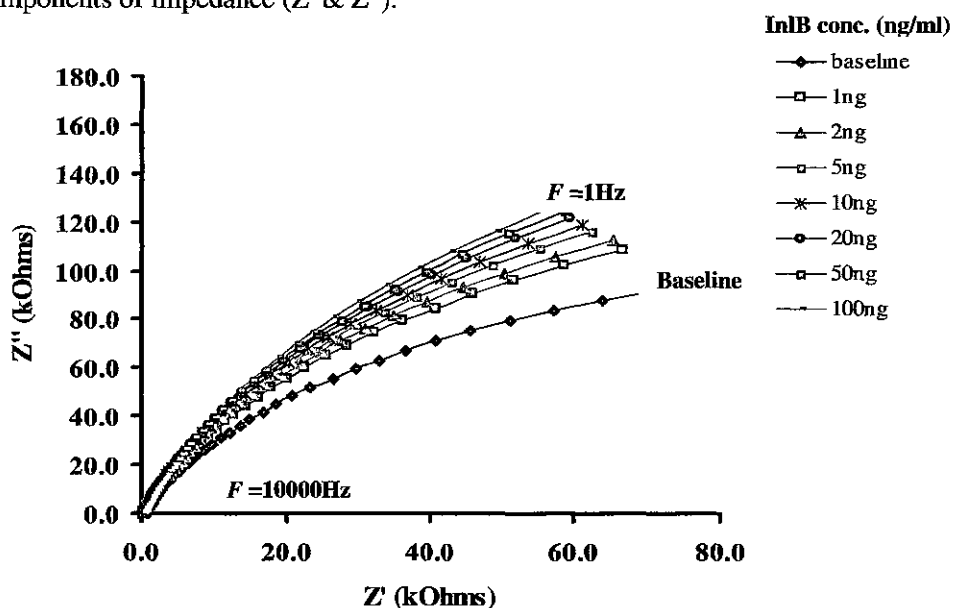


Figure 5.17 Nyquist plot showing the faradaic component (Z') against the capacitive component (Z'') for PANI-films on carbon electrodes, containing no antibody, following exposure to various concentrations of InlB (1-100ng/ml).

It was immediately obvious that even though no antibody has been immobilised within the PANI thin-film, an almost identical response was observed to that when anti-IgG-doped sensors were exposed to InlB. These results suggest that the impedance changes encountered were not solely due to the specific interaction of antibody with antigen and subsequent complex formation. It is proposed that irreversible non-specific adsorption of antigen to the PANI thin-film surface had occurred and this partially accounted for the changes (increases) in both the resistive (Z') and capacitive (Z'') components of the system impedance. It was also observed that this non-specific adsorption increased with exposure to increasing antigen concentration. This was likely due to the nature of recombinant InlB protein, in that it inherently has a high affinity for adsorption to surfaces.

Another possibility is that there may have been underlying conformational and structural changes within the PANI thin-films themselves over time, when exposed to the buffered antigen solutions, that may be responsible for the impedance changes observed (Myler *et al.*, 2004 and 2005). These may include the proton doping of films, wet-up and polymer swelling (Eggins, 1996) all of which can have an effect on the impedimetric response of the thin-film, causing non-specific increases in impedance over time, even in the presence of no antibody. However, the observed responses for the sample sensors with respect to the control responses were significantly smaller, which allowed deduction of a true signal based on the specific impedimetric response of the sample sensors (as a result of antibody-antigen binding). Any effects as a result of non-specific interactions were reduced in two ways: by blocking with BSA and by correcting the specific impedance response by subtracting the control plots (IgG) from the sample (InlB) plots.

Figure 5.18 shows that although anti-IgG-doped PANI thin-films show a degree of interaction with InlB antigen, it is sufficiently lower than those of the anti-InlB-doped sensors, thus allowing deduction of the sample signal and construction of a calibration curve for the detection of InlB.

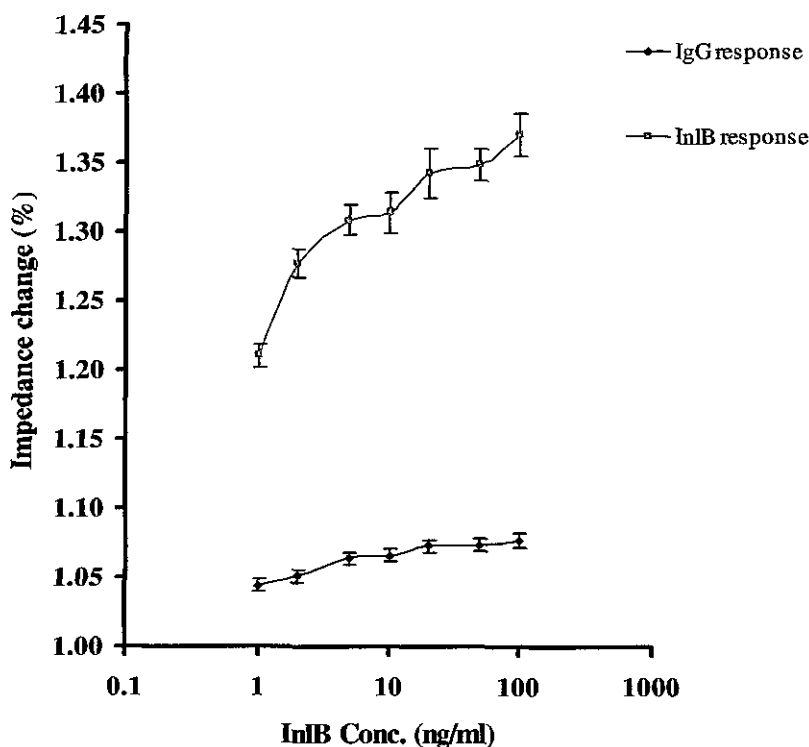


Figure 5.18 Calibration curve showing the percentage impedance change from the baseline trace for increasing InlB antigen concentrations, at a frequency of 1Hz (5mV a.c) for both sample (InlB response) and control (IgG response) sensors. Error bars are calculated from the standard deviations of the mean value of three replicates on two separate electrodes (six replicates in total).

By subtracting the control response (IgG) from the sample response (InlB), the background signal could be eliminated and a true representation of the events occurring at the sensor surface could be deduced. This corrected response (sample data minus control data) is shown in Figure 5.19.

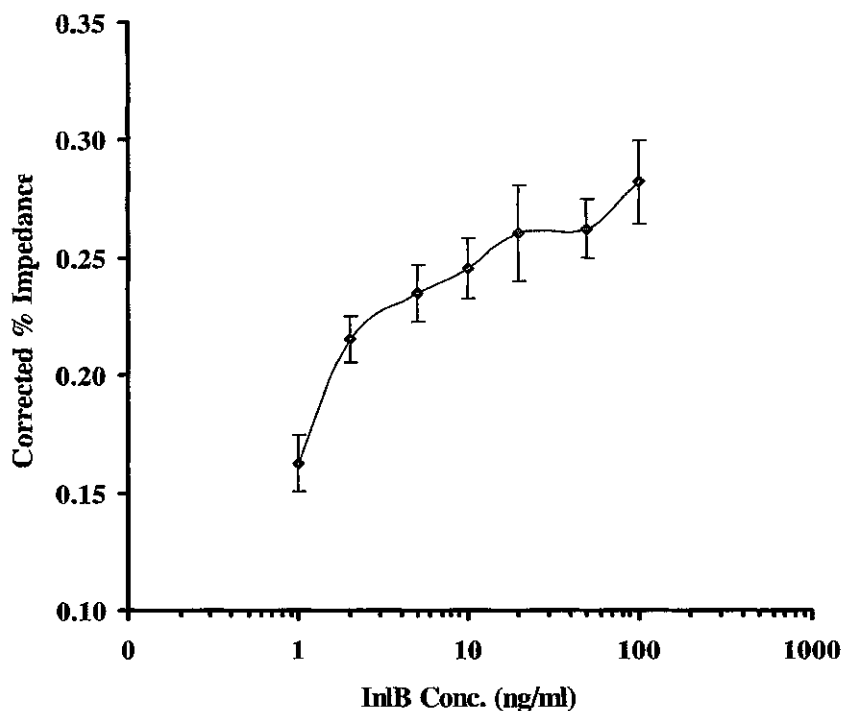


Figure 5.19 Corrected calibration curve showing the percentage impedance change from the baseline trace for increasing InlB antigen concentrations, at a frequency of 1Hz (5mV a.c). Error bars are calculated from the standard deviations of the mean value of three replicates on two separate electrodes (six replicates in total).

Figure 5.18 shows both the specific and control responses of the antibody-doped sensors for the concentration range 1-100ng/ml. However, there is a significant difference between the two curves at 1ng/ml, which indicates that there was some useful range to be explored below that concentration. Indeed, taking into account the data presented in the corrected calibration curve shown in Figure 5.19, it seems that the slope of the curve is highest at lower concentrations. It is reasonable to expect the full plot to be S shaped and, therefore, there is some space at lower concentrations to be explored. The Nyquist plot in Figure 5.7 confirms this, showing that the sensor was saturating towards the upper concentrations and that a significant gap between the baseline response and the response at the lowest concentration of 1ng/ml was present. This suggested that the sensor strategy could be useful for exploring picogram levels of Internalin B and so a range of lower concentrations were examined.

5.2.9 Investigation of specific InlB response at lower concentrations

Experiments were performed in exactly the same way as before except that lower concentrations of antigen were investigated (1-100pg/ml). Anti-InlB antibody at a final concentration of 1 mg/ml was incorporated into the thin-films of electrodeposited PANI at planar carbon electrodes, via affinity immobilisation as before (Sections 2.11.3 and 2.11.4). Following the immobilisation of antibody, EIS was then performed to interrogate the sensor electrodes. Antibody-loaded PANI thin-film electrodes were then exposed for 30 minute time periods to increasing concentrations of antigen. After 30 minutes exposure to a single concentration, the working electrode was flushed with phosphate buffer and the impedance trace was then recorded in phosphate buffer alone between 1Hz to 10000Hz. This process was then repeated for the full range of antigen concentrations (1-100pg/ml). A representative Nyquist plot depicting the variation of the resistive (Z') and capacitive (Z'') components of the vector quantity impedance is shown in Figure 5.20, for the anti-InlB-doped thin-film carbon sensors following exposure to increasing concentrations of InlB antigen (1-100pg/ml). The baseline trace was recorded after a 30-minute stabilisation period in the buffer alone to reduce polymer swelling and wet-up.

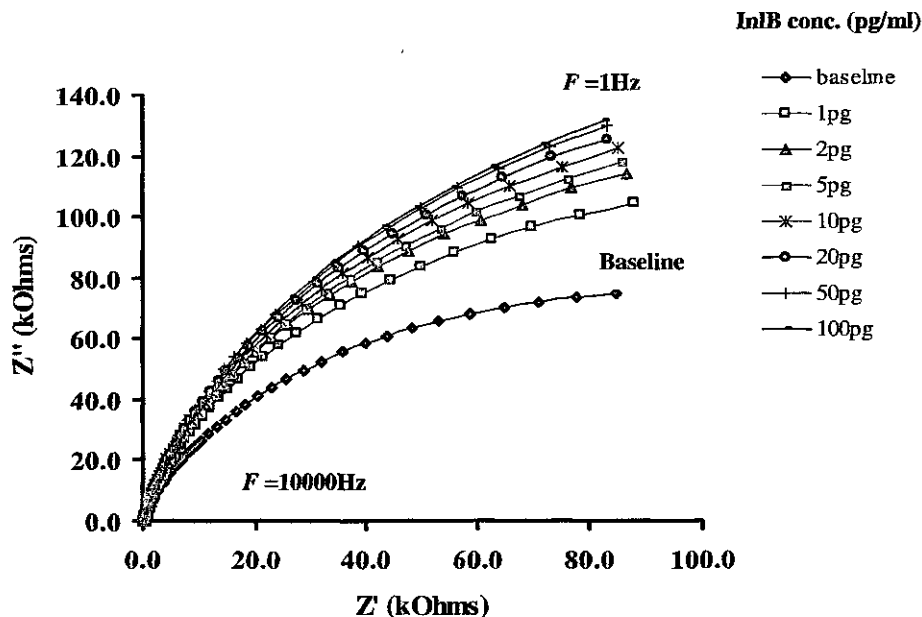


Figure 5.20 Nyquist plot showing the faradaic component (Z') against the capacitive component (Z'') for anti-InlB-doped (sample) PANI-films on carbon electrodes, following exposure to various concentrations of InlB (1-100pg/ml).

Figure 5.20 shows that there were increases over time for both resistive (Z') and capacitive (Z'') components of impedance. Both of these components increased with increasing antigen concentration exposure. The greatest impedance changes were observed at the lower frequencies with the highest impedance changes from the baseline response, measured at 1Hz. The spectra obtained are generally indicative of a modified electrode where the impedance is controlled by the interfacial electron transfer within the entire range of the applied frequencies (Katz and Willner, 2003).

Figure 5.20 does, however, display spectral responses that tend slightly more towards those of a modified electrode where the impedance is mainly controlled by diffusion of the redox species. It can be seen from Figure 5.20 that the resistive component of impedance (Z') has a negligible increment for increasing InlB concentration at 1Hz. However, the capacitive component (Z'') is seen to increase, again at 1Hz, following exposure to increasing antigen concentrations (1-100pg/ml). It can therefore be deduced that the specific interactions of antibody and antigen resulted in a charge transfer mechanism and this charge transfer mechanism was responsible for the observed changes in the Z' and more evidently the Z'' component of the measured impedance. Buffer solution effects were minimised by including a 30-minute stabilisation period, whereby the electrodes were left in buffer for 30 minutes prior to the recording of any impedance measurements. This allowed the electrodes to stabilise within the buffer solution and hence, any observed increases in Z' and more evidently Z'' after this stabilisation period, could only be attributed to the specific interaction of antibody and antigen at the polymer surface.

Figure 5.21 shows a calibration curve representing the total impedance of the system plotted against InlB concentration (1-100pg/ml).

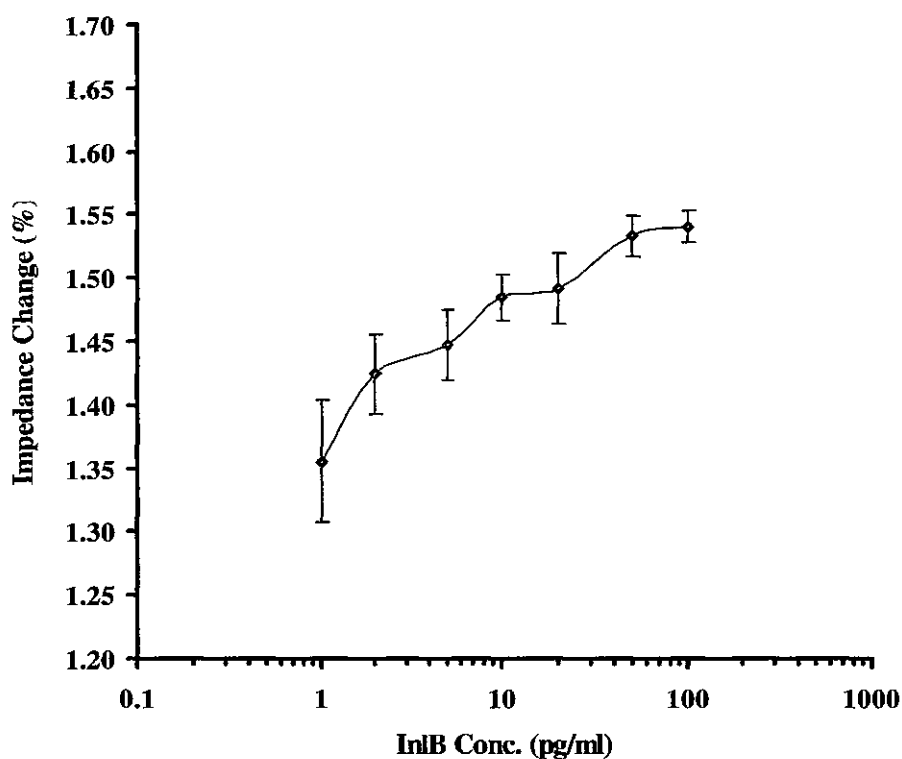


Figure 5.21 Calibration profile showing percentage impedance response against InlB concentrations (1-100 pg/ml) for anti-InlB-doped PANI-coated electrodes at 1Hz. Error bars are calculated from the standard deviations of the mean value of three replicates on two separate electrodes (six replicates in total).

Figure 5.21 shows that there is a quasi-linear response for the percentage impedance change when measured against InlB concentration in the picogram range. This technique therefore, offers a viable approach for the detection and subsequent quantification of InlB over a range of concentrations (1-100pg/ml). Data were fitted to a 4-parameter equation using Biaevaluation™ software and a limit of detection of 1.3pg/ml was found using the 3 sigma method. However this limit of detection only took into account the uncorrected response of the system, whereby the background signal from the anti-IgG-doped (control) sensors had not been subtracted. This meant that the influence of non-specific interactions on the total impedance of the system was not represented, and background impedance could still be contributing to the

overall signal. In order to eliminate the background impedance (and as such the non-specific response of the system) the impedimetric response from the control (IgG) sensors was subtracted from the sample (InIB) sensors and the corrected response of the system determined. A calibration profile showing the percentage change in impedance against antigen concentration for both the sample (InIB response) and control (IgG response) sensors was first constructed, (Figure 5.22).

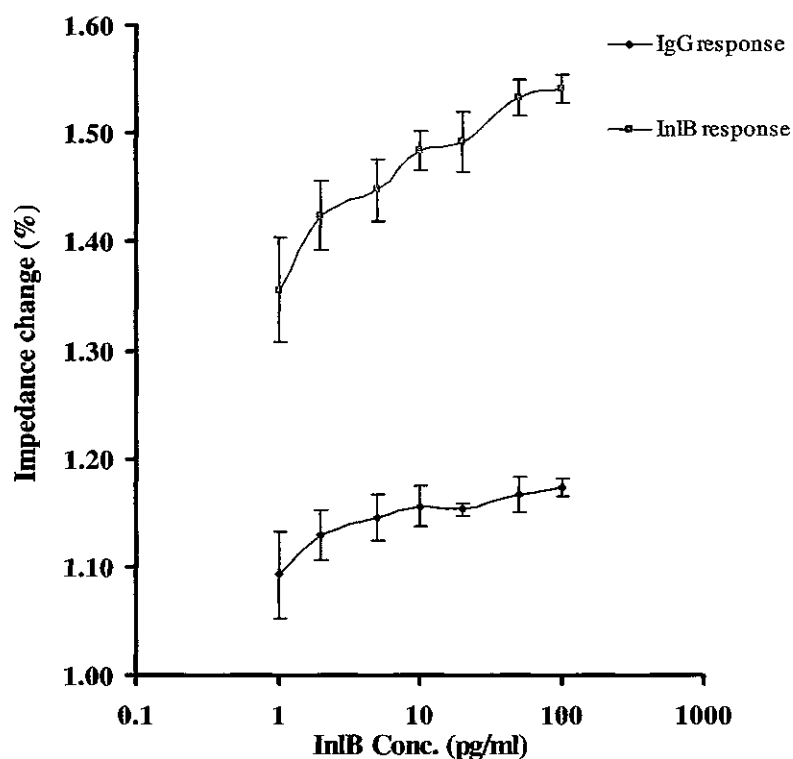


Figure 5.22 Calibration curve showing the percentage impedance change from the baseline trace for increasing InIB antigen concentrations, at a frequency of 1Hz (5mV AC) for both sample and control doped sensors in the picogram range. Error bars are calculated from the standard deviations of the mean value of three replicates on two separate electrodes (six replicates in total).

The signal from the control sensors (6 replicates) was then subtracted from the sample response (6 replicates) and a corrected limit of detection of the system was calculated. Figure 5.23a shows the corrected response (sample minus control) of the impedimetric sensor for InlB detection. The lower limit of detection of the system was calculated using the 3 sigma method and the data fitted to a 4-parameter equation using Biaevaluation™ software. This is shown in figure 5.23b.

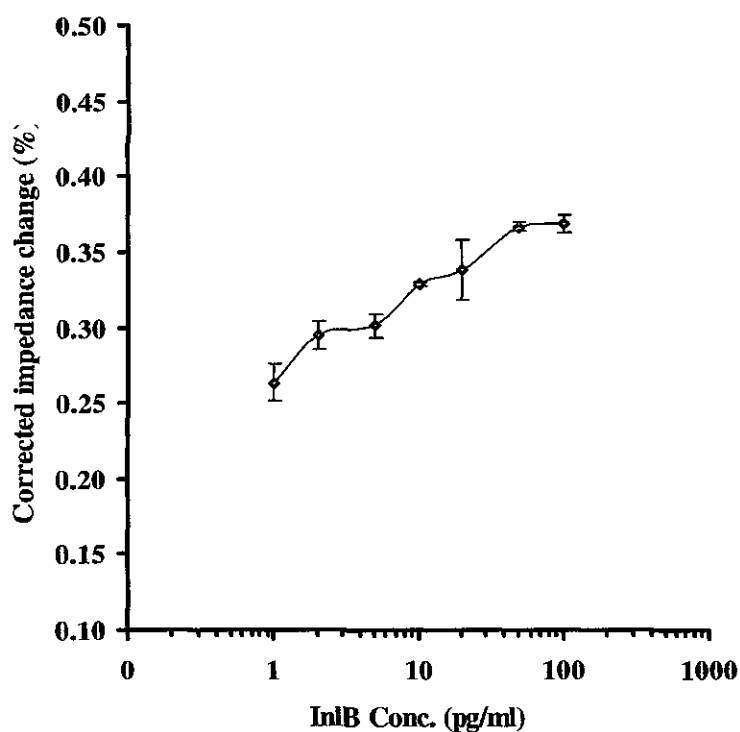


Figure 5.23a Corrected calibration curve showing the percentage impedance change from the baseline trace for increasing InlB antigen concentrations (1-100pg/ml), at a frequency of 1Hz. Error bars are calculated from the standard deviations of the mean value of three replicates on two separate electrodes (six replicates in total) for both the sample and control sensors. The corrected percentage change in impedance was calculated by plotting the difference between the sample and control sensors (calculated by subtraction) against InlB concentration (pg/ml).

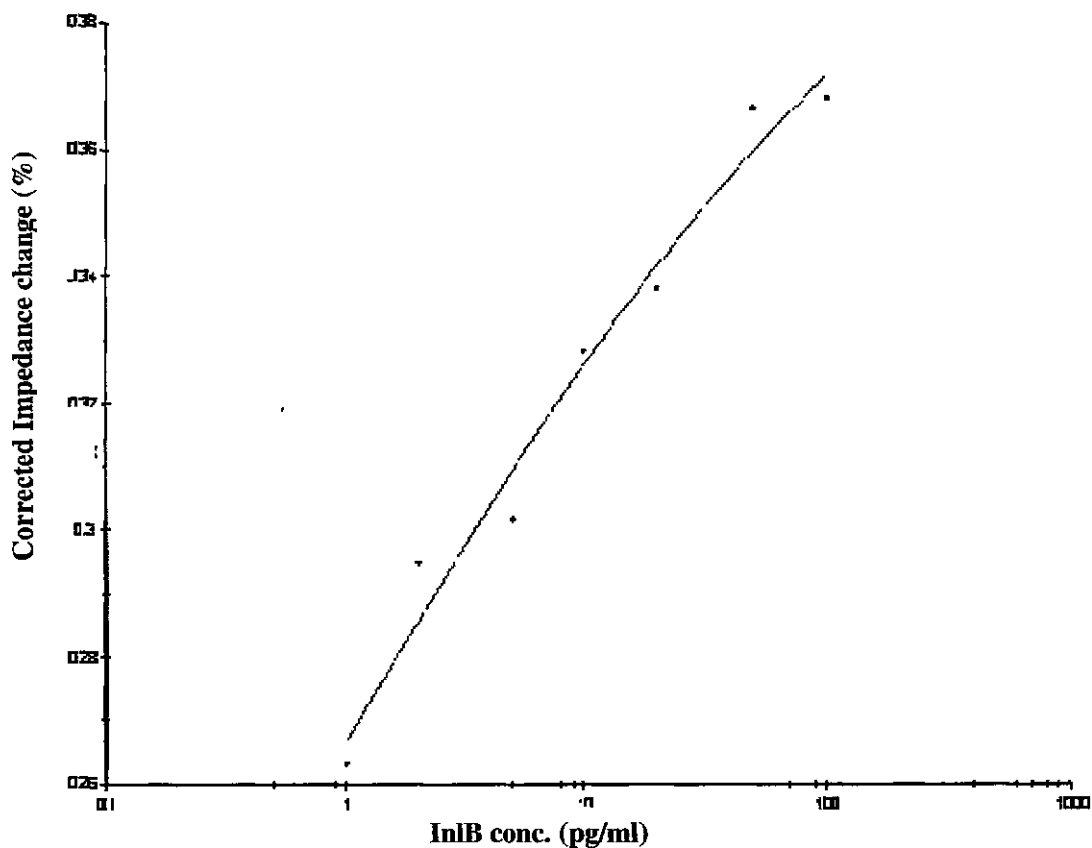


Figure 5.23b Calibration curve showing the corrected response of the system for InlB detection. The data were fitted to 4-parameter equation using Biaevaluation software, for calculation of lower limit of detection using the 3 sigma method. The curve displays total impedance (Z) against InlB concentration. The lower limit of detection (LOD) is equal to 4.1pg/ml

The results were favourable suggesting that the anti-InlB antibody/InlB F3 antigen pair tested in the lower concentration range (picogram) yielded a viable technique for labelless impedimetric immunosensing of InlB, where the lower limit of detection for the corrected response was determined to be 4.1pg/ml.

5.3 Discussion

The development of a generic platform for the 'labelless' transduction of binding events was examined in this chapter. The InlB protein fragment F3 was used in association with an anti-InlB polyclonal antibody for 'labelless' sensing of InlB binding using an electrochemical immunosensor. Polyaniline was successfully laid down as a conductive thin-film layer on planar carbon electrode surfaces, which facilitated antibody immobilisation within the thin-film. Sensor modification with neutravidin and biotin allowed site-specific coupling of the antibody to the polyaniline matrix. Formation of antibody-antigen complexes on conductive supports yielded a chemically modified film on the surface which altered the impedance features of the interface (Pritchard *et al.*, 2004). The preparation of stable sensor surfaces is an important consideration for reproducibility, and in order to measure low protein concentrations, a thin sensing layer with a high capacitance is required. The formation of the antibody/antigen complex on such a surface perturbs the double-charged layer existing at the electrode/electrolyte interface, resulting in an increase of its thickness and the insulation of the electrode. This causes both capacitance changes and electron transfer resistance changes at the interface (Katz *et al.*, 1998 and 2001).

Impedimetric interrogation of the thin-film carbon sensors yielded positive results with more rigorous, reproducible data collected at the lower end of the frequency range (1-10Hz). The specific interactions and resultant complexes formed gave rise to an overall increase in terms of impedance change from the baseline response, at the electrode/solution interface. Impedances were recorded by multiple interrogations of both sample and control sensors (6 replicates), with InlB-F3 antigen. Plots of the real (Z') and imaginary (Z'') components of the impedance, at a specific frequency (1Hz), provided information for construction of calibration curves. Initial investigations of this sensor system explored the labelless detection of InlB in the nanogram range. However, there was significant evidence that lower detection levels could be achieved so further exploration of the sensor strategy was performed. Lower concentrations of antigen were examined under the same conditions and a detection range of 1-100pg/ml was found. The results were favourable suggesting that detection of the anti-InlB/InlB pair in the picogram range was a suitable method for the labelless impedimetric immunosensing of InlB, where the lower limit of detection for the corrected response was determined to be 4.1pg/ml.

Affinity sensors employing electrochemical methods, offer good possibilities for the sensitive detection of unlabelled biomolecules such as proteins and peptides. Sargent and Sadik (1999) described a method for the detection of human serum albumin (HSA) using conducting polypyrrole electrodes and impedance spectroscopy techniques. They studied the capacitive behaviour of antibody-doped thin-film electrodes in the presence of antigen, as was demonstrated in this chapter. The theory of charge generation in the polymeric domains are predominantly responsible for the analytical signals observed in such investigations and form the basis of the labelless immunosensor presented in this chapter.

Lillie *et al.* (2001) developed a labelless bioaffinity sensor for the detection of luteinising hormone using polypyrrole-doped interdigitated electrodes and cyclic voltammetry. They demonstrated that immobilised protein in a conducting film could be indirectly recognised using electrochemical methods, allowing the sensitive transduction of binding events following exposure to the desired analyte. This suggested that the thin-film structure of antibody-doped electrodes is altered upon occurrence of a bioaffinity reaction and the monitoring of the resulting electrochemical events, permits the sensitive detection of analytes on such surfaces. Alfonta *et al.* (2001), reported on the use of faradaic impedance spectroscopy and chronopotentiometry as transduction methods for biorecognition events at modified electrode surfaces for the detection of enzymes, DNA and antibodies. This system focused on the biocatalysed precipitation of insoluble product produced on electrode supports and subsequent transduction of the precipitation process using faradaic impedance spectroscopy and chronopotentiometry. Information on the electron-transfer resistances of the electrodes covered by the insoluble product can be derived thus providing vital information on the total electrode resistances at the conducting supports. Katz *et al.* (2001) describe a similar strategy for the development of an affinity sensor based on the bio-catalysed precipitation of an insoluble product on modified electrodes. The precipitation of the product onto the electrode allows amplification of the underlying biorecognition event occurring on the electrode surface. Therefore, the amount of precipitate generated is controlled by the original concentration of antibody-antigen and the time interval for precipitation, allowing sensitivity to be controlled by these parameters.

Direct immunosensors based on impedance measurements have also been developed, using antibodies or antigens immobilised at electroactive polymer-coated electrodes. Kharitonov *et al.* (2001) presented a similar study based on the electrochemical probing of bioaffinity interactions using both impedance spectroscopy and chronopotentiometry. Grant *et al.* (2003) describe a label-free, reagentless immunosensor for the detection of BSA, with a linear response from 0-75ppm reported while Myler *et al.* (2004 and 2005) showed the development of microelectrode arrays for the immunosensing of ethanol. Electrochemical immunosensors offer good possibilities for sensitive detection of unlabeled proteins, with potential for reusability possible. The most significant problem encountered with these sensors, however, is the contribution of non-specifically adsorbed proteins to the overall signal. In many cases, this contribution is disregarded; however, methods to correct for the specificity of the signal have been described, (Ameur *et al.*, 1997), whereby the control sensor response to antigen probing can be subtracted from the sample signal to give corrected response. This technique was adapted for the affinity sensing of InlB, described in this chapter.

Sensors based on the immobilisation or entrapment of immunomolecules (antibodies or antigens) onto modified electrode surfaces, for subsequent detection using electrochemical methods are becoming increasingly popular for rapid and sensitive detection of biologically important analytes. In conclusion, tremendous improvement in the sensitivity of immunosensing can be achieved using 'labelless' affinity sensors, such as the one presented here for the direct and specific detection of InlB. This technique could be further developed for the rapid detection of bacterial protein markers in real samples using a multiplexed set-up. Antibodies directed against a number of protein markers specific for the detection of different bacterial pathogens could be immobilised on electrode surfaces, thus enabling the rapid and sensitive detection of such pathogens using 'labelless' impedimetric techniques. The potential of the 'labelless' affinity sensor, described here as viable method for the detection of biomolecules, highlights the importance of impedance-based detection in the evolving field of immunosensors.

Chapter 6:
Conclusions

6.1 Overall conclusions and future work

The aim of this thesis was to develop novel biosensing strategies for the detection of biologically important analytes using both optical and electrochemical methods. A number of transduction approaches were investigated for improved immunodetection of a small hapten, bacterial proteins, whole cells and IgG. The specific targets chosen for immunoassay development were Internalin B, an invasion-associated protein of *Listeria monocytogenes*; parvovirus B19, the first human parvovirus; warfarin, the ninth most prescribed drug in the world and human IgG.

Biosensing methods rely on a number of key elements for successful operation and these include; biomolecule immobilisation strategy, analyte biorecognition, platform design, presence or absence of labels, detection strategy and system used. Each of these components plays an important role in the ability of the sensor to sensitively detect the analyte under investigation. Therefore, the work described in this thesis focused on a number of topics associated with these elements in order to generate novel assays for improved detection of target molecules. The generation of novel reagents using molecular cloning techniques, for improved detection of the bacterial protein Internalin B from *L. monocytogenes* was assessed. Novel fluorescent labels with better optical properties were also examined and the advantages of such probes in the development of novel immunoassay formats were discussed. Fluorescence and impedance-based detection systems were studied and a number of platforms were assessed including microtitre plates, polymer chips with enhanced fluorescence capture capabilities and screen-printed electrodes incorporating electroactive thin-films. Sensor platforms, incorporating specially designed materials for enhanced immobilisation and thus biorecognition can be used for the improved detection of analytes (Pavlickova *et al.*, 2004; Wingren *et al.*, 2005). In the research described in this thesis, chemical, electrochemical and physical modifications were investigated. Surface modification of polymer substrates for biochip applications, electropolymerisation of electrodes for immunoassay development and the thin-film deposition of biocompatible surfaces for implants were studied. The development of new and improved biosensing strategies, incorporating novel transduction methods, both labelled (fluorescence-based) and un-labelled (impedance-based) were evaluated.

Chapter 3 focused on exploring a key element in immunosensor design, biorecognition. The development of new and improved antigens and antibodies using antibody engineering and recombinant protein techniques, promotes biorecognition at sensor surfaces, by generating highly specific targets and tailored antibodies with increased affinities and specificities. The cloning and subsequent high-level expression of the recombinant InlB fragments F3, F4 and F5 created alternative InlB antigenic determinants for immunoassay development. The InlB recombinant protein, that was previously cloned and expressed (Leonard, 2003), was sub-divided into three shorter overlapping peptide fragments which were cloned into the Qiagen pQE-60 expression vector for His-tag purification and expressed in *E. coli*. The protein fragments were optimised for maximum expression and purified using IMAC. The purified proteins were characterised SDS-PAGE and Western blotting. The His-tagged protein fragments (pQE-60) were assessed for immunoreactivity with a panel of anti-InlB antibodies to see which portion of the recombinant InlB protein contained the epitope for antibody binding. Through a series of Western blotting experiments the antibody-binding region was located in the first 248 amino acids of the protein (F3 fragment), near the 'leucine-rich' repeats (Section 3.3.7). Freiberg *et al.* (2004) reported that this region is highly stable against thermal denaturation and plays a critical role in the *in vivo* stability of Internalin B. The F3 fragment was thus used for all further assay development and characterisation since it was defined as the most immunoreactive portion of the entire InlB protein. This made antigen preparation far simpler, eliminating the need to grow and purify the rest of the protein.

The InlB fragments were also successfully cloned into the pAC4 expression vector for *in vivo* biotinylation. The *in vivo* biotinylated fragments were expressed in *E. coli* and purified using monomeric avidin affinity chromatography. The purified fragments were characterised using fluorescence-based immunoassays with streptavidin-linked fluorescent probes and Biacore (Section 3.4.2). The *in vivo* biotinylated F3 fragment was successfully immobilised onto a CM5-dextran chip that had been modified with neutravidin for the specific capture of the protein fragment. The immobilised surface was subsequently used in a Biacore-based inhibition assay for the detection of InlB. The biotinylated F3 fragment was also shown to be a useful reagent for fluorescence-based detection using fluorescent labels such as Cy5, FITC and quantum dots. This

highlighted the potential role of the *in vivo* biotinylated InlB fragments in the further development and optimisation of both fluorescence-based and Biacore-based assays for the detection of Internalin B protein and *L. monocytogenes* cells.

Chapter 4 focused on fluorescence-based detection and alternative platform designs. Fluorescence-based detection is a highly sensitive and safe method for the sensing of target molecules. The evaluation fluorescence-based methods for detection of analytes were therefore examined on two different platforms; microtitre plates and polymer chips with cone assemblies. Fluorophores can be covalently attached to macromolecules and the emission of these fluorescent probes can be from UV to NIR. Probes are available with short (nanosecond) to long (micro to millisecond) life-times. Current trends in fluorescent labelling for biological applications lie with a number of emerging technologies e.g. quantum dots and nanocrystals. The evolution of these tags coupled with advances in functionalisation methods for biomolecule attachment gives rise to a new generation of sophisticated labels suitable for high throughput screening in diagnostics. The use of novel probes such as quantum dots and porphyrin labels for the detection of InlB and warfarin in plate-based competitive assays was successfully demonstrated (Sections 4.3 and 4.4). Future work could include further optimisation of conditions to improve assay sensitivity and limits of detection for warfarin and Internalin B and subsequent assessment of fluorescence-based assay sensitivities using real sample analysis (Findlay *et al.*, 2000). In the case of warfarin, spiked urine samples could be assayed to investigate if the fluorescently-labelled antibodies could detect warfarin in a complex matrix of clinical significance (Capitan-Vallvey *et al.*, 1999). While, for InlB detection, real sample analysis in chocolate milk could be examined, since it is the most common source of *L. monocytogenes* in food (Dogana, 2003).

Quantum dots were also used in an immunostaining application for the imaging of whole *L. monocytogenes* cells (Section 4.5), where photostability and brightness are key factors. Future work could include the multiplexing of quantum dots with other labels for immunostaining applications, thus allowing the multiple staining of cells with a single excitation source.

Nanoparticles are another group of inorganic probes that are highly complex, spectroscopically tailored tags that can be used to improve assay sensitivity, reproducibility and multiplexing capabilities. The synthesis and characterisation of ruthenium-doped nanoparticles was shown (*Section 4.6*). The use of such particles for the detection of biological molecules (in this case human IgG), in fluorescence-based immunoassay formats was successfully demonstrated. Nanoparticles can be easily functionalised for biomolecule attachment and are consistently brighter and more robust than traditional fluorescent probes. The ruthenium-nanoparticles described in this thesis were up to 20,000 brighter than their constituent dye and provided a 60 fold increase in sensitivity for the detection of human IgG, when compared with ruthenium-labeled antibody. The potential of dye-doped nanoparticles as important reagents for the future of fluorescence-based detection is apparent, especially if coupled with the chip-based methods described in the following paragraphs.

The use of polymer chips with cone assemblies as suitable platforms for the chip-based detection of InlB and the parvovirus capsid protein VP2 was examined (*Sections 4.4.5 and 4.7*). The establishment of preliminary assays on the optical enhancement structures was successful, and, although significant optimisation is still required, the methodology looks promising to bring about signal enhancement and ultimately, increased sensitivity. Significant developments have been ongoing within the NCSR to further improve the optical enhancement structures. These have included a change in the material used for fabrication and a change in the design of the cone to a paraboloid structure, increasing the light collection efficiency still further, and improved precision leading to better defined optical performance. Further improvements in the detection system to allow the incorporation of suitable filters and excitation sources, would permit the use of novel fluorescent labels such as nanoparticles and quantum dots in chip-based assays. This will have a significant influence in the area of fluorescence-based analysis in the near future.

Chapter 5 examined the use of a 'labelless' impedance-based sensor for the detection of InIB. Polyaniline was successfully laid down as a conductive thin-film layer on planar carbon electrode surfaces. This facilitated the immobilisation of antibody within the conducting thin-film at the electrode surface. Sensor modification with avidin and biotin allows site-specific coupling of the antibody to the polyaniline matrix. Impedimetric interrogation of the thin-film carbon sensors yielded positive results, whereby data at the lower end of the frequency range (1-10 Hz) showed the greatest consistency. The specific interactions and resultant stable complex formed gave rise to an overall increase in terms of impedance change from the baseline response at the electrode assembly/solution interface. This indicated that impedance-based detection was a suitable method for the labelless immunosensing of InIB, where the lower limit of detection for the corrected response was determined to be 4.1 pg/ml.

Future work on this sensor system could include further investigation of the specific protein interactions occurring at the antibody-doped thin-film sensor surface, in order to enhance antibody orientation and therefore improve immune complex formation. This would provide the possibility to control and improve the composition of the biomolecule-polymer layer and particularly the biomolecule loading. The loss of biomolecule in the aqueous electrolyte during polymer formation can be determined by measuring the biological activity or the protein content of the electrolyte medium. Therefore the real quantity of biomolecule entrapped could be determined by looking at the difference between the initially deposited amount and the amount loss to the electrolyte. Optimisation of antibody-loading in such a way would enhance the operational capabilities of the sensor. Further work could also include testing the 'labelless' impedimetric sensor in real samples for the detection of *L.monocytogenes* cell surface proteins i.e. spiked milk and food samples. By examining the sensors using representative samples, a rough estimate of the systems applicability with real-world samples for the detection of Internalin B, could be examined.

In conclusion, the key merit of the work presented in this thesis lies in the demonstrated potential applications of novel antibody-based biosensors for the detection of haptens, proteins and whole cells. The results clearly emphasise the possible use of novel antigens (Chapter 3), novel labels and associated detection platforms (Chapter 4), and novel transduction strategies (Chapter 5) in the development of improved sensing techniques for the detection of clinically significant targets. The methods shown for enhanced fluorescence-based detection could be further improved by combining the described fluorescence-based assays using novel fluorescent labels (quantum dots and nanoparticles) with the polymer chip platforms (with cone structures for optical enhancement), in order to develop highly sensitive and reproducible methods for the detection of InlB, warfarin, VP2, hIgG and many other analytes. The results also show the successful integration of an improved antigen for InlB sensing (F3), within a 'labelless' impedance-based sensor platform to facilitate the sensitive detection of InlB. The results highlight the suitability of InlB F3 as a marker for the specific immunodetection of InlB and the potential use of impedance-based transduction for the detection of many targets using a non-invasive 'labelless' technique.

Chapter 7: References

A

Aalberse, R. C., Kleine, Budde, I., Stapel, S. O and van Ree, R (2001). Structural aspects of cross-reactivity and its relation to antibody affinity *Allergy*, **67**, 27-29.

Aizawa, M. (1994). Immunosensors for clinical analysis. *Adv. Clin. Chem.*, **31**, 247–75.

Akerman, M. E., Chan, W. C., Laakkonen, P., Bhatia, S. N. and Ruoslahti, E. (2002) Nanocrystal targeting *in vivo*. *Proc. Nat. Acad. Sci USA*, **99** (20), 12617-12621.

Alfonta, L., Bardea, A., Khersonsky, O., Katz, E. and Willner, I. (2001). Chronopotentiometry and Faradaic impedance spectroscopy as signal transduction methods for the biocatalytic precipitation of an insoluble product on electrode supports: routes for enzyme sensors, immunosensors and DNA sensors *Biosens. Bioelectron.*, **16**, 675-687.

Alfthan, K. (1998) Surface plasmon resonance biosensors as a tool in antibody engineering *Biosens. Bioelectron.*, **13** (6), 653-663.

Alivisatos, P. (2004) The use of nanocrystals in biological detection *Nat. Biotechnol.*, **22** (1), 47-52.

Ameur, S., Maupas, H., Martelet, C., Jaffrezic-Renault, N., Ben Ouada, H , Cosnier, S. and Labbe, P (1997) *Mat Sci. and Eng.*, **5**, 111-119.

Anderson, L.J. (1987) Human parvovirus infections. *J. Virol. Methods*, **17** (1-2), 175-181.

Anonymous. (1990). Public Health Laboratory Service Working Party on Fifth Disease. Prospective study of human Parvovirus (B19) infection in pregnancy. *Br. Med J.*, **300**,166-170.

Anonymous. (1998). Stability of Nunc-immuno Maxi-Sorp™ surfaces. *Nunc Bulletin*, **6**, 6-8.

Anonymous. (2005). Pierce Biotechnology Inc. Instruction manual # 20227.

Anonymous. (2007). Technology Note #23. *GE Healthcare, Biacore AB.*

Anzai, J., Kobayashi, Y., Yasuhiro, S., Takeshita H Chen, Q., Osa, T. and Hoshi, T. (1998). Enzyme sensors prepared by layer-by-layer deposition of enzymes on a platinum electrode through avidin–biotin interaction. *Sens. Actuat. A-Phys.*, **52** (1-2), 3-9.

Aoyagi, S. and Kudo, M. (2005). Development of fluorescence change-based, reagent-less optic immunosensor. *Biosens. Bioelectron.*, **20** (8), 1680-1684.

Arnold, F.H. (1991). Metal-affinity separations: a new dimension in protein processing. *Biotechnol. N.Y.*, **9** (20), 151-156.

Ashwin, H.M., Stead, S L , Taylor, J.C., Startin, J.R , Richmond, S.F., Homer, V., Bigwood, T. and Sharman, M. (2005). Development and validation of screening and confirmatory methods for the detection of chloramphenicol and chloramphenicol glucuronide using SPR biosensor and liquid chromatography–tandem mass spectrometry. *Anal. Chim. Acta*, **529** (24), 103-108.

Ausubel, F.M., Brent, R., Kingston, R.E., Moore, D.D., Seidman, J.G., Smith, J and Struhl, K. (1994). *Current Protocols in Molecular Biology*. John Wiley and Sons, New York, USA

Awais, M., Sato, S. and Umezawa, Y (2007). A fluorescent indicator to visualize ligand-induced receptor/coactivator interactions for screening of peroxisome proliferator-activated receptor γ ligands in Irving cells. *Biosens. Bioelectron.*, **22** (11), 2564-2569.

Azzazy, H. and Highsmith, W (2002). Phage display technology: clinical applications and recent innovations. *Clin. Biochem.*, **35**, 425 – 445

B

Bagwe, R.P., Hilliard, L.R., Tan, W. (2006). Surface modification of silica nanoparticles to reduce aggregation and nonspecific binding. *Langmuir*, **22**, (9), 4357-4362.

Bakaltcheva, I.B., Shriver-Lake, L.C. and Ligler, F.S. (1998). Fiber optic biosensor for multianalyte detection: importance of preventing fluorophore aggregation. *Sens. Actuat. B - Chem.*, **51**, 46-51.

Bakker, E., Bühlmann, P. and Pretsch, E (2004) The phase-boundary potential model. *Talanta*, **63** (1), 3-20.

Barbas, C., Kang, A., Lerner, R. and Benkovic, S. (1991) Assembly of combinatorial antibody libraries on phage surfaces. the geneIII site. *Proc Nat. Acad Sci. USA*, **88**, 7978 - 7981.

Barbas, C.F.I., Burton, D.R. and Scott, J.K. (2001). In *Phage Display : A Laboratory Manual*. Cold Spring Harbour Laboratory Press, New York, USA.

Barbero, C., Kötzt, R., Kalaji, M., Nyholm, L. and Peter, L. M. (1993). Ion exchange and memory effects in polyaniline. *Synthetic Met.*, **55** (2-3), 1545-1551.

Bard, A.J. and Faulkner, L.R. (1980). *Electrochemical Methods Fundamentals and Applications* (1st Edn.) John Wiley and Sons, New York, USA

Bart, M., Stigter, E. C , Stapert, H. R., de Jong, G. J. and van Bennekom, W. P. (2005). On the response of a label-free interferon-gamma immunosensor utilizing electrochemical impedance spectroscopy *Biosens. Bioelectron.*, **21** (1), 49-59.

Barton, A., Collyer, S.D., Davis, F., Gornall, D., Law, K.A., Lawrence, E.C.D., Mills, D W., Myler, S , Pritchard, J.A , Thompson, M., and Higson, S.P.J. (2004). Sonochemically fabricated microelectrode arrays for biosensors offering widespread applicability: Part I. *Biosens. Bioelectron.*, **20** (2), 328-337.

Basheer, M.C., Santhosh, U., Alex, S., George Thomas, K , Suresh, C.H. and Das, S. (2007). Design and synthesis of squaraine based near infrared fluorescent probes. *Tetrahed.*, **63** (7), 1617-1623.

Bashir, R., (2004). BioMEMS: state-of-the-art in detection, opportunities and prospects. *Adv. Drug Deliver.Rev.*, **56** (11), 1565-1586.

Baylis, R.M., Doak, S.H., Holton, M.D. and Dunstan, P.R. (2007). Fluorescence imaging and investigations of directly labelled chromosomes using scanning near-field optical microscopy. *Ultramicro.* **107** (4-5), 308-312.

Beckett, D., Kovaleva, E and Schatz, P.J. (1999). A minimal peptide substrate in biotin holoenzyme synthetase-catalyzed biotinylation. *Protein Sci.*, **8** (4), 921-9.

Beersma, M.F.C., Claas, E.C.J., Sopaheluakan, T. and Kroes, A (2005). Parvovirus B19 viral loads in relation to VP1 and VP2 antibody responses in diagnostic blood samples. *J.Clin.Virol.*, **34**(1), 71-75.

Behnisch, J., Hollander, A., Tyczkowski, J., Gazicki, M., Pela, I and Ledzion, R. (1998). Formation of hydrophobic layers on biologically degradable polymeric foils by plasma polymerization. *Surf Coat. Tech.*, **98** (1-3), 872-874.

Ben-Dov, I., Willner, I. and Zisman, E. (1997). Piezoelectric immunosensors for urine specimens of *Chlamydia trachomatis* employing quartz crystal microbalance microgravimetric analyses *Anal. Chem.*, **69** (17), 3506-3512.

Benjamini, E., Coico, R. and Sunshine, G. (2000) Immunology: a short course, (4th edn.) Wiley and Sons, New York, USA.

Berger, C.E.H., Beumer, T A.M., Kooyman, R P.H. and Greve, J. (1998). Surface plasmon resonance multisensing. *Anal.Chem.*, **70**, 703-706.

Berggren, C. and Johansson, G. (1997). Capacitance measurements of antibody-antigen interactions in a flow system *Anal.Chem.* **69** (18), 3651-3657.

Berney, H. C., Alderman, J., Lane, W. A. and Collins, J. K (1998). Development of a capacitive immunosensor: a comparison of monoclonal and polyclonal capture antibodies as the primary layer. *J Mol. Recognit.*, **11** (1-6), 175-177.

Bessette, P.H., Aslund, F., Beckwith, J. and Georgiou, G. (1999). Efficient folding of proteins with multiple disulfide bonds in the *Escherichia coli* cytoplasm. *Proc. Nat Acad. Sci. USA*, **96** (24), 13703-13708

Betty, C.A., Lal, R., Sharma, D.K., Yakhmi, J.V. and Mittal, J.P (2004). Macroporous silicon based capacitive affinity sensor—fabrication and electrochemical studies. *Sensor. Actuat. B - Chem.*, **97** (2-3), 334-343

Bierne, H. and Cossart, P. (2002). InlB, a surface protein of *Listeria monocytogenes* that behaves as an invasin and a growth factor. *J. Cell Sci.*, **115** (17), 3357-3367.

- Blawas, A. S.** and Reichert, W.M. (1998) Protein patterning *Biomaterials*, **19**, 595-609.
- Blue, R.,** Kent, N., Polerecky, L., McEvoy, H., Gray, D. and MacCraith, B D. (2005). Platform for enhanced detection efficiency in luminescence-based sensors. *Electron. Letts.* **41** (12), 682-684.
- Blum, L.J.** and Coulet, P.R. (1991). Biosensor principles and applications. Marcel Dekker, New York, USA.
- Borrebaeck, C.A.K.** (2000). Antibodies in diagnostics - from immunoassays to protein chips. *Imm. Today*, **21**, (8), 379-382.
- Branden, C.** and Tooze, J. (1991). Introduction to Protein Structure, Garland Publishing, New York, USA
- Brennan, J.,** Dillon, P and O’Kennedy, R. (2003). Production, purification and characterisation of genetically derived scFv and bifunctional antibody fragments capable of detecting illicit drug residues. *J Chromatog. B*, **786**, 327 – 342.
- Brett, C. M. A.** and Oliveira Brett, A.M (1993) Electroanalysis. Oxford University Press, Oxford, UK.
- Brown, K.E.** (2004). Detection and quantitation of parvovirus B19 *J Clin.Virol.*, **31** (1), 1-4.
- Bruchez, M. Jr.,** Moronne, M., Gin, P, Weiss, S. and Alivisatos, A. P. (1998). Semiconductor nanocrystals as fluorescent biological labels. *Science*, **281** (5385), 2013-2016.
- Buchwalow, I.G.,** Minin, E.A. and Boecker, W. (2005). A multicolor fluorescence immunostaining technique for simultaneous antigen targeting. *Acta Histochem.*, **107** (2), 143-148.
- Buerk, D.G.** (1993). Biosensors Theory and Applications. Technomic Publications, Lancaster, UK.

Bujard, H., Gentz, R., Lanzer, M., Stuebber, D., Mueller, M., Ibrahimi, I., Haeuptle, M. and Dobberstein, B. (1987) A T5 promoter-based transcription-translation system for the analysis of proteins *in vitro* and *in vivo*. *Method Enzymol.*, **115**, 416 – 433

Burton, D.R. and Barbas III, C.F. (1993). Monoclonal Fab Fragments from Combinatorial Libraries Displayed on the Surface of Phage. *J. Immunol. Methods*, **3** (3), 155-163.

Byfield, M.P. and Abuknesha, A. (1994). Biochemical aspects of biosensors. *Biosens. Bioelectron.*, **9**, 373-400

C

Cao, Y. and Lam, L. (2003) Bispecific antibody conjugates in therapeutics. *Adv. Drug Deliv. Rev.*, **55** (2), 171-197.

Capitán-Vallvey, L.F., Deheldel, M.K.L. and Avidad, R. (1999). Determination of warfarin in waters and human plasma by solid phase room-temperature transmitted phosphorescence. *Arch. Environ. Contam. Toxicol.* **37**, 1.

Casaedi, J., Powell, M.J. and Kenten, J.H. (1990). Expression and Secretion of Aequorin as a Chimeric Antibody by Means of a Mammalian Expression Vector. *Proc. Nat. Acad. Sci. USA*, **87**, 2047-2051

Casey, J., Keep, P., Chester, K, Robson, L., Hawkins, R. and Begent, R. (1995). Purification of bacterially expressed single chain Fv antibodies for clinical applications using metal chelate chromatography. *J Immunol. Methods*, **179**, 105 – 116.

Castellano, F., Dattelbaum, J.D. and Lakowicz, J.R. (1998). Long-lifetime Ru (II) complexes as labeling reagents for sulfhydryl groups. *Anal. Biochem* **255**, 165-170.

Chakraborty, T., Ebel, F. and Domann, E. (1995). A focal adhesion factor directly linking intracellularly motile *Listeria monocytogenes* and *Listeria ivanovi* to the actin-based cytoskeleton of mammalian cells. *EMBO J.*, **14** (7), 1314-1321

Chan, W.C.W. and Nie, S.M. (1998). Quantum dot bioconjugates for ultrasensitive nonisotopic detection. *Science*, **281**, 2016–2018.

Chan, W.C.W., Maxwell, D.J., Gao, X, Bailey, R.E., Han, M. and Nie, S. (2002). Luminescent quantum dots for multiplexed biological detection and imaging. *Curr. Opin. Biotechnol.*, **13**, 40–46.

Charles, P. T., Goldman, E R., Rangasammy, J. G , Schauer, C L., Chen, M. S. and Tatt, C. R. (2004). Fabrication and characterization of 3D hydrogel microarrays to measure antigenicity and antibody functionality for biosensor applications. *Biosens. Bioelectron.*, **20** (4), 753-764.

Cheng, T.J., Lin, T.M. and Chang, H.S (2002). Physical adsorption of protamine for heparin assay using a quartz crystal microbalance and electrochemical impedance spectroscopy. *Anal Chim. Acta*, **462** (2), 261-273.

Cho, W.K., Sohn, U. and Kwak, J.K. (2000). Production and in vitro refolding of a single-chain antibody specific for human plasma apolipoprotein A-I. *J Biotechnol.*, **77** (2-3), 169-178.

Choi, W.C., Kim, M.Y., Suh, C.W. and Lee, E. (2005) Solid-phase refolding of inclusion body protein in a packed and expanded bed adsorption chromatography. *Process Biochem*, **40** (5), 1967-1972.

Chowdhury, P.S. and Wu, H. (2005). Tailor-made antibody therapeutics. *Methods* , **36** (1), 11-24.

Cloutier, S.M., Couty, S., Terskikh, A., Marguerat, L., Crivelli, V., Pugnieres, Mani, J.C , Leisinger, H J., Mach, J P. and Deperthes, D (2000). Streptabody, avidity molecule made by tetramerization of in vivo biotinylated, phage display-selected scFv fragments on streptavidin. *Mol. Immunol.*, **37**, 1067-1077.

Cooke, D., Fitzpatrick, B., O’Kennedy, R , McCormack, T., Egan, D. (1997). In: O’Kennedy, R. and Thornes, R.D., (Eds). *Coumarins Biology, Applications and Mode of Action*. John Wiley and Sons Ltd., Chichester, UK

Coon, D. (2003). Parvovirus B19: Characteristics, diseases and diagnosis. *Chn. Microbiol. Newslett.*, **25** (21), 161-167.

Cossart, P. (2002). Molecular and cellular basis of the infection by *Listeria monocytogenes*. an overview. *Int. J. Med. Microbiol.*, **291**,401-409.

Cossart, P., Pizarro-Cerda, J and Lecuit, M. (2003). Invasion of mammalian cells by *Listeria monocytogenes*: functional mimicry to subvert cellular functions. *Trends Cell. Biol.*, **13**, 3-31.

Cossart, Y.E., Field, A.M., Cant, B and Widdows, D. (1975). Parvovirus-like particles in human sera. *Lancet*, **1**, 7898, 72-73.

Cui, X., Pei, R. and Wang, Z. (2003), Layer-by-layer assembly of multilayer films composed of avidin and biotin-labeled antibody for immunosensing. *Biosens. Bioelectron.*, **18** (1), 59-67

Cullum, B. M. and Vo-Dinh, T. (2000). The development of optical nanosensors for biological measurements *Trends Biotechnol.*, **18** (9), 388-393.

D

Dahint, R., Trileva, E., Acunman, H., Konrad, U., Zimmer, M., Stadler, V. and Himmelhaus, M. (2007). Optically responsive nanoparticle layers for the label-free analysis of biospecific interactions in array formats. *Biosens. Bioelectron.*, **22** (12), 3174-3181.

Dalton, C.B., Austin, C.C, Sobel, J., Hayes, P.S., Bibb, W.F., Graves, L M., Swaminathan, B., Proctor, M. and Griffin, P.M. (1997). An outbreak of Gastroenteritis and fever due to *Listeria monocytogenes* in milk. *New Engl. J Med.*, **336**,100-105.

Dancette, O.P., Taboureau, J.L., Tournier, E, Charcosset, C. and Blond, P. (1999). Purification of immunoglobulins G by protein A/G affinity membrane chromatography. *J. Chromatog. B.*, **723** (1-2), 61-68.

Darmanin-Sheehan, A., Quinn, J., Daly, S., Dillon, P. and O’Kennedy, R. (2003) The development of novel miniaturised immuno-sensing devices: A review of a small technology with a large future. *Anal. Lett.*, **36** (3), 511-537.

Davis, F. and Higson, S. P (2005). Structured thin films as functional components within biosensors. *Biosens. Bioelectron.*, **21** (1), 1-20.

De Leij, L., Poppema, S. and The, T.H. (1983). Cryopreservation of newly formed hybridomas. *J. Immunol. Methods*, **62** (1), 69-72.

De Jong, E., de Haan, T., Kroes, A., Beersma, M., Oepkes, O. and Walther, F. (2004). Parvovirus B19 infection in pregnancy. *J. Clin. Virol.* **36**, (1), 1-7.

Delves, P.J. (1997). General Introduction, in Antibody production- essential techniques. Rickwood, D. (Ed.), John Wiley and Sons, West Sussex, UK.

Deng, T., Wang, H., Li, J.S., Hu, S.Q., Shen, G.L. and Yu, R.Q. (2004). A novel immunosensor based on self-assembled chitosan/alginate multilayers for the detection of factor B. *Sens. Actuat. B-Chem.*, **99** (1), 123-129.

Dercksen, D.P., Brinkhof, J.M.A., Dekker-Norren, T., van Maanen, K., Bode, C.F., Baird, G and Kamp, E.M. (2000). A comparison of four serological tests for the diagnosis of caseous lymphadenitis in sheep and goats. *Vet. Microbiol.* **75**, 167-175

De Valk, H., Vaillant, V., Jacquet, C., Rocourt, J., Le Querrec, F., Stainer, F., Quelquejeu, N, Pierre, O., Pierre, V., Descenclos, J.-C. and Goulet, V. (2001). Two consecutive nationwide outbreaks of listeriosis in France, October 1999-February 2000. *Am. J. Epidemiol.*, **154**, 944-950.

Dillon, P., Manning, B., Daly, S., Killard, T. and O’Kennedy, R. (2003). Production of recombinant anti-morphine-3-glucuronide single-chain variable fragments (scFv) antibody for the development of a “real-time” biosensor-based immunoassay. *J. Immunol. Methods.*, **276**, 151-161.

Doganay, M. (2003). Listeriosis: clinical presentation. *FEMS Immunol. Medical Microbiol.*, **1485**, 1-3.

Domen, P.L., Nevens, J.R., Mallia, A.K., Hermanson, G.T. and Klenk, D.C. (1990). Site-directed immobilization of proteins. *J. Chromatog. B*, **510**, 293-302.

Dong, Y. and Shannon, C (2000). Heterogeneous Immunosensing Using Antigen and Antibody Monolayers on Gold Surfaces with Electrochemical and Scanning Probe Detection. *Anal. Chem.*, **72**, 2371-2376.

Dong, D., Zheng, D and Wang, F. Q. (2004). Quantitative photoelectrochemical detection of biological affinity reaction: biotin-avidin interaction. *Anal. Chem.* **76** (2), 499-501.

Dotsikas, Y. and Loukas, Y L. (2004). Employment of 4-(1-imidazolyl) phenol as a luminol signal enhancer in a competitive-type chemluminescence immunoassay and its comparison with the conventional antigen-horseradish peroxidase conjugate-based assay. *Anal.Chim Acta*, **509**, 103-109.

Doyle, S., Kerr, S., O Keeffe, G , O.Carroll, D , Daly, P. and Kilty, C. (2000) Detection of parvovirus B19 IgM by antibody capture enzyme immunoassay *J. Virol Methods*, **90**, (2),143-152

Drams, S., Biswas I, Magun, E., Braun, L., Mastroeni, P. and Cossart, P. (1995). Entry of *Listeria monocytogenes* into hepatocytes requires expression of InlB, a surface protein of the internalin multigene family. *Mol. Microbiol.*, **16**, 251-61.

Dunbar, S.A., Vander Zee, C.A., Oliver, K.G., Karem, K L. and Jacobson, J.W. (2003). Quantitative, multiplexed detection of bacterial pathogens: DNA and protein applications of the Luminex LabMAP™ system *J. Microbiol. Meth.*, **53** (2), 245-252.

Doyle, S., Kerr, S., O'Keeffe, G., O'Carroll, D., Daly, P. and Kilty, C. (2000). Detection of parvovirus B19 IgM by antibody capture enzyme immunoassay: receiver operating characteristic analysis *J. Virol. Methods*, **90** (2), 143-152.

E

Eastwood, D. and Gouterman, M. (1970). Porphyrins : XVIII. Luminescence of (Co), (Ni), Pd, Pt complexes. *J. Mol. Spectrosc.*, **35**, 359-375

Eggins, B. (1996). Biosensors an Introduction, (1st ed.) John Wiley and Sons Ltd. Chicester.

Ekins, R. and Chu, R (1993). Multianalyte testing. *Clin. Chem.*, **39**, 369-370.

Ekins, Roger P. (1999). Microarrays: their origins and applications. *TibTech*, **17**, 217-218.

Espina, V., Woodhouse, E.C., Wulfkuhle, J., Asmussen, H.D., Petricoin III, E.F. and Liotta, L.A. (2004). Protein microarray detection strategies: focus on direct detection technologies. *J. Immunol. Methods*, **290**, 121-133

F

Fahrner, R.L., Blank, G.S. and Zapata, G.A. (1999) Expanded bed protein A affinity chromatography of a recombinant humanized monoclonal antibody: process development, operation, and comparison with a packed bed method. *J. Biotechnol.*, **75** (2-3), 273-280.

Fang, A., Tee Ng, H. and Yau Li, S.F. (2003). A high-performance glucose biosensor based on monomolecular layer of glucose-oxidase covalently immobilised on indium-tin oxide surface. *Biosens. Bioelectron.*, **19** (1), 43-49.

Feldstein, M.J., Golden, J.P., Rowe, C.A., MacCraith, B.D. and Ligler, F.S. (1999). Array biosensor: optical and fluidics systems. *J. Biomed. Microdev.*, **1** (2), 139-153.

Figueiro, S.D., Macedo, A.A.M, Melo, M.R.S., Freitas, A.L.P., Moreira, R.A., de Oliveira, R.A., Goes, J.C. and Sombra, A.S.B. (2006). On the dielectric behaviour of collagen-algal sulfated polysaccharide blends: Effect of glutaraldehyde crosslinking. *Biophys. Chem.*, **120**, 154-159

Findlay, J.W.A., Smith, W.C., Lee, J.W., Nordblom, G.D., Das, I., DeSilva, B.S., Khan, M.N. and Bowsher, R.R. (2000). Validation of immunoassays for bioanalysis. a pharmaceutical industry perspective. *J. Pharm. Biomed. Anal.*, **21** (6), 1249-1273.

Fitzpatrick, B. and O'Kennedy, R. (2004). The development and application of a surface plasmon resonance-based inhibition immunoassay for the determination of warfarin in plasma ultrafiltrate. *J. Immunol. Methods*, **291**, (1-2), 11-25.

Fletcher, S. (2001). The two-terminal equivalent network of a three-terminal electrochemical cell. *Electrochem Commun.*, **3** (12), 692-696.

Freiberg, A., Machner, M.P, Pfeil, W., Schubert, W-D., Heinz, D.W. and Seckler, R. (2004). Folding and stability of the leucine-rich repeat domain of Internalin B from *Listeria monocytogenes*. *J. Mol. Biol.*, **337**, 453-461.

G

- Gao, X.** and Nie, S (2003). Molecular profiling of single cells and tissue specimens with quantum dots. *Trends Biotechnol.*, **21** (9), 371-373.
- Gardas, A.** and Lewartowska, A. (1988). Coating of proteins to polystyrene ELISA plates in the presence of detergents. *J. Immunol. Methods*, **106** (2), 10, 251-255
- Georgiou, G.** and Valax, P (1996). Expression of correctly folded proteins in *Escherichia coli*. *Curr. Opin Biotechnol.*, **7**, 190-197.
- Ghindilis, A.L** and Kurochkin, I N (1994). Glucose potentiometric electrodes based on mediatorless bioelectrocatalysis A new approach. *Biosens. Bioelectron.*, **9** (4-5), 353-357.
- Ghindilis, A.L.**, Atanasov, P., Wilkins, M. and Wilkins, E. (1998) Immunosensors: electrochemical sensing and other engineering approaches. *Biosens. Bioelectron.*, **13** (1), 113-131.
- Glockler, J.** and Angenendt, P. (2003). Protein and antibody microarray technology. *J. Chromatog. B*, **797**, 229-240.
- Goepel, W.** and Heiduschka, P. (1995). Interface analysis in biosensor design. *Biosens. Bioelectron.*, **10**, 853-883
- Goldman, E. R.**, Clapp, A. R. and Anderson, G P. (2004) Multiplexed toxin analysis using four colors of quantum dot fluororeagents. *Anal. Chem.*, **76** (3), 684-688.
- Goldman, E. R.**, Mattoussi, H., Anderson, G. P., Medintz, I. L. and Mauro, J. M. (2005). Fluoroimmunoassays using antibody-conjugated quantum dots. *Meths. Mol. Biol.*, **303**, 19-34.
- Goldman, E. R.**, Medintz, I. L and Mattoussi, H. (2006). Luminescent quantum dots in immunoassays. *Anal. Bioanal. Chem* , **384** (3), 560-563.
- Gospodinova, N.** and Terlemezyan L. (1998). Conducting polymers prepared by oxidative polymerization polyaniline. *Prog Polym. Sci.*, **23**, 1443-1484.

Grant, S., Pritchard, J.A., Davis, F, Higson, S.P.J. and T Gibson, T. (2003). Labelless and reversible immunosensor assay based upon an electrochemical current transient protocol. *Anal. Chim Acta.*, **495**, (1-2), 21-32

Grant, S., Davis, F., Law, K.A , Barton, A.C , Collyer, S D., Higson, S.P J. and Gibson, T.D. (2005). Label-free and reversible immunosensor based upon an ac impedance interrogation protocol *Anal. Chim. Acta.*, **537**, 163-168

Green, N.M. (1965) A spectrophotometric assay for avidin and biotin based on binding of dyes by avidin. *Biochem. J.*, **94**, 23c-24c.

Grennan, K., Killard, A.J., Hanson, C.J., Cafolla, A.A. and Smyth, M.R (2006). Optimisation and characterisation of biosensors based on polyaniline. *Talanta.*, **68** (5), 1591-1600

Gretch, D. R., Suter, M and Stinski, M. F. (1987) The use of biotinylated monoclonal antibodies and streptavidin affinity chromatography to isolate herpesvirus hydrophobic proteins or glycoproteins. *Anal. Biochem.*, **163** (1), 270-277.

Guan, J.G., Miao, Y.Q. and Zhang, Q.J., J. (2004). Impedimetric biosensors. *J Biosci Bioeng.*, **4**, 219-226.

Gudgin-Dickson, E. F., Pollak, A. and Diamandis, E. P. (1995). Ultrasensitive bioanalytical assays using time-resolved fluorescence detection. *Pharmacol. Therapeut.*, **66** (2), 207-235.

Gurland, H.J., Davison, A.M., Bonomini, V., Falkenhagen, D., Hansen, S., Kishimoto, T., Lysaght, M.J., Moran, J. and Valek, A. (1994). Definitions and terminology in biocompatibility. *Nephrol. Dial. Transpl.* **9**, (2), 4-10

H

Hadas, E. and Theilen, G. (1987). Production of monoclonal antibodies: The effect of hybridoma concentration on the yield of antibody-producing clones *J. Immunol. Methods*, **96**, 3-6.

Hall, M., Kazakova, I. and Yao, Y-M. (1999). High Sensitivity Immunoassays Using Particulate Fluorescent Labels *Anal. Biochem.* **272**, 165-170.

Handl, H.L. and Gillies, R.J. (2005). Lanthanide-Based Assays for Ligand-Receptor Interactions. *Life. Sci.*, **77**, 361-371.

Hannig, G. and Makrides, S. (1998). Strategies for optimising heterologous protein expression in *Escherichia coli*. *TibTech*, **16**, 54 –60.

Harrison, R. (2000). Expression of soluble heterologous proteins via fusion with NusA protein. *inNovations*, **11**, 4-7.

Hayakawa, T., Yoshinari, M. and Nemoto, K. (2004). Characterization and protein-adsorption behavior of deposited organic thin film onto titanium by plasma polymerization with hexamethyldisiloxane. *Biomater.*, **25**, 119.

Hayhurst, A., Georgiou, G. (2001). High-throughput antibody isolation. *Curr. Opin Chem Biol.*, **5** (6), 683-689.

Hays, H. C. W., Millner, P. A and Prodromidis, M. I. (2006). Development of capacitance based immunosensors on mixed self-assembled monolayers. *Sens. Actuat. B-Chem.*, **114** (2), 1064-1070.

Hearty, S., Leonard, P., Quinn, J., O’Kennedy, R. (2006). Production, characterisation and potential application of a novel monoclonal antibody for rapid identification of virulent *Listeria monocytogenes*. *J. Microbiol. Meths*, **66**, 294-312.

Heggeness, M. H. and Ash, J. F. (1977). Use of the avidin-biotin complex for the localization of actin and myosin with fluorescence microscopy. *J. Cell Biol.*, **73** (3), 783-788

Hemmilá, I. and Mukkala, I.V. (2001). Time-Resolution in Fluorometry Technologies, Labels, and Applications in Bioanalytical Assays. *Crit. Rev. Clin Lab Sci.*, **38** (6), 441-519.

Hermanson, G. T. (1996). Bioconjugate Techniques. Academic Press, London, UK.

Hernández-Caraballo, E.A and Marcó-Parra, L.M. (2003). Direct analysis of blood serum by total reflection X-ray fluorescence spectrometry and application of an artificial neural network approach for cancer diagnosis. *Spectrochim. Acta. B*, **58** (12), 2205-2213.

Hirsh, J., Dalen, J.E. and Anderson D.R. (2001). Oral anti-coagulants: mechanism of action, clinical effectiveness, and optimal therapeutic range. *Chest*, **119**, 8S–21S.

Hochuli, E., Dobeli, H. and Schacher, A. (1987). New metal chelate adsorbent selective for proteins and peptides containing neighbouring histidine residues *J. Chromatog.B.*, **411**, 177-184.

Hock, B. (1997). Antibodies for immunosensors a review. *Anal. Chim. Acta.*, **347**, (1-2), 177-186.

Hockney, R.C. (1994). Recent developments in heterologous protein production in *E. coli*. *Trends Biotechnol.*, **12** (11), 456-463.

Hof, H. (2003). History and epidemiology of listeriosis. *FEMS Immunol Medical Microbiol.*, **1489**,1-4.

Hollingsworth, P. (1999). A proactive approach to safety issues. *Food Technol.*, **53**, 26.

Homola, J., Yee, S.S. and Gauglitz, G. (1999). Surface plasmon resonance sensors: review. *Sens. Actuat. B*, **54**, 3-15.

Hoogenboom, H.R., de Bruijn, A.P., Hufton, S.E., Hoet, R.N., Arends, J-W., Roovers, R.C. (1998). Antibody phage display technology and its applications. *Immunotechnol.*, **4**,1-20.

Hoshina, Y., Yamada, Y., Tanaka, H., Doi, T. and Takahashi, T (2007). Synthesis of fluorescent-labeled aeruginosin derivatives for high-throughput fluorescence correlation spectroscopy assays. *Bioorgan. Med. Chem. Letts.*, **17** (10), 2904-2907.

Hou, J. Zheng, J. and Shamsi, S.A. (2007). Separation and determination of warfarin enantiomers in human plasma using a novel polymeric surfactant for micellar electrokinetic chromatography–mass spectrometry. *J Chromatog. A*, **1159** (1-2), 208-216.

Huang, J.G., Lee, C.L., Lin, H.L., Chuang, T.L., Wang, W.S., Juang, R.H., Wang, C.H., Lee, C.K., Lin, S.M., Lin, C.W. (2006). Miniaturized germanium-doped silicon dioxide-based surface plasmon resonance waveguide sensor for immunoassay detection. *Biosens. Bioelectron.*, **22**, 519–525.

Humphreys, D.P., Sehdev, M., Chapman, A P , Ganesh, R., Smith, B J., King, L.M., Glover, D.J , Reeks, D.G. and Stephens, P (2000) High-level periplasmic expression in *E. coli* using a eukaryotic signal peptide: Importance of codon usage at the 5'-end of the coding sequence. *Protein Expres.Purif.*, **20** (2), 252-264

Hun, X. and Zhang, Z. (2007). Fluoroimmunoassay for tumor necrosis factor- α in human serum using Ru(bpy)₃Cl₂-doped fluorescent silica nanoparticles as labels. *Talanta*, **73**, (2), 366-371.

Huse, K., Böhme, H.J and Scholz, G (2002) Purification of antibodies by affinity chromatography. *J. Biochem. Bioph. Meth.*, **51** (3), 217-231.

I

Inoue, H., Nojima, H. and Okayama, H. (1990). High efficiency transformation of *Escherichia coli* with plasmids. *Gene*, **96**, 23-28.

Ireton, K. and Cossart, P. (1997). Host-pathogen interactions during entry and actin-based movement of *Listeria monocytogenes*. *Annu. Rev. Genet.*, **31**,113-138.

J

Jain, M., Kamal, N. and Batra, S.K. (2007). Engineering antibodies for clinical applications. *Trend. Biotechnol.*, **25**, 7, 307-316.

Jaiswal, J. K., Goldman, E. R., Mattoussi, H. and Simon, S. M. (2004). Use of quantum dots for live cell imaging. *Nat. Methods*, **1** (1), 73-78.

Jaiswal, J. K., Mattoussi, H., Mauro, J. M. and Simon, S. M. (2003). Long-term multiple color imaging of live cells using quantum dot bioconjugates. *Nat. Biotechnol.* **21** (1), 47-51.

Jamieson, T., Bakhshi, R., Petrova, D., Pocock, R., Imani, M. and Seifalian, A.M. (2007). Biological applications of quantum dots. *Biomaterials*, **28** (31), 4717-4732.

Janeway, C.A., Jr., Travers, P., Walport, M. and Capra, J. (1999). The recognition of antigen, p79-113, in *Immunobiology: the immune system in health and disease* (4th edition) Austin, P. and Lawrence, E. (Eds.). Garland Publishing, New York, USA.

Janocha, B., Hegemann, D., Oehr, C., Brunner, H., Rupp, F. and Geis-Gerstorfer, J. (2001). Adsorption of protein on plasma-polysiloxane layers of different surface energies *Surf. Coat. Technol.* **142-144**, 1051-1055.

Jensen, A., Frederiksen, W. and Gerner-Smidt, P. (1994). Risk factors for Listeriosis in Denmark, 1989-1990. *Scand. J. Infect. Dis.*, **26**, 171-178.

Ji, X., He, Z., Ai, X., Yang, H. and Xu, C. (2006). Determination of clenbuterol by capillary electrophoresis immunoassay with chemiluminescence detection. *Talanta*, **70** (2), 353-357.

Jin, W., Wang, Y.F., Ge, R.L., Shi, H.M., Jia, C.Q. and Tu, P.F. (2007). Simultaneous analysis of multiple bioactive constituents in *Rheum tanguticum* Maxim. ex Balf. by high-performance liquid chromatography coupled to tandem mass spectrometry. *Rapid Commun. Mass Sp.*, **21** (14), 2351-2360.

Jo, B-H., Van Lerberghe, L.M., Motsegood, K.M. and Beebe, D.J. (2000). Three-dimensional micro-channel fabrication in polydimethylsiloxane (PDMS) elastomer. *J. Microelectromech. Syst.*, **9**, 76-81.

Jones, D. and Seeliger, H. (1992) The genus *Listeria*, p1595-1616, in *The Prokaryotes* 2nd Edn., Balows, C.A., Truper, H.G., Dworkin, M., Harder, W. and Schleur, K-H. (Eds.), Springer Verlag, Heidelberg, Germany.

Jonquieres, R., Bierne, H., Fiedler, F., Gounon, P. and Cossart, P. (1999). Interaction between the protein InlB of *Listeria monocytogenes* and lipoteichoic acid: a novel mechanism of protein association at the surface of gram-positive bacteria. *Mol. Microbiol.*, **34**, 902-914.

Jordan C.E. and Corn, R.M. (1997). Surface plasmon resonance imaging measurements of electrostatic biopolymer adsorption onto chemically modified gold surfaces. *Anal. Chem.*, **69** (7), 1449-1456.

Jordan, J. (1996). Identification of human parvovirus B19 infection in idiopathic nonimmune hydrops fetalis. *Am. J. Obstet. Gynecol.*, **174**, 37-42.

Jung, S., Honegger, A. and Pluckthun, A. (1999). Selection for improved protein stability by phage display. *J. Mol Biol.*, **294**, 163-80.

K

Kameswara-Rao, V., Rai, G.P., Agarwal, G.S. and Suresh, S. (2005). Amperometric immunosensor for detection of antibodies of *Salmonella typhi* in patient serum. *Anal. Chim. Acta*, **531**, 173–177.

Kane, J.F. (1995) Effects of rare codon clusters on high-level expression of heterologous proteins in *Escherichia coli*. *Curr. Opin. Biotech.*, **6** (5), 494-500.

Kang, J.H., Choi, H.J., Hwang, S.Y., Han, S.H., Jeon, J.Y. and Lee, E.K. (2007). Improving immunobinding using oriented immobilization of an oxidized antibody. *J. Chromatog. A*, **1161**, (1-2), 9-14.

Karlsson, R., Kullman-Magnusson, M., Hamalainen, M.D., Remaeus, A., Andersson, K., Borg, P., Gyzander, E. and Deinum, J. (2000) Biosensor analysis of drug target interactions: Direct and competitive binding assays for investigation of interactions between thrombin and thrombin inhibitors. *Anal. Biochem.* **278**, 1-13.

Katz, E., Heleg-Shabtai, V., Bardea, A., Willner, I., Rau, H. K. and Haehnel, W. (1998). Fully integrated biocatalytic electrodes based on bioaffinity interactions. *Biosens. Bioelectron.* **13**, (7-8), 741-756.

Katz, E., Alfonta, L. and Willner, I. (2001). Chronopotentiometry and Faradaic impedance spectroscopy as methods for signal transduction in immunosensors. *Sens. Actuat. B- Chem.*, **76** (1-3), 134-141.

Katz, E. and Willner, I. (2003). Probing biomolecular interactions at conductive and semiconductive surfaces by impedance spectroscopy. Routes to impedimetric immunosensors, DNA-sensors, and enzyme biosensors *Electroanal.*, **15**, 913-947.

Kaufmann, B., Baxa, U., Chipman, P.R., Rossmann, M.G., Modrow, S. and Seckleret, R. (2005). Parvovirus B19 does not bind to membrane-associated globoside in vitro. *Virology*, **332** (1), 189-198.

Kerman, K., Endo, T., Tsukamoto, M., Chikae, M., Takamura, Y. and Tamiya, E. (2007). Quantum dot-based immunosensor for the detection of prostate-specific antigen using fluorescence microscopy *Talanta*, **71**, 1494–1499.

Kharitonov, A.B., Alfonta, L., Katz, E. and Willner, I (2000). Probing of bioaffinity interactions at interfaces using impedance spectroscopy and chronopotentiometry. *J. Electroanal. Chem.*, **487**, 133-141

Killard, A.J., Deasy, B., O'Kennedy, R. and Smyth, M.R. (1995). Antibodies: production, functions and applications in biosensors. *Trends Anal. Chem.* **14**, 257-267.

Kim, J.H., Cho, J.H., Cha, G S., Lee C.W., Kim, H.B. and Paek, S.H. (2000). Conductimetric membrane strip immunosensor with polyaniline-bound gold colloids as signal generator. *Biosens. Bioelectron.*, **14**, **12**, 907-15.

King, S.H.P., Joslin, M.A., Raudibaugh, K., Pieniaszek jr., H.J. and Benedek, I.H. (1995). Dose-dependent pharmacokinetics of warfarin in healthy volunteers. *Pharm. Res.*, **12** (12), 1874.

Kipriyanov, S.M., Moldenhauer, G. and Little, M. (1997). High level production of soluble single chain antibodies in small-scale *Escherichia coli* cultures. *J. Immunol. Methods.*, **200**, 69-77.

Kobe, B. and Kajava, A.V. (2001). The leucine-rich repeat as a protein recognition motif *Curr. Opin. Struc. Biol.*, **11**, 725-732.

Köhler, G. and Milstein, C. (1975). Continuous cultures of fused cells secreting antibody of predefined specificity *Nature*, London, **256**, 495-497.

Krebber, A., Bornhauser, S., Burmester, J, Honegger, A., Willuda, J., Bosshard, H and Pluckthun, A. (1997). Reliable cloning of functional antibody variable domains from hybridomas and spleen cell repertoires employing a reengineered phage display system. *J. Immunol. Methods.*, **201**, 35-55

Krepkiy, D., Wong, K., Gawrisch, K. and Yeliseev, A. (2006). Bacterial expression of functional, biotinylated peripheral cannabinoid receptor CB2. *Protein Expres.Purif.*, **49** (1), 60-70.

Kricka, L.J. (2003). Clinical applications of chemiluminescence. *Anal.Chim.Acta*, **500**, (1-2), 279-286.

Kukar, T., Eckenrode, S., Gu, Y., Lian, W., Megginson, M., She, J.X. and Wu, D. (2002) Protein Microarrays to Detect Protein-Protein Interactions Using Red and Green Fluorescent Proteins. *Anal. Biochem.* **306** (1), 50-54.

Kumar, P., Colston, J.T., Chambers, J.P., Rael, E.D. and Valdes, J.J. (1994). Detection of *botulinum* toxin using an evanescent wave immunosensor. *Biosens. Bioelectron.* **9**, 57-63.

L

Lackowicz, J.R. (1999). Principles of Fluorescence spectroscopy (2nd Ed.). Kluwer Academic/Plenum Publishers, New York, USA

Laemmli, U. (1970). Cleavage of structural proteins during assembly of the head of bacteriophage T4. *Nature*, London, **227**, 680-685

Lainé, S., Salhi, S. and Rossignol, J.M. (2002). Overexpression and purification of the hepatitis B antigen precursor. *Curr. Opin Biotech.*, **103** (1), 67-74.

Lamtore, J.B., Iverson, B. and Hogan, M.E. (1996). An intensely luminescent polymeric lanthanide chelator for multiple fluorescence labeling of biomolecules. *Tetrahed. Letts.*, **37** (36), 6483-6486.

La Vallie, E., DiBlasio, E., Kovacic, S., Grant, K., Schendel, P. and McCoy, J. (1993). A thioredoxin gene fusion system that circumvents inclusion body formation in the *E. coli* cytoplasm. *Bio/Technol.* **11**, 187 – 193.

Lefranc, G. and Lefranc, M.P. (1990). Antibody engineering and perspectives in therapy. *Biochimie*, **72** (9), 639-651.

Leonard, P. (2003). Production of antibodies for use in a biosensor-based assay for *Listeria monocytogenes*. PhD Thesis, School of Biotechnology, Dublin City University

Leonard, P., Hearty, S., Quinn, J. and O'Kennedy, R (2005). Development of a surface plasmon resonance-based immunoassay for the direct detection of *Listeria monocytogenes*. *J. Food Protect* , **68** (4),728-735.

Leung, A., Shankar, P.M. and Mutharasan, R. (2007) A review of fiber-optic biosensors. *Sens. Actuat. B-Chem*, **125**, (2), 688-703.

Li, C. M., Sun, C Q., Chen, W. and Pan, L (2005). Electrochemical thin film deposition of polypyrrole on different substrates. *Surf. Coat Technol*, **198** (1-3), 474-477.

Li, D.J., Cui, F.Z. and Zhao, G.J. (1998). Ion-beam-induced biomedical behavior of hexamethyldisiloxane films on deposited polyetherurethanes. *App. Surf. Sci.* **126**, 1-10

Li, J., Wang, H., Deng, T., Wu, Z , Shen, G. and Yu, R. (2004). A Plasma-polymerized film for capacitance immunosensing. *Biosens. Bioelectron.*, **20** (4), 841-847.

Lian, W., Litherland, S.A., Badrane, H., Tan, W., Wu, D., Baker, H.V., Gulig, P A , Lim, D.V and Jin, S. (2004). Ultrasensitive detection of biomolecules with fluorescent dye-doped nanoparticle. *Anal. Biochem*, **334**, 135-144.

Liedberg, B., Nylander, C. and Lundstrom, I. (1995). Biosensing with surface plasmon resonance - how it all started. *Biosens. Bioelectron.*,**10**, 1-9.

Lillie, G., Payne, P.A. and Vadgama, P (2001). Electrochemical impedance spectroscopy as a platform for reagentless bioaffinity sensing *Sensor. Actuat. B- Chem.*, **78**, 249-256.

Liu^a, L.J., Hu, J.M., Pei, R.J. and Hu, Y. (1999). Development of a piezoelectric immunosensor for the detection of factor B. *Chem. J. Chun. Univ*, **6**, 887-889.

Liu, Y.M., Mu, H.B., Zheng, Y L., Wang, C.Q., Chen, Y.H , Li, F.R., Wang, J.H. and Cheng, J K. (2007). Capillary electrophoretic immunoassay for alpha-fetoprotein with chemiluminescence detection. *J Chromatog B* (In press).

Liu^b, X., Zhang, S., Pan, X. and Wang, C. (1999). A novel method for increasing production of mature proteins in the periplasm of *Escherchia coli*. *Protein. Sci.*, **8**, 2085 – 2089.

Lochner, N., Lobmaier, C., Wirth, M., Leitner, A., Pittner, F. and Gabor, F. (2003). Silver nanoparticle enhanced immunoassays. one step real time kinetic assay for insulin in serum. *Eur. J. Pharm. and Biopharm*, **56**, 469-477.

Losito, H., De Giglio, E., Cioffi, N. and Malitesta, C. (2001). Spectroscopic investigation on polymer films. *J. Mater. Chem*, **11**, 1812-1817.

Lower, S.K. (1994). Electrochemistry' Chem1 virtual textbook, Simon Fraser University, Vancouver, Canada. (online at www.chem1.com).

Lu, B., Smyth, M.R. and O'Kennedy, R. (1996). Immunological activities of IgG antibody on pre-coated Fc receptor surfaces. *Anal. Chim. Acta*, **331** (1-2), 97-102.

Lu, B., Iwuoha, E.I., Smyth, M.R. and O'Kennedy, R. (1997). Development of an "electrically wired" amperometric immunosensor for the determination of biotin based on a non-diffusional redox osmium polymer film containing an antibody to the enzyme label horseradish-peroxidase. *Anal. Chim. Acta*, **345**(1-3), 59-66.

Lucas, L.J., Chesler, J.N. and Yoon, J Y. (2007). Lab-on-a-chip immunoassay for multiple antibodies using microsphere light scattering and quantum dot emission. *Biosens. Bioelectronics*, **23**, (5), 675-681.

Lundberg, E., Sundberg, M., Graslund, T., Uhlén, M. and Svahn, H.A. (2007). A novel method for reproducible fluorescent labeling of small amounts of antibodies on solid phase. *J. Immunol. Meths.*, **322** (1-2), 40-49.

Luo, L., Zhang, Z., Hou, L., Wang, J. and Tian, W. (2007). The study of a chemiluminescence immunoassay using the peroxyoxalate chemiluminescent reaction and its application. *Talanta*, **72** (4), 1293-1297.

Luppa, P.B., Sokoll, L.J. and Chan, D.W. (2001) Immunosensors--principles and applications to clinical chemistry. *Chn. Chim. Acta*, **314**, 1-26.

M

Macdonald, J.R., (Ed.). (1987) Impedance Spectroscopy Emphasizing Solid Materials and Systems. John Wiley and Sons, New York, USA.

Majerus, P.W., Broze, G J, Miletich, J.P. and Tollefsen, D.M. (1996). Anticoagulant thrombolytic, and antiplatelet drugs. In: Hardman JG, Limbird LE, (Eds). Goodman and Gilman's *The pharmacological basis of therapeutics*. (9th Edn.) McGraw-Hill New York, 1347-51.

Makrides, S.C. (1996). Strategies for achieving high-level expression of genes in *Escherichia coli* *Microbiol Rev.*, **60**, 512-538.

Manger, R., Woodle, D., Berger, A. and Hungerford, J. (2007). Flow cytometric detection of saxitoxins using fluorescent voltage-sensitive dyes. *Anal. Biochem* , **336** (2), 149-155.

Markgren, P.O., Lindgren, M.T., Gertow, K., Karlsson, R., Hamalainen, M and Danielson, U H. (2001). Determination of interaction kinetic constants for HIV-1 protease inhibitors using optical biosensor technology. *Anal Biochem*. **291**, 207–218 .

Marquette, C.A. and Blum, L.J. (2006). State of the art and recent advances in immunoanalytical systems. *Biosens. Bioelectron.*, **21** (8), 1424-1433.

Marquette, C.A., Hezard, P., Deguli, A and Blum, L J (2006). Macro-molecular chemiluminescent complex for enhanced immuno-detection onto microtiter plate and protein biochip. *Sens. Actuat B-Chem.*, **113** (2), 664-670.

Martsev, S.P., Preygerzon, V.A., Mel'nikova, Y.I., Kravchuk, Z.I., Ponomarev, G.V , Lunev, V E. and Savitsky (1995). Modification of monoclonal and polyclonal IgG with palladium (II) coproporphyrin I: Stimulatory and inhibitory functional effects induced by two different methods. *J. Immunol. Methods.*, **186**, 293-304.

Mason, W.T. (Ed). (1993). Fluorescent and luminescent probes for biological activity: a practical guide to technology for quantitative real-time analysis. Academic Press, London, UK.

Mattheakis, L.C., Dias, J.M., Choi, Y.J., Gong, J., Bruchez, M.P., Liu, J. and Wang, E. (2004). Optical coding of mammalian cells using semiconductor quantum dots. *Anal Biochem.*, **327** (2), 200-208.

Mattoussi, H., Mauro, J.M., Goldman, E.R., Anderson, G.P., Sundar, V.C., Mikulec, F.V and Bawendi, M.G. (2000). Self-assembly of CdSe-ZnS quantum dot bioconjugates using an engineered recombinant protein. *J. Am. Chem. Soc.*, **122**, 12142-12150.

Matz, M. V., Fradkov, A. F. and Labas, Y. A. (1999). Fluorescent proteins from nonbioluminescent Anthozoa species. *Nat. Biotechnol.*, **17** (10), 969-973.

Mauriz, E., Calle, A., Manclus, J.J., Montoya, A., Hildebrandt, A., Barcelo, D. and Lechuga, L.M. (2007). Optical immunosensor for fast and sensitive detection of DDT and related compounds in river water samples. *Biosens. Bioelectron* , **22** (7), 1410-1418.

Mayer, R.J. and Walker, J.H. (1987). *Immunochemical Methods in Cell and Molecular Biology*. Academic Press, London, UK.

Mayforth, R.D. (1993). Antibody structure, p 4-23, in *Designing Antibodies*. Academic Press, London, UK.

Maynard, J. and Georgiou, G. (2000). Antibody engineering. *Ann. Rev. Biomed. Eng.*, **2**, 339-376.

Mazuet, C., Lerouge, D., Poul, M.A. and Blin, N. (2006). Breast carcinoma specific antibody selection combining phage display and immunomagnetic cell sorting. *Biochem. Biophys. Res. Commun.*, **348** (2), 550-559.

McCafferty, J., Griffiths, A., Winter, G. and Chiswell, D. (1990). Phage antibodies: filamentous phage displaying antibody variable domains. *Nature London*, **348**, 552-554.

Medintz, I. L., Uyeda, H. T., Goldman, E. R. and Mattoussi, H. (2005). Quantum dot bioconjugates for imaging, labelling and sensing. *Nat. Mater.*, **4** (6), 435-446.

Mena, C., Almeida, G., Carneiro, L., Teixeira, P., Hogg, T. and Gibbs, P.A. (2004). Incidence of *Listeria monocytogenes* in different food products commercialized in Portugal. *Food Microbiol.*, **21** (2), 213-216.

Michalzik, M., Wilke, R. and Buttgenbach, S. (2005). Miniaturized QCM-based flow system for immunosensor application in liquid. *Sens. Actuat. B-Chem.*, 111-112, 410-415.

Morrin, A., Guzman, A., Killard, A.J., Pingarron, J.M. and Smyth, M.R. (2003). Characterisation of horseradish peroxidase immobilisation on an electrochemical biosensor by colorimetric and amperometric techniques *Biosens. Bioelectron.* **18**, 715-720.

Mueller, R.L. (2004). First-generation agents. aspirin, heparin and coumarins. *Best Pract. Res. Clin. Haematol.*, **17** (1), 23-53.

Müller, K.M., Arndt, K.M., Bauer, K. and Plückthun, A. (1998). Tandem immobilised metal-ion affinity chromatography/immunoaffinity purification of His-tagged proteins; Evaluation of two anti-His tag monoclonal antibodies. *Anal. Biochem.*, **259**, 54-61.

Muller-Renaud, S., Dupont, D. and Duheu, P. (2004). Quantification of beta casein in milk and cheese using an optical immunosensor. *J.Agric.Food Chem.*, **52** (4), 659-664.

Mullett, W.M., Lai, E.P.C. and Yeung, J.M. (2000). Surface plasmon resonance-based immunoassays. *Methods*, **22**, 77-91.

Mulvaney, S.P., Mattoussi, H.M. and Whitman, L.J. (2004). Incorporating fluorescent dyes and quantum dots into magnetic microbeads for immunoassays. *BioTechniques*, **36**, (4), 602-609.

Murby, M., Uhlén, M. and Ståhl, S. (1996). Upstream strategies to minimize proteolytic degradation upon recombinant production in *E. coli*. *Protein Express. Purif.* **7** (2), 129-136.

Murer, L., Zacchello, G. and Bianchi, D. (2000). Thrombotic microangiopathy associated with parvovirus B 19 infection after renal transplantation. *J. Am. Soc. Nephrol.*, **11**, 1132-1137.

Muronetz, V.I. and Korpela, T. (2003) Isolation of antigens and antibodies by affinity chromatography. *J. Chromatog , B*, **790** (1-2), 53-66.

Myler, S., Collyer, S. D., Davis, F., Gornall, D. D. and Higson, S. P. (2005). Sonochemically fabricated microelectrode arrays for biosensors. Part III. AC impedimetric study of aerobic and anaerobic response of alcohol oxidase within polyaniline. *Biosens. Bioelectron.*, **21** (4), 666-671.

Myler, S., Davis, F., Collyer, S. D. and Higson, S. P. (2004). Sonochemically fabricated microelectrode arrays for biosensors--part II. Modification with a polysiloxane coating. *Biosens Bioelectron.*, **20** (2), 408-412.

Myong Song, J., Culha, M., Kasli, P.M , Griffin, G.D. and Vo-Dinh, T. (2005). compact CMOS biochip immunosensor towards the detection of a single bacteria. *Biosens. Bioelectron.* , **20**, 2203-2209.

N

Nahir, T.M. and Bowden, E.F. (1996). The distribution of standard rate constants for electron transfer between thiol-modified gold electrodes and adsorbed cytochrome c. *J. Electroanal Chem.*, **410** (1), 9-13.

Nakanishi, K., Muguruma, H. and Karube, I (1996). A novel method of immobilizing antibodies on a quartz crystal microbalance using plasma-polymerized films for immunosensors. *Anal. Biochem.*, **68**, 1695-1700.

Nimeri, G., Augustinsson, A., Lassen, B., Stendahl, O., Ohman, L. and Elwing, H. (1994) The chemiluminescence response of neutrophils on polymer surfaces made by glow discharge plasma polymerization *J. Biomater Sci. Polym. Ed* , **6** (8), 741-749.

Nimeri, G., Ohman, L., Elwing, H., Wettero, J. and Bengtsson, T. (2002). The influence of plasma proteins and platelets on oxygen radical production and F-actin distribution in neutrophils adhering to polymer surfaces. *Biomaterials* **23** , 1785-1795.

Nisnevitch, N., Kolog-Gulco, M., Trombka, D., Green, B.S. and Firer, M A. (2000). Immobilization of antibodies onto glass wool. *J. Chromatog. B.*, **738** (2), 217-223.

O

O' Kennedy, R., Leonard, P., Hearty, S., Daly, S., Dillon, P., Brennan, J., Dunne, L., Darmanin Sheehan, A., Stapleton, S., Tully, L., Quinn, J. and Chakraborty, T. (2005). Advances in biosensors for the detection of pathogens in food and water In: *Rapid Methods for Biological and Chemical Contaminants in Food and Feed*, 85-104. Van Amerongen, A., Barug, D. and Lauwaars, M (Eds) Wageningen Academic Publishers, The Netherlands.

O'Riordan, T. C., Soini, A. E. and Papkovsky, D. B. (2001). Monofunctional derivatives of coproporphyrins for phosphorescent labeling of proteins and binding assays. *Anal Biochem.*, **290** (2), 366-375.

O'Riordan, T. C., Soini, A. E., Soini, J T and Papkovsky, D B. (2002). Performance evaluation of the phosphorescent porphyrin label solid-phase immunoassay of alpha-fetoprotein. *Anal Chem.*, **74** (22), 5845-5850.

Osman, A., Arbring, K. and Lindahl, T.L. (2005). A new high-performance liquid chromatographic method for determination of warfarin enantiomers. *J. Chromatog. B*, **826** (1-2), 75-80.

Ouerghi, O., Touhami, A , Jaffrezic-Renault, N., Martelet, C., Ben Ouada, H. and Cosnier, S. (2002). Impedimetric immunosensor using avidin-biotin for antibody immobilization. *Bioelectrochem.*, **56**, 131-133.

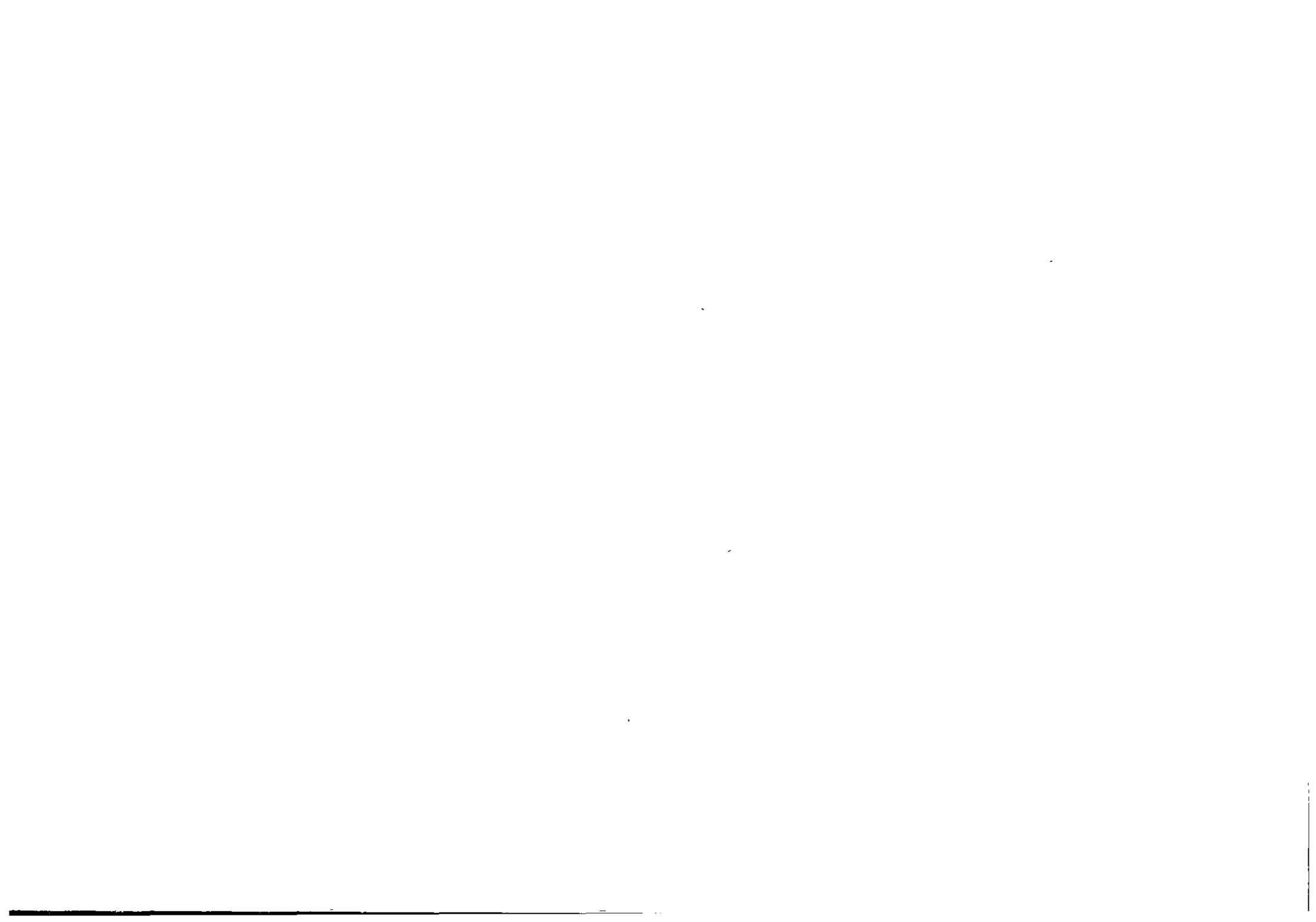
Ow, H., Larson, D.R., Srivastava, M., Baird, B.A., Webb, W.W. and Wiesner, U. (2005). Bright and stable core-shell silica fluorescent nanoparticles. *Nanolett.*, **5**, (1), 113-117.

P

Padoa, C.J. and Crowther, N.J. (2006). Engineered antibodies: A new tool for use in diabetes research. *Diabetes Res. Clin. Prac.*, **74** (2), 1, S51-S62

Pan, J. (2007). Direct and rapid monitoring the biochemical reaction of interleukin-6 in human using a flow-injection capacitive immunosensor in clinical immunoassay. *Sens. Actuat. B*, **125** (2), 517-525.

Papkovsky, D.B. (1991) Luminescent porphyrins probes. *Appl. Fluor Technol.* **3**, 16-24.



Papkovsky, D.B. (1993). Luminescent porphyrins as probes for optical (bio)sensors. *Sens. Actuat. B-Chem.*, **11**, (1-3), 293-300.

Papkovsky, D. B. and O'Riordan, T. C. (2005). Emerging applications of phosphorescent metalloporphyrins. *J. Fluoresc.*, **15** (4), 569-584.

Pardo-Yissar V., Katz, E., Wasserman, J. and Willner, I. (2003). Acetylcholine esterase-labeled CdS nanoparticles on electrodes. photoelectrochemical sensing of the enzyme inhibitors. *J. Am. Chem Soc.*, **125** (3), 622-623.

Pavlickova, P., Schneider, E.M. and Hug, H. (2004). Advances in recombinant antibody microarrays. *Clin. Chim. Acta*, **343**, (1-2), 17-35.

Peiró, G., Aranda, F.I, Adrover, E., Niveiro, M., Alenda, C., Payá, A. and Seguí, J. (2007). Analysis of HER2 by chromogenic in situ hybridization and immunohistochemistry in lymph node-negative breast carcinoma: prognostic relevance. *Hum. Path.*, **38** (1), 26-34.

Pejic, B. and DeMarco, R (2006). Impedance spectroscopy: Over 35 years of electrochemical sensor optimization. *Electrochim. Acta*, **51** (28), 6217-6229.

Peterlana, D., Puccetti, A., Corrocher, R. and Lunardi, C. (2006). Serologic and molecular detection of human Parvovirus B19 infection. *Clin. Chim. Acta*, **372**, (1-2), 14-23.

Pham, K.N, Fullston, D. and Sagoe-Crentsil, K. (2007). Surface modification for stability of nano-sized silica colloids. *J Coll Interfa. Sci.* **315**, 1, 123-127

Pohanka, M., Pavli, O and Skl'adal, P (2007). Diagnosis of tularemia using piezoelectric biosensor technology. *Talanta*, **71**, 981-985.

Porath, J., Carlsson, J, Olsson, I and Belfrage, G. (1975). Metal chelate affinity chromatography, a new approach to protein fractionation. *Nature London*, **258**, 598-599.

Posner, B., Lee, I., Itoh, T., Pyati, J., Graff, R., Thorton, G.B., La Polla, B. and Benkovic, S.J.(1993). A revised strategy for cloning antibody gene fragments in bacteria. *Gene*, **128** (1), 111-117

Prandoni, A. and Wright, I.S. (1942). The anti-coagulants heparin and the dicoumarin 3,30-methylene-bis (-4-hydroxycoumarin). *Bull NY Acad Med.*, **18**, 433-458

Prasad, B. and Lal, R. (1999). A capacitive immunosensor measurement system with a lock-in amplifier and potentiostatic control by software. *Meas. Sci. Technol* , **10**, 1097-1104

Prasad, G.R., Daniels, S., Cameron, D.C., McNamara, B.P , Tully E. and O'Kennedy, R (2005). PECVD of biocompatible coatings on 316L stainless steel. *Surf Coat. Technol.*, **200** (1-4), 1031-1035.

Pritchard, J., Law, K., Vakurov, A.; Millner, P. Higson, S P. (2004). Sonochemically fabricated enzyme microelectrode arrays for the environmental monitoring of pesticides *Biosens Bioelectron.*, **20** (4), 765-772.

Prowse, C., Ludlam, C.A. and Yap, P.L. (1997). Human parvovirus B19 and blood products. *Vox. Sang.*, **72**, 1-10.

Purvis, D., Leonardova, O., Farmakovsky, D and Cherkasov, V. (2003). An ultrasensitive and stable potentiometric immunosensor. *Biosens. Bioelectron* , **18**, 1385-1390.

Q

Qhobosheane, M., Santra, S., Zhang, P and Tan, W. (2001). Biochemically functionalized silica nanoparticles *Analyst*, **126** (8), 1274-1278

Qiagen Ltd. (2000). In *The QIA Expressionist: A handbook for the high-level expression and purification of 6 His-tagged proteins* QIAgen Ltd., West Sussex, UK.

Quinn, J. and O'Kennedy, R (1999) Transduction platforms and biointerfacial design of biosensors for 'real-time' biomolecular interaction analysis. *Anal. Letters*, **32**, 1475-1517.

R

Raitman, O.A., Katz, E, Buckmann, AF and Willner, I (2002). Integration of polyaniline/poly(acrylic acid) films and redox enzymes on electrode supports: an in situ electrochemical/surface plasmon resonance study of the bioelectrocatalyzed oxidation of glucose or lactate in the integrated bioelectrocatalytic systems. *J. Am. Chem. Soc.*, **124** (22), 6487-6496.

Ramanavičius, A., Ramanavičiene, A. and Malinauskas, A. (2006). Electrochemical sensors based on conducting polymer-polypyrrole. *Electrochim. Acta*, **51** (27), 6025-6037.

Rao, L., Jones, D.P., Nguyen, Lam H., McMahan, Scott A. and Burgess, R.A. (1996). Epitope mapping using histidine-tagged protein fragments: Application to *E. coli* RNA polymerase σ^{70} . *Anal. Biochem.*, **241**, 173-179.

Rea, M.C., Cogan, T.M. and Tobin, T. (1992). Incidence of pathogenic bacteria in raw milk in Ireland. *J. Appl. Bacteriol.*, **73**, 331-336.

Rodil, S.E., Olivares, R., Arzate, H. and Muhl, S. (2003). Properties of carbon films and their biocompatibility using in-vitro tests. *Diamond Relat. Mater.*, **12**, (3-7), 931-937.

Rodil, S. E., Olivares, R. and Arzate, H. (2005). In vitro cytotoxicity of amorphous carbon films. *Biomed. Mater. Eng.*, **15** (1-2), 101-112.

Rogers, K.R. (2000). Principles of affinity-based biosensors. *Mol. Biotechnol.*, **14**, 109.

Roitt, I. M. (1994), Essential immunology - 8th ed., Blackwell Scientific Publications, Oxford, UK.

Roque, A.C.A., Silva, C.S O. and Taipa, M.A. (2007). Affinity-based methodologies and ligands for antibody purification: Advances and perspectives. *J. Chromatog. A*, **1160**, (1-2), 44-55.

Rowe^a, C. A., Scruggs, S B., Feldstein, M. J, Golden, J. P. and Ligler, F. S. (1999). An array immunosensor for simultaneous detection of clinical analytes. *Anal Chem.* **71**, 433-439.

Rowe^b, C.A., Tender, L.M., Feldstein, M.J., Golden, J.P., Scruggs, S.B., MacCraith, B.D., Cras, J.J. and Ligler, F.S. (1999). Array biosensor for simultaneous identification of bacterial, viral, and protein analytes. *Anal. Chem.*, **71**, 3846-3852.

Rowe-Taitt, C.A., Golden, J.P, Feldstein, M.J., Cras, J.J., Hoffman, K.E. and Ligler, F.S. (2000). Array biosensor for detection of biohazards. *Biosens.Bioelectron.*, **14**, (10-11), 785-794.

Rubina, A.Y., Dyukova, V.I. Dementieva, E.I., Stomakhin, A.A., Nesmeyanov, V.A., Grishin, E.V. and Zasedatelev, A.S (2005). Quantitative immunoassay of biotoxins on hydrogel-based protein microchips. *Anal. Biochem* , **340**(2), 317-329.

Rucker, V. C., Havenstrite, K. L, and Herr, A.E. (2005). Antibody microarrays for native toxin detection. *Anal. Biochem.* **339** (2), 262-270.

Ryan, O., Smyth, M.R. and O’Fagan, C. (1994). Horseradish peroxidase the analyst's friend. *Essays Biochem.*, **28**, 129-146.

S

Sadik, O. A., Xu, H. and Gheorghiu, E. (2002). Differential impedance spectroscopy for monitoring protein immobilization and antibody-antigen reactions. *Anal. Chem.*, **74** (13), 3142-3150.

Santala, V. and Lammunmäki, U. (2004) Production of a biotinylated single-chain antibody fragment in the cytoplasm of *Escherichia coli*. *J. Immunol. Methods.*, **284**, 165-175.

Santra, S., Zhang, P., Wang, K., Tapeç, R. and Tan, W. (2001). Conjugation of biomolecules with luminophore-doped silica nanoparticles for photostable biomarkers. *Anal. Chem.*, **73** (20), 4988-4993

Sapsford, K.E., Charles, P.T , Patterson, C.H and Ligler, F.S. (2002). Demonstration of four immunoassay formats using the array biosensor *Anal. Chem* , **74** (5), 1061-1068

Sapsford, K.E., Ngundi, M.N., Moore, M.H., Lassman, M.E., Shriver-Lake, L.C., Taitt, C.R and Ligler, F.S (2006) Rapid detection of foodborne contaminants using an Array Biosensor *Sens. Actuat. B-Chem.*, **113** (2), 599-607.

Sargent, A. and Sadik, O.A, (1999). Monitoring antibody–antigen reactions at conducting polymer-based immunosensors using impedance spectroscopy. *Electrochim. Acta*, **44**, 4667-4675.

Satoh, H., Hayashi, M. and Satoh, S. (1982). Anti-warfarin antibody preparation and its characterization for radioimmunoassay. *J. Pharm. Pharmacol.*, **34** (7), 429-433

- Schatz, P.J.** (1993). Use of peptide libraries to map the substrate specificity of a peptide-modifying enzyme: a 13 residue consensus peptide specifies biotinylation in *Escherichia coli* *Biotechnology*, **10**, 1138-1143.
- Schettters, H.** (1999). Avidin and streptavidin in clinical diagnostics. *Biomol. Eng.*, **16**, 73–8.
- Schneider, B.H.**, Dickinson, E.L., Vach, M.D., Hoijer, J.V. and Howard, L.V. (2000). Highly sensitive optical chip immunoassays in human serum. *Biosens Bioelectron.* **15**, 13–22.
- Schubert, W-D.**, Gobel, G., Diepholz, M., Darji, A., Kloer, D., Hain, T., Chakraborty, T., Wehland, J., Domann, E. and Heinz, D.W. (2001). Internalins from the human pathogen *Listeria monocytogenes* combine three distinct folds into a contiguous Internalin domain. *J Molec. Biol.*, **312**, 783-794.
- Schultze, J.W.** (2000). Electrochemical Materials Science: An introduction to Symposium 4 of the 50th Anniversary of ISE Electrochemistry and Materials: Synthesis and Characterization. *Electrochim.Acta*, **45** (20), 3193-3203.
- Scouten, W.H.**, Luong, J.H.T. and Brown, R.S. (1995). Enzyme or protein immobilization techniques for applications in biosensor design. *Trends Biotechnol.*, **3**, 178.
- Sethi, R.S.** (1994). Transducer aspects of biosensors. *Biosens. Bioelectron* , **9** (3), 243-264.
- Seveus, L.**, Vaisala, M., Hemmila, I., Kojola, H., Roomans, G. M. and Soini, E. (1994). Use of fluorescent europium chelates as labels in microscopy allows glutaraldehyde fixation and permanent mounting and leads to reduced autofluorescence and good long-term stability *Microsc.Res.Tech.*, **28** (2), 149-154.
- Seydack, M.** (2005). Nanoparticle labels in immunosensing using optical detection methods. *Biosens. Bioelectron.*, **20** (12), 2454-2469.
- Sibler, A.P.**, Kempf, E., Glacet, A., Orfanoudakis, G., Bourel, D. and Weiss, E. (1999). In vivo biotinylated recombinant antibodies: high efficiency of labelling and application to the cloning of active anti-human IgG1 Fab fragments. *J. Immunol. Methods.*, **224**, 1-2,129-140.

Skladal, P., Morozova, N O and Reshetilov, A.N. (2002) Amperometric biosensors for detection of phenol using chemically modified electrodes containing immobilized bacteria *Biosens. Bioelectron.*, **17** (10), 867-873.

Skottrup, P., Hearty, S., Frøkiær, H., Leonard, P, Hejgaard, J, O'Kennedy, R., Nicolaisen, M and Justesen, A.F. (2007). *Biosens. Bioelectron.*, **22**, 2724–2729.

Slavík, R., Homola, J and Brynda, E. (2002). A miniature fiber optic surface plasmon resonance sensor for fast detection of staphylococcal enterotoxin B. *Biosens Bioelectron.*, **17**,6-7, 591-595.

Smith, D. and Johnson, K. (1988) Single-step purification of polypeptides expressed in *Escherichia coli* as fusions with glutathione S-transferase. *Gene*, **67**, 31 – 40.

Smith, G.P. (1985) Filamentous fusion phage: novel expression vectors that display cloned antigens on the virion surface. *Science*, **228**, 1315-1317.

Smith, J.E., Wang, L. and Tan, W. (2006). Bioconjugated silica-coated nanoparticles for bioseparation and bioanalysis. *Trends Anal.Chem.*, **25** (9), 848-855.

Soderlind, E., Ohlin, M and Carlsson, R. (1999). Complementarity-determining region (CDR) implantation: a theme of recombination. *Immunotechnol* , **4**, 279-285.

Song, F., Peng, X., Lu, E., Zhang, R, Chen, X. and Song, B (2004). Syntheses, spectral properties and photostabilities of novel water-soluble near-infrared cyanine dyes. *J. Photochem Photobiol.A* **168** (1-2), 53-57.

Souteyrand, E., Martin, J. R. and Martelet, C. (1994). Direct detection of biomolecules by electrochemical impedance measurements. *Sens. Actuat. B-Chem.*, **20** (1), 63-69.

Southwick, F.S. and Purich, D.L. (1996). Intracellular Pathogenesis of listeriosis. *New Engl. J. Med.*, **334**, 770-775.

Stapleton, S., Tully, E. and O'Kennedy, R. (2004). Immunoassays: the production of antibodies. *Encyclopedia of Analytical Science*, (2nd Edition), Townsend, A. (Ed). Academic Press, New York, USA, pp306-316.

Stoynov, Z.B., Grafov, B., Stoynova, B. and Elkin, V. (1991). Electrochemical Impedance. *Nauka, Moscow*.

Stoynov, Z. (1989). Structural spectral analysis of electrochemical impedance *Electrochim. Acta*, **34** (8), 1187-1192.

Stranik, O., McEvoy, H. M, McDonagh, C. and MacCrath, B. D. (2005). Plasmonic enhancement of fluorescence for sensor applications *Sens. Actuat B-Chem.*, **107** (1), 148-153.

Stuber, D., Bannwarth, W., Meloen, R. and Matile, H. (1990). New B cell epitopes in the *Plasmodium falciparum* malaria circumsporozoite protein. *Eur. J. Immunol.*, **20**, 819 – 824.

Sukhanova, A., Devy, J., Venteo, L., Kaplan, H , Artemyev, M., Oleinikov, V., Klinov, D., Pluot, M., Cohen, J.H.M. and Nabiev, I. (2004). Biocompatible fluorescent nanocrystals for immunolabeling of membrane proteins and cells. *Anal. Biochem.*, **324** (1), 60-67.

Sun, B., Xie, W., Yi, G., Chen, D., Zhou, Y. and Cheng, J. (2001). Microminiaturized immunoassays using quantum dots as fluorescent label by laser confocal scanning fluorescence detection. *J. Immunol. Methods*, **249**, 85-89.

Sun, Y., Lu, M., Yin, X-F. and Gong, X-G. (2006). Intracellular labeling method for chip-based capillary electrophoresis fluorimetric single cell analysis using liposomes *J Chromatog. A*, **1135** (1), 109-114.

Suresh-Kumar, R., Prabhune, A.A., Pundle, A.V., Karthikeyan, M. and Suresh, C.G. (2007). A tryptophan residue is identified in the substrate binding of penicillin G acylase from *Kluyvera citrophila*. *Enzym. Microb. Technol.*, **40**, 1389–1397.

Sutherland, A.J. (2002). Quantum dots as luminescent probes in biological systems. *Curr. Opin Solid State Mater. Sci.*, **6** (4), 365-370.

Székács, A., Trummer, N., Adányi, N., Váradi, M. and Szendro, I. (2003). Development of a non-labeled immunosensor for the herbicide trifluralin via optical waveguide lightmode spectroscopic detection. *Anal. Chim. Acta*, **487**, (1), 31-42.

Szymańska, I., Radecka, H., Radecki, J. and Kaliszan, R. (2007). Electrochemical impedance spectroscopy for study of amyloid β -peptide interactions with (-) nicotine ditartrate and (-) cotinine. *Biosens. Bioelectron.*, **22** (9-10), 1955-1960.

T

Tan^a, L.P., Lue, R.Y.P., Chen, G.Y.J and Yao, S.Q. (2004). Improving the intein-mediated, site-specific protein biotinylation strategies both *in vitro* and *in vivo* *Bioorgan. Med Chem Letts.*, **14** (24), 6067-6070.

Tan^b, W., Wang, K. and He, X (2004) Bionanotechnology based on silica nanoparticles. *Med. Res. Rev.*, **24** (5), 621-638.

Tatsumi, H., Fukuda S, Kikuchi M. and Koyama Y. (1996) Construction of biotinylated firefly luciferases using biotin acceptor peptides. *Anal. Biochem.*, **1, 243** (1), 176-180.

Taylor, R.F. (1991) Immobilized antibody and receptor-based biosensors. Protein Immobilization, Fundamentals and Applications, Marcel Dekker, New York, USA.

Tijssen, P. (1985) Practice and theory of enzyme immunoassays. Elsevier, New York,, USA.

Tirat, A., Freuler, F., Stettler, T., Mayr, L.M. and Leder, L. (2006). Evaluation of two novel tag-based labelling technologies for site-specific modification of proteins. *Int. J. Biol Macromols.*, **39**, (1-3), 66-76.

Todman, M.G., Han, S.K. and Herbison, A.E. (2005). Profiling neurotransmitter receptor expression in mouse gonadotropin-releasing hormone neurons using green fluorescent protein-promoter transgenics and microarrays. *Neuroscience*, **132**(3), 703-712.

Trau, D., Yang, W., Seydack, M., Caruso, F. and Yu, N.T (2002). Nanoencapsulated microcrystalline particles for superamplified biochemical assays. *Anal. Chem.*, **21**, 5480-5486.

Tsien, R.Y. (1998). The green fluorescent protein. *Annu. Rev. Biochem.*, **67**, 509-544.

Tully, E., Hearty, S., Leonard, P. and O'Kennedy, R. (2006). The development of rapid fluorescence-based immunoassays, using quantum dot-labelled antibodies for the detection of *Listeria monocytogenes* cell surface proteins. *Int J. Biol. Macromol.*, **39**, (1-3), 127-134.

Turková, J. (1999). Oriented immobilization of biologically active proteins as a tool for revealing protein interactions and function. *J. Chromatog. B.*, **722**, (1-2), 11-31.

Turner, A.P.F., Karube, I. and Wilson, G.S (Eds). (1986). *Biosensors: fundamentals and applications*. Oxford University Press, Oxford, UK.

Turner A.P.F., Karube I. and Wilson, G.S. (1989). *Biosensors fundamentals and Applications* - Chapter 6. Immobilisation of the biological component of biosensors. Oxford Science Publications, Oxford, UK.

V

Valeur-Jensen, A.K., (1999). Risk factors for parvovirus B19 infection in pregnancy *J. Amer. Med. Assoc.*, **281**, 1099-1105.

Van Emon, J.M., Seiber, J.N and Hammock, B.D. (1989). Immunoassay techniques for pesticide analysis. In: Sherma, J. (ed.), *Analytical methods for pesticides and plant growth regulators* (Volume XVII: Advanced analytical techniques). Academic Press, San Diego, pp217-261.

Vaughan, T., Williams, A., Pritchard, K., Osbourn, J , Pope, A., Earnshaw, J , McCafferty, J., Hodits, R., Wilton, J. and Johnson, K. (1996). Human antibodies with sub-nanomolar affinities isolated from a large non-immunised phage display library *Nature Biotechnol.*, **14**, 309-314

Vautin-Ul, C., Boisse-Laporte, C., Bennisad, N., Chausse, A., Leprince, P. and Messina, R. (2000). Hexamethyldisiloxane (HMDSO)-plasma-polymerised coatings as primer for iron corrosion protection: influence of RF bias. *Prog. Org. Coat.*, **38**, 9.

Villa, R., Ortiz, C.R , Tapia, S., Gonzalez, G., Trillo, E., Garza, K.M., Stafford, S.W. and Murr. L.E. (2002). *In vitro* biocompatibility studies of fibroblast cells on Ti-Ta alloys. *Mater. Trans.* **43**, (12), 2991-2994.

Vo-Dinh, T., Cullum, B.M. and Stokes, D.L. (2001). Nanosensors and biochips: frontiers in biomolecular diagnostics *Sens. Actuat. B-Chem.*, **74**, (1-3), 2-11.

W

Wacker, R., Schroder, H. and Niemeyer, C.M. (2004). Performance of antibody microarrays fabricated by either DNA-directed immobilization, direct spotting, or streptavidin-biotin attachment: a comparative study. *Anal. Biochem.*, **330**, 281-287.

Wadkins, R.M., Golden, J.P., Pritsiolas, L.M. and Ligler, F.S. (1998). Detection of multiple toxic agents using a planar array immunosensor. *Biosens Bioelectron.*, **13**, 407-15

Wang, L.Y., Zhao, C. Q., Zhu, C. Q. and Wang, L. (2004). Syntheses and spectral studies of functionalized ZnS nanoparticles as fluorescence probes. *Guang Pu Xue Yu Guang Pu Fen Xi*, **24** (1), 98-101.

Wang^a, W., Jin, Q and Luo, G. (2003). A novel sandwich immunosensing method for measuring cardiac troponin I in sera. *Anal. Biochem.*, **321** (2), 209-216.

Wang^b, H., Li, J., Ding, Y, Lei, C., Shen, G and Yu, R. (2004). Novel immunoassay for *Toxoplasma gondii*-specific immunoglobulin G using a silica nanoparticle-based biomolecular immobilization method. *Anal. Chim Acta*, **501**, (1) , 37-43.

Wei, J., Mu, Y., Song, D., Fang, X., Liu, X, Bu, L., Zhang, H., Zhang, G.Ding, J. Wang, W., Jin, Q. and Luo, G. (2003). A novel sandwich immunosensing method for measuring cardiac troponin I in sera. *Anal. Biochem.*, **321**, (2), 209-216

West, J. L., and Halas, N.J. (2000). Applications of nanotechnology to biotechnology commentary. *Curr Opin. Biotechnol.*, **11**, (2), 215-217.

Westwood, O.M.R. and Hay, F.C., (Eds.), (2001). Epitope mapping: a practical approach. Oxford University Press, Oxford, UK.

Wilchek, M. and Bayer, E.A. (1988). The avidin-biotin complex in bioanalytical applications *Anal. Biochem.*, **171**, 1-32.

Willner, I. and Katz, E. (2000). Integration of Layered Redox Proteins and Conductive Supports for Bioelectronic Applications *Angew Chem Int Ed.*, **39**, 1180-1218

Willner, I., Katz, E. and Willner, B. (2000). Biosensors and their applications. (Eds: Yang VC, Ngo TT). Kluwer Academic publishers New York, **4**, 47

Willner, I. (2002). Tech.Sight. Bioelectronics. Biomaterials for sensors, fuel cells, and circuitry *Science*, **298**, 2407-2408

Wingren, C., Steinhauer, C., Ingvarsson, J., Persson, E., Larsson, K. and Borrebaeck, C.A K. (2005). Microarrays based on affinity-tagged single chain Fv antibodies: Sensitive detection of analyte in complex proteomes. *Proteomics*, **5**, 1281-1291.

Winter, G., Griffiths, A.D., Hawkins, R.E. and Hoogenboom, H.R. (1994). Making antibodies by phage display technology *Ann. Rev. Immunol.*, **12**, 433-55.

Wolfbeis, O.S. (Ed.). (1993). Fluorescence Spectroscopy. New methods and applications. Springer-Verlag, Heidelberg, Germany

Wong, S. and Brown, K.E. (2006). Development of an improved method of detection of infectious parvovirus B19. *J. Clin. Virol.*, **35** (4), 407-413.

Wu, P., Hoglebe, P. and Granger, D.W. (2006). DNA and protein microarray printing on silicon nitride waveguide surfaces. *Biosens. Bioelectron.*, **21** (7), 1252-1263.

Wu, Z., Yan, Y, Shen, G. and Yu, R (2000) A novel approach of antibody immobilization based on n-butyl amine plasma-polymerized films for immunosensors. *Anal. Chim.Acta*, **412**, (1-2), 29-35.

X

Xu, Z., Chen, X. and Dong, S. (2006) Electrochemical biosensors based on advanced bioimmobilization matrices *TrAC.*, **25** (9), 899-908.

Y

Yamaguchi, Y., Kim, H., Kato, K., Masuda, K., Shimada, I. and Arata, Y. (1995). Proteolytic fragmentation with high specificity of mouse immunoglobulin G mapping of proteolytic cleavage sites in the hinge region. *J. Immunol. Methods*, **181** (2), 259-267.

Yang, M., McGovern, M.E. and Thompson M. (1997). Genosensor technology and the detection of interfacial nucleic acid chemistry. *Anal. Chim. Acta*, **346** (3), 259-275.

Ye, Z., Tan, M., Wang, G. and Yuan, J. (2005). Development of functionalized terbium fluorescent nanoparticles for antibody labeling and time-resolved fluoroimmunoassay application. *Talanta*, **65**, 206-210.

Yoto, Y., Kudoh, T., Haseyama, K., Suzuki, N., Oda, T., Katoh, T., Takahashi, T., Sekiguchi, S. and Chiba, S. (1995). Incidence of human parvovirus B19 DNA detection in blood donors. *Br J. Haematol.*, **91**, 1017-1018.

Young, N., MacKenzie, C., Narang, S., Oomen, R. and Baenziger, J. (1995). Thermal stabilization of a single-chain Fv antibody fragment by introduction of a disulphide bond. *FEBS Letts.*, **377** (2), 135 - 139.

Young, N.S. and Browne, K.E. (2004) Parvovirus B19. *N Engl. J. Med.*, **350**, (6), 586-597.

Yuan, J. and Wang, G. (2006). Lanthanide-based luminescence probes and time-resolved luminescence bioassays. *TrAC*, **25** (5), 490-500.

Z

Zayats, M., Kharitonov A.B., Katz, E., Buckmann, A.F. and Willner, I. (2000) An integrated NAD⁺-dependent enzyme-functionalized field-effect transistor (ENFET) system: development of a lactate biosensor. *Biosens. Bioelectron.*, **15**, (11-12), 671-680

Zhang, X., Guan, R.F., Zhang, F. and Chan, K.Y. (2006). Ordered amino-functionalized mesoporous silica thin films for high-density DNA probes. *Script. Material*, **54** (9), 1651-1654

Zhao, X., Bagwe, R.P. and Tan, W. (2004). Development of organic-dye-doped silica nanoparticles in a reverse microemulsion. *Adv. Mater.*, **16** (2), 173-176.

Zheng, D., Wang, N 7 Wang, F. (2004). Sensitive chemically amplified electrochemical detection of ruthenium tris-(2,2'-bipyridine) on tin-doped indium oxide electrode. *Anal.Chim.Acta*, **508** (2), 225-231.

Zotti, G., Cattarin, S. and Comisso, N. (1988). Cyclic potential sweep electropolymerization of aniline. The role of anions in the polymerization mechanism. *J. Electroanal. Chem.*, **239**, 387-396.

Appendix:
**PECVD of Biocompatible coatings on 316L
stainless steel for arterial stent applications.**

A1 Introduction

This section describes the strategies involved in assessing the biocompatibility of silica-like thin films, deposited on stainless steel by Plasma Enhanced Chemical Vapor Deposition (PECVD). The main application of such coatings is the fabrication of arterial stents and, therefore, biocompatibility of the material is a key issue. *Medical devices are subject to stringent controls and safeguards, under EU law and are subject to rigorous testing prior to use.* The component materials of medical devices may leach compounds, or have undesirable surface characteristics, which render them unsuitable for clinical use. Biocompatibility is defined as 'the ability of a material, device or system to perform without a clinically significant host response in the specific application' (Gurland, 1994). Preliminary biocompatibility studies in the early R&D stage of a biomaterial, generally employs the use of cell culture models for initial characterisation.

A2 Thin film composition & behaviour

SiO_xCyHz films are produced by plasma polymerization of hexamethyldisiloxane and oxygen. This study details the variation of the SiO_xCyHz film properties deposited on 316L stainless steel in a RF reactor. The films were characterized for their hardness, hydrocarbon content and wettability. The film properties are found to be dependent on the Oxygen/HMDSO flow ratio and RF power. The film-tissue interaction depends on the hydrophobicity or hydrophilicity of the film; therefore, the wettability of the film was measured by contact angle analysis. Preliminary biocompatibility studies were carried out using Rat Aortic Smooth Muscle (RASM) cells. The data collected for assessment of cell proliferation, viability and toxicity are presented.

The biomedical behaviour of implanted material can be altered by modifying its surface properties, without affecting the bulk mechanical properties (Li *et al.*, 1998). Plasma polymerized hexamethyldisiloxane (HMDSO) films deposited by PECVD is found to improve the cell activity at the implant-tissue interface (Hayakawa *et al.* 2004). The success of a biomaterial depends on the nature and composition of the first adsorbed protein layer and its activation rather than on the surface chemistry of the implant (Nimeri *et al.*, 2002). The protein adsorption and implant-tissue interaction is

dependent on the hydrophobicity and hydrophilicity of the surface (Janocha *et al.*, 2001). Several studies have reported the possibility of tuning the film properties by varying the O₂/HMDSO ratio and RF power, (Vautin-UI *et al.*, 2000) but less attention has been paid to the contact angle variation with plasma parameters (Behnisch *et al.*, 1998) We have investigated the variation of water contact angle with O₂/HMDSO ratio, pressure and RF power. Preliminary characterisation to assess the biocompatibility of the films has been carried out and initial results of cell proliferation, viability and toxicity is presented for different O₂/HMDSO ratio.

A3 Biocompatibility testing

To study the bioresponse of the films, rat aortic smooth muscle (RASM) cells were cultured in standard 75cm² cell culture flasks in a cell culture medium composed of Dulbecco's modified Eagle's medium (DMEM) supplemented with 10% (v/v) fetal calf serum (FCS), 2% (v/v) L-glutamine and appropriate antibiotics (Detailed in Section 2.12.1). The cells were grown at 37°C in a humidified atmosphere with 5% CO₂. The thin film coated samples were seeded in 24 well culture plates at a density of 10,000cells/ml (Villa *et al.*, 2002). Each batch of samples was plated in triplicate for both the MTT assay and cell proliferation and viability determination, with appropriate controls. Assays were conducted on Days 2, 4 and 6.

A4 Cell proliferation & viability

Cells were grown (Section 2.12.1). On day 2, 4 and 6 of the experiment, samples were removed for morphological analysis post incubation in culture and the cultured cells assessed for cell proliferation and viability, by Trypan blue vital dye staining. The trypsinised cells were counted as per Section 2.12.3 and viability calculated. This process was repeated on days 4 and 6 of the experiment and the data compiled graphically (Figure A1). The cells from wells containing untreated substrates and no substrate were also tested as controls.

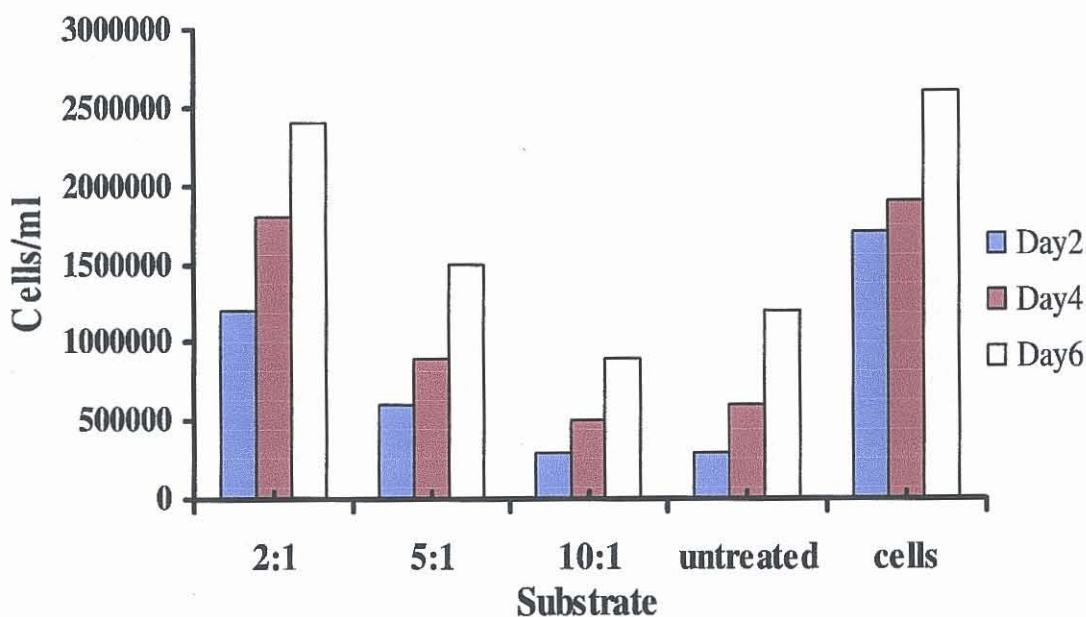


Figure A1 Initial results of the cell proliferation & viability tests, which are determined by Trypan blue staining and counting with a Neubauer haemocytometer. The lowest ratio of Oxygen to HMDSO (2:1) showed the greatest proliferation, almost comparable to the growth of cells seeded in absence of any substrate. The cell viability tests are based on the ability of dead cells to take up Trypan blue dye, where as live healthy cells remain white. Percentage viability was calculated to be > 90% in all cases except for the negative control, latex, where the % viability was < 10%.

It is clear from Figure A1 that the film surface does not adversely affect the growth of the cells, and that the RASM cells do not die off in culture in the presence of these materials. In fact the growth of the cells with coated substrates is comparable to those seeded without substrates. Films with varying wettability were deposited by varying the O₂/HMDSO ratio. The hydrocarbon content decreases with increasing O₂/HMDSO ratio and RF power. This leads to an increase in the film hardness as the film becomes 'silica-like' at high O₂/HMDSO ratio and high RF power. The high O₂/HMDSO ratio films show a temporal effect exhibiting high hydrophilicity immediately after deposition but the hydrophilicity decreases with time. The low O₂/HMDSO ratio (2:1) films show a higher proliferation rate than the high O₂/HMDSO ratio (10:1) film.

A5 Cytotoxicity testing

A commercial MTT assay kit (Roche Diagnostics) was used to assess cytotoxicity of the cells in culture, post-incubation with the coated substrates, as described in section 2.12.5. MTT (3-[4,5-dimethylthiazol-2-yl]-2,5-diphenyltetrazolium bromide) is a yellow tetrazolium salt that cleaved by metabolically active cells to form purple formazan salt crystals. An increase in the number of living cells results in an increase in the total metabolic activity in the sample. This increase directly correlates to the amount of purple formazan crystals formed, as monitored by the absorbance (Rodil *et al.*, 2003). The MTT test was performed for each substrate in 8 separate wells and each experiment was repeated for the full set of samples on three occasions

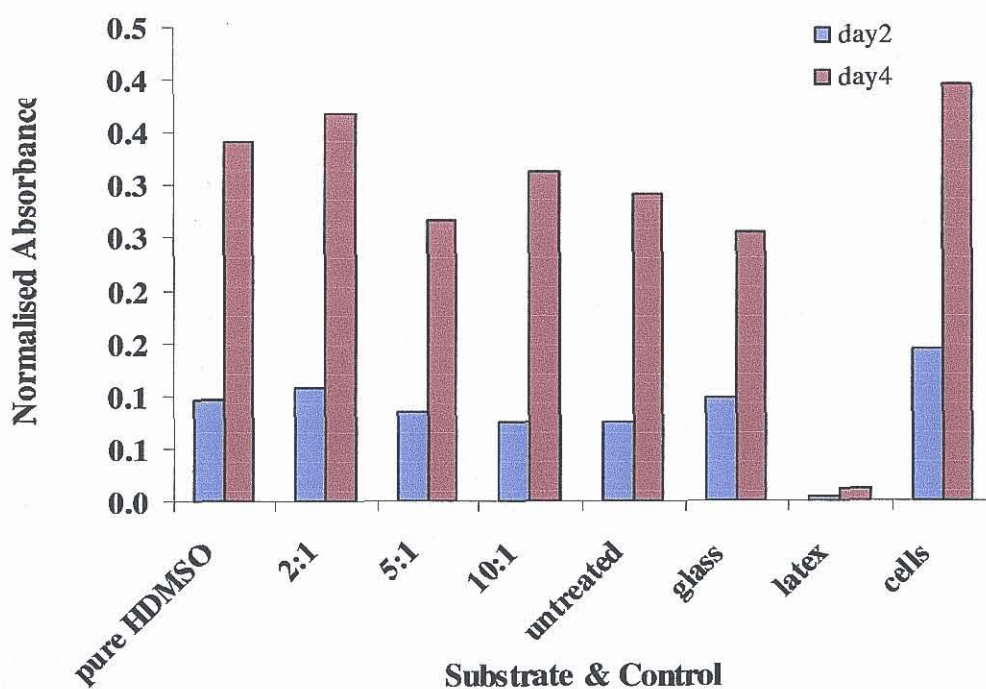


Figure A2 Initial results of the cytotoxicity tests, which are determined by MTT assay. The lowest ratio of oxygen to HDMSO (2:1) showed the greatest proliferation, almost comparable to the growth of cells seeded in absence of any substrate. The cell viability tests were based on the ability of dead cells to take up Trypan blue dye, where as live healthy cells remained white. Percentage viability was calculated to be >90% in all cases except for the negative control, latex, which is know to be highly toxic to cells.

It is clear from Figure A2 that the film surface does not adversely effect the growth of the cells, and that the RASM cells do not die off in culture in the presence of these foreign materials. In fact the growth of the cells with coated substrates is comparable to those seeded without substrates.

A6 SEM analysis of substrates post incubation in culture with RASM cells.

Substrates were removed from culture and cells fixed with glutaraldehyde and osmium tetroxide (*Section 2.12.7*) prior to examination using Scanning Electron Microscopy (SEM). Figure A3 (A-D) shows SEM pictures for each ratio of $O_2/HDMSO$ tested.

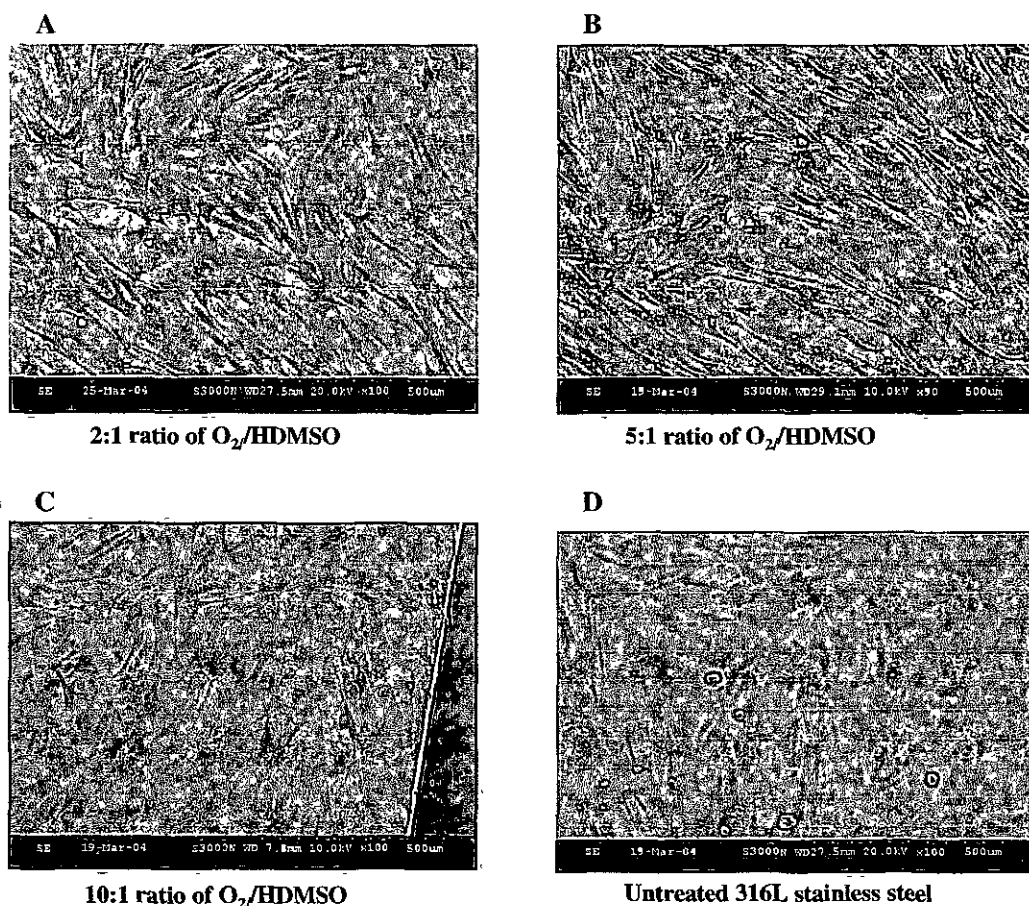


Figure A3 SEM images of stainless steel substrates post incubation in culture with varying ratios of HDMSO/ O_2 . Cell adhesion and proliferation is greatest on the films with lowest ratio of oxygen to HDMSO (2:1). Higher magnification and examination of a greater sample set would give more detail as to the actual effect of the thin film on the stainless steel substrates.

A7 Discussion

The films do not seem to adversely affect the growth of the cells. The RASM cells do not die off in culture in the presence of the coated stainless steel. The growth of the cells with coated substrates is comparable to those seeded with no substrates. A small sample set was used to conduct these preliminary investigations. For a more complete assessment of the biocompatibility of these thin films, a greater sample set and larger number of replicates for each experiment would be necessary.

Future work on this project could include the assessment of the biocompatibility of PECVD thin-film coated polymers such as PMMA, PDMS and Polycarbonate. Protein absorption analysis of thin film coated polymers for biochip application could also be investigated. Directed cell attachment on various substrates using biocompatible thin films and the incorporation of various fluorescent labels into such cells via immunostaining, would allow the monitoring of the cell growth on the films using fluorescent microscopy.